

Tong-Cun Zhang
Pingkai Ouyang
Samuel Kaplan
Bill Skarnes *Editors*

Proceedings of the 2012 International Conference on Applied Biotechnology (ICAB 2012)

Volume 2

Lecture Notes in Electrical Engineering

Volume 250

For further volumes:
<http://www.springer.com/series/7818>

Tong-Cun Zhang · Pingkai Ouyang
Samuel Kaplan · Bill Skarnes
Editors

Proceedings of the 2012 International Conference on Applied Biotechnology (ICAB 2012)

Volume 2

 Springer

Editors

Tong-Cun Zhang
College of Bioengineering
Tianjin University of Science
and Technology
Tianjin
People's Republic of China

Samuel Kaplan
Department of Microbiology, Houston
Medical School
University of Texas
Texas, TX
USA

Pingkai Ouyang
Nanjing University of Technology
Nanjing
People's Republic of China

Bill Skarnes
Wellcome Trust Sanger Institute
Cambridge
UK

ISSN 1876-1100

ISSN 1876-1119 (electronic)

ISBN 978-3-642-37921-5

ISBN 978-3-642-37922-2 (eBook)

DOI 10.1007/978-3-642-37922-2

Springer Heidelberg New York Dordrecht London

Library of Congress Control Number: 2013945796

© Springer-Verlag Berlin Heidelberg 2014

This work is subject to copyright. All rights are reserved by the Publisher, whether the whole or part of the material is concerned, specifically the rights of translation, reprinting, reuse of illustrations, recitation, broadcasting, reproduction on microfilms or in any other physical way, and transmission or information storage and retrieval, electronic adaptation, computer software, or by similar or dissimilar methodology now known or hereafter developed. Exempted from this legal reservation are brief excerpts in connection with reviews or scholarly analysis or material supplied specifically for the purpose of being entered and executed on a computer system, for exclusive use by the purchaser of the work. Duplication of this publication or parts thereof is permitted only under the provisions of the Copyright Law of the Publisher's location, in its current version, and permission for use must always be obtained from Springer. Permissions for use may be obtained through RightsLink at the Copyright Clearance Center. Violations are liable to prosecution under the respective Copyright Law. The use of general descriptive names, registered names, trademarks, service marks, etc. in this publication does not imply, even in the absence of a specific statement, that such names are exempt from the relevant protective laws and regulations and therefore free for general use.

While the advice and information in this book are believed to be true and accurate at the date of publication, neither the authors nor the editors nor the publisher can accept any legal responsibility for any errors or omissions that may be made. The publisher makes no warranty, express or implied, with respect to the material contained herein.

Printed on acid-free paper

Springer is part of Springer Science+Business Media (www.springer.com)

Preface

2012 International Conference on Applied Biotechnology (ICAB2012) was organized by Tianjin University of Science and Technology, Tianjin Institute of Industrial Biotechnology, Chinese Academy of Sciences was held from October 18th to 19th, 2012 in Tianjin, China.

The conference served as a forum for exchange and dissemination of ideas and the latest findings among all parties involved in any aspects of applied biotechnology. The following distinguished professors gave keynote speeches: Hassan Ashktorab (Howard University, U.S.A), William Carl Skarnes (The Wellcome Trust Sanger Institute, U.K), Hiroyuki Takenaka (Kyushu Kyoritsu University, Japan) and Xueli Zhang (Tianjin Institute of Industrial Biotechnology, Chinese Academy of Sciences, China). The conference was complemented by talks given by other 51 professors and investigates.

More than 200 authors from 44 different universities, institutes and companies submitted conference papers. A lot of fields have been covered, ranging from fermentation engineering, cell engineering, genetic engineering, enzyme engineering and protein engineering.

Special thanks are given to Academic Committee, Organizing Committee and Secretary Staff of the conference for the commitment to the conference organization. We would like also to thank all the authors who contributed with their papers to the success of the conference.

This Book gathers a selection of the papers presented at the conference; it contains contributions from both academic and industrial researchers providing a unique perspective on the research and development of applied biotechnology from all over the world. The scientific value of the papers also helps the researchers in this field to get more valuable results.

Tianjin, China

Tong-Cun Zhang
Pingkai Ouyang
Samuel Kaplan
Bill Skarnes

Committees

Sponsor

Chinese Society of Biotechnology

Organizers

Tianjin University of Science and Technology
Key Lab of Industrial Fermentation Microbiology, Ministry of Education
Tianjin Institute of Industrial Biotechnology, Chinese Academy of Sciences

Co-organizers

Tianjin Society for Microbiology
Tianjin International Joint Academy of Biotechnology and Medicine
College of Biotechnology and Pharmaceutical Engineering, Nanjing University of Technology
College of Life Science, Nankai University
School of Biotechnology, Jiangnan University
College of Life Science and Technology, Beijing University of Chemical Technology
School of Bioscience and Bioengineering, South China University of Technology
College of Biotechnology, Chongqing University
State Key Laboratory of Bioreactor Engineering, East China University of Science and Technology
School of Biological Engineering, Dalian Polytechnic University
School of Food and Bioengineering, Shandong Polytechnic University

Academic Committee

Chairman

Pingkai Ouyang, Academician, Nanjing University of Technology, China

Executive Chairman

Zixin Deng, Academician, Shanghai Jiaotong University, China

Baoguo Sun, Academician, Beijing Technology and Business University, China

Tianwei Tan, Academician, Beijing University of Chemical Technology, China

Prof. George Fu Gao, Institute of Microbiology of Chinese Academy of Sciences, China

Prof. Xiaohong Cao, Tianjin University of Science and Technology, China

Prof. Jian Chen, Jiangnan University, China

Prof. Yanhe Ma, Tianjin Institute of Industrial Biotechnology, Chinese Academy of Sciences, China

Members

Prof. Baishan Fang, Xiamen University, China

Prof. Cheng Yang, Tianjin International Joint Academy of Biotechnology and Medicine, China

Prof. Cunjiang Song, Nankai University (Tianjin Society for Microbiology), China

Prof. Danqun Huo, Chongqing University, China

Prof. Fang Liu, Nankai University, China

Prof. Fuping Lu, Tianjin University of Science and Technology, China

Prof. Guocheng Du, Jiangnan University, China

Prof. He Huang, Nanjing University of Technology, China

Prof. Hongzhang Chen, Institute of Process Engineering, Chinese Academy of Sciences, China

Prof. Jianhe Xu, East China University of Science and Technology, China

Prof. Jianjiang Zhong, Shanghai Jiaotong University, China

Prof. Jianjun Liu, Shandong Academy of Food and Fermentation Industries, China

Prof. Jibin Sun, Tianjin Institute of Industrial Biotechnology, Chinese Academy of Sciences, China

Prof. Lirong Yang, Zhejiang University, China

Prof. Longjiang Yu, Huazhong University of Science and Technology, China

Prof. Min Wang, Tianjin University of Science and Technology, China

Prof. Muyi Cai, China National Research Institute of Food and Fermentation Industries, China

Prof. Ning Chen, Tianjin University of Science and Technology, China
Prof. Qipeng Yuan, Beijing University of Chemical Technology, China
Prof. Ruiming Wang, Shandong Polytechnic University, China
Prof. Shiru Jia, Tianjin University of Science and Technology, China
Prof. Shuyi Qiu, Guizhou University, China
Prof. Shuangjiang Liu, Institute of Microbiology of Chinese Academy of Sciences, China
Prof. Youshu Xia, Sichuan Academy of Food and Fermentation Industries, China
Prof. Siliang Zhang, East China University of Science and Technology, China
Prof. Tong-Cun Zhang, Tianjin University of Science and Technology, China
Prof. Xianzhen Li, Dalian University of Technology, China
Prof. Xiaolei Wu, Beijing University, China
Prof. Xinhui Xing, Tsinghua University, China
Prof. Xueming Zhao, Tianjin University, China
Prof. Yin Li, Institute of Microbiology of Chinese Academy of Sciences, China
Prof. Yinbo Qu, Shandong University, China
Prof. Ying Lin, South China University of Technology, China

Organizing Committee

Chairman

Prof. George Fu Gao, Vice Dean, Beijing Institutes of Life Science, Chinese Academy of Sciences, China

Executive Chairman

Prof. Shuheng Ma, Vice Dean, Tianjin Institute of Industrial Biotechnology, Chinese Academy of Sciences, China
Prof. Dongguang Xiao, Dean, Tianjin University of Science and Technology, China

Members

Yinhua Wan, Deputy Secretary General, Chinese Society of Biotechnology, China
Lei Ma, Director, President's Office, Tianjin University of Science and Technology, China
Feng Wen, Secretary of the Party Committee, College of Bioengineering, Tianjin University of Science and Technology, China

Dingcheng Liu, Vice Dean, Division of Science and Technology, Tianjin University of Science and Technology, China
Cunjiang Song, Secretary General, Tianjin Society of Microbiology, China
Cheng Yang, Vice Dean, Tianjin International Joint Academy of Biotechnology and Medicine, China

Secretariat

Secretary General

Prof. Shuheng Ma, Vice Dean, Tianjin Institute of Industrial Biotechnology, Chinese Academy of Sciences, China

Deputy Secretary General

Prof. He Huang, Dean, Division of Science and Technology, Nanjing University of Technology, China
Prof. Cunjiang Song, Secretary General, Tianjin Society of Microbiology, China
Prof. Tong-Cun Zhang, Director, Key Laboratory of Industrial Fermentation Microbiology (Tianjin University of Science and Technology), Ministry of Education, China

Members

Yue Wang, Juke Wang, Hongling Wang, Jiaming Wang, Yanbing Shen, Yihan Liu, Jian Zhang, Chaozheng Zhang, Kui Lu, Hao Zhou, Xuegang Luo, Cheng Zhong, Qingyang Xu, Bin Jia, Xuewu Guo, Zhilei Tan

Contents

Part III Pharmaceutical Biotechnology

- 66 Promising Biomarkers: MicroRNAs at Diagnosis, Therapy and Prognostic Evaluation of Breast Cancer 649**
Dalin Lu, Nan Wang, Xinghua Liao, Xuan Huang, Jianhua Zhang, Zhenyu Wang, Lian Duan, Jiajie Liu, Baoshu Jin, Yue Wang and Tong-Cun Zhang
- 67 Dimerization of Chemokine Receptors and its Novel Roles in Drug Discovery 657**
Mingqing Wang, Baosheng Ge and Fang Huang
- 68 The Mechanism of Apoptosis in Adenocarcinoma of Lung Cancer A549 Cells Induced by Albumin-Derived from Peanut 669**
Minhui Long, Yuejun Sun, Ni Chen, Zimin Zhang, Wen Chu, Yue Ma, Shenheng Luo, Zhongpeng Zhao and Aipo Diao
- 69 Serum miR-124 and TNF- α are Biomarkers of Ischemic Cerebrovascular Disease 681**
Jiajie Liu, Xinghua Liao, Nan Wang, Jun Zhou, Lian Duan, Dalin Lu, Zhipeng Liu, Tingbao Yan, Deyun Ma, Xiumei Dong, Xueguang Sun and Tong-Cun Zhang
- 70 A New Process for Preparation of Hydroxytyrosol 689**
Yinghao Gao, Xijuan Liang, Yuanmou Chen, Fei Hu, Weizhu Liu, Peng Yu and Erbing Hua
- 71 Design and Synthesis of 2-Arylbenzimidazole Analogues as Novel SIRT1 Activators for the Treatment of Type II Diabetes 697**
Fei Hu, Yuanmou Chen, Yinghao Gao, Shaolong Jia, Weizhu Liu, Peng Yu and Erbing Hua

72	Design and Synthesis of SRT1 Activators for Potential Lead Compounds of Treatment of Diabetes	705
	Weizhu Liu, Qiuyue Wang, Fei Hu, Yinghao Gao, Yingying Wang, Peng Yu and Erbing Hua	
73	Synthesis of 1,3-benzodioxol-5-ethanol and Its Derivatives	715
	Na Ji, Yinghao Gao, Yuanmou Chen, Shaolong Jia, Fei Hu, Peng Yu and Erbing Hua	
74	Tetrandrine Inhibits Proteasomal Chymotrypsin-Like Activity and Induces Apoptosis in Human PC-3 Cells	723
	Li Zhang, Wanxin Shi, Weihua Cao, Xiangru Liang, Yufu Hu, Mo Chen and Guoqing Shi	
75	The Purifying Effect of Apocynum Venetum Seedlings on Estuarine Water	733
	Yangcang Xu, Tao Yu, Yunshan Zhong and Xiaoyan Wang	
76	Expression, Purification, and Activity Assay of Chicken Interferon-Alpha	741
	Yue Ma, Minhui Long and Aipo Diao	
77	Synthesis and Controlled Release of 5-Fluorouracil from Hydroxyethylchitosan: Based Polymer Prodrug	749
	Yanfei Peng, Wanshun Liu, Baoqin Han and Ruixue Zhou	
78	Telomerase is Significant as an Early Diagnostic Marker and Therapeutic Target	757
	Lian Duan, Nan Wang, Xinghua Liao, Jun Zhou, Dalin lu, Jiajie Liu, Xueguang Sun and Tong-Cun Zhang	
79	Isolation, Identification, Antibacterial Effects of Antibiotic Drugs, and Chinese Herbal Extracts to the Pathogenic Bacteria of Swollen Abdomen from <i>Scophthalmus maximus</i> in Vitro	765
	Xuan Wu, Dongqing Bai, Guoxia Zhu, Yanbin Ji, Zhichao Jia and Peng Zhou	
80	Lichen: A Potential Anticancer Official Resource	773
	Meirong Ren, Feng Xu and Xinli Wei	

- 81 Clinical Significance of Screening Impaired Glucose Tolerance in Essential Hypertension Patients** 783
Jun Zhu, Peiqing Feng, Shu Guo, Xinghua Liao, Jiajie Liu,
Junfang Zhang, Tingbao Yan, Yue Wang and Tong-Cun Zhang
- 82 Cardiac Hypertrophy-Specific Genes are Synergistic Activated by Myocardin and CREB-binding protein (CBP) p300** 789
Zhenyu Wang, Xuehua Zhao, Mingzhe Li, Dongsun Cao
and Tong-Cun Zhang
- 83 Design, Synthesis, and Biological Evaluation of the Novel Antitumor Agent 2-benzyl-3, 4-dihydroisoquinolin-1(2H)-one and Its Derivatives** 797
Jian Lv, Lei Lv, Xiaomin Zhang, Yao Zhou, Kui Lu, Yifei lu,
Yuou Teng, Hua Sun and Peng Yu
- 84 Using Water Miscible Ionic Liquid to Improve the Efficiency of 15 α -hydroxylation of 13-ethyl-gon-4-en-3,17-dione by *Penicillium raistrickii*** 805
Shuhong Mao, Na Wang, Zhijiang Ge, Boyuan Hua,
Yanqing Li and Fuping Lu
- 85 Nuclear Receptor Property of E2F1 for Novel Anticancer Drug Discovery** 811
Ning Zhang, Jin Li and Aimin Meng
- 86 MRTF-A Promotes Migration of MCF-7 Breast Cancer Cells via Transactivation of CYR61** 821
Xuegang Luo, Chunling Zhang, Wenwen Zhao, Lei Liu,
Shu Guo, Zhipeng Liu, Jing Wang and Tong-Cun Zhang
- 87 The Analysis of the Inhibition Effect of Cholic Acid Derivatives on the Proliferation of Breast Cancer Cells** 827
Xuegang Luo, Jing Wang, Xiangchao Gu, Chunling Zhang,
Xiangzheng Hu and Tong-Cun Zhang
- 88 Design, Synthesis and Biological Evaluation of the Novel Antitumor Agent 5-Bromobenzofuran-3(2H)-One and its Derivatives** 835
Lei Lv, Xiaomin Zhang, Jian Lv, Yao Zhou, Weiguo Hu,
Peng Yu and Yuou Teng

- 89 Preliminary Study on the Mechanism of Cartilage Polysaccharide Inducing H22 Cell to Engender Immunogenicity 843**
Guoqiang Zheng, Pan Li, Anguo Teng, Jie Zheng, Wenhang Wang and Anjun Liu
- 90 Design and Synthesis of Novel 20-Substituted Hydroxycamptothecin Derivatives 853**
Shaopeng Wen, Dewu Quan, Yao Zhou, Haiyong Jia, Peng Yu, Hua Sun and Na Guo
- 91 Design and Synthesis of 5-Azacytidine Analogs 861**
Jianbo Xing, Hua Sun, Xijuan Liang, Yuou Teng, Peng Yu and Kui Lu
- 92 Stigmasterol from the Flowers of *Trollius chinensis* 867**
Mengmeng Zhou, Min Wang, Daoqing Xu and Qin Pan
- 93 Design, Synthesis and Primary Biological Evaluation of the Novel Antitumor Agent Indoline-3-One and Its Derivatives 875**
Haiyong Jia, Guojun Pan, Yiqian Wang, Shaopeng Wen, Qiannan Guo, Weiguo Hu, Peng Yu, Hua Sun and Yuou Teng
- 94 Research Progress on the Anti-Rheumatoid Arthritis Drugs. 883**
Peng Wang, Xuegang Luo, Chongxi Wang, Xinjia Wang, Guang Hu and Tong-Cun Zhang
- 95 Design and Synthesis of 1H-2,3-Dihydro-1-Pyrrolizinones Derivatives 893**
Changhai Sun and Jing Cao
- 96 Inhibition of iNOS to Protect Intermittent Hypoxia-Induced Hippocampal Neurons Impairment by *Astragalus* Extract in Rat 899**
Qiang Zhang, Wenyuan Gao, Shuli Man, Yun Zhang and Baoyun Chen
- 97 Prepared and Characterization of 12 β ,15 α -Dihydroxy-16 α ,17-Epoxyprogesterone 907**
Yibo Wang, Yanbing Shen, Jiajia Ren, Jianmei Luo and Min Wang

**Part IV Agriculture, Environmental, Marin Biotechnology
and Bio-energy Technology**

- 98 Structure Elucidation of Two Triterpenoid Saponins from Leaves of *Schima superba* Gardn. et Champ 915**
Guanghua Huo, Changling Zhang and Yingjun Zhang
- 99 Study on Extraction of Xylan from Bamboo Shoot Shell 923**
Nengfu Yu, Nengliang Wu, Yu Wang and Yegou Tu
- 100 Study on Preparation of Low Alcoholic Wine from Tomato 931**
Kai-ye Deng and Er-na Li
- 101 Effects of Glucose Assimilation on Lutein and Chlorophyll Biosyntheses in the Green Alga *Chlorella pyrenoidosa* 943**
Tao Li, Yi-han Liu, Fu-ping Lu and Yue Jiang
- 102 RNA Interference and Applications in Plants. 955**
Yunrong An, Zhongyou Pei, Nan Xin and Haifeng Wang
- 103 Isolation, Identification and Degradation Characteristics of Three Thick Oil Degrading Bacteria Strains 963**
Chan Tian, Shengyan Tian, Xianbin Liu and Lulu Qin
- 104 Effect of Anti-Nematode Preparations on Physiological Traits of Cucumber Leaves Affected by Root-Knot Nematode 973**
Shuchang Lu
- 105 Enzymolysis and Microbial Transformation of Geniposide in *Gardenia Jasminoides* into Genipin by *Aspergillus niger*. 981**
Yu Li, Wenbin Jin, Wei Jing, Mengcheng Yao,
Yanyang Tang and Fuping Lu
- 106 Study on the Application of a Thermotolerant *Saccharomyces cerevisiae* in the Production of Bio-ethanol 993**
Yueqiang Li, Yefu Chen, Jian Dong, Xinxin Zhang,
Tong Shen and Dongguang Xiao
- 107 Different Chemicals Stimulate Diapause Termination of *Artemia* Embryos 1003**
Yuqing Chen and Bo Zhang

108	Dominant Bacteria TCCC15005 Used for Treatment of Alkaline Wastewater from Oil Refinery in a SBR	1011
	Jing Yang, Hua Zhao, Xi Wang, Xin Feng and Xinhua Wang	
109	Isolation and Characterization of a New Moderately Halophilic Bacterium Strain SM. 200-5 from Solar Saltern Ponds	1023
	Gaochao Xu, Yuangao Deng, Donghui Song and Liying Sui	
110	Preparation of Wetting Powder for Biocontrol <i>Bacillus subtilis</i>	1033
	Fang Chen, Shangjing Guo, Haiying Shi, Deduo Han, Yuanjun Kang, Yu Zheng and Min Wang	
111	Isolation and Characterization of s-Butanol Tolerant Microorganisms	1041
	Litao Shi, Hongjiang Yang, Qian Li and Xuying Qin	
112	Application of Support Vector Machine in Base Liquor Classification	1051
	Junsen Lu, Liping Du, Haimei Ding, Ziping Du and Dongguang Xiao	
113	Isolation and Characterization of n-Butanol Tolerant Microorganisms	1057
	Yue Yu, Hongjiang Yang, Qun Li and Xuying Qin	
114	Effects of Dual-Frequency Ultrasound with α-amylase on the Properties and Structure of Mung Bean Starch.	1067
	Aijun Hu, Jing Lu, Jie Zheng, Xiaoqing Zhang, Ying Zhang, Tong Zhang, Qian Li and Lin Yang	
115	Relationship Between Diet and Stable Carbon and Nitrogen Isotope Composition in Beef Tissues	1075
	Fengmei Sun, Guangyu Shi, Huiwen Wang and Shuming Yang	
116	Expression and Sequence Analysis of <i>ChRpS3</i>, a Ribosomal Protein S3 cDNA, and its Potential Role in Ovary Development of <i>Cymbidium hybridum</i>	1083
	Xiaoqiang Chen, Xiulan Li, Ning Sun and Wenqin Song	

- 117 Lichen Flora on the Genera *Alectoria*, *Pseudephebe*, and *Sulcaria* (Lichenized Ascomycota, Parmeliaceae) from the Hengduan Mountains in China (4)** 1095
Xinyu Wang, Dong Liu, Jianwen Li, Hiroshi Harada and Lisong Wang
- 118 Discussion on the New and the Old Country Mark in Detecting the Coliform Bacteria** 1107
Lin Huang, Chunxia Wang, Ying Zhang, Fan Mei, Yan Huang, Jinpeng Wang and Bo Zheng
- 119 Screening Autotetraploid Plantlets of *Glycyrrhiza uralnesis* *Fisch* by Colchicine-Treated Bud Culture** 1117
Xinglin Li, Junting Lu, Xuefei Cao, Na Zhao, Yang Han, Aijia Cao, Jie Ding and Jun Zhao
- 120 Screening of Antimicrobial Marine Microorganisms and Purifying of Its Bioactive Substances** 1125
Zhiwen Liu, Qiankun Ruan, Sirigulen Qian and Lina Cong
- 121 Determination of Dichloromethane in Waste Water Using Headspace Gas Chromatography** 1137
Chaozheng Zhang, Huijing Xu, Yutao Li and Fuhai Wang
- 122 Simulation of Bio-syngas Production from Biomass Gasification via Pressurized Interconnected Fluidized Beds** 1145
Fei Feng, Guohui Song, Laihong Shen and Jun Xiao
- 123 Research on Salt-tolerant Gene *GPD1* in *Zygosaccharomyces rouxii*** 1157
Lihua Hou, Yanfei Yu, Cong Wang and Chunling Wang
- 124 Mutagenic Research on Ciliary Neurotrophic Factor (CNTF) in *Escherichia coli* After Heavy Ions Irradiation** 1165
Xiaodong Jin, Qingfeng Wu, Xinguo Liu, Yan Liu, Yong Chen, Jian Lu and Lin Jiang
- 125 Molecular Characterization and Expression of Ribosomal Protein L15 Gene (*RPL15*) From *Arachis hypogaea*** 1171
Qi Wu, Xiuzhen Wang, Hongtao Yu, Yufei Ding, Fenggao Cui, Jiancheng Zhang, Yueyi Tang and Chuantang Wang
- 126 Optimization of Extraction Conditions for Glycosaminoglycan from *Urechis unicinctus* by Response Surface Methodology** 1183
Chunying Yuan, Xu Han, Qingman Cui and Ping Liu

127 Quantitative Trait Loci Mapping of Unstripped Germ Rate in Milled Rice 1191
 Shengbin Liu, Fang Wang, Zetian Hua, Meng Meng, Fei Zhao and Xin Liu

128 The Application of the GSI in the Preservation and Quality Control of Oat Beverage 1197
 Yuzhu Liu and Min Zhang

129 The Effect of Carbon Nanotubes on Rice Seed Germination and Root Growth 1207
 Yumei Jiang, Zetian Hua, Yiqing Zhao, Qindai Liu, Fang Wang and Qin Zhang

130 Study on the Accumulation Laws of Protein in *Japonica* Rice Seed During Development 1213
 Fang Wang, Bolian Sun, Chunkai Gu, Jiajia Mi, Qin Zhang and Zetian Hua

131 Prevalence Investigation of Tetracycline Resistant Bacteria in Raw Milk 1219
 Xiaomei Zhang and Hongjiang Yang

132 Study on Biological Denitrification Removal Technologies Treating Eutrophication Water 1229
 Zongzheng Yang, Huan Zhang, Deqiang Zhang and Jinzhao Pang

133 Study on Decolorization Effect of Biological Strengthening the Activated Carbon with White Rot Fungi 1237
 Zongzheng Yang, Junxia Xu, Peng Yu and Jinzhao Pang

134 The Removal of Crude Oil in Waste Drilling Muds by a Constructed Microbial Consortium 1245
 Yunkang Chang, Xingbiao Wang, Yifan Han, Manman Wang, Chenggang Zheng, Yongli Wang and Zhiyong Huang

135 Isolation and Identification of Saline Tolerance Phosphate-Solubilizing Bacteria Derived from Salt-affected Soils and Their Mechanisms of P-solubilizing 1259
 Yang Han, Chunmei Wang, Xinglin Li, Xuefei Cao, Aijia Cao and Na Zhao

136 Isolation and Characterization of a *Bacillus* Strain for Alkaline Wastewater Treatment 1267
 Kun Chen, Wenyu Shi, Jing Yang, Tong Zhang and Hua Zhao

Part III
Pharmaceutical Biotechnology

Chapter 66

Promising Biomarkers: MicroRNAs at Diagnosis, Therapy and Prognostic Evaluation of Breast Cancer

Dalin Lu, Nan Wang, Xinghua Liao, Xuan Huang, Jianhua Zhang, Zhenyu Wang, Lian Duan, Jiajie Liu, Baoshu Jin, Yue Wang and Tong-Cun Zhang

Abstract MicroRNAs (miRNAs) are small noncoding RNAs with regulatory functions, which play an important role in malignancies. An increasing amount of experimental evidence has shown that many miRNAs are aberrantly expressed in breast cancer and influence breast cancer behavior and progression. Furthermore, miRNAs can act either as tumor suppressors or as oncogenes, depending on the targets they regulate, and measurements of miRNAs expression in breast cancer have diagnostic and prognostic implications. Thus, this implies that miRNAs have huge potential as biomarkers. In addition, their extreme stability and ease of detection further support the idea that miRNAs have great potential to evolve into effective biomarkers in the clinic. The objective of this review is to update current realization regarding that miRNAs are promising candidates at diagnostic, therapeutic and prognostic evaluation aspects of clinical application.

Keywords Breast cancer · miRNAs · Diagnosis · Therapy · Prognosis

D. Lu, X. Liao, and X. Huang contributed equally to this work and are nominated as the first author.

D. Lu (✉) · X. Liao · Z. Wang · L. Duan · J. Liu · T.-C. Zhang (✉)
Medical school, Wuhan University of Science and Technology, Wuhan 430000,
People's Republic of China
e-mail: tony@tust.edu.cn

D. Lu · N. Wang · X. Liao · Y. Wang · T.-C. Zhang
Key Laboratory of Industrial Fermentation Microbiology, Ministry of Education
and Tianjin, College of Biotechnology, Tianjin University of Science and Technology,
Tianjin 300457, People's Republic of China

D. Lu · J. Zhang · B. Jin
The Second Artillery General Hospital PLA, Beijing 100000, People's Republic of China

X. Huang
Medical School, Nanchang University, Nanchang 330006, People's Republic of China

66.1 A Brief Introduction to MicroRNAs

‘Noncoding’ or ‘non-messenger’ RNAs are various molecules with structural, enzymatic, and regulatory functions. Among these RNAs with regulatory activity are miRNAs, which are about 22 nucleotides in length [1]. The majority of animal miRNAs are imprecisely matching to their target mRNAs, and then they hinder protein synthesis by unknown mechanisms. Some studies even suggest that the translationally repressed target mRNAs remain related with ribosomes [2–4]. In addition, computational algorithms have estimated that miRNAs could target more than 30 % of the human genome [5]. Significantly, a single miRNAs can regulate more than one gene, and equally a particular gene can be regulated by compound miRNAs. Thus, miRNAs, can regulate diverse biological processes, for example, development, angiogenesis, differentiation, immune cell function, proliferation, apoptosis and wound healing, and so on [6].

An increasing number of deregulated miRNAs has been detected in breast cancer, and many of them are closely associated with cancer metastasis and poor prognosis, and reduce survival time of breast cancer patients. For example, the high-expressed miRNA, miR-21, has been reported to be associated with advanced stage, node positivity. Meanwhile, miRNA-21 knock-down in cell-line models have been related to increased sensitivity to topotecan and taxol. All of them suggest an important role of miRNAs in oncogenesis, diagnosis, therapy, and prognosis of breast cancer [7–11].

In this review, we discuss miRNAs as potential biomarkers used in breast cancer, emphasizing that miRNAs can be effectively used in these aspects of diagnosis, therapy, and prognostic valuation in the clinical setting. Our efforts are to research and recommend more effective methods to improve the quality of life and survival time.

66.2 Potential Use of miRNAs as Biomarkers for Breast Cancer

miRNAs expression profiles derived from large-scale analyses of tumor samples have been shown to serve as phenotypic signatures of particular cancer types. For example, seven independent studies have analyzed the miRNA profile of breast cancer tissues or cell lines, compared to normal tissues or cell-lines. These studies described a general down-regulation of miRNAs in breast cancer tissues or cell lines compared to normal breast cancer tissues or cell-lines [7, 12–17].

Up to now, most profiling studies have paid attention to deregulated miRNAs either in the primary breast cancer tissue or in breast cancer cell lines. miRNAs expression profile analyses from all kind of breast cancer or cell lines analyzed by

miRNAs profiling have revealed considerably different miRNA profiles (for mature or precursor miRNAs) compared with normal cells from the same tissue. A review of the published large-scale miRNA profiles reveals that several constantly deregulated miRNAs in tumors from breast cancer patients together with their clinical correlations are listed in Table 66.1. Undeniably, many of these miRNAs, such as let-7a, miR-10b, miR-21, miR-31, miR-145, and miR-155 are deregulated in various types of cancer, including breast, prostate, colon, lung, liver cancers, and melanoma [17–21]. In addition, the overexpression of several miRNAs such as miR-21 and so on in human breast cancer is associated with advanced clinical stage, lymph node metastasis, and patient poor prognosis [14]. Furthermore, Zhao et al. have demonstrated that circulating miRNAs in plasma could potentially serve as novel minimally invasive biomarkers for early detection of breast cancer [22]. Heneghan and his colleagues surveyed a panel of 7 candidate miRNAs in whole blood RNAs from 148 breast cancer patients and 44 specific miRNA, miR-195, only high-expressed in breast cancer. Additionally, they observed a significant reduction of miR-195 in postoperative whole blood compared with the preoperative samples of the same patients [17]. Thus, it could be applied not only to directly detect breast tumors, but also perceive breast cancer relapse.

Besides, due to their resistance to degradation, blood miRNAs appear to be very stable, and there is budding interest in profiling circulating miRNAs either as diagnostic noninvasive agent markers or as therapeutic measures. Circulating miRNAs have been widely reported to be drastically elevated in the blood of cancer patients compared with healthy controls, and levels of these miRNAs are associated with the primary tumors. The elimination of the primary tumor leads to the recover of deregulated circulating miRNAs, implying that many of these elevated circulating miRNAs are ‘tumor-derived’ and cancer-specific [6]. The current belief is that these ‘tumor-derived’ circulating miRNAs are released from the primary tumor via exosome vesicles and apoptotic bodies although the exact mechanisms of release are still emerging [23–25]. Although there will be technical difficulties, all these miRNAs’ properties imply that miRNAs as clinical biomarkers will have a promising prospect.

66.3 miRNAs Profiling to Advance Development of Diagnosis, Therapy, and Prognostic Evaluation

There is increasing evidence to support that miRNAs are closely associated with a huge proportion of breast cancer heterogeneity. Many miRNAs have been shown to be deregulated in breast cancer [7, 13, 26, 27] and specific miRNAs functioning as regulators of tumorigenicity, invasion, and metastasis have been documented [8, 9, 28, 29]. In addition, miRNAs that can regulate ER, PR, and HER2/neu,

Table 1 Commonly regulated miRNAs, their targets, and pathway in breast cancer

miRNA	Tumor expression level	References	Validated targets	Pathways	References
miR-21	↑	[7]	HER2, BCL2, TPML, TIMP3, PDCD4, PTEN, MASPIN, RHOB, MMP3	Apoptosis, invasion, metastasis	[14, 28, 34–38]
miR-155	↑	[7]	Caspase3, FOXO3A, SOCS1, RHOA	Proliferation, TGF- β , signaling	[39–42]
miR-191	↑	[7, 43]			
miR-196a	↑	[7, 43]	ANXA1	Proliferation, apoptosis	[44]
miR-10b	↓	[7]	RHOC, TIAM, HOXD10	Migration, invasion, metastasis	[8, 45, 46]
miR-302b	↑	[47]	p21	Invasion, Migration	[47]
miR-425	↑	[9]	DICER1		[47]
miR-100	↓	[48]			
miR-125b	↓	[7, 43, 48]	HER2, HER3, CRAF, MUC1, BAK, ERA, RTKN	Proliferation, apoptosis, migration	[26, 30, 49, 50]
miR-145	↓	[7, 48]	TP53, PUMA, c-Myc, MUC1, ER α , RTKN	Proliferation, apoptosis, invasion	[51–54]
miR-205	↓	[26]	HER3, VEGF-A, EMT	Proliferation, invasion	[7, 55, 56]

This table represents miRNAs whose expressions are notably regulated in clinical samples (tumors of human patients)

known to be of diagnostic value, therapeutic worth, and prognostic significance in breast cancer, has been demonstrated [30, 31].

At present, miRNAs expression profiling can be used to evaluate clinicopathological variables to categorize breast tumors. To predict disease progression and prognosis using miRNAs expression profiling analysis is of particular interest. First of all, profiling features the potential to identify novel prognostic indicators, which may contribute to improve patients for adjuvant therapy. This approach has already shown promise with genomic signatures, and miRNA profiles appear to have superior accuracy to mRNA profiling [32]. Besides, the measurement of miRNAs with regulatory roles, distinct breast tumor samples could identify novel targets for therapeutic manipulation. For example, miRNA-221 and 222 are negatively correlated with ER α protein expression and the knockdown of miRNA-221/222 can effectively restore ER α protein expression [33]. Of course, there are more miRNAs associated with PR and HER2. Here, we do not list all of them.

In conclusion, all these findings discussed in this report suggest that miRNAs detected are promising as novel biomarkers and useful for the elimination of false positives, false negatives of conventional various classifiers, and prognostic evaluation. Moreover, clinician could apply gene therapies to change expression of miRNAs to remedy breast cancer.

Acknowledgments This work was financially supported by National Natural Science Foundation of China (No. 30970615, 31071126) and Program for Changjiang Scholars and Innovative Research Team in University of Ministry of Education of China (IRT1166) and the Key Project of Chinese Ministry of Education (212010) and Hubei key project of Science and Technology Research (No. D20111102) and Hubei Natural Science Foundation (No.2010CDB03506).

References

1. Bartel DP (2004) MicroRNAs: genomics, biogenesis, mechanism and function. *Cell* 116:281–297
2. Olsen PH, Ambros V (1999) The lin-4 regulatory RNA controls developmental timing in *Caenorhabditis elegans* by blocking LIN-14 protein synthesis after the initiation of translation. *Dev Biol* 216:671–680
3. Seggerson K, Tang L, Moss EG (2002) Two genetic circuits repress the *Caenorhabditis elegans* heterochronic gene *lin-28* after translation initiation. *Dev Biol* 243: 215–225
4. Griffiths-Jones S, Saini HK, van Dongen S et al (2008) miRBase: tools for microRNA genomics. *Nucl Acids Res* 36:154–158
5. Lewis BP, Burge CB, Bartel DP (2005) Conserved seed pairing, often flanked by adenosines, indicates that thousands of human genes are microRNA targets. *Cell* 120:15–20
6. Andorfer CA, Necela BM, Thompson EA et al (2011) MicroRNA signatures: clinical biomarkers for the diagnosis and treatment of breast cancer. *Trends in Molecular Medicine* 17(6):313–319
7. Iorio MV, Ferracin M, Liu CG et al (2005) MicroRNA gene expression deregulation in human breast cancer. *Cancer Res* 65:7065–7070
8. Ma L, Teruya-Feldstein J, Weinberg RA (2007) Tumour invasion and metastasis initiated by microRNA-10b in breast cancer. *Nature* 449:682–688

9. Tavazoie SF, Alarcón C, Oskarsson T et al (2008) Endogenous human microRNAs that suppress breast cancer metastasis. *Nature* 451:147–152
10. Silveri L, Tilly G, Vilotte JL et al (2006) MicroRNA involvement in mammary gland development and breast cancer. *Reprod Nutr Dev* 46:549–556
11. Corcoran C, Friel AM, Duffy MJ et al (2011) Intracellular and Extracellular MicroRNAs in Breast Cancer. *Clin Chem* 57(1):18–32
12. Sempere LF, Christensen M, Silahatoglu A et al (2007) Altered MicroRNA expression confined to specific epithelial cell subpopulations in breast cancer. *Cancer Res* 67:11612–11620
13. Volinia S, Calin GA, Liu CG et al (2006) A microRNA expression signature of human solid tumors defines cancer gene targets. *PNAS* 103:2257–2261
14. Yan LX, Huang XF, Shao Q et al (2008) MicroRNA miR-21 over-expression in human breast cancer is associated with advanced clinical stage, lymph node metastasis and patient poor prognosis. *RNA* 14:2348–2360
15. Fassan M, Baffa R, Palazzo JP et al (2009) MicroRNA expression profiling of male breast cancer. *Breast Cancer Res* 11:R58
16. Lehmann U, Streichert T, Otto B et al (2010) Identification of differentially expressed microRNAs in human male breast cancer. *BMC Cancer* 10:109
17. Heneghan HM, Miller N, Lowery AJ et al (2010) Circulating microRNAs as novel minimally invasive biomarkers for breast cancer. *Ann Surg* 251:499–505
18. Selcuklu SD, Donoghue MT, Spillane C (2009) miR-21 as a key regulator of oncogenic processes. *Biochem Soc Trans* 37:918–925
19. Faraoni I, Antonetti FR, Cardone J et al (2009) miR-155 gene: a typical multifunctional microRNA. *Biochim Biophys Acta* 1792(6):497–505
20. Wang Y, Lee CG (2009) MicroRNA and cancer: focus on apoptosis. *Cell Mol Med* 13:12–23
21. Valastyan S, Reinhardt F, Benaich N et al (2009) A pleiotropically acting microRNA, miR-31, inhibits breast cancer metastasis. *Cell* 137(6):1032–1046
22. Zhao H, Shen J, Medico L et al (2010) A pilot study of circulating miRNAs as potential biomarkers of early stage breast cancer. *PLoS ONE* 5(10):e13735
23. Iguchi H, Kosaka N, Ochiya T (2010) Secretory microRNAs as a versatile communication tool. *Commun Integr Biol* 3:478–481
24. Kosaka N, Iguchi H, Ochiya T (2010) Circulating microRNA in body fluid: a new potential biomarker for cancer diagnosis and prognosis. *Cancer Sci* 101:2087–2092
25. Kosaka N, Iguchi H, Yoshioka Y et al (2010) Secretory mechanisms and intercellular transfer of microRNAs in living cells. *J Biol Chem* 285:17442–17452
26. Mattie MD, Benz CC, Bowers J et al (2006) Optimized high-throughput microRNA expression profiling provides novel biomarker assessment of clinical prostate and breast cancer biopsies. *Mol Cancer* 5:24
27. Blenkinson C, Goldstein LD, Thorne NP et al (2007) MicroRNA expression profiling of human breast cancer identifies new markers of tumor subtype. *Genome Biol* 8:R214
28. Zhu S, Wu H, Wu F et al (2008) MicroRNA-21 targets tumor suppressor genes in invasion and metastasis. *Cell Res* 18:350–359
29. Bhaumik D, Scott GK, Schokrpur S et al (2008) Expression of microRNA-146 suppresses NF- κ B activity with reduction of metastatic potential in breast cancer cells. *Oncogene* 27:5643–5647
30. Scott GK, Goga A, Bhaumik D et al (2007) Coordinate suppression of ERBB2 and ERBB3 by enforced expression of micro-RNA miR-125a or miR-125b. *J Biol Chem* 282:1479–1486
31. Adams BD, Furneaux H, White BA (2007) The micro-ribonucleic acid (miRNA) miR-206 targets the human estrogen receptor-alpha(ER α) and represses ER α messenger RNA and protein expression in breast cancer cell lines. *Mol Endocrinol* 21:1132–1147
32. Lu J, Getz G, Miska EA et al (2005) MicroRNA expression profiles classify human cancers. *Nature* 435:834–838

33. Zhao JJ, Lin J, Yan H et al (2008) miRNA-221/222 negatively regulates estrogen receptor and is associated with tamoxifen resistance in breast cancer. *J Biol Chem* 283(45):31079–31086
34. Qi L, Bart J, Tan LP et al (2009) Expression of miR-21 and its targets (PTEN, PDCD4, TM1) in flat epithelial atypia of the breast in relation to ductal carcinoma in situ and invasive carcinoma. *BMC Cancer* 9:163
35. Huang GL, Zhang XH, Guo GL et al (2008) Expression of microRNA-21 in invasive ductal carcinoma of the breast and its association with phosphatase and tensin homolog deleted from chromosome expression and clinicopathologic features. *Zhonghua Yi Xue Za Zhi* 88:2833–2837
36. Qian B, Katsaros D, Lu L et al (2009) High miR-21 expression in breast cancer associated with poor disease-free survival in early stage disease and high TGF-beta1. *Breast Cancer Res Treat* 117:131–140
37. Song B, Wang C, Liu J et al (2010) MicroRNA-21 regulates breast cancer invasion partly by targeting tissue inhibitor of metalloproteinase 3 expression. *J Exp Clin Cancer Res* 29:29
38. Huang TH, Wu F, Loeb GB et al (2009) Up-regulation of mir-21 by her2/neu signaling promotes cell invasion. *J Biol Chem* 284:18515–18524
39. Kong W, He L, Coppola M et al (2010) MicroRNA-155 regulates cell survival, growth, and chemo-sensitivity by targeting FOXO3a in breast cancer. *J Biol Chem* 285:17869–17879
40. Jiang S, Zhang HW, Lu MH et al (2010) MicroRNA-155 functions as an OncomiR in breast cancer by targeting the suppressor of cytokine signaling 1 gene. *Cancer Res* 70:3119–3127
41. Kong W, Yang H, He L et al (2008) MicroRNA-155 is regulated by the transforming growth factor beta/Smad pathway and contributes to epithelial cell plasticity by targeting RhoA. *Mol Cell Biol* 28:6773–6784
42. Ovcharenko D, Kelnar K, Johnson C et al (2007) Genome-scale microRNA and small interfering RNA screens identify small RNA modulators of trail-induced apoptosis pathway. *Cancer Res* 67:10782–10788
43. Hui AB, Shi W, Boutros PC et al (2009) Robust global micro-RNA profiling with formalin-fixed paraffin-embedded breast cancer tissues. *Lab Invest* 89:597–606
44. Luthra R, Singh RR, Luthra MG et al (2008) MicroRNA-196a targets annexin A1: a microRNA-mediated mechanism of annexin A1 down-regulation in cancers. *Oncogene* 27:6667–6678
45. Ma L, Reinhardt F, Pan E et al (2010) Therapeutic silencing of miR-10b inhibits metastasis in a mouse mammary tumor model. *Nat Biotechnol* 28:341–347
46. Moriarty CH, Pursell B, Mercurio AM (2010) miR-10b targets Tiam1: implications for Rac activation and carcinoma migration. *J Biol Chem* 285:20541–20546
47. Esquela-Kerscher A, Slack FJ (2006) Oncomirs-microRNAs with a role in cancer. *Nat Rev Cancer* 6:259–269
48. Navon R, Wang H, Steinfeld I et al (2009) Novel rank-based statistical methods reveal microRNAs with differential expression in multiple cancer types. *PLoS ONE* 4(11):e8003
49. Zhou M, Liu Z, Zhao Y et al (2010) MicroRNA-125b confers the resistance of breast cancer cells to paclitaxel through suppression of pro-apoptotic Bcl-2 antagonist killer 1 (Bak1) expression. *J Biol Chem* 285:21496–21507
50. Hofmann MH, Heinrich J, Radziwill G et al (2009) A short hairpin DNA analogous to miR-125b inhibits C-Raf expression, proliferation, and survival of breast cancer cells. *Mol Cancer Res* 7:1635–1644
51. Spizzo R, Nicoloso MS, Lupini L et al (2010) miR-145 participates with TP53 in a death-promoting regulatory loop and targets estrogen receptor- α in human breast cancer cells. *Cell Death Differ* 17:246–254
52. Sachdeva M, Zhu S, Wu F et al (2009) p53 represses c-Myc through induction of the tumor suppressor miR-145. *PNAS* 106(9):3207–3212
53. Sachdeva M, Mo YY (2010) MicroRNA-145 suppresses cell invasion and metastasis by directly targeting mucin 1. *Cancer Res* 70:378–387

54. Wang S, Bian C, Yang Z et al (2009) miR-145 inhibits breast cancer cell growth through RTKN. *Int J Oncol* 34:1461–1466
55. Wu H, Zhu S, Mo YY (2009) Suppression of cell growth and invasion by miR-205 in breast cancer. *Cell Res* 19:439–448
56. Gregory PA, Bert AG, Paterson EL et al (2008) The miR-200 family and miR-205 regulate epithelial to mesenchymal transition by targeting ZEB1 and SIP1. *Nat Cell Biol* 10:593–601

Chapter 67

Dimerization of Chemokine Receptors and its Novel Roles in Drug Discovery

Mingqing Wang, Baosheng Ge and Fang Huang

Abstract G-protein-coupled receptors (GPCRs) comprise the largest family of integral membrane proteins and mediate most of the transmembrane signal transduction. Approximately 50 % of all marketed drugs target GPCRs, which makes this protein family the most important drug targets. Chemokine receptors belong to GPCRs, which were perceived as monomers decades ago. However, recently there are growing evidences indicating that most of GPCRs can form dimers or higher order oligomers. Some chemokine receptors are also found existing as homodimers or heterodimers. A large number of studies have suggested that homodimers or heterodimers may exhibit specific functions, which are different from their monomeric counterparts. Meanwhile, the appearance of dimers with new signaling properties gives new chance in the search for novel drug targets. In this review, we will mainly summarize the current knowledge of the dimerization of chemokine receptors and its potential roles in drug discovery.

Keywords Chemokine receptor · Dimerization · Drug discovery · GPCRs

67.1 Introduction

G-protein-coupled receptors (GPCRs) comprise the largest family of integral membrane proteins and mediate most of the transmembrane signal transduction [1]. GPCRs are important drug targets and account for about 50 % of all the drugs on the market [2]. Chemokine receptors are a subgroup of the GPCRs superfamily. To date, totally 22 chemokine receptors have been discovered in human genome [3]. Chemokine receptors and their chemokines play an important role in the immune

M. Wang · B. Ge · F. Huang (✉)

Center for Bioengineering and Biotechnology, China University of Petroleum (East China),
Qingdao 266580, People's Republic of China

e-mail: fhuang@upc.edu.cn

defense by directing the migration of leukocytes. In addition to their normal roles, chemokine receptors are involved in many diseases, including inflammatory diseases, cancer, AIDS, and so on [4]. Hence chemokine and receptors are deemed as important drug targets. The first small molecule successfully targeting the chemokine receptor was the CCR5 antagonist, for the prevention of HIV infection, approved by the Federal Drug Administration (FDA) in 2007. Besides, a CXCR4 antagonist was approved by the FDA in 2008 for hematopoietic stem cell mobilization [5]. The existence of dimers or oligomers of GPCRs has been confirmed in the past decades. The structure of chemokine receptor dimers is different from the monomeric form, so it is possible that the dimers function in specific signaling pathways. Moreover, the dimers may take part in ligand binding and distinct signal transduction. The specificity of dimerization may give new opportunity to find novel drugs [6, 7]. Chemokine receptor dimerization and its role in drug discovery are reviewed in this paper.

67.2 Chemokines and Chemokine Receptors

Chemokines are small proteins, which mediate cell migration during inflammation and development. Based on the cysteine (Cys) in the N-terminal domain, chemokines are divided into four classes (CC, CXC, CX3C, XC) [8]. The nomenclature of chemokine is characterized by combination of “L” and an Arabic number, such as CCL1. In the CC class, the two Cys residues are adjacent, and there are 28 known members in human genome. In the CXC class, there is an additional amino acid between the two Cys residues and 17 known CXC chemokines have been discovered till now. The CX3C chemokine has only one known member, with three additional amino acids between the two Cys residues. XC class contains only one cysteine and there are two known members [9, 10].

There are totally 22 known chemokine receptors in human genome [3], and 19 of which works as signaling receptors. The classification of chemokine receptors is based on the ligands which they bind. For example, CC receptors bind CC ligands. The other three chemokine receptors (D6, CCX-CKR, DARC) are atypical receptors, which are unable to directly mediate leukocyte migration. They are thought to regulate chemokine distribution or abundance to control chemokine-derived leukocyte migration. Many chemokines bind multiple receptors and most receptors bind multiple chemokines (Table 67.1). Despite of the pivotal roles in the immune system, chemokine receptors are associated with many diseases, such as atherosclerosis, rheumatoid arthritis, asthma, and cancer (Table 67.1). In addition, CXCR4 and CCR5 are the primary co-receptor for X4 and R5 HIV-1 isolates.

Table 67.1 Chemokine receptor binding their ligands and related to diseases

Chemokine receptor	Binding chemokine	Related to diseases
CXCR1	CXCL6,7,8	Sepsis, atherosclerosis [48]
CXCR2	CXCL1,2,3,5,6,7,8	Sepsis, rheumatoid arthritis [48]
CXCR3	CXCL9,10,11	Transplant, psoriasis, cancer [49]
CXCR4	CXCL12	HIV, cancer [50, 51]
CXCR5	CXCL13	
CXCR6	CXCL16	
CXCR7	CXCL11,12	Cancer [52]
CCR1	CCL3,5,7,8,13,14,15,16,23	Psoriasis, cancer [53]
CCR2	CCL2,7,8,13,16	Diabetes, obesity, cancer [54]
CCR3	CCL5,7,8,11,13,15,16,24,26,28	Allergic diseases, Asthma1 [55]
CCR4	CCL17,22	Asthma, skin disease
CCR5	CCL3,4,5,8,11,14,16	HIV, transplant, cancer [56]
CCR6	CCL20	Asthma [57]
CCR7	CCL19,21	Cancer [58]
CCR8	CCL1	
CCR9	CCL25	Irritable bowel disease [58]
CCR10	CCL27,28	
XCR1	XCL1,2	
CX3CR1	CX3CL1	Atherosclerosis [59]
D6	CCL2,3,4,5,7,8,11,13,14,17,22	
CCX-CKR	CCL19,21,25	
DARC	CCL2,7,8,11,13,14,16,17,18; CXCL1,5,6,7,8,9,11,13	

67.3 Methods to Study GPCR Dimerization

In 1996, Hebert firstly demonstrated that β 2-adrenergic receptors could form homodimers by using Co-immunoprecipitation [11]. Since then, many methods have been used to detect the dimerization or higher order oligomerization of many GPCRs [12]. Biochemical techniques are traditional methods to study the dimerization of GPCRs, including SDS–Polyacrylamide Gel Electrophoresis (SDS-PAGE), Cross-linking experiments, Co-immunoprecipitation (Co-IP) and western blot [13]. However, such biochemical techniques can not be used to probe the dimerization of GPCRs in living cells. In the past decade, there was a shift toward using resonance energy transfer techniques to study the dimerization. Applications of bioluminescence resonance energy transfer (BRET) and fluorescence resonance energy transfer (FRET) can exhibit advantages over many more traditional techniques because they can detect both intracellular and cell surface expressed dimers in intact living cells [14]. BRET and FRET are based on the nonradioactive transfer of energy from a donor molecule to an acceptor molecule in a close distance (less than 10 nm), which have overlapping excitation and emission spectra. Bimolecular fluorescence complementation (BiFC) has also been used to detect the dimerization. BiFC is based on the association between two nonfluorescent fragments of a

Table 67.2 Methods to study GPCR dimerization

Biochemical techniques	Biophysical techniques
SDS-PAGE,	Fluorescence resonance energy transfer (FRET),
Cross-linking experiments,	Bioluminescence resonance energy transfer (BRET),
Western blot,	Biomolecular fluorescence complementation (BiFC),
Co-immunoprecipitation (Co-IP)	Atomic force microscopy (AFM)

fluorescent protein, which could be fused to two GPCRs. If the two GPCRs can interact, then the nonfluorescent fragments can be brought close to each other and thus form a fluorescent protein. In addition, the dimerization and higher order oligomerization of rhodopsin in native retinal disks was studied by using atomic force microscopy [15] (Table 67.2).

67.4 Chemokine Receptor Dimerization and their Functions

GPCRs were considered to exist and function as monomers which can interact with G-proteins in 1:1 stoichiometry. However, in the past decades, the hypothesis was challenged. The growing evidences indicate that GPCRs can physically interact with each other. They can form dimers or even oligomers. In 1998, Jones et al. found the GABAB (a member of class C GPCR) could exist and function as a heterodimer [16]. Both GABABR1 and GABABR2 are nonfunctional when individually expressed in cells, because GABABR1 is retained in the endoplasmatic reticulum (ER), GABABR2 can not bind the ligand [17, 18]. The class C GPCR including sweet and umami taste receptors can function in the form of heterodimer [19, 20].

67.4.1 Chemokine Receptor Homodimerization and Heterodimerization

Some chemokine receptors can exist as homodimers. In the early research, ligands were thought to induce the homodimerization. For example, CXCL12 induced CXCR4 homodimerization [21], while CCL2 and CCL5 could induce the homodimerization of CCR2 and CCR5, respectively [22, 23]. Recent studies suggest that CCR2 [24], CCR5 [25], CXCR1 [26], CXCR2 [27], CXCR4 [28, 29], CXCR7 [30], and DARC [31] can form constitutive homodimerization.

Some chemokine receptors can also form heterodimers. Mellado et al. first reported CCR2/CCR5 heterodimerization as ligand dependent. His study suggested that CCR2/CCR5 heterodimerization was induced by costimulation of CCL2 and CCL5. El-Asmar et al. found CCR5 and CCR2 could heterodimerized

with the similar efficiency as they could homodimerize using BRET. And there was no cooperative signaling after costimulation by CCL2 or CCL5 [32]. This result was very different from Mellado's study. Different research methods in the two studies may cause the different results. Mellado et al. used cross-linking agent before addition of ligand, which is prior to cell lysis and immunoprecipitation in an effort to stabilize receptor interaction, but El-Asmar et al. did not use. The cross-linking agent could induce association of receptors and the ligand could also help enhance the cross-linking effort. More experiments suggested that CCR2 and CCR5 formed constitutive homodimerization and heterodimerization. The role of ligand in CCR2/CCR5 dimerization is unclear [32]. In addition, CXCR1/CXCR2 [26], CXCR4/CCR2 [33], CXCR4/CXCR7 [30], CXCR4/CCR5 [34], DARC/CCR5 [31] can form constitutive heterodimerization (Table 67.3).

67.4.2 The Functions of Chemokine Receptor Dimerization

In contrast to class C GPCRs in which dimerization is strictly necessary for their functions [35], while some chemokine receptors can exist and function as monomeric form. The homodimers or heterodimers of chemokine receptors may have novel functions, which is possibly different from the monomers (Table 67.3). The acknowledgment on dimerization of chemokine receptors may help find novel drug targets for therapy.

Human immunodeficiency virus type 1(HIV-1) infection is mediated by binding of the viral protein gp120 to two proteins on the surfaces of target cells, CD4 and a co-receptor. The co-receptors are normally chemokine receptors, typically either CCR5 or CXCR4. HIV-1 strains can be divided into three major groups based on

Table 67.3 Functions of chemokine receptors dimerization

	Functions of dimerization
CCR2/CCR2	Important for migration
CCR2/CCR5	Alter signaling [60]
CCR2V64I/CCR5	Delayed HIV progression [61]
CCR2V64I/CXCR4	Delayed HIV progression [61]
CCR2/CXCR4	Transinhibition of chemotaxis and calcium response [62]
CCR5/CCR5	Important for migration
CCR5/CXCR4	T cell costimulation and alternative signaling [63]
CCR5/CCR5 Δ 32	HIV resistance [64]
CXCR4/CCR5 Δ 32	HIV resistance [64]
CXCR1/CXCR1	Important for migration and signaling [65]
CXCR2/CXCR2	Important for migration and signaling [65]
CXCR1/CXCR2	No effect on CXCL1-induced signaling [65]
CXCR4/CXCR7	Delayed ERK activation [66]
CXCR4/CXCR4	Important for migration and signaling [66]
DARC/CCR5	Transinhibition of chemotaxis and calcium response [31]

their co-receptor specificity as follows: R5 (CCR5-tropic), X4 (CXCR4-tropic), and R5X4 (able to use either CCR5 or CXCR4) [36]. CCR5 Δ 32 is a 32-bp deletion in the portion of the human CCR5 open reading frame (ORF) that encodes the second extracellular loop [37, 38]. CCR5 Δ 32 encodes a truncated protein, which is not detected on the cell surface and therefore could not function as a co-receptor with HIV [39, 40]. Only a small population of individuals have the allelic truncation variant CCR5 Δ 32. People with CCR5 Δ 32 homozygotes can resist HIV-1. Agrawal et al. evidence that expression of recombinant CCR5 Δ 32 protein confers broad protection against R5 and X4 strains of HIV-1 [41]. The mechanism was that CCR5 Δ 32 protein can heterodimerize with intracellular wide type CCR5 and CXCR4. They can form heterodimerization and thus CCR5 Δ 32 protein can act as a negative regulator of wide type CCR5 and CXCR4. The heterodimerization can reduce the cell surface expression of the major HIV co-receptors and thus can resist entry of HIV. Understanding the mechanism of CCR5 Δ 32 protein heterodimerized with CCR5 and CXCR4 may lead to new cues into the relationships of these receptors. Then novel therapeutic drugs which induce resistance to HIV-1 can be developed.

CCR2-V64I is a polymorphism in CCR2 in which Val 64 is replaced by Ile. People with CCR2-V64I have four-year delay in the progress to AIDS [42]. However, relatively few virus strains that can use CCR2 in conjunction with CD4 to infect cells have been reported. Mellado et al. find that CCR5 and CXCR4 can form heterodimerization with CCR2-V64I. The heterodimers can delay the HIV progress [43].

WHIM (Warts, Hypogammaglobulinemia, Infections, and Myelokathexis) syndrome is an immune deficiency, where dimerization is thought to result in abnormal function of the CXCR4 receptor. The expression of C-terminal truncation mutants of CXCR4 results in uncommon genetic immunodeficiency disease. The studies show that CXCR4(wt)/CXCR4(mu) heterodimers are at least twice as much as their homodimers, when two receptors coexist in the same cell at the same concentration, thus suggesting that CXCR4(wt)/CXCR4(mu) heterodimers are dominant in the cells of patients with WHIM [44].

Some chemokine receptors are reported to take part in cancer metastasis (Table 67.1). For example, CXCR4 is reported to be expressed in a variety of cell types, including peripheral blood lymphocytes and monocytes. CXCR4 is also highly expressed in 28 human cancers, including prostate cancer, lung cancer, and pancreatic cancer, metastases, and malignant breast tumors. Wang et al. found constitutive dimers of CXCR4 in malignant living cell using FRET [45]. Lipid raft microdomains are important in directed migration of cancer cells by maintaining receptor dimer conformation. An 18 residue peptide which is as the same as the TM4 of CXCR4, reduce the energy transfer between protomers of CXCR4 dimer then block CXCR4-mediated cancer cell migration. Therefore, it is possible to use peptides to specifically control migration of cancer cells and to decrease the number of CXCL12 attracted tumor-associated macrophages, which could promote tumor metastasis. The study of TM4 peptide from CXCR4 suggested that chemokine receptor dimers were potential important targets for effective cancer

therapy. It is possible to block cancer metastases through drugs like TM4 peptide that interferes with dimeric receptor structures [7, 45]. More efforts are needed to address the structure of dimerization of chemokine receptors and their signaling role in HIV-1 infections, immunity, cancer biology and therapy, allergic conditions, and various inflammatory.

CXCR7 is a novel chemokine receptor, which has two natural ligands CXCL11 and CXCL12. CXCL12 is also the ligand of CXCR4. In addition, CCX771 is a small specific antagonist of CXCR7, similar to CXCL11. CXCR7 is different from other receptors in signaling. Ligand activation of CXCR7 cannot trigger Gi-mediated signaling and induced cell migration. The stimulation of ligands can induce CXCR7 to associate with β -arrestin2, which is a unique signaling properties of CXCR7. CXCR4, and CXCR7 could form constitutive heterodimer [46]. Because CXCR4 and CXCR7 are linked to many cancers, the study of the role of CXCR4/CXCR7 heterodimer is a hot spot. CXCR7 is important for CXCL12-mediated transendothelial migration (TEM) in CXCR4 + CXCR7 + tumor cells. CXCR7 can help tumor cells pass through endothelial cells. Moreover, although the TEM is mediated by CXCL12/CXCR4, CXCL11, and CCX771 (belonging to ligands of CXCR7) can potently block TEM. CCX771 is more efficient in blocking TEM than the CXCR4 antagonist AMD3100, but it does not change the binding affinity of CXCL12 for CXCR4 [47]. These results suggest that ligands of CXCR7 can inhibit CXCL12-mediated transendothelial migration. The research suggested CXCR7 could be a novel cancer therapeutic target.

67.5 Prospects

The growing evidence supports the concept that chemokine receptor dimers or oligomers may have more novel functions. The dimers or oligomers are probably the basic functional unit of some chemokines. The dimerization of chemokine receptors may have novel specificity and have less or even no side effect, which makes them a promising new generation of drug targets. Synthetic peptides of transmembrane region of chemokines may be an effective tool to study the role of receptor dimerization. The synthetic peptides and their modified forms may be useful for the treatment of cancers, infectious disease, and inflammatory conditions. Interfering of HIV-1 infection can be achieved by drugs targeting dimerization of co-receptor CCR5, CXCR4. Above all, the research on chemokine receptors dimerization will bring a new dawn in the treatment of cancers, AIDS, asthma, and so on.

Acknowledgments This work was financially supported in part by the National Key Basic Research Program of China (2012CB518000), the National Natural Science Foundation of China (No. 31000377), Shandong Province Natural Science Foundation (No. ZR2010BQ016), the Natural Science Foundation for Distinguished Young Scholar of Shandong Province (No. JQ201008), and the Fundamental Research Funds for the Central Universities (No. 11CX04030A).

References

1. Vassilatis DK, Hohmann JG, Zeng H et al (2003) The G protein-coupled receptor repertoires of human and mouse. *Proc Natl Acad Sci USA* 100:4903–4908
2. Drews J (2000) Drug discovery: a historical perspective. *Science* 287:1960–1964
3. Allen SJ, Crown SE, Handel TM (2007) Chemokine: receptor structure, interactions, and antagonism. *Annu Rev Immunol* 25:787–820
4. Gerard C, Rollins BJ (2001) Chemokines and disease. *Nat Immunol* 2:108–115
5. O'Hayre M, Salanga CL, Handel TM (2010) Emerging concepts and approaches for chemokine-receptor drug discovery. *Expert Opin Drug Discov* 5:1109–1122
6. Mandriks I, Petrovska R, Klovins J (2010) Evidence for constitutive dimerization of niacin receptor subtypes. *Biochem Biophys Res Commun* 395:281–287
7. Wang J, Norcross M (2008) Dimerization of chemokine receptors in living cells: key to receptor function and novel targets for therapy. *Drug Discovery Today* 11:625–632
8. Liddiard K, Jones E (2001) Chemokine/chemokine receptor nomenclature. *J Leukoc Biol* 70:465–466
9. Jaerve A, Muller HW (2012) Chemokines in CNS injury and repair. *Cell Tissue Res* 349:229–248
10. Massimo L, Raffaella B, Corsi MM (2005) Chemokines and Their Receptors. *Pathology Patterns Reviews* 123(Suppl 1):S82–S95
11. Hebert TE, Moffett S, Morello JP et al (1996) A peptide derived from a beta2-adrenergic receptor transmembrane domain inhibits both receptor dimerization and activation. *J Biol Chem* 271:16384–16392
12. Milligan G (2007) G protein-coupled receptor dimerisation: molecular basis and relevance to function. *Biochim Biophys Acta* 1768:825–835
13. Milligan G, Bouvier M (2005) Methods to monitor the quaternary structure of G protein-coupled receptors. *FEBS J* 272:2914–2925
14. Boute N, Jockers R, Issad T (2002) The use of resonance energy transfer in high-throughput screening: BRET versus FRET. *Trends Pharmacol Sci* 23:351–354
15. Fotiadis D, Liang Y, Filipek S et al (2003) Atomic-force microscopy: Rhodopsin dimers in native disc membranes. *Nature* 421:127–128
16. Jones KA, Borowsky B, Tamm JA et al (1998) GABA(B) receptors function as a heteromeric assembly of the subunits GABA(B)R1 and GABA(B)R2. *Nature* 396:674–679
17. Margeta-Mitrovic M, Jan YN, Jan LY (2001) Function of GB1 and GB2 subunits in G protein coupling of GABA(B) receptors. *Proc Natl Acad Sci U S A* 98:14649–14654
18. Galvez T, Duthey B, Kniazeff J et al (2001) Allosteric interactions between GB1 and GB2 subunits are required for optimal GABA(B) receptor function. *EMBO J* 20:2152–2159
19. Li X (2009) TIR receptors mediate mammalian sweet and umami taste. *Am J Clin Nutr* 90:733S–737S
20. Zhao GQ, Zhang Y, Hoon MA et al (2003) The receptors for mammalian sweet and umami taste. *Cell* 115:255–266
21. Vila-Coro AJ, Rodriguez-Frade JM, Martin DA et al (1999) The chemokine SDF-1alpha triggers CXCR4 receptor dimerization and activates the JAK/STAT pathway. *FASEB J* 13:1699–1710
22. Rodriguez-Frade JM, Vila-Coro AJ, Ana AM et al (1999) The chemokine monocyte chemoattractant protein-1 induces functional responses through dimerization of its receptor CCR2. *Proc Natl Acad Sci U S A* 96:3628–3633
23. Hernanz-Falcon P, Rodriguez-Frade JM, Serrano A et al (2004) Identification of amino acid residues crucial for chemokine receptor dimerization. *Nat Immunol* 5:216–223
24. Percherancier Y, Berchiche YA, Slight I et al (2005) Bioluminescence resonance energy transfer reveals ligand-induced conformational changes in CXCR4 homo- and heterodimers. *J Biol Chem* 280:9895–9903

25. Issafras H, Angers S, Bulenger S et al (2002) Constitutive agonist-independent CCR5 oligomerization and antibody-mediated clustering occurring at physiological levels of receptors. *J Biol Chem* 277:34666–34673
26. Wilson S, Wilkinson G, Milligan G (2005) The CXCR1 and CXCR2 receptors form constitutive homo- and heterodimers selectively and with equal apparent affinities. *J Biol Chem* 280:28663–28674
27. Trettel F, Di Bartolomeo S, Lauro C et al (2003) Ligand-independent CXCR2 dimerization. *J Biol Chem* 278:40980–40988
28. Babcock GJ, Farzan M, Sodroski J (2003) Ligand-independent dimerization of CXCR4, a principal HIV-1 coreceptor. *J Biol Chem* 278:3378–3385
29. Rodriguez D, Gutierrez-de-Teran H (2012) Characterization of the homodimerization interface and functional hotspots of the CXCR4 chemokine receptor. *Proteins* 80:1919–1928
30. Sierro F, Biben C, Martinez-Munoz L et al (2007) Disrupted cardiac development but normal hematopoiesis in mice deficient in the second CXCL12/SDF-1 receptor, CXCR7. *Proc Natl Acad Sci U S A* 104:14759–14764
31. Chakera A, Seeber RM, John AE (2008) The duffy antigen/receptor for chemokines exists in an oligomeric form in living cells and functionally antagonizes CCR5 signaling through hetero-oligomerization. *Mol Pharmacol* 73:1362–1370
32. El-Asmar L, Springael JY, Ballet S et al (2005) Evidence for negative binding cooperativity within CCR5-CCR2b heterodimers. *Mol Pharmacol* 67:460–469
33. Sohy D, Parmentier M, Springael JY (2007) Allosteric transinhibition by specific antagonists in CCR2/CXCR4 heterodimers. *J Biol Chem* 282:30062–30069
34. Contento RL, Molon B, Boularan C et al (2008) CXCR4-CCR5: a couple modulating T cell functions. *Proc Natl Acad Sci U S A* 105:10101–10106
35. Johnston JM, Aburi M, Provasi D et al (2011) Making structural sense of dimerization interfaces of delta opioid receptor homodimers. *Biochemistry* 50:1682–1690
36. Agrawal L, Alkhatib G (2001) Chemokine receptors: emerging opportunities for new anti-HIV therapies. *Expert Opin Ther Targets* 5:303–326
37. Dean M, Carrington M, Winkler C et al (1996) Genetic restriction of HIV-1 infection and progression to AIDS by a deletion allele of the CKR5 structural gene. Hemophilia Growth and Development Study, Multicenter AIDS Cohort Study, Multicenter Hemophilia Cohort Study, San Francisco City Cohort. ALIVE Study. *Science* 273:1856–1862
38. Huang Y, Paxton WA, Wolinsky SM et al (1996) The role of a mutant CCR5 allele in HIV-1 transmission and disease progression. *Nat Med* 2:1240–1243
39. Samson M, Libert F, Doranz BJ et al (1996) Resistance to HIV-1 infection in caucasian individuals bearing mutant alleles of the CCR-5 chemokine receptor gene. *Nature* 382:722–725
40. Zimmerman PA, Buckler-White A, Alkhatib G et al (1997) Inherited resistance to HIV-1 conferred by an inactivating mutation in CC chemokine receptor 5: studies in populations with contrasting clinical phenotypes, defined racial background, and quantified risk. *Mol Med* 3:23–36
41. Agrawal L, Lu X, Qingwen J et al (2004) Role for CCR5Delta32 protein in resistance to R5, R5X4, and X4 human immunodeficiency virus type 1 in primary CD4 + cells. *J Virol* 78:2277–2287
42. Smith MW, Dean M, Carrington M et al (1997) Contrasting genetic influence of CCR2 and CCR5 variants on HIV-1 infection and disease progression. Hemophilia Growth and Development Study (HGDS), Multicenter AIDS Cohort Study (MACS), Multicenter Hemophilia Cohort Study (MHCS), San Francisco City Cohort (SFCC). ALIVE Study. *Science* 277:959–965
43. Mellado M, Rodriguez-Frade JM, Vila-Coro AJ (1999) Chemokine control of HIV-1 infection. *Nature* 400:723–724
44. Lagane B, Chow KY, Balabanian K et al (2008) CXCR4 dimerization and beta-arrestin-mediated signaling account for the enhanced chemotaxis to CXCL12 in WHIM syndrome. *Blood* 112:34–44

45. Wang J, He L, Combs CA (2006) Dimerization of CXCR4 in living malignant cells: control of cell migration by a synthetic peptide that reduces homologous CXCR4 interactions. *Mol Cancer Ther* 5:2474–2483
46. Levoye A, Balabanian K, Baleux F (2009) CXCR7 heterodimerizes with CXCR4 and regulates CXCL12-mediated G protein signaling. *Blood* 113:6085–6093
47. Zabel BA, Wang Y, Lewen S et al (2009) Elucidation of CXCR7-mediated signaling events and inhibition of CXCR4-mediated tumor cell transendothelial migration by CXCR7 ligands. *J Immunol* 183:3204–3211
48. Godessart N, Kunkel SL (2001) Chemokines in autoimmune disease. *Curr Opin Immunol* 13:670–675
49. Vicari AP, Caux C (2002) Chemokines in cancer. *Cytokine Growth Factor Rev* 13:143–154
50. Amin K, Janson C, Harvima I (2005) CC chemokine receptors CCR1 and CCR4 are expressed on airway mast cells in allergic asthma. *J Allergy Clin Immunol* 116:1383–1386
51. Muller A, Homey B, Soto H et al (2001) Involvement of chemokine receptors in breast cancer metastasis. *Nature* 410:50–56
52. Miao Z, Luker KE, Summers BC et al (2007) CXCR7 (RDC1) promotes breast and lung tumor growth in vivo and is expressed on tumor-associated vasculature. *Proc Natl Acad Sci USA* 104:15735–15740
53. Luboshits G, Shina S, Kaplan O et al (1999) Elevated expression of the CC chemokine regulated on activation, normal T cell expressed and secreted (RANTES) in advanced breast carcinoma. *Cancer Res* 59:4681–4687
54. Peters W, Charo IF (2001) Involvement of chemokine receptor 2 and its ligand, monocyte chemoattractant protein-1, in the development of atherosclerosis: lessons from knockout mice. *Curr Opin Lipidol* 12:175–180
55. Suzuki K, Morokata T, Morihira K et al (2006) In vitro and in vivo characterization of a novel CCR3 antagonist, YM-344031. *Biochem Biophys Res Commun* 339:1217–1223
56. Wenzel J, Henze S, Worenkamper E et al (2005) Role of the chemokine receptor CCR4 and its ligand thymus- and activation-regulated chemokine/CCL17 for lymphocyte recruitment in cutaneous lupus erythematosus. *J Invest Dermatol* 124:1241–1248
57. Reibman J, Hsu Y, Chen LC (2003) Airway epithelial cells release MIP-3alpha/CCL20 in response to cytokines and ambient particulate matter. *Am J Respir Cell Mol Biol* 28:648–654
58. Papadakis KA, Prehn J, Moreno ST et al (2001) CCR9-positive lymphocytes and thymus-expressed chemokine distinguish small bowel from colonic Crohn's disease. *Gastroenterology* 121:246–254
59. Greaves DR, Hakkinen T, Lucas AD et al (2001) Linked chromosome 16q13 chemokines, macrophage-derived chemokine, fractalkine, and thymus- and activation-regulated chemokine, are expressed in human atherosclerotic lesions. *Arterioscler Thromb Vasc Biol* 21:923–929
60. Mellado M, Rodriguez-Frade JM, Vila-Coro AJ et al (2001) Chemokine receptor homo- or heterodimerization activates distinct signaling pathways. *EMBO J* 20:2497–2507
61. O'Byrne PM, Inman MD, Parameswaran K (2001) The trials and tribulations of IL-5, eosinophils, and allergic asthma. *J Allergy Clin Immunol* 108:503–508
62. Ting PC, Lee JF, Wu J et al (2005) The synthesis of substituted biperidine amide compounds as CCR3 antagonists. *Bioorg Med Chem Lett* 15:1375–1378
63. Erin EM, Williams TJ, Barnes PJ (2002) Eotaxin receptor (CCR3) antagonism in asthma and allergic disease. *Curr Drug Targets Inflamm Allergy* 1:201–214
64. Flood-Page P, Menzies-Gow A, Phipps S et al (2003) Anti-IL-5 treatment reduces deposition of ECM proteins in the bronchial subepithelial basement membrane of mild atopic asthmatics. *J Clin Invest* 112:1029–1036
65. Berkman N, Ohnona S, Chung FK (2001) Eotaxin-3 but not eotaxin gene expression is upregulated in asthmatics 24 hours after allergen challenge. *Am J Respir Cell Mol Biol* 24:682–687

66. Struyf S, Menten P, Lenaerts JP et al (2001) Diverging binding capacities of natural LD78beta isoforms of macrophage inflammatory protein-1alpha to the CC chemokine receptors 1, 3 and 5 affect their anti-HIV-1 activity and chemotactic potencies for neutrophils and eosinophils. *Eur J Immunol* 31:2170–2178

Chapter 68

The Mechanism of Apoptosis in Adenocarcinoma of Lung Cancer A549 Cells Induced by Albumin-Derived from Peanut

Minhui Long, Yuejun Sun, Ni Chen, Zimin Zhang, Wen Chu,
Yue Ma, Sheng Luo, Zhongpeng Zhao and Aipo Diao

Abstract Peanut albumin which possesses protease inhibitor activity could be used as an anticancer reagent. This paper would discuss the effect and mechanism of apoptosis induced by peanut albumin on human adenocarcinoma lung cancer A549. MTT assay was used to evaluate the inhibition of peanut albumin on 11 kinds of cancer cells. Compared with other cells, there was the great significant change in A549 cells. Morphological structures were detected by fluorescence microscope, and cell cycle was measured by flow cytometry (FCM). Annexin V/PI was used to detect cell cycle of A549 treated with peanut albumin. The differential expressions between the group treated with peanut albumin and the control were detected by Western-blot and quantitative-PCR. It was found that peanut albumin could inhibit proliferation of A549 cells, and induce apoptosis of A549. The possibility apoptosis of A549 cells induced by peanut albumin maybe correlated with mitochondrial apoptosis pathway.

Keywords Peanut albumin · A549 · Apoptosis · Mitochondrial pathway

Note: Y. Sun and M. Long are joint primary author.

M. Long · Y. Sun · W. Chu · Y. Ma · S. Luo · A. Diao (✉)
College of Biotechnology, Tianjin University of Science and Technology, Tianjin 300457,
People's Republic of China
e-mail: diaoaiipo@tust.edu.cn

M. Long (✉) · N. Chen · Z. Zhang
College of Life Science, South China Normal University, Guangzhou 510631,
People's Republic of China
e-mail: longminhui2006@yahoo.com.cn

Z. Zhao
State Key Laboratory of Pathogen and Biosecurity, Institute of Microbiology and
Epidemiology, Academy of Military Medical Sciences, Beijing 100071,
People's Republic of China

68.1 Introduction

Much epidemiologic evidence indicates that diets containing legumes products, such as peanuts and soybeans, are relevant low cancer incidence and mortality rates, particularly with respect to colon, breast, prostates cancer [1–5]. Protease inhibitors in these products are effective suppressors of carcinogenesis and have ability to prevent carcinogen-induced transformation [6–10]. Albumins are major groups of seed storage proteins widely distributed in both mono- and di-cotyledonous plants, such as peanuts and soybeans. In addition to the storage protein function of albumins, recent findings have demonstrated that albumins have protease inhibitor activity/or anti-proliferative activity and can also play a protective role in plants as defensive weapons against fungal attack/or anti-bacteria [11–13].

Previous work from our laboratory demonstrated that albumins-derived from peanut exerts trypsin inhibitor activity. Interestingly, this activity is stronger than Bowman-Birk trypsin inhibitor, a candidate for anti-cancer, which has been reported to exert powerful anti-carcinogenic activity [14–17]. Studies have been verified that the inhibition of various types of cancers is one of anti-cancer characteristics of BBI [18]. Much evidence shows that many different trypsin inhibitors in their pure forms suppress carcinogenesis. Although some data from in vitro studies suggest that peanut-derived isoflavones and other compounds may have anti-carcinogenic activity, there is a scarcity of published studied in a pure form [19]. Albumin in peanut has the character of trypsin inhibitor, it is supposed that the albumin is one of constitutes which can inhibit carcinogenesis in peanut.

This study will demonstrate that albumin in peanut is responsible for the anti-carcinogenesis and will find which kind of mechanisms of albumin is in action. On the basis of this knowledge, several kinds of tumor cells will be used with respect to the application of such constitute to verify its anti-carcinogenesis.

68.2 Materials and Methods

68.2.1 *Extraction Albumins of Peanut*

Local peanut cultivars were provided by the ShanDong Agricultural Institute in ShanDong Province in china. Peanut was pulverized in the presence of liquid nitrogen, 1 g peanut fine power was mixed with 6 ml of N-hexane for 24 h at –20 °C, filtered with filter paper and dried with vacuum pump, then mixed with phosphate buffer (10 mM, pH 7.9) at 4 °C for overnight according to 10 ml/g, and centrifuged (Beckman Coulter, Krefeld, Germany) at 8,000 g for 20 min to collect supernatant. To gain the protein, the supernatant was homogenized in 65 % ammonium sulfate and kept at 4 °C for 4 h, centrifuged for 20 min (12,000 g, 4 °C). Part of the protein precipitated here and the supernatant was discarded after centrifugation. The sediment was dissolved in phosphate buffer as described before.

68.2.2 Assay of Trypsin Inhibitor Activity Using BAPNA as Substrate

A reaction mixture of 200 μl containing protein(0–0.01 mg) and 0.25 mg trypsinase in reaction buffer (50 mM Tris, 20 mM CaCl_2 , pH 7.5) was incubated at 37 °C for 30 min., then added 1 ml of BAPNA solution containing 0.2 g BAPNA (Sigma) in reaction buffer was incubated at 37 °C for 10 min. The reaction was stopped with 200 μl of cold 30 % acetic acid, incubated in ice for 10 min, and centrifuged at 10,000 g for 10 min. To the supernatant, the A410 was taken. One unit of trypsin was arbitrarily defined as the amount that increased A410 by 0.01 under the assay conditions. One unit of TI was defined as the amount that inhibited one unit of trypsin.

68.2.3 Cell Cultures

The A549, HGP-2, Hele, 786O, MCF-7, BGC-823, DU-145, CaCo-2, Colo 320, Ramos, U-87MG, cell lines were kindly provided by Dr WenYan. HE and Professor DongGang XU (Institute of Basic Medical Science Academy of Military Medical Sciences, Beijing, China). The cells were cultured in DMEM-Hams's F-12 (1:1) supplemented with 50 $\text{mg} \cdot \text{mL}^{-1}$ gentamicin, 50 $\text{mg} \cdot \text{mL}^{-1}$ kanamycin, 10 mg/ml.

68.2.4 MTT Assay for Albumins Application

The solution of albumins was poured into bag filter for renaturation in PBS at 4 °C. The albumins were added to the cell culture medium at a concentration of 50–200 $\mu\text{g} \cdot \text{mL}$ in different cell lines as described before and incubated for 6–48 h. Then MTT was added to the medium 500 $\mu\text{g} \cdot \text{mL}$ and incubated for 4 h. The medium was removed, and the Formazan was diluted in dimethyl sulphoxide (DMSO). After vibration, the formazane concentration of the supernatant was measured by determination of the absorbance at 490 nm.

68.2.5 Total RNA Preparation and Real-Time PCR(qPCR) Assay

RNA pure reagent kit for rapid extraction of ultrapure RNA (Biomed, China) was used to extract the total RNA from the A549 cells-treated with/without albumin for 6 h, respectively, according to the operation manual. PrimerScript Reverse

Table 68.1 The follow primers are used in qPCR assay

Caspase 3	CAS3-1	5'-CTGCCGGAGTCTGACTTGGAA-3'
	CAS3-2	5'-ATCAGTCCCAGTGTCTGTCTCAATG-3'
Caspase 9	CAS9-1	5'-ACCAGCTGGATGCTGTGTCAAG
	CAS9-2	5'-TGCTCCAGAATGCCATCCAA-3'
Caspase 8	CAS8-1	5'-GGACATGTTGTCCATCCTGA-3'
	CAS8-2	5'-TTTCTTGGTCAGCGTGTAGC-3'
Bcl-2	Bcl-2-1	5'-ATGAGCGATGAGTTTGAGGGTTC-3'
	Bcl-2-1	5'-CGATCCCACCAGGACTGGATA-3'
Bax	Bax-1	5'-TTTGCTTCAGGGTTTCATCC-3'
	Bax-2	5'-CAGTTGAAGTTGCCGTCAGA-3'

Transcriptase (TaKaRa Biotechnology Co. Ltd. (Dalian)) was used for the reverse-transcription of 1 µg total RNA of each group by strictly following the operation manual enclosed with the kit. The resulted cDNA should be used for QPCR that was carried out by using the fluorescent MaximaTMSYBR Green/ROX qPCR Master Mix (2×) in Mx3000QPCR Systems (Agilent Technologies Stratagene Products Division, USA), and the reaction system (20 µl) should be used respectively to detect the mRNA expression levels of caspase3, 8, 9, Bcl-2 and Bax in A549 cells (primers information was shown in Table 68.1).

68.2.6 Protein Extraction and Immunoblot Analysis

The A549 cells of various group-treated with/without 100 µg·mL for 12 h were rinsed with the pre-cooled phosphate buffer (1 × PBS) for three times, then from which the cell total protein was extracted by RIPA lysis buffer (Applygen Technologies Inc., China) and quantified by the Protein Detection Kit with Lowry's method (KeyGEN Biotechnology Co., China).

Cell protein was separated by electrophoresis on 15 %SDS-PAGE, and then transferred onto a PVDF membrane of 0.2 µm aperture (Immobilon™ Millipore, USA) by Western blotting. The nonspecific binding sites on PVDF membrane should be blocked by 5 % defatted milk powder dissolute in Tris-buffered saline/1%Tween20 (TBS-T) at 4 °C for overnight. Then, the specific antibodies (1st antibody) against caspase3, 8, 9 (Cell Signaling Technology Inc., USA), and Bcl-2, Bax (Cell Signaling Technology Inc., USA) were prepared with 5 % defatted milk powder, and diluted for 1,000 times (1:1000). Finally, SuperSignal West Femto Substrate (Thermo Scientific, USA) was used for development in a dark room, and the house-keeping gene GAPDH (Cwbiotech Inc., China) as internal reference.

68.2.7 Measurement of Apoptosis

Double staining method with Annexin V-FITC/Propidium iodide (PI) (Nanjing Keygen Biotech Co, Ltd.) was used to detect the phosphatidylserine (PS) at the cell surface to evaluate the apoptotic cell number. A549 cells were inoculated I at the concentration of 6×10^5 /well into a 6 well-plate, which were divided into untreated (control) group, negative group (BSA), treated with albumins at concentrations of 100 μg . The cells were collected after the treatment with albumins for 24 h, digested with 0.25 % trypsin without EDTA (invitrogen, USA) and washed with phosphate buffer for two times to which 500 μl Binding Buffer and 5 μl Annexin V-FITC were added, 5 μl PI-suspended cells were mixed homogeneously, and reacted in dark for 15 min. The stained cells were counted and analyzed by flow cytometry (FACSCalibur, BD Bioscience). The above-mentioned tests should be repeated for three times.

68.2.8 Statistics

All the parameters were expressed as mean \pm SD, the softwares: Student *t* test, one-way ANOVA, SPSS13.0, and MxPro 3000- QPCR were used for statistical analysis. * $p < 0.05$ and ** $p < 0.01$ were used to express the statistically significant difference.

68.3 Results and Discussion

68.3.1 The Trypsin Inhibitor Activity of Albumins in Peanut

The protein was extracted with 10-mM phosphate buffer, pH 7.9. The TI activity of this protein was tested and compared to BBI and bovine TI. The change in turbidity in every sample was measured by turbidimeter. The turbidity of albumins decreased from 31 to 15 at equal concentration. BBI and Bovine TI also showed similar pattern with turbidity being reduced from 33 to 10 and from 33 to 14, respectively. TI assay done with BSA as control showed no activity (Fig. 68.1). The turbidity, therefore, decreased by 51, 61, and 55 % for purified protein, BBI, Bovine TI respectively at a concentration of 100 $\mu\text{g} \cdot \text{ml}^{-1}$. Although the decrease in turbidity was better in case of BBI and Bovine TI, the protein also showed significant and comparable TI activity (Fig. 68.1).

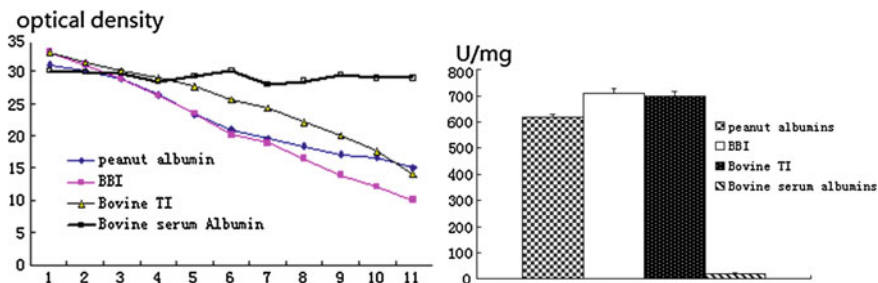


Fig. 68.1 TI activity of purified peanut albumin protein along with BBI and Bovine TI. The bovine serum albumin was used as a control. All experiments were done three times and averaged. Collumn 1 Bovine TI; Collumn 2 BBI; Collumn 3 albumins; Collumn 4 BSA

68.3.2 The Effects of Peanut's Albumins on Different Tumor Cell Lines

BBI are responsible for anti-cancer or inhibitor tumor cells growth, migration, differentiation [14–18]. BBI have the ability of anti-cancer, but some types of tumors are highly resistant to these BBI therapy or BBI treatment [20]. Albumins maybe have the similarity to BBI. We have therefore tested ability of 2 s albumins to inhibit the different types of tumor cells. A549, HGP-2, Hele, 786O, MCF-7, BGC-823, DU-145, CaCo-2, Colo 320, Ramos, U-87MG cells were grown for 4 days in DMED and harvested. 1×10^5 cells for every kind of cell line were plated in 96-well dishes, then treated with 100 $\mu\text{g}/\text{mL}$ of albumins for 24 h and then subjected to MTT assay. The MTT assay is a convenient colorimetric assay of mitochondrial viability that assesses the number of viable cells versus the number of dead cell in a given sample. Figure 68.2 shows that the A549, MCF-7, Colo 320, Romos cells are more sensitive to albumins. These phenomena maybe due to

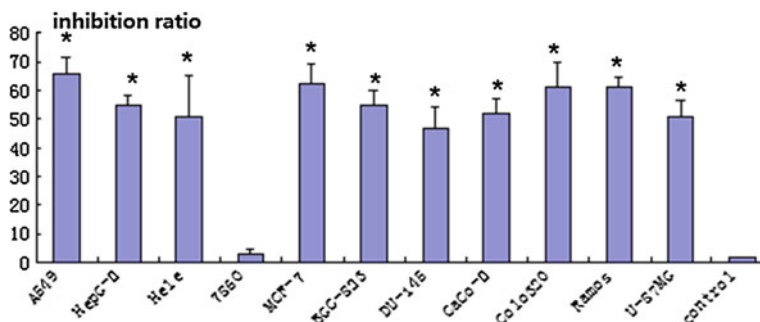


Fig. 68.2 Effects of peanut albumins treatment on the growth of 11 kinds of tumor cell lines. Different cells were incubated with 100 $\mu\text{g}/\text{ml}$ peanut albumin for 24 h. The color intensity was measured using a microtiter plate reader (Bio-Rad model 550) at 490 nm. All the cell lines could be inhibited by peanut albumin except 786O

the fact that those cells were stimulated to apoptosis by peanut albumins more easily than the others. Similar results were achieved by treating the cells with the peanut albumins for 1 h and subjecting the samples to an MTT assay 24 h later (data not shown). These data have been confirmed with other techniques such as measurement of cell viability by trypan blue exclusion cell-count before and after peanut albumins treatment, as well as by flow-cytometry analysis (data not shown). Interestingly, the 786O cells had an overall resistance to any dose of the peanut albumins, whether above or below the assessed LD₅₀. However, A549 and MCF-7 are the most sensitive to albumins. The results showed albumins enhanced A549, MCF-7 cell death even at doses well below the LD₅₀(refer to BBI), suggesting that albumins could easily simulate A549 and MCF-7 cell to die, maybe used to lower the necessary dose of albumins treatments for patients.

Surprisingly, the Hele, BGC-823, DU-145, CaCo-2, Colo 320, Ramos, U-87MG, cells were sensitive to treatments with 2S albumins. However, the affect of albumins on those cells were more less than A549, MCF-7.

68.3.3 Changes of A549 Cell Mitochondrial Pathway and the Apoptosis and Proliferation of Tumor Cell After Treatment with Peanut Albumin

There were some interactions between tumor cells and peanut albumin when tumor cells were incubated with peanut albumin in previous experiment, and the A549 cells were the most sensitive to albumins. For the further exploring the effect of on A549 cells growth when they were treated with peanut albumin, different concentrations of peanut albumin were incubated with A549 cell, and the expression change of Bcl-2, Bax, Caspase3, Caspase9, and Caspase8 were monitored. Then the finding expression of Bax, Caspase3, Caspase9 displayed a significant increasing tendency ($p < 0.05$), and the level of Caspase8 expression was not significantly changed, while Bcl-2 mRNA expression was significantly decreased ($p < 0.05$), and its protein expression was also significantly decreased (Fig. 68.3a, b). These results suggested that peanut albumin as a new anti-tumor candidate could induce A549 cells to apoptosis which displayed a character similar to the action produced by BBI, which might be related with its trypsin inhibitor activity. We also observed the influence of both on cell apoptosis, and found that the cell apoptosis rate (42.5 %) was significantly higher than the control group (3.6 %), further verifying that peanut albumin possesses the promotion effect on cell apoptosis (Fig. 68.3c). This study demonstrated that the albumin in peanut can regulate A549 cells' function, and demonstrated the promotion effect to cell apoptosis possibly through mitochondrial pathway.

Our goal was to find whether components of the peanut proteins, when they were added into media, would inhibit the growth of the tumor cell or induce tumor cell to death. We also hoped to find which type of tumor cells that response to

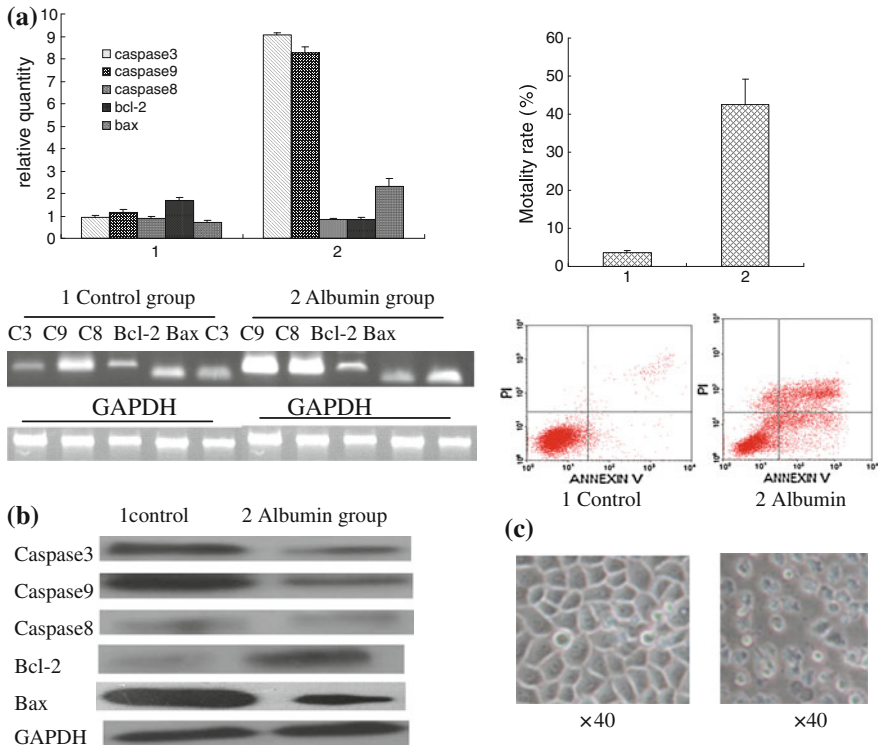


Fig. 68.3 The expression and protein levels change of above-mentioned various cytokines in cytoplasm were observed after A549 cell lines were treated with peanut albumin. A. The expression levels change of Bcl-2, Bax, Caspase3, Caspase9, Caspase8 in intra-cellular were detected by qPCR. B. The expression of Bcl-2, Bax, Caspase3, Caspase9, Caspase8 in protein levels were detected. C. A549 cells apoptosis was detected by flow cytometry

peanut albumins at the time of culture, though in practice our screen was more effective for finding the former. We chose different cell lines imaging to read out our screening assay, an information rich method that facilitated monitoring of multiple phenotypes. Typically, an imaging screen for cellular appearances would be performed as a fixed endpoint assay in microplates with DAPI staining for DNA and perhaps also apoptosis. The advantage of this method lies in ease of image analysis; however, fixed endpoint imaging would limit our ability to quantify both the cell growth and apoptosis responses, since they are separated by ~ 24 h. Other potential drawbacks of a fixed endpoint DAPI assays include demarcation of the necrosis and apoptosis cell as well as potential loss of weakly adherent cells and distortion of cellular structures during fixation. Hence, to assess whether peanut albumins-induced cell death, MTT assay was used to measure the relative survival of cells. When A549, HGP-2, Hele, MCF-7, BGC-823, DU-145, CaCo-2, Colo 320, Ramos, and U-87MG cells were incubated with increasing concentrations of peanut albumins and the proteins caused a dose-dependent inhibition of

cell proliferation (data not shown) except 786O cells, whereas the inhibitory effect of peanut albumins was approximately twofold higher than that of BBI with concentrations ranging from 30 to 40 μg . Some components in peanut albumins are family of trypsin inhibitors isolated from plant seeds that exhibit anti-bacterial and anti-fungal properties [21, 22]. Few studies show they have the capacity to induce cell death in human cancer cells. In this report, we first used A549 cell lines as models for assay and found that albumins which possess the activity of trypsin inhibitor inhibited the growth of this cell lines in vitro. Most significantly, A549 cells were more sensitive to albumin than normal pneumonocyte with lower concentration of albumins, indicating A549 cells might be potentially model for investigating the anticancer of peanut albumin (data not shown). Furthermore, peanut albumins induced a form of apoptotic cell death in A549 cells, which was characterized by extensive vacuolization, surface exposure of PS, and loss of mitochondrial membrane. Moreover, the A549 cells apoptotic process induced by peanut albumin was caspase-dependent. Caspase3, one member of caspases which are a family of proteases involved in the execution of apoptosis, is known to be an important molecule in the cellular suicide cascade. It can be activated by stimuli with a membrane (receptor-activated) or mitochondrial origin [23]. In fact, caspase3 is a downstream response factor of caspase9, which, in turn, is activated by cytochrome c released by mitochondria or by caspase8 that is activated by membrane death receptors [23]. Pro- and anti-apoptotic genes of the Bcl2 family act by stabilizing (Bcl2-like) or destabilizing (Bax-like) the mitochondrial membrane, thus altering the release of cytochrome c that, in turn, activates caspase9 and caspase3 sequentially [24]. On the other hand, membrane-dependent stimuli such as Fas/FasL or tumor necrosis factor α (TNF- α)/TNF- α R interaction may trigger caspase8 activation, which eventually leads to caspase3 activation [23]. Over high level of mRNA expression of caspase3, caspase9, Bax occurred in A549 cells in this study and we observed that caspase3, caspase9, Bax also has the similar changing tendency at protein level. Our study also found that peanut albumin can inhibit Bcl-2 mRNA transcription, and decrease the expression of anti-apoptotic protein Bcl-2 in A549 cell strain and little effect on caspase8 when A549 cells were stimulated by peanut albumin, demonstrating that peanut albumin displayed an effect of promotion of A549 cell's apoptosis.

68.4 Conclusion

In summary, cell death pathway induced by peanut albumins was main characteristic of mitochondrial pathway in A549 cells for great changes in expression of caspase3, caspase9, Bcl-2, Bax ($P < 0.05$), and for little change of caspase8 was observed ($P = 0.974$). The anti-tumor function of ($P < 0.05$) peanut albumin was further understood, laid the theoretical basis for subsequent research and provided a new idea for the research and development of the drugs against cancer.

References

1. Park SY, Murphy SP, Wilkens LR et al (2008) Legume and isoflavone intake and prostate cancer risk: the multiethnic cohort study. *Int J Cancer* 123(4):927–932
2. Adlercreutz H, Honjo H, Higashi A et al (1991) Urinary excretion of lignans and isoflavonoid phytoestrogens in Japanese men and women consuming a traditional Japanese diet. *Am J Clin Nutr* 54:1093–1100
3. Adlercreutz H, Markkanen H, Watanabe S (1993) Plasma concentrations of phyto-oestrogens in Japanese men. *Lancet* 342:1209–1210
4. Hebert JR, Hurley TG, Olendzki BC et al (1998) Nutritional and socioeconomic factors in relation to prostate cancer mortality: a cross-national study. *J Natl Cancer* 90(1637–1647):9
5. Jacobsen BK, Knutsen SF, Fraser GE (1998) Does high soy milk intake reduce prostate cancer incidence? The adventist health study (United States). *Cancer Causes Control* 9:553–557
6. Sarkar FH, Li Y, Wang Z et al (2010) Lesson learned from nature for the development of novel anti-cancer agents: implication of isoflavone, curcumin, and their synthetic analogs. *Curr Pharm Des* 16(16):1801–1812
7. Li Y, Wang Z, Kong D et al (2008) Regulation of Akt/FOXO3a/GSK-3beta/AR signaling network by isoflavone in prostate cancer cells. *J Biol Chem* 283:27707–27716
8. Su Y, Simmen RC (2009) Soy isoflavone genistein upregulates epithelial adhesion molecule E-cadherin expression and attenuates beta-catenin signaling in mammary epithelial cells. *Carcinogenesis* 30:331–339
9. Su Y, Simmen FA, Xiao R et al (2007) Expression profiling of rat mammary epithelial cells reveals candidate signaling pathways in dietary protection from mammary tumors. *Physiol Genomics* 30:8–16
10. Wagner J, Lehmann L (2006) Estrogens modulate the gene expression of Wnt-7a in cultured endometrial adenocarcinoma cells. *Mol Nutr Food Res* 50:368–372
11. Wu Y, Wang W, Messing J (2012) Balancing of sulfur storage in maize seed. *BMC Plant Biol* 12:77
12. Mandal S, Kundu P, Roy B et al (2002) Precursor of the inactive 2S seed storage protein from the Indian mustard *Brassica juncea* is a novel trypsin inhibitor. characterization, post-translational processing studies, and transgenic expression to develop insect-resistant plants. *J Biol Chem* 277(40):37161–37168
13. Pelegri PB, Noronha EF, Muniz MA et al (2006) An antifungal peptide from passion fruit (*Passiflora edulis*) seeds with similarities to 2S albumin proteins. *Biochim Biophys Acta* 1764(6):1141–1146
14. Clemente A, Sonnante G, Domoney C (2011) Bowman-Birk inhibitors from legumes and human gastrointestinal health: current status and perspectives. *Curr Protein Pept Sci* 12(5):358–373
15. Clemente A, Moreno FJ, Marín-Manzano Mdel C et al (2010) The cytotoxic effect of Bowman-Birk isoinhibitors, IBB1 and IBBD2, from soybean (*Glycine max*) on HT29 human colorectal cancer cells is related to their intrinsic ability to inhibit serine proteases. *Mol Nutr Food Res* 54(3):396–405
16. Marín-Manzano MC, Ruiz R, Jiménez E et al (2009) Anti-carcinogenic soyabean Bowman-Birk inhibitors survive faecal fermentation in their active form and do not affect the microbiota composition in vitro. *Br J Nutr* 101(7):967–971
17. Tang M, Asamoto M, Ogawa K et al (2009) Induction of apoptosis in the LNCaP human prostate carcinoma cell line and prostate adenocarcinomas of SV40T antigen transgenic rats by the Bowman-Birk inhibitor. *Pathol Int* 59(11):790–796
18. Palavalli MH, Natarajan SS, Wang TT (2012) Imbibition of soybean seeds in warm water results in the release of copious amounts of Bowman-Birk protease inhibitor, a putative anticarcinogenic agent. *J Agric Food Chem* 60(12):3135–3143

19. Yeh CC, You SL, Chen CJ (2006) Peanut consumption and reduced risk of colorectal cancer in women: a prospective study in Taiwan. *World J Gastroenterol* 12(2):222–227
20. Dittmann KH, Dikomey E, Mayer C (2000) The Bowman-Birk protease inhibitor enhances clonogenic cell survival of ionizing radiation-treated nucleotide excision repair-competent cells but not of xeroderma pigmentosum cells. *Int J Radiat Biol* 76(2):223–229
21. Wang T, Zhang E, Chen X et al (2010) Identification of seed proteins associated with resistance to pre-harvested aflatoxin contamination in peanut. *BMC Plant Biol* 10:267
22. Ye XY, Ng TB (2001) Hypogin, a novel antifungal peptide from peanuts with sequence similarity to peanut allergen. *J Pept Res* 57(4):330–337
23. Ashkenazi A, Dixit VM (1998) Death receptors, signaling and modulation. *Science* 281:1305–1308
24. Green DR, Reed JC (1998) Mitochondria and apoptosis. *Science* 281(5381):1309–1312

Chapter 69

Serum miR-124 and TNF- α are Biomarkers of Ischemic Cerebrovascular Disease

Jiajie Liu, Xinghua Liao, Nan Wang, Jun Zhou, Lian Duan, Dalin Lu, Zhipeng Liu, Tingbao Yan, Deyun Ma, Xiumei Dong, Xueguang Sun and Tong-Cun Zhang

Abstract MicroRNAs are small non-coding RNAs with 19-22 nucleotides. MiR-124 expresses abundantly in brain tissue and is involved in the development of ischemic cerebrovascular disease (ICVD). Tumor necrosis factor-alpha (TNF- α) is one of the important factors of the inflammatory reaction after cerebral ischemia. To explore the roles of miR-124 and TNF- α in the process of ICVD, here, we collected the serum of 15 patients with ICVD and 5 normal individuals. The levels of miR-124 and TNF- α were detected by real-time PCR and ELISA. The results showed that compared with the normal individuals, the levels of miR-124 and TNF- α in serum were upregulated in the patients, while they were downregulated after clinical treatment, suggesting that these two factors could be used as good biomarkers for the diagnosis and prognosis of ICVD. Besides, our research also provided a theory foundation for understanding the mechanism of inflammatory response in cerebral ischemia mediated by miR-124.

Keywords Ischemic cerebrovascular disease (ICVD) · Inflammation · miR-124 · Tumor necrosis factor-alpha (TNF- α)

The first two authors contributed equally to the project.

J. Liu · X. Liao · J. Zhou · L. Duan · D. Lu · X. Dong · T.-C. Zhang (✉)
College of Medicine, Wuhan University of Science and Technology,
Wuhan 430065, People's Republic of China
e-mail: tony@tust.edu.cn

X. Liao · N. Wang · Z. Liu · T. Yan · D. Ma · X. Sun · T.-C. Zhang
Key Laboratory of Industrial Microbiology, Ministry of Education and Tianjin City,
College of Biotechnology, Tianjin University of Science and Technology,
Tianjin 300457, People's Republic of China

69.1 Introduction

Ischemic cerebrovascular disease (ICVD) is a group of brain dysfunctions related to disease of the blood vessels supplying the brain. The most common forms of ICVD are transient ischemic attack (40 % of cases) and cerebral embolism (30 %), followed by cerebral thrombosis (20 %) [1]. Cerebrovascular disease is commonly known as activity limitations (also referred to as “disabilities”), mostly in elderly patients, manifested as paralysis, weakness, aphasia, and mental health changes. Stroke is a leading cause of mortality and permanent disability, with two-thirds of onsets due to ischemia. Major modifiable risk factors of ICVD include hypertension, smoking, obesity, and diabetes .

MicroRNAs are a class of small non-coding RNAs that can regulate gene expression and play a critical role in many biological and pathological processes [2, 3]. Although the total number of microRNAs remains controversial [4–7], and the roles of some specific microRNAs need to be defined, recent research has shown that expression of microRNAs in diverse tumors is significantly different from normal tissue [8–10]. Present studies have indicated that specific MicroRNAs played important roles in ICVD occurrence and development process. MicroRNAs may also provide a new strategy for the preservation and diagnosis of ischemic stroke [11].

MiR-124 expresses abundantly in brain tissue and is involved in the development of the ICVD. Besides, stroke-induced inflammatory reaction and the level of tumor necrosis factor- α (TNF- α) in serum would be increased during inflammatory. These results lead to invasion of leukocytes into the evolving brain infarct, seeming to play a key role in the deterioration of ICVD [12, 13]. In order to understand the mechanism of inflammatory response in cerebral ischemia and the roles of miR-124 and TNF- α played in such process, in the present study, the level of miR-124 and TNF- α is tested in the serum of 15 ICVD patients and 5 normal individuals.

69.2 Materials and Methods

69.2.1 Clinical Data

The study was conducted on 15 patients with first-ever ICVD stroke (mean age 63.4 ± 5.2 years, 66 % men). ICVD was confirmed by either MRI or CT imaging of the brain, and the risk factors were characterized based on the ancillary blood and other biochemical examinations. The study excluded the patients with hemorrhage stroke. Patients with concurrent diseases or conditions interfering with the result of the study, like infections, type 2 diabetes mellitus (T2DM), hematological disorders, autoimmune diseases, myocardial infarctions, severe liver disease, malignancies, undergoing surgical interventions within the past 12 months, and

Table 69.1 Clinical data of patients

Group	ICVD	Control
N	15(10/5) (M/F)	5(3/2) (M/F)
Average age	63.4 \pm 5.2	60.2 \pm 3.7

M male, *F* female

those on immunosuppressive drugs were also excluded. All the patients presented completed ICVD stroke, defined as clinical symptoms persisting for more than 48 h. All patients with acute stroke had symptoms confined to the carotid artery territory. The diagnosis of acute stroke was confirmed by tomography of the brain performed immediately after admission. Blood samples were obtained for white blood cell (WBC) counts within the first 24 h after the attack of stroke [14–16]. Five healthy volunteers without risk factors (mean age \pm SD—60.2 \pm 3.7 years, 3 men, and 2 women) served as a control group. The study was performed on the basis of the written consent of each patient and approval of the Ethics Committee of the University School of Medicine in Wuhan.

The age and sex distribution of these 20 cases are shown in Table 69.1.

69.2.2 Blood Specimen Collection

The blood was respectively obtained on the morning of the first day and on the seventh day after attack, and all serum was obtained by the initial centrifugation of the blood samples at 3,000 g for 15 min at 4 °C (Centrifuge 5810R; Eppendorf). Supernatants were collected and immediately stored at -80 °C until use [15].

69.2.3 Real-Time Polymerase Chain Reaction (PCR)

The level of miR-124 was tested by real-time PCR according to manufacturer's instructions (TIANGEN). The three operation step kits (miRcutemiRNA isolation kit, miRcutemiRNA first-strand cDNA synthesis kit, miRcutemiRNA qPCR detection kit (SYBR Green)) were provided. First, total RNA was isolated from serum lysis buffer. Then Poly (A) was added to the 3' terminal of miRNA before reverse transcription. Real-time PCR was performed in the StepOne™ Real-Time PCR System (Applied Biosystems, Inc., Carlsbad, USA). Fast SYBR® Green Master Mix was obtained from Applied Biosystems. The experimental steps were strictly in accordance with the instructions [17]. U6 snRNA was used for the normalization.

69.2.4 Enzyme Linked Immunosorbent Assay (ELISA)

The levels of TNF- α in serum were measured by a human TNF- α ELISA kit (Quantikine, R&D Systems, Minneapolis, USA). A standard curve for quantitative basis was first drawn with five different contents of TNF- α standard samples, and then the serum samples were detected and the concentration of TNF- α calculated using the standard curve. The minimum detectable concentrations in our laboratory were 7 pg/mL for TNF- α .

69.2.5 Statistical Analysis

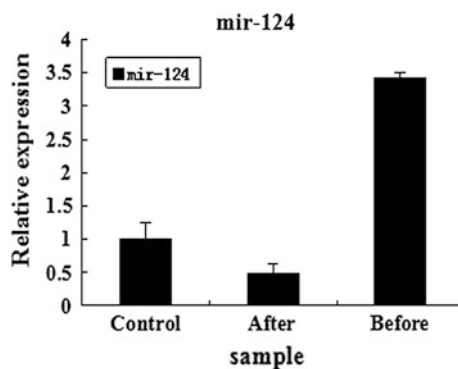
All statistical analyses were computed using SPSS statistical software, and the level of significance was set at $P < 0.05$. The data are reported as mean \pm standard error of the mean.

69.3 Results and Discussion

69.3.1 The Change in mRNA Level of Serum miR-124 in ICVD

To understand the role of miR-124 in ICVD, we used real-time PCR to determine the expression of miR-124 in serum of ICV patients. Compared with patients after clinical treatment and controls, the circulatory miR-124 level of patients before clinical treatment was increased, and compared with the controls, the patients after clinical treatment were significant downregulated (Fig. 69.1). In this experiment, one and a half times greater than the differences were considered as significant difference criterion.

Fig. 69.1 The mRNA level of miR-124 in serum of the ICVD patients and normal persons Control: normal person; After: ICVD patients after clinical treatment; Before: ICVD patients before clinical treatment



69.3.2 The Change in Expression of Serum TNF- α in ICVD

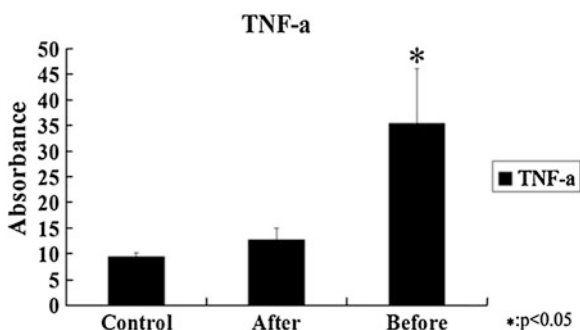
In addition to test the serum concentrations of TNF- α in patients with ICVD before and after clinical treatment and that in control group, the TNF- α level of the samples were measured by ELISA. Results: $X \pm \text{SEM}$. TNF- α value was significantly higher in serum of ICVD patients before clinical treatment than that in normal person ($p = 0.016$, $P < 0.05$) (Table 2, Fig. 69.2). After the clinical treatment, the level of TNF- α in the serum of patients decreased but was still a little higher than that in normal person (Table 69.2, Fig. 69.2). This study showed that increased serum TNF- α level was present in ICVD patients compared with age-matched controls. TNF- α is engaged in the formation of damaged brain cells during the acute cerebrovascular disease period [18–20].

The diagnosis and prognosis of ICVD are dependent on the clinical history and physical examination. Many patients have seizures discontinued when treated, so detailed inquiry seizures is more important. The development of modern imaging technology provides great help for cerebrovascular disease diagnosis, but it cannot apply more vital signs. Functional study of MicroRNAs has developed rapidly recent years in the field of life sciences. A recent study determined that the expression changes in some MicroRNAs and TNF- α in human serum or plasma may be diagnostic markers for certain diseases or physiological changes. At present, a variety of MicroRNAs has been found involved in the pathological process of ICVD. It has been reported that miR-124 was related to the differentiation of neural stem and precursor cells, and was significantly upregulated in the acute phase of ICVD. The present study indicates that expression of circulatory miR-124 was upregulated in serum of ICVD patients before clinical treatment, and

Table 69.2 The expression of TNF- α in serum of the ICVD patients and normal persons (TNF- α /pg/ml, $X \pm \text{SEM}$)

Group	<i>n</i>	TNF- α
Control	5	9.50 \pm 0.68
Patients(after clinical treatment)	15	12.81 \pm 2.15
Patients(before clinical treatment)	15	35.50 \pm 10.53

Fig. 69.2 The expression of TNF- α in serum of ICVD patients and normal persons (TNF- α /pg/ml, $X \pm \text{SEM}$)
Control: normal person;
After: ICVD patients after clinical treatment; Before: ICVD patients before clinical treatment



downregulated after clinical treatment, compared to the controls. The finding may have implications for the development of a desirable biomarker and therapy for ischemic stroke. Since this study utilized serum, tested miR-124 and TNF- α levels in system circulatorium, it would be beneficial for the elucidation of this disease diagnosis method or treatment targets. Serum microRNA is stable and not easy to be degraded, taken from the blood it is convenient, no tissue damage, quick and simple, serum microRNA can be used as a new clinical diagnosis method.

69.4 Conclusion

Our results show that compared with normal serum, the level of serum miR-124 and TNF- α were upregulated in the patients before clinical treatment, while miR-124 and TNF- α were downregulated after clinical treatment, suggesting that these two factors could be used as good biomarkers for the diagnosis and prognosis of ICVD. Besides, our research also provided a theory foundation for understanding the mechanism of inflammatory response in cerebral ischemia mediated by miR-124.

Acknowledgments This work was financially supported by National Natural Science Foundation of China (No. 30970615, 31071126) and Program for Changjiang Scholars and Innovative Research Team in University of Ministry of Education of China (IRT1166) and the Key Project of Chinese Ministry of Education (212010) and Outstanding Young Talent Project of Scientific Research Plan of Education Department in Hubei province (Q20101111).

References

1. Thomas T, Stephen B, Colin M (2000) The global burden of cerebrovascular disease. *Global Burden Dis* 21(06):06
2. Shlomit G, Eti M, Yariv Y et al (2008) Serum MicroRNAs are promising novel biomarkers. *Serum MicroRNA Biomark* 3(9):e3148
3. Soifer HS, Rossi JJ, Saetrom P (2007) MicroRNAs in disease and potential therapeutic applications. *Mol Ther* 15(12):2070–2079
4. Pheasant M, Mattick JS (2007) Raising the estimate of functional human sequences. *Genome Res* 17(9):1245–1253
5. Bentwich I, Avniel A, Karov Y, Aharonov R et al (2005) Identification of hundreds of conserved and nonconserved human microRNAs. *Nat Genet* 37(7):766–770
6. Berezikov E, Plasterk RH (2005) Camels and zebrafish, viruses and cancer: a microRNA update. *Hum Mol Genet.* 14(2):R183–R190
7. Ng Tsui NB, Ng EK, Lo YM (2002) Stability of endogenous and added RNA in blood specimens, serum, and plasma. *Clin Chem* 48(10):1647–1653
8. Calin GA, Croce CM (2006) MicroRNA signatures in human cancers. *Nat Rev Cancer* 6(11):857–866
9. Cummins JM, He Y, Leary RJ et al (2006) The colorectal microRNAome. *Proc Natl Acad Sci USA* 103(10):3687–3692
10. Bartel DP (2009) MicroRNAs: target recognition and regulatory functions. *Cell* 136(2):215–233

11. Maddahi A, Edvinsson L (2010) Cerebral ischemia induces microvascular pro-inflammatory cytokine expression via the MEK/ERK pathway. *J Neuroinflammation* 7:14
12. Zaremba J, Losy J (2001) The levels of TNF-alpha in cerebrospinal fluid and serum do not correlate with the counts of the white blood cells in acute phase of ischaemic stroke. *Folia Morphol (Warsz)* 60(2):91–97
13. Meda L, Cassatella MA, Szendrei GI et al (1995) Activation of microglial cells by beta-amyloid protein and interferon-gamma. *Nature* 374(6523):647–650
14. Gan CS, Wang CW, Tan KS (2012) Circulatory microRNA-145 expression is increased in cerebral ischemia. *Genet Mol Res* 11(1):147–152
15. Fischer CP, Perstrup LB, Berntsen A et al (2005) Elevated plasma interleukin-18 is a marker of insulin-resistance in type 2 diabetic and non-diabetic humans. *Clin Immunol* 117(2):152–160
16. Bansal BC, Gupta RR, Bansal MR et al (1975) Serum lipids and uric acid relationship in ischemic thrombotic cerebrovascular disease. *Stroke* 6(3):304–307
17. Kroh EM, Parkin RK, Mitchell PS et al (2010) Analysis of circulating microRNA biomarkers in plasma and serum using quantitative reverse transcription-PCR (qRT-PCR). *Methods* 50(4):298–301
18. Alvarez XA, Franco A, Fernández-Novoa L et al (1996) Blood levels of histamine, IL-1 β , and TNF- α in patients with mild to moderate Alzheimer disease. *Mol Chem Neuropathol* 29(2–3):237–252
19. Arican O, Aral M, Sasmaz S et al (2005) Serum levels of TNF- α , IFN- γ , IL-6, IL-8, IL-12, IL-17, and I L-18 in patients with active psoriasis and correlation with disease severity. *Mediators Inflamm* 5:273–279
20. Bi Y, Liu G, Yang R (2009) MicroRNAs: novel regulators during the immune response. *J Cell Physiol* 218(3):467–472

Chapter 70

A New Process for Preparation of Hydroxytyrosol

Yinghao Gao, Xijuan Liang, Yuanmou Chen, Fei Hu, Weizhu Liu, Peng Yu and Erbing Hua

Abstract Hydroxytyrosol is one of the major natural phenolic compounds, mainly in virgin olive oil and the wastewater generated from olive oil processing. Based on its strong antioxidation, hydroxytyrosol is widely used in medical treatment, food, beauty, and other industries. Its diverse biological activities have for a long time attracted considerable interest of synthetic and pharmacological areas. In this paper, the new process of hydroxytyrosol synthesis has been explored, which starts from catechol protection, followed by Friedel–Crafts reaction with ethyl oxalyl monochloride, then the Wolff–Kishner–Huang reaction and reduction reaction with LAH, and finally deprotection. The target compound was obtained by five-step reaction with an overall yield of 23 %. The title compound was characterized on the basis of ^1H NMR spectral.

Keywords Natural · Hydroxytyrosol · Synthesis · New process

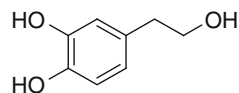
70.1 Introduction

Hydroxytyrosol (3,4-dihydroxyphenylethanol) is primarily found in fruits and leaves of olive and has been reported to exert several biological and pharmacological activities [1]. It was first discovered and extracted from the wastewater that resulted when green olives were rinsed in the process of making olive oil [2–4] (Fig. 70.1).

For decades olive oil has been known for its many healthy properties. It has long been noted that the Mediterranean diet has been associated with a lower

Y. Gao · X. Liang · Y. Chen · F. Hu · W. Liu · P. Yu · E. Hua (✉)
Key Laboratory of Industrial Microbiology, Ministry of Education, College of Biotechnology, Tianjin University of Science & Technology, Tianjin 300457, People's Republic of China
e-mail: huarb@tust.edu.cn

Fig. 70.1 Structures of hydroxytyrosol



incidence of cardiovascular disease and certain cancers than the diet of other Western countries [5]. And since extra-virgin olive oil is the principal source of fat in the Mediterranean diet and has been identified as an important contributor to the reduced mortality associated with this diet, researchers began studying olive oil, looking for the compound that was responsible for the anti-inflammatory and cholesterol-lowering effects [6].

That's when they found hydroxytyrosol—the polyphenol thought to be responsible for olive oil's anti-inflammatory and antioxidant effects [7]. Its ability to absorb free radicals and protect cells and mitochondria [8] from damage is quite impressive.

The antioxidant activity is the most studied property of hydroxytyrosol. The interest of hydroxytyrosol is based on its remarkable pharmacological and antioxidant activities. Reactive oxygen species, which are continuously being formed as a result of metabolic processes in the organism, may cause oxidation and damage of cellular macromolecules, and therefore, may contribute to the development of degenerative diseases, such as atherosclerosis, cancer, diabetes, rheumatoid arthritis, and other inflammatory diseases [9].

The high antioxidant efficiency of hydroxytyrosol, attributed to the presence of the *o*-dihydroxyphenyl moiety, is due to its high capacity for free radical scavenging during the oxidation process and to its reducing power on Fe^{3+} [10].

In numerous human, animal, and *in vitro* studies, hydroxytyrosol has been shown to:

- (1) Decrease markers or indicators of inflammation including PEG-1, IL-10, C-reactive protein, TNF- α , COX-2, iNOS, and others [11].
- (2) Significantly increasing ATP energy production and supporting healthy mitochondrial function [12].
- (3) Improve the quality of life for osteoporosis patients. Hydroxytyrosol may have critical effects on the formation and maintenance of bone, and can be used as effective remedies in the treatment of osteoporosis symptoms [13].
- (4) Reduce the risk of macular degeneration and improve eye health [14].
- (5) Boost significant and rapid reductions in LDL or 'bad' cholesterol [15].
- (6) Have a treatment effect on the cardiovascular system [16].

Additional research shows that hydroxytyrosol holds great promise for a wide variety of potential health benefits.

Hydroxytyrosol is the most powerful natural antioxidant currently known. Well-documented studies confirm its anti-inflammatory, antibacterial, antioxidant, and cardioprotective health benefits. Although it is not familiar to most people, hydroxytyrosol promises to soon become a staple in natural health care. Its biological activities and beneficial effects on human health have stimulated the

development of different procedures for the chemical and enzymatic synthesis of hydroxytyrosol. In this paper, we designed a new, economically effective, technically attractive process for preparation of hydroxytyrosol starting from catechol, because catechol is commercially available.

70.2 Materials and Methods

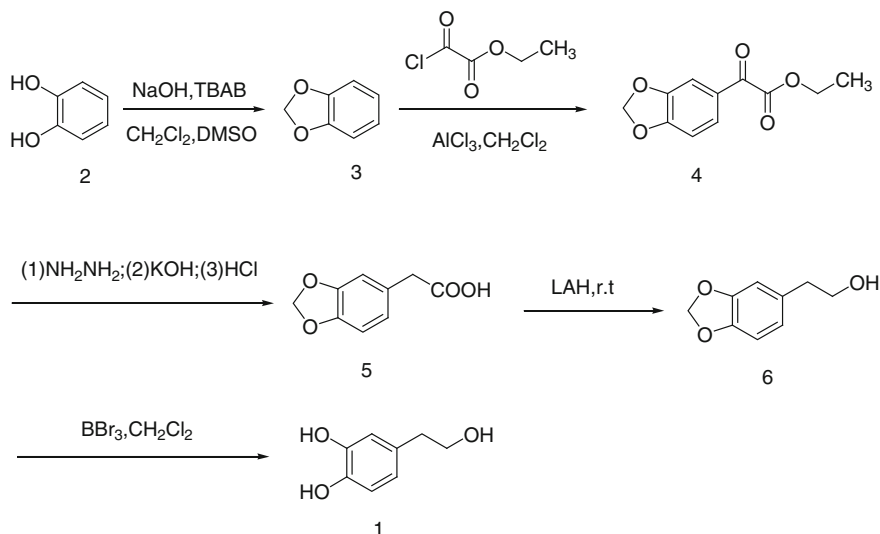
70.2.1 Materials and Measurements

All reagents and solvents used were of reagent grade. Reaction temperatures were controlled by oil bath temperature modulator. Thin layer chromatography (TLC) was performed using E. Merck silica gel 60 GF254 pre-coated plates (0.25 mm). Silica gel (particle size 200–400 mesh) was used for flash chromatography. ^1H spectra were recorded on Bruker AM-400 NMR spectrometers in deuterated chloroform.

70.2.2 General procedures

The route to prepare hydroxytyrosol was presented in Scheme 70.1 .

General procedure for the preparation of 1,2-methylenedioxybenzene(3) [17]



Scheme 70.1 Synthesis of hydroxytyrosol

A mixture of DMSO (80 ml), dichloromethane (20 mL), and tetrabutyl ammonium bromide (1.9 g, 6 mmol) was rigorously stirred and heated to reflux. Then a solution of catechol (11 g, 0.1 mol) in DMSO (60 mL) and a solution of sodium hydroxide (8 g, 0.2 mol) in water (8 mL) were added dropwise at the same time at such a rate that the addition was complete after 2 h. After the addition was complete, the reaction mixture was stirred and refluxed for a further hour.

Then water (100 mL) was slowly added to the reaction mixture. The reaction mixture was heated and the distillates were accumulated from 99 to 104° C. The distillates were 1,2-methylenedioxybenzene (3) and water. The distillates were poured into separator funnel and separated. Then 1,2-methylenedioxybenzene(3) was obtained in 81.7 % yield.

$^1\text{H-NMR}(\text{CDCl}_3)$: δ/ppm 5.96-5.97 (2H, s, $\underline{\text{CH}_2}$), 6.85-6.88 (4H, s, ArH)

General procedure for the preparation of ethyl 2-(benzo[d] [1, 3] dioxol-6-yl)-2-oxoacetate(4) [18]

In a three-necked round-bottomed flask mounted with a cooler system under inert conditions, AlCl_3 (11.7 g, 0.086 mol) was suspended in CH_2Cl_2 (120 mL) at 0 °C. To this mixture ethyl oxalyl monochloride (11.7 g, 0.086 mol) was added dropwise in about 10–15 min. After 10 min the stirred suspension became a pale yellow solution. At 0 °C 1,2-methylenedioxybenzene (3) (10 g, 0.082 mol) was added dropwise in about 10 min. Then the solution was stirred at r.t. for 1 h. To this reaction mixture the three fold volume of H_2O was carefully added. Extraction was performed with EtOAc (5 × 60 mL). The organic layers were collected and washed with saturated NaCl solution (2 × 100 mL), dried over Na_2SO_4 , and concentrated in vacuo. The crude product was purified by column chromatography on silica gel eluted with (PE/EtOAc80:1) to give the compound 4 (10.2 g, 56.7 %) as a pale yellow oil.

$^1\text{H-NMR}(\text{CDCl}_3)$: δ/ppm 1.41-1.45 (3H, t, CH_2CH_3), 4.42-4.47 (2H, m, CH_2CH_3), 6.10 (2H, s, $\underline{\text{CH}_2}$), 6.90-6.92 (1H, d, ArH), 7.49-7.50 (1H, d, ArH), 7.62-7.64(1H, dd, ArH).

General procedure for the preparation of 3,4-(methylenedioxy)phenylacetic acid(5) [19]

In a three-necked round-bottomed flask compound 4(6.7 g, 0.03 mol) and 85 %-hydrazine hydrate (8.85 g, 0.15 mol) was dissolved in ethylene glycol (60 mL). The reaction mixture was stirred and heated at 120 ° C for 2 h then it was cooled to room temperature and KOH (5 g, 0.09 mol) was added in. The reaction mixture was heated at 180 ° C for 2 h to remove low-boiling point compounds then refluxed for 4 h. When the reaction mixture was cooled to room temperature, the pH was adjusted to around 3 by progressively adding hydrochloric acid (6 mol/L). To this reaction mixture H_2O (60 mL) was added. Extraction was performed with EtOAc (5 × 40 mL). The organic layers were collected and washed with saturated NaCl solution (2 × 50 mL), dried over Na_2SO_4 , and concentrated in vacuo. The crude product was purified by column chromatography on silica gel eluted with (PE/EtOAc5:1) to give the compound 5 (3.39 g, 62.8 %) as a white solid.

$^1\text{H-NMR}(\text{CDCl}_3)$: δ/ppm 3.59 (2H, s, $\underline{\text{CH}_2\text{COOH}}$), 5.97 (2H, s, $\underline{\text{CH}_2}$), 6.73-6.75 (1H, dd, ArH), 6.78 (1H, s, ArH), 6.80-6.81 (1H, d, ArH).

General procedure for the preparation of 3,4-(methylenedioxy)phenethyl alcohol(6)

In a round-bottomed flask compound 5(3 g, 0.017 mol) was dissolved in dry THF (30 mL) at 0 ° C. To this mixture LiAlH₄ (1.7 g, 0.05 mol) was carefully added. The mixture was stirred at room temperature for 1 day. When the reaction was complete, the reaction mixture was quenched with 10 % HCl at 0 ° C until evolution of gas stopped. For work-up, the mixture was diluted with H₂O(50 mL). Extraction was performed with EtOAc (5 × 20 mL). The organic layers were collected and washed with saturated NaCl solution (2 × 30 mL), dried over Na₂SO₄, and concentrated in vacuo. The crude product was purified by column chromatography on silica gel eluted with (PE/EtOAc3:1) to give the compound 6 (1.28 g, 46 %) as a colorless oil.

¹H-NMR(CDCl₃): δ/ppm 1.55 (1H, s, CH₂CH₂OH), 2.79-2.82 (2H, t, CH₂CH₂OH), 3.82-3.85 (2H, t, CH₂CH₂OH), 5.95 (2H, s, CH₂), 6.69-6.71 (1H, dd, ArH), 6.74-6.75 (1H, d, ArH), 6.77-6.79 (1H, d, ArH).

General procedure for the preparation of hydroxytyrosol(1) [20]

In a round-bottomed flask compound 6 (0.2 g, 1.20 mmol) was dissolved in dry CH₂Cl₂ (25 mL) at -40 ° C. To this mixture a solution of BBr₃ (0.7 g, 2.4 mmol) in CH₂Cl₂ (2 mL) was carefully added via syringe. The mixture was stirred at room temperature for 2 h. When the reaction was completely detected by TLC, the reaction mixture was quenched with CH₃OH (5 mL) at 0 ° C. For work-up, the mixture was diluted with H₂O (30 mL). Extraction was performed with EtOAc (3 × 20 mL). The organic layers were collected and washed with saturated NaCl solution (2 × 30 mL), dried over Na₂SO₄, and concentrated in vacuo. The crude product was purified by column chromatography on silica gel eluted with (PE/EtOAc1:1) to give the compound 1 (0.141 g, 76 %).

¹H-NMR(CDCl₃): δ/ppm 3.03-3.07 (2H, t, CH₂CH₂OH), 3.49-3.53 (2H, t, CH₂CH₂OH), 5.04 (1H, s, ArOH), 5.14 (1H, s, ArOH), 6.64-6.66 (1H, dd, ArH), 6.73-6.74 (1H, d, ArH), 6.80-6.82 (1H, d, ArH).

70.3 Results and Discussion

In this work, a novel and efficient method based on Friedel–Crafts reaction and Wolff-Kishner-Huang reaction to synthesize hydroxytyrosol has been developed. This process has several advantages compared with the traditional pathway for the synthesis of hydroxytyrosol. This method has fewer steps with lower cost which uses cheap catechol as the starting material. In this procedure, catechol was reacted with CH₂Cl₂ in DMSO at 140 ° C to obtain 1,2-methylenedioxybenzene. Then 1, 2-methylenedioxybenzene was converted into ethyl2-(benzo[d][1,3]dioxol-6-yl)-2-oxoacetate(4) by Friedel–Crafts reaction. Compound 4 was subsequently reduced with hydrazine hydrate to obtain 3,4-(methylenedioxy)phenylacetic acid(5) which was readily separated by column chromatography in a high yield. Finally hydroxytyrosol was obtained by reduction of compound 5 with LiAlH₄ and

deprotection with BBr_3 . The target compound was obtained by five-step reaction with an overall yield of 23 %. Although this method involves several steps, it can be easily performed in large scale and the starting material is inexpensive.

70.4 Conclusion

In conclusion, we have introduced a new method for accessing hydroxytyrosol, by utilizing catechol as a starting material. The overall procedure involves commercial available and inexpensive materials, using standard experimental procedures, wherein all intermediates are stable and isolatable in moderate and good to yields.

Acknowledgments This work was supported by National Natural Science Foundation of China (No: 81072521), the Science & Technology Project of Tianjin (11ZCGHHZ00400), International Science & Technology Cooperation Program of China (2013DFA31160) and Tianjin University of Science and Technology (No: 20100411).

References

1. Tuck KL, Hayball PJ (2002) Major phenolic compounds in olive oil: metabolism and health effects. *J Nutr Biochem* 13:636–644
2. Capasso R, Evidente A, Avolio S et al (1999) A highly convenient synthesis of hydroxytyrosol and its recovery from agricultural waste waters. *J Agric Food Chem* 47:1745–1748
3. Fernández-Bolaños J, Rodríguez G, Rodríguez R et al (2002) Production in large quantities of highly purified hydroxytyrosol from liquid-solid waste of two phase olive oil processing or Alperujo. *J Agric Food Chem* 50:6804–6811
4. Allouche N, Fki I, Sayadi S (2004) Toward a high yield recovery of antioxidants and purified hydroxytyrosol from olive mill wastewaters. *J Agric Food Chem* 52:267–273
5. Perrinjaquet-Moccetti T, Busjahn A, Schmidlin C et al (2008) Food supplementation with an olive (*Olea europaea* L.) leaf extract reduces blood pressure in borderline hypertensive monozygotic twins. *Phytother Res* 22:1239–1242
6. Tripoli E, Giammanco M, Tabacchi G et al (2005) The phenolic compounds of olive oil: structure, biological activity and beneficial effects on human health. *Nutr Res Rev* 18:98–112
7. Ragione FD, Cucciolla V, Borroello A et al (2000) Hydroxytyrosol, a natural molecule occurring in olive oil, induces cytochrome c-dependent apoptosis. *Biochem Biophys Res Commun* 278(3):733–739
8. Hao JJ, Shen WL, Yu GL et al (2010) Hydroxytyrosol promotes mitochondrial biogenesis and mitochondrial function in 3T3-L1 adipocytes. *J Nutr Biochem* 7:634–644
9. Clara B, Anna A (2009) Antioxidant effects of natural bioactive compounds. *Curr Pharm Des* 15:3063–3073
10. Torres de Pinedo A, Peñalver P, Morales JC (2007) Synthesis and evaluation of new phenolic-based antioxidants: structure-activity relationship. *Food Chem* 103:55–61
11. Sanchez-Fidalgo S, Sanchez de Ibarguen L, Cardeno A et al (2012) Influence of extra virgin olive oil diet enriched with hydroxytyrosol in a chronic DSS colitis model. *Eur J Nutr* 51(4):497–506

12. Liu ZB, Sun LJ, Zhu L, Xu J et al (2007) Hydroxytyrosol protects retinal pigment epithelial cells from acrolein-induced oxidative stress and mitochondrial dysfunction. *J Neurochem* 103(6):2690–2700
13. Hagiwara K, Goto T, Araki M et al (2011) Olive polyphenol hydroxytyrosol prevents bone loss. *Eur J Pharmacol* Jul 15;662(1-3):78-84
14. Zhu L, Liu ZB, Feng ZH et al (2010) Hydroxytyrosol protects against oxidative damage by simultaneous activation of mitochondrial biogenesis and phase II detoxifying enzyme systems in retinal pigment epithelial cells. *J Nutr Biochem* 21(11):1089–1098
15. Gonzalez-Santiago M, Martín-Bautista E, Carrero JJ et al (2006) One-month administration of hydroxytyrosol, a phenolic antioxidant present in olive oil, to hyperlipemic rabbits improves blood lipid profile, antioxidant status and reduces atherosclerosis development. *Atherosclerosis* Sep;188(1):35-42
16. Vazquez-Velasco M, Esperanza Díaz L, Lucas R et al (2011) Effects of hydroxytyrosol-enriched sunflower oil consumption on CVD risk factors. *Br J Nutr* May;105(10):1448-52
17. Bashall P, Collins F (1975) A convenient, high-yielding method for the methylation of catechols. *Tetrahedron Lett* 16:3489–3490
18. Ianni A, Waldvogel SR (2006) Reliable and versatile synthesis of 2-aryl-substituted cinnamic acid esters. *Synthesis* 13:2103–2112
19. Guoxin Y, Gang C, Yong L et al (2010) An alternative process for preparation of 3, 4-dimethoxyphenylacetic acid. *Chinese Journal of Pharmaceuticals* 41(10):730–730
20. Alvarez E, Chahboun R, Haidour B (2009) Method for the preparation of hydroxytyrosol and 3-(3, 4-dihydroxyphenyl) propanol from methylene dioxybenzenes. WO: 2009153374, 2009-12 -23

Chapter 71

Design and Synthesis of 2-Arylbenzimidazole Analogues as Novel SIRT1 Activators for the Treatment of Type II Diabetes

Fei Hu, Yuanmou Chen, Yinghao Gao, Shaolong Jia, Weizhu Liu,
Peng Yu and Erbing Hua

Abstract SIRT1, an NAD⁺-dependent sirtuin deacetylase, has emerged as potential therapeutic target for treatment of human illnesses such as type II diabetes, cancer, cardiovascular and neurodegenerative diseases. Resveratrol, a naturally occurring small molecule activator of SIRT1, has been demonstrated to improve metabolism and glucose tolerance. SRT1720, an imidazothiazole derivative, recently made as the most potent SIRT1 activator is structurally unrelated to resveratrol. In this work, we design and synthesize a series of compounds as novel potential SIRT1 activators through a two-step convenient synthetic procedure. Fourteen 2-Arylbenzimidazole analogues were characterized on the basis of ¹H NMR spectra. Tests for biological activity of these compounds are underway.

Keywords Synthesis · SIRT1 activator · Type II diabetes · 2-Arylbenzimidazole analogues

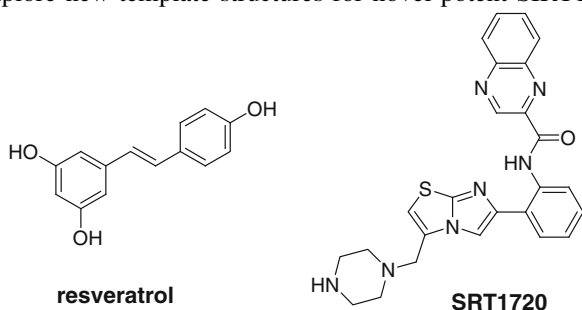
71.1 Introduction

The prevalence of metabolic syndrome associated with increased risk for cardiovascular disease, type II diabetes, or cancer has been increasing over the past decade [1, 2]. The metabolic syndrome was a complex process and can be regulated by genetic alterations and calorie restriction [3]. Recently, a growing list of evidence implicates mammalian sirtuins in the regulation of various aspects of CR responses, namely, glucose homeostasis [4], insulin secretion [5, 6], fat metabolism [7], stress resistance [8–12], and physical activity [13]. There has been much

F. Hu · Y. Chen · Y. Gao · S. Jia · W. Liu · P. Yu · E. Hua (✉)
Key Laboratory of Industrial Microbiology, Ministry of Education, College of
Biotechnology, Tianjin University of Science and Technology, Tianjin 300457,
People's Republic of China
e-mail: huarb@tust.edu.cn

interest in developing pharmacological agents that mimic the effects of calorie restriction. SIRT1, an NAD⁺-dependent deacetylase, has been implicated as one of the key downstream regulators of CR in yeast, rodents, and humans [14–16]. Small molecule activators of SIRT1 have been identified that exhibit efficacy in animal models of diseases typically associated with aging including type II diabetes [17]. Resveratrol, a polyphenolic SIRT1 activator, mimics the anti-aging effects of calorie restriction in lower organisms and in mice fed a high-fat diet ameliorates insulin resistance, increases mitochondrial content, and prolongs survival [18, 19]. Milne et al. identified SRT1720 as potent SIRT1 activators, which are structurally unrelated to but 1,000-fold more active than resveratrol toward improving glucose homeostasis, increasing insulin sensitivity, and increasing mitochondrial function in rodent models of type II diabetes [20]. Thus, SIRT1 activation is a promising new therapeutic approach for treating diseases of aging such as type II diabetes.

On this basis, numerous efforts have been devoted to discover novel activators of SIRT1. We synthesis 2-Arylbenzimidazole as new scaffold instead of the nuclear structure of SRT1720, then fourteen 2-Arylbenzimidazole analogues as the novel potential SIRT1 activators were synthesized. The aim of this work is to explore new template structures for novel potent SIRT1 activators.



71.2 Materials and Methods

71.2.1 Materials and Measurements

All reagents and solvents used were of reagent grade. Reaction temperatures were controlled by oil bath temperature modulator. Thin layer chromatography (TLC) was performed using E. Merck silica gel 60 GF₂₅₄ precoated plates (0.25 mm). Silica gel (particle size 200–400 mesh) was used for flash chromatography. ¹H spectra were recorded on Bruker AM-400 NMR spectrometer in deuterated chloroform and deuterated DMSO.

71.2.2 Experimental Methods

The route to prepare the 2-Arylbenzimidazole analogues was presented in Fig. 71.1.

The methods of synthesizing and purifying intermediate 1 were as follows.

To a flask 1, 2-diaminobenzene (3.24 g, 30 mmol), 3-Aminobenzoic acid (4.93 g, 36 mmol), and PPA (33 g) were added, then the reaction mixture was allowed to be heated to 200 °C by oil bath and kept reflux for 5 h. After the reaction was completely finished, the reaction mixture was slowly poured into ice water and the resulting mixture is basified with solid NaOH and NaHCO₃. At pH8-10 the precipitate was filtered, washed with water, and dried to obtain the crude product, which purified by flash column chromatography (silica gel, pure CH₂Cl₂) to afford intermediate 1. The synthesis and purity methods of intermediate 2 were the same as the method for intermediate 1.

The second step b: two scaffolds (intermediate 1 and intermediate 2) with aromatic carboxylic acid by acylation reaction.

In a round-bottomed flask, aromatic carboxylic acid (1.2 mmol) was dissolved in suitable amount of CH₂Cl₂ (25 mL), followed by adding EDCI (1.5 mmol), Et₃N (2 mmol), DMAP (0.5 mmol), and intermediate 1 (1 mmol). Then the reaction mixture was allowed to be heated to 80 °C and kept reflux for 6 h. After cooling, the reaction mixture was poured into a 100 mL separating funnel, then water was added, then extracted by CH₂Cl₂, the organic layer was washed by water, saturated salt water, and dried by sodium sulphate. The organic phase was evaporated under vacuum to remove the solution CH₂Cl₂, providing the crude product. Then it was purified by flash column chromatography to afford 2-Arylbenzimidazole compounds.

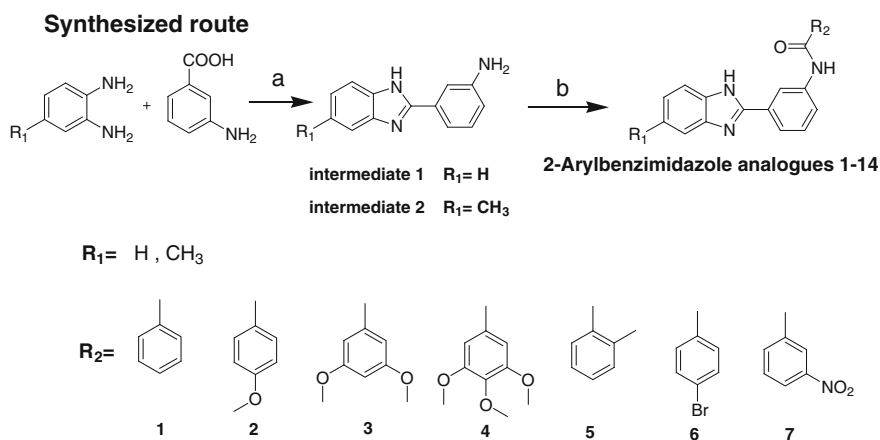


Fig. 71.1 Reagents and conditions: **a** PPA, 200 °C, 5 h (yield 87-90 %); **b** CH₂Cl₂, EDCI, DMAP, Et₃N, 80 °C, 6 h (yield 35-86 %)

71.2.3 Syntheses

2-(2'-aniline) benzimidazole (intermediate 1)

A white solid, 87.4 % yield.

^1H NMR (400 MHz DMSO): δ /ppm 12.682 (s, 1H), 7.555 (s, 2H), 7.438–7.429 (t, 1H), 7.293–7.273 (d, 1H), 7.195–7.156 (m, 3H), 6.699–6.675 (dd, 1H), 5.286–5.284(d, 2H).

2-Arylbenzimidazole analogue 1

A white solid, 62.2 % yield.

^1H NMR (400 MHz CDCl_3): δ /ppm 8.418–8.410 (t, 1H), 8.080 (s, 1H), 7.878–7.856 (m, 3H), 7.648–7.625 (m, 3H), 7.593–7.557 (m, 1H), 7.518–7.480 (m, 2H), 7.449–7.410 (t, 1H), 7.291–7.248 (m, 3H).

2-Arylbenzimidazole analogue 2

A white solid, 59.4 % yield.

^1H NMR (400 MHz DMSO): δ /ppm 12.778–12.740 (d, 1H), 10.430 (s, 1H), 8.682 (s, 1H), 8.037–8.019 (d, 2H), 7.860–7.841 (m, 2H), 7.639–7.314 (m, 6H), 7.063–7.011 (m, 1H), 2.443–2.426 (m, 3H).

2-Arylbenzimidazole analogue 3

A white solid, 45.8 % yield.

^1H NMR (400 MHz CDCl_3): δ /ppm 8.338 (s, 1H), 8.110 (s, 1H), 7.826–7.806 (d, 1H), 7.714–7.666 (m, 2H), 7.403–7.363 (t, 1H), 7.252–7.237 (m, 1H), 6.955–6.950 (d, 2H), 6.603–6.592 (t, 1H), 3.796 (s, 6H).

2-Arylbenzimidazole analogue 4

A white solid, 72.6 % yield.

^1H NMR (400 MHz CDCl_3): δ /ppm 8.767 (s, 1H), 8.270 (s, 1H), 7.730–7.696 (t, 2H), 7.552–7.531 (dd, 2H), 7.283 (s, 1H), 7.270–7.231 (t, 1H), 7.220–7.197(m, 2H), 3.873 (s, 3H), 3.753 (s, 6H).

2-Arylbenzimidazole analogue 5

A white solid, 47.9 % yield.

^1H NMR (400 MHz CDCl_3): δ /ppm 9.883 (s, 1H), 8.460 (s, 1H), 7.904–7.885 (d, 1H), 7.812 (s, 1H), 7.645 (d, 2H), 7.506–7.486 (m, 3H), 7.396 (t, 1H), 7.303–7.270 (m, 4H), 2.533 (s, 3H).

2-Arylbenzimidazole analogue 6

A white solid, 86.1 % yield.

^1H NMR (400 MHz CDCl_3): δ /ppm 8.416–8.406 (t, 1H), 7.923 (s, 1H), 7.876–7.857 (d, 1H), 7.776–7.754 (m, 3H), 7.681–7.659(m, 2H), 7.546–7.506 (t, 1H), 7.322–7.260(m, 3H).

2-Arylbenzimidazole analogue 7

A white solid, 35.1 % yield.

^1H NMR (400 MHz DMSO): δ /ppm 12.952 (s, 1H), 10.791 (s, 1H), 8.889–8.880 (t, 1H), 8.717–8.709 (t, 1H), 8.488–8.461 (dd, 2H), 7.938–7.860 (m, 3H), 7.686–7.668 (d, 1H), 7.595–7.535 (dd, 2H), 7.239–7.200 (m, 2H).

2-(2'-aniline) -5-methyl-benzimidazole (intermediate 2).

A white solid, 90.3 % yield.

^1H NMR (400 MHz CDCl_3): δ /ppm 9.337 (s, 1H), 7.468–7.461(t, 1H), 7.291–7.244 (m, 4H), 7.107–7.083 (dd, 1H), 6.786–6.758 (m, 1H), 3.804 (s, 2H), 2.487(s, 3H).

2-Arylbenzimidazole analogue 8

A white solid, 67.6 % yield.

^1H NMR (400 MHz CDCl_3): δ /ppm 10.445 (s, 1H), 8.482 (s, 1H), 8.008 (s, 1H), 7.927–7.911 (d, 1H), 7.886–7.864 (d, 2H), 7.822 (s, 1H), 7.559 (s, 1H), 7.521–7.489 (d, 2H), 7.262 (m, 2H), 7.021–6.998 (d, 2H), 3.896 (s, 3H).

2-Arylbenzimidazole analogue 9

A white solid, 65.7 % yield.

^1H NMR (400 MHz CDCl_3): δ /ppm 8.393 (s, 1H), 7.987 (s, 1H), 7.865–7.835 (m, 3H), 7.637–7.617 (d, 1H), 7.554–7.534 (d, 1H), 7.464–7.424 (t, 1H), 7.404 (s, 1H), 7.110–7.089 (d, 1H), 7.003–6.981 (d, 2H), 3.887 (s, 3H), 2.485 (s, 3H).

2-Arylbenzimidazole analogue 10

A white solid, 44.2 % yield.

^1H NMR (400 MHz CDCl_3): δ /ppm 8.406–8.397 (t, 1H), 8.021 (s, 1H), 7.875–7.855 (d, 1H), 7.657–7.633 (dd, 1H), 7.552 (s, 1H), 7.493–7.453 (t, 2H), 7.406 (s, 1H), 7.115–7.092 (dd, 1H), 6.999–6.993 (d, 2H), 6.651–6.640 (t, 1H), 3.861 (s, 6H), 2.489 (s, 3H).

2-Arylbenzimidazole analogue 11

A white solid, 73.2 % yield.

^1H NMR (400 MHz CDCl_3): δ /ppm 8.347–8.338 (t, 1H), 8.073 (s, 1H), 8.817–7.768 (m, 2H), 7.545 (s, 1H), 7.504–7.464 (t, 2H), 7.404 (s, 1H), 7.110 (m, 3H), 3.940 (s, 6H), 3.925 (s, 3H), 2.491 (s, 3H).

2-Arylbenzimidazole analogue 12

A white solid, 56.3 % yield.

^1H NMR (400 MHz CDCl_3): δ /ppm 8.750–8.736 (dd, 2H), 8.475–8.451 (dd, 2H), 8.409–8.387 (dd, 2H), 7.637–7.596 (dt, 2H), 7.479–7.458 (t, 1H), 7.447 (s, 1H), 7.426 (s, 1H), 7.416–7.415 (d, 1H), 7.396 (s, 1H), 2.684 (s, 6H).

2-Arylbenzimidazole analogue 13

A white solid, 85.7 % yield.

^1H NMR (400 MHz CDCl_3): δ /ppm 8.350 (s, 1H), 8.117 (s, 1H), 7.859–7.813 (dd, 3H), 7.610–7.607 (dd, 1H), 7.587–7.509 (m, 2H), 7.498–7.461 (t, 2H), 7.404–7.365 (t, 2H), 7.088–7.065 (dd, 1H), 2.460 (s, 3H).

2-Arylbenzimidazole analogue 14

A white solid, 37.4 % yield.

^1H NMR (400 MHz DMSO): δ /ppm 12.814–12.774 (d, 1H), 10.775 (s, 1H), 8.885–8.882 (d, 1H), 8.675 (s, 1H), 8.484–8.457 (m, 2H), 7.941–7.856 (m, 3H), 7.579–7.323 (m, 3H), 7.070–7.014 (m, 1H), 2.448–2.429 (d, 3H).

Table 71.1 Effect of the ratio of aromatic carboxylic acid

Entry	Acid: diamine	Yield (%)
1	1	76.5
2	1.1	83.5
3	1.2	90.6
4	1.3	91.1
5	1.4	91.6

71.3 Results and Discussion

In this work, we synthesized intermediate from 1,2-diaminobenzene and 3-Aminobenzoic acid with PPA under solvent-free conditions. In this reaction, the temperature is very important. In our initial attempts, when temperature was under 180 °C, the reaction produced a complicated composition and made the separation difficult. When 200 °C, the reaction can react completely and easily work up to afford pure product. Interestingly, the ratio of aromatic carboxylic acid can affect on this reaction yield (Table 71.1). We found the increased yield with higher ratio of acid, but when the ratio is higher than 1.2, the yield is not increased obviously. In addition, the excess aromatic carboxylic acid can bring a side reaction and this material is not cheap. So the ratio of 1.2 is the best choice.

In the step b, fourteen 2-Arylbenzimidazole analogues were synthesized by acylation reaction. In our initial attempts, we use HATU as the catalyst but TLC showed two main spots, the HATU may induce reaction within aniline and imidazole acylations whatever the ratio of aromatic carboxylic acid to aniline was changed. Without HATU the reaction directed to a major product and excessive acid can increase the yield of reaction. In all, we take 1.2 equivalent acids in this reaction. The total yield was 31–77 %; this method was lower cost, simple, and convenient.

2-Arylbenzimidazole analogues have the similar structure with SIR1720, to choose benzimidazole as structural template is due to its important pharmacophore in modern drug discovery [21]. Benzimidazole derivatives have exhibited significant activity against several viruses such as HIV [22, 23], herpes (HSV-1) [24], and human cytomegalovirus (HCMV) [23]. Benzimidazole and its derivatives have been used as angiotensin II inhibitors [25], potential antitumor agents [26], and antimicrobial agents [27].

71.4 Conclusion

In summary, we have synthesized two kinds of 2-arylbenzimidazole compounds with moderate yield from relevant 1, 2-diaminobenzene and aromatic carboxylic acids through two steps for imidazole formation and acylation. The imidazole formation was conducted only in the present of PPA without using solvent. The

salient features of this reaction are mild reaction conditions, moderate yields, and clean work-up procedure. These advantages should render the synthesis of 2-arylbenzimidazole analogues more efficient and environmental friendly.

Acknowledgments Funding for this study was provided by National Natural Science Foundation of China (No: 81072521), Tianjin University of Science & Technology (No: 20100411), International Science & Technology Cooperation Program of China (2013DFA31160) and the Science & Technology Project of Tianjin (11ZCGHHZ00400).

References

1. Dekker JM, Girman C, Gieln R, Nijpels G, Stehouwer CDA, Bouter LM, Heine RJ (2005) Metabolic syndrome and 10-year cardiovascular disease risk in the hoorn study. *Epidemiology* 112:666–673
2. Russo A, Autelitano M, Bisanti L (2008) Metabolic syndrome and cancer risk. *Eur J Cancer* 44(2):293–7
3. Guarente Leonard (2006) Sirtuins as potential targets for metabolic syndrome. *Nature* 444:868–874
4. Rodgers, JT Carlos Lerin, Wilhelm Haas, Steven P Gygi Bruce. M, Spiegelman. (2005) Nutrient control of glucose homeostasis through a complex of PGC-1 α and SIRT1. *Nature* 434:113–118
5. Bordone L, Motta MC, Picard F, Robinson A, Ulupi SJ, Apfeld J (2006) Sirt1 regulates insulin secretion by repressing UCP2 in pancreatic beta cells. *PLoS Biol* 4(2):e31
6. Moynihan KA, Grimm AA, Bernal-Mizrachi E, Plueger MM, Ford E, Cras-Méneur C, Permutt MA, Imai S (2005) Increased dosage of mammalian Sir2 in pancreatic beta cells enhances glucose-stimulated insulin secretion in mice. *Cell Metab* Aug; 2(2):105–17
7. Picard F, Kurtev M, Chung N et al (2004) SIRT1 promotes fat mobilization in white adipocytes by repressing PPAR- γ *Nature* 429:771–776
8. Brunet A et al (2004) Stress-dependent regulation of FOXO transcription factors by the SIRT1 deacetylase. *Science* 303:2011–2015
9. Luo J et al (2001) Negative control of p53 by Sir2a promotes cell survival under stress. *Cell* 107:137–148
10. Motta MC et al (2004) Mammalian SIRT1 represses forkhead transcription factors. *Cell* 116:551–563
11. Vaziri H et al (2001) hSIR2 (SIRT1) functions as an NAD-dependent p53 deacetylase. *Cell* 107:149–159
12. Wang C et al (2006) Interactions between E2F1 and SirT1 regulate apoptotic response to DNA damage. *Nat Cell Biol* 8:1025–1031
13. Chen D et al (2005) Increase in activity during calorie restriction requires Sirt1. *Science* 310:1641
14. Cohen HY et al (2004) Calorie restriction promotes mammalian cell survival by inducing the SIRT1 deacetylase. *Science* 305:390–392
15. Bordone L, Guarente L (2005) Calorie restriction, SIRT1 and metabolism: understanding longevity. *Nature Rev Mol Cell Biol* 6:298–305
16. Barzilai N, Banerjee S, Hawkins M, Chen W, Rossetti L (1998) Caloric restriction reverses hepatic insulin resistance in aging rats by decreasing visceral fat. *J Clin Invest* 101:1353–1361
17. Smith JJ, Gagne DJ, Galonek HL (2009) Small molecule activators of SIRT1 replicate signaling pathways triggered by calorie restriction in vivo. *BMC Syst Biol* 3:31

18. Baur JA et al (2006) Resveratrol improves health and survival of mice on a high-calorie diet. *Nature* 444:337–342
19. Wood JG et al (2004) Sirtuin activators mimic caloric restriction and delay ageing in metazoans. *Nature* 430:686–689
20. Milne JC, Philip D, Lambert, David P, Carney et al (2007) Small molecule activators of SIRT1 as therapeutics for the treatment of type 2 diabetes. *Nature* 29 450(7170):712–6
21. Tebbe MJ, Spitzer WA, F Victor S.C. Miller CC, Lee TR, Sattelberg E, Mckinney, Tang CJ (1997) Antirhino/enteroviral vinylacetylene benzimidazoles: a study of their activity and oral plasma levels in mice. *J Med Chem* 40 (24):3937–3946
22. Porcari AR, Devivar RV, Kucera LS, Drach JC, Townsend LB (1998) Design, synthesis, and antiviral evaluations of 1-(substituted benzyl)-2-substituted-5, 6-dichloro-benzimidazoles as nonnucleoside analogues of 2, 5, 6-trichloro1-((-d-ribofuranosyl)benzimidazole. *J Med Chem* 41:1251
23. Roth M, Morningstar ML, Boyer PL, Hughes SH, Bukheit RW, Michejda CJ (1997) Synthesis and biological activity of novel nonnucleoside inhibitors of HIV-1 reverse transcriptase. 2-Aryl-Substituted Benzimidazoles. *J Med Chem*40(26): 4199–4207
24. Migawa MT, Giradet JL, Walker JA, Koszalka GW, Chamber-Lain SD, Drach JC, Townsend LB (1998) Design, synthesis, and antiviral activity of α -Nucleosides: D- and L-Isomers of Lyxofuranosyl- and (5-Deoxylyxofuranosyl) benzimidazoles. *J Med Chem* 41(8):1242–1251
25. Nadaf RN, Siddiqui SA, Daniel T, Lahoti RJ, Srinivasan KV (2004) Room temperature ionic liquid promoted regioselective synthesis of 2-arylbzimidazoles, benzoxazoles and benzthiazoles under ambient conditions. *J Mol Catal A: Chem* 214:155
26. Denny WA, Rewcastle GW, Baguley BC (1990) Structure-activity relationships for 2-phenylbenzimidazole-4-carbo-xamides, a new class of “minimal” DNA-intercalating agents which may not act via topoisomerase II. *J Med Chem* 33(2):814–819
27. Forseca T, Gigante B, Gilchrist TL (2001) A short synthesis of phenanthro[2,3-d]imidazoles from dehydroabiatic acid. Application of the methodology as a convenient route to benzimidazoles. *Tetrahedron* 57(9):1793–1799

Chapter 72

Design and Synthesis of SIRT1 Activators for Potential Lead Compounds of Treatment of Diabetes

Weizhu Liu, Qiuyue Wang, Fei Hu, Yinghao Gao, Yingying Wang, Peng Yu and Erbing Hua

Abstract Sirtuins catalyze NAD⁺-dependent protein deacetylation and are key regulators of transcription, apoptosis, metabolism, and aging. There are seven human sirtuins (SIRT1–7), and SIRT1 has been proven as a key mediator of the pathways downstream of calorie restriction that has been shown to delay the onset and the incidence of age-related diseases such as type II diabetes. Increasing SIRT1 activity, either by transgenic over expression of the SIRT1 gene in mice or by pharmacological activation by small molecule activator SIRT1720, has shown beneficial effects in rodent models of type II diabetes. In this paper, several small molecules were designed and synthesized through a convenient synthetic procedure. Ten newly synthesized compounds were characterized on the basis of ¹H NMR.

Keywords Sirt1 · Activator · 2-phenylbenzo[*d*]thiazole · 2-phenylbenzo[*d*]oxazole · Synthesis

72.1 Introduction

Silent information regulator 2(Sir2) was first identified as a gene that is required to maintain cell mating type in *Saccharomyces cerevisiae* by repressing the transcription of mating type genes [1]. It leads to a decrease in histone acetylation [1, 2] and an increase in lifespan in yeast [3]. Extensive researches show that four sirtuins (Hst1-4) in addition to Sir2 in *Saccharomyces cerevisiae*, and seven homologs (SIRT1-7) have been identified in mammals. Among the seven members

W. Liu · Q. Wang · F. Hu · Y. Gao · Y. Wang · P. Yu · E. Hua (✉)
Key Laboratory of Industrial Microbiology of Ministry of Education,
College of Biotechnology, Tianjin University of Science and Technology,
Tianjin 300457, People's Republic of China
e-mail: huarb@tust.edu.cn

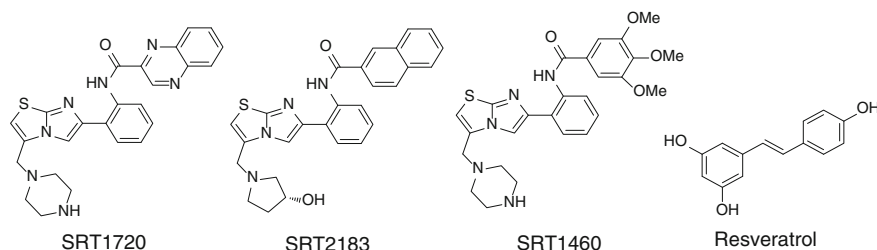


Fig. 72.1 Structures of SRT1720, SRT2183, SRT1460 and Resveratrol [24]

of the homologs, the nuclear SIRT1 is the closest homolog of yeast Sir2 [4]. SIRT1, an NAD^+ -dependent deacetylase [5], is critical regulators of transcription and playing important roles in the regulation of apoptosis, differentiation, metabolism, and chromatin remodeling [6–14]. SIRT1 has shown to be activated by fasting and Calorie restriction [15, 16]. SIRT1 is a principal modulator of pathways downstream of calorie restriction that produces beneficial effects on glucose homeostasis and insulin sensitivity in adipose tissue, skeletal muscle, and liver [17–20]. On this basis, activation of SIRT1 could serve as a novel approach to treat type II diabetes.

Resveratrol, a naturally occurring small molecule activator of SIRT1, has been reported to improve insulin sensitivity, increase mitochondrial content, and prolong survival of mice fed a high fat, high calorie diet [21–23]. So it indicates that SIRT1 may represent an attractive therapeutic target for the treatment of type II diabetes. Recently, SRT1720, SRT2183, and SRT1460 were described by Sirtris Pharmaceuticals as SIRT1 activators [24] (Fig. 72.1). They are structurally unrelated to resveratrol. SRT1720, the strongest activator of the series, was reported that it could improve glucose homeostasis, increase insulin sensitivity, and increase mitochondrial function in rodent models of type II diabetes [23, 24]. According to the structure of SRT1720, We have tried change the core structure of SRT1720 from imidazo[1,2-*b*]thiazoles into 2-phenylbenzo[*d*]thiazole or 2-phenylbenzo[*d*]oxazole. Ten new compounds were synthesized. In this paper, we mainly explore a kind of new structures of potential SIRT1 activators.

72.2 Experimental

72.2.1 Materials and Measurements

All reagents and solvents used were of reagent grade. Reaction temperatures were controlled by oil bath temperature modulator. Thin layer chromatography (TLC) was performed using E. Merck silica gel 60 GF₂₅₄ precoated plates (0.25 mm). Silica gel (particle size 200–400 mesh) was used for flash chromatography.

^1H spectra were recorded on Bruker AM-400 NMR spectrometers in deuterated chloroform and deuterated DMSO.

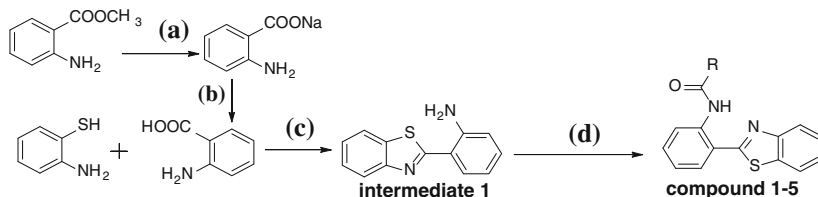
72.2.2 Experimental Procedure

The route to Synthesis of 2-phenylbenzo[*d*]thiazole and 2-phenylbenzo[*d*]oxazole analogs was presented in Fig. 72.2.

72.2.2.1 The Procedure of Reaction *a* and *b*

The reaction *a* and *b* was used for the preparation of 2-aminobenzoic acid from 2-aminobenzoate. In a round-bottomed flask, 2-aminobenzoate (6.3 g, 41.6 mmol) was dissolved in ethanol (30 ml). Then add 10 % NaOH solution (20 ml) in the flask. The reaction mixture was warmed up to 60 °C for 5 h. After the reaction was completely finished by the addition of suitable amount of 10 % HCl solution, white solid appears at PH 5-7 and vacuum dried . The crude product was used directly for the next step without further purification.

The first route



The second route

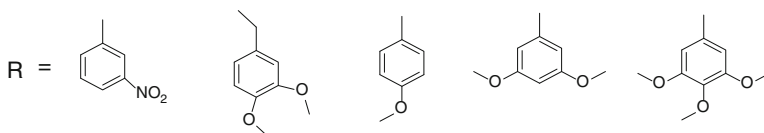
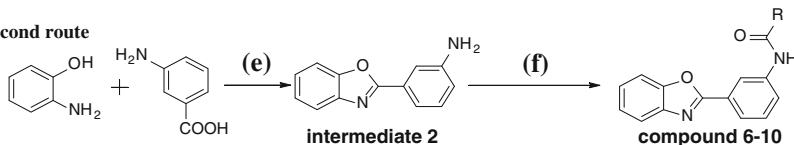


Fig. 72.2 Reagents and conditions: **a** NaOH, EtOH, 60 °C; **b** HCl; **c** PPA, 200 °C, 6 h; **d** CH_2Cl_2 , EDCI, Et_3N , DMAP, Et_3N , 80 °C, 8 h; **e** PPA, 200 °C; **f** $\text{C}_5\text{H}_5\text{N}$, EDCI, Et_3N , 90 °C, 5 h

72.2.2.2 The Procedure of Reaction *c* and *e*

The methods of synthesizing and purifying intermediate 2 were the same as intermediate 1, the experimental procedure are as follows [25]. To a flask which contained 2-aminobenzenethiol (4 g, 29.6 mmol), 2-aminobenzoic acid (4.5 g, 32.8 mmol) from last step and PPA (44 g, 130.6 mmol). Then the reaction mixture was allowed to be heated to 200 °C and kept reflux for 6 h. After the reaction was completely finished, the reaction mixture was slowly poured into ice water and the resulting mixture basified with solid NaOH. At pH 5-6 the precipitate was filtered, washed with water, and dried to give the intermediate 1.

72.2.2.3 The Procedure of Reaction *d*

In a round-bottomed flask, RCOOH (1.2 mmol) was dissolved in suitable amount of CH₂Cl₂, followed by adding EDCI (1.5 mmol), Et₃N (1.5 mmol) for stirring for 20 min, then DMAP (0.5 mmol) and intermediate 1(1 mmol) was added. The reaction mixture was allowed to be heated to 80 °C and kept reflux for 8 h. After cooling the reaction mixture was poured into a 100 ml separating funnel, then water was added and extracted by CH₂Cl₂, the organic layer was washed by water and brine. The Solvent was dried under vacuum to offer the crude product. The crude product was purified by flash column chromatography to afford 2-phenylbenzo[*d*]thiazole analogs.

72.2.2.4 The Procedure of Reaction *f*

In a round-bottomed flask, RCOOH (1.2 mmol) was dissolved in suitable amount of C₅H₅N, followed by adding EDCI (1.5 mmol), Et₃N (1.5 mmol) for stirring for 20 min, then intermediate 2(1 mmol) was added. Then the reaction mixture was allowed to be heated to 90 °C and kept reflux for 5 h. After the reaction was completely finished, the mixture was filtered. The solid was recrystallized from methanol and hexane to yield the pure product.

72.2.3 Syntheses

2-(benzo[*d*]thiazol-2-yl)aniline (Intermediate 1)

This compound was prepared in 80.2 % yield by following reaction *a*, *b*, and *c*. light yellow solid.

¹H NMR (400 MHz CDCl₃): δ/ppm 7990, 7.985 (d, *J* = 2 HZ, 1H), 7.891, 7.871 (d, *J* = 8 HZ, 1H), 7.750–7.737 (t, *J* = 4 HZ, 1H), 7.501–7.475 (dd, *J* = 0.64, 0.18 HZ, 1H), 7.402–7.377 (t, *J* = 5.2 HZ, 1H), 7.273–7.246 (m, 1H), 6.836, 6.823 (d, *J* = 5.2 HZ, 1H), 6.798–6.773 (t, *J* = 5.2 HZ, 1H), 6.451 (s, 2H).

N-(2-(benzo[d]thiazol-2-yl)phenyl)-3-nitrobenzamide (Compound 1)

This compound was prepared in 40.7 % yield by following reaction *a*, *b*, *c*, and *d*. white solid.

¹H NMR (400 MHz CDCl₃): δ/ppm 13.521 (s, 1H), 8.804, 8.783 (d, *J* = 2 Hz, 1H), 9.043–9.020 (q, *J* = 4 Hz, 1H), 8.607, 8.587 (d, *J* = 8.4 Hz, 1H), 8.500–8.476 (dd, *J* = 7.2, 1.3 Hz, 1H), 8.163, 8.142 (d, *J* = 8.4 Hz, 1H), 7.967–7.934 (m, 2H), 7.818–7.778 (t, *J* = 8.4 Hz, 1H), 7.598–7.548 (m, 2H), 7.484–7.446 (t, *J* = 8.1 Hz, 1H), 7.282–7.244 (t, *J* = 8.5 Hz, 1H).

N-(2-(benzo[d]thiazol-2-yl)phenyl)-2-(3,4-dimethoxy-phenyl)acetamide (Compound 2)

This compound was prepared in 36.8 % yield by following reaction *a*, *b*, *c*, and *d*. light yellow solid.

¹H NMR (400 MHz CDCl₃): δ/ppm 12.341 (s, 1H), 8.805–8.782 (dd, *J* = 8.0, 8 Hz, 1H), 7.929–7.899 (q, *J* = 4 Hz, 2H), 7.843–7.820 (dd, *J* = 6.4, 1.2 Hz, 1H), 7.548–7.416 (m, 3H), 7.177–7.136 (t, *J* = 7.6 Hz, 1H), 7.967–7.934 (m, 2H), 7.818–7.778 (t, *J* = 8.0 Hz, 1H), 7.012–6.987 (dd, *J* = 6.1 Hz, 1H), 6.949, 6.945 (d, *J* = 2 Hz, 1H), 6.823, 6.802 (d, *J* = 8.5 Hz, 1H), 3.829 (s, 1H), 3.801 (s, 1H), 3.791 (s, 1H).

N-(2-(benzo[d]thiazol-2-yl)phenyl)-4-methoxybenzamide (Compound 3)

This compound was prepared in 25.1 % yield by following reaction *a*, *b*, *c*, and *d*. white solid.

¹H NMR (400 MHz CDCl₃): δ/ppm 13.257 (s, 1H), 9.052, 9.031 (d, *J* = 8.4 Hz, 1H), 8.224, 8.202 (d, *J* = 8.8 Hz, 2H), 8.027, 8.007 (d, *J* = 8 Hz, 1H), 7.955–7.904 (dd, *J* = 8.4, 1.6 Hz, 2H), 7.573–7.513 (q, *J* = 7.2 Hz, 2H), 7.472–7.431 (t, *J* = 8.4 Hz, 1H), 7.260–7.167 (t, *J* = 6.8 Hz, 1H), 7.097, 7.075 (d, *J* = 8.9 Hz, 2H), 3.936 (s, 3H).

N-(2-(benzo[d]thiazol-2-yl)phenyl)-3,5-dimethoxybenzamide (Compound 4)

This compound was prepared in 23.5 % yield by following reaction *a*, *b*, *c*, and *d*. white solid.

¹H NMR (400 MHz CDCl₃): δ/ppm 13.384 (s, 1H), 9.052, 9.031 (dd, *J* = 8.4 Hz, 1H), 8.187, 8.167 (d, *J* = 8.4 Hz, 1H), 7.946–7.915 (m, 2H), 7.564–7.525 (m, 2H), 7.466, 7.446 (d, *J* = 8.4 Hz, 1H), 7.422–7.417 (d, *J* = 2 Hz, 2H), 7.229–7.188 (t, *J* = 8.4 Hz, 1H), 6.700–6.689 (t, *J* = 2 Hz, 1H), 3.915 (s, 6H).

N-(2-(benzo[d]thiazol-2-yl)phenyl)-3,4,5-trimethoxybenzamide (Compound 5)

This compound was prepared in 20.6 % yield by following reaction *a*, *b*, *c*, and *d*. white solid.

¹H NMR (400 MHz CDCl₃): δ/ppm 13.170 (s, 1H), 9.001, 8.980 (d, *J* = 8.4 Hz, 1H), 8.187, 8.167 (d, *J* = 8.4 Hz, 1H), 7.975–7.917 (q, *J* = 8.4 Hz, 3H), 7.572–7.499 (m, 2H), 7.460–7.422 (t, *J* = 8.4 Hz, 1H), 7.396 (s, 1H), 7.234–7.197 (t, *J* = 8.4 Hz, 1H), 3.962 (s, 9H).

3-(benzo[d]oxazol-2-yl)aniline (Intermediate 2)

This compound was prepared in 82 % yield by following reaction *e* light yellow solid.

¹H NMR (400 MHz CDCl₃): δ/ppm 7.785–7.740 (m, 1H), 7.660–7.635 (dt, *J* = 8.4, 1.2 Hz, 1H), 7.588–7.560 (m, 2H), 7.369–7.326 (m, 2H), 7.306, 7.286 (d, *J* = 8.4 Hz, 1H), 6.864–6.836 (ddd, *J* = 8.4, 2.4, 1.2 Hz, 1H), 3.842 (s, 2H).

N-(3-(benzo[d]oxazol-2-yl)phenyl)-3-nitrobenzamide (Compound 6)

This compound was prepared in 68.3 % yield by following reaction *e* and *f* light yellow solid.

¹H NMR (400 MHz DMSO): δ /ppm 10.862 (s, 1H), 8.879 (s, 1H), 8.783 (s, 1H), 8.484, 8.464 (d, *J* = 8.4 HZ, 2H), 8.075, 8.055 (d, *J* = 8.4 HZ, 1H), 7.999, 7.980 (d, *J* = 7.2 HZ, 1H), 7.904–7.864 (t, *J* = 8.4 HZ, 1H), 7.862–7.818 (m, 2H), 7.664–7.624 (t, *J* = 8.4 HZ, 1H), 7.488–7.416 (m, 2H).

N-(3-(benzo[d]oxazol-2-yl)phenyl)-2-(3,4-dimethoxyphenyl)acetamide (Compound 7)

This compound was prepared in 64.7 % yield by following reaction *e* and *f* white solid.

¹H NMR (400 MHz CDCl₃): δ /ppm 8.074 (s, 1H), 7.984, 7.964 (d, *J* = 8.4 HZ, 1H), 7.905, 7.885 (d, *J* = 8.4 HZ, 1H), 7.757–7.734 (m, 1H), 7.586–7.563 (m, 1H), 7.488–7.448 (t, *J* = 8.4 HZ, 1H), 7.377–7.329 (m, 2H), 7.310 (s, 1H), 6.938–6.888 (q, *J* = 4 HZ, 2H), 6.853 (s, 1H).

N-(3-(benzo[d]oxazol-2-yl)phenyl)-4-methoxybenzamide (Compound 8)

This compound was prepared in 50.5 % yield by following reaction *e* and *f* light yellow solid.

¹H NMR (400 MHz CDCl₃): δ /ppm 8.408 (s, 1H), 8.047, 8.007 (t, *J* = 8.4 HZ, 2H), 7.894, 7.872 (d, *J* = 8.8 HZ, 3H), 7.788–7.766 (m, 1H), 7.607–7.576 (m, *J* = 8.8 HZ, 1H), 7.562–7.522 (d, *J* = 8.4 HZ, 1H), 7.380–7.357 (dd, *J* = 6, 3.2 HZ, 2H), 7.019, 6.997 (d, *J* = 8.8 HZ, 2H), 3.894 (s, 3H).

N-(3-(benzo[d]oxazol-2-yl)phenyl)-2-(3,5-dimethoxyphenyl)acetamide (Compound 9)

This compound was prepared in 57.8 % yield by following reaction *e* and *f* white solid.

¹H NMR (400 MHz CDCl₃): δ /ppm 8.421 (s, 1H), 8.057, 8.037 (d, *J* = 8.4 HZ, 1H), 8.004–7.973 (t, *J* = 12.4 HZ, 2H), 7.785–7.762 (m, 1H), 7.602–7.579 (m, 1H), 7.563–7.523 (d, *J* = 8.4 HZ, 1H), 7.378–7.356 (m, 2H), 7.019, 7.013 (d, *J* = 2.4 HZ, 2H), 6.648–6.636 (t, *J* = 2.4 HZ, 1H), 3.862 (s, 1H).

N-(3-(benzo[d]oxazol-2-yl)phenyl)-2-(3,4,5-trimethoxyphenyl)acetamide (Compound 10)

This compound was prepared in 60.3 % yield by following reaction *e* and *f* white solid.

¹H NMR (400 MHz CDCl₃): δ /ppm 8.380 (s, 1H), 8.082–8.037 (m, 2H), 7.948 (s, 1H), 7.787–7.765 (m, 1H), 7.607–7.539 (m, 2H), 7.386–7.363 (m, 2H), 7.125 (s, 2H), 3.954, 3.928 (d, *J* = 10.4 HZ, 9H).

72.3 Results and Discussion

In this work, the core structure of SRT1720 has been changed from imidazo [1,2-*b*]thiazoles to 2-phenylbenzo[*d*]thiazole or 2-phenylbenzo[*d*]oxazole. At the same time, ortho-amide bond is shifted to meta-position one to check if these changes could bring significant SAR improvement.

Table 72.1 The yield (%) of reaction under condition 1 and 2

Compounds	Condition 1	Condition 2
1	40.7	26.5
2	36.8	22.3
3	32.1	24.4
4	35.5	20.9
5	28.6	19.6
6	46.7	68.3
7	38.6	64.7
8	30.5	50.5
9	36.7	57.8
10	31.2	60.3

As to the reaction *c* and *d*, the temperature is a very important factor. In our initial attempts, when temperature under 170 °C, the reaction produced a complicated composition and made the separation difficult. When increased to over 200 °C, the reaction can complete for easy work-up to afford pure product.

In addition, as to reaction *e* and *f* acylation, when reaction condition was CH₂Cl₂ and DCC, all our reactions gave the yield among 14–19 %. We set up other two new conditions: 1. CH₂Cl₂, EDCl, and DMAP as catalyst, Et₃N, 80 °C, and 8 h; 2. C₅H₅N as solvent, EDCl, Et₃N, 90 °C, and 5 h. Interestingly, two different yield for this two different type reaction were observed (Table 72.1). In Table 72.1, for compound 1–5 of 2-phenylbenzo[*d*]thiazole analog, yield under condition 1 is higher than under condition 2; whereas for compound 6–10 of 2-phenylbenzo[*d*]oxazole analog, yield under condition 2 is higher than under condition 1. Especially, compound 6–10 was formed as precipitation under condition 2 for making the isolation easy.

72.4 Conclusion

In summary, the two suitable conditions for quick synthesis of different kinds of compounds such as 2-phenylbenzo[*d*]thiazole and 2-phenylbenzo[*d*]oxazole were developed, which offered overall yield 30–69 %. All compounds synthesized in this paper are core-changed partially similar to the structure of SRT1720. The aim of the work is to find suitable fragments for a further structural expansion for seeking a lead compound with a potential biological activity toward Sirt1.

Acknowledgments Sponsor and financial support acknowledgments are provided by National Natural Science Foundation of China (No: 81072521), Tianjin University of Science & Technology (No: 20100411), International Science & Technology Cooperation Program of China (2013DFA31160) and the Science & Technology Project of Tianjin (11ZCGHHZ00400).

References

1. Kong Xingxing, Wang Rui, Liu Xiaojun, Zhu Liuluan, Shao Di, Fang Fu-De et al (2009) Function of SIRT1 in physiology. *Biochemistry (Moscow)* 74:703–708
2. Braunstein M, Rose AB, Holmes SG, Allis, Broach JR (1993) Transcriptional silencing in yeast is associated with reduced nucleosome acetylation. *Genes Dev* 7:592–604
3. Kaeberlein M, McVey M, Guarente L (1999) The SIR2/3/4 complex and SIR2 alone promote longevity in *Saccharomyces cerevisiae* by two different mechanisms. *Genes Dev* 13:2570–2580
4. Frye RA (2000) Phylogenetic classification of prokaryotic and eukaryotic Sir2-like proteins. *Biochem Biophys Res Commun* 273:793–798
5. Michan S, Sinclair D (2007) Sirtuins in mammals: insights into their biological function. *Biochem J* 404:1–13
6. Starai VJ, Celic I, Cole RN, Boeke JD, Escalante-Semerena JC (2002) Sir2-dependent activation of acetyl-CoA synthetase by deacetylation of active lysine. *Science* 298:2390–2392
7. Rusche LN, Kirchmaier AL, Rine J (2003) The establishment, inheritance, and function of silenced chromatin in *Saccharomyces cerevisiae*. *Annu Rev Biochem* 72:481–516
8. Gasser SM, Cockell MM (2001) The molecular biology of the SIR proteins. *Gene* 279:1–16
9. Dryden SC, Nahhas FA, Nowak JE, Goustin AS, Tainsky MA (2003) Role for human SIRT2 NAD-dependent deacetylase activity in control of mitotic exit in the cell cycle. *Mol Cell Bio* 23:3173–3185
10. Wood JG, Rogina B, Lavu S, Howitz K, Helfand SL (2004) Sirtuin activators mimic caloric restriction and delay ageing in metazoans. *Proc Natl Acad Sci USA* 101:15998–16003
11. Tissenbaum HA, Guarente L (2001) Increased Dosage of a sir-2 gene extends lifespan in *Caenorhabditis elegans*. *Nature* 410:227–230
12. Vaziri H, Dessain SK, Ng Eaton E, Imai SI, Frye RA, Pandita TK, Guarente L, Weinberg RA (2001). Hsir2^{SIR1} Functions as an NAD-Dependent P53 Deacetylase. *Cell* 107(2):149–159
13. Luo J, Nikolaev AY, Imai S, Chen D, Su F, Shiloh A, Guarente L, Gu W (2001) Negative control of p53 by Sir2 [alpha] promotes cell survival under stress. *Cell* 107:137–148
14. Langley E, Pearson M, Faretta M, Bauer UM, Frye RA, Minucci S, Pelicci PG, Kouzarides T (2002) Human SIR2 deacetylates p53 and antagonizes PML/p53-induced cellular senescence. *EMBO J* 21:2383–2396
15. Cohen HY, Miller C, Bitterman KJ, Wall NR, Hekking B, Kessler B, Howitz KT, Gorospe M, de Cabo R, Sinclair DA (2004) Calorie restriction promotes mammalian cell survival by inducing the SIRT1 deacetylase. *Science* 305:390–392
16. Heilbronn LK, Civitarese AE, Bogacka I, Smith SR, Hulver M, Ravussin E (2005) Glucose tolerance and skeletal muscle gene expression in response to alternate day fasting. *Obes Res* 13:574–581
17. Milne JC, Lambert PD, Schenk S, Carney DP, Smith JJ (2007) Small molecule activators of SIRT1 as therapeutics for the treatment of type 2 diabetes. *Nature* 450:712–716
18. Bordone L, Guarente L (2005) Calorie restriction, SIRT1 and metabolism: understanding longevity. *Nature Rev Mol Cell Biol* 6:298–305
19. Cohen HY, Miller C, Bitterman KJ, Wall NR et al (2004) Calorie restriction promotes mammalian cell survival by inducing the SIRT1 deacetylase. *Science* 305:390–392
20. Heilbronn LK et al (2005) Glucose tolerance and skeletal muscle gene expression in response to alternate day fasting. *Obes Res* 13:574–581
21. Baur JA, Pearson KJ, Price NL, Jamieson HA, Lerin C, Kalra A, Prabhu VV, Allard JS, Pistell PJ, Poosala S, Gwinn D, Wang M, Ramaswamy S, Fishbein KW, Spencer RG, Lakatta EG, LeCouteur D, Shaw RJ et al (2006) Resveratrol improves health and survival of mice on a high-calorie diet. *Nature* 444:337–342
22. Lagouge M, Argmann C, Gerhart-Hines Z, Meziane H, Lerin C, Daussin F, Messadeq N, Milne J, Lambert P, Elliott P, Geny B, Laakso M, Puigserver P, Auwerx J (2006) Resveratrol

- improves mitochondrial function and protects against metabolic disease by activating SIRT1 and PGC-1 [alpha]. *Cell* 127:1109–1122
23. Milne JC, Lambert PD, Schenk S, Carney DP, Smith JJ, Gagne DJ, Jin L, Boss O, Perni RB, Vu CB, Bemis JE, Xie R, Disch JS, Ng PY, Nunes JJ, Lynch AV, Yang H, Galonek H (2007) Israelian, and Westphal, C.H. *Nature* 450:712–716
 24. Pacholec M, Bleasdale JE, Chrnyk B, Cunningham D, Flynn D, Garofalo RS, Griffith D, Griffor M, Loulakis P, Pabst B, Qiu X, Stockman B, Thanabal V, Varghese A, Ward J, Withka J, Ahn K (2010) SRT1720, SRT2183, SRT1460, and resveratrol are not direct activators of SIRT1. *J. Biol Chem* 285:8340–8351
 25. OXFORD GLYCOSCIENCES (UK) LTD; SCOPES, David, Ian, Carter; WO2003/74516;(2003); (A1) English

Chapter 73

Synthesis of 1,3-benzodioxol-5-ethanol and Its Derivatives

Na Ji, Yinghao Gao, Yuanmou Chen, Shaolong Jia, Fei Hu,
Peng Yu and Erbing Hua

Abstract It has been reported that resveratrol can enhance Sirt1 expression and has the activation effect on the proteins related to insulin signaling. It can also ameliorate insulin tolerance in order to achieve the function of preventing and curing diabetes. In this work, we designed a new series of analogs related to the structure of resveratrol such as 1,3-benzodioxol-5-ethanol, which is synthesized from 1,3-benzodioxole by the reactions of Friedel-Crafts reaction, Wolff-Kishner-Huang and reduction. In addition, seven new 1,3-benzodioxol-5-ethanol derivatives were obtained through esterification with different substituents of organic acid. All compounds were characterized by $^1\text{H-NMR}$. Yields of derivatives are from 13.2 to 78.8 %.

Keywords 1,3-benzodioxol-5-ethanol · 1,3-benzodioxole derivatives · Pharmaceutical intermediate · Synthesis

73.1 Introduction

It is a global problem that metabolic syndrome is a threat to human health. The key point to treat metabolic syndrome is improving insulin resistance because it is the pathogenesis of type II diabetes, obesity, and primary hypertension [1]. It has been reported that Sirt-1 plays an important role [2, 3] in increasing insulin secretion [4]. Resveratrol is the agonist of Sirt-1 and some derivatives have enhanced effect on it [5]. In this paper, we aim to introduce 1,3-benzodioxole and design a new series of analogs related to the structure of resveratrol. In the field of medicine

N. Ji · Y. Gao · Y. Chen · S. Jia · F. Hu · P. Yu · E. Hua (✉)

Key Laboratory of Industrial Microbiology of Ministry of Education, College of Biotechnology, Tianjin University of Science and Technology, Tianjin 300457, People's Republic of China
e-mail: huarb@tust.edu.cn

synthesis, compounds with the group of 1,3-benzodioxole is not only the important intermediates of berberine [6], but also the significant material to synthesis quinolone drugs. Meanwhile good activity were found in the field of antitumor 1,3-benzodioxole derivatives [7, 8]. Thus, a series of active compounds and high value added pharmaceutical intermediates derived from 1,3-benzodioxole is bound to be more widely applied in the field of drug discovery in the future.

Economic and security synthetic technology of 1,3-benzodioxol-5-ethanol has not been reported. The traditional method is from 1,3-benzodioxole by the reaction of chloromethylation, nitrile, hydrolysis, and reduction [9]. However, the virulent sodium cyanide used in this synthetic method is harmful to both environment and experimenters, it is not an environmental friendly and safe process. Wang Yuanxing [10] and his colleagues developed a relative safe synthetic method using methyl methylthiomethyl sulfo (FAMSO) as an equivalent reagent of carbonyl group. They gained 1,3-benzodioxol-5-acetic acid from piperonal with three-steps reactions but it took a high production cost. In order to meet the needs of developing new drugs, we have designed an economic and safe synthetic route by using inexpensive 1,3-benzodioxole as the starting material. According to the structure-activity relationship, we got seven new 1,3-benzodioxol-5-ethanol derivatives.

73.2 Materials and Methods

73.2.1 Materials and Measurements

^1H NMR spectra were recorded on Bruker AM-400 NMR spectrometers using deuterated chloroform as solvent and tetramethylsilane as an internal standard. Reaction temperatures were controlled by oil bath temperature modulator. Thin layer chromatography (TLC) was performed using E. Merck silica gel 60 GF₂₅₄ precoated plates (0.25 mm). Visualization was made with ultraviolet light. Column chromatography was performed on silica gel (particle size 200–400 mesh). All reagents and solvents used in the present were of reagent grade.

73.2.2 Experimental Methods

The route to prepare the 1,3-benzodioxol-5-ethanol and derivatives was presented in Fig. 73.1.

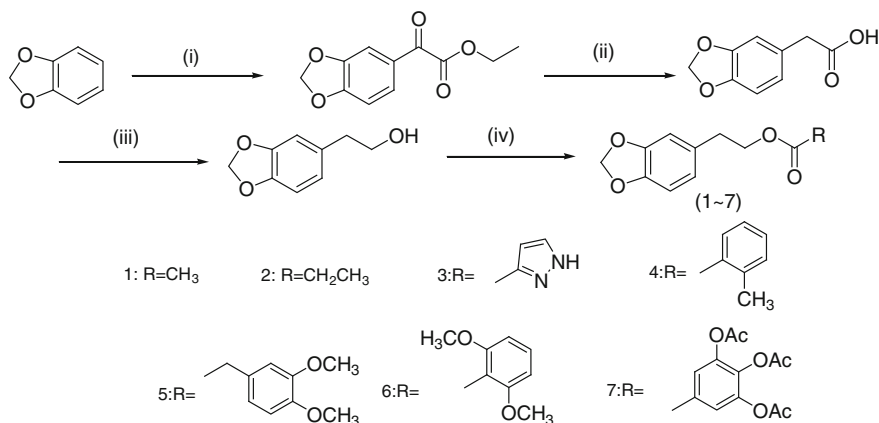


Fig. 73.1 Reagents and conditions: (i) C₄H₅ClO₃, AlCl₃, CH₂Cl₂, rt; (ii) N₂H₄·H₂O, EG, KOH, HCl, 180 °C; (iii) LAH, THF, rt; (iv) EDCI, DMAP, TEA, CH₂Cl₂, rt

73.2.2.1 Ethyl 2-(benzo[1,3]dioxole-5-yl)-2-oxoacetate [11]

In a three-necked round-bottomed flask mounted with a cooler system, AlCl₃ (11.7 g, 0.089 mol) was suspended in CH₂Cl₂ (100 ml) under 0 °C. To this stirred mixture ethyl chlorooxoacetate (11.76 g, 0.086 mol) was slowly added in about 15 min. After 10 min the suspension became a pale yellow solution. 1,3-benzodioxole (10 g, 0.082 mol) was added dropwise at 0 °C in about 10 min. Then the reaction mixture was stirred at room temperature for 1 h. After the reaction was completely finished, the threefold volume of H₂O was slowly added. Extraction was performed with ethyl acetate (3 × 30 mL). The organic phase was washed with saturated NaCl solution, filtered, dried (Na₂SO₄), and concentrated in vacuo. The crude residue was purified by silica gel column chromatography (petroleum ether/ethyl acetate 40:1) to give 10.2 g as yellow oil.

73.2.2.2 1,3-benzodioxol-5-acetic acid [12]

A mixture of ethyl 2-(benzo[1,3]dioxole-5-yl)-2-oxoacetate (10.2 g, 0.046 mol), 85 % hydrazine hydrate (13.55 g, 0.23 mol), and ethanediol (100 ml) was stirred at 120 °C for 2 h. To the mixture was added KOH (7.65 g, 0.138 mol), then heated to 180 °C and kept reflux for 4 h. Cooling it to room temperature, dilute HCl solution (6 mol/L) was poured into the mixture to adjust the pH value to 2–3. After a while the mixture separated out a large amount of white solid. Filtered and collected the crude product (5.18 g, 62.8 %), it was used directly for the next step without further purification.

73.2.2.3 1,3-benzodioxol-5-ethanol [13–15]

In a round-bottomed flask, lithium aluminum hydride (2.93 g, 0.086 mol) was added to 1,3-benzodioxol-5-acetic acid (5.18 g, 0.029 mol) stirred in anhydrous THF (50 mL) in ice bath. The mixture was warmed up to room temperature for overnight. Ice water (20 mL) was added slowly to the mixture to quench reaction and flocks were resolved by dilute HCl (10 %). The mixture was washed with ethyl acetate (3 × 20 mL) and we used saturated NaHCO₃ solution to neutralize residual HCl. Dried (Na₂SO₄), filtered, concentrated in vacuo, and then purified by silica gel column chromatography (petroleum ether/ethyl acetate 20:1) to afford 1,3-benzodioxol-5-ethanol 2.2 g.

73.2.2.4 General Procedure 1 (GP1) for 1,3-benzodioxole Derivatives (1 ~ 7) [16–19]

In a round-bottomed flask, 1,3-benzodioxol-5-ethanol (0.2 g, 1.2 mmol) was added to a mixture of organic acid (1.46 mmol), EDCI (0.28 g, 1.46 mmol), DMAP (0.03 g, 0.25 mmol), and triethylamine (0.15 g, 1.48 mmol) were stirred in anhydrous dichloromethane (20 mL) at room temperature. The organic layer was washed with water (3 × 20 mL) and then dried over anhydrous Na₂SO₄. The solution was concentrated and the residue was purified by silica gel column chromatography, eluting with petroleum ether-ethyl acetate mixture.

73.2.3 Syntheses

73.2.3.1 Ethyl 2-(benzo[1,3]dioxole-5-yl)-2-oxoacetate

Yellow oil, 56.7 % yield.

¹H-NMR(CDCl₃)δ: 1.412–1.448 (3H,t,CH₂CH₃), 4.417–4.471 (2H,m,CH₂CH₃), 6.101 (2H,s,CH₂), 6.896–6.917 (1H,d,ArH), 7.490–7.494 (1H,d, ArH), 7.618–7.643 (1H,dd, ArH).

73.2.3.2 1,3-benzodioxol-5-ethanol

Yellow oil, 46.0 % yield.

¹H-NMR(CDCl₃)δ: 1.552(1H,s,CH₂CH₂OH), 2.793–2.825(2H,t, CH₂CH₂OH), 3.819–3.851(2H,t, CH₂CH₂OH), 5.953(2H,s, CH₂), 6.686–6.710(1H,dd, ArH), 6.743–6.747 (1H,d, ArH), 6.771–6.791 (1H,d, ArH).

73.2.3.3 1,3-benzodioxole derivative 1

Yellow oil, 77.2 % yield.

$^1\text{H-NMR}(\text{CDCl}_3)$ δ : 2.038 (3H,s,CH₂CH₂OCOCH₃), 827–2.862 (2H,t,CH₂CH₂OCOCH₃), 4.206–4.241 (2H,t,CH₂CH₂OCOCH₃), 5.928 (2H,s,CH₂), 6.646–6.6751 (3H,m,ArH).

73.2.3.4 1,3-benzodioxole derivative 2

Yellow oil, 78.8 % yield.

$^1\text{H-NMR}(\text{CDCl}_3)$ δ : 1.105–1.143 (3H,t,COCH₂CH₃), 2.288–2.345 (2H,q,COCH₂CH₃), 2.830–2.865 (2H,t,CH₂CH₂OCO), 4.215–4.250 (2H,t,CH₂CH₂OCO), 5.931 (2H,s,CH₂), 6.648–6.752 (3H,m,ArH).

73.2.3.5 1,3-benzodioxole derivative 3

White solid, 19.2 % yield.

$^1\text{H-NMR}(\text{CDCl}_3)$ δ : 2.978–3.013 (2H,t,CH₂CH₂OCO), 4.480–4.516 (2H,t,CH₂CH₂OCO) 5.930 (2H,s,CH₂), 6.717–6.762 (3H,m,ArH), 6.837–6.842 (1H,d,PyrazoleH), 7.660–7.665 (1H,d,PyrazoleH), 11.643 (1H,s,NH).

73.2.3.6 1,3-benzodioxole derivative 4

Yellow oil, 76.5 % yield.

$^1\text{H-NMR}(\text{CDCl}_3)$ δ : 2.557 (3H,s,ArCH₃), 2.969–3.003 (2H,t,CH₂CH₂OCO), 4.443–4.478 (2H,t,CH₂CH₂OCO), 5.928 (2H,s,CH₂), 6.708–6.771 (3H,m,ArH), 7.215–7.253 (2H,m,ArH), 7.362–7.403 (1H,t,ArH), 7.850–7.870 (1H,d,ArH).

73.2.3.7 1,3-benzodioxole derivative 5

White solid, 62.5 % yield.

$^1\text{H-NMR}(\text{CDCl}_3)$ δ : 2.807–2.841 (2H,t,CH₂CH₂OCO), 3.536 (2H,s,COCH₂), 3.852 (3H,s,ArOCH₃), 3.867 (3H,s,ArOCH₃), 4.236–4.270 (2H,t,CH₂CH₂OCO) 5.921 (2H,s,CH₂), 6.573–6.577 (1H,d,ArH), 6.593 (1H,s,ArH), 6.693–6.712 (1H,d,ArH), 6.771–6.823 (3H,m,ArH).

73.2.3.8 1,3-benzodioxole derivative 6

Yellow oil, 37.3 % yield.

$^1\text{H-NMR}(\text{CDCl}_3)$ δ :2.979–2.997 (2H,t, $\underline{\text{CH}_2\text{CH}_2\text{OCO}}$), 3.802 (6H,s, $\underline{\text{OCH}_3}$), 4.473–4.508 (2H,t, $\underline{\text{CH}_2\text{CH}_2\text{OCO}}$), 5.918 (2H,s, $\underline{\text{CH}_2}$), 6.541–6.562 (2H,d, $\underline{\text{ArH}}$), 6.723–6.809 (3H,m, $\underline{\text{ArH}}$), 7.261–7.277 (1H,m, $\underline{\text{ArH}}$).

73.2.3.9 1,3-benzodioxole derivative 7

Brown oil, 13.2 % yield.

$^1\text{H-NMR}(\text{CDCl}_3)$ δ :2.305 (9H,s, $\underline{\text{ArCOOCH}_3}$), 2.946–2.983 (2H,t, $\underline{\text{CH}_2\text{CH}_2\text{O}}$ CO), 4.437–4.472 (2H,t, $\underline{\text{CH}_2\text{CH}_2\text{OCO}}$), 5.936 (2H,s, $\underline{\text{CH}_2}$), 6.687–6.745 (3H,m, $\underline{\text{ArH}}$), 7.765 (2H,s, $\underline{\text{ArH}}$).

73.3 Result and Discussion

The key of experiment is to find a method with good selective substituted at 5-position and high yield. There are two methods reported. One is that 1,3-benzodioxol-5-ethanol was acquired through bromination at 5-position of 1,3-benzodioxol and then ethylene oxide treated with Grignard reagents which were prepared from bromo-substituted intermediate. The other is 1,3-benzodioxol as raw material to get 1,3-benzodioxol-5-acetic acid after three-step reaction or form piperonal through two-steps by using FAMSO then through reduction by Lithium aluminum hydride to get target compound. After trying these two methods, we found that the condition of operation was strict and got 5,6-disubstituted. Therefore, we used ethyl chlorooxoacetate to get the substitution product at 5-position without 5,6-disubstituted because of the steric effect. However, the yield of this step has yet to be improved. Because a large amount of reddish brown sticky substance contained in the products brought difficulties to separation. This problem still remains to be solved by further experiments.

In addition, the reduction from 1,3-benzodioxol-5-acetic acid to 1,3-benzodioxol-5-ethanol was incomplete. Enhancing temperature and extending reaction time could help finish this reaction. We tried to rise yield by esterifying 1,3-benzodioxol-5-acetic acid to relative acetate followed by reduction to 1,3-benzodioxol-5-ethanol, but this method increased difficulty during work-up.

Esterification on hydroxyl group of 1,3-benzodioxol-5-ethanol made this 1,3-benzodioxole derivatives structurally similar to resveratrol. Aromatic acids with different substituent groups have different reaction activity because of directing effects of various substituent groups on activation. In order to achieve the goals of promoting reaction and improving yields, we elevated temperature and prolonged reaction time. In addition, charging sequence affected an extent of reaction. The suitable charging sequence was aromatic acids, EDCI, TEA, DMAP, and 1,3-benzodioxol-5-ethanol.

73.4 Conclusion

In this article, a novel synthetic method was developed to synthesize 1,3-benzodioxol-5-ethanol and its derivatives. This process has several advantages such as fewer steps, good selectivity, safe, and environmental friendly compared with the mainly used synthetic routes. We also afforded seven 1,3-benzodioxole derivatives as potential active compounds for treatment of diabetes and cancer. This method would provide a much better way for synthesis of new 1,3-benzodioxole derivatives.

Acknowledgments This work was supported by National Natural Science Foundation of China (No: 81072521), Tianjin University of Science & Technology (No: 20100411), International Science & Technology Cooperation Program of China (2013DFA31160) and the Science & Technology Project of Tianjin (11ZCGHHZ00400).

References

1. Gordon BA, Benson AC, Bird SR et al (2009) Resistance training improves metabolic health in type 2 diabetes: A systematic review. *Diabetes Res Clin Pr* 83:157–175
2. Carles C, Johan A (2009) Caloric restriction, SIRT1 and longevity. *Trends Endocrin Met* 20:325–331
3. Hye-Sook K, Melanie O (2008) The ups and downs of SIRT1. *Trends Biochem Sci* 33:517–525
4. Yang T, Fu M, Pestell R et al (2006) SIRT1 and endocrine signaling. *Trends Endocrin Met* 17:86–91
5. Kaerberlein M, Mc Donagh T, Heltweg B et al (2005) Substrate specific activation of sirtuins by resveratrol. *J Biol Chem* 280:17038–17045
6. Yang ZY, Liu ZL, Liu HW et al (2011) Synthesis of 1,3-benzodioxole. *Fine Specially Chem* 19:23–26
7. deM Moreira DR, Leite ACL, Ferreira PMP (2007) Synthesis and anti-tumor evaluation of peptidyl-like derivatives containing the 1,3-benzodioxole system. *Eur JMed Chem* 42:351–357
8. Since M, Terme T, Vanelle P (2009) Original TDAE strategy using α -halo carbonyl derivatives. *Tetrahedron* 65:6128–6134
9. Zhou LJ, He QG, Liu ZC et al (2002) Synthesis of 1,3-benzodioxol-5-acetic acid. *Chem Ind Forest Prod* 22:80–82
10. Wang YX, Fang ZJ, Han XL (2007) A convenient synthesis of 3,4-(methylenedioxy) phenylacetic acid. *Chem Reagent* 29(751–752):755
11. Ianni A, Waldvogel SR (2006) Reliable and versatile synthesis of 2-aryl-substituted cinnamic acid esters. *Chem Inform* 13:2103–2112
12. Yao GX, Chen G, Lu Y et al (2010) An alternative process for preparation of 3,4-dimethoxyphenylacetic acid. *Chin J Pharm* 41:730–731
13. Elger B, Huth A, Neuhaus R et al (2005) Novel α -Amino-3-hydroxy-5-methyl-4-isoxazole propionate (AMPA)receptor antagonists of 2,3-benzodiazepine type: chemical synthesis, in vitro characterization, and in vivo prevention of acute neurodegeneration. *J Med Chem* 14:4618–4627
14. Shahane S, Louafi F, Moreau J et al (2008) Synthesis of alkaloids of *Galipea officinalis* by alkylation of an α -aminonitrile. *Eur J Org Chem* 27:4622–4631

15. Capuano B, Crosby IT, Podloucka A et al (2003) Synthesis and preliminary pharmacological evaluation of 4'-arylalkyl analogues of clozapine. II. effect of the nature and length of the linker. *Aus J Chem* 56:875–886
16. Lai CC, Brian GC (2007) Kinetics of amide formation through carbodiimide/N-Hydroxybenzotriazole (HOBt) couplings. *J Org Chem* 72:8863–8869
17. Jiang WL, Jutta W, Richard JL et al (2002) Total synthesis of the ramoplanin A2 and ramoplanose aglycon. *J Am Chem Soc* 124:5288–5290
18. Hwa-Ok K, Hiroshi N, Min SL et al (2000) Design and synthesis of novel conformationally restricted peptide secondary structure mimetics. *Org Lett* 2:301–302
19. Bryan KSY, Dale LB (2003) Synthesis of isochrysohermidin-distamycin hybrids. *J Org Chem* 68:5249–5253

Chapter 74

Tetrandrine Inhibits Proteasomal Chymotrypsin-Like Activity and Induces Apoptosis in Human PC-3 Cells

Li Zhang, Wanxin Shi, Weihua Cao, Xiangru Liang, Yufu Hu, Mo Chen and Guoqing Shi

Abstract The ubiquitin-proteasome pathway has been accepted as a promising target for cancer therapy, as it plays a vital role in cell cycle, function, and survival. In this research, *in silico* study by molecular docking predicted that Tetrandrine(TET), a compound from the roots of *Stephania tetrandra* S Moore, could bind to the active site of the proteasome $\beta 5$ subunit. In vitro assay proved that TET inhibits the chymotrypsin-like (CT) activity of purified human 20S proteasome in a dose-dependent manner with IC_{50} of $0.8 \mu\text{mol/L}$. After exposed to TET for 24 h, the CT activity in human prostate cancer PC-3 cells was inhibited with IC_{50} of $35 \mu\text{mol/L}$, and the ubiquitinated proteins were accumulated in dose-dependent manner. This inhibition was further proved by the accumulation of GFP-CL proteins, which is an indicator of proteasome inhibition in pEGFP-CL1 transferred PC-3 cells. The proteasomal activity inhibition by TET leads to apoptosis like morphological changes and activation of caspase-3 activity in dose-dependent manner in PC-3 cells. Based on these results, we suppose that TET is a proteasome inhibitor and induces cell apoptosis.

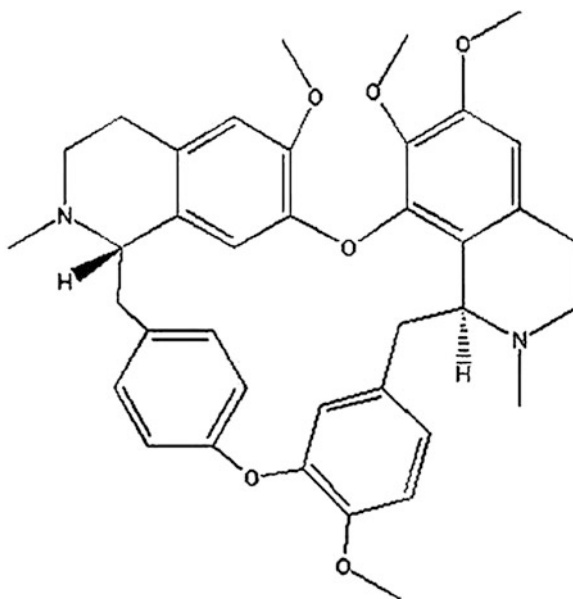
Keywords Apoptosis · Tetrandrine (TET) · Proteasomal activity · PC-3 cells

74.1 Introduction

Tetrandrine (TET) is a purified vasoactive bisbenzylisoquinoline alkaloid derived from the roots of *Stephania tetrandra* S Moore, a medicinal plant widely distributed in China. The structure is shown in Fig. 74.1.

L. Zhang · W. Shi · W. Cao · X. Liang · Y. Hu · M. Chen · G. Shi (✉)
School of Chemistry and Biological Engineering, University of Science and Technology,
Beijing 100083, People's Republic of China
e-mail: shiguqing@ustb.edu.cn

Fig. 74.1 The structure of tetrandrine



TET has been used traditionally for the treatment of congestive circulatory disorder [1] and inflammatory diseases [2]. Many studies have shown that TET has anti-tumor activity [3]. TET induces apoptosis in various cell types such as A549, HepG2 [4], HL60 [5], HCT116 [6], and U937 [7] cells, etc. There have been many mechanisms reported about TET-induced apoptosis. Byeong-Churl Jang [8] shows that tetrandrine-induced apoptosis is mediated by activation of caspases and PKC- δ in U937 cells; Tetrandrine-mediated responses of cell proliferation and cytotoxicity may be correlated with the tetrandrine-induced large-conductance Ca^{2+} -activated K^+ (BK) channel block [9]. Recent studies show that TET induces apoptosis by activating reactive oxygen species and repressing Akt activity in human hepatocellular carcinoma [10]. But the specific mechanisms remain unclear.

Ubiquitin-proteasome system is responsible for a vast majority of protein degradation in eukaryotic cells, which plays an important role in cell cycle and apoptosis [11]. The 26S proteasome is composed of the 20S core catalytic complex flanked on both sides by the 19S regulatory complexes; The 20S proteasome has three catalytic active sites: chymotrypsin-like(CT), trypsin-like(TL), and post-glutamyl peptide hydrolase-like (PGPH), which are located in $\beta 5$, $\beta 2$, and $\beta 1$ subunits, respectively [12]. Inhibition of the proteasomal CT activity can lead to apoptosis in most tumor cell lines [13].

74.2 Materials and Methods

74.2.1 Materials

1. Cells

Human prostate cells PC-3 were obtained from the Cell Culture Center, Institute of Basic Medical Sciences, Chinese Academy of Medical Sciences.

2. Materials

Cell culture medium Ham's F12 and serum were obtained from Hyclone Inc. Tetrandrine was purchased from sigma; A 50 mmol/L stock solution of TET dissolved in 1 mol/L HCl and regulated PH with saturated NaHCO₃ to 7.0 was stored at -20 °C. Purified human 20S proteasome was from BIOMOL International LP. Antibody against ubiquitin (P4D1), actin (C-11), and horseradish peroxidase (HRP)-conjugated secondary anti-rabbit and anti-mouse IgG were from Santa Cruz Biotechnology Inc. Fluorogenic peptide substrate Suc-LLVY-AMC (for the proteasomal chymotrypsin-like activity) was from Enzo Life Sciences Inc.

74.2.2 Methods

1. Proteasomal activity assay

The proteasome activity assay was performed as described [14]. PC-3 cells were treated with different concentrations of TET for 24 h, after which, the cells were harvested and lysed. Incubate the lysate with 40 μmol/L of fluorogenic peptide substrates for 2 h at 37 °C in 100 μL assay buffer (25 mmol/L Tris-HCl, pH 7.4). After incubation, cleaved fluorescent products were measured using fluorescence plate reader with an excitation filter of 380 nm and an emission filter of 460 nm.

2. Western blotting analysis

The Western blotting analysis was performed as described previously [15]. Cell lysates (40 μg) were separated by SDS-PAGE and transferred onto PVDF membrane. The membrane was blocked by 5 % nonfat milk, and the membrane was then probed with antibodies overnight at 4 °C. After the unbinding antibodies were washed, the membrane was incubated with horseradish peroxidase (HRP)-conjugated secondary anti-rabbit or anti-mouse IgG for additional 4 h, followed by the detection of the antibody-bound proteins using the ECL detection kit.

3. PC-3-GFP-CL1 cells construction and exposure

The PC-3-GFP-CL1 cell line was constructed as described previously [16]. GFP-CL1 is consist of a short peptide degron fused to the carboxyl-terminus of green fluorescent protein (GFP-CL1) [17, 18], which is known to be degraded by proteasome, only when the proteasome was inhibited or the UPS crushed,

will the GFP level accumulate and can be detected by fluorescence microscope. PC-3-GFP-CL1 cells were exposed to 50 $\mu\text{mol/L}$ TET for designed time and then pictured by fluorescence microscopy.

74.3 Results and Discussion

74.3.1 Molecular Docking

First of all, Autodock 4.0 software was used to predict the possible interaction between TET and 20S proteasome [19]. The results showed that the lowest “estimated free energy of binding” between $\beta 5$ subunit and TET was -6.28 kcal/mol. The predicted binding conformations were shown in Figs. 74.2a, b.

From Fig. 74.2a, it was shown that TET has a close binding with the active site of proteasome $\beta 5$ subunit, and TET was inlaid with 20S proteasomal cavity with a close distance to the Thr1 residue at $\beta 5$ subunit [20] (marked by red), which is responsible for the proteasomal CT activity; Fig. 74.2b showed that the major binding power between TET and $\beta 5$ subunit was hydrophobic interactions. Based on these, we suppose that TET may be a kind of proteasomal inhibitor.

74.3.2 TET Inhibits Proteasomal CT Activity Both *in Vitro* and *in Vivo*

TET inhibits purified 20S CT-like activity. In order to confirm the results predicted by *in silico* study, the CT activity change of purified 20S proteasome was

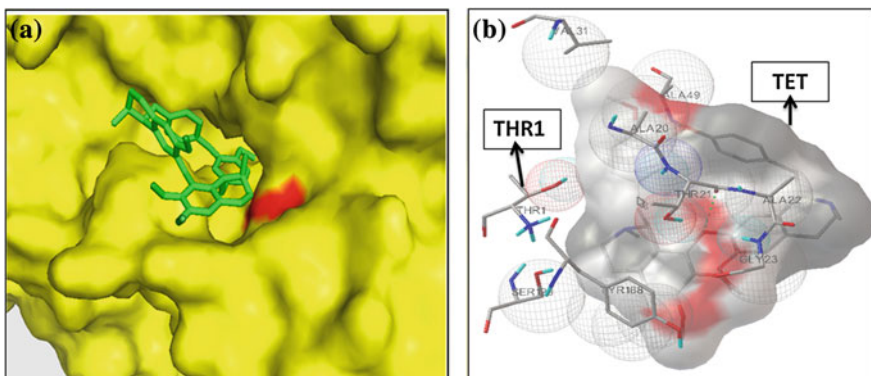
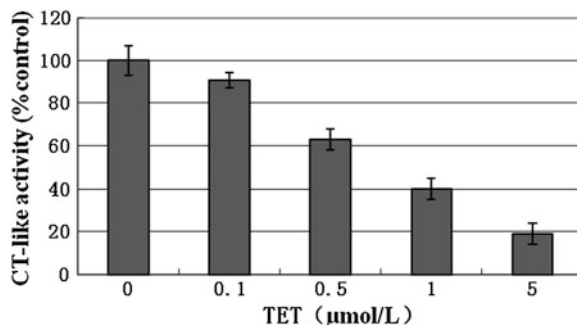


Fig. 74.2 Molecular docking of TET to $\beta 5$ subunit

Fig. 74.3 TET inhibits purified 20S CT-like activity



investigated in different concentrations of TET. The results were shown in Fig. 74.3. TET inhibited 20S proteasomal CT activity in a dose-dependent manner with IC_{50} of 0.8 $\mu\text{mol/L}$.

TET inhibits proteasomal CT-like activity in PC-3 cells. In order to investigate whether TET inhibits tumor cellular proteasome activity, PC-3 cells were treated with different concentrations of TET, followed by measuring proteasome inhibitory effect by the cellular proteasomal chymotrypsin-like activity assay and accumulation of ubiquitinated proteins. As it was shown in Fig. 74.4, TET significantly inhibited the proteasomal chymotrypsin-like activity in PC-3 cells in a concentration-dependent manner (Fig. 74.4); at 50 $\mu\text{mol/L}$ it reached of 70 % inhibition. Coincidentally, levels of ubiquitinated proteins were accumulated in PC-3 cells treated with TET in a concentration-dependent manner (Fig. 74.5).

Fig. 74.4 TET inhibits proteasomal CT-like activity in PC-3 cells

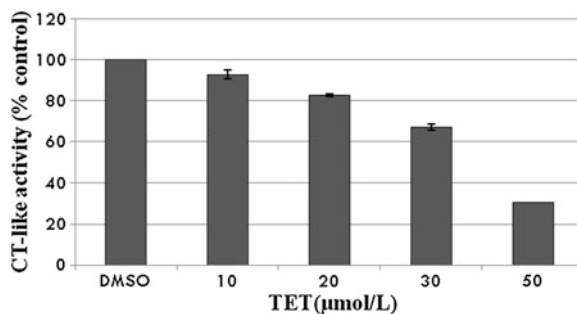
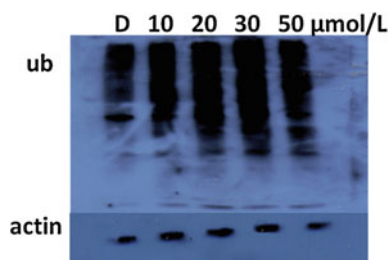


Fig. 74.5 TET induces ubiquitinated proteins accumulated



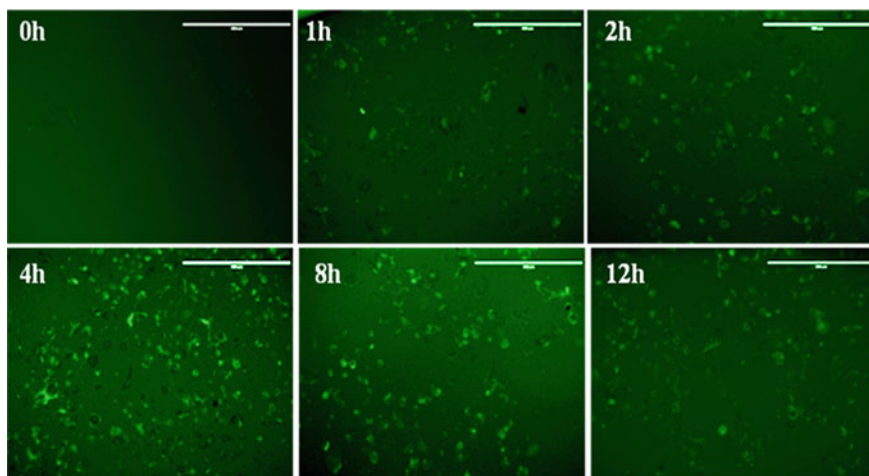


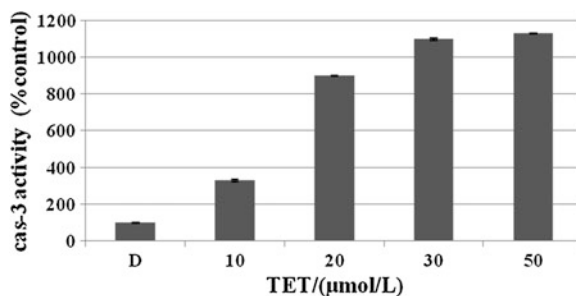
Fig. 74.6 TET induces GFP level accumulated in PC-3-GFP-CL1 cells

Furthermore, the PC-3-GFP-CL1 cells were exposed to 50 $\mu\text{mol/L}$ TET for 0, 1, 2, 4, 8, 12 h and pictured by fluorescence microscopy as shown in Fig. 74.6, which showed the GFP levels were accumulated with the time increased, and after 8 h the GFP level was decreased because of apoptosis, which further indicated that the proteasome was inhibited by TET. These results indicate that TET is an inhibitor of 20S proteasome.

74.3.3 Inhibition of Cellular Proteasomal Activity by TET is Associated with Apoptosis in PC-3 Prostate Cancer Cells

Many studies have shown that inhibition of cellular proteasome activity induces apoptosis [21, 22]. The Caspase-3 activity and cellular apoptotic morphologic changes (condensation and fragmentation) were detected to evaluate the apoptosis

Fig. 74.7 TET activates caspase-3 activity in PC-3 cells



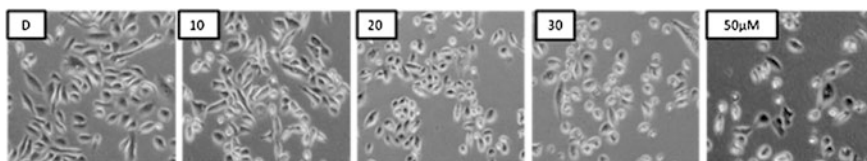
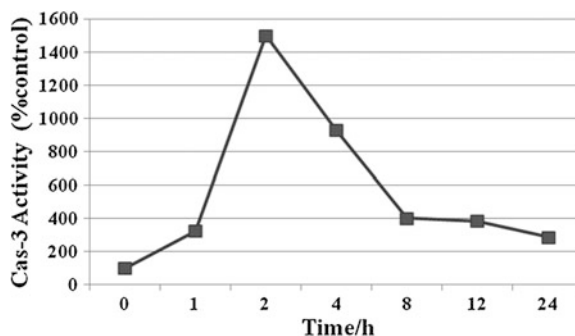


Fig. 74.8 PC-3 cells apoptosis after treated TET(DMSO, 10, 20, 30, 50 $\mu\text{mol/L}$) for 2 h

Fig. 74.9 TET activates caspase-3 activity



of cells. TET at 50 $\mu\text{mol/L}$ induced caspase-3 activity by 11.3-fold after 2 h of exposure (Fig. 74.7). Morphologically, the TET-treated cells turned to round and had serious shrinks, moreover, the floating cells increased with the concentration increased (Fig. 74.8). The results show that with the concentration of TET increased cells' apoptosis aggravate.

PC-3 cells were treated with TET for 0, 1, 2, 4, 8, 12, 24 h, respectively, and then caspase-3 activity was detected. The results are shown in Fig. 74.9. It shows that as early as 2 h the caspase-3 reached the peak by 15-fold. These results show that the inhibition of TET to proteasome CT activity is associated with cell apoptosis.

74.4 Conclusion

Molecular docking shows that proteasome subunit $\beta 5$ has a low combined energy with the natural small molecules tetrandrine. There is a closed conformation between them; TET can significantly inhibit purified 20S proteasome CT activity in a dose-dependent manner. Using prostate cancer cells PC-3 as cell model to examine the inhibition of TET to 20S proteasome shows that: TET inhibits 20S proteasome in PC-3 cells in a dose-dependent manner, 50 $\mu\text{mol/L}$ TET has a significant inhibition of 70 % in 24 h, and the ubiquitinated proteins obviously accumulated, and TET induces the GFP level accumulated in PC-3-GFP-CL1 cells. These results suggest that TET is a potential proteasome inhibitor.

50 $\mu\text{mol/L}$ TET induces caspase-3 activated by 15-fold in 2 h, and lead to obvious apoptotic morphologic changes, which indicates the inhibition of TET to proteasome CT activity is associated with cell apoptosis.

Acknowledgments This work was supported by the National Natural Science Foundation (20977007), and Program for New Century Excellent Talents in University (NCET-11-0581).

References

1. Kwan CY, Achike FI (2002) Tetrandrine and related bis-benzylisoquinoline alkaloids from medicinal herbs: cardiovascular effects and mechanisms of action. *Acta Pharmacol Sin* 23(12):1057–1068
2. Choi HS, Kim HS, Min KR et al (2000) Anti-inflammatory effects of fangchinoline and tetrandrine. *J Ethnopharmacol* 69(2):173–179
3. Chen YJ (2002) Potential role of tetrandrine in cancer therapy. *Acta Pharmacol Sin* 23(12):1102–1106
4. Cheng Z, Wang K, Wei J et al (2010) Proteomic analysis of anti-tumor effects by tetrandrine treatment in HepG2 cells. *Phytomedicine* 17(13):1000–1005
5. Dong Y, Yang MM, Kwan CY (1997) In vitro inhibition of proliferation of HL-60 cells by tetrandrine and coriolus versicolor peptide derived from Chinese medicinal herbs. *Life Sci* 60(8):L135–L140
6. He BC, Gao JL, Zhang BQ et al (2011) Tetrandrine inhibits Wnt/beta-catenin signaling and suppresses tumor growth of human colorectal cancer. *Mol Pharmacol* 79(2):211–219
7. Lai YL, Chen YJ, Wu TY et al (1998) Induction of apoptosis in human leukemic U937 cells by tetrandrine. *Anticancer Drugs* 9(1):77–81
8. Jang BC, Lim KJ, Paik JH et al (2004) Tetrandrine-induced apoptosis is mediated by activation of caspases and PKC-delta in U937 cells. *Biochem Pharmacol* 67(10):1819–1829
9. Wang G, Lemos JR, Iadecola C (2004) Herbal alkaloid tetrandrine: from an ion channel blocker to inhibitor of tumor proliferation. *Trends Pharmacol Sci* 25(3):120–123
10. Liu C, Gong K, Mao X et al (2011) Tetrandrine induces apoptosis by activating reactive oxygen species and repressing akt activity in human hepatocellular carcinoma. *Int J Cancer* 129(6):1519–1531
11. Ciechanover A (1998) The ubiquitin-proteasome pathway: on protein death and cell life. *EMBO J* 17(24):7151–7160
12. Coux O, Tanaka K, Goldberg AL (1996) Structure and functions of the 20S and 26S proteasomes. *Annu Rev Biochem* 65:801–847
13. Almond JB, Cohen GM (2002) The proteasome: a novel target for cancer chemotherapy. *Leukemia* 16(4):433–443
14. Sun F, Anantharam V, Latchoumycandane C et al (2005) Dieldrin induces ubiquitin-proteasome dysfunction in alpha-synuclein overexpressing dopaminergic neuronal cells and enhances susceptibility to apoptotic cell death. *J Pharmacol Exp Ther* 315(1):69–79
15. Shi G, Chen D, Zhai G et al (2009) The proteasome is a molecular target of environmental toxic organotins. *Environ Health Persp*. 117(3):379
16. Sui XY, Liang XR, Hu YF et al (2012) The construction of a cellular model to monitor intracellular proteasome activity. *Adv Mater Res* 518:5586–5589
17. Gilon T, Chomsky O, Kulka RG (1998) Degradation signals for ubiquitin system proteolysis in *saccharomyces cerevisiae*. *EMBO J* 17(10):2759–2766
18. Link CD, Fonte V, Hiester B et al (2006) Conversion of green fluorescent protein into a toxic, aggregation-prone protein by C-terminal addition of a short peptide. *J Biol Chem* 281(3):1808–1816

19. Shi GQ, Sun Q, Yang HJ et al (2010) Molecular modeling for the interaction between proteasome beta 5 subunit and organotin compounds. *Sci China Chem* 53(11):2387–2393
20. Heinemeyer W, Fischer M, Krimmer T et al (1997) The active sites of the eukaryotic 20 S proteasome and their involvement in subunit precursor processing. *J Biol Chem* 272(40):25200–25209
21. An WG, Hwang SG, Trepel JB et al (2000) Protease inhibitor-induced apoptosis: accumulation of wt p53, p21WAF1/CIP1, and induction of apoptosis are independent markers of proteasome inhibition. *Leukemia* 14(7):1276–1283
22. Shinohara K, Tomioka M, Nakano H et al (1996) Apoptosis induction resulting from proteasome inhibition. *Biochem J.* 317(Pt 2):385–388

Chapter 75

The Purifying Effect of *Apocynum Venetum* Seedlings on Estuarine Water

Yangcang Xu, Tao Yu, Yunshan Zhong and Xiaoyan Wang

Abstract The water in Bohai Bay has become more and more eutrophic, causing a frequent red tide bloom. How to decrease eutrophication of this sea area is a pressing problem. The seawater often enters the estuary by flood tide, so the estuary may be a good place to remove eutrophic compounds from the seawater. This paper reported *apocynum venetum* seedlings growth status in water from Beitang estuary and its effects on nutrient removal. The results showed that *apocynum venetum* seedlings could grow both in flood tide water and in ebb tide water from Beitang estuarine, and the content of nitrogen and phosphorus in the water was significantly decreased by *apocynum venetum* seedlings, and the decrease level was largest for nitrite nitrogen in flood tide water. These results indicated that the eutrophic water in Bohai Bay was probably purified by *apocynum venetum* growing in ecological floating boat at estuarine.

Keywords *Apocynum venetum* · Beitang estuary · Eutrophication · Removal · Water quality

75.1 Introduction

The Bohai Bay is a semi-enclosed bay, located in the western region of Bohai Sea in northern China. Due to the poor self-purification and increasing pollution emission from land, pollution of the water body of Bohai Bay has become a

Y. Xu (✉) · T. Yu · Y. Zhong · X. Wang
College of Marine Science and Engineering, Tianjin University of Science and Technology,
Tianjin 300457, People's Republic of China
e-mail: xuyc@tust.edu.cn

Y. Xu
Tianjin Key Laboratory of Marine Resources and Chemistry, Tianjin 300457, People's
Republic of China

serious problem [1]. Eutrophication in seawater would often cause a red tide bloom [2]. There were several ways of purifying eutrophic water. Due to some special advantages, more attention has been paid to the ecological floating bed, gradually applied in the treatment of eutrophic water [3]. However, most studies have been focused on purifying eutrophic fresh water [4]. Is it possible to purify eutrophic seawater by ecological floating bed technology? The higher salinity in seawater, which inhibits the growth of many higher plants, restricts the technology application in this field. Estuaries are transition zones between freshwaters and seawater where large amounts of eutrophication compounds are discharged [5]. Therefore, the ecological floating bed technology may be applied in this zone. In this paper, we studied whether the *apocynum venetum* seedlings could grow in the medium of Beitang estuarine water and whether it could effectively remove the eutrophic compounds in this water.

75.2 Materials and Methods

75.2.1 Estuarine Water Collection and Treatment

The water samples were collected respectively during flood tide and ebb tide in June at Beitang estuarine of Tianjin, China. Then the water samples were filtered by cotton wool.

75.2.2 Plant Material and Growth Condition

The seeds of *apocynum venetum* were collected in the Binhai New Area, Tianjin, China. After sterilization by sodium hypochlorite, the seeds were germinated and cultured in a Hoagland solution. Seeds were allowed to germinate and develop in a controlled growth room. The growth chamber was set at relative humidity 50–80 %, day/night temperatures of 20/16 °C, 16 h photoperiod (350 mol quanta/m².s.P.A.R.) supplied by fluorescent lamps with tungsten supplement. After 15 d of growth, the seedlings were divided into three groups. One group was still cultured in the Hoagland solution, and another two groups were transplanted into the flood tide estuarine water, or the ebb tide estuarine water.

75.2.3 Water Quality Determination

The pH, salinity, conductivity, and dissolved oxygen in estuarine water were determined by water quality detector CX-401 (made by China).

75.2.4 Growth Rate Determination

The growth rate of the apocynum venetum seedlings was calculated by the variations of leaf length and the seedlings' dry weight.

75.2.5 The Phosphate Content was Analyzed by Ascorbic Acid-Molybdenum Blue Spectrophotometric Method [6]

75.2.6 Nitrate Nitrogen Content was Determined by Zinc and Cadmium Reduction Method [7]

75.2.7 Ammonium Nitrogen Content was Determined by a Salicylate Spectrophotometric Method [8]

75.2.8 Statistical Analysis

Data was analyzed by analysis of variance and Student's t test. The data shown were mean and standard deviation (S.D.) of five repetitive tests. The statistical significance for all tests was set at the $P \leq 0.05$ confidence level.

75.3 Results and Discussion

75.3.1 The Water Quality of Beitang Estuary

Beitang estuary is created where the Bohai Bay, the Yongdinghe River, the Newchaobaihe River, and the Jiyunhe River join together. There, the flood tide and ebb tide occurred daily. Table 75.1 showed that dissolved oxygen content was lower in flood tide water than that in ebb tide water, but the salinity and the

Table 75.1 The water quality in Beitang estuary (n = 5)

Sample	DO(mg/L)	SA(%)	CD(ms/cm)	pH
FT	3.85 ± 0.11	3.18 ± 0.13	49.6 ± 2.2	8.23 ± 0.11
ET	4.80 ± 0.21	2.80 ± 0.10	43.5 ± 1.6	8.10 ± 0.13

Note: DO: dissolved oxygen. SA: salinity. CD: conductivity. FT: flood tide, ET: ebb tide

Table 75.2 The nutrients in Beitang estuary (n = 5)

Sample	NN(mg/L)	AN(mg/L)	TP(mg/L)
FT	1.11 ± 0.09	0.47 ± 0.07	0.38 ± 0.09
ET	0.23 ± 0.11	0.41 ± 0.12	0.45 ± 0.11

Note: AN: ammonium nitrogen. NN: nitrate nitrogen. TP: total phosphate. FT: flood tide, ET: ebb tide

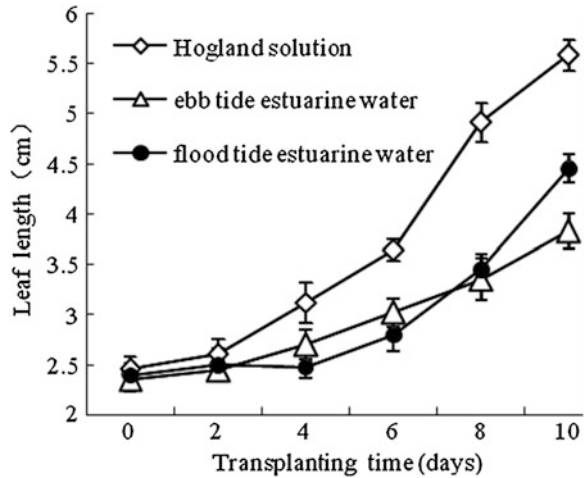
conductivity were higher in the former than that in the later. These results were consistent with those reported by Zhong [9]. There was no significant difference in the pH between the flood tide water and the ebb tide water.

Nitrogen and phosphorus were the main eutrophic component of water body [10]. Table 75.2 showed that nitrate nitrogen content was distinctly higher in the flood tide water than that in the ebb tide water, but there was no significant difference in ammonium nitrogen and phosphate content between flood tide water and ebb tide water. The flood tide water had more seawater than the ebb tide water [11]. The higher nitrate nitrogen in flood tide water indicated the nitrate nitrogen in the seawater of the Bohai Bay was higher than that in nearby rivers. The Bohai Bay is a semi-enclosed bay in which the water body exchange capacity with ocean water was poor [1]. However, About 1 billion tons of wastewater was discharged into the bay from Beijing, Tianjin, and Hebei Province every year [12]. Therefore, the eutrophic compounds such as nitrate from these rivers easily accumulated in the bay. This may be the main reason why the nitrate content in the seawater of the Bohai Bay was higher than that in nearby rivers.

75.3.2 *The Growth Status of Apocynum Venetum Seedlings in Beitang Estuarine Water*

Apocynum venetum was Apocynaceae perennial herb. It was widely distributed in the temperate zones of Eurasia and North America, especially in saline-alkali land, river banks, fluvial plains and sandy soils [13]. Considering its hostile environment, *apocynum venetum* is highly tolerant to salt and drought stress, and can resist strong winds and sands [14]. It could grow in the soil of pH 7.07–9.21 [15] and salt content 8.32 % [16]. The pH of the Beitang estuary water body varied

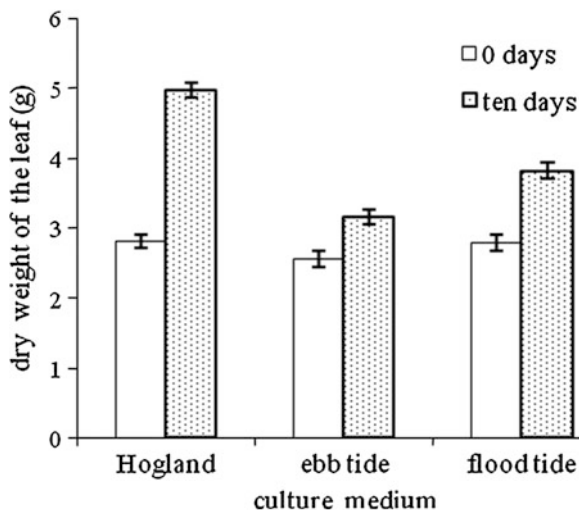
Fig. 75.1 The variation of the leaf length of apocynum venetum seedlings cultured in different medium



from 8.10 to 8.23 and the salinity varied from 2.80 ‰ to 3.18 ‰ (Table 75.1). It is therefore possible for apocynum venetum to grow in the Beitang estuary water body.

In order to prove the above view, a culture experiment was conducted. Fifteen day old apocynum venetum seedlings were divided into three groups, one group was still cultured in a Hogland solution, and another two groups were transplanted into flood tide estuarine water, or ebb tide estuarine water. From the 4th day, the length of leaves in the Hogland solution became longer than that in the other mediums (Fig. 75.1). And the leaf length had no significant change at first 3 days or first 6 days for the apocynum venetum seedlings that grew in the ebb tide water, or in the flood tide water respectively compared to that at day zero. The higher salinity in the flood tide estuarine water probably made the apocynum venetum seedlings have longer lag phase. On the tenth day, the leaf length cultured in the Hogland solution, the flood tide estuarine water, and the ebb tide estuarine water increased by 126.8, 85.4, and 63.0 %, respectively compared to that at day zero (Fig. 75.1). The dry weight of the apocynum venetum seedlings grown in different medium was also measured at day zero and the tenth day of transplanting. It was clear that the dry weight of the seedlings grown in the flood tide water was heavier than that in the ebb tide water (Fig. 75.2). After adapting to the new growth environment, the apocynum venetum seedlings grew quicker in the flood tide water than in the ebb tide water. This is probably ascribed to more inorganic nitrogen in the flood tide water than that in the ebb tide water (Table 75.1). The above results indicated that the apocynum venetum seedlings could grow both in flood tide estuarine water and in ebb tide estuarine water.

Fig. 75.2 The change of the dry weight of apocynum venetum seedlings cultured in different medium

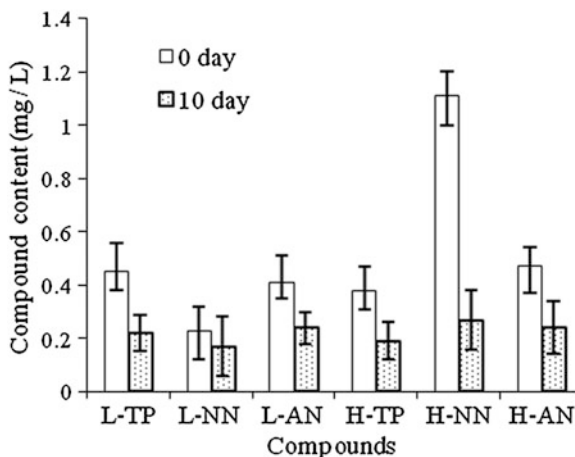


75.3.3 The Effect of Apocynum Venetum Seedlings Removing Inorganic Nitrogen Compounds and Phosphate in Beitang Estuarine Water

Fifteen day old apocynum venetum seedlings were transplanted into the Beitang estuarine water, and 10 days later, the nitrate nitrogen, ammonium nitrogen, and phosphate in medium were determined. The content of phosphate and ammonium nitrogen in the ebb tide estuarine water was decreased by 51.1 and 41.5 % respectively, but the nitrate nitrogen content had no significant change. The content of phosphate, ammonium nitrogen, and nitrate nitrogen in flood tide estuarine water was decreased by 50.0, 75.7, and 48.9 %, respectively by the apocynum venetum seedlings (Fig. 75.3). It indicated that the apocynum venetum seedlings effectively removed nitrogen and phosphate in the Beitang estuarine water body.

Eutrophication is one of the biggest environmental problems in enclosed water areas. The seawater in the Bohai Bay has become increasingly eutrophic during the past several years as a result of runoff from land-base agriculture, industrial, and other anthropogenic activities [17–20]. There are currently not many treatment methods for purifying eutrophic waters. Existing in situ methods such as precipitation of phosphorus have not been successful. Wetland treatments have been used for the removal of nutrients from eutrophic water, but their efficiency has not been proven for (phosphorous) P removal [21]. It has been shown that ecological floating bed effectively remove eutrophic matter in fresh water bodies [3]. Here, we found that salt-tolerant apocynum venetum seedlings also effectively removed eutrophic matter in estuarine water bodies in laboratory conditions. Hence, as long as the ecological floating bed is favorable to the estuarine environment, the apocynum venetum seedlings can grow in this bed and purify the eutrophic

Fig. 75.3 The variation of nutrient content in Beitang estuarine water after planting apocynum venetum seedlings. Note: TP, total phosphate. NN, nitrate nitrogen. AN, ammonium nitrogen. L, ebb tide estuarine water. H, flood tide estuarine water. L-TP means total phosphate in ebb tide estuarine water. The others were same



estuarine water. The estuarine water elevation often changed because of flood tide and ebb tide. Maybe an ecological floating boat would be favorable equipment for purifying eutrophic estuarine water.

75.4 Conclusion

The Bohai Bay is one of the most polluted sea areas in China. The main pollutants were inorganic nitrogen and phosphate [10]. How to control Bohai Bay pollution is a pressing problem. Apocynum venetum is perennial which is widely distributed in saline-alkali wasteland and has strong salt resistance. In this paper, we reported that apocynum venetum seedlings could grow in Beitang estuarine water with the salinity from 2.80 to 3.18 ‰ and the pH from 8.10 to 8.23. What is more, it could effectively remove nitrogen and phosphate in Beitang estuarine water. Therefore, it is possible that nitrogen and phosphate compounds in eutrophic water of the Bohai Bay are removed by apocynum venetum growing in ecological floating boat.

Acknowledgments This work was supported by the Foundation (No. 201102) of Tianjin Key Laboratory of Marine Resources and Chemistry (Tianjin University of Science and Technology), P. R. China and the Scientific Research Foundation for the Returned Overseas Chinese Scholars, State Education Ministry (the forty fourth times). We are grateful to Carlos Arboleda for revising the manuscript in writing.

References

1. Zhao X, Li D (2009) Pollution prediction of Bohai Sea basing on the BP neural network: taking example of Laizhou Bay. *Ecol Econ* 213:139–141 (in Chinese)

2. Lin FA, Lu XW, Luo H et al (2008) History, status and characteristics of red tide in Bohai Sea. *Mar Environ Sci* 27:S1–S5 (in Chinese)
3. Li M, Sun YK, Zhang JK (2010) The application research of ecological floating bed technology. *Ind Saf Environ Prot* 36:35–36 (in Chinese)
4. Zhan JX, Zhi CY, Xia PH (2011) Mechanism and research progresses of purification of wastewater with aquatic plants. *Southwest China J Agric Sci* 24:352–355 (in Chinese)
5. Waelles M, Tanguy V, Lespes G et al (2008) Behavior of colloidal trace metals (Cu, Pb and Cd) in estuarine waters: An approach using frontal ultrafiltration (UF) and stripping chronopotentiometric methods (SCP). *Estuar Coast Shelf Sci* 80:538–544
6. GB/T 12763.4–2007/9 (2011) The specification for oceanographic survey–Part 4: Observations of chemical parameters in sea water. Beijing: Chinese Standard Press (in Chinese)
7. Duan SW, Zhang S, Chen X (2000) Concentrations of nitrogen and phosphorus and nutrient transport to estuary of the Yangtze River. *Chin J Environ Sci* 21:53–56 (in Chinese)
8. Liu LB (2011) Comparison of determination method for ammonia-nitrogen content in water. *Guangzhou chem* 39:110–111 (in Chinese)
9. Zhong YC, Li YH, Zhang LG (1984) Preliminary ecological survey of zoology of the zooplanktons in the beitung estuary. *Acta Ecol Sinica* 4:393–400 (in Chinese)
10. Zhang ZF, He X, Zhang Z et al (2012) Eutrophication status, mechanism and its coupling effect with algae blooming in Bohai. *Mar Environ Sci* 31:465–483 (in Chinese)
11. Shen LJ, Chen DX, Huang HM (2009) Impact of reclamation project on the water exchange capacity of the estuaries in Wenzhou. *J Mar Sci* 27:72–76 (in Chinese)
12. Duan L, Song J, Li X et al (2010) Distribution of selenium and its relationship to the environment in Bohai Bay seawater. *Mar Chem* 121:87–99 (in Chinese)
13. Editorial Committee of the Flora of China of Chinese Academy of Science (1977) *Flora of China*. Science Press, Beijing (in Chinese)
14. Xie WY, Zhang XY, Wang T et al (2012) Botany, traditional uses, phytochemistry and pharmacology of *Apocynum venetum* L. (Luobuma): A review. *J Ethno Pharmacol* 141:1–8
15. Gao XH, Liu H, Liu SX et al (2002) Chemometrics analysis on the saline-alkali components of some main wild-hemp growing soils in Xingjia. *J Yunnan Univ* 24:218–222 (in Chinese)
16. Xi JB, Zhang FS, Mao DR et al (2003) The utilization of halophytes for traditional medicine in Xin jiang. *Rev China Agric Sci Technol* 5:43–48 (in Chinese)
17. Liu SG, Lou S, Kuang CP et al (2011) Water quality assessment by pollution-index method in the coastal waters of Hebei Province in western Bohai Sea, China. *Mar Pollut Bull* 62:2220–2229
18. Liu SM, Li LW, Zhang ZN (2011) Inventory of nutrients in the Bohai. *Cont Shelf Res* 31:1790–1797
19. Peng S, Dai M, Hu Y et al (2009) Long-term(1996–2006) variation of nitrogen and phosphorus and their spatial distributions in Tianjin Coastal Seawater. *Bull Environ Contam Toxicol* 83:416–421
20. Zhang J (1996) Nutrient elements in large Chinese estuaries. *Cont Shelf Res* 16:1023–1045
21. Inoue T, Fukue M, Mulligan CN et al (2009) In situ removal of contaminated suspended solids from a pond by filtration. *Ecol Eng* 35:1249–1254

Chapter 76

Expression, Purification, and Activity Assay of Chicken Interferon-Alpha

Yue Ma, Minhui Long and Aipo Diao

Abstract In this paper, Chicken alpha interferon (IFN- α) gene was cloned into pHis-NusA expression vector, then the recombinant expression vector was transformed into host bacteria *E. coli* BL21. The recombinant chicken IFN- α was induced to express by IPTG, then the protein expression was analyzed with SDS-PAGE. Under the condition that the recombinant protein was induced to express with 0.1 mM IPTG at 16 °C, the expressed protein was soluble. Recombinant Chicken IFN- α was purified by Ni-metal chelate affinity chromatography. The expressed protein was shown to inhibit the replication of Hand foot and mouth disease virus in vero cells.

Keywords Chicken interferon-alpha · Prokaryotic expression · Protein purification · Antiviral activity

76.1 Introduction

Interferon (IFN) belongs to a class of natural proteins that can inhibit virus replication [1, 2]. IFNs constitute a large group of cytokines that are best known for their ability to induce cellular resistance to viral pathogens. They also play a critical role in the response to microbial infections by modulating the innate and adaptive immune system. Furthermore, they are potent regulators of cell growth and have anti-inflammatory effects. IFNs are commonly grouped into two types, type I and type II. Type I IFNs form a still growing family of cytokines that comprises IFN- α , IFN- β [3–5]. Type II IFN is IFN- γ [6]. IFNs had already been characterized, and possess broad-spectrum antiviral activity [7–11].

Y. Ma · M. Long · A. Diao (✉)
College of Biotechnology, Tianjin University of Science and Technology,
Tianjin 300457, People's Republic of China
e-mail: diaoaiipo@tust.edu.cn

In this study, chicken alpha interferon (IFN- α) gene was cloned into pHis-NusA expression vector, then the recombinant expression vector was transformed into host bacteria *E. coli* BL21 [12]. The expressed protein was shown to inhibit replication of hand, foot, and mouth disease virus in vero cells.

76.2 Materials and Methods

76.2.1 Materials

76.2.1.1 Strains and Vector

E. coli TOP10 and BL21 (RILP) kept in our laboratory were used for cloning or expression host. The pHis-NusA vector was a gift from Dr. Eddie McKenzie (The University of Manchester, UK).

76.2.1.2 Virus, Cells and Enzymes

Hand, foot, and mouth disease virus and vero cell line were provided by the Academy of Military Medical Sciences of the Chinese PLA. PCR kit, restriction enzymes EcoR I and BamH I, T4 DNA ligase were purchased from Fermentas, Ni-charged resin was from GenScript.

76.2.2 Measurements

76.2.2.1 Construction of Recombinant Expression Vector pHis-NusA-chIFN- α

Chicken alpha interferon (IFN- α) gene (504 bp in length) was amplified by PCR and digested with restriction enzymes EcoR I and BamH I, ligated into the expression plasmid pHis-NusA and then transformed into *E. coli* TOP10-competent cells. Finally, the nucleotide sequences of the selected clones were confirmed by DNA sequencing. The positive clones with the correct sequence were named as pHis-NusA-chIFN- α .

76.2.2.2 Expression and Purification of chIFN- α

The recombinant plasmid pHis-NusA-chIFN- α was transformed into *E. coli* strain BL21(RILP) and plated on LB-agar supplemented with ampicillin and

chloramphenicol. The transformant was grown for 4 h at 37 °C in LB medium supplemented with ampicillin and chloramphenicol. When the OD₆₀₀ nm reached 0.6, 0.1 mM IPTG was added to induce expression of target protein with the incubation at 16 °C overnight. The cells were harvested by centrifugation at 4,000 rpm for 10 min at 4 °C, re-suspended in Na₂PO₃ lysis buffer (pH 8.0) and subjected to sonication with pulse 2 s and interval 9 s for 10 min. Then the lysate was centrifuged at 10,000 rpm for 10 min at 4 °C, the supernatant was collected and stored at 20 °C. A 12 % SDS-PAGE was engaged to detect the expression of target protein. The expressed protein was visualized by staining with Coomassie brilliant blue (CBB). The Ni-metal chelate affinity chromatography was used to purify recombinant protein His-NusA-chIFN- α [13, 14].

76.2.2.3 Bioactivity of Recombinant chIFN- α Against Hand, Foot, and Mouth Disease Virus

The antiviral activity of purified recombinant chIFN- α was assayed by its activity to inhibit the cytopathic effect caused by hand, foot, and mouth disease virus (HFMDV) in vero cells [15–17]. Vero cells were grown in DMEM high glucose supplemented with 10 % serum and seeded into 96-well plates (2 * 10⁵ cells/well) until the cells formed a compact monolayer after incubation for 12 h at 37 °C with 5 % CO₂ atmosphere environment. A ten-step serial dilution of recombinant chIFN- α was added into the cultures, and the dilutions were from 10¹ to 10⁷.

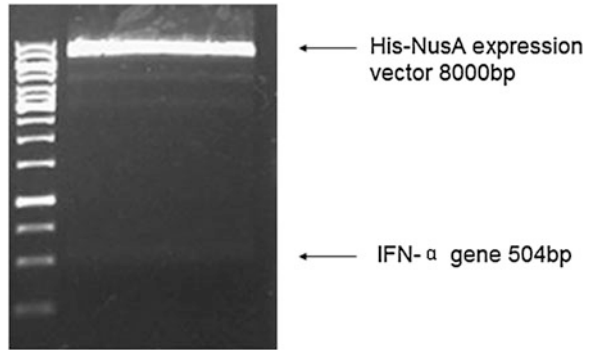
After 12 h incubation, the culture media were removed from the vero cells monolayer in 96-well plate and then vero cells were challenged with HFMDV of 100 TCID₅₀. Wells where the serial dilution (10¹–10⁷) of recombinant chIFN- α was added but without adding HFMDV were used as negative control, and wells where 100 TCID₅₀ HFMDV was added but without adding the recombinant chIFN- α were used as positive control. All cells in the 96-well plate were incubated under the above culture conditions of monolayer cells for 24 h. When pathological changes were formed by HFMDV in more than 50 % vero cells at positive control, the antiviral activity of the recombinant chIFN- α was determined in accordance with the proportion of the percentage cells with pathological changes to all the cells in the same well.

76.3 Results and Discussion

76.3.1 Cloning and Sequencing of pHis-NusA-chIFN- α

Chicken alpha interferon (IFN- α) gene was amplified by PCR, the complete IFN- α sequence consisted of 504 bp, the IFN- α gene fragment was digested with restriction enzymes EcoR I and BamH I, and inserted into the expression plasmid

Fig. 76.1 The pHis-NusA-chIFN- α was digested with restriction enzymes EcoR I and BamH I



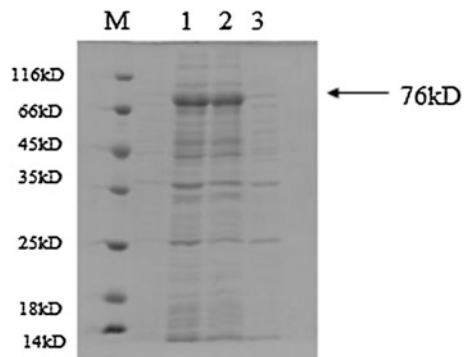
pHis-NusA, which was digested with the same restriction enzymes. As shown in Fig. 76.1, a specific DNA fragment about 504 bp was generated. The result of DNA sequencing showed that the chIFN- α gene was correctly inserted into the expression vector.

76.3.2 Expression and Purification of chIFN- α

Optimization of the expression conditions was performed to improve the expression of the soluble IFN- α protein in *E. coli*. To examine the temperature effect on IFN- α soluble expression, two groups of recombinants were cultured at 16 and 37 °C, respectively. The lysate was centrifugated at 10,000 rpm for 5 min, the pellet and supernatant were collected. T, P, S were indicated total protein of *E.coli*, protein in pellet, protein in supernatant, respectively.

As shown in Fig. 76.2, the recombinant protein was induced with 0.1 mM IPTG at 37 °C. A large amount of target protein at a molecular mass of approximately 76 kDa was generated, and the chIFN- α protein was mainly in the pellet.

Fig. 76.2 The recombinant protein was induced to express with 0.1 mM IPTG at 37 °C. M. protein marker (14/18/25/35/45/66/116kDa) 1. IFN- α -Total; 2. IFN- α - Pellet; 3. IFN- α - Supernatant



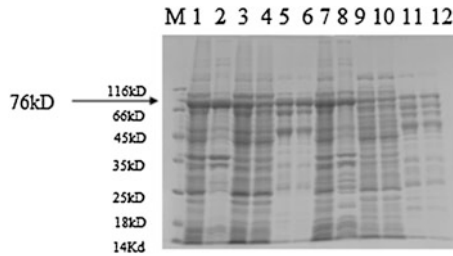


Fig. 76.3 Expression and purification of His-NusA-chIFN- α . The recombinant protein was induced with 0.1 mM IPTG and 0.5 mM IPTG at 16 °C. M. protein marker (14/18/25/35/45/66/116kDa). 0.1 mM IPTG induction: 1. IFN- α -Total, 2. IFN- α - Pellet, 3. IFN- α - Supernatant, 4. IFN- α -unbound, 5. IFN- α -E1 (Protein was eluted by eluting buffer with 250 mM imidazole), 6. IFN- α -E2 (Protein was eluted by eluting buffer with 500 mM imidazole) 0.5 mM IPTG induction, 7. IFN- α -Total, 8. IFN- α - Pellet, 9. IFN- α - Supernatant, 10. IFN- α -unbound, 11. IFN- α -E1 (Protein was eluted by eluting buffer with 250 mM imidazole), and 12. IFN- α -E2 (Protein was eluted by eluting buffer with 500 mM imidazole)

As shown in Fig. 76.3, the recombinant protein was induced with 0.1 mM IPTG at 16 °C, a large amount of target protein at a molecular mass of approximately 76 kDa was generated and it was soluble. Moreover, the protein expression level was higher with 0.1 mM IPTG than that with 0.5 mM IPTG. The Ni-metal chelate affinity chromatography was used to purify recombinant His-NusA-chIFN- α .

76.3.3 Antivirus Activity

To determine whether the recombinant chIFN- α could possess biological activity, the resistance of HFMDV reproduction in vero cells was evaluated using the CPE reduction method [18]. The concentration of chIFN- α was 0.99 mg/ml. According to the calculations of the Reed-Muench's methods, 100TCID₅₀ of HFMDV was $10^{-3.6}$. The vero cells in the positive control were destroyed more than 50 %, the treatment of recombinant chIFN- α could obviously inhibit the reproduction of HFMDV in vero cells [19, 20]. 100 % vero can be protected from 100TCID₅₀ of HFMDV attack when the concentration of chIFN- α was about 1.65×10^{-4} mg/ml (Fig. 76.4). 62.5 % vero can be protected from 100TCID₅₀ of HFMDV attack when the concentration of chIFN- α was about 1.65×10^{-5} mg/ml (Fig. 76.4). 12.5 % vero can be protected from 100TCID₅₀ of HFMDV attack when the concentration of chIFN- α was about 1.65×10^{-6} mg/ml (Fig. 76.4). Vero cells could not be protected from 100TCID₅₀ of HFMDV attack totally when the concentration of chIFN- α was about 1.65×10^{-7} mg/ml (Fig. 76.4). The results showed that chIFN- α had biological activity against HFMDV when the concentration of chIFN- α was about 9.28×10^{-6} mg/ml and the 100TCID₅₀ of HFMDV was $10^{-3.6}$.

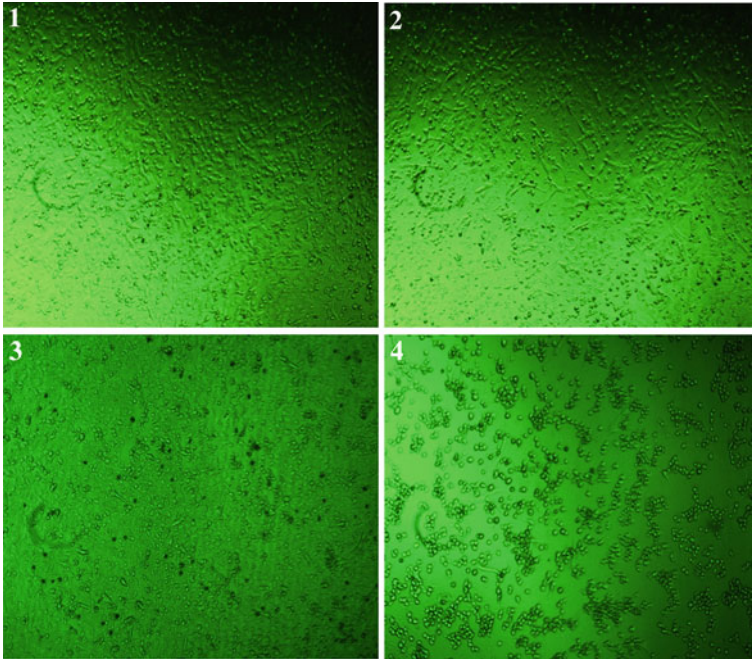


Fig. 76.4 The vero cells were protected from HFMDV by different concentrations of chIFN- α . 1. The concentration of chIFN- α is 1.65×10^{-4} mg/mL. 2. The concentration of chIFN- α is 1.65×10^{-5} mg/mL. 3. The concentration of chIFN- α is 1.65×10^{-6} mg/mL. 4. The concentration of chIFN- α is 1.65×10^{-7} mg/mL

76.4 Conclusion

In this study, the IFN- α was cloned into pHis-NusA expression vector, and the recombinant expression vector was transformed into host bacteria *E. coli* BL21. The recombinant chicken IFN- α was induced to express, and the molecular weight of the expressed protein is about 76 kDa. Under the condition that the recombinant protein was induced to express with 0.1 mM IPTG at 16 °C, the expressed protein was soluble. Recombinant ChIFN- α had biological activity against HFMDV when the concentration of chIFN- α was about 9.28×10^{-6} mg/ml and the 100TCID₅₀ of HFMDV was $10^{-3.6}$.

Acknowledgments This research is supported by the program for Changjiang Scholars and innovative Research Team in University (RIT1166).

References

1. Maeda S, Kawai T, Obinata M et al (1985) Production of human a-interferon in silkworm using a baculovirus vector. *Nature* 315:592–594
2. Smith GE, Summers MD, Fraser, et al (1983) Production of human b-interferon in insect cells infected with a baculovirus expression vector. *Mol Cell Biol* 3:2156–2165
3. Song KD, Lillehoj HS, Choi KD et al (1997) Expression and functional characterization of recombinant chicken interferon-gamma. *Vet Immunol Immunop* 58:321–333
4. Weining KC, Schultz U, Münster U, et al (1996) Biological properties of recombinant chicken interferon-g. *Eur J Immunol* 26:2440–2447
5. Matsuura Y, Tatsumi M, Enami K, et al (1991) Biological function of recombinant IL-6 expressed in a baculovirus system. *Lymphokine Cytokine Res* 10:201–205
6. Smith GE, Ju G, Ericson BL, Moschera J, Lahm H, Chizzonite R, Summers MD (1985) Modification and secretion of human interleukin-2 produced in insect cells by a baculovirus vector. *P Natl Acad Sci USA* 82:8404–8408
7. Mark G, David L, Bruce S, Janice C, Dennis A, Daniel J, Darrell R, Spackman E (2004) Development of a real-time reverse-transcription per for detection of newcastle disease virus rna in clinical samples. *J Clin Microbiol* 42:329–338
8. Ealick SE, Cook WJ, Vijay-Kumar S, Carson M, Nagabhushan TL, Trotta PL, Bugg CE (1991) Three-dimensional structure of recombinant human interferon-gamma. *Science* 252:698–702
9. Michael DR, Bryan SB, Francis VC (2004) Lambda interferon inhibits hepatitis B and C virus replication. *J Virol* 79:3851–3854
10. Wheelock EF (1965) Interferon-like virus-inhibitor induced in human leukocytes by phytohemagglutinin. *Science* 149:310–311
11. Wang LF, Baker ML (2011) Type III IFNs in pteropid bats: differential expression patterns provide evidence for distinct roles in antiviral immunity. *J Immunol* 186:3138–3147
12. Isaacs A, Lindenmann J (1957) Virus interference. I. the interferon. *P Roy Soc Lond* 147:258–267
13. Nakayama A, Yamamoto K, Tabata S (2000) High expression of glycosyltransferase enzyme in *Escherichia coli* and its competent purification method. *Protein Expres Purif* 19:298–303
14. Park TJ, Kim JS, Choi SS, Kim Y (2009) Cloning, expression, isotope labeling, purification, and characterization of bovine antimicrobial peptide, lactophorin in *E. coli*. *Protein Expres Purif* 65:23–29
15. Kadowaki N, Antonenko S, Lau JY, Liu YJ (2000) Natural interferon alpha/beta-producing cells link innate and adaptive immunity. *J Exp Med* 192:219–226
16. Lillehoj HS, Li GX (2004) Nitric oxide production by macrophages stimulated with *Coccidia* sporozoites, lipopolysaccharide, or interferon-gamma, and its dynamic changes in SC and TK strains of chickens infected with *Eimeria tenella*. *Avian Dis* 48:244–253
17. Meager A (2002) Biological assays for interferons. *J Immunol Methods* 261:21–36
18. Espion D, De Henau S, Letellier C, Wemers CD, Brasseur R, Young JF, Gross M, Rosenberg M, Meulemans G, Burny A (1987) Expression at the cell surface of native fusion protein of the Newcastle Disease Virus (NDV) strain Italian from cloned cDNA. *Arch Virol* 95:79–95
19. Carr DJ, Alkhatib K, James CM, Silverman R (2003) Interferon-b suppresses herpes simplex virus type I replication in trigeminal ganglion cells through an Rnase L-dependent pathway. *J Neuroimmunol* 141:40–46
20. Koyama AH, Arakama T, Adachi A (1999) Comparison of an antiviral activity of recombinant consensus interferon with recombinant interferon-alpha-2b. *Microbes and Infect* 1:1073–1077

Chapter 77

Synthesis and Controlled Release of 5-Fluorouracil from Hydroxyethylchitosan: Based Polymer Prodrug

Yanfei Peng, Wanshun Liu, Baoqin Han and Ruixue Zhou

Abstract A novel water-soluble hydroxyethylchitosan-based polymer prodrug of 5-fluorouracil (HECS-5-Fu) was synthesized through acetyl spacer via ester bond. The conjugated content of 5-Fu was 12.2 % (w). In phosphate buffer solution (pH 7.4) at 37 °C, HECS-5-Fu slowly hydrolyzed to release 5-fluorouracil-1-yl acetic acid as characterized by RP-HPLC and LC-MS. The controlled release of drug from HECS-5-Fu powder sustained for more than 25 days. The in vitro experiment indicated that 5-fluorouracil-1-yl-acetic acid at concentration of 400 ug/mL inhibited the proliferation of about 40.0 % mouse fibroblast cell line L929. HECS-5-Fu could have a potential application as an antimetabolic material in glaucoma filtration device implantation.

Keywords Hydroxyethyl chitosan · 5-Fluorouracil · Prodrug · Release · Fibroblast

77.1 Introduction

5-fluorouracil (5-Fu), as an antimetabolite has shown significant antitumor activities. However, its short plasma circulation half-life, serious systemic toxicities, and poor tumor-targeting make it important to screen out more clinically efficient derivatives of 5-Fu, alternatively to prepare controlled and site-specific drug release system.

Polymer materials like peptides, polysaccharides, and other natural products have recently attracted much attention as biodegradable drug carriers. A variety of macromolecular prodrugs of 5-Fu have been developed [1]. In most cases, the bioactivities are due to the free 5-Fu released by a nonspecific chemical hydrolysis

Y. Peng (✉) · W. Liu · B. Han · R. Zhou
College of Marine Life Sciences, Ocean University of China, Qingdao 266003, China
e-mail: yanfeipeng@ouc.edu.cn

of the ester, carbamate, amide bonds between the drug and the polymer backbone [2–5]. 5-Fu-polymer conjugates have also been reported to be able to provide site-specific release of 5-Fu by a step-wise enzymatic and chemical cleavage of chemical bonds under the environmental conditions of target cells [6, 7].

Chitosan and its water-soluble derivatives have been extensively used in developing drug release systems in view of their good biocompatibility, biodegradability, nontoxicity, antibacterial, antitumor, and other bioactivities. Many reports are available on preparation of chitosan-based drug capsules, microspheres, nanoparticles, beads, gels, and films. Chitosan prodrug, in which drug is covalently linked onto chitosan chain has been found to be bioactive in the field of anti-bacteria, anticancer, and antioxidant [8]. Our previous studies show that a blend membrane based on hydroxyethylchitosan (HECS) has good biodegradability and histocompatibility, and can potentially be used as a carrier for corneal endothelial cell transplantation [9, 10]. A novel drug loaded membrane made of N-succinyl-hydroxyethyl chitosan and mitomycin C could inhibit efficiently the in vitro proliferation of fibroblast cell L929 [11]. In an effort to decrease the side effects and potential danger of 5-Fu, and meanwhile prolong the useful life of filtering bleb following trabeculectomy, we reported here a novel synthesis and controlled release of conjugated 5-Fu from HECS prodrug. The inhibitory effect of the released substance against fibroblast cell was evaluated in vitro.

77.2 Materials and Methods

77.2.1 Materials and Reagents

5-Fluorouracil was purchased from Beijing Chemical Reagents Company (Beijing, China). Chloroacetyl chloride and N-methylpyrrolidone (NMP) were purchased from Shanghai Medpep Co., Ltd. (Shanghai, China). 3-(4,5-dimethylthiazol-2-yl)-2,5-diphenyltetrazolium bromide (MTT) was purchased from Sigma Chemical Co.(USA). Materials for cell culture including Dulbecco's Modified Eagle Medium (DMEM), fetal bovine serum (FBS), penicillin and streptomycin were from Gibco Co (USA). Tissue culture flasks and 96-well plates were obtained from Corning Co. (USA). All other chemicals and reagents were commercially available and used as received.

77.2.2 Synthesis of Hydroxyethylchitosan -5-Fu Conjugate (HECS-5-Fu)

Hydroxyethylchitosan (HECS) with molecular weight of 12.5×10^4 and substitution degree of 3.0 was synthesized in our laboratory for the following experiment.

1.0 g HECS was dissolved in 40 mL N-methylpyrrolidone, and 0.8 mL chloroacetyl chloride was added droplet to the solution in an ice-bath. The mixture was then kept stirring at room temperature for 3 h. The chloroacetylated HECS (Cl-HECS, 1.5 g) was obtained by ether precipitation, anhydrous alcohol washing, and vacuum drying. Then 1.0 g chloroacetylated HECS was dissolved in 30 mL re-stilled dimethylsulfoxide, 0.9 g 5-Fu and 0.7 mL triethylamine were added. The whole solution was kept in 50 °C for 24 h under stirring. After that, 60 mL acetone was poured into, and the resultant precipitate was collected, washed with alcohol, and dried in vacuum. 0.9 g HECS-5-Fu conjugate (HECS-5-Fu) was obtained as a white powder.

5-fluorouracil-1-acetic acid (5-FuAA) was prepared according to the method reported previously [12].

The content of 5-Fu in HECS-5-Fu was 12.7 % as determined by measuring the amount of 5-Fu-1-acetic acid released from the conjugate placed in 2.0 mol/L NaOH solution for 2 h at 40 °C, and the unconjugated 5-Fu was 0.5 % by measuring the amount of 5-Fu released in distilled water in parallel [13, 14].

77.2.3 Characterization

UV–Vis absorption spectra were recorded with Tu-1800 UV–Vis spectrophotometer (PGeneral, Beijing, China) between 190 and 400 nm. The infrared spectra (KBr pellets) were recorded on Nicolet NEXUE470 FTIR in a range of 400–4,000 cm^{-1} . HPLC profiles of the released medium collected in intervals were determined on a Shimadzu LC-10A HPLC system equipped with a Waters Symmetry C18 column (2.1 mm \times 100 mm, 3.5 μm) and a SPD-10A UV detector at 266 nm at 30 °C. The mobile phase was water: methanol 98:2 (v/v) with a flow rate of 0.3 mL/min. LC–MS analyses of the released medium collected in the first week were done with a Micromass LCT time-of-flight mass spectrometer equipped with an electro-spray ionization source.

77.2.4 In Vitro Release Studies

The in vitro release was carried out in a sealed plastic tube at 37 °C in phosphate buffer (pH 7.4) solution. HPCS-5-Fu powders (100 mg) were suspended in 7.0 mL of release medium and stirred at 100 rpm. At each selected time, the mixture was firstly centrifuged at 10,000 rpm for 10 min, and then 5.0 mL of the supernatant was removed and replaced by the same volume of fresh medium. The amount of 5-FuAA in the samples withdrawn was determined with an UV spectrometer at 274 nm as compared with the standard curve of 5-FuAA. The release experiment was performed in triplicate. The curve of cumulative percent drug release as a function of time was plotted.

77.2.5 In Vitro Effect on the Growth of Mouse Fibroblast Cell Line L929

L929 cell line were cultured in DMEM supplemented with 10 % (v/v) fetal bovine serum, 1 % penicillin and streptomycin solution. Cells seeded at 4×10^3 cells per well (96-well culture plates) were maintained at 37 °C in a humidified incubator with 5 % CO₂ atmosphere for 24 h, the culture medium was removed, fresh medium (200 μL/well, control group), or 5-Fu (200 μL/well, prepared in cultural medium at a final concentration of 20, 10, 5, and 2.5 ug/mL), or 5-FuAA (200 μL/well, prepared in cultural media at a final concentration of 400, 200, 100, and 50 ug/mL) was then added. The plate was returned for incubation for 72 h. Cytotoxicity of samples was evaluated by the 3-(4, 5-dimethylthiazole-2-yl)-2, 5-diphenyltetrazolium bromide (MTT) assay. The in vitro inhibition ratio was calculated with the following formula:

Inhibition ratio = $(\text{ODO} - \text{ODS}) / (\text{ODO} - \text{ODC}) \times 100\%$, where ODO, ODS, and ODC were the average OD value at 490 nm of five wells in parallel of the control (with the cultural medium), sample treated group and the blank (without cell), respectively.

77.3 Result and Discussion

77.3.1 Synthesis of HECS-5-Fu

Based on the good solubility of HECS in N-methylpyrrolidone, a mild reaction route for chloroacylation of HECS was developed in this report. Figure 77.1 shows the FTIR of HECS and HECS-5-Fu conjugate. In the IR spectrum of the HECS, both the OH groups at C-6 and C-3 and the NH₂ group of chitosan were hydroxyethyl substituted in view of the disappearance of the absorption peaks at 1,030 and 1,160 cm⁻¹ and the weakening at 1,599 cm⁻¹. As for HECS-5-Fu conjugate, new signal at 1247 cm⁻¹ assigned to the stretching vibration of C–N of 5-Fu appeared, and the νC = O moved to 1,670 cm⁻¹ due to the covalent conjugation of 5-Fu into HECS. The peak at 1,747 (C = O) and 771 cm⁻¹ (C–Cl) indicated not all the C–Cl group of chloroacetylated HECS reacted with 5-Fu.

77.3.2 Structure of the Released Substance

During the in vitro release experiment, it was found that the peak absorption in UV spectra of released medium moved from the initial 265 nm to 274 nm. From the HPLC profiles (Fig. 77.2) of the released medium collected in different time interval, it was obvious that the released substances were firstly a mixture,

Fig. 77.1 FTIR spectra of HECS and HECS-5-Fu conjugate

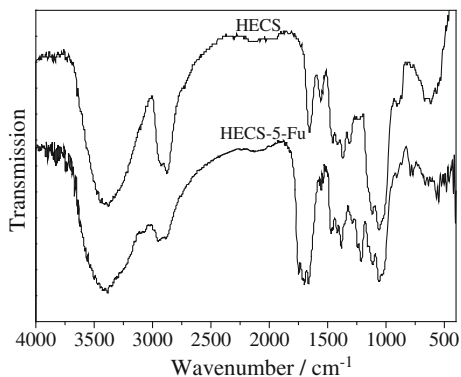
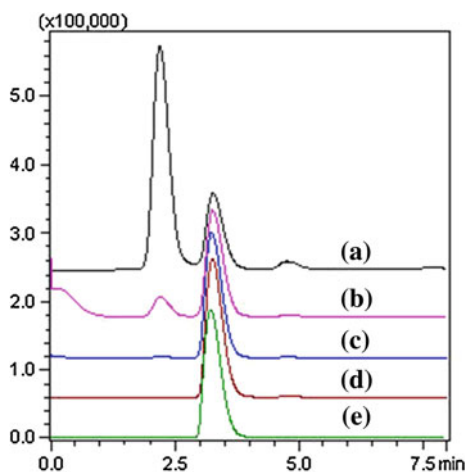


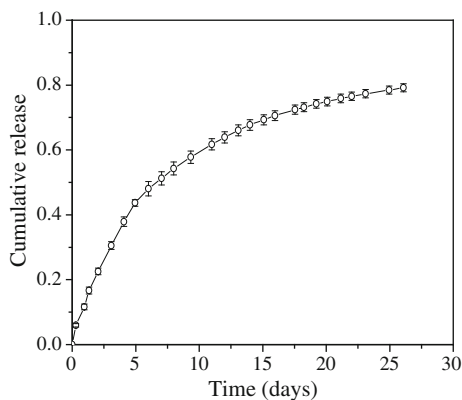
Fig. 77.2 HPLC profiles of the released medium collected in the first day **a**, the 2-7 days **b**, the second week **c**, the third week, and **d** the fourth week **e**



followed by a pure molecule, implying that chemical conjugation of HECS and 5-Fu could make changes of the released target substance.

To determine the structure of the molecules released, released sample collected in the first week was analyzed by ESI-Q-TOFMS/MS. The first eluted substance with $[M + H]^+$ of 131 was proved to be 5-Fu, and the second one to be 5-Fu-1-yl-acetic acid (5-FuAA). It means that HECS-5-Fu conjugate released were no longer pure 5-Fu but a mixture of 5-Fu and its derivatives. 5-Fu released in the beginning might be those unconjugated, and just being embedded during the precipitation of HPES-5-Fu from the reaction solution, while the conjugated 5-Fu released existed as 5-FuAA. It was reported that the release of 5-Fu from conjugates was strongly dependent on the pH of the dissolution medium [15]. The ester bond linking 5-Fu and HECS were firstly broken down to release 5-FuAA, which could be further hydrolyzed to give 5-Fu quickly in alkali solution, while remained unchanged in neutral and acidic environment. Therefore, 5-FuAA was released in the slightly basic medium as we chose.

Fig. 77.3 The release profile of HECS-5-Fu conjugate in phosphate buffer (pH 7.4) at 37 °C



77.3.3 Release Behavior of HECS-5-Fu Conjugate

The release profile of 5-Fu from the conjugate in PBS medium was shown in Fig. 77.3. The conjugate was quiet stable and gave a slow and steady release of 5-FuAA in 26 days we followed. There was not a phenomenon of burst-release usually observed in the initial period. The cumulative release was 43 % in the first 5 days and reached to 73 % in 22 days.

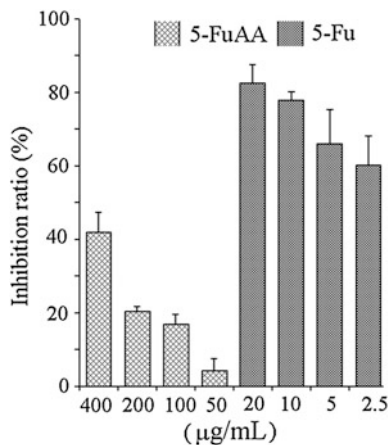
Mechanism for controlled release of bioactive agents from polymer matrices has been well described in literature, suggesting the erosion, diffusion and swelling followed by diffusion, etc. [16, 17]. In case of in vitro release of HECS-5-Fu conjugate, the water-insoluble nature of the conjugate might govern the release pattern. Although HECS adopted was originally hydrophilic and water-soluble, while after chloroacetylation it could form crosslink as a result of the side reactions between violable groups ($-\text{OH}$, $-\text{NH}_2$) and the adjacent chloracetyl group in the polymer chain. The conjugate firstly swelled in the slightly alkali medium, the release was swelling-controlled. After the achievement of swelling equilibrium, the release turned to a diffusion-controlled mechanism. The swelled particles served as a reservoir for drug release.

77.3.4 Inhibitory Effect on the Proliferation of Mouse Fibroblast Cell L-929

It has been reported that 5-FuAA could efficiently inhibit the in vitro proliferation of several tumor cells including leukemia cells, sarcoma 180, hepatic carcinoma and ehrlich ascites tumor [18]. 5-FuAA as the main released substance from HECS-5-Fu conjugate, its antimetabolite effect had to be evaluated firstly.

The effect of 5-FuAA and 5-Fu on the proliferation of mouse fibroblast cell L-929 was shown in Fig. 77.4. Obviously, 5-Fu at a concentration of 20–2.5 $\mu\text{g}/\text{mL}$ could

Fig. 77.4 Effect of 5-FuAA and 5-Fu on the proliferation of mouse fibroblast cell L929



inhibit the proliferation of over 60.0 % fibroblast. As for 5-FuAA, the efficient concentration was much higher than 5-Fu. When 400 ug/mL of 5-FuAA was employed, the inhibition ratio reached to be 42.0 %. Therefore, higher concentration of 5-FuAA must be provided for efficient anti-proliferation of fibroblast cells at the target site, especially in the first two weeks after trabeculectomy. This, however, could be fulfilled due to the relative high 5-Fu content (12.7 %) and good release efficiency of HECS-5-Fu. The unconjugated 5-Fu, which was released from HECS-5-Fu in the beginning, could be another kind of help for the whole inhibition against fibroblast cells.

Due to the effect of possible inflammatory effect of implanted material on drug release from conjugate, the exact antimetabolite effect of HECS-5-Fu conjugate needs to be checked in animal models in future.

77.4 Conclusion

In this study, a novel 5-Fu prodrug based on hydroxyethyl chitosan was synthesized. In phosphate buffer solution, the HECS-5-Fu conjugate released 5-FuAA, and a small amount of 5-Fu at the beginning. The controlled drug release could sustain more than 25 days. Although less efficient than 5-Fu, 5-FuAA could inhibit the in vitro proliferation of mouse fibroblast cell L-929 when higher concentration was employed. The relative high drug loading, sustained release in long period and good release efficiency made HECS-5-Fu conjugate a potential site specific anti-metabolite material in glaucoma filtration device implantation.

Acknowledgments This work was financially supported by the National Natural Sciences Foundation of China (No.30800193). Dr. Joensuu Päivi from University of Oulu is appreciated for the expert help with mass spectrometry.

References

1. Nichifora M, Schachta EH, Seymour LW (1997) Polymeric prodrugs of 5-fluorouracil. *J Control Release* 48:165–178
2. Akashi M, Takemoto K (1990) New aspects of polymer drugs. *Adv Polymer Sci* 97:108–146
3. Ouchi T, Fujino A, Tanaka K et al (1990) Synthesis and antitumor activity of conjugates of poly(α -malic acid) and 5-fluorouracil bound via ester, amide or carbamoyl bonds. *J Control Release* 12:143–153
4. Ouchi T, Hagihara Y, Takahashi K et al (1992) Synthesis and anti-tumor activity of poly(ethylene glycol)s linked to 5-fluorouracil via urethane or urea bonds. *Drug Design Disc* 9:93–105
5. Ouchi T, Banba T, Matsumoto T et al (1990) Synthesis and anti-tumor activity of conjugates of 5-fluorouracil and chito-oligosaccharides involving a hexamethylene spacer group and carbamoyl bonds. *Drug Design Del* 6:281–287
6. Bundgaard H (1989) The double prodrug concept and its application. *Adv Drug Del Rev* 3:39–65
7. Amsberry KL, Borchardt RT (1991) Amine prodrugs which utilise hydroxy amide lactonization. I. a potential redox-sensitive amide prodrug. *Pharm Res* 8:323–330
8. Vinsovam J, Vavrikova E (2008) Recent advances in drugs and prodrugs design of chitosan. *Curr Pharm Design* 14:1311–1326
9. Liang Y, Liu W, Han B et al (2011) Fabrication and characters of a corneal endothelial cells scaffold based on chitosan. *J Mater Sci Mater Med* 22:175–183
10. Liang Y, Liu W, Han B et al (2011) An in situ formed biodegradable hydrogel for reconstruction of the corneal endothelium. *Colloid Surface B* 82:1–7
11. Li M, Han B, Liu W (2011) Preparation and properties of a drug release membrane of mitomycin C with N-succinyl-hydroxyethyl chitosan. *J Mater Sci Mater Med* 22:2745–2755
12. Udo K, Hokonohara K, Motoyama K et al (2010) 5-Fluorouracil acetic acid/beta-cyclodextrin conjugates: drug release behavior in enzymatic and rat cecal media. *Int J Pharm* 388:95–100
13. Wang Q, Liu X, Liu L et al (2007) Synthesis and evaluation of the 5-fluorouracil- pectin conjugate targeted at the colon. *Med Chem Res* 16:370–379
14. Luo Q, Wang P, Miao Y et al (2012) A novel 5-fluorouracil prodrug using hydroxyethylstarch as a macromolecular carrier for sustained release. *Carbohydr Polym* 87:2642–2647
15. Zhang Z, Zhang Q, Wang J (2010) Synthesis and drug release in vitro of porphyran carrying 5-fluorouracil. *Carbohydr Polym* 79:628–632
16. Peppas L (1997) Polymers in controlled drug delivery. *Med Plast Biomater* 4:34–44
17. Prabakaran M, Reis R, Mano J (2007) Carboxymethyl chitosan-graft-phosphatidylethanolamine: amphiphilic matrices for controlled drug delivery. *React & Funct Polym* 67:43–52
18. Yang Z, Wang L, Yang X et al (2000) Pharmacological study on antitumor activity of 5-fluorouracil 1-acetic acid and its rare earth complexes. *J Rare Earth* 18:140–143

Chapter 78

Telomerase is Significant as an Early Diagnostic Marker and Therapeutic Target

Lian Duan, Nan Wang, Xinghua Liao, Jun Zhou, Dalin lu, Jiajie Liu, Xueguang Sun and Tong-Cun Zhang

Abstract Breast cancer, a hormone-dependence disease, is the most common malignant tumor in women. Breast cancer incidence rates increase with age. Telomerase is a ribonucleoprotein that maintains chromosome ends and endows cells with unlimited proliferative potential. Activation of telomerase maintains a relatively stable telomere length, confers immortality on some cells, and may even lead to cancer. It has been reported that, in the tissues of the breast, the activity of telomerase can be detected in more than 90 % of invasive breast cancers, while not in adjacent normal tissues. Thus, telomerase activation plays a critical role in development of breast cancer. Telomerase has been proposed as a biomarker with diagnostic and prognostic potential in breast cancer as well as a basis for the targeted therapy of breast cancer.

Keywords Breast cancer · Telomerase · Chromosome ends · Telomere

This work was financially supported by National Natural Science Foundation of China (No.30970615,31071126) and Program for Changjiang Scholars and Innovative Research Team in University Education of China (IRT1166) and the Key Project of Chinese Ministry of Education (212010) and Outstanding Young Talent Project of Scientific Research Plan of Education Department in Hubei province (Q20101111).

L. Duan · X. Liao · J. Zhou · D. lu · J. Liu · T.-C. Zhang (✉)
College of Medicine, Wuhan University of Science and Technology, Wuhan 430065,
People's Republic of China
e-mail: tony@tust.edu.cn

N. Wang · X. Liao · X. Sun · T.-C. Zhang
Key Laboratory of Industrial Microbiology, Ministry of Education and Tianjin City,
College of Biotechnology, Tianjin University of Science and Technology,
Tianjin 300457, People's Republic of China

78.1 Introduction

Breast cancer, a most common cancer mainly diagnosed in women, is the second leading cause of death in the world. In 2008, breast cancer caused 458,503 deaths worldwide (13.7 % of cancer deaths in women); this is due to difficulty in diagnosing at an early stage. Despite the improvements in diagnostic imaging techniques such as computed tomography, magnetic resonance imaging, etc., the early diagnosis of breast cancer is still difficult. Some reports indicate that telomerase activity play a crucial role in cellular senescence and tumor initiation. So, the detection of telomerase activity has been proposed to be a useful tool in the diagnosis of pancreatic cancer.

Telomerase is a ribonucleoprotein enzyme that specifically restores telomere sequences lost during replication by means of activity the catalytic subunit of human telomerase reverse transcriptase (hTERT), and a telomerase RNA template (hTR) [1]. It is activated in most immortal cell lines and in most malignant tumors that is detected in 85–90 % of human cancer specimens. Telomerase activity is found in breast cancer and pre-invasive lesions of the breast, such as ductal carcinoma in situ (DCIS), suggesting that telomerase activity is activated early in breast carcinogenesis [2]. Since telomerase activity is present in a vast majority of human cancers, it might have a role in the diagnosis and treatment of cancer. In this paper, we mainly review the relationship between telomerase and early diagnosis and therapy of breast cancer.

78.2 Function and Structure of the Telomeres and Telomerase

The ends of linear eukaryotic chromosomes contain specialized structures called telomeres. In humans, telomeres consist of long and repeated TTAGGG sequence, which are associated with a variety of telomere-binding proteins. Telomere DNA is dynamic, being progressively lost with each cell division due to incomplete replication of the termini of linear DNA molecule [3]. After a finite number of replications, the telomere reaches a critical length, and in turn induces replicative senescence [4].

Recently, some researchers find that telomere integrity and function need to bind to telomere response protein, such as telomeric repeat binding factor 1 (TRF1) and telomeric repeat binding factor 2 (TRF2) [5]. TRF1 is a negative regulator of telomere length. Early reports indicated that overexpression of wild-type TRF1 will decrease telomere length, whereas overexpression of mutant TRF1 will lead to telomere elongation. TRF2 also plays an important role in chromosome stabilization. Recent studies have found that overexpression of mutant TRF2 leads to the loss of TRF2 bound at the telomere, induction of the p53-dependent damage pathway, end fusion, and growth arrest as in replication senescence [6, 7].

Although other mechanisms to maintain telomere stability are possible, the mechanism for lengthening telomeres in humans is almost always by the reactivation or upregulation of telomerase. It consists of two core function components hTERT and hTR. These components jointly form the telomerase active site. hTR contributes by binding the telomere end and acts as template for polymerization, while hTERT catalyzes the addition of telomeric repeat [8].¹ Telomerase functions include addition of telomeric repeats, stabilization and maintenance of telomere length, overall spatial orientation, structural integrity, and stability of the chromosome [9]. It is only expressed in a small number of proliferating cell types, such as germ line and somatic stem cells. Most normal human cells lack telomerase activity and their telomeres shorten with each cell division, until they enter replicative senescence. Cells that lose critical cell-cycle checkpoint functions escape this initial growth arrest and divide until they enter crisis when chromosome end fusions and apoptosis occur. Cells remain in this crisis period acquires telomerase expression, that can maintain telomeres is then able to grow continuously (i.e., becomes immortal) and this is generally believed to be a critical step toward cancer progression [10].

78.3 Effects of Telomerase Activity in Breast Cancer

Regulation of telomerase activity during normal cell development and tumorigenesis is highly important in setting cell proliferative lifespan. A number of mechanisms have been revealed to regulate telomerase activity that includes gene transcriptional regulation, alternative splicing, and post-translational modifications of hTERT. The tight correlation between hTERT mRNA expression and telomerase activity in cells suggests that transcriptional regulation of hTERT is one of the primary regulatory mechanisms in regulating telomerase activity. Characterization of the hTERT gene promoter has revealed a number of potential sites for transcriptional regulation, including two typical E-boxes and several GC-boxes for the transcription factors c-Myc and Sp1, respectively. Especially an imperfect estrogen response element (ERE) has also been identified within the hTERT promoter, providing a platform for action of the sex steroid hormone estrogen with estrogen receptor (ER) in regulating hTERT gene transcription and cell proliferative lifespan [11].

Breast cancer is an estrogen-dependent disease. Studies *in vitro* show that estrogen can upregulate the hTERT gene expression and telomerase activity in MCF-7 cells, further studies suggest the imperfect palindromic ERE (GGTCAGGCT-GATC) at -2677 of the hTERT gene promoter (differing from the consensus sequence by one nucleotide (GGTCAN3TGACC)). Deletion of this ERE dramatically reduces estrogen-induced activation of telomerase. Interestingly, mutation of

¹ Tong-cun Zhang: E-mail: tony@tust.edu.cn

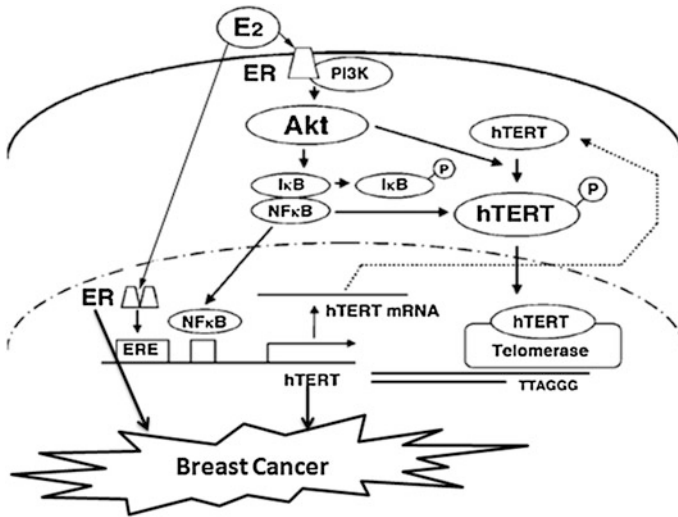


Fig. 78.1 Schematic model. In breast cancer, estrogen can promote the upregulation of telomerase activity directly through binding to both nuclear and nonnuclear ER signal transduction that activated Akt pathway

two c-Myc binding sites located within the proximal 181 bp region completely blocks estrogen activation of telomerase activity. These findings suggest that estrogen-responsive element is responsible for transcriptional activation by ligand-activated ER and c-Myc/Max play additional roles in estrogen-induced transactivation of hTERT [12]. The recent study shows that the activation of telomerase induced by estrogen is due not only to transcriptional regulation of hTERT via an ERE-dependent mechanism and a PI3 K/Akt/NF- κ B cascade, but also to post-translational regulation via phosphorylation of hTERT and association with NF- κ B in MCF-7 cells (Fig. 78.1), that is also true of the mechanism by which cytokines modulate telomerase activity.

78.4 Telomerase: A Diagnostic Marker in Breast Cancer

There were multiple methods to detect telomerase in the breast cancer tissue. The telomere repeat amplification protocol (TRAP) assay usually has detected telomerase activity. This sensitive polymerase chain reaction (PCR)-based assay can detect as few as 1–10 positive cells or 0.01 % positive cells in a mixed population. Kaori Saito et al. examined 38 breast cancer samples and 16 noncancerous breast samples by TRAP that detected telomerase activity in 65.8 % (25/38) of breast cancers, but no telomerase activity in any noncancerous sample [13]. He Guoping detected telomerase activity in 47 of the 52 breast cancer samples (93.8 %), in 15

of 52 adjacent nonmalignant breast tissues (28.85 %) and in 10 of the 32 benign lesions (31.25 %), but no activity was detected all of 14 normal mammary gland tissues [14]. Expression of the hTERT mRNA can also be detected using real-time reverse transcription polymerase chain reaction (RT-PCR). Mohammad et al. measured the mRNA of hTERT in 65 breast cancer patients, and found that 53 (81.54 %) patients exhibited hTERT expression positive and 12 (18.46 %) exhibited expression negative [15]. AE Elkak also tested the expression of hTERT protein by immunohistochemical and confirmed that hTERT expression was positive in 27 (71 %) of 38 tumors [16].

With the increasing number of breast cancers detected by screening procedures, a marker is needed to stratify the risk of subsequent invasive cancer. Blanca Murillo et al. found a significant correlation between telomerase activity and tumor size, lymph node status, and stage. Specially, they found a significant correlation between low levels of telomerase activity and a lack of ER β expression ($p = 0.03$), while telomerase activity was not related to ER α expression ($p = 0.61$) [17]. A significant association between telomerase-positive infiltrating breast carcinomas and lymphovascular invasion, a fundamental step in breast cancer metastasis and a predictor of survival, has also been observed, making telomerase a useful prognostic marker [18].

These assays provide highly sensitive methods for breast cancer diagnosis, but have limitation. Consequently, for the diagnosis of breast cancer, these biomarkers should be combined with other diagnostic technology to avoid false-positive and false-negative results, and better tumor grade and tumor classification can be given. Based on these results, reasonable therapeutic schedule is designed.

78.5 Telomerase: A Potential Therapeutic Target in Breast Cancer

The average telomere length in breast cancer cells is usually well below that of normal cells. Furthermore, most stem cells are quiescent, and telomere shortening normally occurs only with cell division. Since most breast cancer cells have very short telomeres, treatment with telomerase inhibitors should lead to growth arrest and cell death. Thus, telomerase and telomeres offer a variety of potential targets for the development of anticancer therapies. The telomerase protein complex allows for multiple sites for inhibition. Recent research includes targeting the RNA component of the telomerase, inhibition of the catalytic subunit, immunotherapy, and small molecule inhibitors [19].

78.5.1 HTR

Telomerase uses intrinsic RNA subunit as a template for synthesis of new telomere repeats at the chromosome termini. Inhibiting hTR can block elongation of telomere to suppress activation of telomerase. Include antisense oligonucleotides and ribozyme.

78.5.2 Inhibit TERT

The enzymatic activity of telomerase may be inhibited by various telomerase inhibitors, with the induction of accelerated senescence and cell death. The most widely used reverse transcriptase inhibitor is 3 ϵ -azido-3 ϵ -deoxythymidine (AZT). Melana et al. observed that AZT inhibited the growth of breast cancer cells and telomerase activity at lower doses than in normal breast cells [20].

78.5.3 Immunotherapy

There is the elimination of telomerase expressing cells by immune effectors. TERT-positive cells express TERT in association with major histocompatibility complex on cell surfaces. Cells can then be recognized and eliminated by CD8+ cytotoxic T cells. This would provide the rapid elimination of tumor cells with no delay effect. However, TERT-expressing normal cells also would be affected [21].

78.5.4 Small Molecule Inhibitor

One method of specific inhibition of telomerase is through RNA interference (RNAi). Since its discovery, RNAi has been shown as a potent posttranscriptional gene silencing mechanism. Introduction of small interfering RNAs (siRNAs) can mediate the specific degradation of the mRNA, whose sequence is present in the siRNAs. It has been reported that RNAi against hTERT could successfully inhibit telomerase activity in several cancer cell lines. The study from Xue demonstrated the potential of inhibiting telomerase as an effective treatment of breast cancer by siRNA [22].

78.6 Conclusion

Ontogeny and progress of breast cancer were involved in several regulation of the pathway. Although telomerase activation plays a role, the mechanism may involve other regulation factors accompanied. It is expressed in over 90 % of breast cancer cells, while it is not expressed in most normal cells. Recent research showing test of telomerase has sensitivity toward diagnosis of breast cancer, but the guidance of individualized radiation therapy, chemotherapy, and surgical treatment has limitation. Research of telomerase inhibitors is increasing. Combining telomerase inhibitors with current therapies to reduce tumor burden may provide a better regimen to target breast cancer.

References

1. Ortiz BM, De la Vega HA, Medina SC et al (2006) Telomerase activity, estrogen receptors (α , β), Bcl-2 expression in human breast cancer and treatment response. *BMC Cancer* 6:206
2. Xu JH, Chen YH, Olopade O (2010) MYC and breast cancer. *Genes and Cancer* 6(1):629–640
3. Martin-Ruiz CM, Gussekloo J, Van Heemst D et al (2005) Telomere length in white blood cells is not associated with morbidity or mortality in the oldest old: a population-based study. *Aging Cell* 4(6):287–290
4. Wai LK (2004) Telomeres, telomerase, and tumorigenesis – a review. *Med Gen Med* 6(3):19
5. Blasco MA (2003) Mammalian telomeres and telomerase: why they matter for cancer and aging. *Eur J Cell Biol* 82(9):441–446
6. Greider CW (1999) Telomeres do D-loop-T-loop. *Cell* 97:419–422
7. Shay JW (1999) At the end of the millennium, a view of the end. *Nat Gen* 23:382–383
8. Natarajan S, Chen Z, Wanciewicz EV, Monia BP et al (2004) Telomerase reverse transcriptase (hTERT) mRNA and telomerase RNA (hTR) as targets for downregulation of telomerase activity. *Oligonucleotides* 14(4):263–273
9. Saldanha SN, Andrews LG, Tollefsbol TO (2003) Analysis of telomerase activity and detection of its catalytic subunit, hTERT. *Anal Biochem* 315(1):1–12
10. Chiu CP, Harley CB (1997) Replicative senescence and cell immortality: the role of telomeres and telomerase. *Biol. Med* 214(2):99–106
11. Sharyn B, Liu JP (2005) Hormones and growth factors regulate telomerase activity in ageing and cancer. *MCE* 240(1–2):11–22
12. Kyo S, Takakura M, Kanaya T et al (1999) Estrogen activates telomerase. *Cancer Res* 59:5917–5921
13. Saito K, Yagihashi A, Nasu S, Izawa Y et al (2002) Gene expression for suppressors of telomerase activity (telomeric-repeat binding factors) in breast cancer. *Cancer Sci* 93(3):253–258
14. He GP, Shui QL, Zhang LJ, Huang Y (2003) Semi-quantification of telomerase activity and its relationship with pathological indexes in breast carcinoma. *Chin J Exp Surg* 11(20):986–988
15. Yamchi MR, Zarghami N, Rahbani et al (2011) Plasma leptin, hTERT gene expression, and anthropometric measures in obese and non-obese women with breast cancer. *Breast Cancer* 5:27–35

16. Elkak AE, Meligonis G, Salhab M et al (2005) hTERT protein expression is independent of clinicopathological parameters and c-Myc protein expression in human breast cancer. *J Carcinog* 4:17
17. Kawagoe J, Ohmichi M, Takahashi et al (2003) Raloxifene inhibits estrogen-induced up-regulation of telomerase activity in a human breast cancer cell line. *JBC* 287(34):43363–43372
18. Mokbel KM, Parris CN, Ghilchik M, Amerasinghe CN et al (2000) Telomerase activity and lymphovascular invasion in breast cancer. *Eur J Surg Oncol* 26:30–33
19. Herbert BS, Wright WE, Shay JW (2007) Telomerase and breast cancer. *Breast Cancer Res* 3:146–149
20. White LK, Wright WE, Shay JW (2001) Telomerase inhibitors. *Trends Biotechnol* 19(3):114–120
21. Domchek SM, Recio A, Mick R et al (2007) Telomerase-specific T-Cell immunity in breast cancer: effect of vaccination on tumor immunosurveillance. *Cancer Res* 67:10546
22. Dong XJ, Liu A, Zer C et al (2009) siRNA inhibition of telomerase enhances the anti-cancer effect of doxorubicin in breast cancer cells. *BMC Cancer* 9:133

Chapter 79

Isolation, Identification, Antibacterial Effects of Antibiotic Drugs, and Chinese Herbal Extracts to the Pathogenic Bacteria of Swollen Abdomen from *Scophthalmus maximus* in Vitro

Xuan Wu, Dongqing Bai, Guoxia Zhu, Yanbin Ji, Zhichao Jia and Peng Zhou

Abstract The pathogenic bacteria was isolated from Turbot (*Scophthalmus maximus*) with swollen abdomen, and proved to be the pathogenic bacteria by the infection experiment. In this research, VITEK-2 compact system was used to identify the pathogenic bacteria, and test the antibacterial effects of antibiotic drugs, paper diffusion method was used to evaluate the antibacterial effects of three kinds of Chinese herbal extracts on the pathogenic bacteria of swollen abdomen from Turbot in Vitro. The results showed that the pathogenic bacteria of swollen abdomen from Turbot was *Stenotrophomonas maltophilia*, and the separation purity was 99 %. Without Trimethoprim, *S. maltophilia* had no CLSI salient point to the antibiotics of Ampicillin, Amikacin, Aztreonam, Cefazolin, Cefepime, Cefuroxime, Cefuroxime Axetil, Cefotetan, Ceftazidime, Ceftriaxone, Ciprofloxacin, Piperacillin, Imipenem, Gentamicin, Levofloxacin, Nitrofurantoin, Sulbactam, Tazobactam. Extract of the scutellaria and honeysuckle had different antibacterial effects to the *S. maltophilia*, and then the best bacteriostatic (MIC) and bactericidal (MBC) effects were 3.125 mg/mL and 6.25 mg/mL, respectively. However, the best MIC and MBC effects to extract from polygonum cuspidate were 100 mg/mL and 200 mg/mL, MIC and MBC effects lower than that extract from the scutellaria and honeysuckle. The results can provide reference materials for the clinical use of aquaculture and aquatic animal health cultivation.

Keywords Turbot (*Scophthalmus maximus*) · *Stenotrophomonas maltophilia* · Isolation and identification · Antimicrobial susceptibility · Chinese herbal medicine

X. Wu · D. Bai (✉) · G. Zhu · Y. Ji · Z. Jia · P. Zhou
Tianjin Key Lab of AQUA-Ecology and Aquaculture, Department of Fishery Science,
Tianjin Agricultural University, Tianjin 300384, People's Republic of China
e-mail: baidongqing@tjau.edu.cn

79.1 Introduction

Turbot (*S. maximus*) is one of the most economically important marine cultured fish in the world. The fish mainly distributes in the west of Pacific Ocean. At present, Turbot has become an important commercial species to the industrialized culture in the coastal areas of north of Chinese. But with high density of culture, disease outbreaks have occurred and caused heavy economic losses. Swollen abdomen is the main disease in the Turbot. It was a comprehensive disease that can cause infections to most of the aquatic organisms. The diseased fishes appeared slightly with enlargement of liver and spleen and obviously bloated abdomen. The anatomy of the diseased fishes show that mass ascites with pus in the abdominal cavity, and severe cases may have gastrointestinal bleeding [1, 2]. Some researches have studied swollen abdomen of Turbot, and made some achievements [3–5]. In this study, mainly isolated pathogenic bacteria from Turbot (*S. maximus*) with swollen abdomen, and to identify it. Test the antibacterial effects of antibiotic drugs and antibacterial effects of Chinese herbal extracts for the pathogenic bacteria. In order to provide reference materials for the clinical use of aquaculture and aquatic animal health cultivation.

79.2 Materials and Methods

79.2.1 Bacterial Isolation

For bacterial isolation, samples taken from abdominal cavity of diseased Turbot ($n = 30$, body length 4.2 ± 0.6 cm) were directly streaked on agar plates (5 g/l bacteriological peptone, 1 g/l yeast extract, 1 g/l KH_2P_04 , 30 g/l NaCl, 15 g/l agar, pH 7.2–7.4) [6]. After incubation for 48 h at 28 °C, the dominant colonies were picked and streaked for purity onto the same medium and incubated for 24 h at 28 °C. The pure isolates were saved on agar slopes and were routinely grown. Meanwhile isolates were stored in a medium 15 % (v/v) glycerol at -80 °C until use.

79.2.2 Induced Infection Assays

In order to confirm the bacteria was the pathogenic bacteria of swollen abdomen to the Turbot, 50 μl the dosages of 1.0×10^6 CFU with suspensions of pure cultures suspended in sterilized physiological saline, and injected to the health Turbot. While fish in the control group was injected with 0.85 % NaCl.

79.2.3 Biochemical Identification and Antibiotic Susceptibility Test

The VITEK test method by the automated microbe identification analyzer (VITEK 2 compact, bioMérieux, France) was used to identify and characterize the isolates further. The GN (Gram-negative) and AST-GN04 (antimicrobial susceptibility testing) cards were employed for the biochemical identification and antibiotic susceptibility test respectively. The test was done as reported by [7].

79.2.4 Antibacterial Activity Assay of Chinese Herbal Extracts

A disk diffusion method [8] was used to assay the pathogenic bactericidal activity of the Chinese herbal extracts from scutellaria, honeysuckle, and polygonum cuspidate.

The Chinese herbal extracts were dissolved in sterile saline solution (0.85 % NaCl) in double dilutions: at 400, 200, 100, 50, 25, 12.5, 6.25, 3.125 mg/ml. After dilution, antibacterial activity assay was carried out immediately. Bacteria were suspended respectively in sterile saline solution and were diluted to 1.0×10^6 CFU. The suspension (100 μ l) was spread on the medium along the blank paper disk (6 mm diameter) containing different levels of saturated Chinese herbal extract. Blank paper disk with sterile saline solution was offered as control.

The inoculated plates were incubated at 27 °C for 24 h. Antibacterial activity of minimum inhibitory concentration (MIC) was evaluated by measuring the distance of inhibition zone of the tested bacteria. The diameter of inhibition zone below 13 mm was regarded as resistant, between 13 mm and 17 mm moderately susceptible, and above 17 mm susceptible. Tests were performed in triplicate for each test concentration.

The Chinese herbal extracts were dissolved in agar medium in double dilutions: at 400, 200, 100, 50, 25, 12.5, 6.25, 3.125 mg/ml, and then emptied to the plate. 100 suspensions was spread on the plate, the inoculated plates were incubated at 27 °C for 24 h. The MBC is defined as the lowest concentration of the essential oils at which inoculated microorganism was completely killed (99.99 %). Tests were performed in triplicate for each test concentration.

79.3 Results

79.3.1 Bacterial Isolation

Pathogenic bacteria of swollen abdomen were isolated from the abdominal cavity of diseased Turbot, and it was identified as Gram-negative bacteria.

During 5 days of the infection experiments, the Turbot of the control groups did not show any disease signs. All of the treated Turbot showed different disease signs similar to the original diseases. During the infection experiments, high mortality was observed.

79.3.2 Characterization and Identification of Pathogenic Bacteria

The results of biochemical identification test of pathogenic bacteria by VITEK-2 compact system were shown in Table 79.1 indicated that it was *S. maltophilia* with 99 % probability, which was considered as “a excellent identification” by the system. The biochemical details were showed in Table 79.1.

Table 79.1 Biochemical details of pathogenic bacteria

Biochemical details		Biochemical details	
Ala-Phe-Pro-Arylamidase (APPA)	+	Saccharose/Sucrose (SAC)	-
Adonitol (ADO)	-	D-Tagatose (dTAG)	-
L-Pyrrolydonyl-Arylamidase (PyrA)	-	D-Trehalose (dTRE)	-
L-Arabitol (IARL)	-	Citrate (Sodium) (CIT)	-
D-Cellobiose (dCEL)	-	Malonate (MNT)	+
Beta-Galactosidase (BGAL)	-	5-Keto-D-Gluconate (5 KG)	-
H ₂ s Production (H ₂ S)	-	L-Lachate alkalization (ILATk)	+
Beta-N-Acetyl-Glucosaminidase (BNAG)	-	Beta-N-Acetyl-Galactosaminidase (NAGA)	+
Glutamyl Arylamidase pNA (AGLTp)	-	Succinate alkalization (SUCT)	+
D-Glucose (dGLU)	-	Alpha-Glucosidase (AGLU)	-
Gamma-Glutamyl-Transferase (GGT)	+	Alpha-Galactosidase (AGAL)	-
Fermentation/Glucose (OFF)	-	Phosphatase (PHOS)	+
Beta-Glucosidase (BGLU)	+	Glycine Arylamidase (GlyA)	-
D-Maltose (dMAL)	-	Ornithine Decarboxylase (ODC)	-
D-Mannitol (dMAN)	-	Lysine Decarboxylase (LDC)	-
D-Mannose (dMNE)	-	Decarboxylase Base (0DEC)	-
Beta-Xylosidase (BXYL)	-	L-Histidine assimilation (IHISa)	-
Beta-Alanine arylamidase pNA(BAlap)	-	Courmarate (CMT)	-
L-Proline Arylamidase (ProA)	+	Beta-Glucuronidase (BGUR)	-
LipaseI (LIP)	-	O/129 Resistance (O129R)	-
Palatinose (PLE)	-	Glu-Gly-Arg-Arylamidase (GGAA)	-
Tyrosine Arylamidase (TyrA)	-	L-Malate assimilation (IMLTa)	-
Urease (URE)	-	Ellman (ELLM)	-
D-Sorbitol (dSOR)	-	L-Lactate assimilation (ILATa)	-

+, Positive; -, negative

79.3.3 Antibiotic Susceptibility Assay

Use VITEK-2 compact system test antibiotic susceptibility revealed that without Trimethoprim, *s. maltophilia* had no CLSI salient point to the antibiotics of Ampicillin, Amikacin, Aztreonam, Cefazolin, Cefepime, Cefuroxime, Cefuroxime Axetil, Cefotetan, Ceftazidime, Ceftriaxone, Ciprofloxacin, Piperacillin, Imipenem, Gentamicin, Levofloxacin, Nitrofurantoin, Sulbactam, Tazobactam (Table 79.2).

79.3.4 Antibacterial Activity Assay of the Chinese Herbal Extracts

The in vitro antimicrobial activities of Chinese herbal extracts from scutellaria, honeysuckle, and polygonum cuspidate against the *s. maltophilia* and their activity potentials were qualitatively and quantitatively assessed by the presence or absence of inhibition zones, zone diameters, bacteriostatic (MIC), and bactericidal (MBC) values. Although the MICs and MBCs results varied between microorganisms tested, in the most cases the MICs was less than the MBCs.

Table 79.2 Antibiotic susceptibility information of *s. maltophilia*

Antimicrobial	MIC	Interpretation
Ampicillin(AM)	–	–
Ampicillin/Sublactam(SAM)	–	–
Ticarcillin/Clavulanic Acid(TCC)	–	–
Piperacillin(PIP)	–	–
Piperacillin/Tazobactam(TZP)	–	–
Cefazolin (CZ)	–	–
Cefuroxime(CXM)	–	–
Cefuroxime Axetil	–	–
Cefotetan(CTT)	–	–
Ceftazidime(CAZ)	–	–
Ceftriaxone(CRO)	–	–
Cefepime(FEP)	–	–
Aztreonam(ATM)	–	–
Imipenem(IPM)	–	–
Amikacin(AN)	–	–
Gentamicin(GM)	–	–
Tobramycin(TM)	–	–
Ciprofloxacin(CIP)	–	–
Levofloxacin(LEV)	–	–
Nitrofurantoin(FT)	–	–
Trimethoprim/Sulfamethoxazole(SXT)	≤20	S

MIC = minimum inhibitory concentration. S = sensitive, R = resistant, and I = intermediate

Table 79.3 Antimicrobial activity of the Chinese herbal extracts (1.0×10^6 CFU)

Chinese herbal extracts	Bacteriostatic(MIC)	Bactericidal effects (MBC)
Scutellaria	3.125	6.25
Honeysuckle	3.125	6.25
Polygonum Cuspidate	100	200

Results obtained from disk diffusion method, followed by measurements of MIC and MBC, indicate that extract of the scutellaria and honeysuckle had different antibacterial effects to the *S. maltophilia*, and then the best MIC and MBC effects were 3.125 mg/mL and 6.25 mg/mL, respectively. However, the best MIC and MBC effects to extract from polygonum cuspidate were 100 mg/mL and 200 mg/mL, MIC and MBC effects lower than that of extract from the scutellaria and honeysuckle (Table 79.3) .

79.4 Discussion

In our study, we isolated pathogenic bacteria of swollen abdomen from the abdominal cavity of diseased Turbot. And identified it was *S. maltophilia* (*S. maltophilia*).

S. maltophilia is a Gram-negative, nonenterobacteriaceae, nonfermentative, aerobic *bacillus* [9] that was formerly classified in the genus *Xanthomonas* [10]. The most common reported that this organism could infections to the human, mammals, and many marine animals [11–15]. In recent years, *S. maltophilia* of swollen abdomen has caused huge economic losses. It has been reported that at Channel catfish (*Ictalurus Punctatus*), yellow catfish (*Pelteobagrus fulvidraco*), Turbot (*S. maximus*), and so on [5, 16]. According to the research, the action mechanism of *S. maltophilia* to the swollen abdomen was to produce exotoxin, and then destroyed to cell membrane, finally disruption and dissolution of cell [17].

However, some scholar claims that swollen abdomen of Turbot is caused by other pathogenic bacteria [1, 2]. It can be explained that swollen abdomen of Turbot is comprehensive caused by many kinds of bacteria, such as *Edwardsiella tarda*, *Vibriobal* *inolyticus*, *Aeromonas hydrophila*. While only one kind of pathogenic bacteria are to be found in our study.

It was well-known *S. maltophilia* that has resistance to most of the antibiotics. *S. maltophilia* has wide resistance to the antibiotics, has only sensitivity to trimethoprim, gatifloxacin, and Levofloxacin [18, 19] has improved that *S. maltophilia* has no salient point to the antibiotics of cafteroline. Levofloxacin and trimethoprim were of the first choice for infection caused by *S. maltophilia*, others have not significant difference [20]. The above-mentioned results in our research were similar.

Scutellaria, honeysuckle, and polygonum cuspidate have been used traditionally as medicinal herbs for the treatment of gastrointestinal infections in China. In this study, the result showed that extract of the scutellaria, honeysuckle, and polygonum cuspidate had antibacterial effects to the *S. maltophilia*. In addition, several studies showed that these medicinal herbs and extracts can be effective for treating microbial infections. Zhang Bin [21] has shown scutellaria and honeysuckle has different significant effect to resistance, the Edwardsiella ictaluri. The antibacterial activity of rhus chinesis, scutellaria, and honeysuckle against Aeromonas hydrophila has been also reported [22]. Chinese medicinal herbs, such as Galla chinensis, scutellaria, Pericarpium granat have synergistic inhibition for V ibrion splendidus, Edwardsiella tarda, V ibrion parahaemolyticus, Aeromonas salmonicida, V ibrion harveryi [23]. Schizandrae Fructus has also been found to have antimicrobial activity against Bacillus spp, S. aureus, as well as viral infections [24]. At present, it has not reported sensitivity to *S. maltophilia* by Scutellaria, honeysuckle, and polygonum cuspidate. So these results will provide fundamental data for future research.

Acknowledgments This research was financially supported by the Tianjin Agricultural Science and Technology Achievements Transformation and Extension Project (Grant NO. 201004040).

References

1. Li Y, Yan XH, Chen JX et al (2006) Studies on the characteristics of pathogenic edwardsiella tarda isolated from diseased *scophthalmus maximus*. Periodical Ocean Univ Chin 36(4):649–654
2. Xue SX, Feng SM, Sun JS (2006) Isolation and identification of pathogenic bacteria in swollen abdomen of cultured turbot (*scophthalmus maximus*) and flounder (*paralichthys olivaceus*). Oceanologia Etlimnologia Sin 6(37):548–554
3. Zhang L, Wang J, Dong HJ et al (2011) The study of formalin-killed edwardsiella tarda vaccination on the turbot (*scophthalmus maximus*). J Aquac 7(32):22–25
4. Fan RF, Wang YG, Liang Y et al (2011) Screening and identification of a eurythermal probiotic bacterium in the intestine of cultured *scophthalmus maximus*. Prog Fishery Sci 1(32):40–46
5. Xue SX, Sun JS (2008) Detection of Pathogenic Bacterial (Edwardsiella Tarda and V ibrion Alginolyticus) Associated with Swollen Abdomen of Cultured Turbot (*Scophthalmus maximus*) and Flounder (*Paralichthys olivaceus*) by Nested PCR. Acta Hydrobiol Sin 6(32):856–860
6. Mouton JW (2003) Impact of pharmacodynamics on breakpoint selection for susceptibility testing. Infect Dis Clin North Am 17:579–598
7. Garcia-Garrote F, Cercenado E, Bouza E (2000) Evaluation of a new system, VITEK2, for identification and antimicrobial susceptibility testing of enterococci. J Clin Microbiol 38:2108–2111
8. Parekh J, Chanda SV (2008) Antibacterial activity of aqueous and alcoholic extracts of 34 indian medicinal plants against some staphylococcus species. Turk J Biol 32:63–71
9. Bruckner DA, Colonna P (1995) Nomenclature for aerobic and facultative bacteria. Clin Infect Dis 21:263–272

10. Palleroni NJ, Bradbury JF (1993) *Stenotrophomonas*, a new bacterial genus for *xanthomonas maltophilia*. *Int J Syst Bacterio* 143:606–609
11. Marshall WF, Keating MR, Anhalt JP et al (1989) *Xanthomonas maltophilia*: an emerging nosocomial pathogen. *Mayo Clin Proc* 54:1097–1104
12. Gutiérrez Rodero F, Masia MM, Cortés J et al (1996) Endocarditis caused by *stenotrophomonas maltophilia*: case report and review. *Clin Infect Dis* 23:1261–1265
13. Cornwell EErd, Willey P, Belzberg H et al (1996) Characteristics of *xanthomonas* infections in critically ill surgical patients. *Am Surg* 62:478–480
14. Papadakis KA, Vartivarian SE, Vassilaki ME et al (1997) *Stenotrophomonas maltophilia* meningitis report of two cases and review of the literature. *Clin Infect Dis* 87:106–108
15. Vartivarian SE, Papadakis KA, Palacios JA et al (1994) Mucocutaneous and soft-tissue infections caused by *xanthomonas maltophilia*. a new spectrum. *Ann Intern Med* 121:969–973
16. Geng Y, Wang K, Xiao D et al (2008) Pathological studies on channel catfish induced by extracellular products of *stenotrophomonas maltophilia*. *Acta Hydrobiol Sin* 2(34):345–352
17. Huang Y, Wang K, Zheng J et al (2010) Preparation and characterization of monoclonal antibodies against pathogenic *stenotrophomonas maltophilia*. *Chin Vet Sci* 40(9):907–912
18. Zhao Y, Liu Q, Xin X (2008) Identification and antimicrobial susceptibility test for *stenotrophomonas maltophilia*. *Chin J Mis diagn* 18(28):6956–5957
19. Er H, Zhang Y, Wang J et al (2012) Distribution and antimicrobial susceptibility assay for *stenotrophomonas maltophilia*. *Chin J Clinicians (Electronic Edition)* 6(11):3117–3118
20. Zhou T, Dai P, Xie Y et al (2006) Evaluation of the susceptibility test methods and analysis of the antimicrobial resistance of *stenotrophomonas maltophilia*. *Lab Med* 21(1):25–27
21. Zhang B, Hang T, Chen M et al (2010) Antimicrobial susceptibility test and bacteriostatic of chinese herbals to the *edwardsiella ictaluri*. *Fish Sci Technol Inf* 37(6):282–287
22. Cao L, Li Y (2009) Chinese medicinal herbs sensitivity test on the pathogen of bacterial septicemia from *ictalurus punctatus* in vitro. *J Hydroecology* 2(1):95–97
23. Li H, LI Q, Fu L (2011) Antibacterial action of several chinese herbal medicines to major marine pathogenic bacteria. *J Dalian Ocean Univ* 1(26):6–11
24. Sinclair S (1998) Chinese herbs: a clinical review of *astragalus*, *ligusticum*, and *schizandrae*. *Altern Med Rev* 3:338–344

Chapter 80

Lichen: A Potential Anticancer Official Resource

Meirong Ren, Xinli Wei and Feng Xu

Abstract Many natural products, which derived from plants, animals, and microorganisms, have been isolated as bioactive compounds with great therapeutic potential for cancer, but as a fungus, lichen has long been neglected in this area. The special symbiotic form of fungi and algae and worldwide distribution even extreme habitat of lichen contribute to its biological and chemical diversity, so, lichen becomes an amazing resource for the discovery of new anticancer drugs. The aim of this review is to show the value of lichen as a potential resource of anticancer drugs, especially highlight several lichen metabolisms and their derivatives, which can show the potentials to inhibit cellular proliferation or cytotoxicity and trigger apoptosis of cancer cells. To identify the new lead-compounds from lichen and elucidate the active principles with therapeutic potential for cancer, it is essential to establish a high-throughput screening program and dedicated collaboration among lichenologists, chemists, pharmacologists, and biologists.

Keywords Anticancer · Cytotoxicity · Lichen · Secondary metabolisms

M. Ren (✉)

College of Life Science, Southwest Forestry University, Kunming 650224, People's Republic of China
e-mail: xiaohei504@hotmail.com

F. Xu

HeBei ZhiTong Biological Pharmaceutical Co., Ltd, Baoding 072656, People's Republic of China

X. Wei (✉)

State Key Laboratory of Mycology, Institute of Microbiology, Chinese Academy of Sciences, Beijing 100101, People's Republic of China
e-mail: weixl@im.ac.cn

80.1 Introduction

Cancer is a class of disease characterized by out-of-control cell growth. It is a major health problem in the world, which is the second most common cause of death disease for all ages [1]. The number of new cancer cases diagnosed has been increasing steadily in recent decades, while the mortality of cancer patients is decreasing. Earlier diagnosis and various treatments, especially chemotherapy, have improved cure rates for malignancy and reduced risk of death. Natural products and their derivatives, especially those from plants, animal, and microorganisms, have long been a traditional source of drug which contributes not less than 60 % drugs. Some of them, such as vinca alkaloid, vincristine, taxol, fumiquinazolines, and rebeccamycin, etc. [2–4], show the strong anti-cancer activity.

Lichens are a unique life form of symbiosis composed of fungi and algae and or cyanobacteria. As pioneers, lichens show a worldwide distribution even various extreme environmental conditions which were unfavorable to the survival of the individual partners, from arctic to tropical regions, and from the plains to the highest mountains (approximately 8 % of terrestrial ecosystems are lichen-dominated) [5, 6]. It is not known how many species inhabit the earth; however, it is becoming increasingly clear that the number of microbial species is many times larger than estimated. For example, as conservatively estimated, there would be at least 1.5 million species of fungi [7, 8], but up to now only 65,000 species are known [9], accounting for less than 5 % of the total. The known lichen species is about 13,500–17,000 [10], which only account for about 1 % of the total fungi species.

In response to fancy physiological character and strong adaptability to extreme conditions, there are great variety of secondary metabolites which are often structurally unique produced by lichen, among which only a small number were found in other fungi and higher plants [11]. Over 700 lichen metabolites have been identified so far [12], only few of which are commercially available and the most of known compounds are poorly investigated for their bioactivities and medicinal potential [13]. Therefore increasing research on lichen natural resource may provide good results for exploiting and developing valuable natural products which benefit for human.

In 2000, 57 % of all drugs in clinical trails for cancer were either natural products or their derivatives. Most of the important antitumor compounds used for chemotherapy of tumors are microbial-produced antibiotics [14]. As fungi, for the past 20–30 years, some studies with lichen, even with the limited screening effort, have indicated the frequent occurrence of metabolites with antibiotic [15], anti-bacterial [16], antiviral [17], anti-HIV [18], antiproliferation [19], and antioxidant [20] properties. Recently, many researchers have been particularly interested in the antineoplastic activities of lichen and have obtained some promising and interesting results, which will be discussed in detail in this review.

80.2 The History of Lichen as Traditional Medicine

Throughout the ages, lichens have been used for various purposes, in particular as dyes, perfumes, and remedies in folk medicines. The topical use of lichen extracts has its origin in ancient Egyptian times [21]. The most important application of lichens is to treat diseases of animals and humans as traditional medicine, which can be traced back to the 18th dynasty (1700–1800 BC) when *Evernia furfuracea* (L.) Mann was first used as a drug [22]. Wei [23] published the book “Lichens Officinales Sinenses” to describe the lichen usage as Chinese traditional medicine. Spanish folk medicine has documented use of lichens in various medical ailments. Tea prepared from *Flavocetraria nivalis* (L.) Kärnefelt & Thell is used in the treatment of motion-sickness and heart attacks of by natives of Qollahuaya Andeans in Poland [24]. *Lethariella zahlbruckneri* (Du Rietz) Krog can be found only at high elevation and has been used for long term as a traditional tea and medicine in Tibet, and for lowering blood pressure and body fat in Yunnan of China. Local ethnic people believed it to be useful for anti-inflammation [25]. *Cetraria islandica* (L.) Ach. commonly known also as ‘Islandic moss’ is probably one of the best known alpine lichens used in folk medicine. Until now, it is still sold annually in European pharmacies for treatment of minor ailments. This species is traditionally used as reconstituent after tuberculosis and anticatarrhal by the Italians [26]. Studies in Germany developed tablets of *C. islandica* extracts containing polysaccharides and lichen acids, along with pediatric lozenges containing *C. islandica* for the prophylaxis of coughs and catarrh [27]. *Ramalina thrausta* (Ach.) Nyl. is used in Finland for treatment of wounds, athlete’s foot, or other skin diseases and taken to relieve sore throat and toothache [28].

80.3 Cytotoxicity/Antiproliferation on Cancer Cell of Lichen Extract

Some lichen species have been used in screening cytotoxicity since early 1980s. The results obtained guaranteed for the potential application of these lichen in the near future. The cytotoxicity/antiproliferation of lichen has been studied in various cell lines and primarily cultured cells, including multiple tumor cell lines and normal cells. Recent reviews have discussed the anticancer pharmaceutical potential of lichen substances [27, 29, 30].

Since the distribution of bioactive compounds differs according to the lichen used, different solvents were used to extract these compounds from different lichens correspondingly. The methanol extract of *Xanthoria parietina* (L.) Beltr. showed potent antimyeloma activity against P3X63-Ag8.653 cell line [31]. The acetone extract of *L. zahlbruckneri* exhibited significant antiproliferative activity by time- and dose-dependent manners and inducing apoptosis on HT-29 cell lines by caspase-dependent and -independent pathways [19]. A potent cytotoxic activity

was also reported for the hexane extract of *Parmelia caperata* (L.) Ach. against different cancer cell lines and the diethyl ether extract of *Cladonia convoluta* (Lamkey) Anders demonstrated high cytotoxic activity ($IC_{50} < 1 \mu\text{g/ml}$) against 3LL cell line [32]. According to wide screening of cytotoxicity of lichen extracts, it seems that cancer cell growth inhibitions can vary within the lichen extract, solvent used for extraction.

A study monitored cytotoxic activity on 69 species of lichens from New Zealand and showed their inhibitory effect against two cell lines: murine leukemia cells P388 and monkey kidney cell BSC [33]. A high proportion of the lichen extracts showed cytotoxic activity against one or both of the mammalian cell lines. Bézinvin et al. reported that eight lichens *C. convoluta*, *C. rangiformis* Hoffm., *Ramalina cuspidata* (Ach.) Nyl., *Platismatia glauca* (L.) W.L. Culb. & C.F. Culb., *Parmelia perlata* (Huds.) Ach., *P. caperata*, *Usnea rubicunda* Stirt., *Evernia prunastri* (L.) Ach. were extracted successively with *n*-hexane, diethyl ether, and methanol and demonstrated interesting activities particularly on human cancer cell lines [32]. Also, Mitrović [20] evaluated methanol extracts of 5 different species and determined potent antiproliferative activity. Recently, Ranković [34] studied the anticancer activity of extracts from *Cladonia furcata*, *Lecanora atra*, *L. muralis*. All extracts were found to be strong anticancer activity toward both cell lines with IC_{50} values ranging from 8.51 to 40.22 $\mu\text{g/ml}$. Thus, the screening results of crude extracts produced very useful information that lichen species mainly focuses on the family *Parmeliaceae* Zenker, *Cladoniaceae* Zenker, *Lecanoraceae* Körb., *Lobariaceae* Chevall., *Ramalinaceae* C. Agardh, *Sphaerophoraceae* Fr., *Teloschistaceae* Zahlbr., *Umbilicariaceae* Chevall. However, it is difficult to determine the contribution of individual components for the overall anticancer effect with crude extract of lichen. Often, the activity of the extracts may be the result of a synergistic effect of several compounds.

80.4 Anticancer of Lichen Metabolites

80.4.1 Usnic Acid

Usnic acid is the most extensively studied lichen metabolite since its first isolation in 1844 and was originally discovered as a mycobacterial product with weak antifungal activity against rust fungi. Antitumor activity of usnic acid was shown for the first time by Kupchan and Kopperman (1975) against Lewis lung carcinoma in mice [35]. Since then, many researchers pay more attention to the anticancer effect of usnic acid. Expression of caspase-3 revealed induction of apoptosis by usnic acid on L1210 cell line [32, 36]. Unchanged morphology in microtubules or non-increase in the mitotic index on two cancer cell lines suggested that the antineoplastic activity of usnic acid is not related to alterations in the formation and/or stabilization of microtubules [37]. Usnic acid derivative did

not escape from the massive research to identify new potential anti-tumor compounds. Cytotoxicity of nine usnic acid–amine conjugates was evaluated on murine and human cancer cell lines. The author found the more active derivative induced apoptosis via independent of the polyamine transport system (PTS) and diaminoctane chain was a good vector to improve the cytotoxicity of usnic acid [36].

80.4.2 Polysaccharides

Lichens have been used for medicinal purposes and are beneficial to some extent being correlated with polysaccharides. Among the known lichen species, less than 100 species have been investigated for polysaccharides [38]. As plant and other natural resource of polysaccharides, lichen polysaccharides have been known to exert antitumor activity [39]. Japanese scientists were full of enthusiasm at this area and their research show the lowering of non-toxic characteristic of lichen polysaccharides. A lichen-derived polysaccharide CFP-2 reduced the viability of HL-60 and K562 cells due to apoptotic pathway and telomerase activity, suggesting its possible therapeutic potential against cancer [40].

80.4.3 Depsides and Depsidones

Depsides and depsidones, a class of compounds formed by condensation of a phenolic carboxylic acid (such as gallic acid) with a similar compound, have been isolated from plants, but most often found in lichens. Four depsides and nine depsidones got from lichen were tested along with tridepside gyrophoric acid for their cytotoxicity on lymphocytes. Compound pannarin, 1'-cloro pannarin, and sphaerophorin have a cytotoxic effect stronger than positive control colchicine. The activity of other compounds is moderate in degree except vicanicin and variolaric acid. The results could provide useful information for determination of the minimum structural requirements for the production of biological response by these compounds, indicating that the presence of COOH or CHO groups adjacent to an OH group appears to be indispensable [41]. Pannarin and sphaerophorin are also reported to inhibit cell growth and to induce apoptosis in human prostate carcinoma DU-145 [42] and human melanoma M14 cells [43]. Lobaric acid, an orcinol depsidone isolated from *Stereocaulon alpinum* Laur., was shown to cause a significant reduction of DNA synthesis on three malignant cell lines (from erythro-leukemia) [44]. Gissurarson [45] reported the inhibition of cysteinyl-leukotrienes, which are potent mediators of inflammation and constrictors of smooth muscles in humans, with an effective dose of 5.5 μ M.

80.4.4 Others

A diphenyl ether, buellin, present in *Diploicia canescens* (Dicks) A Massal was also found to act as cytotoxicity against B16 and HaCaT cell lines ($IC_{50} = 0.25 \mu\text{M}$ for B16 murine melanoma cell line, lower than $IC_{50} = 0.28 \mu\text{M}$ of positive control etoposide) [46]. The antiproliferative activities of protolichesterinic acid (butyrolactone) isolated from *Cetraria islandica* showed inhibition of growth of breast cancer cell lines and mitogen stimulated lymphocytes [43]. Ernst-Russell [47] reported the isolation of hybocarpace, a naphthazarin-derived pentacycle, from the cultured lichen mycobiont of *Lecanora hybocarpa* (Tuck). Brodo which was collected from woodland in Louisiana, USA. It was found to possess potent cytotoxicity against the murine mastocytoma P815 cell line and IC_{50} value of $0.15 \mu\text{g/ml}$. A new aryl-hydrazide L-glutamic acid derivative, pygmeine, was isolated from amethanolic extract of *Lichina pygmaea*, marine lichen. The *ortho*-, *meta*-, and *para*-hydroxyl isomers along with their respective benzyl intermediates, and a natural methoxylated analog were synthesized and cytotoxicity of them were evaluated on murine and human melanoma cells (B16, A375). The *para*-hydroxyl isomer was found to be the most active ($IC_{50} = 1.6 \mu\text{M}$) on B16 cells [48]. Liu [49] and his colleague isolated the retigeric acid B, a natural pentacyclic triterpenic acid from lichen and found retigeric acid B exerted its antitumor effect by targeting the NF- κ B pathway in prostate cancer cells, and this could be a general mechanism for the antitumor effect of retigeric acid B in other types of cancers as well.

80.5 Conclusions

The above-mentioned activities clearly indicated the potential of lichen compounds for pharmaceutical purposes, but some properties of lichen metabolites still need consideration. Structure of more than 700 lichen substances are available, but due to the slow growth of lichen, their availability is insufficient in quantity and difficulty in large-scale industrial production, lichens were frequently ignored by pharmaceutical industries. As known, the secondary metabolites of lichen which are deposited on the surface of mycelium were usually produced by fungi, therefore it become possible that cultured mycobionts could replace the lichen. In addition, advances in high-throughput screening technologies, have been a dramatic increasing in interest by the pharmaceutical and biotechnology industries. Although many of lichen products are not likely to become therapeutics, the information gained from studying them is likely lead to the development and understanding of novel molecular targets and chemical synthesis or chemical modification of natural metabolites, which in turn may lead to the development of new classes of therapeutic agents. As alternative method, computer drug design and the transfer of genes responsible for production of lichen metabolites may help

development of new synthetics with enhanced pharmacological potency. Eventually, a collaborative effort among lichenologists, chemists, pharmacologists, and biologists should be another pivotal point for the new drug development.

Acknowledgments This work was financially supported by the Scientific Research Foundation for Ph.D, Southwest Forestry University and the Youth Innovation Promotion Association, Chinese Academy of Sciences

References

1. Micheli A, Mugnol E, Krogh V et al, the Europrevail Working Group (2002) Cancer prevalence in European reistry areas. *Ann Oncol* 13:840–865
2. Da Rocha AB, Lopes RM, Schwartsmann G (2001) Natural products in anticancer therapy. *Curr Opin Pharmacol* 1:364–369
3. Sun YY, Xun KL, Wang YT et al (2009) A systematic review of the anticancer properties of berberine a natural product from Chinese herbs. *Anti-Canc D* 20:757–769
4. Sánchez C, Zhu LL, Braña AF et al (2005) Combinatorial biosynthesis of antitumor indolocarbazole compounds. *PANS* 102:461–466
5. Nash TH (1996) Lichen biology. Cambridge: Cambridge University Press 1–7
6. Guschina IA, Dobson G, Harwood JL (2003) Lipid metabolism in cultured lichen photobionts with different phosphorus status. *Phytochem* 64:209–217
7. Hawksworth DL (1991) The fungal dimension of biodiversity: magnitude, significance, and conservation. *Mycol Res* 95:641–655
8. Hawksworth DL (2001) The magnitude of fungal diversity: the 1.5 million species estimate revisited. *Mycol Res* 105:1422–1432
9. DePriest PT (2004) Early molecular investigations of lichen-forming symbionts: 1986–2001. *Annu Rev Microbiol* 58:273–301
10. Nash TH (2008) Lichen biology, 2nd edn. Cambridge University Press, New York
11. Stocker-Wörgötter E (2008) Metabolic diversity of lichen forming ascomycetous fungi: culturing, polyketide and shikimate metabolite production, and PKS genes. *Nat Prod Rep* 25:188–200
12. Huneck S (1999) The significance of lichens and their metabolites. *Naturwissenschaften* 86:559–570
13. Bézivin C, Tomasi S, Lohézic-Le Dévéhat F, Boustie J (2003) Cytotoxic activity of some lichen extracts on murine and human cancer cell lines. *Phytomed* 10:499–503
14. Tomasz M (1995) Mitomycin C: small, fast and deadly (but very selective). *Curr Biol* 2:575–579
15. Lauterwein M, Oethinger M, Belsner K et al (1995) In vitro activities of the lichen secondary metabolites vulpinic acid, (+)-usnic acid, and (–)-usnic acid against aerobic and anaerobic microorganisms. *Antimicrob Agents Chemother* 39:2541–2543
16. Honda NK, Pavan FR, Coelho RG et al (2010) Antimycobacterial activity of lichen substances. *Phytomedicine* 17:328–332
17. Fazio AT, Adler MT, Bertoni MD et al (2007) Lichen secondary metabolites from the cultured lichen mycobionts of *teloschistes chrysophthalmus* and *ramalina celastri* and their antiviral activities. *Z Naturforsch C* 62:4360–4365
18. Neanati N, Hong HX, Mazumder A et al (1997) Depsides and depsidones as inhibitors of HIV-1 integrase: discovery of novel inhibitors through 3D database searching. *J Med Chem* 40:942–952
19. Ren MR, Hur JS, Seo KI et al (2009) Anti-proliferative effects of *Lethariella zahlbruckneri* extracts in HT-29 human colon cancer cells. *Food Chem* T47:2157–2162

20. Mitrović T, Stamenković S, Marković S et al (2011) Antioxidant, antimicrobial and antiproliferative activities of five lichen species. *Int J Mol Sci* 12:5428–5448
21. Mitrović T, Stamenković S, S. tojičić D et al (2011) Lichen as source of versatile bioactive compounds. *Biolog Nys-san* 2:1–6
22. Zambare VP, Christopher LP (2012) Biopharmaceutical potential of lichens. *Pharm Biol* 50:778–798
23. Wei JC, Wang XY, Hou JL et al (1982) *Lichenes officinales sinenses*. Science Press, Beijing
24. Bastien JW (1983) Pharmacopoeia of the qollahuaya andeans. *J Ethnopharmacol* 8:97–111
25. Wang LS, Takao N, William LC et al (2001) Ethnic uses of lichens in Yunnan, China. *Bryologist* 104:345–349
26. Lokar LC, Poldini L (1998) Herbal remedise in the traditional medicine of the Venezia Giulia Region (north east Italy). *J Ethnophar* 22:231–178
27. Podterob AP (2008) Chemmical composition of lichen and their medical applications. *Pharm Chem J* 42:32–38
28. Vartia KO (1973) Antibiotics in lichens. In: Ahmadjian V, Hale ME (eds) *The lichens*. Academic Press, New York 547–569
29. Boustie J, Tomasi S, Grube M (2011) Bioactive lichen metabolites: alpine habitats as an untapped source. *Phytochem Rev* 10:287–307
30. Müller K (2001) Pharmaceutically relevant metabolites from lichens. *Appl Microbiol Biotechnol* 56:9–16
31. Triggiani I D, Ceccarelli D, Loppi S et al (2009) Antiproliferative activity of lichen extracts on murine myeloma cells. *Biologia* 64:59–62
32. Bézinvin C, Tomasi S, Boustie J et al (2003) Cytotoxic activity of some lichen extracts on murine and human cancer cell lines. *Phytomed* 10:499–503
33. Perry NB, Benn MH, Tangney RS et al (1999) Antimicrobial, antiviral and cytotoxic aktivty of New Zealand lichens. *Lichenologi* 31:627–636
34. Ranković BR, Kosanić MM, Stanjkvić TP (2011) Antioxidant, antimicrobial and anticancer activity of the lichens *Cladonia furcata*, *Lecanora atra* and *Lecanora muralis*. *CAM* 11:97–104
35. Kupchan M, Kopperman HL (1975) Usnic acid: tumor inhibitor isolated from lichens. *Experientia* 31:625
36. Bazin MA, Le Lamer AC, Delcros JG (2008) Synthesis and cytotoxic activities of usnic acid derivatives. *Bioorg Med Chem* 16:8737–8744
37. O'Neill MA, Mayer M, Appleyard VCL et al (2010) Does usnic acid affect microtubules in human cancer cells? *Braz. J. Biol* 70:659–664
38. Olafsdóttir ES, Lngólfssdóttir K (2001) Polysaccharides from lichens: structural characteristics and biological activity. *Planta Med* 67:199–208
39. Whistler RL, Bushway AA, Singh PP (1976) Noncytotoxic, antitumour polysaccharides. *Adv Carbohydr Chem Biochem* 32:235–275
40. Chihara G, Hamuro J, Maeda YY (1970) Fractionation and purification of the polysaccharides with marked antitumor activity, especially lentinan, from lentinus edodes (berk.) sing. (an edible mushroom). *Cancer Res* 30:2776–2781
41. Correche E, Carrasco M, Enriz D et al (2002) Cytotoxic screening activity of secondary lichen metabolites. *Acta Farm Bonaerense* 4:273–278
42. Russo A, Piovano M, Lombardo L (2006) Pannarin inhibits cell growth and induces cell death in human prostate carcinoma DU145 cells. *Anti-canc D17*:1163–1169
43. Ogmundsdóttir HM, Zoega GM, Gissurarson SR (1998) Anti-proliferative effects of lichen-derived inhibitors of 5- lipoxigenase on malignant cell-lines and mitogenstimulated Lymphocytes. *J Pharm Pharmacol* 50:107–115
44. Haralsdóttir S, Guolaugsdóttir E, Ogmundsdóttir HM et al (2004) Anti-proliferative effects of lichen-derived lipoxigenase inhibitors on twelve human cancer cell lines of different tissue origin in vitro. *Planta Med* 70:1098–1110

45. Gissurarson SR, Sigurdsson SB, Ingólfssdóttir K et al (1997) Effect of lobaric acid on cysteinyl- leukotriene formation and contractile activity of guinea pig taenia coli. *J Pharmacol Exp Ther* 280:770–773
46. Millot M, Tomasi S, Boustie J et al (2009) Cytotoxic constituents of the lichen *Diploicia canescens*. *J Nat Prod* 72:2177–2180
47. Ernst-Russell MA, Elix JA, Nash IIITH et al (1999) Hybocarpace, a novel cytotoxicity naphthazarin derivative from mycobiont cultures of the lichen *Lecanora hybocarpa*. *Tetrahedr L* 40:6321–6324
48. Roullier C, Chollet-Krugler M, Boustie J et al (2010) A novel aryl-hydrazide from the marine lichen *Lichina pygmaea*: isolation, synthesis of derivatives and cytotoxicity assays. *Bioorg Med* 20:4582–4586
49. Liu YQ, Hu XY, Lou HX et al (2012) Rentigeric acid B exhibits antitumor activity through suppression of nuclear factor- κ B signaling in Prostate cancer cells in vitro and in vivo. *PLoS ONE* 7:1–11

Chapter 81

Clinical Significance of Screening Impaired Glucose Tolerance in Essential Hypertension Patients

Jun Zhu, Peiqing Feng, Shu Guo, Xinghua Liao, Jiajie Liu,
Junfang Zhang, Tingbao Yan, Yue Wang and Tong-Cun Zhang

Abstract Objective: Monitoring data of patients with essential hypertension associated with impaired glucose tolerance then provide clinical basis for the intervention of diabetes and reduce cardiovascular and cerebrovascular disease risk factors. Method: Select 158 patients without sugar metabolic abnormalities previously, whose fasting plasma glucose is <5.6 mmol/L and diagnosed as essential hypertension. Results: After OGTT, in 158 patients, there are 99 cases (62.7 %) with normal glucose tolerance, 45 patients (28.4 %) with impaired glucose tolerance, and 14 cases (8.9 %) with confirming diabetes. Conclusion: The primary hypertensive patients with impaired glucose tolerance abnormalities show a high proportion in hypertensive patients. With metabolic syndrome, patients should be monitored regularly and actively fasting glucose and after 2 h of OGTT to detect and intervene in diabetes earlier, reduce the risk factors of severe cardiovascular and cerebrovascular complications.

Keywords Diabetes · Hypertension · IGT · OGTT

J. Zhu · P. Feng

The First People's Hospital of Qingdao Economic and Technological Development Zone,
Qingdao 266555, People's Republic of China

J. Zhu · P. Feng · S. Guo · X. Liao · J. Liu · T. Yan · Y. Wang · T.-C. Zhang (✉)

Key Laboratory of Industrial Microbiology, Ministry of Education and Tianjin City,
College of Biotechnology, Tianjin University of Science and Technology,

Tianjin 300457, People's Republic of China

e-mail: tony@tust.edu.cn

J. Zhang

The Community Service Center of Tanggu Development Zone in Tianjin, Tianjin 300457,
People's Republic of China

81.1 Introduction

Metabolic abnormalities were observed in the early duration of hypertension, previous studies found that patients with essential hypertension have significant differences in TC, TG, HDL-C, blood insulin levels, and fasting plasma glucose compared with normal ones [1]. Early detection of glucose tolerance abnormalities and therapeutic intervention for hypertensive patients may reduce insulin resistance in phase of impaired glucose tolerance [2, 3], which is key point to prevent and delay the development of T2DM and reduce cardiovascular complications [4–6]. In this study, blood sugar of essential hypertensive patients with normal fasting plasma glucose was detected 2 h after OGTT, thus providing the basis for intervention in the incidence of diabetes and reducing the risk factors of severe complications of cardiovascular and cerebrovascular.

81.2 Materials and Methods

81.2.1 Object of Study

Investigate 586 cases of patients with essential hypertension tested by OGTT in our hospital from May 2007 to 2008. Inclusion criteria: patients who have been confirmed as essential hypertension by outpatient wards, fasting plasma glucose < 5.6 mmol/L, without regarding the merger of other cardiovascular and cerebrovascular risk factors; outpatients with essential hypertension. Exclusion criteria: acute cardiovascular and cerebrovascular complications, severe trauma patients with infection; long-term diuretics used patients; long-term hormones used patients; thyroid function, kidney function, urine, B-mode ultrasonography of abdominal renal artery, adrenal CT, serum renin—angiotensin—aldosterone levels, catecholamine, and other tests were carried out to rule out endocrine hypertension, renal hypertension, renal vascular hypertension, secondary hypertension.

81.2.2 Methods

Try fasting plasma glucose and glucose 2 h after OGTT of eligible patients are monitored by recommended method according to WHO. Patients whose glucose ≥ 7.8 mmol/L 2 h after OGTT must be tested for the second time. If glucose ≥ 11.1 mmol/L 2 h after the second OGTT, they are diagnosed as diabetes; plasma glucose ≤ 7.8 mmol/L and ≥ 11.1 mmol/L 2 h after second OGTT are diagnosed as abnormal glucose tolerance. The patients were divided into three groups according to blood glucose results 2 h after the OGTT: glucose < 7.8 mmol/L is the normal group (NG group), plasma glucose < 7.8 and ≥ 11.1 mmol/L is impaired glucose

tolerance group (IGT group), glucose ≥ 11.1 mmol/L is the diabetes group (DM). We selected NG group as the control. Data analyzed include age, BMI, systolic blood pressure, diastolic blood pressure, uric acid, TG, TC, HDL-C, and influence of HDL-C toward glucose 2 h after the OGTT.

81.2.3 Statistical Analysis

Measurement data show as $x \pm S$, count data expressed as a percentage, measurement data using analysis of deviation.

81.3 Results and Discussion

81.3.1 Basic Situation of Patients

(Table 81.1) we selected includes 158 patients in which 88 cases (55.7 %) were male patients and 70 cases (44.3 %) were female patients. There are 12 cases of patients with coronary heart disease, 32 cases of cerebrovascular disease, 72 cases of metabolic syndrome patients. In OGTT, 199 cases (62.7 %) of them are normal in glucose tolerance, 45 cases (28.4 %) are IGT, 14 cases (8.9 %) are confirmed as diabetes (Table 81.2).

81.3.2 Comparison of Risk Factors in Combined Patients with Different Sugar Metabolic Status

Results showed that there were statistically significant differences among patients of different glucose metabolism status like age, fasting plasma glucose, serum uric acid, LDL-C level. Except for fasting plasma glucose, any other two groups were statistically significant in the rest three groups ($P < 0.01$). There is not statistical

Table 81.1 Basic situation of Patients($x \pm s$)

Item	Parameter
Number (M/F)	88/70
Age (Year)	52.6 ± 13.2
Fasting plasma glucose mmol/L	4.8 ± 0.4
Systolic blood pressure mmHg	145.8 ± 20.0
Diastolic blood pressure mmHg	90.4 ± 13.5
BMI(kg/m)	26.5 ± 3.7

Table 81.2 Comparison of risk factors in combined patients with different sugar metabolic status

Item	NG	IGT	DM	P	F
Age (Year)	51.5 ± 13.3	54.6 ± 12.7	56.0 ± 12.5	0.002	6.121
Fasting plasma glucose mmol/L	4.7 ± 0.4	4.9 ± 0.4	5.16 ± 0.3	0.000	27.552
Systolic blood pressure mmHg	144.1 ± 19.0	148.6 ± 20.9	151.9 ± 24.3	0.008	4.887
Diastolic blood pressure mmHg	90.2 ± 13.6	90.5 ± 12.9	92.7 ± 15.3	0.532	0.633
BMI(kg/m)	26.4 ± 3.8	26.6 ± 3.4	26.7 ± 3.3	0.811	0.210
UA	326.0 ± 90.7	348.9 ± 95.4	340.7 ± 92.2	0.027	3.644
TG	1.8 ± 1.2	1.8 ± 1.0	1.8 ± 0.9	0.871	0.138
TC	4.8 ± 0.8	4.8 ± 0.9	5.0 ± 1.0	0.284	1.261
HDL-C	1.0 ± 0.2	1.0 ± 0.3	1.0 ± 0.2	0.993	0.007
LDL-C	3.1 ± 0.8	3.2 ± 0.9	3.9 ± 0.4	0.001	7.412

significance in age, systolic blood pressure, LDL-C level between the DM group, and the NG group with the NG group ($P > 0.05$).

81.4 Discussion

Impaired glucose tolerance (IGT) population is at high risk of diabetes. IGT patients are prone to develop into diabetes, IGT is also the independent risk factor for cardiovascular and cerebrovascular complications [7–10]. The DECODE study further confirmed that relationship of coronary heart disease mortality and 2-hour postprandial blood glucose are more close than fasting plasma glucose. Early detection of glucose tolerance abnormalities and therapeutic intervention for hypertensive patients may reduce insulin resistance in phase of impaired glucose tolerance, which is key point to prevent and delay the development of T2DM and reduce cardiovascular complications.

In this study, there are 45 cases of impaired glucose tolerance in all selected hypertensive patients accounted for 28.4 %, diagnosed diabetes cases accounted for 8.9 %, indicating that the proportion of abnormal glucose metabolism in hypertensive patients is relatively high, especially over the age of 35. Difference between NG group and IGT group is statistically significant and also statistically significant between NG group and DM group, and the trend for glucose is growing, illustrating that the abnormality of fasting plasma glucose and glucose after 2 h of OGTT are closely related.

The results indicated that high level of systolic blood pressure, uric acid, and LDL-C in patients with abnormal glucose metabolism may be associated with their own metabolic abnormalities. This study shows that there was no significant difference between the DM group and the NG group in age, systolic blood pressure, LDL-C level, which may be caused by a high proportion of metabolic syndrome in selected populations.

Results of glucose metabolism survey in Chinese hospitalized patients with coronary heart show that coronary heart disease combined with impaired glucose tolerance and patients with high blood sugar after 2 h of single OGTT accounted for 54.6 % [11–17]. Investigation and screening results of the Chinese hypertensive glucose metabolism status in 218 cases of patients whose fasting plasma glucose was <5.6 mmol/L show that 2 h after OGTT patients whose plasma glucose ≥ 7.8 mmol/L accounted for 22 % [18–20].

81.5 Conclusion

The above studies have shown patients of primary hypertension with no history of diabetes in newly diagnosed glucose metabolism abnormalities are very common. For hypertensive patients, monitoring fasting plasma glucose, especially by OGTT, has significant meaning in understanding of glucose metabolism status, early detection of hypertensive patients with metabolic syndrome, and intervention of abnormal glucose metabolism positively. Meanwhile, it may reduce the risk factors of cardiovascular and cerebrovascular disease more effectively.

References

1. Arauz-Pacheco C, Parrott MA, Raskin P, American Diabetes Association. (2004) Hypertension management in adults with diabetes. *Diabetes Care*. 27(Suppl 1):S65–S67
2. Wang J, Geiss LS, Cheng YJ et al (2011) Long-term and recent progress in blood pressure levels among U.S. adults with diagnosed diabetes, 1988–2008. *Diabetes Care* 34(7):1579–1581
3. UK Prospective Diabetes Study Group (1998) Tight blood pressure control and risk of macrovascular and microvascular complications in type 2 diabetes: UKPDS 38 *BMJ* 317(7160):703–713
4. King H, Aubert RE, Herman WH (1998) Global burden of diabetes, 1995–2025: prevalence, numerical estimates, and projections. *Diabetes Care* 21(9):1414–1431
5. Bartnik M, Malmberg K, Hamsten A et al (2004) Normal glucose tolerance—a common risk factor in patients with acute myocardial infarction in comparison with population-based controls. *J Intern Med* 256(4):288–297
6. Gu D, Reynolds K, Duan X, et al InterASIA Collaborative Group (2012) Erratum to: Prevalence of diabetes and impaired fasting glucose in the Chinese adult population: International collaborative study of cardiovascular disease in Asia (InterASIA). *Diabetologia*
7. Marques-Vidal P, Bastardot F, von Känel R et al (2012) Association between circulating cytokine levels, diabetes and insulin resistance in a population-based sample (CoLaus study). *Clin Endocrinol (Oxf)*. doi: [10.1111/j.1365-2265.2012.04384.x](https://doi.org/10.1111/j.1365-2265.2012.04384.x)
8. Yamagishi S (2011) Cardiovascular disease in recent onset diabetes mellitus. *J Cardiol* 57(3):257–262
9. Bryhni B, Arnesen E, Jenssen TG (2010) Associations of age with serum insulin, proinsulin and the proinsulin-to-insulin ratio: a cross-sectional study. *BMC Endocr Disord* 10:21

10. Nathan AA, Mohan V, Babu SS et al (2011) Glucose challenge increases circulating progenitor cells in Asian Indian male subjects with normal glucose tolerance which is compromised in subjects with pre-diabetes: a pilot study. *BMC Endocr Disord* 11:2
11. Coutinho M, Gerstein HC, Wang Y et al (1999) The relationship between glucose and incident cardiovascular events. A metaregression analysis of published data from 20 studies of 95,783 individuals followed for 12.4 years. *Diabetes Care* 22(2):233–240
12. Epidemiology Study Group (1998) Will new diagnostic criteria for diabetes mellitus change phenotype of patients with diabetes? Reanalysis of European epidemiological data. DECODE Study Group on behalf of the European Diabetes BMJ. 8;317(7155):371–375
13. Bartnik M, Malmberg K, Norhammar A et al (2004) Newly detected abnormal glucose tolerance: an important predictor of long-term outcome after myocardial infarction. *Eur Heart J* 25(22):1990–1997
14. Norhammar A, Tenerz A, Nilsson G et al (2002) Glucose metabolism in patients with acute myocardial infarction and no previous diagnosis of diabetes mellitus: a prospective study. *Lancet* 359(9324):2140–2144
15. Bartnik M, Rydén L, Ferrari R et al (2004) Euro heart survey investigators. the prevalence of abnormal glucose regulation in patients with coronary artery disease across Europe. The euro heart survey on diabetes and the heart. *Eur Heart J* 25(21):1880–1890
16. Hashimoto K, Ikewaki K, Yagi H et al (2005) Glucose intolerance is common in Japanese patients with acute coronary syndrome who were not previously diagnosed with diabetes. *Diabetes Care* 28(5):1182–1186
17. Choi KM, Lee KW, Kim SG et al (2005) Inflammation, insulin resistance, and glucose intolerance in acute myocardial infarction patients without a previous diagnosis of diabetes mellitus. *J Clin Endocrinol Metab* 90(1):175–1780
18. DeFronzo RA, Tobin JD, Andres R (1979) Glucose clamp technique: a method for quantifying insulin secretion and resistance. *Am J Physiol* 237(3):E214
19. Chiu KC, Cohan P, Lee NP et al (2000) Insulin sensitivity differs among ethnic groups with a compensatory response in IS-cell function *Diabetes Care* 23:1353
20. DaYH ChangYP, Jin MY (2006) The relationship between coronaryartery disease and abnormal glucose regulation in China: the ChinaHeart Survey. *Eur Heart J* 27:2573–2579

Chapter 82

Cardiac Hypertrophy-Specific Genes are Synergistic Activated by Myocardin and CREB-binding protein (CBP) p300

Zhenyu Wang, Xuehua Zhao, Mingzhe Li, Dongsun Cao
and Tong-Cun Zhang

Abstract Myocardin is a remarkably potent transcriptional co-activator expressed in a broad range of embryonic and adult tissues, and it can induce cardiac hypertrophy. However, it remains poorly understood about the effects of myocardin in cardiac hypertrophy. Here, we show that the p300, a histone acetyltransferase, enhanced transcriptional activity of myocardin. Conversely, class II histone deacetylases HDAC5 suppress cardiac-special genes activation by myocardin and p300. These findings point that myocardin maybe a nexus for regulation of cardiac hypertrophic-special genes expression by changes in chromatin acetylation. Our results provide novel evidence to explore the roles of myocardin and their co-factors in cardiac hypertrophy for the future studies.

Keywords Myocardin · p300 · Transactivation · Cardiac hypertrophy

Zhenyu Wang and Xuehua Zhao are the two co-first authors.

Z. Wang · M. Li · D. Cao · T.-C. Zhang (✉)
Institute of Life Science, Wuhan University of Science and Technology,
Wuhan 430065, China
e-mail: zhangtongcun@wust.edu.cn

Z. Wang
e-mail: wangzhenyu@wust.edu.cn

X. Zhao · M. Li
Department of Biological Chemistry, College of Medical, Wuhan University of Science
and Technology, Wuhan 430065, China

82.1 Introduction

Hypertrophy is a principal response of the heart to overload from any causes, which include myocardial infarction, dilated cardiomyopathy, valvar heart disease, and hypertension [1]. At the cellular level, the characteristics of cardiac hypertrophy includes that cell size and protein synthesis is increased, and a set of fetal cardiac genes, which are normally expressed in the heart only before birth, are reactivated [2–4]. It suggests that the transcriptional control program of cardiac fetal genes may be redeployed to regulate hypertrophic cardiac growth. However, the molecular mechanisms that regulate cardiac hypertrophy remain poorly understood over the past years.

Serum response factor, SRF, a protein expressed in all tissues and containing conserved MADS (MDM1, agamous, deficiens, SRF) domain, is required for specification of muscle tissue lineages, such as cardiac and smooth muscle [5, 6]. SRF binds CArG box, a highly conserved cis-regulatory element CC(A/T)6GG, and existing in promoters of target genes include cardiac and smooth muscle-specific genes which encodes atrial natriuretic factor (ANF), α -actin, myosin heavy chain (cardiac-MHC), and so on, and plays key role in the expression of these genes [7, 8]. Except binding to specific DNA sequence, SRF can also interact with a wide variety of cell-restricted and/or signal-dependent accessory co-factors.

Until now, myocardin may be the most potent co-factor of the SRF-associated proteins identified [9]. Myocardin is the strongly transcriptional coactivator expressed specifically in cardiac muscle and smooth muscle cells (SMCs) during postnatal development, and is required for cardiomyocyte survival and maintenance of heart function [10]. Myocardin interacts with SRF, and then binds to CArG box motifs to synergistically activate expression of cardiac and smooth muscle-specific genes [8–12], then induces cardiomyocyte hypertrophy [13]. But currently, we still know relatively little about the function of myocardin in the heart and its hypertrophy.

Chromatin remodeling and histone modifications, e.g., histone acetylation/deacetylation play essential roles in heart development and disease by reprogramming gene expression under different pathophysiological conditions [14]. CREB-binding protein (CBP) p300, the most extensively studied histone acetyltransferases (HATs) in muscle, is required for heart muscle development and hypertrophy [15]. The study showed that CBP can be recruited to the SRF-myocardin complex, and acetylates nucleosomal histones surrounding the SRF-binding site, and transactivates differentiation marker genes of SMCs [16]. In cardiac hypertrophy, the interaction between myocardin and p300 and their effects remain poorly understood.

In our studies, we investigated the effect how p300 regulates cardiac hypertrophy-specific genes transcription activated by myocardin. Luciferase reporter assays illustrated that p300 significantly increased synergistic activity of ANF-promoter, α -actin-promoter, and MHC-promoter with myocardin in COS-7 cells and neonatal rat myocytes. Furthermore, we show that co-transfection of myocardin and p300 in

neonatal rat cardiomyocytes could significantly upregulate cardiac hypertrophic gene expression. This study indicates that myocardin and p300 might combine together and play an important role in cardiac hypertrophy.

82.2 Materials and Methods

82.2.1 Plasmids

Plasmids, which were used in this study, have all been reported previously [13, 16], and the expressive plasmid, pcDNA3.1(-)(Invitrogen), was used as a control.

82.2.2 Preparation of Primary Neonatal Rat Myocytes

Cultured cardiomyocytes were obtained from 1–3-day-old SD rats with the following modifications. Briefly, the ventricles were isolated, dissected from major vessels, and cut into small pieces. The heart tissues were then digested through multiple rounds in phosphate buffered solution (PBS), pancreatin (Sigma), and 100 units/mL collagenase (GIBCO) at 37 °C for 15 min. After centrifugation, the cells were resuspended in DMEM/F12 (HyClone) containing 20 % fetal bovine serum (FBS). Afterward, the cells were differentially plated for 1 h to remove contaminating nonmyocytes, and were then plated on dishes with a density of 1×10^6 cells/mL. Cardiomyocytes were cultured in medium supplemented with 20 % FBS for 12 h at 37 °C in a 5 % CO₂ incubator and changed to serum-free DMEM/F12 before transfections and/or treatments.

82.2.3 Transient Transfection and Luciferase Reporter Assays

COS-7 cells and cardiomyocytes were seeded at 1.5×10^4 cells/cm² onto 24-well plates approximately 12 h before transfection. Plasmids were transfected into cells using Fugene HD (Roche Applied Science). 10 µL of extracts (100µL/well) were prepared for luciferase activity assays by using a luciferase reporter assay system according to the manufacturer's directions (Promega). Report gene luciferase activities were normalized to the luciferase activity of the control. Each sample was examined in duplicate, and it was repeated in 3 different experiments.

82.2.4 *Semi-quantitative RT-PCR*

Semi-quantitative RT-PCR analysis was carried out as described previously [13, 16]. To show equal loading of the cDNA samples, GAPDH (glyceraldehyde-3-phosphate dehydrogenase) was used as an internal control. The PCR primer sequences are as follows: GAPDH: Forward-ATTCAACGGCACAGTCAAGG, Reverse-GCAGAAGGGGCGGAGATGA; ANF: Forward-AGAGAGTGAGCCGAGACAGC, Reverse-TCTGAGACGGGTTGACTTCC; α -actin: Forward-CATAGCCAGCAAAGGG, Reverse-CAAGGCACAGA AACCAA; cardiac-MHC: Forward-TGAGACGGACGCCATACAG, Reverse-CCTCATACTTCTGCTTCC ACTC.

82.2.5 *Statistical Analysis*

Data were expressed as mean \pm SE and accompanied by the number of experiments performed independently, and analyzed by *t*-test.

82.3 Results

82.3.1 *The Transcriptional Activity of Myocardin is Modulated by p300*

We tested whether p300, a ubiquitous transcriptional coactivator with intrinsic HAT activity, might modulate myocardin activity. The expression plasmids encoding myocardin and p300 were co-transfected into COS cells, and resulted in synergistic and dose-dependent activation of luciferase reporters linked to the cardiac muscle-specific ANF, cardiac- α -actin, and cardiac-MHC promoters (Fig. 82.1a–c), all controlled by CARG boxes. Similarly, the ability of myocardin activating a luciferase reporter linked to ANF, α -actin, and MHC promoter was enhanced by p300 in cultured neonatal rat myocytes (Fig. 82.1d–f). And, we can see that p300 alone could not stimulate expression of CARG box-dependent reporters, whereas it could augment the promyogenic activity of myocardin, and these suggested that effects of p300 were directed at myocardin, not SRF, the endogenous factor both in COS cells and cardiac myocytes (Fig. 82.1a–f).

To further investigate whether the histone acetylation–deacetylation affects the activation of cardiac muscle gene expression by myocardin, we tested potential involvement of HDAC5, a class II HDAC, in the transcriptional activity of myocardin. Increasing the relative level of p300 could counteract the repressive effect of HDAC5 on the transcriptional activity of myocardin, and vice versa (Fig. 82.1g). In part, the study suggested that p300 and HDAC5 stimulate and

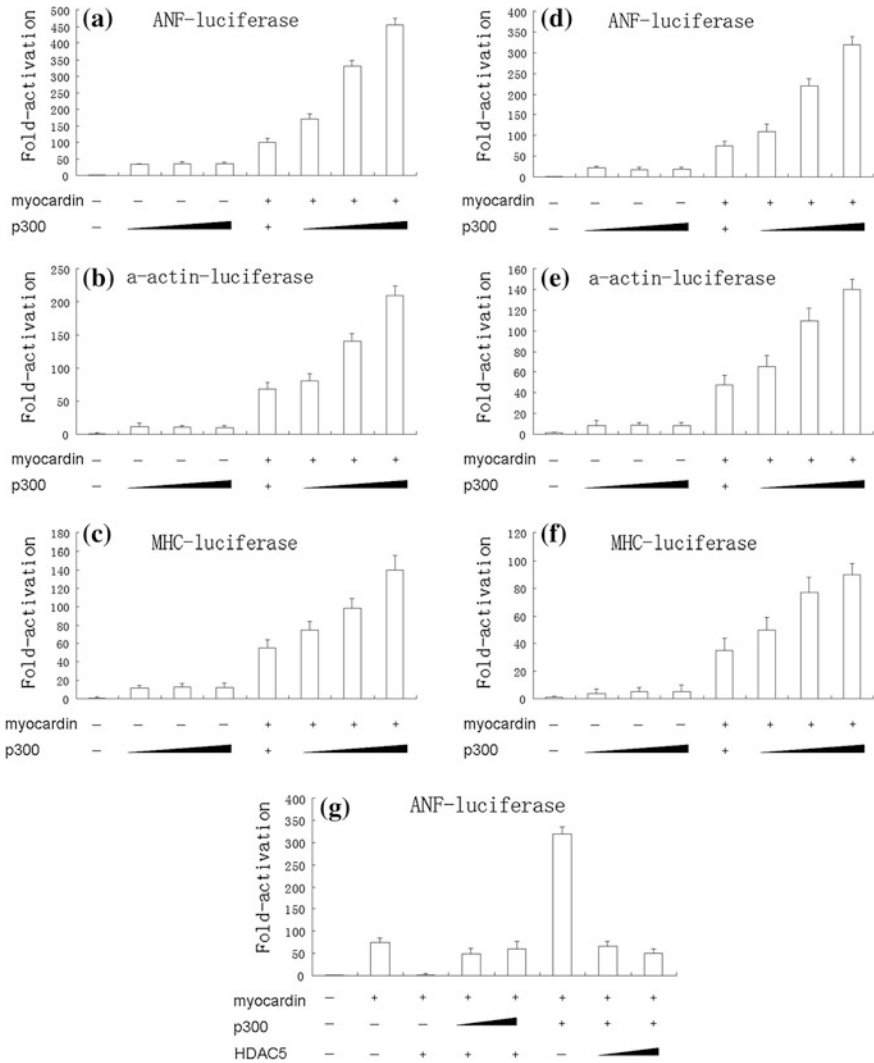


Fig. 82.1 P300 and HDAC5 modulate the transcriptional activity of myocardin. **a–c** Expression vectors encoding myocardin (0.1 μ g) and p300 (0.1, 0.3 and 0.5 μ g) were transiently co-transfected into COS cells and the indicated luciferase reporters as described in Sect. 82.2. **d–f** Expression vectors encoding myocardin (0.2 μ g) and p300 (0.2, 0.6 and 1 μ g) were transiently co-transfected into primary neonatal rat cardiomyocytes and the indicated luciferase reporters as described in Sect. 82.2. **g** Expression vectors encoding myocardin (0.2 μ g), p300 (1 μ g), HDAC5 (0.5 μ g), and increasing amounts of p300 (0.6 and 1 μ g) and HDAC5 (0.5, and 1 μ g), respectively, were transiently transfected into primary neonatal rat cardiomyocytes, and the ANF-luciferase reporter as described in Sect. 82.2

suppress the activity of myocardin respectively, and exert opposing influences on cardiac muscle gene expression.

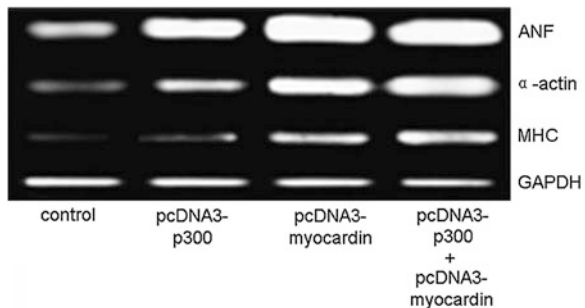
82.3.2 *The Cardiac Hypertrophy-Specific Genes are Regulated by Overexpressing Myocardin and p300 In Vivo*

Xing et al. reported that myocardin might promote cardiomyocyte hypertrophy [13]. To investigate whether p300 enhances the transcriptional activity of myocardin in cardiomyocytes, RT-PCR was carried out to determine changes in cardiac hypertrophy-specific genes expression as a result of co-transfecting expression plasmids of myocardin and p300 into primary neonatal rat myocytes. As shown in Fig. 82.2, ANF, α -actin, and MHC mRNA levels were significantly elevated. Therefore, in partially, p300 plays an important role in cardiac hypertrophy induced by myocardin.

All of these suggest that myocardin and p300 may combine to regulate cardiac-specific genes and induce cardiac hypertrophy. In our study, the results demonstrate that transcription effect of cardiac-specific genes promoter activated by myocardin could be enhanced by p300, and suppressed by HDAC5.

Furthermore, the expression of cardiac gene is induced with co-transfecting myocardin and p300 into neonatal rat cardiomyocytes. Our studies indicate that combined activities of myocardin and p300 may play an important role in cardiac hypertrophy. Our results provide novel evidence to explore the roles of myocardin and its co-factors in cardiac hypertrophy and potential therapeutic targets of heart disease for the future studies.

Fig. 82.2 P300 upregulated the expression of cardiac hypertrophy-specific genes activated by myocardin. Semi-quantitative RT-PCR analysis for ANF, α -actinin, and MHC in cardiomyocytes overexpressing myocardin and p300 at 48 h



82.4 Discussion

Cardiac hypertrophy is regulated by a complex transcription factor interaction. SRF, a highly interactive transcription factor, associates with other known hypertrophic regulatory factors and influences cellular growth [17]. Our previous results show that, in the heart, myocardin, a member of megakaryoblastic leukemia (MKL) family, binds directly to SRF, and activates a subset of cardiomyocyte-specific genes, such as those encoding myofibrillar, cytoskeletal, and structural proteins, and overexpression of these factors induces hypertrophy in neonatal rat cardiomyocytes, whereas their dominant-negative mutants block agonist-induced growth [13].

Histones involve in modulating the structure of chromatin and the accessibility of regulatory DNA sequences to transcriptional activators and repressors, and then controlling gene expression. Acetylation of histones by histone acetyltransferases can relax chromatin structure, and allow access of transcription factors to DNA and then stimulates gene expression [14]. Our previous study shows that p300 enhanced the activity of myocardin, and then induces the acetylation of nucleosomal histones surrounding CArG box in the control regions of smooth muscle genes [16].

Acknowledgments This work was financially supported by national natural science foundation of China (No. 30970615), natural science foundation of Hubei (No. 2010CDB03506), key project of Science and Technology Research of Hubei (No. D20111102), and college students' innovation fund of Wuhan university of Science and Technology (No. 10ZRZ097).

References

1. Levy DK, Anderson M, Savage DD et al (1988) Echocardiographically detected left ventricular hypertrophy: prevalence and risk factors. *Aann Int Med* 108:7–13
2. Akazawa H, Komuro I (2003) Roles of cardiac transcription factors in cardiac hypertrophy. *Circu Res* 92:1079–1088
3. Frey N, Olson EN (2003) Cardiac hypertrophy: the good, the bad, and the ugly. *Ann Rev Physio* 65:45–79
4. Olson EN, Schneider MD (2003) Sizing up the heart: development redux in disease. *Genes Dev* 17:1937–1956
5. Arsenian S, Weinhold B, Oelgeschlager M et al (1998) Serum response factor is essential for mesoderm formation during mouse embryogenesis. *EMBO J* 17:6289–6299
6. Belaguli NS, Schildmeyer LA, Schwartz RJ (1997) Organization and myogenic restricted expression of the murine serum response factor gene. *J Biol Chem* 272:18222–18231
7. Miano JM (2003) Serum response factor: toggling between disparate programs of gene expression. *J Mol Cell Cardiol* 35:577–593
8. Small EM, Warkman AS, Wang DZ et al (2005) Myocardin is sufficient and necessary for cardiac gene expression in *Xenopus*. *Development* 132:987–997
9. McDonald Wamhoff BR, Hoofnagle MH et al (2006) Control of SRF binding to CArG box chromatin regulates smooth muscle gene expression in vivo. *J Clin Invest* 116:36–48

10. Huang J, Lu M, Cheng L et al (2009) Myocardin is required for cardiomyocyte survival and maintenance of heart function. *Proc Natl Acad Sci U S A* 106:18734–187349
11. Wang Z, Wang DZ, Pipes GC et al (2003) Myocardin is a master regulator of smooth muscle gene expression. *Proc Natl Acad Sci U S A* 100:7129–7134
12. Li S, Wang DZ, Wang Z et al (2003) The serum response factor coactivator myocardin is required for vascular smooth muscle development. *Proc Natl Acad Sci U S A* 100:9366–9370
13. Xing W, Zhang TC, Cao D et al (2006) Myocardin induces cardiomyocyte hypertrophy. *Circu Res* 98:1089–1097
14. Backs J, Olson EN (2006) Control of cardiac growth by histone acetylation/deacetylation. *Circu Res* 6:15–24
15. Han P, Hang CT, Yang J et al (2011) Chromatin remodeling in cardiovascular development and physiology. *Circul Res* 108:378–396
16. Cao D, Wang Z, Zhang C et al (2005) Modulation of smooth muscle gene expression by association of histone acetyltransferases and deacetylases 6 with myocardin. *Mol Cell Bio* 25:364–376
17. Oh J, Wang Z, Wang DZ et al (2004) Target gene-specific modulation of myocardin activity by GATA transcription factors. *Mol Cell Biol* 24:8519–8528

Chapter 83

Design, Synthesis and Biological Evaluation of the Novel Antitumor Agent 2-benzyl-3, 4-dihydroisoquinolin-1(2H)-one and Its Derivatives

Jian Lv, Lei Lv, Xiaomin Zhang, Yao Zhou, Kui Lu, Yifei lu, Yuou Teng, Hua Sun and Peng Yu

Abstract Tetrahydroisoquinoline and its derivatives have a wide range of biological activities, such as antitumor, antimicrobial, and analgesic properties and so on. Some tetrahydroisoquinoline alkaloid derivatives have been studied as antitumor drug molecules, but 2-benzyl-7-substituted-ethoxy]-3, 4-dihydro-1(2H)-isoquinolinone series have not been reported yet. In this paper, we would like to report the design, synthesis, and biological evaluation of the novel tetrahydroisoquinoline derivatives. Among those compounds, four new tetrahydroisoquinoline derivatives have not been reported before. All the newly synthesized compounds were characterized by ^1H NMR and their antitumor activities were evaluated by using HT-29, K562 and HepG2 cell line. 2-Benzyl-7-[2-(tert-butyl-4-piperazinecarboxylate) ethoxy]-3, 4-dihydro-1(2H)-isoquinolinone demonstrated good antitumor activity against K562 cancer cell with an IC_{50} of 1.58 μM .

Keywords Tetrahydroisoquinoline derivatives · Synthesis · Antitumor · MTT

83.1 Introduction

Tetrahydroisoquinolines are naturally occurring small molecules belonging to the alkaloids family, which possess a lot of biological activities such as antitumor, antimicrobial, analgesic, and antiarrhythmic [1–3]. Recently, it was reported that

J. Lv · L. Lv · X. Zhang · Y. Zhou · K. Lu · Y. Teng · H. Sun · P. Yu (✉)
Key Laboratory of Industrial Microbiology, Ministry of Education, College of Biotechnology, Tianjin University of Science and Technology, Tianjin 300457, People's Republic of China
e-mail: yupeng@tust.edu.cn

J. Lv · L. Lv · X. Zhang · Y. Zhou · K. Lu · Y. Teng · H. Sun · P. Yu
Tianjin Key Laboratory of Industry Microbiology, College of Biotechnology, Tianjin University of Science and Technology, Tianjin 300457, People's Republic of China

Y. lu
China Pharmaceutical University, Jiangsu 210009, People's Republic of China

animals and humans also have endogenous tetrahydroisoquinolines compounds, which play an important role by acting as the receptor or regulating the activity of enzymes [4].

Cancer is a global public health problem. WHO estimates that there are about 10 million new cancer patients each year. At present, cancer mortality rate is still on the rise. The existing chemotherapy drugs mostly by interfering cell division to kill cancer cells, in clinical practice by using anticancer drugs, the phenomenon of resistance gradually emerged. Thus there is an urgent need for more effective anticancer drugs.

In this paper, we would like to report the design and synthesis of novel tetrahydroisoquinolines derivatives with nucleophilic substitution reaction as the key step. The target compounds (6a–d) were synthesized in six steps through cyclization, nucleophilic substitution reaction, and so on. Biological activity evaluation indicated that 2-Benzyl -7-[2-(tert-butyl-4-piperazinecarboxylate) ethoxy]-3,4-dihydro-1(2H)-isoquinolinone (6d) shows good antitumor activity against K562 and HepG2 cells.

83.2 Materials and Methods

83.2.1 Materials and Measurements

All reagents and solvents used in this paper were of reagent grade. Reaction temperatures were controlled using oil bath temperature modulator. Thin layer chromatography (TLC) was performed using E. Merck silica gel 60 GF254 pre-coated plates (0.25 mm) and visualized using a combination of UV. Silica gel (particle size 200–400 mesh) was used for flash chromatography. ^1H NMR spectra was recorded on Bruker AM-400 NMR spectrometers in deuterated chloroform or deuterated DMSO. The chemical shifts are reported in δ (ppm) relative to tetramethylsilane as internal standard.

83.2.2 Chemistry

Figure 83.1 demonstrates the synthetic approach to the target compound 6a–d.

4-Methoxyphenethylamine was employed to react with ethyl chloroformate in basic condition to provide compound 1 which was then cyclized in PPA at 120 °C to afford the key intermediate 2. In this step, anhydrous conditions and appropriate reaction time were required. If the reaction conditions were not controlled well, almost no desired product or low yield was obtained.

After Compound 2 was charged to benzyl chloride to provide compound 3 in good yield (83 %), it was converted into compound 4 when treated with BBr_3 at -78 °C. With compound 4 in hand, two methods were tried for the preparation of compound

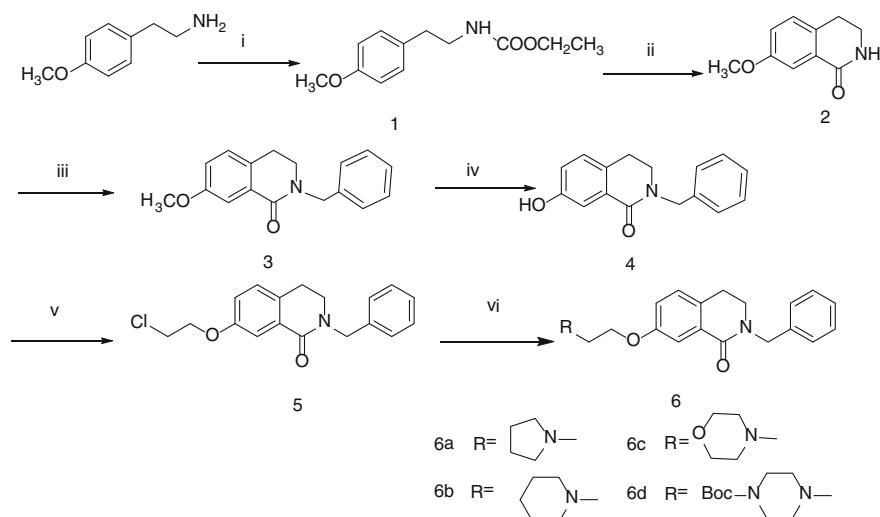


Fig. 83.1 Synthetic route to tetrahydroisoquinolines derivative

5. First, ethylenedichloride was used as reactant, but very low yield was obtained because the bis-alkylated byproduct was generated at the reaction condition. So we changed to the different approach with 1-bromo-2-chloroethane as the reactant which resulted in very good yield for the key intermediate. Compound **5** was then reacted with pyrrolidine, piperidine, morpholine, and 1-Boc-piperazine to afford compound **6a-d** respectively. In order to optimize the reaction condition, different times and temperatures were tested for each target compound, finally it was found that the best condition was 80 °C for 1 h for compound (**6a**) with 84 % yield; 90 °C for 5 h for compound (**6b**) with 54 % yield; 80 °C for 2 h for compound (**6c**) with 82 % yield, and 100 °C for 7 h for compound (**6d**) with 75 % yield, respectively.

Reagents and conditions: (i) ClCO_2Et , Et_3N , CH_2Cl_2 ; (ii) PPA; (iii) NaH, DMF, benzyl chloride; (iv) BBr_3 , CH_2Cl_2 ; (v) K_2CO_3 , DMF, 1-bromo-2-chloroethane; (vi) K_2CO_3 , DMF.

83.2.3 Biological Assay

The inhibition activities of above newly synthesized compounds were tested on the K562, HT-29, and HepG2 cells. The results of compounds **6a-d** were listed in Table 83.1. The results in Table 83.1 indicated that 2-benzyl-7-[2-(tert-butyl)-4-piperazinecarboxylate] ethoxy]-3, 4-dihydro-1(2H)-isoquinolinone (**6d**) demonstrated good antitumor activity against K562 and HepG2 with an IC_{50} of 1.58 μM and 3.86 μM , respectively. But it was not active against HT-29 ($\text{IC}_{50} > 10 \mu\text{M}$) at our test condition.

Table 83.1 Inhibition activity of the compound 6a, 6b, 6c, and 6d

Tested cell	Samples (IC ₅₀)			
	6a	6b	6c	6d
K562	>10	>10	>10	1.58
HepG2	>10	>10	>10	3.86
HT-29	>10	>10	>10	>10

83.3 Results and Discussion

83.3.1 Synthesize and Characterize tetrahydroisoquinolines Derivatives by ¹H NMR

[2-(4-Methoxyphenyl) ethyl]carbamic acid ethyl ester (1) [5, 6] To the 4-Methoxyphenethylamine (4.0 g, 0.026 mol) in dry dichloromethane (50 mL) at 0 °C was added dropwise triethylamine (4.02 g, 0.039 mol). After stirring for 10 min ethyl chloroformate (4.31 g, 40 mmol) was added. The reaction mixture was cooled to 5 °C and stirred at 5 °C for 2 h. The reaction mixture was diluted with dichloromethane (100 mL) and water (50 mL). The phases were separated and the organic layer was washed with water (2 × 100 mL), brine (100 mL), and dried over anhydrous magnesium sulfate. The solvent was removed under vacuum to afford the crude which was purified by flash column chromatography (silica gel, petroleum ether/ethyl acetate 20:1) to yield the compound 1 (5.5 g, 93 %).

¹H NMR (CDCl₃ 400 MHz): δ/ppm 1.22 (t, J = 7.2 Hz, 3H), 2.74 (t, J = 7.2 Hz, 2H), 3.41–3.36 (m, 2H), 3.78 (s, 3H), 4.12–4.07 (q, 2H), 4.72 (s, 1H), 6.86–6.82 (m, 2H), 7.11–7.09 (m, 2H).

7-methoxy-3, 4-dihydro-1(2H)-isoquinolone (2) [7–9] To a flask (50 mL) under Ar was added polyphosphoric acid (PPA) (75.7 g) and stirred for 30 min at 120 °C, then the compound 1 (5.0 g, 22.39 mmol) was rapidly added. The reaction mixture was stirred for 4.5 h at 120 °C. The reaction mixture was cooled to room temperature, poured into ice-water (100 mL), and then extracted with dichloromethane (3 × 100 mL). The combined organic layers were washed with water (2 × 100 mL), brine (100 mL), and dried over anhydrous magnesium sulfate. The solvent was removed under vacuum to afford the crude which was purified by flash column chromatography (silica gel, petroleum ether/ethyl acetate 1:1) to yield compound 2 (2.6 g, 67 %).

¹H NMR (d₆-DMSO 400 MHz): δ/ppm 2.87 (t, J = 6.8 Hz, 2H), 3.37 (t, J = 4.8 Hz, 2H), 3.81 (s, 3H), 7.10–7.07 (m, 1H), 7.28–7.25 (m, 1H), 7.41 (d, J = 2.8 Hz, 1H), 7.97 (s, 1H).

2-Benzyl-7-methoxy-3, 4-dihydro-1(2H)-isoquinolinone (3) [10] To a solution of compound 2 (2.0 g, 11.29 mmol) in dry N, N-Dimethylformamide (8 mL) was added NaH (60 % in oil, 0.54 g, 22.57 mmol) in portions at 0 °C. Benzyl chloride (2.14 g, 16.93 mmol) was added. The mixture was brought to room temperature and stirred until completion (TLC monitor). The reaction mixture was quenched

with saturated solution of NH_4Cl and then extracted with dichloromethane ($3 \times 100 \text{ mL}$). The combined extracts were washed with water ($2 \times 100 \text{ mL}$), brine (100 mL), and dried over anhydrous magnesium sulfate. The solvent was removed under vacuum to provide the crude which was purified by flash column chromatography (silica gel, petroleum ether/ethyl acetate 15:1) to afford compound 3 (2.5 g, 83 %).

^1H NMR (CDCl_3 , 400 MHz): δ/ppm 2.90 (t, $J = 4.4 \text{ Hz}$, 2H), 3.50 (t, $J = 4.4 \text{ Hz}$, 2H), 3.88 (s, 3H), 4.82 (s, 2H), 7.10–7.00 (m, 2H), 7.37–7.29 (m, 5H), 7.72 (d, $J = 1.6 \text{ Hz}$, 1H).

2-Benzyl-7-hydroxy-3, 4-dihydro-1(2H)-isoquinolinone (4) [11] To a solution of compound 3 (1.5 g, 5.61 mmol) in dry dichloromethane (25 mL) at -78°C was added dropwise BBr_3 (5.62 g, 22.44 mmol) and the mixture was brought to room temperature and stirred overnight. MeOH was added at 0°C until the reaction mixture was clear. The solvent was removed in vacuo to give the crude product which was purified by flash column chromatography (silica gel, petroleum ether/ethyl acetate 1:1) to afford compound 4 (1.2 g, 84 %).

^1H NMR (CDCl_3 , 400 MHz): δ/ppm 2.88 (t, $J = 6.4 \text{ Hz}$, 2H), 3.51 (t, $J = 6.8 \text{ Hz}$, 2H), 4.83 (s, 2H), 7.01–6.99 (m, 1H), 7.07–7.05 (m, 1H), 7.36–7.28 (m, 5H), 8.17 (d, $J = 2.4 \text{ Hz}$, 1H).

2-Benzyl-7-(2-chloroethoxy)-3, 4-dihydro-1(2H)-isoquinolinone (5) [12–14] To a solution of compound 4 (2.0 g, 7.90 mmol) in dry N, N-Dimethylformamide (5 mL) was added K_2CO_3 (3.27 g, 23.69 mmol). After stirring for 10 min 1-bromo-2-chloroethane (3.40 g, 23.69 mmol) was added. The reaction mixture was heated to 80°C and refluxed for 24 h. The reaction mixture was cooled to room temperature, and diluted with dichloromethane (100 mL). The organic layers were washed with water (100 mL), brine (100 mL), and dried over anhydrous magnesium sulfate. The solvent was removed under vacuum to afford the crude which was purified by flash column chromatography (silica gel, petroleum ether/ethyl acetate 10:1) to get compound 5 (1.9 g, 76 %).

^1H NMR (CDCl_3 , 400 MHz): δ/ppm 2.90 (t, $J = 6.4 \text{ Hz}$, 2H), 3.50 (t, $J = 6.8 \text{ Hz}$, 2H), 3.85 (t, $J = 5.6 \text{ Hz}$, 2H), 4.33 (t, $J = 6.0 \text{ Hz}$, 2H), 4.82 (s, 2H), 7.06–7.04 (m, 1H), 7.12–7.10 (m, 1H), 7.36–7.30 (m, 5H) 7.70 (d, $J = 2.8 \text{ Hz}$, 1H).

Compounds (6a–d) To a solution of compound 5 (1 equiv) in dry N, N-Dimethylformamide (2 mL) was added K_2CO_3 (3.0 equiv). After stirring for 10 min a-d (1.5 equiv) was added. The reaction mixture was heated to the 80 – 100°C and refluxed for 5 h. The reaction mixture was cooled to room temperature, and diluted with dichloromethane (100 mL). The organic layers were washed with water (100 mL), brine (100 mL), and dried over anhydrous magnesium sulfate. The solvent was removed under vacuum to afford the crude which was purified by flash column chromatography (silica gel, petroleum ether/ethyl acetate 1:1) to get compounds (6a–d).

2-Benzyl-7-[(1-pyrrolidinyl) ethoxy]-3, 4-dihydro-1(2H)-isoquinolinone (6a) [15] Starting from compound 5 (1.5 g, 4.75 mmol) and pyrrolidine (0.51 g, 7.12 mmol), compound 6a was obtained in 84 % yield.

^1H NMR (CDCl_3 , 400 MHz): δ/ppm 1.85–1.82 (m, 4H), 2.68–2.65 (m, 4H), 2.88 (t, $J = 6.4$ Hz, 2H), 2.94 (t, $J = 6.0$ Hz, 2H), 3.45 (t, $J = 6.8$ Hz, 2H), 4.20 (t, $J = 6.0$ Hz, 2H), 4.81 (s, 2H), 7.06–7.03 (m, 2H), 7.35–7.28 (m, 5H), 7.71 (d, $J = 2.8$ Hz, 1H).

2-Benzyl-7-[2-(1-piperidinyl) ethoxy]-3,4-dihydro-1(2H)-isoquinolinone (6b) [16] Starting from compound 5 (2.0 g, 6.33 mmol) and piperidine (0.81 g, 9.50 mmol), compound 6b was obtained in 54 % yield.

^1H NMR (CDCl_3 , 400 MHz): δ/ppm 1.48–1.45 (m, 2H), 1.66–1.60 (m, 4H), 2.55–2.53 (m, 4H), 2.82 (t, $J = 6.0$ Hz, 2H), 2.88 (t, $J = 6.4$ Hz, 2H), 3.49 (t, $J = 6.8$ Hz, 2H), 4.19 (t, $J = 6.0$ Hz, 2H), 4.81 (s, 2H), 7.09–7.00 (m, 2H), 7.36–7.29 (m, 5H), 7.70 (d, $J = 2.8$ Hz, 1H).

2-Benzyl-7-[2-(4-morpholinyl) ethoxy]-3,4-dihydro-1(2H)-isoquinolinone (6c) [17] Starting from compound 5 (1.6 g, 5.07 mmol) and morpholine (0.67 g, 7.60 mmol), compound 6c was obtained in 82 % yield.

^1H NMR (CDCl_3 , 400 MHz): δ/ppm 2.61–2.59 (m, 4H), 2.83 (t, $J = 5.6$ Hz, 2H), 2.88 (t, $J = 6.8$ Hz, 2H), 3.48 (t, $J = 6.8$ Hz, 2H), 3.76–7.40 (m, 4H), 4.19 (t, $J = 5.6$ Hz, 2H), 4.81 (s, 2H), 7.09–6.99 (m, 2H), 7.35–7.30 (m, 5H), 7.70 (d, $J = 2.4$ Hz, 1H).

2-Benzyl-7-[2-(tert-butyl-4-piperazinecarboxylate) ethoxy]-3, 4-dihydro-1(2H)-isoquinolinone (6d) [18] Starting from compound 5 (1.6 g, 5.07 mmol) and 1-Boc-piperazine (1.42 g, 7.60 mmol), compound 6d was obtained in 75 % yield.

^1H NMR (CDCl_3 , 400 MHz): δ/ppm 1.47 (s, 9H), 2.57–2.54 (m, 4H), 2.90–2.84 (m, 4H), 3.50–3.47 (m, 6H), 4.20 (t, $J = 5.6$ Hz, 2H), 4.80 (s, 2H), 7.02–6.99 (m, 1H), 7.09–7.07 (m, 1H), 7.35–7.28 (m, 5H), 7.70(d, $J = 2.8$ Hz, 1H).

83.3.2 Biological assay

The antiproliferative effect of these compounds was determined against K562, HepG2, and HT-29 cells by using MTT assay [19]. The cells were diluted to a density of 5×10^4 cells/mL and added 100 μL to each well of the 96-well plates with a multichannel pipet. After incubating for 24 h, 0.5 μL compounds were added and then cells were further incubated for 48 h (final concentrations of each compound: 0.1, 0.3, 1, 3 and 10 μM). The culture plates were incubated for 4 h after which 20 μL MTT was added to each well, then the medium were removed from the wells and 100 μL DMSO added into each well. After leaving for further 10 min to dissolve the formazan crystals formed, the optical density (OD) was measured at 490 and 630 nm. Cell viability was calculated from measurements of OD value according to the corresponding formula and a graph is plotted of Cell viability (y-axis) against drug concentration (x-axis) [20]. The inhibitory concentrations by 50 % values (IC_{50}) of sample compounds toward test cell proliferation were presented in Table 83.1.

83.4 Conclusion

We report the design and synthesis of novel tetrahydroisoquinolines derivatives, several steps among this route were optimized, such as cyclization, nucleophilic substitution reaction. The nucleophilic substitution reaction was the key step. All the target compounds were synthesized in six steps with the overall yield of 20–25 %, respectively. The structures of these novel targets and all of intermediates were confirmed by ^1H NMR. Biological activity test indicated that 2-Benzyl-7-[2-(tert-butyl-4-piperazinecarboxylate) ethoxy]-3, 4-dihydro-1(2H)-isoquinolinone (6d) has good antitumor activity against K562 and HepG2 cell. In order to improve the antitumor activity further modification base on compound (6d) was undergoing in our lab.

Acknowledgments The authors sincerely thank the financial support from the Tianjin University of Science and Technology (20090431), the Science and Technology Project of Tianjin (10ZCKFSY07700 and 11ZCGHHZ00400), the Natural Science Foundation of Tianjin (11JGYBJC14300) and the High School Science and Technology Development Foundation of Tianjin (20090226).

References

1. Gitto R, Damiano FM, Ferro S (2011) Synthesis and biological profile of new 1, 2, 3, 4-tetrahydroisoquinolines as selective carbonic anhydrase inhibitors. *Bioorg Med Chem* 19:7003–7007
2. Nicolauo KC, Valiulin RA, Pokorski JK (2012) Bio-inspired synthesis and biological evaluation of a colchicine-related compound library. *Bioorg Med Chem Lett* 22:3776–3780
3. Horling A, Mueller C, Barthel R (2012) A new class of selective and potent 7-dehydrocholesterol reductase inhibitors. *J Med Chem* 55:7614–7622
4. Kartnig T, Bucar F, Wagner H et al (1991) Flavonoids from the aboveground parts of *Ruscus aculeatus*. *Planta Med* 57:85
5. Funke U, Fischer S, Hiller A et al (2008) 3-(4-(6-Fluoroalkoxy-3, 4-dihydroisoquinoline-2(1H)-yl)cyclohexyl)-1H-indole-5-carbonitriles for SERT imaging: chemical synthesis, evaluation in vitro and radiofluorination. *Bioorg Med Chem Lett* 18:4727–4730
6. Anderson WK, McPherson HL Jr, New JS et al (1984) Synthesis and murine antineoplastic activity of bis[(carbamoyloxy)methyl] derivatives of pyrrolo[2,1-a]isoquinoline. *J Med Chem* 27:1321–1325
7. Kessar SV, Kulkarni SK, Jain R et al (2009) Preparation of isoquinoline compounds as monoamine re-uptake inhibitor for treating nervous system disorders WO 2009118765
8. Flynn DL, Petillo PA (2008) Preparation of pyrazolyl phenyl ureas as enzyme modulators. US 20080113967
9. Plobeck N, Delorme D, Wei ZY et al (2000) New diarylmethylpiperazines as potent and selective nonpeptidic delta opioid receptor agonists with increased in vitro metabolic stability. *J Med Chem* 43:3878–3894
10. Fisher MJ, Gunn B, Harms Cs et al (1997) Non-peptide RGD surrogates which mimic a Gly-Asp beta-turn: potent antagonists of platelet glycoprotein IIb-IIIa. *J Med Chem* 40:2085–2101
11. Sall DJ, Grunewald GL et al (1987) Inhibition of phenylethanolamine N-methyltransferase (PNMT) by aromatic hydroxy-substituted 1, 2, 3, 4,-tetrahydroisoquinolines: further studies

- on the hydrophilic pocket of the aromatic ring binding region of the active site. *J Med Chem* 30:2208–2216
12. Hardcastle IR, Rowlands MG, Houghton J et al (1995) Rationally designed analogues of tamoxifen with improved calmodulin antagonism. *J. Med.Chem* 38:241–248
 13. Bogomazova AA, Kunakova RV, Zlotskii SS (2010) Reactions of 1,1- and 1,2-dihaloalkanes with substituted phenols. *Bashkirskii Khimicheskii Zhurnal* 17:19–22
 14. Staneva TD, Nacheva EB, Lazarov VK et al (2004) Method for the production of methyl 2-[4-[2-(1-piperidinyl) ethoxy]benzoyl]benzoate hydrochloride BG 107390
 15. Blume E, Winkelmann E, Schaper W et al (1985) 1-(2-Aryl-1,3-dioxolan-2-ylmethyl)azoles, their salts, and their use DE 3410070
 16. Kumar A, Pathak SR, Ahmad P et al (2006) Novel substituted naphthalen-1-yl-methanone derivatives as anti-hyperglycemic agents. *Bioorg Med Chem Lett* 16:2719–2723
 17. Pierce AC, Arnost M, Davies RJ et al (2004) Preparation of 3,5-diamino[1,2,4]triazoles as protein kinase inhibitors WO 2004046120
 18. Hennequin, Laurent Francois Andre (2005) Preparation of quinazolines as inhibitors of VEGF receptor tyrosine kinases. WO 2005014582
 19. Mosmann T (1983) Rapid colorimetric assay for cellular growth and survival: application to proliferation and cytotoxicity assays. *J Immunol Methods* 65:55–63
 20. Haudecoeur R, Ahmed-Belkacem A, Yi W et al (2011) Discovery of naturally occurring aurones that are potent allosteric inhibitors of hepatitis C virus RNA-dependent RNA polymerase. *J Med Chem* 54:5395–5402

Chapter 84

Using Water Miscible Ionic Liquid to Improve the Efficiency of 15 α -hydroxylation of 13-ethyl-gon-4-en-3,17-dione by *Penicillium raistrickii*

Shuhong Mao, Na Wang, Zhijiang Ge, Boyuan Hua, Yanqing Li and Fuping Lu

Abstract Improved efficiency of steroid microbial transformation by co-solvents is generally attributed to their positive effects on the solubility of substrate in aqueous media. Ionic liquids have been widely researched as possible ‘green’ replacements for organic solvents. In this study, the effect of water miscible ionic liquids on the 15 α -hydroxylation of 13-ethyl-gon-4-en-3,17-dione by *Penicillium raistrickii* ATCC 10490 was investigated. The results indicated that the striking improvement of biotransformation of substrates up to 94.46 % were obtained after addition of [BMIM]BF₄ under the optimized conditions. This also resulted in morphological changes of *P. raistrickii* mycelia in the fermentation broth with or without [BMIM]BF₄. Based on the above observations, we therefore conclude that [BMIM]BF₄-induced changes of mycelial morphology of *P. raistrickii* have positive effects on the production of the desired product, thus most likely contributing to the observed higher yield of steroid biotransformation in addition to [BMIM]BF₄ known effects on substrate solubility.

Keywords Biotransformation • Fungal morphology • Ionic liquids • *Penicillium raistrickii*

S. Mao · B. Hua · F. Lu (✉)

Key Laboratory of Industrial Fermentation Microbiology, Ministry of Education, Tianjin University of Science and Technology, Tianjin 300457, People’s Republic of China
e-mail: lfp@tust.edu.cn

N. Wang · Z. Ge · F. Lu

National Engineering Laboratory for Industrial Enzymes, Tianjin University of Science and Technology, Tianjin 300457, People’s Republic of China

Y. Li

Tianjin Key Laboratory of Industrial Microbiology, College of Biotechnology, Tianjin University of Science and Technology, Tianjin 300457, People’s Republic of China

84.1 Introduction

Gestodene is exogenous female sex steroid with extremely potent oral contraceptive. And gestodene appears to cause fewer adverse effects. Therefore, they are commonly used in clinics [1]. In the preparation of gestodene, 15 α -hydroxylation of 13-ethyl-gon-4-en-3,17-dione, an important intermediate product, plays an important role.

In steroid microbial transformation, the dissolution of substrate is the key step [2]. Solubility of steroids in water-containing media is very low, i.e., 10^{-4} – 10^{-5} mol/l. This considerably limits the productivity of the biotransformation systems, where the initial substrate concentration hardly ever exceeds 2×10^{-3} mol/l. Conventional approach to solve this problem is the feeding of substrates in the form of saturated solutions in water-miscible solvents. In fact, there are many literatures on the optimization of co-solvents for the yield improvement of desired product [2–4], and to study the relationship between biotransformation rate and factors influencing this.

Ionic liquids have been widely researched as possible ‘green’ replacements for organic solvents. ILs are salts with unique physical properties, such as a negligible vapor pressure, low viscosity, and high thermal stability. There are many examples for the use of these kinds of ILs in biocatalysis and biotransformations [5]. However, the kinds of biocatalysts used in ionic liquids have been very limited, and most of those reported so far are hydrolytic enzymes such as lipases. To this day, the possibility of whole-cell catalysis in the presence of ILs remains largely unexplored, with only a few published accounts [6–8]. In this study, we investigated the application of four water miscible ILs in 15 α -hydroxylation of 13-ethyl-gon-4-en-3,17-dione catalyzed by *P. raistrickii* ATCC 10490. Besides, the effect of ILs as co-solvents on the morphological changes in the bioconversion was also discussed.

84.2 Materials and Methods

84.2.1 Microorganisms and Medium Format

P. raistrickii ATCC 10490 were maintained on glucose/peptone/agar slants which were incubated at 28 °C for a week, followed by adding 5 ml water to each slant, and scalping the spores from the agar surface. The harvested spore suspensions were inoculated into 50 ml fermentation medium in a 250 ml flask, with a final concentration of 5×10^6 spores/ml. After growth for 21 h on a shaking operating at 28 °C and 180 rpm, 5 % of the seed culture was inoculated in the fermentation medium which contains (g/L) glucose, 20; corn steep liquor, 10; NaNO₃, 2; KH₂PO₄, 1; K₂HPO₄, 2; MgSO₄, 0.5; FeSO₄, 0.02; KCl, 0.5. After 36 h, the substrates with 3 % ILs were added to the fermentation medium to investigate the effects of ILs on the morphology of *P. raistrickii* ATCC 10490.

84.2.2 Chemicals Analysis

The cultures of 500 μl were collected, then extracted 30 min with one volume of ethyl acetate. The extracts were dried in air, and afterwards resolved in 1,000 μl methanol. The determination of substrate and product was carried out by high-pressure liquid chromatography at 241 nm with an isocratic run of methanol/water = 80:20 and a flow of 1 ml/min using ODS-2HPERSIL C18 column.

84.2.3 Morphological Measurement

Pellet particles were analyzed by determining the number of pellet per given volume and pellet size. Images of *P. raistrickii* ATCC 10490 were captured by BX51 microscopy (OLYMPUS Ltd., Japan); the captured images were analyzed by FerAnaForAv software developed by the State Key Laboratory of Bioreactor Engineering, National Research Center for Biotechnology (Shanghai). The size of the pellet was quantified using the diameter corresponding to a circular area equivalent to the pellet projected area.

84.3 Results and Discussion

84.3.1 Effect of ILs on the Production of 15 α -hydroxylation of 13-ethyl-gon-4-en-3,17-dione

ILs are usually added to the fermentation broth to improve the dissolution of substrate in aqueous by the formation of water-solubility agents with substrates [9]. Moreover, hydrophile ILs reduced the polarity of the conversion system and enhanced the transportation of substrates into fungi [5]. Therefore, during the microbial hydroxylation at C-15 of 13-ethyl-gon-4-en-3,17-dione by *P. raistrickii* ATCC 10490, water-miscible ILs and organic solvents such as [BMIM]DCA, [BMIM]Cl, [BMIM]BF₄, [BMIM]Br, and 1,2-propanediol, were used as co-solvents to enhance the solubility of 13-ethyl-gon-4-en-3,17-dione and to improve the yields of desire product.

As shown in Figs. 84.1 and 84.2, the addition of ILs and hydrophile organic solvents plays positive effects on biotransformation. In contrast to the bioconversion system without co-solvents, the conversion rate of the initial substrate concentration of 3.0 g/l, has been improved obviously after the addition of 4 % [BMIM]DCA, [BMIM]Cl, [BMIM]BF₄, [BMIM]Br, and 1,2-propanediol, respectively. Actually, it was found that the conversion rates were higher than 70.0 % after the addition of 4 % [BMIM]DCA, [BMIM]Cl, [BMIM]BF₄, [BMIM]Br, and 1,2-propanediol, separately.

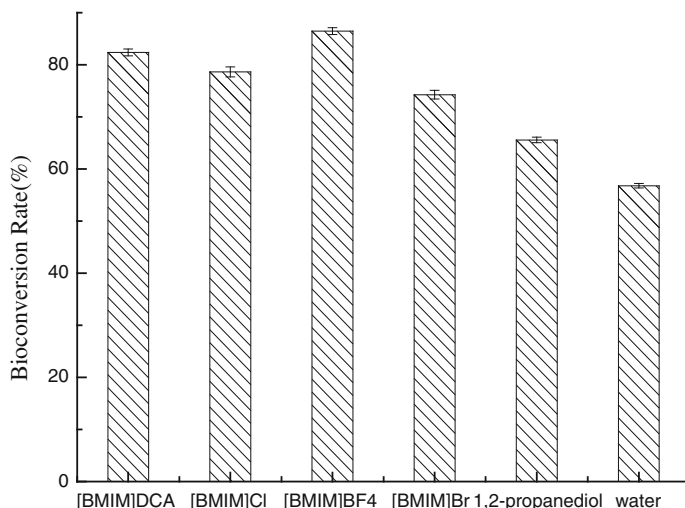


Fig. 84.1 Bioconversion rate of 13-ethyl-gon-4-en-3,17-dione to 15 α -hydroxylation of 13-ethyl-gon-4-en-3,17-dione without co-solvents, and with 4 % [BMIM]DCA, [BMIM]Cl, [BMIM]BF₄, [BMIM]Br, 1,2-propanediol, respectively

Subsequently, the effects of concentration of hydrophile ILs and organic solvent on steroid bioconversion were investigated. As displayed in Fig. 84.2, the maximum conversion rate up to 90.24 % was obtained when 3.0 % [BMIM]BF₄ were added. And then, the conversion rate decreased with the increasement of [BMIM]BF₄. Similar results were also found for [BMIM]DCA, [BMIM]Cl, [BMIM]Br, and 1,2-propanediol.

84.3.2 Fungal Morphology

P. raistrickii ATCC 10490 showed the pellet type of morphology in the fermentation broth under the optimized condition. In this work, morphological characteristics of mycelia grown in the culture media with ILs (3 % [BMIM]BF₄) and without co-solvents were explored, respectively. According to the classification of the pellets [10], the morphology of pellet was characterized as a spherical shape of particle with a dense core zone surrounded by a flurry region, namely, the hairy type.

The frequency distribution of fungal morphology was shown in Fig. 84.3. The size of pellets was in the range of 0.6–4 mm. The pellets grown in both two culture media had narrow size distributions. In case of culture medium with ILs (3 % [BMIM]BF₄), the pellet size was diverse, and pellets bigger than 1.8 mm comprised 88 % of all pellets. Nevertheless, in the fermentation broth without co-solvents, pellets in the same size range comprised only 10 % of all pellets, at the

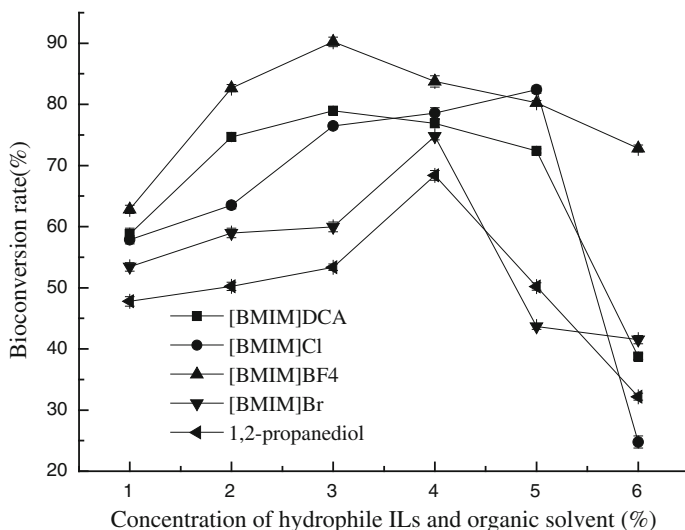
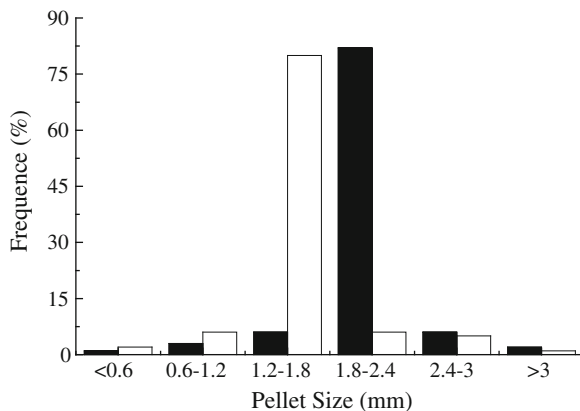


Fig. 84.2 Bioconversion rate of 13-ethyl-gon-4-en-3,17-dione to 15 α -hydroxylation of 13-ethyl-gon-4-en-3,17-dione after addition different concentration of [BMIM]DCA (■), [BMIM]Cl (●), [BMIM]BF₄ (▲), [BMIM]Br (▼), and 1,2-propanediol (◄)

Fig. 84.3 Pellet size distribution of *P. raistrickii* in the culture media with ILs (3% [BMIM]BF₄) (■) and without co-solvents (□)



same time, pellets smaller than 1.8 mm comprised 90%. The larger pellets induced by ILs (3% [BMIM]BF₄), in which mycelial morphologies were plump and symmetry, were benefit to osculation of substrate with pellets and the followed transformation of substrate into the *P. raistrickii* ATCC 10490.

84.4 Conclusion

In conclusion, effects of ILs (3 % [BMIM]BF₄) on the bioconversion to 15- α -hydroxylation of 13-ethyl-gon-4-en-3,17-dione by *P. raistrickii* ATCC 10490 were studied. And the higher yield (94.46 %) of desire product was obtained, as compared with those reported. Furthermore, the morphology changes induced by ILs (3 % [BMIM]BF₄), were first studied. Results indicated that the productive morphology of *P. raistrickii* ATCC 10490 formed, being benefit to mass transfer, occurred after the addition of ILs (3 % [BMIM]BF₄).

Acknowledgments This work was financially supported by National High-tech R&D Program of China (863 Program) “Biotransformation Technology of Steroids” (No. 2011AA02A211), Applied Basic Research Programs of Science and Technology Commission Foundation of Tianjin (No.12JCQJNC06400), Science & Technology Development Project of Tianjin Higher Education (No. 20100601).

References

1. Nevado JJB, Flores JR, Castañeda Peñalvo G (1999) Voltammetric behavior of gestodene using square-wave technique determination in oral contraceptives. *Electroanal* 11:268–273
2. Irrgang S, Schlosser D, Fritscher W (1997) Involvement of cytochrome P-450 in the 15[α]-hydroxylation of 13-ethyl-gon-4-ene-3,17-dione by *Penicillium raistrickii*. *J Steroid Biochem Mol Biol* 60:339–346
3. Li J, Geng X, Weng L et al (2005) Study on fermentation condition of steroid 15 α -hydroxylation by *Penicillium raistrickii*. *Microbiology* 32:87–91
4. Romano A, Romano D, Ragg E et al (2006) Steroid hydroxylations with *Botryodiplodia malorum* and *Colletotrichum lini*. *Steroids* 71:429–434
5. Gangu SA, Weatherley LR, Scurto AM (2009) Whole-cell biocatalysis with ionic liquids. *Curr Org Chem* 13:1242–1258
6. Wu DX, Guan YX, Wang HQ et al (2011) 11 α -Hydroxylation of 16 α , 17-epoxyprogesterone by *Rhizopus nigricans* in a biphasic ionic liquid aqueous system. *Bioresour Technol* 102:9368–9373
7. Mao S, Hua B, Hu X, et al (2012) 11 α Hydroxylation of 16 α , 17-epoxyprogesterone in biphasic ionic liquid/water system by *Aspergillus Ochraceus*. *J Chem Technol Biotechnol*. doi: [10.1002/jctb.3828](https://doi.org/10.1002/jctb.3828)
8. Mao S, Hu X, Sun Y, Hua B et al (2012) 15 α Hydroxylation of 13-ethyl-gon-4-en-3, 17-dione by *Penicillium raistrickii* in an ionic liquid/water biphasic system. *Biotechnol Lett* 34:2113–2117
9. Parvulescu VI, Hardacre C (2007) Catalysis in IL. *Chem Rev* 107:2615–2665
10. Cox PW, Thomas CR (1992) Classification and measurement of fungal pellets by automated image analysis. *Biotechnol Bioeng* 39:945–952

Chapter 85

Nuclear Receptor Property of E2F1 for Novel Anticancer Drug Discovery

Ning Zhang, Jin Li and Aimin Meng

Abstract E2F1, a member of transcription factor superfamily E2F, is similar to nuclear receptors such as estrogen receptor (ER) and peroxisome proliferators-activated receptors (PPARs) in structure and function. However, E2F1 plays a paradoxical role in cancer progression control. Instead of non-transcriptional function, the paradox mainly derives from E2F1 transcriptional function, which determines cell death or survival by different cofactors recruitment. This characteristic of E2F1 establishes itself as a good target for novel anticancer drug discovery and it is promising to develop appropriate small molecules with E2F1 antagonism activity or inverse agonist activity which might be even better for tumor suppression.

Keywords Anticancer effects · Antagonism · E2F1 · Drug target · Transcriptional function

85.1 Introduction

E2F family members are key regulators of genes involved in cell cycle progression, cell fate determination, and apoptosis. E2F1, an E2F family member, is similar to nuclear receptor members (such as PPARs and ER) in structure and function. Structurally E2F1 has similar function domains to nuclear receptor members such as DNA binding domain, transactivation domain, cofactor binding domain, dimerization domain, and can form dimer with DP1 to bind to DNA and initiate gene transcription. Functionally E2F1 regulates many different bioprocesses depending on different cofactors recruited. Besides its transcriptional

N. Zhang · J. Li · A. Meng (✉)

Institute of Radiation Medicine, Peking Union Medical College, Chinese Academy of Medical Sciences, Tianjin 300192, People's Republic of China

e-mail: aiminmeng@irm-cams.ac.cn

function, it also bears non-transcriptional function: being recruited to broken DNA strand for DNA repair.

However, there are paradoxical effects of E2F1 on determination of cell death and survival. E2F1 was initially found to promote cell cycle progression and proliferation [1, 2] but was lately demonstrated to be involved in cell apoptosis induced by DNA damage through p53-dependent and independent pathway [3]. Furthermore, upregulation of E2F1 levels in different kinds of cancers obtained contradictory prognosis [4]. Finally, E2F1 can both contribute to chemoresistance and chemosensitivity of DNA damage agents in cancer treatment [5–8].

Recent observations suggest that E2F1 transcriptional function is regulated by its cofactors and finally results in two different consequences discussed below: one is cell survival and proliferation by recruitment of coactivator; the other is cell cycle arrest and apoptosis by recruitment of corepressor. Moreover some compounds discussed below have directly or indirectly antagonism effects on E2F1 by increasing its corepressor recruitment or coactivator dissociation, has tumor repression effects. These studies suggest that E2F1 is a potential target for anti-cancer drug development.

85.2 E2F Family

E2F family plays an important role in the control of cell cycle progression, development, tissue homeostasis, and apoptosis. To date, eight members of E2Fs (E2F1-8) have been identified in human genome and can be divided into two subgroups according to structural and functional similarities: E2F1, E2F2, and E2F3a are transcriptional activators, whereas E2F4, E2F5, E2F6, E2F7, and E2F8, act as repressors of transcription [9]. Five functional domains of E2Fs have been identified including N-terminal domain (containing a cyclinA/Chk2 binding site), DNA binding domain (DBD), DPs dimerization domain, marked box, transactivation domain. E2F1-3 have all these domains, while E2F4 and E2F5 have the last four domains, E2F6 only have DBD domain and dimerization domain, E2F7 and E2F8 have a duplicate DNA binding domain. Typically, E2F proteins, except E2F7 and E2F8, associate with a dimerization partner (DP1-4) protein to form a heterodimeric complex that binds to the promoter of target genes [10, 11].

E2F family and nuclear receptors (NRs) are all transcriptional factors with similar structural domains. E2F1 is most similar to NRs in structure and function. NRs contain the following domains: (1) N-terminal regulatory domain: contains the activation function 1 (AF-1) which synergize with AF2 to produce a more robust upregulation of gene expression independent of the presence of ligand but normally very weak. (2) DBD: a highly conserved domain contains two zinc fingers that bind to specific sequences of DNA. (3) Hinge region: connects the DBD with the LBD and influences intracellular trafficking and subcellular distribution. (4) Ligand binding domain (LBD): along with the DBD, the LBD contributes to the dimerization interface of the receptor and binds to coactivator and

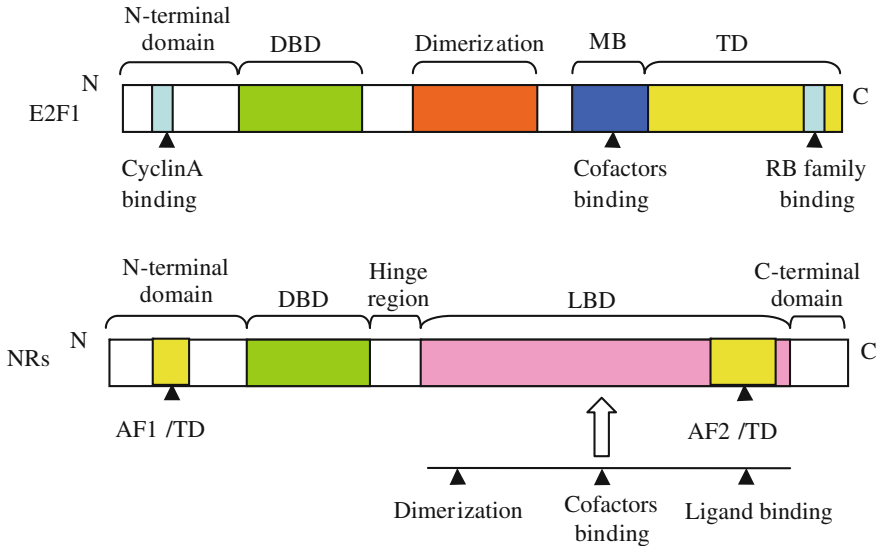


Fig. 85.1 The domains of E2F1 and NRs

corepressor. The LBD also contains the activation function 2 (AF-2) domain whose role is dependent on the presence of bound ligand. (5) C-terminal domain: highly variable in sequence between various NRs [12]. Compared to NRs, E2F1 contains the following domains: (1) N-terminal domain: contains an nuclear localization signal (NLS) signaling for nuclear trafficking functionally similar to the NRs' hinge region and a cyclin A binding domain for cyclinA to recruit Chk2 to mediate E2F1 phosphorylation and transactivation similar to AF1 domain of NRs. (2) DBD: contains conserved DNA sequence to recognize E2F promoters and binds to DNA. (3) Dimerization domain: along with DBD, dimerization domain contributes to the heterodimerization of DP1 and E2F1. (4) Marked box domain: binds cofactors. (5) Transactivation domain (TD): binds cofactors and mediates transactivation. It seems that NRs' LBD includes the functions of dimerization domain, marked box domain, and transactivation domain of E2F1 [13–16], (Fig. 85.1).

85.3 The Transcriptional and Non-transcriptional Function of E2F1

Among E2F members, E2F1 is the only member that considered is as both oncoprotein and tumor suppressor protein because it paradoxically influences human cancer development [17]. The real role of E2F1 gets fiercely debated. According to its transcriptional function, E2F1 associates with DP1 to form a

heterodimer on DNA to regulate downstream gene expression to induce corresponding biological effects. E2F1 is first found to directly upregulate the expression of many cell proliferation related genes, such as cyclin E, cyclin A, c-myc, DNA polymerase, and RBM38 [18–20]. However, E2F1 is also found to directly upregulate the transcription of proapoptosis genes, such as p73, caspase7, p14ARF, Apaf1, PUMA, and DBC2, to induce cell apoptosis [21, 22]. E2F1 also has non-transcriptional activity that E2F1 interacts with proteins and regulates their activity without affecting on cell proliferative or apoptotic genes expression. For example, E2F1 can recruit NBS1 and GCN5 to DNA broken strand for DNA repair [13].

85.4 E2F1 Cofactors

Cofactors, also called coregulators, are proteins that can be recruited to NRs and other transcription factors to alter chromatin and initiate (coactivators) or repress (corepressors) gene expression. Antagonist ligand interacts with NRs and enhances them to recruit corepressors on DNA to prevent gene transcription, while agonist ligand interaction induces the dissociation of corepressor complexes and favors the recruitment of coactivators to initiate gene transcription [23]. Compared to NRs, cofactors that interact with E2F1 to initiate or repress genes induction has been identified and some of them mediate E2F1 distinct bidirectional regulation, being activator in one bioprocess and simultaneously repressor in the opposite bioprocess.

85.4.1 Coactivator

E2F1 coactivators including MDM2, ANCCA, ACTR, nuclear EGFR, AHR, and SIRT1 induce proliferative genes expression and/or repress apoptotic genes expression. Murine double minute 2 (MDM2) is an oncoprotein. Martin K and colleagues first observed that MDM2 directly contacts the transactivation domain of E2F1 using residues conserved in the activation domain of P53 to stimulate E2F1/DP1 formation and augment cell proliferation. Another study also demonstrated that MDM2-E2F1 signaling is essential for melanoma cell proliferation cells and identified E2F1 as a biomarker to consider when stratifying putative candidates for clinical studies of P53-MDM2 [24, 25]. AAA nuclear coregulators cancer associated protein (ANCCA) is an AAA + ATPase and has been strongly implicated to promote tumorigenesis. Revenko and its colleagues first identified ANCCA as an E2F coactivator and demonstrated that its N terminus interacts with both the N and C termini of E2F1-3 to induce E2F target genes expression and a novel mechanism involving ANCCA bromodomain may contribute to cancer cell proliferation [26]. Nuclear epidermal growth factor receptor (EGFR), a nuclear

tyrosine kinase receptor, can promote tumor progression and chemoresistance [27]. Hanada and colleagues have recently found that EGF-activated nuclear EGFR binds to E2F1 to induce B-Myb gene expression and breast tumors proliferation in vivo [28]. ACTR (also named AIB1, SRC-3), a coactivator of NRs, is considered as an oncoprotein. Louie and its colleagues first found that ACTR protein directly interacts with E2F1 through its N-terminal domain and is required for E2F1-mediated breast cancer cells proliferation. Another study found that the ACTR gene expression is also positive regulated by E2F1 [29, 30]. The aryl hydrocarbon receptor (AHR) is a ligand-activated transcription factor and plays an important role in cell cycle progression and tumor progression. AHR ligands include dioxin and related compounds which can induce a bidirectional regulation of E2F1. In the presence of AHR ligand, AHR directly interacts with E2F1 on the E2F promoter of cell proliferative genes to promote cancer cell proliferation, while the complex of AHR and E2F1 can also bind on E2F promoter of apoptotic genes to inhibit Apaf1 and P73 gene expression to inhibit cancer cell apoptosis [31, 32]. SIRT1, an NAD(+)-dependent deacetylase, is a metabolic regulator and recently found to contribute to cancer cell survival [33]. Wang and colleagues found that SIRT1 can directly interact with E2F1 to inhibit response of P73 to DNA damage and rescue DNA damaged cancer cell. Another study found SIRT, PCAF, and E2F1 corecruited in vivo on the P1p73 promoter to repress E2F1 induced P73 expression and contributes to cancer cells survival [34, 35].

85.4.2 Corepressor

RB family members, Alien, Necdin, and RIP140 are considered as corepressors of E2F1 which stimulate apoptosis genes expression and/or repress proliferative genes expression. Retinoblastoma gene (RB) family including RB1, p107, and p130 are potent corepressors of E2F1. There are two different E2F1-RB1 complexes probably formed in response to DNA damage: a repressing complex containing histone deacetylase 1 (HDAC1) and an activating complex containing P/CAF, which cause a bidirectional regulation of E2F1-RB1 that repress cell cycle genes expression but stimulate proapoptotic genes expression to induce cell arrest and apoptosis [36, 37]. P107 and P130 also directly interact with E2F1 and repress its proliferative gene expression in cancer cells [38, 39]. c-Jun activation domain-binding protein-1 (Jab1), is formerly reported as a coactivator of other transcription factors and promotes cell progression but identified as an extremely specific corepressor of E2F1 [40]. Jab1 can selectively interact with the marked box domain of E2F1 and exhibits a significant effect on the E2F1-mediated expression of proapoptotic genes [41, 42]. Receptor-interacting protein of 140 kDa (RIP140) is a cofactor of nuclear receptor involved in reproduction and energy homeostasis. Aurélie and colleagues found that RIP140 can directly interact with E2F1 on E2F target promoters to represses the expression of E2F1 target genes (such as cyclin E and cyclin B2) and found that low RIP140 mRNA expression was associated with

high E2F1-target gene levels and basal-like tumors in analysis of human breast cancers and indicated that RIP140-E2F1 pathway can discriminate human breast tumor subtypes [43]. Necdin (NDN), a member of the melanoma-associated antigen (MAGE) family, is a tumor suppressor protein. Taniura and colleagues found that NDN binds to a C-terminal domain of E2F1, and repress E2F-dependent transactivation *in vivo*, and suppresses the colony formation of RB-deficient SAOS-2 osteosarcoma cells [44, 45]. Alien is a corepressor of several nuclear receptor superfamilies and mediates gene silencing and cell proliferation repression [46]. Tenbaum and colleagues found that Alien interacts with E2F1 *in vivo* on the E2F promoter and inhibits transactivation of E2F1 and endogenous E2F1 gene expression using a proteomic approach. Another two studies also demonstrated that Alien inhibits E2F1 activity to represses proliferative genes expression and reduces cancer cell proliferation [47, 48].

The characteristic of NRs-like regulatory mode and distinct bi-directional transcriptional regulation of E2F1 indicate that compounds with high affinity to E2F1, which recruit corepressors and dissociate coactivators, may have value to develop targeted anticancer drugs.

85.5 Anticancer Compounds Directly Modulate E2F1 Activity

It is unclear whether E2F1 has endogenous ligands. Some compounds are found to repress tumor progression via modulating E2F1 activity. Beta-Lapachone though does not cause DNA damage but can induce cancer cell apoptosis via increasing the amount of RB binding to E2F1 including mutant p53 cancer cells [49, 50]. Nutlin-3 and its enantiomer of nutlin-3a are MDM2 antagonist and potent anticancer compounds. They both can induce apoptosis through inhibiting the interaction between E2F and MDM2 and subsequently p73 and Noxa expression in normal and p53 mutant cancer cell [51, 52]. SU9516 prevents the dissociation of RB from E2F1 and induces cancer cell apoptosis [53, 54]. Esculetin induces G1 arrest in human leukemia U937 cells partially through the enhancement of RB/E2F1 interaction and subsequently cyclin E expression repression [55]. Resveratrol induces E2F1-mediated gene expression of ASPP1, a new member of the apoptosis stimulation protein of p53 (ASPP) family and subsequently apoptosis in MCF-7 and MDA-MB231 breast cancer cells [56]. Amurensin G, a potent natural SIRT1 inhibitor, inhibits angiogenesis and tumor growth of tamoxifen-resistant breast cancer via repressing E2F1 mediated Pin1 gene and protein expression [57, 58]. SAHA and TSA, inhibitors of histone deacetylases, stimulate apoptosis through selectively induction of E2F1-mediated proapoptotic BH3-only protein expression [59].

E2F1 completely or partially participate in the tumor suppression effects of compounds listed above. Some was already been observed directly E2F1

antagonist-like effect with enhancing its corepressors recruitment such as Beta-Lapachon and Esculetin or coactivators dissociation such as MDM2 antagonist. And the others display indirect antagonist-like effect in regulation of E2F1 target genes. So it is feasible to develop little molecules with E2F1 antagonism for cancer treatment.

85.6 Perspectives

The paradoxical effects of E2F1 lie in its NRs-like regulatory mode depending on cofactors recruitment, and can be resolved via properly modulating E2F1. Moreover, P53 and RB protein are often mutated or deficient in malignances, which cause chemoresistance and tumor recurrence [60, 61], while E2F1 is normal in most cancer cells and can induce cancer cell apoptosis both dependent and independent of p53 and RB. In addition, E2F1 has distinct bi-directional regulatory function and some compounds repress tumor progression via direct and indirect antagonist-like regulation of E2F1. These characteristic of E2F1 provide a potent anticancer drug target and it is promising to develop appropriate small molecules with E2F1 antagonism or inverse agonism even better for tumor suppression (Fig. 85.2).

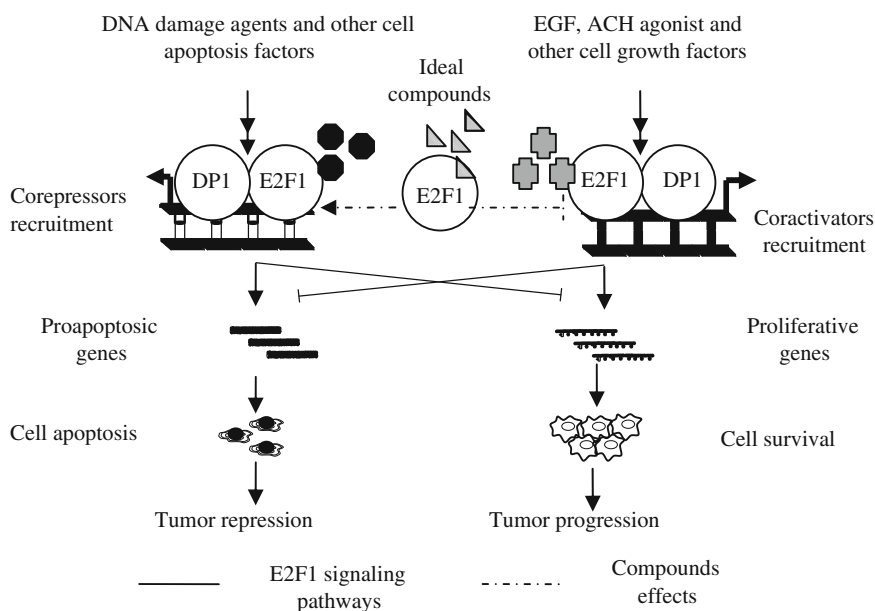


Fig. 85.2 Development compound targeting transcription function of E2F1 for cancer therapy

References

1. Timmers C, Sharma N, Opavsky R et al (2007) E2f1, E2f2 and E2f3 control E2F target expression and cellular proliferation via a p53-dependent negative feedback loop. *Mol Cell Biol* 27:65–78
2. Wu L, Timmers C, Maiti B et al (2001) The E2F1-3 transcription factors are essential for cellular proliferation. *Nature* 414:457–462
3. Engelmann D, Pützer BM (2010) Translating DNA damage into cancer cell death-A roadmap for E2F1 apoptotic signalling and opportunities for new drug combinations to overcome chemoresistance. *Drug Resist Updates* 13:119–131
4. Johnson DG, Degregori J (2006) Putting the oncogenic and tumor suppressive activities of E2F into context. *Curr Mol Med* 6:731–738
5. Engelmann D, Pützer BM (2012) The dark side of E2F1: in transit beyond apoptosis. *Cancer Res* 72:571–575
6. Banerjee D, Schnieders B, Fu JZ et al (1998) Role of E2F1 in chemosensitivity. *Cancer Res* 58:4292–4296
7. Dong YB, Yang HL, McMasters KM (2003) E2F1 overexpression sensitizes colorectal cancer cells to camptothecin. *Cancer Gene Ther* 10:168–178
8. Hao H, Zhou HS, McMasters KM (2009) Chemosensitization of tumor cells: inactivation of nuclear factor-kappa B associated with chemosensitivity in melanoma cells after combination treatment with E2F1 and doxorubicin. *Methods Mol Biol* 542:301–313
9. Lammens T, Li J, Leone G et al (2009) Atypical E2Fs: new players in the E2F transcription factor family. *Trends Cell Biol* 19:111–118
10. DeGregori J, Johnson DG (2006) Distinct and overlapping roles for E2F family members in transcription, proliferation and apoptosis. *Curr Mol Med* 6:739–748
11. Rowland BD, Bernards R (2006) Re-evaluating cell cycle regulation by E2Fs. *Cell* 127:871–874
12. Chris MB, Moray JC (2010) *Nuclear Receptors*. Springer, New York
13. Biswas AK, Johnson DG (2012) Transcriptional and nontranscriptional functions of E2F1 in response to DNA damage. *Cancer Res* 72:3–7
14. Rubin SM, Gall AL, Zheng N et al (2005) Structure of the Rb C-terminal domain bound to E2F1-DP1: a mechanism for phosphorylation-induced E2F release. *Cell* 123:1093–1106
15. Slansky JE, Farnham PJ (1996) Introduction to the E2F family: protein structure and gene regulation. *Curr Top Microbiol Immunol* 208:1–30
16. Cress WD, Nevins JR (1996) A role for a bent DNA structure in E2F-mediated transcription activation. *Mol Cell Biol* 16(5):2119–2127
17. Lazzarini Denchi E, Helin K (2005) E2F1 is crucial for E2F-dependent apoptosis. *EMBO Rep* 6:661–668
18. Ren B, Cam H, Takahashi Y et al (2002) E2F integrates cell cycle progression with DNA repair, replication, and G2/M checkpoints. *Genes Dev* 16:245–256
19. Alonso MM, Alemany R, Fueyo J et al (2008) E2F1 in gliomas: a paradigm of oncogene addiction. *Cancer Lett* 263:157–163
20. Feldstein O, Ben-Hamo R, Bashari D et al (2012) RBM38 is a direct transcriptional target of E2F1 that limits E2F1 induced proliferation. *Mol Cancer Res* 0(9):1169–1177
21. Wu Z, Yu Q (2009) E2F1-mediated apoptosis as a target of cancer therapy. *Curr Mol Pharmacol* 2:149–160
22. Freeman SN, Ma Y, Cress WD (2008) RhoBTB2 (DBC2) is a mitotic E2F1 target gene with a novel role in apoptosis. *J Biol Chem* 283:2353–2362
23. Lonard DM, O'Malley BW (2012) Nuclear receptor coregulators: modulators of pathology and therapeutic targets. *Nat Rev Endocrinol* 8:598–604
24. Martin K, Trouche D, Hagemeyer C et al (1995) Stimulation of E2F1/DP1 transcriptional activity by MDM2 oncoprotein. *Nature* 375:691–694

25. Verhaegen M, Checinska A, Riblett MB et al (2012) E2F1 dependent oncogenic addiction of melanoma cells to MDM2. *Oncogene* 31:828–841
26. Revenko AS, Kalashnikova EV, Gemo AT et al (2010) Chromatin loading of E2F-MLL complex by cancer-associated coregulator ANCCA via reading a specific histone mark. *Mol Cell Biol* 30:5260–5272
27. Brand TM, Iida M, Li C et al (2011) The nuclear epidermal growth factor receptor signaling network and its role in cancer. *Discovery Med* 12:419–432
28. Hanada N, Lo HW, Day CP et al (2006) Coregulation of B-Myb expression by E2F1 and EGF receptor. *Mol Carcinog* 45:10–17
29. Mussi P, Yu C, O'Malley BW et al (2006) Stimulation of steroid receptor coactivator 3 (SRC-3) gene overexpression by a positive regulatory loop of E2F1 and SRC-3. *Mol Endocrinol* 20:3105–3119
30. Louie MC, Zou JX, Rabinovich A et al (2004) ACTR/AIB1 functions as an E2F1 coactivator to promote breast cancer cell proliferation and antiestrogen resistance. *Mol Cell Biol* 24:5157–5171
31. Watabe Y, Nazuka N, Tezuka M et al (2010) Aryl hydrocarbon receptor functions as a potent coactivator of E2F1-dependent transcription activity. *Biol Pharm Bull* 33:389–397
32. Marlowe JL, Fan Y, Chang X et al (2008) The aryl hydrocarbon receptor binds to E2F1 and inhibits E2F1 induced apoptosis. *Mol Biol Cell* 19:3263–3271
33. Knight JR, Milner J (2012) SIRT1, metabolism and cancer. *Curr Opin Oncol* 24:68–75
34. Wang C, Chen L, Hou X et al (2006) Interactions between E2F1 and SirT1 regulate apoptotic response to DNA damage. *Nat Cell Biol* 8:1025–1031
35. Pediconi N, Guerrieri F, Vossio S et al (2009) hSirT1-dependent regulation of the PCAF-E2F1-p73 apoptotic pathway in response to DNA damage. *Mol Cell Biol* 29:1989–1998
36. Julian LM, Palander O, Seifried LA et al (2008) Characterization of an E2F1 specific binding domain in pRB and its implications for apoptotic regulation. *Oncogene* 27:1572–1579
37. Dick FA, Dyson N (2003) pRB contains an E2F1 specific binding domain that allows E2F1 induced apoptosis to be regulated separately from other E2F activities. *Mol Cell* 12:639–649
38. O'Connor RJ, Schaley JE, Feeney G et al (2001) The p107 tumor suppressor induces stable E2F DNA binding to repress target promoters. *Oncogene* 20:1882–1891
39. Dai Y, Hamm TE, Dent P et al (2006) Cyclin D1 overexpression increases the susceptibility of human U266 myeloma cells to CDK inhibitors through a process involving p130-, p107- and E2F-dependent S phase entry. *Cell Cycle* 5:437–446
40. Shackelford TJ, Claret FX (2010) JAB1/CSN5: a new player in cell cycle control and cancer. *Cell Div* 18:26
41. Lu H, Liang X, Issaenko OA et al (2011) Jab1/CSN5 mediates E2F dependent expression of mitotic and apoptotic but not DNA replication targets. *Cell Cycle* 10:3317–3326
42. Hallstrom TC, Nevins JR (2006) Jab1 is a specificity factor for E2F1 induced apoptosis. *Genes Dev* 20:613–623
43. Docquier A, Harmand PO, Fritsch S et al (2010) The transcriptional coregulator RIP140 represses E2F1 activity and discriminates breast cancer subtypes. *Clin Cancer Res* 16:2959–2970
44. Chapman EJ, Knowles MA (2009) Necdin: a multi functional protein with potential tumor suppressor role? *Mol Carcinog* 48:975–981
45. Taniura H, Taniguchi N, Hara M et al (1998) Necdin, a postmitotic neuron-specific growth suppressor, interacts with viral transforming proteins and cellular transcription factor E2F1. *J Biol Chem* 273:720–728
46. Papaioannou M, Melle C, Baniahmad A (2007) The coregulator Alien. *Nucl Recept Signal* 5:e008
47. Tenbaum SP, Papaioannou M, Reeb CA et al (2007) Alien inhibits E2F1 gene expression and cell proliferation. *Biochim Biophys Acta* 1773:1447–1454
48. Hong W, Li J, Wang B et al (2011) Epigenetic involvement of Alien/ESET complex in thyroid hormone-mediated repression of E2F1 gene expression and cell proliferation. *Biochem Biophys Res Commun* 415:650–655

49. Li Y, Sun X, LaMont JT et al (2003) Selective killing of cancer cells by beta-lapachone: direct checkpoint activation as a strategy against cancer. *Proc Natl Acad Sci U S A* 100:2674–2678
50. Choi YH, Kang HS, Yoo MA (2003) Suppression of human prostate cancer cell growth by beta-lapachone via down-regulation of pRB phosphorylation and induction of Cdk inhibitor p21(WAF1/CIP1). *J Biochem Mol Biol* 36:223–229
51. Ambrosini G, Sambol EB, Carvajal D et al (2007) Mouse double minute antagonist Nutlin-3a enhances chemotherapy induced apoptosis in cancer cells with mutant p53 by activating E2F1. *Oncogene* 26:3473–3481
52. Kitagawa M, Aonuma M, Lee SH et al (2008) E2F1 transcriptional activity is a critical determinant of Mdm2 antagonist-induced apoptosis in human tumor cell lines. *Oncogene* 27:5303–5314
53. Yu B, Lane ME, Wadler S (2002) SU9516, a cyclin dependent kinase 2 inhibitor, promotes accumulation of high molecular weight E2F complexes in human colon carcinoma cells. *Biochem Pharmacol* 64:1091–1100
54. Lane ME, Yu B, Rice A et al (2001) A novel cdk2-selective inhibitor, SU9516, induces apoptosis in colon carcinoma cells. *Cancer Res* 61:6170–6177
55. Lee SH, Park C, Jin CY et al (2008) Involvement of extracellular signal-related kinase signaling in esculetin induced G1 arrest of human leukemia U937 cells. *Biomed Pharmacother* 62:723–729
56. Shi Y, Yang S, Troup S et al (2011) Resveratrol induces apoptosis in breast cancer cells by E2F1-mediated up-regulation of ASPP1. *Oncol Rep* 25:1713–1719
57. Oh WK, Cho KB, Hien TT et al (2010) Amurensin G, a potent natural SIRT1 inhibitor, rescues doxorubicin responsiveness via down regulation of multidrug resistance. *Mol Pharmacol* 78:855–864
58. Kim JA, Kim MR, Kim O et al (2012) Amurensin G inhibits angiogenesis and tumor growth of tamoxifen resistant breast cancer via Pin1 inhibition. *Food Chem Toxicol* 50:3625–3634
59. Zhao Y, Tan J, Zhuang L et al (2005) Inhibitors of histone deacetylases target the Rb-E2F1 pathway for apoptosis induction through activation of proapoptotic protein Bim. *Proc Natl Acad Sci U S A* 102:16090–16095
60. Muller PA, Vousden KH, Norman JC (2011) P53 and its mutants in tumor cell migration and invasion. *J Cell Biol* 192:209–218
61. Gordon GM, Du W (2011) Targeting Rb inactivation in cancers by synthetic lethality. *Am J Cancer Res* 1:773–786

Chapter 86

MRTF-A Promotes Migration of MCF-7 Breast Cancer Cells via Transactivation of CYR61

Xuegang Luo, Chunling Zhang, Wenwen Zhao, Lei Liu, Shu Guo, Zhipeng Liu, Jing Wang and Tong-Cun Zhang

Abstract Myocardin-related transcription factor A (MRTF-A) is a transcriptional coactivator of serum response factor (SRF). Recent studies have found that the MRTF–SRF signal pathway might play critical role in Rho-dependent cytoskeletal rearrangements and tumor metastasis. To further explore the detailed molecular mechanisms for MRTF-A-mediated cell migration, in this study, the effect of MRTF-A on the migration of mouse fibroblast NIH3T3 cells and MCF-7 human breast cancer cells was detected using a scratch wound model, and its transcriptional activity on the promoter of Cysteine-rich angiogenic inducer 61 (CYR61) was also analyzed by luciferase assay. The results showed that overexpression of MRTF-A could significantly promote the migration of NIH3T3 cells and drive the transcriptional activity of CYR61 promoter in African green monkey kidney COS-7 cells and strongly enhance upregulation of CYR61 gene. In contrast, RNA interference-mediated knockdown of MRTF-A reduced the migration ability of MCF-7 breast cancer cells. Taken together, our results suggested that MRTF-A is involved in tumor metastasis via transactivation of CYR61.

Keywords MRTF-A · CYR61 · Breast cancer · Migration

X. Luo · C. Zhang · W. Zhao · L. Liu · S. Guo · Z. Liu · J. Wang · T.-C. Zhang (✉)
Key Laboratory of Industrial Microbiology, Ministry of Education, College of
Bioengineering, Tianjin University of Science and Technology, Tianjin, China
e-mail: tony@tust.edu.cn

X. Luo
e-mail: luoxuegang@tust.edu.cn

X. Luo · C. Zhang · W. Zhao · L. Liu · S. Guo · Z. Liu · J. Wang · T.-C. Zhang
Tianjin Key Laboratory of Industrial Microbiology, Tianjin, China

86.1 Introduction

Tumor metastasis is one of the biological characteristics of malignant tumor, and it is the leading cause of death to clinical tumor patients, 90 % of all cancer-related deaths are caused by tumor metastasis. Only by effectively controlling the occurrence and development of tumor metastasis can we overcome tumor. Thus, understanding the regulation of these series of molecular interactions and signal transduction pathways are important in developing new antimetastatic treatment strategies [1].

MRTFs are a group of transcriptional coactivators of serum response factor (SRF) [2–4]. Myocardin, myocardin-related transcription factor-A (MRTF-A), and myocardin-related transcription factor-B (MRTF-B), which are expressed in a broad range of embryonic and adult tissues [5–8]. They all have similar structural features and the transcription initiation function. Studies have demonstrated that: MRTFs associates with SRF via the highly conserved cis-regulatory components of CArG box motifs to synergistically regulate gene transcription [4, 9–11]. One central signal pathway regulating MRTFs is regulated through actin and is closely linked to cytoskeletal rearrangements and tumor metastasis, such as cell polarity, shape, and motility [12–16]. MRTF-A have recently been implicated in tumor cell invasion and metastasis [17]. Suppression of MRTF-A decreased MCF-7 cell motility while cell proliferation was unaffected.

CYR61 is a member of the CCN family, the CYR61 gene of human is located on chromosome 1q22.3, CYR61 have the mosaic multimodule structure and interact with a variety of factors, it is a very important regulatory factor and play critical role in the regulation of cell adhesion, migration, proliferation and angiogenesis, inflammatory response, tissue remodeling, and other important physiological and pathological processes [18–19]. More importantly CYR61 is involved in occurrence and development of tumors, and the function is different in diverse tumors. CYR61 can induce tumor cells proliferation and migration in breast cancer and glioma tumor.

In our studies, to further explore the detailed molecular mechanisms for MRTF-A-mediated cell migration. MRTF-A on the migration of NIH3T3 cells and MCF-7 cells was detected using a scratch wound model, its transcriptional activity on the promoter of CYR61 was analyzed by luciferase assay and RNA interference-mediated knockdown of MRTF-A reduced the migration ability of MCF-7 breast cancer cells.

86.2 Materials and Methods

86.2.1 Cell Culture, Plasmids Used, and Cell Transfection

COS-7 cells, NIH3T3 cells, and MCF-7 cells were cultured at 37 °C in (DMEM)/F12 (HyClone) supplemented with 10 % fetal bovine serum (FBS) in

a 5 % CO₂ incubator. The plasmid encoding human MRTF-A was purchased from Addgene (Cambridge, MA). Promoter of CYR61 was amplified by polymerase chain reaction (PCR) using the genomic DNA isolated from MCF-7 cells as template. For transfection experiments, the cells were cultured in serum medium without antibiotics at 80 % confluence for 24 h, and then transfected with transfection reagent (Turbofect, Thermo) according to manufacturer's instructions. After incubation for 6 h, the medium was removed and replaced with normal culture medium for 24 h. Then, the RT-PCR and Western blotting were performed as follows .

86.2.2 Measurement of Cellular Migration

NIH3T3 cells and MCF-7 cells were grown to confluence in 24 well plates, and then scratched with the narrow end of a sterile pipet tip. The width of the scratch was taken a picture in each well after initial wounding, Medium was immediately replaced with serum-free DMEM/F12 containing MRTF-A to NIH3T3 and sh-MRTFA to MCF-7 cells, and cells were incubated for 72 h at 37 °C in a CO₂-incubator. After 72 h, the scratch width was taken a picture again.

86.2.3 Luciferase Assays

COS-7 cells were grown in 24 well plates, within 24 h of transfection, cells were treated with lysis buffer (Promega), luciferase assays (Promega) were conducted by the GloMax-Multi Detection System.

86.2.4 Semi-Quantitative Reverse-Transcription Polymerase Chain Reaction

Semi-quantitative RT-PCR analysis was performed as previously reported [20]. The total cellular RNA was extracted from cells with Trizol reagent (Invitrogen) and the total RNA was reverse-transcribed with M-MLV reverse transcriptase (Promega) according to the manufacturer's instructions. GAPDH was the internal control.

86.2.5 Statistical Analysis

Data analyzed by *t* test. The difference at $P < 0.05$ was considered statistically significant.

86.3 Results and Discussion

86.3.1 MRTF-A Promote Cell Migration

To investigate whether MRTF-A promotes cell migration, we overexpressed MRTF-A in NIH3T3 cells and RNA interference-mediated knockdown of MRTF-A in MCF-7 cells using a scratch wound model. Within 72 h of transfection, overexpression of MRTF-A caused a concentration-dependent decrease in NIH3T3 cells migration. Cell migration is shown in Fig. 86.1a. In contrast, RNA interference-mediated knockdown of MRTF-A reduced the migration ability of MCF-7 cells, cell migration is shown in Fig. 86.1b.

NIH3T3 cells and MCF-7 cells migration were assessed using a scratch assay. NIH3T3 cells were treated with MRTF-A, and cell migration into cell-free area was assessed after 72 h (a). MCF-7 cells were treated with shMRTF-A, and cell migration into cell-free area was assessed after 72 h (b).

86.3.2 MRTF-A Drive the Transcriptional Activity of CYR61

CYR61 plays a critical role in the regulation of cell adhesion, migration, proliferation, and angiogenesis. To determine whether MRTF-A promotes migration of MCF-7 cells via transactivation of CYR61, we overexpressed MRTF-A in COS7 and MCF-7. Within 24 h of transfection, MRTF-A caused a significant increase in the activity of the CYR61-Luc reporter. The figure is shown in Fig. 86.2a, and mRNA levels in Fig. 86.2b.

Luciferase assay for CYR61-Luc reporter in transfected with MRTF-A plasmid for 24 h in COS-7 (a). RT-PCR analysis for CYR61 in transfected MCF-7 at 24 h (b). (* $P < 0.05$ vs. pcDNA3.1, $n = 3$).

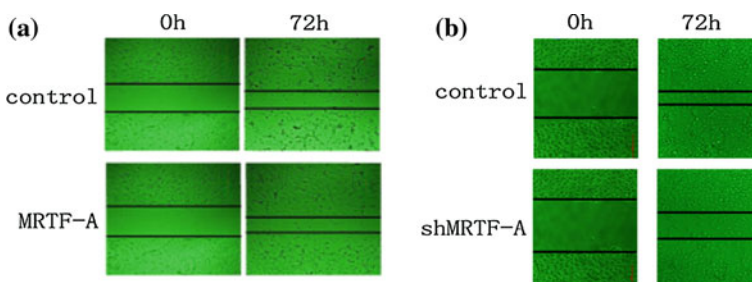


Fig. 86.1 Effect of MRTF-A on cell migration. **a** NIH3T3 cells were treated with MRTF-A, and cell migration into cell-free area was assessed after 72 h. **b** MCF-7 cells were treated with shMRTF-A, and cell migration into cell-free area was assessed after 72 h

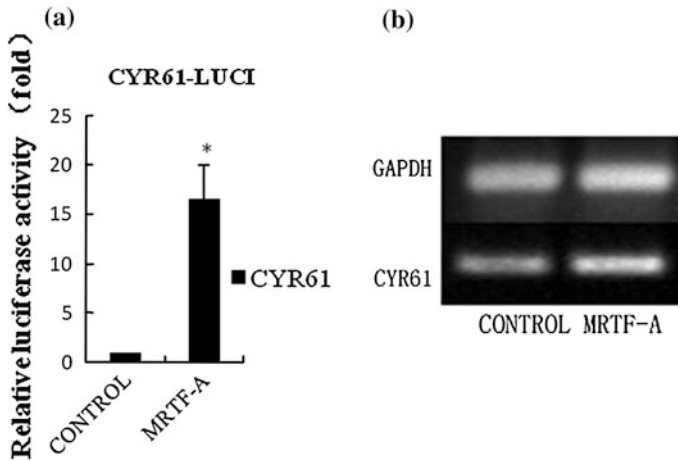


Fig. 86.2 MRTF-A upregulated the expression of CYR61. **a** Luciferase assay for CYR61-Luc reporter in transfected with MRTF-A plasmid for 24 h in COS-7. **b** RT-PCR analysis for CYR61 in transfected MCF-7 at 24 h. (* $P < 0.05$ vs. pcDNA3.1, $n = 3$)

86.4 Conclusion

In summary, our results show that overexpression of MRTF-A promotes migration of NIH3T3 cells and drive the transcriptional activity of CYR61. Furthermore, h-shMRTF-A reduced the migration ability of MCF-7 breast cancer cells. Our studies indicate that MRTF-A promotes migration of MCF-7 breast cancer cells via transactivation of CYR61.

References

1. Diers AR, Dranka BP, Ricart KC et al (2010) Modulation of mammary cancer cell migration by 15-deoxy- Δ 12, 14-prostaglandin J2: implications for anti-metastatic therapy. *Biochem J* 430(1):69–78
2. Arsenian S, Weinhold B, Oelgeschläger M et al (1998) Serum response factor is essential for mesoderm formation during mouse embryogenesis. *EMBO J* 17(21):6289–6299
3. Bass-Zubek AE, Godsel LM, Delmar M et al (2009) Plakophilins: multifunctional scaffolds for adhesion and signaling. *Curr Opin Cell Biol* 21(5):708–716
4. Pipes GCT, Creemers EE et al (2006) The myocardin family of transcriptional coactivators: versatile regulators of cell growth, migration, and myogenesis. *Genes Dev* 20:1545–1556
5. Miralles F, Posern G, Zaromytidou AI et al (1998) Actin dynamics control SRF activity by regulation of its coactivator MAL. *Cell* 2003(113):329–342
6. Mouilleron S, Guettler S, Langer CA et al (2008) Molecular basis for G-actin binding to RPEL motifs from the serum response factor coactivator MAL. *EMBO J* 27:3198–3208
7. Vartiainen MK, Guettler S, Larijani B et al (2007) Nuclear actin regulates dynamic subcellular localization and activity of the SRF cofactor MAL. *Science* 316:1749–1752

8. McDonald OG, Wamhoff BR, Hoofnagle MH et al (2006) Control of SRF binding to CArG box chromatin regulates smooth muscle gene expression in vivo. *J Clin Invest* 116:36–48
9. Wang D, Chang PS, Wang Z et al (2001) Activation of cardiac gene expression by myocardin, a transcription cofactor for serum response factor. *Cell* 105:851–862
10. Cen B, Selvaraj A, Burgess RC et al (2003) Potent transcription coactivator for serum response factor(SRF), is required for serum induction of SRF target genes. *Mol Cell Biol* 23:6597–6608
11. Posen G, Treisman R (2006) Actin' together: serum response factor, its cofactors and the link to signal transduction. *Trends Cell Biol* 16:588–596
12. Li J, Zhu X, Chen M et al (2005) Myocardin-related transcription factor B is required in cardiac neural crest for smooth muscle differentiation and cardiovascular development. *Proc Natl Acad Sci USA* 102:8916–8921
13. Li S, Chang S, Qi X et al (2006) Requirement of a myocardin-related transcription factor for development of mammary myoepithelial cells. *Mol Cell Biol* 26:5797–5808
14. Sun Y, Boyd K, Xu W et al (2006) Acute myeloid leukemia-associated Mkl1 (Mrtf-a) is a key regulator of mammary gland function. *Mol Cell Biol* 26:5809–5826
15. Parmacek MS (2007) Myocardin-related transcription factors: critical coactivators regulating cardiovascular development and adaptation. *Circ Res* 100:633–644
16. Medjkane S, Perez-Sanchez C, Gaggioli C et al (2009) Myocardin-related transcription factors and SRF are required for cytoskeletal dynamics and experimental metastasis. *Nat Cell Biol* 11:257–268
17. Almeida EA, Ilic D, Han Q et al (2000) Matrix survival signalling: from fibronectin via focal adhesion kinase to c-Jun NH(2)-terminal kinase. *J Cell Biol* 149:741–754
18. Babic AM, Kireeva ML, Kolesnikova TV et al (1998) CYR61, a product of a growth factor-inducible immediate early gene, promotes angiogenesis and tumor growth. *Proc Natl Acad Sci USA* 95:6355–6360
19. Tsai MS, Bogart DF, Castaneda JM et al (2002) Cyr61 promotes breast tumorigenesis and cancer progression. *Oncogene* 21:8178–8185
20. Xing W, Zhang TC, Cao D et al (2006) Myocardin induces cardiomyocyte hypertrophy. *Circ Res* 98:1089–1097

Chapter 87

The Analysis of the Inhibition Effect of Cholic Acid Derivatives on the Proliferation of Breast Cancer Cells

Xuegang Luo, Jing Wang, Xiangchao Gu, Chunling Zhang, Xiangzheng Hu and Tong-Cun Zhang

Abstract Cancer is one of the major causes of death worldwide. Many clinical evidences showed that the incidence of colon cancer increased after the cholecystectomy, suggesting that bile acid and its derivatives might play roles in the process of tumorigenesis and its prevention. Bile acid derivative is a kind of good candidates for prodrug design, but there are still few reports of its development for anticancer drugs either domestically or internationally. In the present study, IC₅₀ of 9 bile acid derivatives against MCF-7 human breast cancer cells was detected by MTT assay, and the safety of several bile acid derivatives with high anticancer effect were further analyzed in human umbilical vein endothelial cells. The results showed that among 9 bile acid derivatives, cholic acid n-buthyl ester had lower IC₅₀ against cancer cells, but it did not have cytotoxicity to normal cell at low concentration, indicating that they would be a good candidate for the development of novel anticancer agents.

Keywords Bile acid derivatives · MTT assay · Cholic acid n-buthyl ester

X. Luo · J. Wang · X. Gu · C. Zhang · T.-C. Zhang (✉)
Key Laboratory of Industrial Microbiology, Ministry of Education, College of Bioengineering, Tianjin University of Science and Technology, Tianjin 300457, People's Republic of China
e-mail: tony@tust.edu.cn

X. Luo · J. Wang · X. Gu · C. Zhang · T.-C. Zhang
Tianjin Key Laboratory of Industrial Microbiology, Tianjin 300457, People's Republic of China

J. Wang
The Second People's Hospital of Hengshui City, Hengshui 053000, People's Republic of China

X. Hu
College of Science, Tianjin University of Science and Technology, Tianjin 300457, People's Republic of China
e-mail: hxz0903@yahoo.com.cn

87.1 Introduction

Cancer remains one of the leading causes of morbidity and mortality worldwide [1–4]. Natural products have been used extensively in traditional medicine for treatment of a myriad of diseases including various types of cancers [5]. Investigation of natural products is a research field with great potential [6–8]. Primary bile acids (cholic and chenodeoxycholic acid) are hydrophobic derivatives of cholesterol synthesized in the liver and secreted with bile into the duodenum where they play important role in digestion and absorption of dietary lipids [9]. It not only can promote digestion and absorption of lipids, regulate cholesterol metabolism, but also be used directly as the drug treatment of liver disease, gallstones, and inflammation and other diseases.

Although bile acid derivative is a kind of good candidates for prodrug design, but there are still few reports of its development for anticancer drugs either domestically or internationally. Thus, to screen such novel effective anticancer drugs, in this study, the cytotoxic effect and the 50 % inhibitory concentration (IC₅₀) of 9 bile acid derivatives against human cancer cells and normal cells was detected with MTT assay.

87.2 Materials and Methods

87.2.1 Materials

Bile acid derivatives (Fig. 87.1) were synthesized in our lab. Dulbecco's Modified Eagle Medium (DMEM) and Fetal bovine serum (FBS) were purchased from HyClone (Thermo scientific). DMSO was purchased from Biochem Technology (Shanghai, China). Trypsin and MTT were purchased from Solarbio (Beijing, China).

87.2.2 Cell Culture

Both MCF-7 human breast cancer cells and human umbilical vein endothelial cells (HUVEC) were grown in Dulbecco's Modified Eagle Medium (DMEM) supplemented with 10 % fetal bovine serum at 37 °C in a humidified atmosphere of 5 % CO₂ and 95 % air.

87.2.3 MTT Assay

The MTT assay has proven to be a rapid and reproducible means of estimating cell numbers in various eukaryotic systems [10]. MCF-7 or HUVEC were seeded into

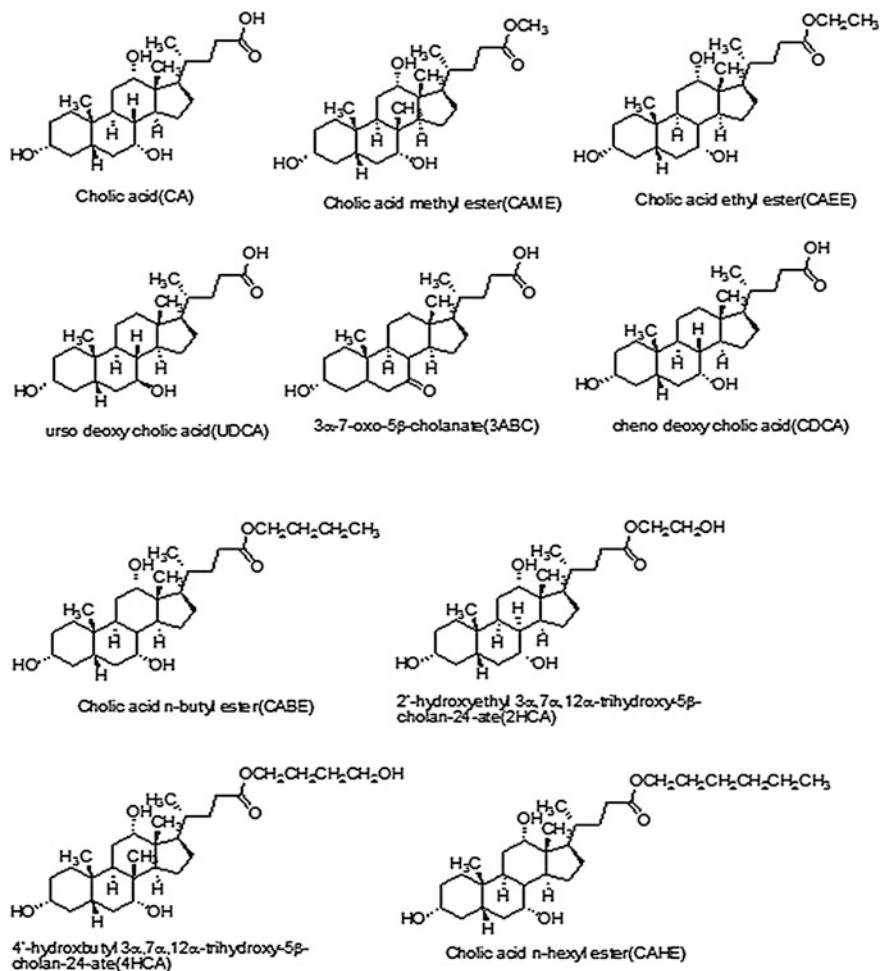


Fig. 87.1 The structure of the bile acid derivatives

96-well dishes at a density of 1×10^4 per well in a fixed volume of 100 μ L and kept under 5 % CO_2 at 37 $^\circ C$ for 12 h. After 12 h, cells were attached as controlled by microscopy and treated with the different bile acid derivatives dissolved with DMSO, which final concentration range from 1 to 625 μ mol/L. After 24 h incubation, 20 μ L of MTT solution (5 mg/mL) were added to each well and incubation with MTT for 4 h. The supernatants were removed and the cells were solubilized in DMSO (100 μ L) for 10 min [11–13]. Finally, the absorbance of the formazan product of MTT reduction was measured at 570 nm using BioTek SynergyTM 4 Hybrid Microplate Reader.

87.2.4 Statistical Analysis

The inhibitory rate was calculated based on the following formula [14, 15]:

$$\text{Inhibition rate (\%)} = \left(1 - \frac{A_{\text{experimental}}}{A_{\text{control}}} \right) \times 100$$

(A means absorbance)

Furthermore, IC₅₀ is the concentration of the cytotoxic agent that led to a decrease of 50 % of the recorded signal. The IC₅₀ was calculated by using SPSS Statistics 19 statistical analysis software.

87.3 Results and Discussion

87.3.1 Effect of Bile Acid Derivatives on Proliferation of MCF-7 Breast Cancer Cells

We first performed a MTT-based proliferation assay to explore how the bile acid derivatives influence the growth of MCF-7 cells, while taxol (paclitaxel) was used as the positive control. Taxol is one of the most effective microtubule-targeting drugs for breast cancer treatment, and it accounts for significant improvements in the survival of breast cancer patient in the last two decades [16]. As shown in Fig. 87.2, all the 9 compounds had remarkable inhibitory effect on the proliferation of MCF-7 cancer cells, and it showed a dose-dependent manner under the concentrations range from 1 to 625 $\mu\text{mol/L}$.

MCF-7 cells were treated with bile acid derivatives (CAME, CAEE, CABE, UDCA, CDCA, 3ABC, 2HCA, 4HCA, CAHE) and taxol. After 24 h, cell number was determined by MTT assay. Data shown were average \pm SE from one typical experiment with 6 replicates out of a series of 3 independent experiments.

The MTT (3-(4, 5-dimethylthiazole-2-yl)-2, 5-diphenyltetrazolium bromide) assays are widespread methods to assess cell viability [17, 18]. MTT is reduced by mitochondrial dehydrogenases in living cells to a blue-magenta-colored formazan precipitate. The absorption of dissolved formazan in the visible region correlates with the number of intact alive cells [19]. In the present study, the results suggested that bile acid derivatives are able to damage and destroy MCF-7 human breast cancer cells, and thus decrease the reduction of MTT to formazan.

Furthermore, to compare the anticancer function among the tested compounds, IC₅₀ values of the bile acid derivatives and taxol were calculated based on the former data. The results showed that the IC₅₀ of CAME, CAEE, CABE, UDCA, CDCA, 3ABC, 2HCA, 4HCA, CAHE, and taxol were 56.272, 72.289, 13.685, 418.279, 395.918, 372.743, 182.356, 36.767, 104.081, 32.134 $\mu\text{mol/L}$, respectively (Fig. 87.3). The results showed that among 9 bile acid derivatives, CABE

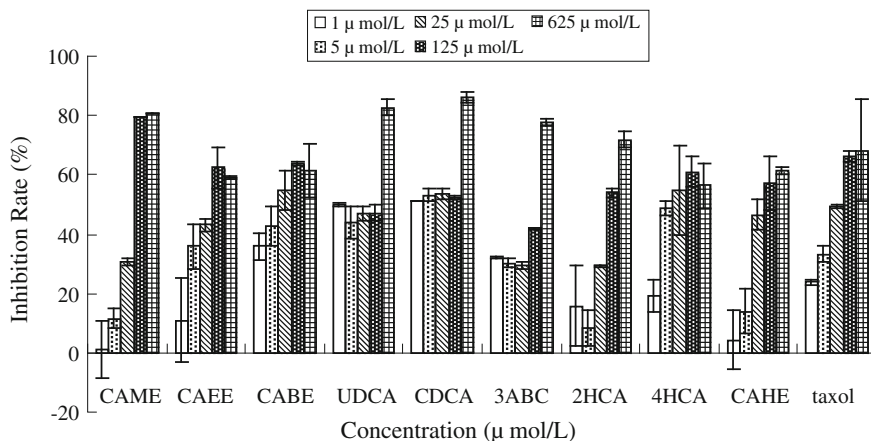


Fig. 87.2 Effects of bile acid derivatives on the proliferation of MCF-7 cells

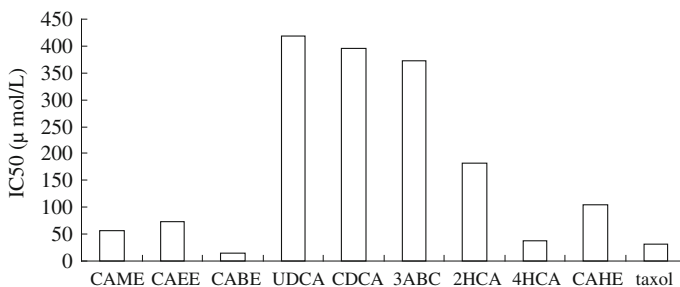


Fig. 87.3 IC₅₀ of bile acid derivatives against MCF-7 cells

had the lowest IC₅₀ against MCF-7 cells, and it was even lower than the IC₅₀ values of taxol, indicating that CABB might be powerful anticancer agents.

87.3.2 Effect of Bile Acid Derivatives on Proliferation of HUVEC

Human umbilical vein endothelial cells (HUVEC) are a kind of human body endothelial cells [20]. Therefore, we chose HUVEC as the normal cell lines to assess the safety of bile acid derivatives with high anticancer effects. As shown in Fig. 87.4, CAEE, 2HCA, CABB, 4HCA, CAHE were quite safe to the normal cells, especially CABB and CAEE, which could even promote the proliferation of HUVEC when the concentration was lower than 5 μmol/L.

HUVEC cells were treated with bile acid derivatives (CAEE, CABB, 2HCA, 4HCA, CAHE). After 24 h cell number was determined by MTT assay. Data

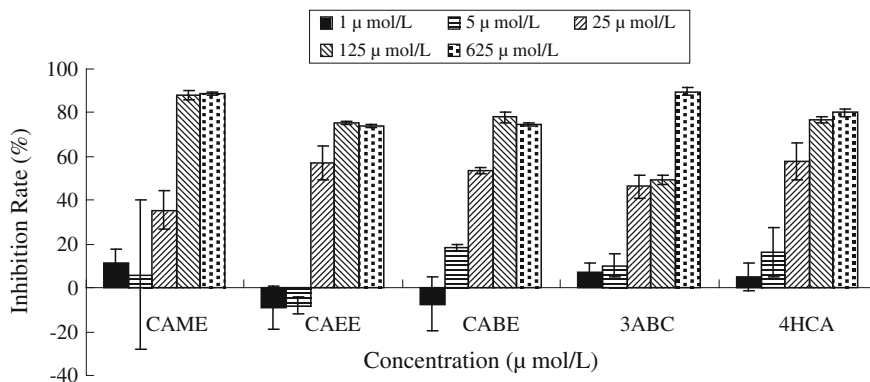


Fig. 87.4 Effects of bile acid derivatives on the proliferation of HUVEC

shown were average \pm SE from one typical experiment with 6 replicates out of a series of 3 independent experiments.

87.4 Conclusions

Our results strongly suggest that bile acid derivatives can be promising sources of potential anticancer activity. The present results will form the basis for selection of bile acid derivatives for further investigation in the potential drug discovery of new natural bioactive compounds. Among 9 bile acid derivatives tested in the present study, cholic acid ethyl ester and cholic acid n-butyl ester had high anticancer activity but low toxic effect on normal cells, indicating that these two compounds would be a good candidate for the development of novel bile acid-derived anticancer agents. Our future work will further confirm the *in vivo* anticancer activity of them and explore its detailed mechanism.

Acknowledgments This work was financially supported by the National Basic Research Program of China (973 Program) (NO. 2009CB825504), the National Natural Science Foundation of China (NO. 31000343, NO. 31071126), the Science & Technology Project of Tianjin (No. 10JCZDJC22500, 10ZXCSY10100), and the High School Science & Technology Development Foundation of Tianjin (NO.20090602).

References

1. Kanavos P (2006) The rising burden of cancer in the developing world. *Ann Oncol* 6(17):15–23
2. Shibuya K, Mathers CD, Pinto BC (2002) Global and regional estimates of cancer mortality and incidence by site: II. results for the global burden of disease 2000. *BMC Cancer* 2:37

3. Salminen E, Izewska J, Andreo P (2005) IAEA's Role in the global management of cancer-focus on upgrading radiotherapy services. *Acta Oncol* 44:816–824
4. Sener SF, Grey N (2005) The global burden of cancer. *Surg Oncol* 92:1–3
5. Sudhakar C, Sabitha P, Shashi KR (2007) Betulinic acid inhibits prostate cancer growth through inhibition of specificity protein transcription factors. *Cancer Res* 67:2816–2823
6. García SR, Ng C, Anderson H et al (2011) Synergistic drug combinations for tuberculosis therapy identified by a novel high-throughput screen. *Antimicrob Agents Ch* 55(8):3861–3869
7. Aydee CE, Syrovets T, Pitterle K et al (2010) Tirucallic acids are novel pleckstrin homology domain-dependent Akt inhibitors inducing apoptosis in prostate cancer cells. *Mol Pharmacol* 3(77):378–387
8. Gaube F, Wolff S, Pusch L et al (2007) Gene expression profiling reveals effects of *cimicifuga racemosa* (L.) NUTT. (black cohosh) on the estrogen receptor positive human breast cancer cell line MCF-7. *BMC Pharmacol* 7:11
9. Pai R, Tarnawski AS, Tran T (2004) Deoxycholic acid activates β -catenin signaling pathway and increases colon cell cancer growth and invasiveness. *Mol Biol Cell* 15:2156–2163
10. Lazaro JE, Gay F (1998) *Plasmodium falciparum*: in vitro cytotoxicity testing using MTT. *J Biomol Screen* 1(3):49–53
11. Hida T, Ueda R, Takahashi T et al (1989) Chemosensitivity and radiosensitivity of small cell lung cancer cell lines studied by a newly developed 3-(4,5-dimethylthiazol-2-yl)-2,5-diphenyltetrazolium bromide (MTT) hybrid assay. *Cancer Res* 9(49):4785–4790
12. Noguchi K, Tani MI, Nakamura M (2005) Evaluation of chemosensitivity testing with highly purified tumor cells in 435 patients with gastric carcinoma using an MTT assay. *Anticancer Res* 25:931–938
13. Montoro E, Lemus D, Echemendia M et al (2005) Comparative evaluation of the nitrate reduction assay, the MTT test, and the resazurin microtitre assay for drug susceptibility testing of clinical isolates of mycobacterium tuberculosis. *J Antimicrob Chemth* 2(55):500–505
14. Akiri SR, Sareddy GR, Phanithi PB et al (2010) The antioxidant and antiproliferative activities of methanolic extracts from njavara rice bran. *BMC Complem Altern M* 10:4
15. Pieters R, Loonen AH, Huismans DR et al (1990) In vitro drug sensitivity of cells from children with leukemia using the MTT assay with improved culture conditions. *Blood* 11(76):2327–2336
16. Lu J, Tan M, Huang WC et al (2009) Mitotic deregulation by survivin ErbB2-overexpressing breast cancer cells contribute to taxol resistance. *Clin Cancer Res* 15(4):1326–1334
17. Nakamura R, Saikawa Y, Kubota T et al (2006) Role of the MTT chemosensitivity test in the prognosis of gastric cancer patients after postoperative adjuvant chemotherapy. *Anticancer Res* 26:1433–1438
18. Mueller H, Kassack MU, Wiese M (2004) Comparison of the usefulness of the MTT, ATP, and calcein assays to predict the potency of cytotoxic agents in various human cancer cell lines. *J Biomol Screen* 9(6):506–515
19. Mosmann T (1983) Rapid colorimetric assay for cellular growth and survival: application to proliferation and cytotoxicity assays. *J Immunol Methods* 65:55–63
20. Mukherjee P, Anthony CF, Laura M et al (2008) Ganglioside GM3 suppresses the proangiogenic effects of vascular endothelial growth factor and ganglioside GD1a. *J Lipid Res* 2(49):929–938

Chapter 88

Design, Synthesis, and Biological Evaluation of the Novel Antitumor Agent 5-Bromobenzofuran-3(2H)-One and its Derivatives

Lei Lv, Xiaomin Zhang, Jian Lv, Yao Zhou, Weiguo Hu, Peng Yu, Hua Sun and Yuou Teng

Abstract Aurones and auronols are naturally occurring 2-benzylidenebenzofuranone-3(2H)-one derivatives. Aurones have a limited occurrence in fruits, vegetables, and bright yellow color to flowers such as cosmos and coreopsis. Aurones possess a wide range of biological activities, such as antitumor, anti-fungal, phytoalexin, and so on. Some aurone derivatives have been studied as antitumor drug molecules, but 2-benzylidene-5-bromobenzofuranone-3(2H)-one series have not been reported yet. In this paper, we'd like to report the design, synthesis, and biological evaluation of the novel aurone derivatives. All the newly synthesized compounds were characterized by ^1H NMR and their antitumor activities were evaluated by using MTT method in HT-29, K562, and HepG2 cell lines. 5-bromo-2-(4-nitrobenzylidene) benzofuran-3(2H)-one demonstrated good antitumor activity against K562 cells with an IC_{50} of 0.37 μM .

Keywords Aurone derivatives · Synthesis · Antitumor · MTT

L. Lv · X. Zhang · J. Lv · Y. Zhou · P. Yu · H. Sun · Y. Teng (✉)
Key Laboratory of Industrial Microbiology, Ministry of Education, College of Biotechnology, Tianjin University of Science and Technology, Tianjin 300457, People's Republic of China
e-mail: tyo201485@tust.edu.cn

L. Lv · X. Zhang · J. Lv · Y. Zhou · P. Yu · H. Sun · Y. Teng
Tianjin Key Laboratory of Industry Microbiology, College of Biotechnology, Tianjin University of Science and Technology, Tianjin 300457, People's Republic of China

W. Hu
North China Pharmaceutical Co. Ltd, Hebei 050015, People's Republic of China

88.1 Introduction

Aurones, a class of flavonoids found in fruits and flowers [1], possess a lot of biological activities such as antitumor, antifungal, and phytoalexin [2–4]. Their occurrence in marine organisms has been recently reported [5]. Compared to flavones, the medicinal literature on aurones is in its infancy with trends and design are just now emerging [6, 7].

Cancer is a global public health problem. Cancer chemoprevention aimed at reducing the risk of cancer by avoiding exposure to cancer-causing agents, enhancing the host defense capacity, adjusting lifestyle, supplementing with chemopreventive agents that inhibit, reverse, or block tumorigenesis [8–10]. In clinical practice with the usage of anticancer drugs, the phenomenon of resistance gradually emerged, thus a tremendous effort will be made to enhance the intracellular accumulation of antitumor agents in resistant cells [11, 12].

Aurones are recently attracting the interest of an increasing number of research groups. In this paper, we report our works made on the design and synthetic routes toward a series of functionalized aurones. The target compounds (6a–6e) were synthesized in six steps through esterification reaction, nucleophilic substitution reaction, aldol reaction [13], and so on. We also detected their antitumor activity against K562, HT29, and HepG2 cancer cells. Their biological activity results indicated that 5-bromo-2-(4-nitrobenzylidene) benzofuran-3(2H)-one (6a) shows good antitumor activity against K562 cells.

88.2 Materials and Methods

88.2.1 Materials and Measurements

All reagents and solvents used in this paper were of reagent grade. Reaction temperatures were controlled using oil bath temperature modulator. Thin layer chromatography (TLC) was performed using E. Merck silica gel 60 GF254 pre-coated plates (0.25 mm) and visualized using a combination of UV. Silica gel (particle size 200–400 mesh) was used for flash chromatography. ^1H NMR spectra was recorded on Bruker AM-400 NMR spectrometers in deuterated chloroform and deuterated DMSO. The chemical shifts are reported in δ (ppm) relative to tetramethylsilane as internal standard.

88.2.2 Chemistry

The synthetic approaches of target compound 6a–6e were demonstrated in Fig. 88.1.

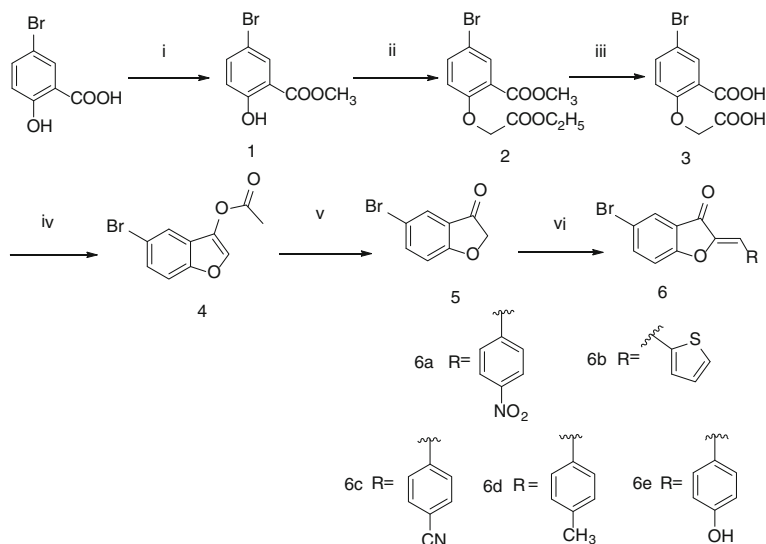


Fig. 88.1 Synthetic route of aurone derivatives

5-Bromosalicylic acid was employed to react with methanol at 80 °C to provide compound 1 which was then reacted with Ethyl chloroacetate at 70 °C to afford the key intermediate 2. Compound 2 was reacted with 10 % aqueous NaOH at 60 °C to provide compound 3 in good yield (81 %), then it was converted into compound 4 when treated with Ac₂O, CH₃COONa at 160 °C for 4 h. A mixture of compound 4, methanol, water, and 1 N HCl was heated to reflux for 3 h to obtain compound 5. Compound 5 was then reacted with 4-Nitrobenzaldehyde, 2-Thenaldehyde, 4-Cyanobenzaldehyde, 4-methylbenzaldehyde, and 4-Hydroxybenzaldehyde to afford compound 6a, 6b, 6c, 6d, and 6e.

88.2.3 Biological Assay

The anticancer activities for newly synthesized compounds were tested on the K562, HT-29, and HepG2 cells by using MTT method. The results of compounds (6a–6e) were listed in Table 88.1 which indicated that 5-bromo-2-(4-nitrobenzylidene)-benzofuran-3(2H)-one (6a) demonstrated good antitumor activity against K562 and HT-29 with an IC₅₀ of 0.37 μM and 7.19 μM, respectively. But it was not active against HepG2 (IC₅₀ > 10 μM) at our test condition.

Reagents and conditions: (i) CH₃OH, conc H₂SO₄; (ii) ClCH₂COOC₂H₅, K₂CO₃, acetone; (iii) 10 % NaOH, H₂O, then HCl; (iv) Ac₂O, HAc, CH₃COONa; (v) CH₃OH, HCl; and (vi) HAc, conc HCl.

Table 88.1 Inhibition Activity of the compound 6a, 6b, 6c, 6d, and 6e

Tested cell	Samples (IC ₅₀)				
	6a	6b	6c	6d	6e
K562	0.37	4.14	>10	>10	>10
HepG2	>10	>10	>10	>10	>10
HT-29	7.19	>10	>10	>10	>10

88.3 Results and Discussion

88.3.1 Synthesis and Characterize Aurones Derivatives by ¹H NMR

2-hydroxy-5-bromobenzoic acid methyl ester (1) [14]. The conc. H₂SO₄ (6 mL) was added dropwise into 5-Bromosalicylic acid (6.0 g, 27.65 mmol) in methanol (180 mL) at 0 °C. After stirring for 10 min, the reaction mixture was heated to 80 °C for 12 h. The solvent was removed under vacuum to afford the crude which was purified by flash column chromatography (silica gel, petroleum ether/ethyl acetate 25:1) to yield the compound 1 (5.7 g, 89 %).

¹H NMR (CDCl₃ 400 MHz): δ/ppm 3.98 (s, 3H), 6.90 (d, J = 8.8 Hz, 1H), 7.55 (dd, J = 8.8 Hz, 2.41 Hz, H), 7.97 (d, J = 2.8 Hz, 1H), 10.71(s, 1H).

Methyl 2-((Ethoxycarbonyl)methoxy)-5-bromobenzoate(2). To a solution of 2-hydroxy-5-bromobenzoic acid methyl ester (4.8 g, 20.78 mmol) in acetone (120 mL) was added K₂CO₃ (8.64 g, 62.33 mmol) and ethylchloroacetate(5.1 g, 41.55 mmol).The mixture was stirred for 5 h at 70 °C. After the solvent was evaporated, the residue was dissolved in water and extracted with ethyl acetate, the organic layer was dried over Na₂SO₄. The solvent was removed under vacuum to provide the crude which was purified by flash column chromatography (silica gel, petroleum ether/ethyl acetate 10:1) to afford compound 2 (5.8 g, 87 %).

¹H NMR (d₆-DMSO 400 MHz): δ/ppm 1.29 (t, J = 9.6 Hz, 3H), 3.92 (s, 3H), 4.28(q, J = 9.6 Hz, 2H), 4.71 (s, 2H), 6.80 (d, J = 12.0 Hz, 1H), 7.55 (d, J = 8.4 Hz, 1H), 7.96 (s, 1H).

2-(Carboxymethoxy)-5-bromobenzoic Acid (3) [15]. To a solution of compound 2 (4.6 g, 14.49 m mol) in 1 N aqueous NaOH (262 mL), the mixture was stirred for 4 h at 60 °C. The product formed by adding 1 N HCl was filtered to give 3.18 g of compound 3 (80 %).

¹H NMR (d₆-DMSO 400 MHz): δ/ppm 4.79 (s, 2H), 6.99 (d, J = 9.2 Hz, 1H), 7.64 (dd, J = 2.8 Hz, 8.8 Hz, 1H), 7.75 (d, J = 2.4 Hz, 1H), 13.1 (broad, s, 1H).

5-Bromo-3-acetoxybenzofuran(4). A mixture of acetic anhydride(170 mL), acetic acid(157 mL), anhydrous sodium acetate(20 g, 240 mmol), and compound 3 was heated to reflux for 4 h. Saturated aqueous sodium carbonate was then added, and the mixture was extracted with CH₂Cl₂. The solvent was removed in vacuo to give the crude product which was purified by flash column

chromatography (silica gel, petroleum ether/ethyl acetate 8:1) to afford compound 4 (2.4 g, 81.7 %).

$^1\text{H NMR}$ (CDCl_3 , 400 MHz): δ/ppm 2.37 (s, 3H), 7.33 (d, $J = 12.0$ Hz, 1H), 7.43 (dd, $J = 4.8$ Hz, 2.8 Hz 1H), 7.71 (s, 1H), 8.02 (s, 1H).

5-Bromobenzofuran-3(2H)-one (5). A mixture of compound 4 (2.4 g, 9.54 mmol), methanol (50 mL), water (30 mL) and 1 N HCl (60 mL) was heated to reflux for 3 h. The precipitate formed was collected by filtration, washed with water, and dried under vacuum to get compound 5 (1.9 g, 86 %).

$^1\text{H NMR}$ (CDCl_3 , 400 MHz): δ/ppm 4.67(s, 2H), 7.06 (d, $J = 12.0$ Hz, 1H), 7.69 (dd, $J = 2.8$ Hz, 2.8 Hz, 1H), 7.79 (d, $J = 2.8$ Hz, 1H).

Compounds (6a–6e) [16]. To a solution of compound 5 (1 equiv) and 1.2 equiv of appropriate benzaldehyde derivatives in 10 mL of glacial acetic acid, 2 drops of concentrated hydrochloric acid was added at the room temperature, the reaction was stirred at the same temperature for 3 h. The reaction mixture was poured into ice–water and filtered. The filter cake was purified by flash column chromatography (silica gel, petroleum ether/ethyl acetate 30:1–20:1) to get compounds (6a–6e).

5-bromo-2-(4-nitrobenzylidene) benzofuran-3(2H)-one (6a). Starting from compound 5 (0.2 g, 0.94 mmol) and 4-Nitrobenzaldehyde (0.17 g, 1.13 mmol), compound 6a was obtained in 66 % yield.

$^1\text{H NMR}$ (CDCl_3 , 400 MHz): δ/ppm 6.90 (s, 1H), 7.30 (s, 1H), 7.82–7.79(dd, $J = 8.8$ Hz, 2.4 Hz, 1H), 7.95 (d, $J = 2.0$ Hz, 1H), 8.05 (d, $J = 8.8$ Hz, 2H), 8.26 (d, $J = 4.4$ Hz, 2H).

5-bromo-2-(thiophen-2-ylmethylene) benzofuran-3(2H)-one (6b). Starting from compound 5 (0.2 g, 0.94 mmol) and 2-Thenaldehyde (0.13 g, 1.13 mmol), compound 6b was obtained in 71 % yield.

$^1\text{H NMR}$ (CDCl_3 , 400 MHz): δ/ppm 7.17–7.14 (m, 1H), 7.19 (s, 1H), 7.23 (s, 1H), 7.55 (d, $J = 3.6$ Hz, 1H), 7.63 (d, $J = 5.2$ Hz, 1H), 7.74–7.71 (dd, $J = 8.4$ Hz, 2 Hz, 1H), 7.90 (d, $J = 2.0$ Hz, 1H).

5-bromo-2-(4-cyanobenzylidene) benzofuran-3(2H)-one (6c). Starting from compound 5 (0.2 g, 0.94 mmol) and 4-Cyanobenzaldehyde (0.15 g, 1.13 mmol), compound 6c was obtained in 54 % yield.

$^1\text{H NMR}$ (CDCl_3 , 400 MHz): δ/ppm 6.85 (s, 1H), 7.29 (s, 1H), 7.73 (d, $J = 8.4$ Hz, 2H), 7.79 (dd, $J = 8.8$ Hz, 2 Hz, 1H), 7.93 (d, $J = 2.0$ Hz, 1H), 7.98 (d, $J = 10.4$ Hz, 2H).

5-bromo-2-(4-methylbenzylidene) benzofuran-3(2H)-one (6d). Starting from compound 5 (0.2 g, 0.94 mmol) and 4-methylbenzaldehyde (0.14 g, 1.13 mmol), compound 6d was obtained in 88 % yield.

$^1\text{H NMR}$ (CDCl_3 , 400 MHz): δ/ppm 2.41 (s, 3H), 6.91 (s, 1H), 7.23 (s, 1H), 7.28 (d, $J = 6.8$ Hz, 2H), 7.73 (dd, $J = 8.8$ Hz, 2 Hz, 1H), 7.80 (d, $J = 8.0$ Hz, 2H), 7.96 (d, $J = 2.0$ Hz, 1H).

5-bromo-2-(4-hydroxybenzylidene) benzofuran-3(2H)-one (6e). Starting from compound 5 (0.2 g, 0.94 mmol) and 4-Hydroxybenzaldehyde (0.14 g, 1.13 mmol), compound 6e was obtained in 65 % yield.

¹H NMR (d6-DMSO 400 MHz): δ /ppm 6.91 (d, $J = 8.8$ Hz, 2H), 6.96 (s, 1H), 7.55 (d, $J = 8.4$ Hz, 1H), 7.87–7.94 (m, 4H), 10.30 (s, 1H).

88.3.2 Anticancer Activity Assay

All the above compounds were tested for their in vitro anticancer activity against HT-29, K562, and HepG2 cells by MTT-Based assay. The cells were diluted to a density of 5×10^4 cells/mL and added 100 μ L to each well of the 96-well plates with a multichannel pipet. After incubating for 24 h, 0.5 μ L compounds were added and then cells were further incubated for 48 h (final concentrations of each compound: 0.1, 0.3, 1, 3, and 10 μ M). The culture plates were incubated for 4 h after which 20 μ L MTT was added to each well, then the medium was removed from the wells and 100 μ L DMSO was added into each well. After leaving for further 10 min to dissolve the formazan crystals formed, the optical density (OD) was measured at 490 and 630 nm. Cell viability was calculated from measurements of OD value according to the corresponding formula and a graph is plotted of Cell viability (y-axis) against drug concentration (x-axis). The given values are mean values of three experiments. The IC₅₀ concentration represents the concentration which results in a 50 % decrease in cell growth after 2 days incubation. The results were presented in Table 88.1.

88.4 Conclusion

We report the design and synthesis of novel aurone derivatives. Several steps among this route were optimized, such as cyclization, nucleophilic substitution reaction, aldol reaction, and so on. The cyclization reaction was the key step. All the target compounds were synthesized in six steps with the overall yield of 25–30 %, respectively. The structures of these novel targets and all of intermediates were confirmed by ¹H NMR. Biological activity test indicated that 5-bromo-2-(4-nitrobenzylidene) benzofuran-3(2H)-one (6a) has good antitumor activity against K562 and HT-29 cells. In order to improve the antitumor activity, further modification based on compound (6a) was undergone in our lab.

Acknowledgments The authors sincerely thank the financial support from the Tianjin University of Science and Technology (20110406, 20110115), the Natural Science Foundation of Tianjin (11JGYBJC14300), the Science and Technology Project of Tianjin (11ZCGHHZ00400) and the Natural Science Foundation of Tianjin (12JCYBJC31600).

References

1. Harborne JR (1994) The flavonoids: advances in research since 1986. Chapman and Hall, London, pp 341–399
2. Brooks CJW, Watson DG (1985) Phytoalexins. *Nat Prod Rep* 2:427–459
3. Aufmkolk M, Koerhle J, Hesch RD et al (1986) Inhibition of rat liver iodothyronine deiodinase. Interaction of aurones with the iodothyronine ligand-binding site. *J Biol Chem* 261:11623
4. Kayser O, Kiderlen AF, Folkens U et al (1999) In vitro leishmanicidal activity of aurones. *Planta Med* 65:316
5. Choudhary MI, Hayat S, Khan AM et al (2001) Two new aurones from marine brown alga *spatoglossum variabile*. *Chem Pharm Bull* 49:105–107
6. Boumendjel A (2003) Aurones: a subclass of flavonoids with promising biological potential. *Curr Med Chem* 10:2621–2630
7. Lawrence NJ, Rennison D, McGown AT et al (2003) The total synthesis of an aurone isolated from *Uvaria hamiltonii*: Aurones and flavones as anticancer agents. *Bioorg Med Chem Lett* 13:3759–3763
8. Sporn MB, Liby KT (2005) Cancer chemoprevention: scientific promise, clinical uncertainty. *Nat Clin Pract Oncol* 2:518–525
9. Hail NJ, Cortes M, Drake EN et al (2008) Cancer chemoprevention: a radical perspective. *Free Rad Biol Med* 45:97–110
10. Chen C, Kong AN (2005) Dietary cancer-chemopreventive compounds: from signaling and gene expression to pharmacological effects. *Trends Pharmacol Sci* 26:318–326
11. Ford JM (1996) Experimental reversal of P-glycoprotein-mediated multidrug resistance by pharmacological chemosensitizers. *Eur J Cancer* 32:991–1001
12. Wiese M, Pajeva IK (2001) Structure-activity relationships of multidrug resistance reversers. *Curr Med Chem* 8:685–713
13. Lee CY, Chew EH, Go ML (2010) Functionalized aurones as inducers of NAD(P)H: quinone oxidoreductase 1 that activate AhR/XRE and Nrf2/ARE signaling pathways: synthesis, evaluation and SAR. *Eur J Med Chem* 45:2957–2971
14. Ohkata K, Tamura Y, Shetuni BB et al (2004) Stereoselectivity control by oxaspiro rings during Diels-Alder cycloadditions to cross-conjugated cyclohexadienones: the syn oxygen phenomenon. *J Am Chem Soc* 126:16783–16792
15. Cheng C, Zhu SF, Liu B et al (2007) Highly enantioselective insertion of carbenoids into O-H bonds of phenols: an efficient approach to chiral alpha-aryloxy-carboxylic esters. *J Am Chem Soc* 129:12616–12617
16. Cheng H, Zhang L, Liu Y et al (2010) Design, synthesis and discovery of 5-hydroxyaurone derivatives as growth inhibitors against HUVEC and some cancer cell lines. *Eur J Med Chem* 45:5950–5957

Chapter 89

Preliminary Study on the Mechanism of Cartilage Polysaccharide Inducing H22 Cell to Engender Immunogenicity

Guoqiang Zheng, Pan Li, Anguo Teng, Jie Zheng, Wenhong Wang and Anjun Liu

Abstract It was discussed that the apoptosis product of H22 hepatocarcinoma cells induced by cartilage polysaccharide (CP) could activate the body immune system to antitumor. The mice's survival time, life extension rate (LER) and livability were measured by animal experiment. Lymphocyte proliferation was determined by MTT. The immune serum titer was identified by ELISA. The tumor protein antigen was analyzed by SDS-PAGE, Western blot, 2-D, and mass spectrometry analysis (MS). Compared with the model group, there was a significant improvement on the survival time, LER, livability, thymus index, spleen index, and stimulation index in immune group. The serum had high antibody titer which was up to 1:6,400. The tumor-specific antigen was tubulin alpha chain by MS and molecular weight is 50 KDa. The apoptosis product of H22 induced by CP had immunogenicity and could activate the immune system of the mouse to antitumor.

Keywords Cartilage · Polysaccharide · Immunogenicity · Tumor-specific antigen · Antitumor

89.1 Introduction

Immunotherapy is an approach to induce immune responses to tumor-associated antigens. Yet, the immunogenicity of tumor antigen is generally weak requiring an adjuvant which stimulates the immune system against tumor [1]. Several studies have applied cytokines as adjuvant in vaccine [2], but in recent years

G. Zheng · P. Li · A. Teng · J. Zheng · W. Wang · A. Liu (✉)
College of Food Engineering and Biotechnology, Tianjin University of Science and Technology, Tianjin 300457, People's Republic of China
e-mail: laj@tust.edu.cn

polysaccharide has been shown to be a good biological response modifier (BRM) without the adverse side effects compared to traditional agents [3]. There are more than 220 kinds of antitumor polysaccharides extracted from *Ganoderma lucidum*, *Lentinus edodes*, *Grifola frondosa*, and others [4–6]. Previous studies confirmed in our lab that cartilage polysaccharide (CP) isolated from porcine cartilage could significantly induce cell apoptosis and inhibit tumor growth in vivo and extend the survival rate of mice. The pathogenesis of systemic lupus erythematosus (SLE) had close relation with cell apoptosis that apoptotic body could denature their own tissue and engender immunogenicity of proteins antigen in mice immune system [7]. Due to the discovery of tumor antigen with immunogenicity, some people attempted to search the high expression tumor-associated protein as tumor antigen [8]. In this study, H22 hepatocarcinoma cells were treated with CP to investigate whether its apoptosis product as the tumor cell vaccine could protect the immune mice from tumor or not.

89.2 Materials and Methods

89.2.1 Cell Line and Experimental Animal

The murine H22 hepatocarcinoma cells line was purchased from Tianjin Medical Sciences University. The animals were female BALB/c mice, 6–8 weeks of age, 20 g in weight, and purchased from Chinese Academy of Military Medical Sciences Experimental Animal Center.

89.2.2 Preparation of the Tumor Vaccine

The H22 hepatocarcinoma cells (2.5×10^8 cells) were cultured in 8 ml RPMI1640 medium with 10 % FBS and mixed with 400 $\mu\text{g}/\text{mL}$ CP for 48 h. Cells were harvested by centrifugation (12,000 r/min for 20 min). The pellet was suspended in distilled water and then subjected to six repeated freeze–thaw cycles in liquid nitrogen as vaccine. The vaccine was injected in back subcutaneous once a week, amount to four times. After 4 weeks, H22 hepatocarcinoma cells ($2 \times 10^6/0.2$ mL) were injected in armpits.

89.2.3 Animal Immune Experiment

Animal trials were undertaken using groups of 20 animals for each treatment (control, model, and immune group). The model group was immunized with equal

amount of 0.9 % saline. Trials were performed over a 30-day period with the survival time, life extension rate (LER), and livability of each group.

89.2.4 Spleen Index and Thymus Index

The mice body weight was measured and then they were sacrificed. Organs (spleen and thymus) were removed and weighed.

89.2.5 Lymphocyte Proliferation Experiment

Lymphocytes proliferation experiment was assayed by MTT. The fresh spleen of each group was ground into single cell suspension, about 5×10^6 cells/ml. The H22 cells (100 μ l/well) were cultured in the 96-well microplate and simultaneously treated with ConA and LPS for 48 h, whose concentration is 5 μ g/ml respectively. The cells were added MTT solution (0.5 mg/ml in $1 \times$ PBS pH 7.4) for 4 h and DMSO simultaneously shaking for 2 min. The culture medium and the untreated cells were used as controls. The optical absorption at 570 nm was measured and the stimulation index (Si) was calculated.

89.2.6 Preparation of Immune Serum

After 4 weeks, blood was taken from the eyeball of immunized mice and incubated at 4 °C for 3 h. The serum was subsequently collected by centrifugation (5,000 r/min, 10 min) and stored in liquid nitrogen prior to analysis.

89.2.7 SDS-PAGE and Western Blot

The proteins were extracted from the H22 cells treated with CP (24, 48, and 72 h) respectively, and the control cells by RIPA lysis buffer. One SDS-PAGE gel was stained with Coomassie Brilliant Blue R-250. The other duplicate SDS-PAGE gel was transferred to a nitrocellulose membrane (NC) and subsequently treated with blocking reagent (5 % w/v skimmed milk powder) for 2 h at 4 °C. The NC membrane was then reacted with immunized serum at 1:150 dilution and incubated overnight at 4 °C followed by incubation with goat anti-mouse IgG labelled with HRP at a dilution of 1:2,500 for 1 h at 37 °C. Immunodetection was accomplished by enhanced ECL and autoradiography on Kodak film.

89.2.8 2D-PAGE and MS

To perform 2-D PAGE, first, proteins (1 mg) were applied to isoelectric focusing (IEF), the IPG strips (17 cm, pH 3–10) were rehydrated overnight. Secondly, IPG strips were equilibrated twice in the equilibration buffer (0.375 M Tris-HCl [pH 8.8], 6 M urea, 20 % glycerol, 2 % sodium dodecyl sulfate [SDS]) for 15 min. In the first equilibration, 200 mg of DTT was dissolved in 10 ml buffer. In the second equilibration 250 mg iodoacetamide was added. Strip was then transferred to the 12 % SDS-PAGE gels and covered with 0.5 % low melting agarose. The gel was stained with Coomassie Brilliant Blue R-250 and then used for MS analysis.

89.2.9 Statistical Analysis

One Way Analysis of variance (ANOVA) was performed to determine differences in life extension rate and livability. A P value of <0.05 was considered significant.

89.3 Results

89.3.1 Survival Status was Improved in Immunized Mice

The survival time (30.06 ± 0.84 d) was increased in immune group compared with model group (18.0 ± 0.91 d) ($P < 0.05$) (Table 89.1). The life extension rate (66.87 %) and livability (70 %) in immune group were significantly different from model group ($p < 0.01$). The result showed that the immunized mice were generated immunogenicity by tumor vaccine, which activated the immune system and enhanced immunity to provide protection against tumor intrusion.

89.3.2 Thymus and Spleen were Protected by Tumor Vaccine

The thymus was severely atrophied and spleen was swollen obviously in model group compared with blank group, but in immune group thymus atrophy and

Table 89.1 Survival status of the mice ($\bar{x} \pm s$)(n = 20)

Groups	Survival time(d)	Life extension rate (%)	Livability (%)
Blank group	–	–	–
Model group	18.0 ± 0.91	0	0
Immune group	$30.06 \pm 0.84^*$	66.87**	70**

*P < 0.05 vs. model group; **P < 0.01 vs. model group

Table 89.2 Spleen and thymus indexes of the mice in different groups ($\bar{x} \pm s$) ($n = 20$)

Groups	Thymus index (Ti)	Spleen index (Si)
Blank group	4.17 \pm 0.98	4.86 \pm 0.47
Model group	0.49 \pm 0.32	9.35 \pm 0.41
Immune group	3.43 \pm 0.24**	4.41 \pm 0.71**

**P < 0.01 vs. model group

splenomegalia were changed slightly, which was close to normal mice (Table 89.2). The result showed that, to a certain extent, immune organ in the immune group was protected after treatment with vaccine. The reasons for splenomegalia are required further study in model group.

89.3.3 Lymphocyte was Activated with Tumor Vaccine

From Table 89.3, compared with the model group, B and T cells' stimulation index (SI) of the immune group had increased remarkably ($P < 0.01$). Although the immunized mice had extreme gap with the blank group, it had much improvement contrast with the model group. Results revealed that tumor vaccine could activate lymphocyte to protect mice to resist the tumor cells.

89.3.4 High Level Antibody was Detected in Immunized Mice

The serum of the immune group had higher antibody titer than the blank group ($> 1:6,400$) (Fig. 89.1). The result showed the tumor vaccine treated with CP adjuvant could produce tumor antigen or enhance the immunogenicity of tumor-specific antigen which could generate antibody to enhance humoral immune. Thus the tumor vaccine could generate antibody to inhibit tumor cell proliferation.

89.3.5 A 50 kDa Tumor Protein Antigen was Found by SDS-PAGE and Western Blotting

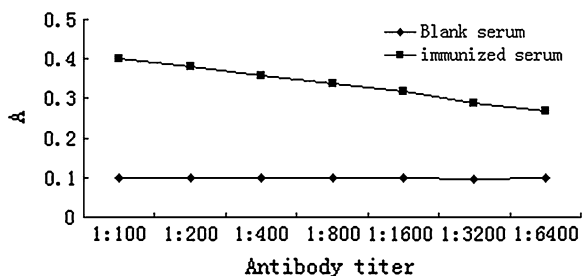
A tumor protein antigen band emerged at 50 kDa, which showed strong reaction with immunized serum rather than the blank serum. We presumed that the tumor

Table 89.3 Lymphocyte proliferation of each group ($\bar{x} \pm s$, $n = 20$)

Group	Con A	LPS
Blank group	10.29 \pm 0.68	9.86 \pm 0.32
Model group	1.26 \pm 0.15	1.74 \pm 0.18
Immune group	5.87 \pm 0.41**	4.29 \pm 0.71**

**P < 0.01 vs. model group

Fig. 89.1 The absorbance of serum antibody titer



protein antigen could activate the immune responses due to the changes in antigen protein's expression, which could combine with these specific antibodies. It could be the tumor protein antigen producing these specific antibodies to stop the invasion of tumor cells (Fig. 89.2).

89.3.6 The Tumor Antigen was Tubulin Alpha Chain by 2-D-PAGE and MS

The total protein extracted from H22 cell mixed CP for 48 h and the untreated H22 cells were analyzed in at least three independent experiments. The result showed that a protein was up-regulated obviously in treated H22 cells with CP in Fig. 89.3. According to MS analysis, the protein is tubulin alpha chain (Accession Number:

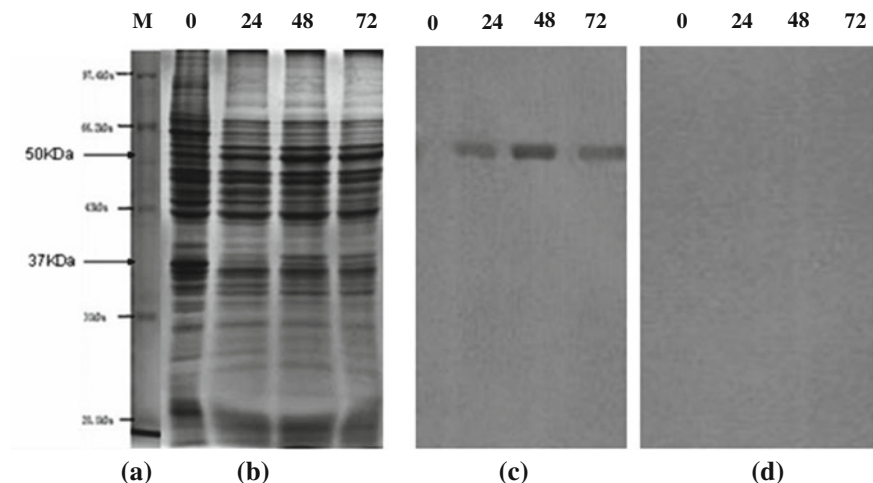


Fig. 89.2 Result of tumor-specific antigen by Western blotting. **a** Marker; The numbers above are for H22 cells treated with the CP for 0, 24, 48, and 72 h, respectively; **b** SDS-PAGE; **c** The result of western blot incubated with the immunized serum; **d** blank serum

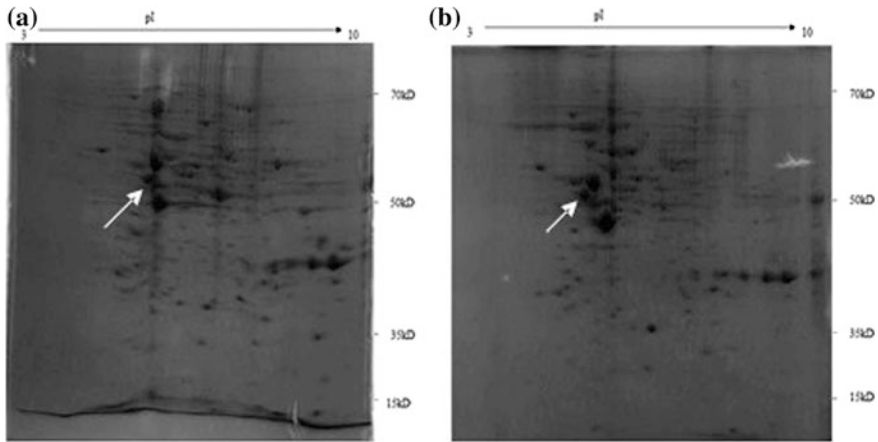


Fig. 89.3 Result of 2-D PAGE stained by Coomassie blue. **a** The protein from the untreated H22 cells. **b** The protein from the treated H22 cells with CP for 48 h

gil549052). Its pI is 4.94 and molecular weight is 50.81 kDa. The result of the 50 kDa protein was consistent with previous results of SDS-PAGE and Western Blot.

89.4 Discussion

The primary cause of CP that inhibited cell proliferation and induced cell apoptosis was used as a blocker in cell cycle which was blocked in the G1 and S phase and could not inverse to the G2 phase; the changes in cellular morphology such as nuclear condensation and fragmentation occurring upon CP treatment was also observed [1].

This study tried to evaluate the effect of tumor vaccine treated with CP for 48 h. Compared with model groups, there was an evident improvement in survival time, life extension rate, and livability in the immune group. Thymus index and spleen index were also demonstrated as available protection for immune organ. Lymphocyte proliferation experiment had increased remarkably in comparison with model group. These results revealed that the tumor vaccine could significantly stimulate the homologous antitumor immune responses, containing cellular immunity and humoral immunity. Western blot and 2D-PAGE showed the expression of a tumor antigen at an estimated molecular mass of 50 kDa, was up-regulated after treatment with CP, and the tumor antigen was tubulin alpha chain by MS. Tubulin alpha chain was the component of the microtubule involved in maintaining the cell morphology, mitotic progression, and chromosomal segregation. Tubulin alpha chain binding the drug could promote cell apoptosis by inhibiting mitotic program. Some studies illustrated that tubulin alpha chain had a

certain effect on occurrence, development, and prognosis in lung cancer. With the development of the tumor, the expression of tubulin alpha chain increased gradually, so that controlling tubulin alpha chain in cancer cells had vital significance on the treatment of cancer [9].

In our opinion, the expression of tumor-specific antigen (TSA) in H22 hepatocarcinoma cells was controlled by CP. We may deduce a conclusion that the immunogenicity of the tumor vaccine was increased due to the high expression of protein or post-translational protein modification by CP. When the tumor vaccine was injected into mice, the antitumor immune responses were activated, so that the mice could keep from invasion of tumor cells. The identification of TSA led to the development of immunotherapy aimed at augmenting antitumor immune responses [10]. From this fact we could conclude that TSA might be a therapeutic target. Tumor vaccines based on TSA played a key role in cancer prevention. Active immunotherapy with cancer vaccines could induce humoral and cellular immune responses and the development of immunological memory which may substantially reduce the relapse of the tumor [11, 12].

Acknowledgments This work was supported by grants from China National Natural Science Foundation (No.31271975 and No.20776113).

References

1. Liu A, Gao Y, Zhang H et al (2011) Immunologic mechanism of the anti-tumor immunity responses induced by the altogether culture medium of porcine cartilage polysaccharide and S180 ascites lump cells as a tumor vaccine. *ICBBE*:1–5
2. Richard M (2010) Antibody and cell-mediated immunity to *Streptococcus pneumoniae*: implications for vaccine development. *J Mol Med* 88:135–142
3. Tzianbos O (2000) Polysaccharide immunomodulators as therapeutic agents: Structural aspects and biologic function. *Clin Micro Rev* 13(4):523–533
4. Wei D, Li N, Wei D et al (2009) Tumor-inhibitory and liver-protective effects of *Phellinus igniarius* extracellular polysaccharides. *World J Microbiol Biotechnol* 125:633–638
5. Zhang L, Liu W, Han B et al (2008) Isolation and characterization of antitumor polysaccharides from the marine mollusk *Ruditapes philippinarum*. *Eur Food Res Technol* 227:103–110
6. Maria L, Daniel P, Ana P et al (2009) In vivo growth-inhibition of Sarcoma 180 by an α -(1 → 4)-glucan- β -(1 → 6)-glucan-protein complex polysaccharide obtained from *Agaricus blazei* Murill. *J Nat Med* 63:32–40
7. Li H, Wang J (2005) Cell apoptosis and systemic lupus erythematosus. *Shandong Med J* 45(16):4–6
8. Ke X, Wang J, Yang X (2006) The new concept of tumor antigen and the importance of immunotherapy in lymphoma and other tumors. *J Exp Hematol* 14(3):151–154
9. Chen Q, Jiang Z, Wu L (2010) Relativity expression of Tubulin alpha chain and MDR1 with lung cancer biology. *Chinese J Oncol* 32(4):278–282
10. Constantin N, Baxevasis S, Perez M (2009) Combinatorial treatments including vaccines, chemotherapy and monoclonal antibodies for cancer therapy. *Cancer Immunol Immunother* 58:317–324

11. Neelapu S, Kwak L (2007) Vaccine therapy for B-cell lymphomas: next-generation strategies. American Society of Hematology education program book. Atlanta GA:243–249
12. Paula W, Olga R, Jennifer B et al (2009) Her-2 DNA versus cell vaccine: immunogenicity and anti-tumor activity. *Cancer Immunol Immunother* 58:759–767

Chapter 90

Design and Synthesis of Novel 20-Substituted Hydroxycamptothecin Derivatives

Shaopeng Wen, Dewu Quan, Yao Zhou, Haiyong Jia, Peng Yu,
Hua Sun and Na Guo

Abstract Camptothecin (CPT) is a potent antitumor alkaloid isolated in 1966 by M.E. Wall. Clinical use of camptothecin in cancer therapy, however, was limited by its poor water solubility. Recently, there is a growing tendency to develop some new methods for the synthesis of novel derivatives to solve the problem. In this paper, we'd like to report the design and synthesis of a novel series of 20-substituted Hydroxycamptothecin to increase the water solubility. All the five products have never been reported before. All the products and important intermediates were characterized by ¹HNMR and LC-MS spectra.

Keywords Hydroxycamptothecin derivatives · Water solubility

90.1 Introduction

Camptothecin is a pentacyclic alkaloid, which was first isolated in 1966 from the extract of a Chinese plant, *Camptotheca acuminata*, by M.E. Wall [1], and soon it was found that CPT possess good inhibitory activity against a broad spectrum of tumors. Interest in CPT derivatives was revitalized in 1985 by the discovery that CPT exhibits a unique mechanism of action because it targets the nuclear enzyme topoisomerase I [2–4]. CPT forms a ternary complex with topoisomerase I and

S. Wen · D. Quan · Y. Zhou · H. Jia · P. Yu · H. Sun · N. Guo (✉)
Key Laboratory of Industrial Microbiology, Ministry of Education,
College of Biotechnology, Tianjin University of Science and Technology,
Tianjin 300457, People's Republic of China
e-mail: guona@tust.edu.cn

S. Wen · D. Quan · Y. Zhou · H. Jia · P. Yu · N. Guo
Tianjin Key Laboratory of Industry Microbiology, College of Biotechnology,
Tianjin University of Science and Technology, Tianjin 300457,
People's Republic of China

DNA, and the stabilization of these complex results in DNA breaks by preventing DNA relegation [5–7].

Initial clinical trials with CPT were limited by its poor solubility in physiologically compatible media [8]. Early attempts to form a water-soluble sodium salt of CPT by opening the lactone ring with sodium hydroxide resulted in a compound with poor antitumor activity [9–11]. It was later reported that the closed lactone form is an absolute requisite for antitumor activity [12, 13]. Intensive efforts in medicinal chemistry over the past several decades have provided a large number of camptothecin analogues, of which topotecan and irinotecan [14] are among those clinically approved for the treatment of cancers.

In order to increase the water solubility, we added some water soluble groups in appropriate position of hydroxycamptothecin. In this paper, we would like to report the design and synthesis of novel 20-substituted hydroxycamptothecin derivatives. The target compounds (**4a–4e**) were synthesized through four steps.

90.2 Results and Discussion

90.2.1 Chemistry

Figure 90.1 demonstrates the synthetic approach to the target compounds **4a–4e**. Hydroxycamptothecin reacted with Di-tert-butyl dicarbonate in DMF generated compound **1**, which was then reacted with 4-Nitrophenyl chloroformate under argon to afford the key intermediate compound **2**. In this step, anhydrous and anaerobic conditions were required because low yield was observed when the reaction conditions were not well controlled. Compound **2** respectively reacted with diethylamine, propylamine, n-Butylamine, morpholine and pyrrolidine to get compounds **3a–3e**. Compounds **3a–3e** in dichloromethane was allowed to react with trifluoroacetic acid to produce the target compounds **4a–4e**.

90.3 Experimental

90.3.1 Materials and Measurements

All reagents and solvents used in this paper were of reagent grade. Thin layer chromatography (TLC) was performed using E. Merck silica gel 60 GF254 pre-coated plates (0.25 mm) and visualized using a combination of UV. Silica gel (particle size 200–400 mesh) was used for flash chromatography. ¹H NMR spectra was recorded on Bruker AM-400 NMR spectrometers in CDCl₃ or *d*₆-DMSO. The chemical shifts are reported in δ (ppm) relative to tetramethylsilane as internal standard.

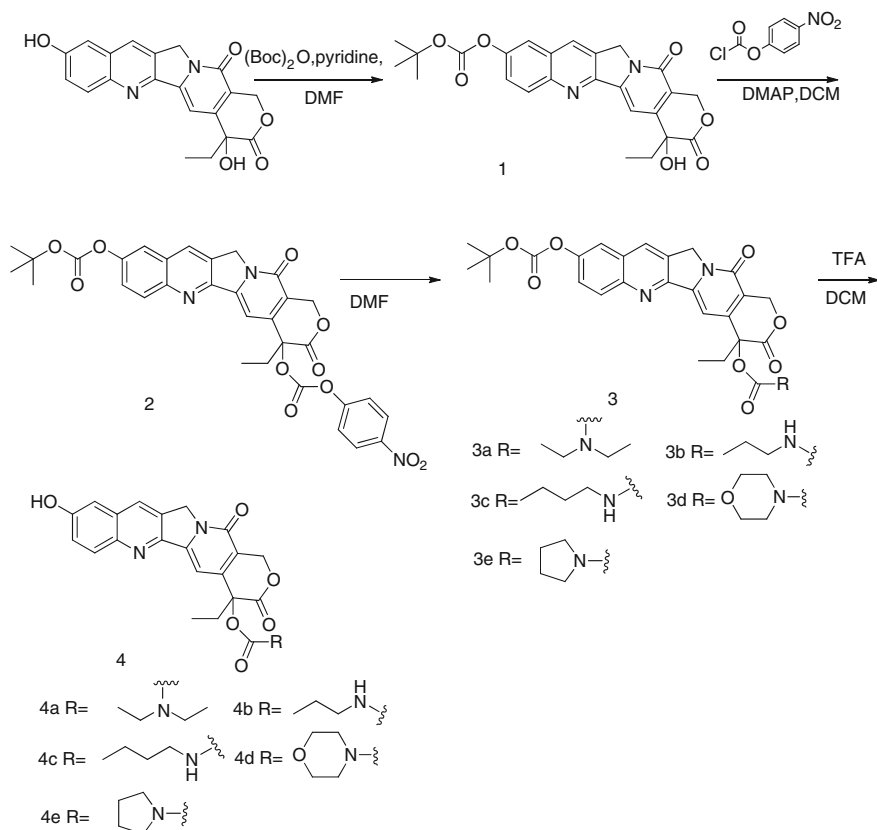


Fig. 90.1 Synthetic route of 20-substituted hydroxycamptothecins derivatives

90.3.2 Experimental Section

tert-butyl(4-ethyl-4-hydroxy-3,14-dioxo-3,4,12,14-tetrahydro-1H-pyrano[3',4':6,7]indolizino[1,2-b]quinolin-9-yl) carbonate (1). To the hydroxycamptothecin (12 g, 0.055 mol) in dry N,N-Dimethylformamide (137 mL) at 0 °C was added Di-tert-butyl dicarbonate (10 g, 0.027 mol). The reaction mixture was stirred at room temperature for 10 h. The reaction mixture was diluted with dichloromethane (800 mL). The phases were separated and the organic layer was washed with water (3 × 300 mL), 1 N HCl (3 × 100 mL) and dried over anhydrous magnesium sulfate. The solvent was removed under vacuum to afford the crude, which was purified by flash column chromatography (silica gel, dichloromethane/methanol 20:1) to yield the compound **1** (14.5 g, 95 %).

^1H NMR (CDCl_3 400 MHz): δ /ppm 1.06 (t, $J = 6$ Hz, 3H), 1.62 (s, 9H), 1.91 (m, $J = 6$ Hz, 2H), 5.30 (s, 2H), 5.31 (d, $J = 16.5$ Hz, 1H), 5.75 (d, $J = 16.5$ Hz,

1H), 7.66 (dd, $J = 2.4$ Hz, 1H), 7.67 (s, 1H), 7.75 (d, $J = 2.4$ Hz, 1H), 8.21 (s, 1H), 8.25 (s, 1H), 8.34 (s, 1H).

tert-butyl(4-ethyl-3,14-dioxo-3,4,12,14-tetrahydro-1H-pyrano[3',4':6,7]indolizino[1,2-b]quinoline-4,9-diyl) (4-nitrophenyl) dicarbonate (2). To the compound **1** (4.0 g, 8.4 mmol) in dry dichloromethane (400 mL) at 0 °C was added 4-Dimethylaminopyridine (1.52 g, 42 mmol) slowly. The reaction mixture was stirred at 0 °C for 10 min, then 4-nitrophenylchloroformate (5.2 g, 25.1 mmol) was added. The reaction mixture was stirred for 10 h at room temperature. The reaction mixture was diluted with dichloromethane (100 mL). The phases were separated and the organic layer was washed with water (2 × 100 mL), brine (100 mL), and dried over anhydrous magnesium sulfate. The solvent was removed under vacuum to afford the crude which was purified by flash column chromatography (silica gel, dichloromethane/methanol 120:1) to yield the compound **2** (3.3 g, 60 %).

¹H NMR (*d*₆-DMSO 400 MHz): δ /ppm 1.06 (t, $J = 6$ Hz, 3H), 1.54 (s, 9H), 2.26 (m, 2H), 5.28 (s, 2H), 5.56 (d, $J = 6.4$ Hz, 2H), 7.28 (s, 1H), 7.52 (d, $J = 12$ Hz, 2H), 7.66 (dd, $J = 9.2$ Hz, 2 Hz, 1H), 8.01 (s, 1H), 8.21 (d, $J = 9.2$ Hz, 1H), 8.28 (d, $J = 9.2$ Hz, 2H), 8.68 (s, 1H).

9-((tert-butoxycarbonyl)oxy)-4-ethyl-3,14-dioxo-3,4,12,14-tetrahydro-1H-pyrano[3',4':6,7]indolizino[1,2-b]quinolin-4-yl diethylcarbamate (3a). To a solution of compound **2** (1.0 g, 1.59 mmol) in dry N,N-Dimethylformamide (8 mL) was added diethylamine (0.23 g, 3.18 mmol). The reaction mixture was stirred for 30 min at room temperature. The reaction mixture was diluted with dichloromethane (25 mL). The phases were separated and the organic layer was washed with water (2 × 50 mL), brine (100 mL), and dried over anhydrous magnesium sulfate. The solvent was removed under vacuum to afford the crude which was purified by flash column chromatography (silica gel, dichloromethane/methanol 175:1) to yield the compound **3a** (0.3 g, 60 %).

¹H NMR (*d*₆-DMSO 400 MHz): δ /ppm 0.97 (m, 6H) 1.06 (t, $J = 6$ Hz, 3H), 1.54 (s, 9H), 2.26 (m, 2H), 3.40 (m, 4H), 5.28 (s, 2H), 5.56 (d, $J = 6.4$ Hz, 2H), 7.28 (s, 1H), 7.66 (dd, $J = 9.2$ Hz, 2 Hz, 1H), 8.01 (s, 1H), 8.21 (d, $J = 9.2$ Hz, 1H), 8.68 (s, 1H).

9-((tert-butoxycarbonyl)oxy)-4-ethyl-3,14-dioxo-3,4,12,14-tetrahydro-1H-pyrano[3',4':6,7]indolizino[1,2-b]quinolin-4-yl propylcarbamate (3b). To a solution of compound **2** (1.0 g, 1.59 mmol) in dry N,N-Dimethylformamide (8 mL) was added propylamine (0.19 g, 3.18 mmol). The reaction mixture was stirred for 30 min at room temperature. The reaction mixture was diluted with dichloromethane (25 mL). The phases were separated and the organic layer was washed with water (2 × 50 mL), brine (100 mL) and dried over anhydrous magnesium sulfate. The solvent was removed under vacuum to afford the crude which was purified by flash column chromatography (silica gel, dichloromethane/methanol 175:1) to yield the compound **3b** (0.3 g, 60 %).

¹H NMR (*d*₆-DMSO 400 MHz): δ /ppm 0.90 (m, 3H) 1.06 (t, $J = 6$ Hz, 3H), 1.54 (s, 9H), 1.60 (m, 2H), 2.26 (m, 2H), 3.18 (m, 2H), 3.40 (m, 4H) 5.28 (s, 2H),

5.56 (d, $J = 6.4$ Hz, 2H), 7.28 (s, 1H), 7.66 (dd, $J = 9.2$ Hz, 2 Hz, 1H), 8.01 (s, 1H), 8.21 (d, $J = 9.2$ Hz, 1H), 8.68 (s, 1H).

9-((tert-butoxycarbonyl)oxy)-4-ethyl-3,14-dioxo-3,4,12,14-tetrahydro-1H-pyrano[3',4':6,7]indolizino[1,2-b]quinolin-4-yl butylcarbamate (3c). To a solution of compound **2** (1.0 g, 1.59 mmol) in dry N,N-Dimethylformamide (8 mL) was added n-Butylamine (0.23 g, 3.18 mmol). The reaction mixture was stirred for 30 min at room temperature. The reaction mixture was diluted with dichloromethane (25 mL). The phases were separated and the organic layer was washed with water (2×50 mL), brine (100 mL) and dried over anhydrous magnesium sulfate. The solvent was removed under vacuum to afford the crude which was purified by flash column chromatography (silica gel, dichloromethane/methanol 175:1) to yield the compound **3c** (0.3 g, 60 %).

$^1\text{H NMR}$ (d_6 -DMSO 400 MHz): δ /ppm 0.90 (m, 5H) 1.06 (t, $J = 6$ Hz, 3H), 1.54 (s, 9H), 1.60 (m, 2H), 2.26 (m, 2H), 3.18 (m, 2H), 3.40 (m, 4H) 5.28 (s, 2H), 5.56 (d, $J = 6.4$ Hz, 2H), 7.28 (s, 1H), 7.66 (dd, $J = 9.2$ Hz, 2 Hz, 1H), 8.01 (s, 1H), 8.21 (d, $J = 9.2$ Hz, 1H), 8.68 (s, 1H).

9-((tert-butoxycarbonyl)oxy)-4-ethyl-3,14-dioxo-3,4,12,14-tetrahydro-1H-pyrano[3',4':6,7]indolizino[1,2-b]quinolin-4-yl morpholine-4-carboxylate (3d). To a solution of compound **2** (1.0 g, 1.59 mmol) in dry N,N-Dimethylformamide (8 mL) was added morpholine (0.23 g, 3.18 mmol). The reaction mixture was stirred for 30 min at room temperature. The reaction mixture was diluted with dichloromethane (25 mL). The phases were separated and the organic layer was washed with water (2×50 mL), brine (100 mL) and dried over anhydrous magnesium sulfate. The solvent was removed under vacuum to afford the crude which was purified by flash column chromatography (silica gel, dichloromethane/methanol 175:1) to yield the compound **3d** (0.3 g, 60 %).

$^1\text{H NMR}$ (d_6 -DMSO 400 MHz): δ /ppm 0.90 (t, $J = 6$ Hz, 3H), 1.54 (s, 9H), 1.81 (m, 2H), 1.91 (m, 2H), 2.11 (m, 2H), 3.17 (m, 2H), 3.61 (m, 2H), 5.28 (s, 2H), 5.56 (d, $J = 6.4$ Hz, 2H), 7.28 (s, 1H), 7.66 (dd, $J = 9.2$ Hz, 2 Hz, 1H), 8.01 (s, 1H), 8.21 (d, $J = 9.2$ Hz, 1H), 8.68 (s, 1H).

9-((tert-butoxycarbonyl)oxy)-4-ethyl-3,14-dioxo-3,4,12,14-tetrahydro-1H-pyrano[3',4':6,7]indolizino[1,2-b]quinolin-4-yl pyrrolidine-1-carboxylate (3e). To a solution of compound **2** (1.0 g, 1.59 mmol) in dry N,N-Dimethylformamide (8 mL) was added pyrrolidine (0.24 g, 3.18 mmol). The reaction mixture was stirred for 30 min at room temperature. The reaction mixture was diluted with dichloromethane (25 mL). The phases were separated and the organic layer was washed with water (2×50 mL), brine (100 mL) and dried over anhydrous magnesium sulfate. The solvent was removed under vacuum to afford the crude which was purified by flash column chromatography (silica gel, dichloromethane/methanol 175:1) to yield the compound **3e** (0.3 g, 60 %).

$^1\text{H NMR}$ (d_6 -DMSO 400 MHz): δ /ppm 0.90 (t, $J = 6$ Hz, 3H), 1.54 (s, 9H), 1.81 (m, 2H), 1.91 (m, 2H), 2.11 (m, 2H), 3.17 (m, 4H), 3.65 (m, 4H), 5.28 (s, 2H), 5.56 (d, $J = 6.4$ Hz, 2H), 7.28 (s, 1H), 7.66 (dd, $J = 9.2$ Hz, 2 Hz, 1H), 8.01 (s, 1H), 8.21 (d, $J = 9.2$ Hz, 1H), 8.68 (s, 1H).

4-ethyl-9-hydroxy-3,14-dioxo-3,4,12,14-tetrahydro-1H-pyrano[3',4':6,7]indolizino[1,2-b]quinolin-4-yl diethylcarbamate (4a). To a solution of compound **3a** (0.3 g, 0.53 mmol) in dry dichloromethane (25 mL) at 0 °C was added trifluoroacetic acid (1 mL) and the mixture was brought to room temperature and stirred overnight. The solvent was removed in vacuo to give the crude product which was purified by flash column chromatography (silica gel, dichloromethane/methanol 120:1) to afford compound **4a** (0.12 g, 50 %).

¹H NMR (*d*₆-DMSO 400 MHz): δ/ppm 0.97 (m, 6H) 1.06 (t, *J* = 6 Hz, 3H), 2.26 (m, 2H), 3.40 (m, 4H) 5.28 (s, 2H), 5.56 (d, *J* = 6.4 Hz, 2H), 7.28 (s, 1H), 7.66 (dd, *J* = 9.2 Hz, 2 Hz, 1H), 8.01 (s, 1H), 8.21 (d, *J* = 9.2 Hz, 1H), 8.68 (s, 1H).

4-ethyl-9-hydroxy-3,14-dioxo-3,4,12,14-tetrahydro-1H-pyrano[3',4':6,7]indolizino[1,2-b]quinolin-4-yl propylcarbamate (4b). To a solution of compound **3b** (0.3 g, 0.54 mmol) in dry dichloromethane (25 mL) at 0 °C was added trifluoroacetic acid (1 mL) and the mixture was brought to room temperature and stirred overnight. The solvent was removed in vacuo to give the crude product which was purified by flash column chromatography (silica gel, dichloromethane/methanol 120:1) to afford compound **4b** (0.11 g, 51 %).

¹H NMR (*d*₆-DMSO 400 MHz): δ/ppm 0.90 (m, 3H) 1.06 (t, *J* = 6 Hz, 3H), 1.60 (m, 2H), 2.26 (m, 2H), 3.18 (m, 2H), 3.40 (m, 4H), 5.28 (s, 2H), 5.56 (d, *J* = 6.4 Hz, 2H), 7.28 (s, 1H), 7.66 (dd, *J* = 9.2 Hz, 2 Hz, 1H), 8.01 (s, 1H), 8.21 (d, *J* = 9.2 Hz, 1H), 8.68 (s, 1H).

4-ethyl-9-hydroxy-3,14-dioxo-3,4,12,14-tetrahydro-1H-pyrano[3',4':6,7]indolizino[1,2-b]quinolin-4-yl butylcarbamate (4c). To a solution of compound **3c** (0.3 g, 0.53 mmol) in dry dichloromethane (25 mL) at 0 °C was added trifluoroacetic acid (1 mL) and the mixture was brought to room temperature and stirred overnight. The solvent was removed in vacuo to give the crude product which was purified by flash column chromatography (silica gel, dichloromethane/methanol 120:1) to afford compound **4c** (0.11 g, 53 %).

¹H NMR (*d*₆-DMSO 400 MHz): δ/ppm 0.90 (m, 5H) 1.06 (t, *J* = 6 Hz, 3H), 1.60 (m, 2H), 2.26 (m, 2H), 3.18 (m, 2H), 3.40(m, 4H), 5.28 (s, 2H), 5.56 (d, *J* = 6.4 Hz, 2H), 7.28 (s, 1H), 7.66 (dd, *J* = 9.2 Hz, 2 Hz, 1H), 8.01 (s, 1H), 8.21 (d, *J* = 9.2 Hz, 1H), 8.68 (s, 1H).

4-ethyl-9-hydroxy-3,14-dioxo-3,4,12,14-tetrahydro-1H-pyrano[3',4':6,7]indolizino[1,2-b]quinolin-4-yl morpholine-4-carboxylate (4d). To a solution of compound **3d** (0.3 g, 0.56 mmol) in dry dichloromethane (25 mL) at 0 °C was added trifluoroacetic acid (1 mL) and the mixture was brought to room temperature and stirred overnight. The solvent was removed in vacuo to give the crude product, which was purified by flash column chromatography (silica gel, dichloromethane/methanol 120:1) to afford compound **4d** (0.12 g, 52 %).

¹H NMR (*d*₆-DMSO 400 MHz): δ/ppm 0.90 (t, *J* = 6 Hz, 3H), 1.81 (m, 2H), 1.91(m, 2H), 2.11(m, 2H), 3.17(m, 2H), 3.61(m, 2H), 5.28(s, 2H), 5.56 (d, *J* = 6.4 Hz, 2H), 7.28 (s, 1H), 7.66 (dd, *J* = 9.2 Hz, 2 Hz, 1H), 8.01 (s, 1H), 8.21 (d, *J* = 9.2 Hz, 1H), 8.68 (s, 1H).

4-ethyl-9-hydroxy-3,14-dioxo-3,4,12,14-tetrahydro-1H-pyrano[3',4':6,7]indolizino[1,2-b]quinolin-4-yl pyrrolidine-1-carboxylate (4e). To a solution of compound **3e** (0.3 g, 0.53 mmol) in dry dichloromethane (25 mL) at 0 °C was added trifluoroacetic acid (1 mL) and the mixture was brought to room temperature and stirred overnight. The solvent was removed in vacuo to give the crude product which was purified by flash column chromatography (silica gel, dichloromethane/methanol 120:1) to afford compound **4e** (0.11 g, 50 %).

¹H NMR (d₆-DMSO 400 MHz): δ/ppm 0.90 (t, *J* = 6 Hz, 3H), 1.81 (m, 2H), 1.91 (m, 2H), 2.11 (m, 2H), 3.17 (m, 4H), 3.65 (m, 4H), 5.28 (s, 2H), 5.56 (d, *J* = 6.4 Hz, 2H), 7.28 (s, 1H), 7.66 (dd, *J* = 9.2 Hz, 2 Hz, 1H), 8.01 (s, 1H), 8.21 (d, *J* = 9.2 Hz, 1H), 8.68 (s, 1H).

90.4 Summary

Here we describe the synthesis of a series of novel 20-substituted hydroxycamptothecin derivatives, several steps among this route were optimized, such as the coupling reaction. The coupling reaction was the key step in the entire route. In this step, anhydrous and anaerobic conditions were required. All the target compounds were synthesized through four steps with the overall yield of 12–15 %. Compared with the hydroxycamptothecin, the water solubility has increased a lot. These new target compounds and key intermediates were confirmed by ¹H NMR and LC–MS spectra. The biological activities of these compounds are being evaluated.

Acknowledgments The authors sincerely thank the financial support from the Tianjin University of Science and Technology (20110406, 20110115), the Natural Science Foundation of Tianjin (11JGYBJC14300), the Science & Technology Project of Tianjin (11ZCGHHZ00400) and the Natural Science Foundation of Tianjin (12JCYBJC31600).

References

1. Wall ME, Wani M, Cook C, Palmer KH et al (1996) Sim, Plant antitumor agents. I. The isolation and structure of camptothecin, a novel alkaloidal leukemia and tumor inhibitor from *camptotheca acuminata*. *J Am Chem Soc* 88:3888–3890
2. Hsiang YH, Liu LF, Wall ME et al (1989) DNA topoisomerase I-mediated DNA cleavage and cytotoxicity of camptothecin analogues. *Cancer Res* 49:4385
3. Kawato Y, Aonuma M, Hirota Y et al (1991) Intracellular roles of SN-38, a metabolite of the camptothecin derivative CPT-11, in the antitumor effect of CPT-11. *Cancer Res* 51:4187
4. Loza MC, Wellinger RE (2009) A novel approach for organelle-specific DNA damage targeting reveals different susceptibility of mitochondrial DNA to the anticancer drugs camptothecin and topotecan. *Nucleic Acids Res* 37:e26

5. Han M, He CX, Fang QL et al (2009) A novel camptothecin derivative incorporated in nano-carrier induced distinguished improvement in solubility, stability and anti-tumor activity both in vitro and in vivo. *Pharm Res* 26:926–935
6. Hsiang YH, Liu LF (1988) Identification of mammalian DNA topoisomerase I as an intracellular target of the anticancer drug camptothecin. *Cancer Res* 48:1722–1726
7. Davis ME (2009) Design and development of IT-101, a cyclodextrin-containing polymer conjugate of camptothecin. *Adv Drug Deliv Rev* 61:1189–1192
8. Hsu JL, Ho YF, Li TK et al (2012) Rottlerin potentiates camptothecin-induced cytotoxicity in human hormone refractory prostate cancers through increased formation and stabilization of topoisomerase I-DNA cleavage complexes in a PKC δ -independent pathway. *Biochem Pharmacol* 84:59–67
9. Cao Z, Mendoza J, Kozielski A, Liu X et al (2012) Giovannella, Anticancer Activity of New Haloalkyl Camptothecin Esters against Human Cancer Cell Lines and Human Tumor Xenografts Grown in Nude Mice. *Anti Cancer Agents Med Chem Anti Cancer Agents* 12:818–828
10. Min KH, Park K, Kim YS et al (2008) Hydrophobically modified glycol chitosan nanoparticles-encapsulated camptothecin enhance the drug stability and tumor targeting in cancer therapy. *J Controll Release* 127:208–218
11. Ozeki T, Hashizawa K, Kaneko D et al (2010) Treatment of rat brain tumors using sustained-release of camptothecin from poly (lactic-co-glycolic acid) microspheres in a thermoreversible hydrogel. *Chem Pharm Bull* 58:1142
12. Sapra P, Zhao H, Mehlig M et al (2008) Novel Delivery of SN38 Markedly Inhibits Tumor Growth in Xenografts, Including a Camptothecin-11–Refractory Model. *Clin Cancer Res* 14:1888–1896
13. Swaminathan S, Pastero L, Serpe L et al (2010) Cyclodextrin-based nanospheres encapsulating camptothecin: Physicochemical characterization, stability and cytotoxicity. *Eur J Pharm Biopharm* 74:193–201
14. Li P, Zheng Y, Ran H et al (2012) Ultrasound triggered drug release from 10-Hydroxycamptothecin-loaded phospholipid microbubbles for targeted tumor therapy in mice. *J Controll Release* 162:349–354

Chapter 91

Design and Synthesis of 5-Azacytidine Analogs

Jianbo Xing, Hua Sun, Xijuan Liang, Yuou Teng, Peng Yu
and Kui Lu

Abstract 5-azacytidine is a prescription injectable drug used for the treatment of myelodysplastic syndromes (MDS) and acute myelogenous leukemia (AML). In this paper, we would like to report a new approach to 5-azacytidine analogs from dicyanodiamine and formic acid or benzoic acid through several efficient reactions, such as cyclization reaction, Vorbrüggen coupling, and so on. Among those compounds, two azacytosine analogs and two 5-azacytidine analogs have not been reported yet. All products and important intermediates were characterized by ¹HNMR and MS spectrums.

Keywords 5-azacytidine analogs · Antiproliferative activity · Cyclization reaction and Vorbrüggen coupling

91.1 Introduction

5-azacytidine (5-aza-CR) is well-known DNA methyltransferase inhibitor and has been approved to be prescription injectable drug for the treatment of myelodysplastic syndrome (MDS), chronic myelomonocytic leukemia (CMML) and acute myelogenous leukemia (AML) [1]. 5-azacytidine and its analogs extensively exist in nature and possess lots of biological activities like antiviral, anticancer,

J. Xing · H. Sun · X. Liang · Y. Teng · P. Yu · K. Lu (✉)
Key Laboratory of Industrial Microbiology, Ministry of Education, College of
Biotechnology, Tianjin 300457, China
e-mail: lukui@tust.edu.cn

J. Xing · H. Sun · X. Liang · Y. Teng · P. Yu · K. Lu
Tianjin Key Laboratory of Industry Microbiology, College of Biotechnology,
Tianjin 300457, China

J. Xing · H. Sun · X. Liang · Y. Teng · P. Yu · K. Lu
Tianjin University of Science & Technology, Tianjin 300457, China

anti-HIV, etc. Recently, there is a growing tendency to develop some new methods for the synthesis of 5-azacytidine analogs to study their biological properties [1, 2].

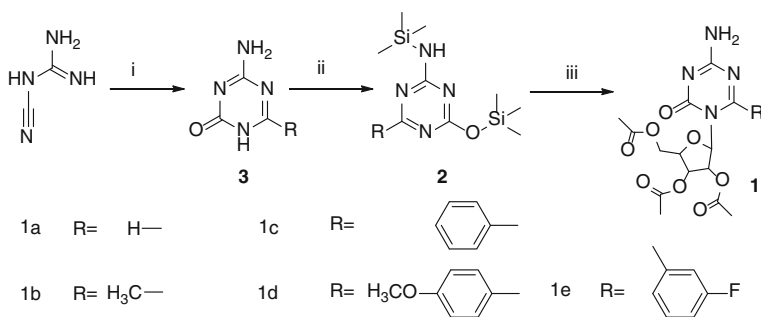
Usually, the azacytosine analogs were synthesized from guanyurea with orthoesters, refluxed with the dimethylformamide [3–5]. In this paper, a new method is developed for the synthesis of azacytosine, we would like to report the design and synthesis of azacytidine analogs with cyclization and Vorbrüggen coupling as the key steps [6, 7]. The target compounds (**1-3**) were synthesized in three steps in 15–40 % overall yield.

91.2 Results and Discussion

91.2.1 Chemistry

As illustrated in Scheme 91.1, the target compounds **1** were synthesized from dicyanodiamine through the intermediate compounds **2** and compound **3**. Compound **3**, 4-Amino-6-1,3,5-triazin-2(1H)-ones, prepared from the reactions of dicyanodiamine and formic acid (or acetic acid, benzoic acid), reacted with hexamethyldisilazane (HMDS) to produce N,O-bistrimethylsilylated-1,3,5-triazinones [8]. Vorbrüggen coupling of compound **2** with acylated sugars in anhydrous acetonitrile in the presence of a Lewis acid catalyst (SnCl_4) gave the acylated nucleosides [9, 10].

Reagents and Conditions: (i) carboxylic acid/anhydrous sodium sulfate/DMF, 145 °C, 70–80 %; (ii) HMDA/ $(\text{NH}_4)_2\text{SO}_4$ /toluene, 130 °C, 85–95 %; and (iii) acylated sugars/ SnCl_4 /acetonitrile, 10–40 %



Scheme 91.1 Synthetic route to azacytidine analogs

91.2.2 Experimental

Materials and Instruments. All reagents and solvents used in this paper were of reagent grade. Reaction temperatures were controlled using oil bath temperature modulator or ice bath. Thin layer chromatography (TLC) was performed using E. Merck silica gel 60 GF254 precoated plates (0.25 mm) and visualized using a combination of UV. Silica gel (particle size 200–400 mesh) was used for flash chromatography. $^1\text{H-NMR}$ spectra was recorded on Bruker AM-400 NMR spectrometers in deuterated chloroform and deuterated DMSO. The chemical shifts are reported in δ (ppm) relative to tetramethylsilane as internal standard. Mass spectra were recorded on LCMS-QP2010 mass instrument.

91.2.2.1 Compounds (3a–3b)

To a flask (100 mL) dicyanodiamine (2 g, 0.12 mol), formic acid (2.2 g, 0.24 mol), or acetic acid (3.3 g, 0.24 mol) were added. The mixture was heated to 120 °C for 20 min, then the system was cool to room temperature, the precipitate was filtered and washed with EtOH to give a white solid. The white solid to was put into a flask (100 mL), and heat to 145 °C for 4 h. Then the reaction system was cooled to 75 °C, and water (30 mL) was added, the mixture was stirred for 5 min, hydrochloric acid was added until the white solid was completely dissolved. The mixture was filtered and the ammonia (aq) was added until the pH = 8–9, the precipitate was filtered to give another white solid which was then put into a flask (100 mL), water (30 mL) and ammonia (aq, 10 mL) was added. The mixture was heated to 75 °C for 10 min. After cooling to room temperature, the mixture was filtered and the filtrate was adjust to pH = 8–9 by hydrochloric acid. The precipitate was filtered to give the pure product as a white solid.

4-Amino-1,3,5-triazin-2(1H)-one(3a). Starting from dicyanodiamine (2 g, 0.12 mol) and formic acid (2.2 g, 0.24 mol), **compound 3a** was obtained (1.73 g, 65 %). $^1\text{H NMR}$ (d_6 -DMSO 400 MHz): δ /ppm 7.26(s, 2H), 8.05 (s, 1H), 11.56 (s, 1H). EMS-MS: m/z 113[M + 1] $^+$.

4-Amino-2-methyl-1,3,5-triazin-one(3b). Starting from dicyanodiamine (2 g, 0.12 mol) and acetic acid (3.3 g, 0.24 mol), **compound 3b** was obtained (1.8 g, 61 %). $^1\text{H NMR}$ (d_6 -DMSO 400 MHz): δ /ppm 2.37 (s, 3H), 7.89 (s, 1H), 11.67 (s, 1H). EMS-MS: m/z 127[M + 1] $^+$, 125[M–1] $^-$.

91.2.2.2 Compounds (3c–3e)

To a flask (100 mL), dicyanodiamine (2 g, 0.12 mol), benzoic acid (2.6 g, 0.12 mol), or 4-methoxybenzoic acid (3.3 g, 0.12 mol) or 3-fluorobenzoic acid (3.3 g, 0.12 mol), anhydrous sodium sulfuric (2 g) were added. The mixture was heated to 145 °C for 6 h. Then the mixture was cool to room temperature for 12 h, the

precipitate was filtered and washed with EtOH to give a white solid. The white solid was put into a flask (100 mL), water (10 mL) was added, the mixture was stirred for 5 min, hydrochloric acid was added until the white solid was completely dissolved. The mixture was filtered and the ammonia (aq) was added until the pH = 8–9, the precipitate was filtered to give another white solid which was then put into a flask (100 mL), water (30 mL) and ammonia (aq, 10 mL) was added. The mixture was heated to 75 °C for 10 min. After cooling to room temperature, the mixture was filtered and the filtrate was adjust to pH = 8–9 by hydrochloric acid. The precipitate was filtered to give the pure product as a white solid.

4-Amino-2-phenyl-1,3,5-triazin-one(3c). Starting from dicyanodiamine (2 g, 0.12 mol) and benzoic acid (2.6 g, 0.12 mol), **compound 3c** was obtained (1.0 g, 23 %). ¹H NMR (d₆-DMSO 400 MHz): δ/ppm 7.49 (s, 1H), 7.51 (t, *J* = 10.4 Hz, 3H), 7.60 (s, 1H), 8.19(d, *J* = 8.8 Hz, 2H) 11.53 (s, 1H). EMS-MS: *m/z* 189.0[M + 1]⁺, 187.1.0[M–1][–].

4-Amino-2-(4-methoxyphenyl)-1,3,5-triazin-one(3d). Starting from dicyanodiamine (2 g, 0.12 mol) and 4-methoxybenzoic acid (3.3 g, 0.12 mol), **compound 3d** was obtained (1.5 g, 29 %). ¹H NMR (d₆-DMSO 400 MHz): δ/ppm 3.85 (s, 3H), 7.06 (d, *J* = 6.2 Hz, 2H), 7.38 (s, 1H), 8.19 (d, *J* = 6.2 Hz, 2H), 11.74 (s, 1H), 11.78 (s, 1H). EMS-MS: *m/z* 219.1[M + 1]⁺, 217.3[M–1][–].

4-Amino-2-(3-fluorophenyl)-1,3,5-triazin-one(3e). Starting from dicyanodiamine (2 g, 0.12 mol) and 3-fluorobenzoic acid (3.3 g, 1.2 mol), **compound 3e** was obtained (2.0 g, 40 %). ¹H NMR (d₆-DMSO 400 MHz): δ/ppm 7.39 (s, 1H), 7.56(d, *J* = 10.0 Hz, 1H), 7.64 (s, H), 8.16 (d, *J* = 9.4 Hz, 1H), 8.21 (s, 1H), 11.26 (s, 1H). EMS-MS: *m/z* 207.1[M + 1]⁺, 205.2[M–1][–].

91.2.2.3 Compounds (1a–1e)

To a solution of **compound 3a–3e** (4.46 mmol) in HMDS (10 mL) was added (NH₄)₂SO₄ (0.01 g). The mixture was refluxed for 12–16 h. After evaporation under vacuum, compound **2a–2e** was obtained. The crude product was used to glycosylation without further purification. **Compound 2a–2e** (1 equiv) was dissolved in anhydrous acetonitrile, 1,2,3,5-tetra-*O*-acetyl-β-D-ribose (1 equiv) and SnCl₄ (2 equiv) in acetonitrile were added. The mixture was stirred at room temperature for 10–18 h, then diluted in chloroform and neutralized with a saturated solution of sodium bicarbonate. The organic layer was separated, dried, and evaporated. The residue was purified by flash column chromatography (CHCl₃-CH₃OH) to give **Compound 1a–1e** as white solids.

1-(2,3,5-tri-*O*-acetyl-β-D-ribose)-4-Amino-1,3,5-triazin-2(1H)-one(1a). Starting from the **compound 3a** (500 mg), **compound 1a** was obtained in (600 mg, 40 %). ¹H NMR (d₆-DMSO 400 MHz): δ/ppm 2.05 (s, 3H), 2.06 (s, 3H), 2.07 (s, 3H), 4.27–4.32 (m, 1H), 5.33 (t, *J* = 11.2 Hz, 1H), 5.43 (t, *J* = 5.1 Hz, 1H), 5.78 (d, *J* = 4.1 Hz, 1H).

1-(2,3,5-tri-*O*-acetyl-β-D-ribose)-4-Amino-2-methyl-1,3,5-triazin-one(1b).

Starting from the **compound 3b** (500 mg), **compound 1b** was obtained

(380 mg, 27 %). ^1H NMR (d6-DMSO 400 MHz): δ/ppm 2.05 (s, 3H), 2.06 (s, 3H), 2.07 (s, 3H), 2.44 (s, 3H), 3.69–3.75 (m, 1H), 4.19–4.29 (m, 2H), 4.50–4.54 (m, 1H), 5.62–5.72 (m, 3H).

1-(2,3,5-tri-O-acetyl- β -D-ribose)-4-Amino-6-phenyl-1,3,5-triazin-one(1c).

Starting from the **compound 3c** (500 mg), **compound 1c** was obtained (237 mg, 20 %). ^1H NMR (d6-DMSO 400 MHz): δ/ppm 2.05 (s, 3H), 2.06 (s, 3H), 2.07 (s, 3H), 4.27–4.37(m, 2H), 4.64 (m, 1H), 5.37 (m, 1H), 5.66 (t, $J = 12.6$ Hz, 1H), 6.54 (s, 2H), 6.83 (d, $J = 11.2$, 1H), 7.46 (t, $J = 10.1$, 2H), 7.55 (d, $J = 9.5$, 1H), 8.41 (d, $J = 9.5$, 2H).

1-(2,3,5-tri-O-acetyl- β -D-ribose)-4-Amino-2-(4-methoxyphenyl)-1,3,5-triazin-one(1d). Starting from the **compound 3d** (500 mg), **compound 1d** was obtained (106 mg, 9 %). ^1H NMR (d6-DMSO 400 MHz): δ/ppm 2.05 (s, 3H), 2.06 (s, 3H), 2.07 (s, 3H), 3.87 (s, 3H), 4.14(m, 2H), 4.64 (m, 1H), 5.35 (m, 1H), 5.63 (t, $J = 12.7$ Hz,1H), 6.46 (s, 2H), 6.80 (d, $J = 11.2$, 1H), 7.09 (m, 2H), 7.34 (t, $J = 10.8$, 1H), 7.94 (s, 1H), 7.99 (d, $J = 9.5$, 1H).

1-(2,3,5-tri-O-acetyl- β -D-ribose)-4-Amino-2-(3-fluorophenyl) -1,3,5-triazin-one(1e). Starting from the **compound 3e** (500 mg), **compound 1e** was obtained in (160 mg, 15 %). ^1H NMR (d6-DMSO 400 MHz): δ/ppm 2.05 (s, 3H), 2.06 (s, 3H), 2.07 (s, 3H), 4.22 (m, $J = 40.4$, 2H), 4.37 (m, 1H), 5.25 (m, 1H), 5.63(t, $J = 12.7$ Hz,1H), 6.41 (s, 2H), 6.80 (d, $J = 11.1$, 1H), 7.23 (m, 1H), 7.40 (m, 1H), 8.09 (d, $J = 11.8$, 1H), 7.99 (d, $J = 9.5$, 1H).

91.3 Summary

In summary, we report the design and synthesis of azacytidine analogs by using cyclization reaction and Vorbrüggen coupling as the key steps. Among this, the cyclization reaction is a new approach to synthesize the azacytosine analogs. With this method in hand, the synthesis of azacytosines becomes easier and cheaper. All the target compounds were synthesized in three steps with the total yield of 15–40 %. These new target compounds and all intermediates were confirmed by ^1H NMR and MS. The biological activities of these compounds are being evaluated.

Acknowledgments The authors sincerely thank the financial support from the Tianjin University of Science & Technology (20110407), the Science & Technology Project of Tianjin (11ZCGHHZ00400), the Natural Science Foundation of Tianjin (11JGYBJC14300), International Science & Technology Cooperation Program of China (2013DFA31160) and Tianjin City High School Science & Technology Fund Planning Project (20110504).

References

1. Griffiths EA, Gore SD (2008) DNA methyltransferase and histone deacetylase inhibitors in the treatment of myelodysplastic syndromes. *Semin Hematol* 45:23–30
2. Grønbaek K, Hother C, Jones PA (2007) Epigenetic changes in cancer. *APMIS* 115: 1039–1059
3. Hartenstein R, Fridovich I (1967) Amidinourea formate, a precursor of 2-amino-4-hydroxy-*s*-triazine. *J Org Chem* 32:1653–1654
4. Piskala A (1967) Synthesis of 5-azacytosine (4-amino-1,2-dihydro-1,3,5-triazin-2-one) and its methyl derivatives. *Coll Czech Chem Commun* 32:3966–3976
5. Hanna NB, Masojdkova M, Fiedler P, Piskala A (1998) Synthesis of some 6-substituted 5-azacytidine. *Collect Czech Chem Commun* 63:222–230
6. Hanna NB, Zajicek J, Piskala A (1997) 6-Methyl-5-azacytidine-synthesis, conformational properties and biological activity, a comparison of molecular conformation with 5-azacytidine. *Nucleos Nucleot* 16:129–144
7. Niedballa U, Vorbruggen H (1974) General synthesis of N-glycoside, synthesis of 5-azacytidines. *J Org Chem* 39:3672–3674
8. Winkey MW, Robins RK (1970) Direct glycosylation of 1,3,5-triazinones. New approach to the synthesis of the nucleoside antibiotic 5-azacytidine (4-amino-1- β -D-ribofuranosyl-1,3,5-triazin-2-one) and related derivatives. *J Org Chem* 35:491–495
9. Pierce AC, Arnost M, Davies RJ, Forster C (2004) Diaminotriazoles useful as inhibitors of protein kinases. WO Patent 2004046120
10. Gaubert G, Mathe C, Imbach JL, Eriksson S, Vincenzetti S, Salvatori D, Vita A, Maury G (2000) Unnatural enantiomers of 5-azacytidine analogues: synthesis and enzymatic properties. *Eur J Med Chem* 35:1011–1019

Chapter 92

Stigmasterol from the Flowers of *Trollius chinensis*

Mengmeng Zhou, Min Wang, Daoqing Xu and Qin Pan

Abstract After being extracted with 75 % ethanol, *Trollius chinensis* extract was obtained by evaporation of its supernatant under vacuum conditions and dissolved with water, followed by extraction with petroleum ether. The petroleum ether part was collected and subjected to silica gel column chromatography and separated individual. Components were further purified by several rounds of silica gel column, followed by recrystallization with methanol. In total, three compounds were isolated from the air-dried flowers of *Trollius chinensis* and identified as β -sitosterol, stigmasterol and hellebore acid based on spectral analysis, NMR experimentation. Among these three compounds, stigmasterol was found for the first time in *Trollius chinensis*.

Keywords *Trollius chinensis* · Ranunculaceae · β -sitosterol · Stigmasterol · Hellebore acid

92.1 Introduction

Thanks to its remarkable curative effect [1, 2], *Trollius chinensis* Bunge (Ranunculaceae), is now widely used for treating upper respiratory infection [3], chronic pharyngitis, laryngitis, and amygdalitis in traditional Chinese medicine.

M. Zhou · M. Wang (✉)

Key Laboratory of Industrial Microbiology, Ministry of Education, National Engineering Laboratory for Industrial Enzymes, Tianjin Key Laboratory of Industrial Microbiology, College of Biotechnology, Tianjin University of Science and Technology, Tianjin 300457, People's Republic of China
e-mail: minw@tust.edu.cn

D. Xu (✉)

Zhongxin Pharmaceuticals, Tianjin 300193, People's Republic of China
e-mail: xudaoqing@vip.sina.com

Q. Pan

Key Laboratory of Chinese Medicine Quality Control Enterprise, Tianjin, R&D Center Tianjin Zhongxin Pharmaceutical, Tianjin 300457, People's Republic of China

Recently, medicines that mainly contain *Trollius chinensis* are more popular [1], such as *Trollius chinensis* Particles, *Trollius chinensis* Capsule, and *Trollius chinensis* Dispersible Tablets. It is also used in cigarette as a spice [4]. The yellow pigment [5] in this plant is now widely used as a natural dyestuff [5]. In agriculture, it plays a role as a natural insecticide because of the active insecticidal ingredients 2''-O-(2 -methylbutyryl)-vitexin and ursolic acid [6]. In the field of food production, it is also used as an antioxidant [7, 8].

The origin habitat of *Trollius chinensis* is in Peru. It prefers to live in the areas that are warm, moist, and full of sunshine. In China, it is mainly distributed in the southwest, northwest, and northeast, especially in Chengde of Hebei province, Neimenggu, Yunnan, and Xinjiang province. The statistical data from Doroszewska in 1974 showed that there are 31 species of *Trollius chinensis* in the whole word.

Previous studies indicate that the main components of *Trollius chinensis* are flavones, organic acids, and alkaloids [9, 10]. It is also reported that the main constituents that contribute to pharmacological function is flavones [11, 12]. Recently, thanks to new technologies, more active ingredients were found from this valuable medicine plant, for example, vitexin, orietin, and their derivatives. Jian-Hua Zou [13] identified four flavone C-glycosides in 2005; Zhan-Lin Li [14] isolated three new flavone C-glycosides in 2008; Shao-Qing Cai in 2006 isolated an antiviral flavonoid-type C-Glycosides [15]. Ru-Feng Wang isolated trollioside [16] in 2003, a new alkaloid [17] in 2004, and a new natural ceramide in 2010. However, little work has been conducted to isolate and identify active ingredients from the petroleum ether part of the *Trollius chinensis* extracts.

In this paper, we report the isolation and structure elucidation of the compounds that obtained from the petroleum ether part, one of the identified compounds was, for the first time, found in this plant, which was a supplement to the composition of the *Trollius chinensis*.

92.2 Materials and Methods

92.2.1 General

NMR spectra were recorded in CDCl₃ with an BRUKER 400 NMR spectrometer with TMS as an internal standard. Silica gel H and silica gel 60–100, 200–300 mesh (both from Qingdao Haiyang Chemical Co., Qingdao, P.R. China) were used for column chromatography.

92.2.2 Plant Material

The air-dried flowers were bought from Anguo Chinese herbal medicine market, Hebei, China, in June 2011. And it is stored in the medicine storage of R&D Center Tianjin Zhong Xin Pharmaceutical.

92.2.3 Extraction and Isolation

The air-dried flowers were extracted (20 kg) with 75 % ethanol three times, soaking for 24 h each time. The supernatant was evaporated in vacuo at 50 °C into small volume and made sure there was no ethanol left. Then dissolve it with water. After that, partition the solution with petroleum ether, ethyl acetate, and n-butyl alcohol one by one [18], and yield petroleum ether extractum 720 g. The petroleum ether extractum dissolved by petroleum ether was subjected to silica gel (200–300 mesh), eluting with a petroleum ether—ethyl acetate gradient to gain 10 fractions judging by the result of TLC. Number them as fraction 1, fraction 2 and so on.

Fraction 4 was set up to silica gel (200–300 mesh), eluting with a petroleum ether—ethyl acetate gradient to give four parts. Then, put the third part to the silica gel, eluting it with a petroleum ether—acetone gradient to yield three sections. Dissolve the last section with the least methanol in 50 °C water bath, then put it into the refrigerator when its temperature was near to the room temperature. In this way, we got both I and II by the method of recrystallization.

Fraction 5 was set up to silica gel (200–300 mesh), eluting with a petroleum ether-ethyl acetate gradient to get 6 parts. The last part was evaporated to small volume, and lay aside at room temperature. Few days later, there was crystal yield, washed it with method, the crystal of III was obtained from the last part.

92.3 Results and Discussion

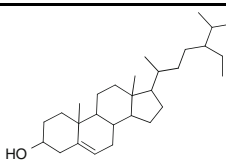
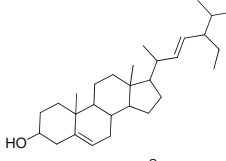
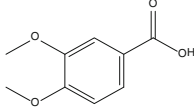
92.3.1 Identification of the Compound I

Compound I was got as a white powder, mp: 135–137 °C; It is easy to be dissolved in CDCl₃, while hard in methanol. ¹³C (400 MHz, CDCl₃) δ(ppm): 140.78(s, C-5), 121.73(d, C-6), 71.83(d, C-3), 56.89(d, C-14), 56.09(t, C-17), 50.16(d, C-9), 45.87(t, C-4), 42.26(s, C-13), 39.71(t, C-12), 38.86(t, C-1), 36.16(s, C-10), 35.89(d, C-20), 33.98(s, C-7), 33.73(d, C-8), 32.43(t, C-22), 30.31(t, C-2), 29.19(t, C-24), 28.26(d, C-25), 26.13(d, C-16), 25.41(t, C-28), 24.38(t, C-15), 21.22(t, C-27), 21.10(t, C-11), 19.82(q, C-26), 19.41(q, C-19), 18.99(q, C-27), 18.79(q, C-21), 11.99(q, C-29), 11.87(q, C-18). Comparing the detail spectral data with that from the literature [19], this compound was identified as β-sitosterol (Table 92.1).

92.3.2 Identification of the Compound II

Compound II was obtained as a white powder, mp: 135 °C ~ 137 °C; It is easy to be dissolved by CHCl₃, while hard in methanol. ¹H (400 MHz, CDCl₃) δ(ppm): 5.36(1H, s, H-6). ¹³C (400 MHz, CDCl₃) δ(ppm): 140.78(C-5), 138.31(C-22),

Table 92.1 Basic information of the compounds I–III

Number	Name	Molecular formula	Structural formula
I	β -sitosterol	C ₂₉ H ₅₀ O	
II	Stigmasterol	C ₂₉ H ₄₈ O	
III	Hellebore acid	C ₉ H ₁₀ O ₄	

129.31(C-23), 121.73(C-6), 71.83(C-3), 56.80(C-17), 55.99(C-14), 51.25(C-24), 50.16(C-9), 42.34(C-4), 42.24(C-13), 40.45(C-20), 39.71(C-12), 37.28(C-1), 36.53(C-10), 31.93(C-2,8,25), 31.69(C-7), 28.91(C-16), 25.41(C-28), 24.38(C-15), 21.22(C-21), 21.10(C-11, 27), 19.41(C-19), 18.99(C-26), 12.25(C-29), 11.87(C-18). Comparing the detail spectral data with the literature [20], identified it as stigmasterol.

92.3.3 Identification of the Compound III

Compound III was obtained as a yellow powder, mp: 179 °C ~ 182 °C; It is easy to be dissolved in CHCl₃. ¹³C (400 MHz, CDCl₃) δ (ppm): 171.88(COOH), 153.92(C-4), 148.87(C-3), 124.76(C-8), 121.85(C-1), 112.52(C-2), 110.51(C-5), 56.23(OCH₃-4), 56.17(OCH₃-3). ¹H (400 MHz, CDCl₃) δ (ppm): 11.806(1H, s, COOH), 7.79(1H, d, 2-H), 7.61(1H, d, 2-H), 6.93(1H, d, 5-H), 3.96(3H, s, 4-OCH₃), 3.95(3H, s, 3-OCH₃). This detail spectral data was compared with literature data [21], as the result, this compound was recognized as hellebore acid (Tables 92.2, 92.3, 92.4).

The petroleum ether part contains a variety of aliphatics and chlorophyll, which made the separation harder. To remove the aliphatics, the experiment was performed in cold temperatures and samples were loaded to the silica gel column, eluted with petroleum ether, ether acetate. The above procedure was repeated as necessary to minimize the amounts of aliphatics. However, each round of silica gel column purification resulted in 10 % loss of contents.

Our results showed that recrystallization with normal hexane are an efficient method to remove chlorophyll in the extracts, as the chlorophyll is very hard to

Table 92.2 ^{13}C NMR (400 MHz) spectral data of compound I

The number of C	δ (ppm)	The number of C	δ (ppm)
1	38.36	16	26.1
2	30.31	17	56.09
3	71.83	18	11.87
4	45.87	19	19.41
5	140.78	20	35.89
6	121.73	21	18.79
7	33.98	22	32.43
8	33.73	23	21.22
9	50.16	24	29.19
10	36.16	25	28.26
11	21.10	26	19.82
12	39.71	27	18.99
13	42.24	28	25.41
14	56.89	29	11.99
15	24.3		

solve in normal hexane. Thus, after silica gel column chromatography, the sections that contain the target compounds were collected and the chlorophyll removed by recrystallization. In addition, part of the chlorophyll also can be removed by silica gel column chromatography. However, the chlorophyll cannot be completely removed by either method. Therefore, effective new methods for chlorophyll removal are needed.

The petroleum ether extractum contains a large variety of sterols and terpenoids, and many of them have the same core structure and only differ in some functional groups. Repeated silica gel chromatography and recrystallization cannot

Table 92.3 ^{13}C NMR (400 MHz) spectral data of compound II

The number of C	δ (ppm)	The number of C	δ (ppm)
1	37.28	16	28.91
2	31.93	17	56.80
3	71.83	18	11.87
4	42.34	19	19.41
5	140.78	20	40.45
6	121.73	21	21.22
7	31.69	22	138.31
8	31.93	23	129.31
9	50.16	24	51.25
10	36.53	25	31.93
11	21.10	26	18.99
12	39.71	27	21.10
13	42.24	28	25.41
14	55.99	29	12.25
15	24.38		

Table 92.4 ^{13}C NMR (400 MHz) spectral data of compound III

The number of C	δ (ppm)
C-1	121.85
C-2	112.52
C-3	148.87
C-4	153.92
C-5	110.51
C-8	124.76
OCH ₃ -3	56.17
OCH ₃ -4	56.23
COOH	171.88

separate them efficiently. And it is essential to develop novel methods to separate the above classes of functional compounds.

The main chemical compositions in the petroleum ether are volatile oils [21], aliphatics [22], chlorophyll, sterols, and terpenoids. Many of them are active ingredients. The currently reported compounds found in the *Trollius chinensis* fail to account for the pharmacological activities of this medicinal plant. Further study of its petroleum ether extracts might help uncover the active ingredient responsible for the curative effects of this valuable medical plant.

92.4 Conclusions

Through silica-gel column chromatography and recrystallization, three compounds were isolated from the air-dried flowers of the *Trollius chinensis*. All three compounds are medicinally active ingredients. Especially, the discovery of stigmasterol is a valuable addition to the list of medicinally active ingredients in the genus *Trollius*. Given that lack of attention to the petroleum ether extracts of *Trollius chinensis*, more efforts are taken to further isolate additional active ingredients that are warranted.

References

1. Pan HF, Xin CL, Li SZ (2007) Study on the effect of *Trollius* beverage in clearing and moistening throat. *Lishizhen Med Mater Med Res* 9:2233–2234
2. Wang P (1996) The observation of the treatment of upper respiratory tract infection by *Trollius chinensis* infusion. *Chin Tradit Pat Med* 3:50
3. Geng JT, Geng YX (1976) The medicine optional of prevention and control in pharyngeal chronic inflammation. *Shanxi Med* 03:37
4. Ji XM, Zhao HX, Li BJ et al (2011) Analysis of volatile components in *Trollius chinensis* bunge extract and its application in cigarette. *Fine Chem* 28(5):467–470
5. Cao LJ, Yi DF (2011) Dyeing of wool with globe flower. *Wool Tex J* 39(8):9–12

6. Yang F, Liu ZY, Liu W et al (2009) Inhibitory effects of three compounds extracted from *Trollius ledebouri* on phenoloxidase of *spodotera exigua*. *Chin J Pestic Sin* 02:235–238
7. Zhao EL, Zhao XH, Fan JF (2008) Study on the extraction and antioxidation of flavone from *Trollius chinensis* bunge. *J Food Sci Biot* 28(1):81–85
8. Yan J, Hu HN, Tian JM et al (2010) The antioxidant action research of the total *Trollius* flavonoids. *Lishizhen Med Mater Med Res* 02:386–387
9. Song DM, Sun QS (2004) Chemical studies on the constituents of *Trollius altaicus* C.A.Mey. China. *J Med Chem* 14(04):233–235
10. Zou JH, Yang JS (2005) Study on chemical constituents of *Trollius ledebouri*. *Chin Pharm J* 10:733–736
11. Su LJ, Wang H, Su ZW et al (2005) Chemical composition and pharmacological action of the *Trollius chinensis*. *World Notes Plant med* 20(1):14–16
12. Li ZL, Li DY, Wang Y et al (2008) Antibacterial constituents from the flowers of *Trollius chinensis* Bunge. *J Shenyang Pharm Univ* 25(8):627–629
13. Zou J, Yang J, Dong Y et al (2005) Flavone glycosides from flowers of *Trollius chinensis*. *China Pharm J* 40(10):1121–1125
14. Li ZL, Li DY, Hua HM et al (2009) Three new acylated flavone C-glycosides from the flowers of *Trollius chinensis*. *Nat Prod Lett J* 5:426–432
15. Cai SQ, Wang RF, Yang XW et al (2006) Antiviral flavonoid-Type C-glycosides from the flowers of *Trollius chinensis*. *Chem Biod* 3(3):343–348
16. Wang RF, Ma CM, Zhang QY et al (2004) Trollioside, a new compound from the flowers of *Trollius chinensis*. *Nat Prod Lett* 6(2):139–144
17. Wang RF, Yang XW, Ma CM et al (2004) A bioactive alkaloid from the flowers of *Trollius chinensis*. *Heterocycles* 63(6):1443–1448
18. Ye SM, Li YL, Yang YT et al (2002) The extraction technology of *Trollius chinensis*. *Chin Med Mat* 06:463–464
19. Luo YJ, Xiao XF, Wang ZL (2009) Studies on chemical constituents of *Stenoloma chusana*(L.)Ching. *Chem Res Appl* 21(1):97–99
20. Zhang XQ, Qi J, Ye WC et al (2004) Chemical constituents from *Xanthium sibiricum*. *J Chin Pharm Univ* 05:18–19
21. Feng XF (1998) Chemical constituents from *Trollius chinensis*. *Chin Tradit Herbal Drugs J* 29(9):587–588
22. Wang RF, Yang XW, Ma CM et al (2010) Analysis of fatty acids from the flowers of *Trollius chinensis*. *Chin Med Mat* 10:1579–1581

Chapter 93

Design, Synthesis and Primary Biological Evaluation of the Novel Antitumor Agent Indoline-3-One and Its Derivatives

Haiyong Jia, Guojun Pan, Yiqian Wang, Shaopeng Wen,
Qiannan Guo, Weiguo Hu, Peng Yu, Hua Sun and Yuou Teng

Abstract Indolinone displays promising antitumor properties by inhibiting various kinase families. In this paper, we'd like to report the design, synthesis, and primary biological evaluation of the novel indoline-3-one and its derivatives. All the newly synthesized compounds including the novel compound 2-(4-(trifluoromethyl)benzylidene)indolin-3-one (5f) were characterized by ^1H NMR and their antitumor activities were evaluated by using MTT method in HT-29, K562, and HepG2 cell lines. 2-(2-nitrobenzylidene)indolin-3-one (5d) demonstrated good antitumor activity against HT-29, K562, and HepG2 with an IC_{50} of 2.04 μM , 2.33 μM , 2.24 μM , respectively. 2-(4-(trifluoromethyl)benzylidene)indolin-3-one(5f) demonstrated good antitumor activity against K562 and HepG2 with an IC_{50} of 2.27 μM , 3.47 μM .

Keywords Indoline-3-one · Synthesis · Antitumor · MTT

H. Jia · G. Pan · Y. Wang · S. Wen · Q. Guo · P. Yu · H. Sun · Y. Teng (✉)
Key Laboratory of Industrial Microbiology, Ministry of Education,
College of Biotechnology, Tianjin University of Science and Technology,
Tianjin 300457, People's Republic of China
e-mail: tyo201485@tust.edu.cn

H. Jia · G. Pan · Y. Wang · S. Wen · Q. Guo · P. Yu · H. Sun · Y. Teng
Tianjin Key Laboratory of Industry Microbiology, College of Biotechnology,
Tianjin University of Science and Technology, Tianjin 300457,
People's Republic of China

W. Hu
North China Pharmaceutical Co. Ltd, Hebei 050015, People's Republic of China

93.1 Introduction

Indolinone displays promising antitumor properties by inhibiting various kinase families [1]. Indolinone tyrosinekinase inhibitors block kit activation and growth of small cell lung cancer cells [2]. Sunitinib is an oral multitarget tyrosine kinase inhibitor with potent antiangiogenic properties, and it possess similar core structure to indolinone. Preclinical data have demonstrated that pancreatic neuroendocrine tumors depend on vascular endothelial growth factor receptors and platelet growth factor receptors-signaling pathways for tumor angiogenesis. Sunitinib has recently been approved for the treatment of patients with advanced, progressive pancreatic neuroendocrine tumors [3–7].

Microtubules are among the most successful targets for anticancer therapies and for the development of new anticancer drugs. A-432411 is a novel small molecule that destabilizes microtubules at high concentration and disrupts normal spindle formation at low concentration. A-432411 is an indolinone that is structurally different from other known synthetic microtubule inhibitors. This compound is efficacious against a variety of human cancer cell lines including drug-resistant HCT-15 that over expresses Pgp170. Biochemical studies show that A-432411 competes with the colchicine-binding site on tubulin and inhibits microtubule polymerization [8, 9]. Receptor tyrosine kinases (RTKs) have been shown to be important mediators of cellular signal transduction in cells [10]. Many RTKs have been shown to be oncogene products implicating their role in the transformation process associated with human cancers [11]. 3-substituted indolin-2-ones have been designed and synthesized as a novel class of tyrosine kinase inhibitors which exhibit selectivity toward different RTKs [12]. We'd like to design, synthesis and biological evaluation of the novel indoline-3-one and its derivatives.

Indolinone are recently attracting the interest of an increasing number of research groups. In this paper, we report our works made on the design and synthetic routes toward a series of functionalized auronones. The target compounds (5a–5f) were synthesized in five steps through hydrolysis reaction, nucleophilic substitution reaction, aldol reaction [13], and so on. We also detected their antitumor activity against K562, HT29, and HepG2 cancer cells. Their biological activity results indicated that 2-(2-nitrobenzylidene)indolin-3-one (5d) demonstrated good antitumor activity against HT-29, K562 and HepG2 with an IC_{50} of 2.04, 2.33, 2.24 μ M, respectively. 2-(4-(trifluoromethyl)benzylidene)indolin-3-one(5f) demonstrated good antitumor activity against K562 and HepG2 with an IC_{50} of 2.27 μ M, 3.47 μ M.

93.2 Materials and Methods

93.2.1 Materials and Measurements

All reagents and solvents used in this paper were of reagent grade. Reaction temperatures were controlled using oil bath temperature modulator. Thin layer chromatography (TLC) was performed using E. Merck silica gel 60 GF254 pre-coated plates (0.25 mm) and visualized using a combination of UV. Silica gel (particle size 200–400 mesh) was used for flash chromatography. ^1H NMR spectra was recorded on Bruker AM-400 NMR spectrometers in deuterated chloroform and deuterated DMSO. The chemical shifts are reported in δ (ppm) relative to tetramethylsilane as internal standard.

93.2.2 Chemistry

The synthetic approaches of target compound 5a–5f were demonstrated in Fig. 93.1.

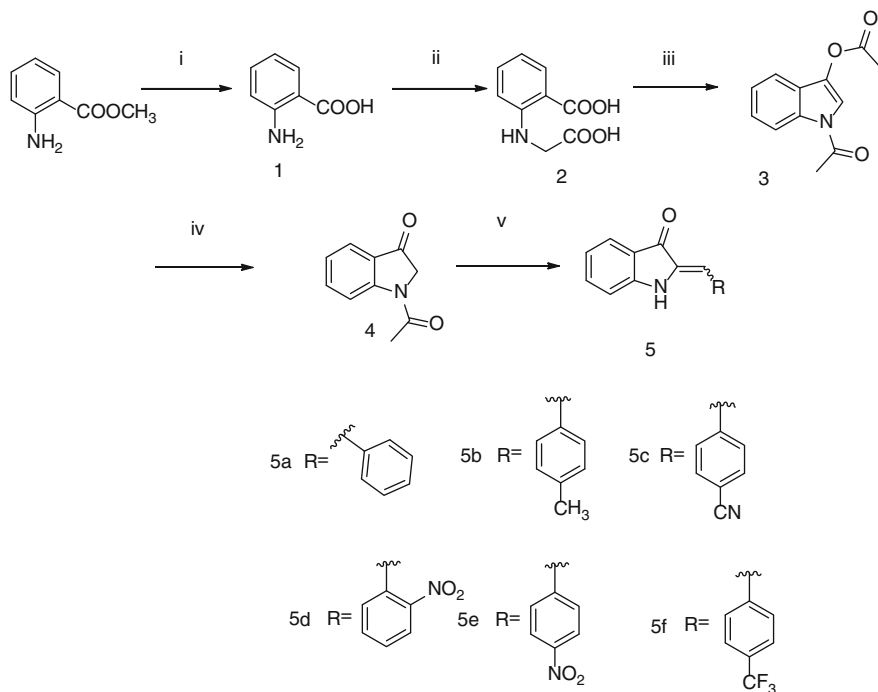


Fig. 93.1 Synthetic route of indolin-3-one derivatives

Table 93.1 Inhibition activity of the compound 6a, 6b, 6c, 6d and 6e (μM)

Tested cell	Samples (IC_{50})					
	5a	5b	5c	5d	5e	5f
K562	>10	>10	>10	2.33	>10	2.27
HepG2	>10	>10	>10	2.24	>10	3.47
HT-29	>10	>10	>10	2.04	>10	>10

Methyl anthranilate was employed to react with 10 % aqueous NaOH at 80 °C to provide compound 1 which was then reacted with chloroacetic at 100 °C to afford the key intermediate 2, then it was converted into compound 3 when treated with Ac_2O , CH_3COONa at 160 °C for 8 h. A mixture of compound 3, Sodium sulfite, water was heated to reflux for 2 h to obtain compound 4. Compound 4 was then reacted with benzaldehyde, 4-methylbenzaldehyde, 4-Cyanobenzaldehyde, 2-Nitrobenzaldehyde, 4-Nitrobenzaldehyde, and 4-(trifluoromethyl) benzaldehyde to afford compound 5a, 5b, 5c, 5d, 5e and 5f.

93.2.3 Biological Assay

The anticancer activities for newly synthesized compounds were tested on the K562, HT-29, and HepG2 cells by using MTT method [14]. The results of compounds (5a–5f) were listed in Table 93.1 which indicated that 2-(2-nitrobenzylidene)indolin-3-one (5d) and 2-(4-(trifluoromethyl)benzylidene)indolin-3-one(5f) demonstrated good antitumor activity against K562 and HepG2 with an IC_{50} of 2.33, 2.24, 2.27, and 3.47 μM , respectively. But it was not active against HT-29 ($\text{IC}_{50} > 10 \mu\text{M}$) at our test condition.

Reagents and conditions: (i) 10%NaOH, H_2O , then HCl; (ii) ClCH_2COOH , Na_2CO_3 , NaOH, H_2O , then HCl; (iii) Ac_2O , HAc, CH_3COONa ; (iv) $\text{C}_2\text{H}_5\text{OH}$, H_2O , Na_2SO_3 ; (v) $\text{C}_2\text{H}_5\text{OH}$, H_2O , conc HCl.

93.3 Results and Discussion

93.3.1 Synthesis Indoline-3-One and Its Derivatives by ^1H NMR

2-aminobenzoic acid (1). To a solution of methyl 2-aminobenzoate (10 g, 66.15 m mol) in 10 % aqueous NaOH (80 mL), the mixture was stirred for 4 h at 80 °C. The product formed by adding 1 N HCl was filtered to give 8.2 g of 1 (90 %).

^1H NMR (CDCl_3 400 MHz): δ /ppm 6.689–6.723 (m, 2H), 7.341 (t, $J = 8.0$ Hz, 1H), 7.962 (d, $J = 8.4$ Hz, 1H).

2-((2-carboperoxyphenyl)amino)acetic acid (2) [15]. To a solution of 2-aminobenzoic acid (10 g, 72.92 mmol) in water (120 mL) was added NaOH (9.33 g, 233.35 mmol), Na₂CO₃ (9.27 g, 87.50 mmol) and chloroacetic (8.27 g, 87.50 mmol). The mixture was stirred for 10 h at 100 °C. The product formed by adding 1 N HCl was filtered to give 11.4 g of 2 (80 %).

¹H NMR (d₆-DMSO 400 MHz): δ/ppm 3.666 (d, J = 4.8 Hz, 2H), 6.464–6.498 (m, 2H), 7.216–7.258 (m, 1H), 7.781–7.805 (dd, J = 8.0 Hz, 1.6, 1H).

1-acetyl-1H-indol-3-yl acetate (3). A mixture of acetic anhydride (100 mL), acetic acid (30 mL), anhydrous sodium acetate (16.81 g, 204.95 mmol), and compound 2 was heated to reflux for 4 h. Saturated aqueous sodium carbonate was then added, and the mixture was extracted with CH₂Cl₂. The solvent was removed in vacuo to give the crude product, which was purified by flash column chromatography (silica gel, petroleum ether/ethyl acetate 15:1) to afford compound 3 (4.45 g, 40 %).

¹H NMR (CDCl₃ 400 MHz): δ/ppm 2.409 (s, 3H), 2.632 (s, 3H), 7.311–7.348 (m, 1H), 7.399–7.440 (m, 1H), 7.564 (d, J = 4.0 Hz, 1H), 7.740 (s, 1H), 8.485 (d, J = 4.0 Hz, 1H).

1-acetylidolin-3-one (4). A mixture of compound 3 (4.0 g, 18.41 mmol), ethanol (40 mL), water (80 mL), and Na₂SO₃ (2.79 g, 22.10 mmol) was heated to reflux for 2 h. Ethanol was removed in vacuo to give the precipitate which was collected by filtration, washed with water, and dried under vacuum to get compound 4 (2.7 g, 90 %).

¹H NMR (CDCl₃ 400 MHz): δ/ppm 2.343(s, 3H), 4.316 (s, 2H), 7.240 (t, J = 7.2 Hz, 1H), 7.666–7.708 (m, 1H), 7.769 (d, J = 4.0 Hz, 1H), 8.582 (d, J = 4.0 Hz, 1H).

Compounds (5a–5f) [16]. To a solution of compound 4 (1 equiv) and 1.2 equiv of appropriate benzaldehyde derivatives in 2.5 mL of water, 2.5 mL of ethanol, 2 drops of concentrated hydrochloric acid was added at the room temperature, the reaction was heated to reflux for 2 h. The reaction mixture was poured into ice-water and filtered. The filter cake was washed with petroleum ether and dried under vacuum to get compounds (5a–5f).

2-benzylideneindolin-3-one (5a). Starting from compound 4 (0.2 g, 1.14 mmol) and benzaldehyde (0.15 g, 1.37 mmol), compound 5a was obtained in 70 % yield.

¹H NMR (CDCl₃ 400 MHz): δ/ppm 6.697 (s, 1H), 6.897 (s, 1H), 6.983–7.030(m, 2H), 7.367 (d, J = 7.2 Hz, 1H), 7.458–7.522 (m, 3H), 7.578 (d, J = 3.6 Hz, 2H), 7.780 (d, J = 4.0 Hz, 1H).

2-(4-methylbenzylidene)indolin-3-one (5b). Starting from compound 4 (0.2 g, 1.14 mmol) and 4-methylbenzaldehyde (0.15 g, 1.37 mmol), compound 5b was obtained in 75 % yield.

¹H NMR (d₆-DMSO 400 MHz): δ/ppm 2.360 (s, 3H), 6.630 (s, 1H), 6.918 (t, J = 7.2 Hz, 1H), 7.150 (d, J = 3.6 Hz, 1H), 7.295 (d, J = 4.0 Hz, 2H), 7.503–7.544 (m, 1H), 7.585 (d, J = 4.0 Hz, 1H), 7.644 (d, J = 4.0 Hz, 1H).

4-((3-oxoindolin-2-ylidene)methyl)benzonitrile (5c). Starting from compound 4 (0.2 g, 1.14 mmol) and 4-Cyanobenzaldehyde (0.18 g, 1.37 mmol), compound 5c was obtained in 50 % yield.

^1H NMR (d₆-DMSO 400 MHz): δ /ppm 6.627 (s, 1H), 6.963 (t, $J = 7.2$ Hz, 1H), 7.149 (d, $J = 4.0$ Hz, 1H), 7.562 (t, $J = 8.0$ Hz, 2 Hz, 1H), 7.610 (d, $J = 4.0$ Hz, 1H), 7.874 (dd, $J = 11.6$ Hz, 3.2 Hz, 4H), 10.058 (s, 1H).

2-(2-nitrobenzylidene)indolin-3-one (5d). Starting from compound 4 (0.2 g, 1.14 mmol) and 2-Nitrobenzaldehyd (0.21 g, 1.37 mmol), compound 5d was obtained in 88 % yield.

^1H NMR (d₆-DMSO 400 MHz): δ /ppm 6.801 (s, 1H), 6.948 (t, $J = 7.2$ Hz, 1H), 7.090 (d, $J = 4.0$ Hz, 1H), 7.549 (t, $J = 7.6$ Hz, 1H), 7.592–7.689 (m, 2H), 7.843 (t, $J = 7.2$ Hz, 1H), 7.931 (d, $J = 4.0$ Hz, 1H), 8.109 (d, $J = 4.0$ Hz, 1H), 10.000 (s, 1H).

2-(4-nitrobenzylidene)indolin-3-one (5e). Starting from compound 4 (0.2 g, 1.14 mmol) and 2-Nitrobenzaldehyd (0.21 g, 1.37 mmol), compound 5e was obtained in 85 % yield.

^1H NMR (d₆-DMSO 400 MHz): δ /ppm 6.663 (s, 1H), 6.976 (t, $J = 7.2$ Hz, 1H), 7.160 (d, $J = 4.0$ Hz, 1H), 7.553–7.594 (m, 1H), 7.619 (d, $J = 4.0$ Hz, 1H), 7.948 (d, $J = 8.8$ Hz, 2H), 8.263 (d, $J = 4.0$ Hz, 2H), 10.155 (s, 1H).

2-(4-(trifluoromethyl)benzylidene)indolin-3-one (5f). Starting from compound 4 (0.2 g, 1.14 mmol) and 4-(trifluoromethyl)benzaldehyde (0.24 g, 1.37 mmol), compound 5f was obtained in 75 % yield.

^1H NMR (d₆-DMSO 400 MHz): δ /ppm 6.664 (s, 1H), 6.957 (t, $J = 7.2$ Hz, 1H), 7.151 (d, $J = 4.0$ Hz, 1H), 7.539–7.622 (m, 1H), 7.795 (d, $J = 4.0$ Hz, 2H), 7.922 (d, $J = 4.0$ Hz, 2H), 9.995 (s, 1H).

93.3.2 Anticancer Activity Assay

All the above compounds were tested for their in vitro anticancer activity against HT-29, K562, HepG2 cells by MTT-based assay. The cells were diluted to a density of 5×10^4 cells/mL and added 100 μL to each well of the 96-well plates with a multichannel pipet. After incubating for 24 h, 0.5 μL compounds were added and then cells were further incubated for 48 h (final concentrations of each compound: 0.1, 0.3, 1, 3, and 10 μM). The culture plates were incubated for 4 h after which 20 μL MTT was added to each well, then the medium were removed from the wells and 100 μL DMSO added into each well. After leaving for further 10 min to dissolve the formazan crystals formed, the optical density (OD) was measured at 490 and 630 nm. Cell viability was calculated from measurements of OD value according to the corresponding formula and a graph is plotted of cell viability (y-axis) against drug concentration (x-axis). The given values are mean values of three experiments. The IC_{50} concentration represents the concentration which results in a 50 % decrease in cell growth after 2 days incubation. The results were presented in Table 93.1.

93.4 Conclusion

We report the design and synthesis of novel indoline-3-one and its derivatives. Several steps among this route were optimized, such as cyclization, nucleophilic substitution reaction, aldol reaction, and so on. The cyclization reaction was the key step. All the target compounds were synthesized in five steps with the overall yield of 25–30 %, respectively. The structures of these novel targets and all of intermediates were confirmed by ^1H NMR. Biological activity test indicated that 2-(2-nitrobenzylidene)indolin-3-one (5d) and 2-(4-(trifluoromethyl)benzylidene)indolin-3-one(5f) have good antitumor activity against K562 and HepG2 cells. In order to improve the antitumor activity, further modifications based on compound (5d) and (5f) were undergoing in our laboratory.

Acknowledgments The authors sincerely thank the financial support from the Natural Science Foundation of Tianjin (12JCYBJC31600), the Science and Technology Project of Tianjin (10ZCKFSY07700, 11ZCGHHZ00400) and Tianjin University of Science and Technology (20110115, 20120117).

References

1. Prakash CR, Raja S (2012) Indolinones as promising scaffold as kinase inhibitors: a review. *Mini Rev Med Chem* 12(2):98–119
2. Krystal GW, Honsawek S, Kiewlich D et al (2001) Indolinone tyrosine kinase inhibitors block Kit activation and growth of small cell lung cancer cells. *Cancer Res* 61(9):3660–3668
3. Wood L (2012) Sunitinib malate for the treatment of renal cell carcinoma. *Expert Opin Pharmacother* 13(9):1323–1336
4. Raymond E, Hammel P, Dreyer C et al (2012) Sunitinib in pancreatic neuroendocrine tumors. *Target Oncol* 7(2):117–125
5. Naraev BG, Strosberg JR, Halfdanarson TR (2012) Current status and perspectives of targeted therapy in well-differentiated neuroendocrine tumors. *Oncology* 83(3):117–127
6. Figlin R, Sternberg C, Wood CG (2012) Novel agents and approaches for advanced renal cell carcinoma. *J Urol* 188(3):707–715
7. Ito T, Igarashi H, Jensen RT et al (2012) Current status and therapeutic strategy for pancreatic neuroendocrine tumors in Japan. *Fukuoka Igaku Zasshi* 103(7):131–137
8. Chen Z, Merta PJ, Lin NH et al (2005) A-432411, a novel indolinone compound that disrupts spindle pole formation and inhibits human cancer cell growth. *Mol Cancer Ther* 4(4):562–568
9. Mulligan JM, Greene LM, Cloonan S et al (2006) Identification of tubulin as the molecular target of proapoptotic pyrrolo-1,5-benzoxazepines. *Mol Pharmacol* 70(1):60–70
10. Halaban R (1991) Growth factors and tyrosine protein kinases in normal and malignant melanocytes. *Cancer Metastasis Rev* 10(2):129–140
11. Bishop JM (1987) The molecular genetics of cancer. *Science* 235(4786):305–311
12. Sun L, Tran N, Tang F et al (1998) Synthesis and biological evaluations of 3-substituted indolin-2-ones: a novel class of tyrosine kinase inhibitors that exhibit selectivity toward particular receptor tyrosine kinases. *J Med Chem* 41(14):2588–2603
13. Lee CY, Chew EH, Go ML (2010) Functionalized aurones as inducers of NAD(P)H:quinone oxidoreductase 1 that activate AhR/XRE and Nrf2/ARE signaling pathways: synthesis, evaluation and SAR. *Eur J Med Chem* 45:2957–2971

14. Islam I, Bryant J, Chou YL et al (2004) Indolinone based phosphoinositide-dependent kinase-1 (PDK1) inhibitors. Part 1: design, synthesis and biological activity. *Bioorg Med Chem Lett* 17(14):3814–3818
15. Nirogi RV, Deshpande AD, Kambhampati R et al (2011) Indole-3-piperazinyl derivatives: novel chemical class of 5-HT(6) receptor antagonists. *Bioorg Med Chem Lett* 21(1):346–349
16. Zhang W, Go ML (2009) Functionalized 3-benzylidene-indolin-2-ones: inducers of NAD(P)H-quinone oxidoreductase 1 (NQO1) with antiproliferative activity. *Bioorg Med Chem* 17(5):2077–2090

Chapter 94

Research Progress on the Anti-Rheumatoid Arthritis Drugs

Peng Wang, Xuegang Luo, Chongxi Wang, Xinjia Wang, Guang Hu and Tong-cun Zhang

Abstract Rheumatoid arthritis (RA) is a chronic systemic autoimmune disease leading to synovial hyperplasia and a series of multisystem comorbidities. Permanent disability usually occurs in 20–30 % of untreated patients within 2–3 years of the disease. Therefore, it is important to diagnose the disease and initiate treatment as early as possible. The drug therapy plays an important role in maintaining a state of very low disease activity and slowing the progression of joint damage. Traditional drug therapy in RA is a pyramid approach, in which nonsteroidal anti-inflammatory drugs (NSAIDs) serve as the base of pyramid and disease-modifying antirheumatic drugs (DMARDs) are employed relatively late. But since this approach is no longer valid, many new drugs used to manage RA have been developed. In this review, we specifically summarize the current drug therapies for the treatment of RA and briefly describe the etiology, pathology and pathogenesis of RA.

Keywords Rheumatoid arthritis · Etiology · Pathology · Pathogenesis · Drug therapy

The first two authors contributed equally to the project.

P. Wang · X. Luo · C. Wang · X. Wang · T.-C. Zhang (✉)
Key Laboratory of Industrial Microbiology, Ministry of Education, College of Bioengineering, Tianjin University of Science and Technology, Tianjin, China
e-mail: tony@tust.edu.cn

X. Luo · C. Wang · X. Wang · G. Hu · T.-C. Zhang
Tianjin Key Laboratory of Industrial Microbiology, Tianjin, China
e-mail: oldmoonlake@gmail.com

G. Hu
Shaoxing Institute of Technology, College of Engineering, Peking University, Shaoxing, Zhejiang, China

94.1 Introduction

Rheumatoid arthritis (RA) is a lifelong chronic inflammatory disease characterized by synovial hyperplasia, eventually, cartilage erosion and bone destruction [1–4]. Although its etiology remains largely unknown, evidence points to a complex interplay between environmental and genetic factors [5]. RA usually attacks joints of the hands, feet, wrists, knees, elbows, ankles, and shoulders symmetrically. Fatigue and weight loss as common symptoms are accompanied by lean blood, slight fever, pericarditis, vasculitis, subcutaneous nodules, etc. Pain and stiffness followed by swelling, redness, and muscle pain in one or more small joints may become worse after a few weeks or months. As the disease progresses, irreversible joint damage may lead to deformity of joint and loss of function. Long-term studies have suggested that disease popularity is estimated to be 1 % all over the world, about 50–70 % of persons with RA become permanently physical disability after 10–15 years of diagnosis [6]. Furthermore, the number of the women suffering from RA is three times more than men, and the disease bedevils all age groups ranging from children to the elderly, but the people in middle age are in supreme danger [7].

Therapeutics options for RA have become more and more. In general, there are four methods in the treatment of RA, i.e., physical therapy, function exercise, drug therapy, and surgical therapy. While physical therapy and function exercise act as adjuvant therapy and work temporarily only for patients in early phase of the disease, surgical therapy is suitable for those with severe disease. However, RA is not simply a joint inflammation but autoimmune disease involved in multiple systems, hence, effective drug therapy is crucial for decreasing the rate of disease progression. A great majority of patients need to change drug types frequently because of efficacy reduction and the lack of significant disease control. Therefore, development of new and better drugs can obtain markedly improved outcomes to patients with RA, with a goal of alleviation of symptoms and improvement of physical function. In the last decade, all kinds of the agents used in the treatment of RA have been developed from immunomodulatory agents to molecules targeting specific cytokines and cells related to the pathogenesis of RA. Fortunately, multiple drug therapies for RA substantially bring about long-term good outcomes for many patients.

94.2 Etiology of Rheumatoid Arthritis

The etiology of RA is not fully known, although quite a lot of researches are ongoing regarding it. For example, it has been determined that the frequency of RA in monozygotic twins is obviously higher than that in the general population [8]. Furthermore, there is a more than 30 % concordance rate of disease in identical twins. The polymorphic human leukocyte antigen DR (HLA-DR) β chain genes (some DR1 and DR4 subtypes) seem to be the mainly identified

susceptibility genes [9, 10]. A recent research of class II genes and molecules of the major histocompatibility complex has showed an increase susceptibility to seropositive RA patients expressing the HLA-DR4 subtypes [11]. It has been indicated that Collagen II and HLA-DR β molecular form dimer complex in order to drive immune responses possibly in the pathogenesis of RA. However, there is not any convincing evidence that a rheumatoid specific antigen has been forthcoming, although some antigens rich in joints, such as collagen II, are possible candidates [12]. An investigation has pointed out that a majority of adult patients present more DR1 antigens than others in the early development of RA [13, 14].

However, nongenetic factors, such as environmental factors, bacteria, viruses, sex hormones, play a major role in initiating and maintaining RA for the majority of patients. A research has showed that a constant stimulus for pathogenesis of RA is peptidoglycan existing in group A *streptococcus*. And a continuous high titer of anti-EB virus antibody was found in the sera and synovial fluids of patients with RA. Furthermore, the number of the women suffering from RA is three times more than men, however, women with RA will go into remission if they are in gestation period or take the pill. It is known to us that many contributors, e.g., cold, damp, fatigue, malnutrition, trauma, mental factor, etc., would give rise to RA. Many patients are very curious to know whether the cause of RA is attributed to improper nutrition, however, by now no investigations have determined that specific nutritional factors are causative agents.

94.3 Pathology and Pathogenesis of Rheumatoid Arthritis

The pathological changes of RA include synovial membrane arthritis, rheumatoid nodules, and rheumatoid vasculitis. Active inflammation is first seen in the synovial membranes of the joints. The normal synovial lining of joint capsule holding the fluid that lubricates the joints is generally two or three cells in thickness. Therefore, thickening of the synovial membranes will gradually cause inflammation and further lead to irreversible damage to joint capsule and articular cartilage because these structures are replaced by scar-like tissue called pannus. After a triggering incident, possibly autoimmune or infectious, synovial macrophages, and fibroblasts begin to proliferate. Then lymphocytes infiltrate perivascular regions and endothelial cells proliferate. It has been suggested that the vascular endothelium plays an active and key role in a variety of immunological processes. In addition, neovascularization occurs and blood vessels are blocked by small clots or inflammatory cells. As time passes, the damaged synovial tissue begins to grow irregularly and then forms pannus tissue. Later, thick and hardened pannus protrudes over the surface of the cartilage and gives rise to joint destruction [15]. Unfortunately, the skin, bones, and muscles adjacent to the joints atrophy from disuse and destruction. Rheumatoid nodules and rheumatoid vasculitis, as severe RA indications, are extra-articular pathological changes of RA and appear in organizations and organs of the whole body.

94.4 Drug Therapy

94.4.1 Nonsteroidal Anti-Inflammatory Drugs

Traditional drug therapy of RA is a pyramid approach, with nonsteroidal anti-inflammatory drugs (NSAIDs) serving as the first-line medicine. Although support for the use of NSAIDs in RA, NSAIDs have lost their historical roles because they cannot be used alone to alter the disease course [16, 17]. NSAIDs are associated with gastropathy, so new NSAIDs were approved and came into broad use in order to decline incidence of NSAIDs gastropathy. In addition, all of these agents, such as nabumetone, etodolac, rofecoxib, etc., were used for initial treatment of RA to reduce joint pain and promoted as being safer than their predecessors.

94.4.2 The Traditional Disease-Modifying Antirheumatic Drugs

Disease-modifying antirheumatic drugs (DMARDs) are very effective for all RA patients to reduce joint swelling and pain, inhibit progressive joint damage, and improve function. The traditional DMARDs consist of methotrexate, hydroxychloroquine, sulfasalazine, leflunomide, etc. MTX is the dominant DMARDs for treatment of RA for many years, SSZ and leflunomide are also widely used. Historically, MTX has been the mainstay of treatment for RA [18], because it slows the progression of joint destruction. However, many trials have showed that methotrexate in combination with another DMARDs is more effective than alone [19].

94.4.3 Biological Agents

Efforts to develop safer and more effective treatments for RA have been achieved through the development of the biologic agents. A few different cellular and cytokine targets have been identified, and some biologics have been approved to treat RA at present, including TNF- α antagonists (adalimumab, etanercept, infliximab), IL-1 antagonist (anakinra), an inhibitor of T cell costimulation (abatacept), and a selective depleter of B cells (rituximab) etc. These biological agents have shown the ability to bring good outcomes for many RA patients.

94.4.3.1 Cytokine Antagonists

Though there are many effective therapeutic targets, inhibition of cytokines seems to be a particular effective approach to controlling inflammation and preventing further joint destruction [20].

TNF Antagonists

TNF- α is a trigger that causes joint tissue damage resulting in bone erosion, so the development of anti-TNF- α monoclonal antibodies alleviates symptoms effectively and prevents the progression of joint damage.

Etanercept (ETN), a soluble tumor necrosis factor (TNF) receptor fusion protein, has been approved for the treatment of RA. TNF- α plays its functions via interaction with its membrane receptors, p55 or TNF receptor I (TNFRI) and p75 (TNFRII), which activate two kinds of completely different signal pathways and cause distinct biological effects. Etanercept, a dimeric human p75-Fc fusion protein, consists of extracellular domains of the human p75 and the constant Fc portion of human IgG1. It has been proved that Etanercept can reduce RA activity for those who have had an inadequate response to other therapies [21–23]. The reason is that Etanercept competitively prevents the binding of TNF- α to cell surface TNF- α receptor, inhibiting the biological activity of TNF [24]. Inhibition of TNF activity may slow or halt progressive joint damage in order to improve the quality of life for patients. Compared with oral methotrexate, subcutaneous etanercept acted more rapidly to decrease disease activity and prevent structural damage in patients with early active RA. The findings indicated that the combination of etanercept and methotrexate was significantly better in decreasing disease activity and slowing joint damage compared with methotrexate or etanercept alone.

Adalimumab (ADA, Humira) is a fully human recombinant immunoglobulin G1 (IgG1) anti-TNF monoclonal antibody, therefore it is thought to be less immunogenic than chimeric antibodies. Adalimumab is suitable for those who have had an inadequate response to DMARDs and also effective in the treatment of patients with moderately to severely RA. Adalimumab, either alone or in combination with methotrexate or standard antirheumatic therapies, has an obvious effect in early treatment of RA. In a key study [25], adalimumab in combination with methotrexate, at a higher dose of 40 mg subcutaneously every 2 weeks, yielded a statistically remarkable improvement compared with methotrexate plus placebo. In general, adalimumab significantly decreased symptoms of active RA and established a long-lasting clinical response in patients, as well as a well-tolerated feature with few patients discontinuing treatment because of side effects.

Infliximab (IFX), a Human-Mouse Chimeric anti-TNF monoclonal antibody, is found to be effective for the treatment of early RA [26]. It is a heterotetrameric protein, and its hypervariable region is murine in origin and the constant domain of the immunoglobulin is made up with a human IgG1 Fc heavy chain and partial k

light chain. Infliximab is usually administered intravenously in an outpatient setting every 4–8 weeks. It has been demonstrated that infliximab plus MTX regimens caused significantly greater improvement in patients with active RA compared with the patients receiving monotherapy with methotrexate.

Golimumab (GLM) is a novel fully human monoclonal antibody to TNF which is used as an immunosuppressive drug. It was derived from hybridomas generated from a transgenic mouse including activated human immunoglobulin genes and inactivated mouse immunoglobulin genes [27]. Golimumab was used as once a month subcutaneous treatment for adults with moderately to severely active RA. The results of GLM administered subcutaneously plus background MTX have suggested a benefit in the long-lasting symptoms reduction of RA [28].

Certolizumab pegol (CZP), lacking a Fc region, is a novel construct consisting of the Fab' antigen binding domain of a humanized anti-TNF mAb and site-specifically attaches to a 40kD molecule of polyethylene glycol (PEG). So it cannot induce complement or antibody-dependent cell mediated cytotoxicity, which has been found in vitro with ADA, ETN and IFX [29]. CZP also increases lengths of disease duration compared with other TNF antagonists. PEG does not cross the placenta, so this drug can be used throughout pregnancy without adverse effects on the fetus. In addition, applicable scope of CZP is very broad, including patients with or without other TNF antagonists, with or without MTX or other DMARDs.

Additional Cytokine Antagonists

A lot of cytokines except TNF are also targets for RA therapy, including IL-1, IL-6 and RANKL etc. Anakinra is the first IL1-receptor antagonist, either alone or in combination with methotrexate, has played a very good efficacy in moderate-to-severe RA. Tocilizumab is a fully humanized mAb targeting the IL6-receptor, now approved for the treatment of RA [30, 31]. However, biologic inhibition of either IL-1 or IL-6 shows no obviously superior outcomes to TNF blockade.

94.4.3.2 B Cell Targets

B lymphocytes are implicated in the pathogenesis of RA. Rituximab (RTX), a chimeric mAb against the protein CD20 which is primarily found on the surface of B cells, effectively destroys B cells in peripheral blood [32]. Several additional agents targeting B cells have been developed, such as ocrelizumab and ofatumumab. Ocrelizumab-a fully human mAb against CD20 can effectively improve symptoms for serum positive patients. Ofatumumab is a complete humanized anti-CD20 antibody, appearing to inhibit early stage B lymphocyte activation. It had been launched by Genmab pharmaceutical company and GlaxoSmithKline (GSK) for the treatment of RA. Although these agents similarly target CD20, ofatumumab can bind to more different antigenic epitopes on CD20

than rituximab or ocrelizumab. All of these compounds targeting B cells cause a reduction in B cell numbers, rheumatoid factors and total immunoglobulin levels in order to preferably control inflammation and prevent joint destruction in the case of inadequate response to anti-TNF- α therapy and conventional therapy.

94.4.3.3 T Cell Targets

Activated CD4⁺ T cells lead to stimulation of osteoclastogenesis and activation of metalloproteinases and further result in joint destruction. Simple activation signal without complementary costimulation signal is unable to achieve full T cell activation. In general, CD80 or CD86 on the surface of antigen-presenting cells (APC) should naturally bind to CD28 on T cells in order to activate T cells. Abatacept (CTLA4-Ig, Orencia), a cytotoxic T-lymphocyte-associated antigen 4-IgG1 fusion protein, contains a high-affinity binding site for CD80 or CD86. As a result, it can effectively prevent the CD80 or CD86-CD28 from delivering costimulatory signal to T cells [33, 34]. The findings indicate that the combination of abatacept and methotrexate was significantly better in improving symptoms of RA and physical function, compared with methotrexate or abatacept alone.

94.4.4 Glucocorticoids

Short-term glucocorticoids (GCs) reduce joint swelling and pain temporarily in a short period when a single inflamed joint contributes to disability acutely. While the long-term steroids may decrease joint damage [35] but have significant side effects, such as osteoporosis, cataracts, cushingoid symptoms, and infection. Besides, increasing evidences show that prudent use of GCs in the treatment of RA should be recommended [36] because of the low risk of adverse effects. In practice, low-dose GCs (less than 10 mg/d) can relieve most patients from pains.

94.4.5 Chinese Herbal Medicine

Previous study has demonstrated that the various active ingredients in Chinese herbal medicine for RA have multiple physiological functions, such as antimicrobial, anti-inflammatory, analgesic, and immunomodulatory activities. In addition, the Chinese herb medicine is effective with higher safety and less adverse effect. *Tripterygium wilfordii* Hook. F (TWHF), a Chinese herbal medicine and a member of the Celastraceae family, has been reported to be a therapeutic agent against a number of autoimmune and inflammatory diseases such as RA. The extractives of TWHF, for instance tripterygium glycosides, can effectively inhibit the production of cytokines by suppressing quite a number of proinflammatory

genes and then induce the apoptosis in lymphocytes and synovial fibroblasts [37]. Patients taking extractives of TWHF frequently developed adverse effects, and occasionally severe toxicity to their livers and kidneys.

94.4.6 Other Agents for RA

Tetracyclines and a number of their semisynthetic derivatives, such as minocycline, have been used as therapeutic agents for RA since the late 1960s. In addition to their antimicrobial activities, antibiotics of the tetracycline family have been further shown to have anti-inflammatory, immunoregulatory, and chondroprotective properties. And anti-inflammatory activity is found to be independent of their antimicrobial properties [38]. The tetracycline compounds directly suppress activities of B and T cells and inhibit matrix metalloproteinase (MMP) by downregulating the expression of type 2 nitric oxide synthase mRNA, an important mediator in collagen degradation.

94.5 Conclusion

In recent decades, development and application of new therapeutic agents for the treatment of RA bring a remarkable development for the treatment of this disease and contribute to research on the pathogenesis of RA. Furthermore, it is very apparent that RA is a multidimensional disease with a highly variable course, so a great majority of patients need to change drug types frequently because of reduction of efficacy and the lack of significant control of disease. RA is a lifelong disease, therefore, it is still necessary to develop novel effective therapeutic approaches against RA in the future. The drugs at present will be replaced by the new drugs which not only target all phases of RA disease progression, but also can be used in combination with other agents. The development of multiple new drugs for RA must be able to bring about long-term good outcomes for many patients.

Acknowledgments This study was financially supported by the Program for Changjiang Scholars and Innovative Research Team in University of Ministry of Education of China (NO. IRT1166).

References

1. Harris ED (1990) Rheumatoid arthritis: pathophysiology and implications in therapy. *New Eng J Med* 322:1277–1289
2. Carmona L, Cross M, Williams B et al (2010) Rheumatoid arthritis. *Best Pract Res Clin Rheumatol* 24:733–745

3. Zvaifler NJ (1983) Pathogenesis of the joint disease of rheumatoid arthritis. *Am J Med* 75:3–8
4. Smolen JS, Aletaha D, Redlich K (2012) The pathogenesis of rheumatoid arthritis: new insights from old clinical data? *Nat Rev Rheumatol* 8:235–243
5. Gregersen PK (1999) Genetics of rheumatoid arthritis: confronting complexity. *Arthritis Res* 1:37–44
6. Schuna AA (1998) Update on treatment of rheumatoid arthritis. *J Am Pharm Assoc* 38:728–735
7. Erhardt CC, Mumford PA, Venables PJ et al (1989) Factors predicting a poor life prognosis in rheumatoid arthritis: an eight year prospective study. *Ann Rheum Dis* 48:7–13
8. Silman AJ, MacGregor AJ, Thomson W et al (1993) Twin concordance rates for rheumatoid arthritis: results from a nationwide study. *Br J Rheumatol* 32:903–907
9. Vaughan JH, Kouri T, Petersen J et al (1988) On the etiology of rheumatoid arthritis. *Scand J Rheumatol Suppl* 74:19–28
10. Gregersen PK, Silver J, Winchester RJ et al (1987) The shared epitope hypothesis: an approach to understanding the molecular genetics of susceptibility to rheumatoid arthritis. *Arthritis Rheum* 30:1205–1213
11. Stastny P (1978) Association of the B-cell alloantigen Dm4 with rheumatoid arthritis. *N Engl J Med* 298:869–871
12. Ronnelid J, Lyscholm J, Engstrom-Laurent et al (1994) Local anti-type II collagen antibody production in rheumatoid arthritis synovial fluid: evidence for an HLA-DR4-restricted IgG response. *Arthritis Rheum* 37:1023–1029
13. Schiff B, Mizrahi Y, Orgad S et al (1982) Association of HLA-Aw31 and HLA-DR1 with rheumatoid arthritis. *Ann Rheum Dis* 41:403–404
14. Woodrow JC, Nichol FE, Zaphiropoulos G (1981) DR antigens and rheumatoid arthritis: a study of two populations. *Br Med J* 283:1287–1288
15. Goldring SR (2000) A 55-year-old woman with rheumatoid arthritis. *JAMA* 283:524–531
16. Scott PA, Kingsley GH, Smith CM et al (2007) Non-steroidal anti-inflammatory drugs and myocardial infarctions: Comparative systematic review of evidence from observational studies and randomised controlled trials. *Ann Rheum Dis* 66:1296–1304
17. Schaffer D, Florin T, Eagle C et al (2006) Risk of serious NSAID-related gastrointestinal events during long-term exposure: a systematic review. *Med J Aust* 185:501–506
18. Donahue KE, Gartlehner G, Jonas DE et al (2008) Systematic review: comparative effectiveness and harms of disease-modifying medications for rheumatoid arthritis. *Ann Intern Med* 148:124–134
19. Kremer JM, Genovese MC, Cannon GW et al (2002) Concomitant leflunomide therapy in patients with active rheumatoid arthritis despite stable doses of methotrexate. *Ann Intern Med* 137:726–733
20. Choy EH, Panayi GS (2001) Cytokine pathways and joint inflammation in rheumatoid arthritis. *N Engl J Med* 344:907–916
21. Lovell DJ, Giannini EH, Reiff A et al (2000) Etanercept in children with polyarticular juvenile rheumatoid arthritis. *N Engl J Med* 342:763–769
22. Moreland LW, Baumgartner SW, Schiff MH et al (1997) Treatment of rheumatoid arthritis with a recombinant human tumor necrosis factor receptor (p75)-Fc fusion protein. *N Engl J Med* 337:141–147
23. Weinblatt ME, Kremer JM, Bankhurst AD et al (1999) A trial of etanercept, a recombinant tumor necrosis factor receptor: Fc fusion protein, in patients with rheumatoid arthritis receiving methotrexate. *N Engl J Med* 340:253–259
24. Mohler KM, Torrance DS, Smith CA et al (1993) Soluble tumor necrosis factor (TNF) receptors are effective therapeutic agents in lethal endotoxemia and function simultaneously as both TNF carriers and TNF antagonists. *J Immunol* 151:1548–1561
25. Keystone EC, Kavanaugh AF, Sharp JT et al (2004) Radiographic, clinical, and functional outcomes of treatment with adalimumab (a human anti-tumor necrosis factor monoclonal

- antibody) in patients with active rheumatoid arthritis receiving concomitant methotrexate therapy: a randomized, placebo-controlled, 52-week trial. *Arthritis Rheum* 50:1400–1411
26. Taylor PC, Steuer A, Gruber J et al (2002) Infliximab attenuates joint destruction in early RA patients with ultrasonographic markers of poor prognosis. *Arthritis Rheum* 46:334
 27. Fishwild DM, O'Donnell SL, Bengoechea T et al (1996) High-avidity human IgG kappa monoclonal antibodies from a novel strain of minilocus transgenic mice. *Nat Biotechnol* 14:845–851
 28. Kremer J, Ritchlin C, Mendelsohn A et al (2010) Golimumab, a new human anti-tumor necrosis factor alpha antibody, administered intravenously in patients with active rheumatoid arthritis: forty-eightweek efficacy and safety results of a phase III randomized, double-blind, placebocontrolled study. *Arthritis Rheum* 62:917–928
 29. Nesbitt A, Fossati G, Bergin M et al (2007) Mechanism of action of certolizumab pegol (CDP870): in vitro comparison with other anti-tumor necrosis factor alpha agents. *Inflamm Bowel Dis* 13:1323–1332
 30. Gomez-Reino JJ, Fairfax MJ, Pavelka K et al (2007) Targeted inhibition of IL-6 with tocilizumab improves quality of life and function in patients with rheumatoid arthritis with inadequate response to a range of DMARDs. *Arthritis Rheum* 56:4234
 31. Genovese M, McKay J, Nasonov E et al (2007) IL-6 receptor inhibition with tocilizumab reduces disease activity in patients with rheumatoid arthritis with inadequate response to a range of DMARDs: the TOWARD Study. *Arthritis Rheum* 56:4309–4310
 32. Dass S, Vital EM, Emery P (2006) Rituximab: novel B-cell depletion therapy for the treatment of rheumatoid arthritis. *Expert Opin Pharmacother* 7:2559–2570
 33. Moreland LW, Alten R, Van den Bosch F et al (2002) Costimulatory blockade in patients with rheumatoid arthritis: a pilot, dose-finding, double-blind, placebo-controlled clinical trial evaluating CTLA-4Ig and LEA29Y eighty-five days after the first infusion. *Arthritis Rheum* 46:1470–1479
 34. Emery P (2003) The therapeutic potential of costimulatory blockade with CTLA-4Ig in rheumatoid arthritis. *Expert Opin Investig Drugs* 12:673–681
 35. Kirwan JR, Bijlsma JW, Boers M et al (2007) Effects of glucocorticoids on radiological progression in rheumatoid arthritis. *The Cochrane Libr* doi: [10.1002/s14651858006356](https://doi.org/10.1002/s14651858006356)
 36. Bijlsma JW, van der Goes MC, Hoes JN et al (2010) Lowdose glucocorticoid therapy in rheumatoid arthritis: an obligatory therapy. *Ann N Y Acad Sci* 1193:123–126
 37. Little C, Parsons T (2000) Herbal therapy for treating rheumatoid arthritis. *The Cochrane Libr*. doi:[10.1002/s14651858002948](https://doi.org/10.1002/s14651858002948)
 38. Alarcon GS (2000) Tetracyclines for the treatment of rheumatoid arthritis. *Expert Opin Investig Drugs* 97:1491–1498

Chapter 95

Design and Synthesis of 1H-2,3-Dihydro-1-Pyrrolizinones Derivatives

Changhai Sun and Jing Cao

Abstract Pyrrolizinone derivatives were discovered showing remarkable anti-inflammatory and analgesic activities. Based on the SAR summarized before, a series of pyrrolizinone derivatives were designed and synthesized in this paper. All the eight target compounds were characterized by ¹HNMR spectra, and the test of anti-inflammatory and analgesic activities is in progress.

Keywords Anti-inflammatory · Analgesic · Pyrrolizinone

95.1 Introduction

Anti-inflammatory drugs has a long history of clinical application, more research showed that inflammation is associated with a variety of diseases. Therefore, the anti-inflammatory drugs is also expected for the treatment of many inflammatory-related diseases, such as atherosclerosis, cancer, stroke, etc., the research of new anti-inflammatory drugs have never been stopped.

Nonsteroidal anti-inflammatory drugs (NSAID) are one of the most important class of anti-inflammatory drugs, widely used in clinic. However, many NSAID could lead to various side effects, for example, the gastrointestinal damage, nephrotoxicity and hepatotoxicity, and so on. Therefore, developing new anti-inflammatory and analgesic agents with lower toxicity have still been the interest of this field [1–8].

C. Sun (✉)

Tianjin Chasesun Pharmaceutical Co. Ltd, Tianjin 301700, People's Republic of China
e-mail: suns-s@vip.163.com

J. Cao

College of Biotechnology, Tianjin University of Science and Technology, Tianjin 300457, People's Republic of China

It has been reported that some *1H*-1, 2-dihydro-1-pyrrolizinone derivatives showed remarkable anti-inflammatory and analgesic activities with new mechanism of action, however, the application of such compounds was restricted due to its toxicity and low activities. In order to improve their activities and reduce the toxicities, a series of new pyrrolizinone derivatives were designed and synthesized based on the SAR reported before [5–8]. Finally, target compounds (*5a–5h*) were obtained and characterized by ^1H NMR and LC–MS spectra.

95.2 Materials and Methods

95.2.1 Materials and Measurements

All reagents and solvents used in this paper were of reagent grade. Reaction temperatures were controlled using oil bath temperature modulator. Thin layer chromatography (TLC) was performed using E. Merck silica gel 60 GF₂₅₄ pre-coated plates (0.25 mm) and visualized using a combination of UV. Silica gel (particle size 200–400 mesh) was used for flash chromatography. ^1H NMR spectra was recorded on Bruker AM-400 NMR spectrometers in deuterated solvent. The chemical shifts are reported in δ (ppm) relative to tetramethylsilane as internal standard.

95.2.2 Chemistry

Figure 95.1 demonstrates the synthetic approach to the target compounds *5a–5h*.

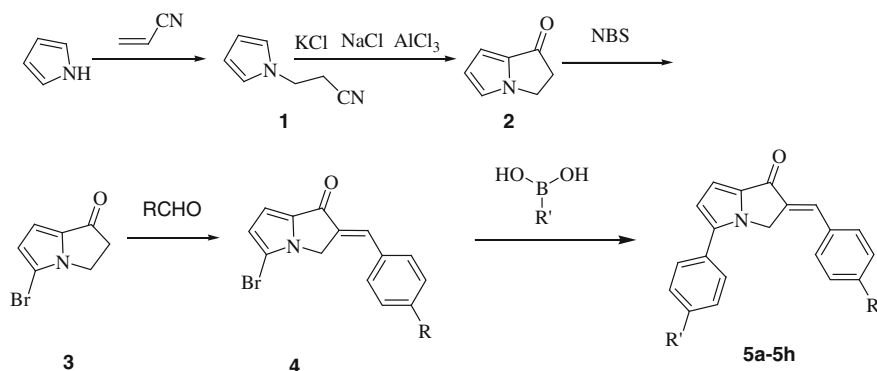


Fig. 95.1 Synthetic route of target compounds *5a–5h*

1H-pyrrole was employed to react with acrylonitrile to provide 3-(1H-pyrrol-1-yl)propanenitrile (compound *1*) which was then cyclized in the presence of Lewis acid to afford the key intermediate *2*. Compound *2* was brominated with NBS in a specific site to provide compound *3*, it was converted into compound *4a–4h* through aldol condensation, *4a–4h* were treated with different boric acid to provide target compounds *5a–5h*.

95.3 Results and Discussion

As described above, eight target compounds (*5a–5h*) were obtained (Table 95.1) with a simple and feasible synthetic route. The evaluation of anti-inflammatory and analgesic activities of these compounds are ongoing right now.

95.4 Experimental

95.4.1 3-(1H-pyrrol-1-yl)propanenitrile (*1*)

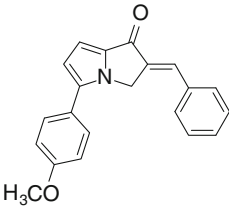
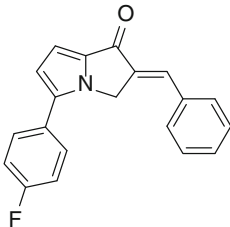
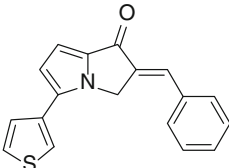
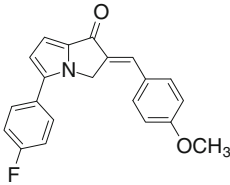
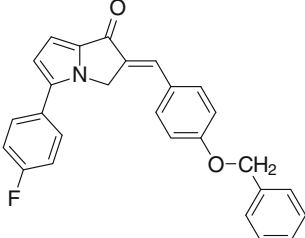
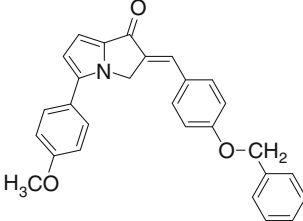
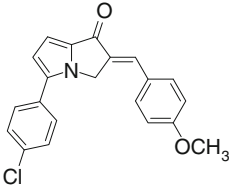
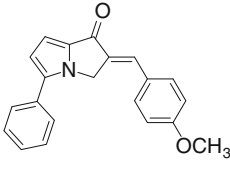
To the 1H-pyrrole (30 g, 0.45 mol) was added 20 % TEBA (6.5 mL), then at 0 °C added acrylonitrile dropwise for about 1 h. After stirring for another 1 h at 35–40 °C, compound *1* was obtained with 80 % yield by distillation in vacuum (130–132 °C/1,066pa, Lit: 132–136 °C/1,066.2pa).

95.4.2 2,3-dihydropyrrolizin-1-one (*2*)

Potassium chloride (5.6 g), sodium chloride (5.6 g), and anhydrous aluminum chloride (28 g) were heated to melt together in a 100 mL round bottom at 140 °C, then the compound *1* was poured into the melted salt mixture, stirred for 35–40 s, the mixture was poured into ice water, adjusted pH to 6–7 with potassium hydroxide, heated with a water bath at 75 °C for 30 min. After cooling, the reaction mixture was extracted with CH₂Cl₂ (50 mL × 3), organic phases were combined and dried over anhydrous magnesium sulfate, purified by flash chromatography using 200–300 mesh silica gel (petroleum ether:ethyl acetate = 8:1), 4.55 g compound *2* was obtained (65 % yield) with m.p 54–55 °C (Lit. :53.5–54 °C).

¹H NMR (CDCl₃, δ):3.11(t, 2H,2-H),4.33(t, 2H, 3-H),6.54(q, 1H, 6-H),6.76 (t, H, 7-H),7.06(d, H, 5-H).

Table 95.1 Structures of target compounds 5a–5h

Compounds no.	Structure	Compounds no.	Structure
5a		5e	
5b		5f	
5c		5g	
5d		5h	

95.4.3 5-bromo-2,3-dihydropyrrolizin-1-one (3)

5.0 g (41.3 mol) of 2,3-dihydropyrrolizin-1-one (2) was dissolved in 20 mL CH_2Cl_2 , the solution of NBS (8.0 g, 45.4 mol) in CH_2Cl_2 was added dropwise to solution of 2 at 0 °C, then stirred at room temperature for 3 h. After the reaction was completed, washing reaction mixture with sodium chloride aqueous solution, organic phases were dried over anhydrous magnesium sulfate. Compound 3 was purified by column chromatography with a yield of 90 % (silica gel 200–300 mesh, petroleum ether: ethyl acetate = 10:1).

$^1\text{H-NMR}$ (CDCl_3 , δ): 3.12(t, 2H, 2-H), 4.2(t, 2H, 3-H), 6.5(d, 1H, 6-H), 6.72(d, H, 7-H).

95.4.4 (E)-2-(4-substitued benzylidene)-5-bromo-2,3-dihydropyrrolizin-1-one (4)

Compound 3 (100 mg) was dissolved in 5 mL ethanol, which was then added with 0.2 mL 10 % sodium hydroxide aqueous solution under ice-bath condition, stirred for 10 min, 4-substitued benzaldehyde ethanol solution was added dropwise, then stirred for 1 h at room temperature. The reaction mixture was filtrated, washed with cold 95 % ethanol 2–3 times, the yellow solid were dried to give the compounds 4 with 58–70 % yield. The following is ^1H NMR example of compounds 4.

(E)-2-benzylidene-5-bromo-2,3-dihydropyrrolizin-1-one: ^1H NMR (CDCl_3 , δ):5.0(d, 2H,3-H),6.53(d, 1H, 6-H),6.89(d, 1H, 7-H),7.47(m, 5H, Ar-H),7.6(s, H, =CH-).

95.4.5 Target Compounds 5a–5h

To a pressure flask-added compounds 4 respectively (1 eq.), 4-substitued phenyl boronic acid (1 eq.), potassium carbonate (1 eq.), triphenylphosphonium (0.05 eq.) and palladium acetate (0.025 eq.). A 3 mL DMF was poured at the condition of N_2 protection, then reacted in a microwave reactor at 130 °C for 1 h, cooled to room temperature, added water, extracted with CH_2Cl_2 three times, combine the organic solution, dried over anhydrous magnesium sulfate, and purified by column chromatography with petroleum ether and ethyl acetate system.

5a (46 % yield): ^1H NMR (CDCl_3 , δ):3.91(s, 3H, $-\text{OCH}_3$),5.3(d, 2H, 3-H),6.69(t, 1H, 6-H),7.02(d, 1H, 7-H),7.06(d, 2H, Ar-H),7.44(m, 5H, Ar-H),7.51(q, 3H, Ar-H and =CH-).

5b (33 % yield): ^1H NMR (CDCl_3 , δ):5.28(d, 2H, 3-H),6.7(d, 1H, 6-H),7(d, 1H, 7-H),7.23(t, 2H, Ar-H),7.45(m, 5H, Ar-H),7.6(q, 3H, Ar-H and =CH-).

5c (40 %): ^1H NMR (CDCl_3 , δ):5.27(d, 2H, 3-H),6.73(d, 1H, 6-H),6.97(d, 1H, 7-H),7.52(m, 8H, Ar-H and Thiophene-H),7.58(s, 1H, =CH-).

5d (38 %): ^1H NMR (CDCl_3 , δ):3.87(s, 3H, $-\text{OCH}_3$),5.21(d, 2H, 3-H),6.70(d, 1H, 6-H),6.95(d, 1H, 7-H),7.0(d, 2H, Ar-H),7.42(d, 2H, Ar-H),7.5(m, 3H, Ar-H and =CH-),7.57(d, 2H, Ar-H).

5e (34 %): ^1H NMR (CDCl_3 , δ):5.16(s, 2H, $-\text{OCH}_2-$),5.30(d, 2H, 3-H),6.76(d, 1H, 6-H),7.02(d, 1H, 7-H),7.09(d, 2H, Ar-H),7.46(m, 8H, Ar-H),7.54(t, 3H, Ar-H and =CH-),7.66(d, 3H, Ar-H).

5f (46 %): ^1H NMR (CDCl_3 , δ):3.87(s, 3H, $-\text{OCH}_3$), 5.05(s, 2H, $-\text{OCH}_2-$),5.15(d, 2H, 3-H),6.63(d, 1H, 6-H),6.88(d, 1H, 7-H),6.98(d, 2H, Ar-H),7.37(m, 11H, Ar-H).

5g (45 %): ^1H NMR (CDCl_3 , δ):3.87(s, 3H, $-\text{OCH}_3$),5.21(d, 2H, 3-H),6.70(d, 1H, 6-H),6.95(d, 1H, 7-H),7.0(d, 2H, Ar-H),7.42(d, 2H, Ar-H),7.5(m, 3H, Ar-H and =CH-),7.57(d, 2H, Ar-H).

5h (48 %): ^1H NMR (CDCl_3 , δ): 3.87(s, 3H, $-\text{OCH}_3$), 5.25(d, 2H, 3-H), 6.74(d, 1H, 6-H), 6.98(t, 3H, Ar-H and 7-H), 7.42(m, 3H, Ar-H), 7.52(t, 3H, Ar-H and =CH-), 7.64(d, 2H, Ar-H).

95.5 Conclusion

Finally, a series of novel 1H-2, 3-dihydro-1-pyrrolizinones Derivatives were designed and synthesized, further SAR research will be carried out in the future.

Acknowledgments The authors sincerely thank Professor Peng Yu and his team in the Tianjin University of Science and Technology for the characterization of compounds and other generous help.

References

1. Morriello GJ, Chicchi G, Johnson T et al (2010) Fused tricyclic pyrrolizinones that exhibit pseudo-irreversible blockade of the NK1 receptor. *Bioorg Med Chem Lett* 20(19):5925–5932
2. Morriello GJ, Mills SG, Johnson T et al (2010) Substituted fused bicyclic pyrrolizinones as potent, orally bioavailable hNK1 antagonists. *Bioorg Med Chem Lett* 20(6):2007–2012
3. Despinoy XL, McNab H (2009) 1-Methoxycarbonylpyrrolizin-3-one and related compounds. *Org Biomol Chem* 7(10):2187–2194
4. Lescot E, Bureau R, Sopkova-de Oliveira Santos J et al (2005) 3D-QSAR and docking studies of selective GSK-3beta inhibitors. comparison with a thieno[2,3-b]pyrrolizinone derivative, a new potential lead for GSK-3beta ligands. *J Chem Inf Model* 45(3):708–715
5. Zhao LQ, Hu YD, Yuan Y et al (2001) Studied on docking of 5,6-diaryl-2,3-dihydro-1-pyrrolizinone derivatives with cyclooxygenase. *Yao Xue Xue Bao* 36(6):415–418
6. Zhao LQ, Yuan Y, Hu YD et al 3D-QSAR of antiinflammatory activities of 5,6-diaryl-2,3-dihydro-1-pyrrolizinone derivatives]. *Yao Xue Xue Bao*. 36(5):343–346
7. Zhao LQ, Yang Z, Zhang SF (2001) 5, 6-diaryl-2, 3-dihydro-1-pyrrolizinone derivatives synthesis and antiinflammatory and analgesic activities. *Yao Xue Xue Bao* 36(4):258–261
8. Zhang SF, Gao WF, Hen HZ (1988) Synthesis of 3H-1, 2-dihydro-1-pyrrolizinone derivatives. *Yao Xue Xue Bao* 23(1):28–33

Chapter 96

Inhibition of iNOS to Protect Intermittent Hypoxia-Induced Hippocampal Neurons Impairment by *Astragalus* Extract in Rat

Qiang Zhang, Wenyuan Gao, Shuli Man, Yun Zhang and Baoyuan Chen

Abstract The aim of this paper is to research the protective effect of *Astragalus* against intermittent hypoxia-induced hippocampal neurons impairment in rat and lay the theoretical foundation for sleep apnea improvement in cognitive function by *Astragalus*. Male Wistar rats were divided into four groups: (1) blank control group; (2) normoxia group; (3) intermittent hypoxia group; (4) *Astragalus* treated intermittent hypoxia group. After 6-week treatment, the expression of iNOS was detected by real-time reverse transcription polymerase chain reaction (RT-PCR) at mRNA level as well as by immunohistochemistry (IHC) and western blot at protein level. As a result, *Astragalus* reduced the expression of iNOS at mRNA and protein levels in hippocampus compared with non-treated groups ($P < 0.05$). In conclusion, *Astragalus* could protect intermittent hypoxia-induced hippocampal neurons impairment in rat.

Keywords *Astragalus* · Intermittent hypoxia · Hippocampus neurons apoptosis · INOS

Q. Zhang (✉) · Y. Zhang · B. Chen
Tianjin Medical University General Hospital, Tianjin Institute of Geriatrics, Anshan Road,
Tianjin 300052, China
e-mail: zhangqianyulv@163.com

W. Gao (✉)
School of Pharmaceutical Science and Technology, Tianjin University, Weijin Road,
Tianjin 300072, China
e-mail: pharmgao@tju.edu.cn

S. Man
Key Laboratory of Industrial Microbiology, Ministry of Education, College
of Biotechnology, Tianjin University of Science and Technology, TEDA, Tianjin 300457,
China

96.1 Introduction

Astragalus extract is an important candidate for the treatment of memory disorders [1]. Previous research reported that *Astragalus* extract has antioxidant activity. In vitro results show that AST-IV protects cardiomyocytes from oxidative stress-mediated injury under hypoxic conditions [2]. *Astragalus membranaceus* can also protect intestinal mucosa against intestinal oxidative damage after hemorrhagic shock [3]. This study aimed to observe the effects of *astragalus membranaceus* to protect intermittent hypoxia-induced hippocampal neurons impairment in rat.

The hippocampus is related with cognitive function. Intermittent hypoxia in hippocampal neurons may cause damages to different systems. *Astragalus* extract modulated the hypoxia/reoxygenation injury of hippocampal neurons and inhibited the apoptosis[4]. Intermittent hypoxia is a hypoxia re-oxygen cycle process. Therefore, we used the intermittent hypoxia (alternating cycles of normoxia (2 min at 21 % O₂) and hypoxia (2 min at 10 % O₂), repeated continuously for 8 h/day during the light portion of the cycle for 6 weeks) to simulate OSA patients and researched whether *Astragalus* could intervene damage progress of hippocampal neurons.

96.2 Materials and Methods

96.2.1 Animal Model

Twenty-four adult male Wistar rats, with body weight around 310 ± 30 g, were provided by the Animal Center of Tianjin Medical University, Tianjin. The animals were randomly divided into four groups ($n = 6$), blank control group, normoxia group, intermittent hypoxia group, and *Astragalus* treated group. All groups had free access to water and food. The hypoxia condition was intermittently induced 30 times per hour (h), and the lowest concentration of oxygen in capsule was 5 %. The capsule inducing hypoxia was circularly charged with nitrogen for 30 s (10 L/min), atmosphere for 40 s (10 L/min) and atmosphere for 50 s (5 L/min), overall 2 min/cycle. The oxygen concentration in capsules ranged from 5 to 21 %. Rats were exposed to alternating cycles of normoxia (2 min at 21 % O₂) and hypoxia (2 min at 10 % O₂), repeated continuously for 8 h/day during the light portion of the cycle for 6 weeks. The experiment was conducted according to the ethics of animal experiments.

96.2.2 *Astragalus* Extraction

Four hundred and twenty g of *Astragalus* were crushed and extracted by 75 % ethanol three times for 3.5 h. The extract was filtered and rotary evaporated, and the remaining part was diluted to 300 mL by distilled water, then the extract

stored at 4 °C. The rats were administrated with 3.5 g/2 mL/kg body weight of *Astragalus* extract once everyday for six months.

96.2.3 Immunohistochemistry

The IHC was performed using Rabbit Anti-Mouse HIF-1 α antibody (Santa, USA), Rabbit Anti-Mouse iNOS antibody (Santa, USA), streptavidin–biotin complex (SABC) kit (Boster, China), and diaminobenzidine (DAB) kit (Boster, China). There was no false positive by setting the blank and replacing the control. Five fields of view without overlapping and at high magnification ($\times 400$) were selected and the average optical density was detected.

96.2.4 Real-Time RT-PCR

The primers of genes were designed by Gene Runner, a comprehensive sequence analysis utility, and no significant homologous sequence was discovered using National Center for Biotechnology Information, The Basic Local Alignment Search Tool (NCBI BLAST). Quantitative real-time RT-PCR was performed according to the protocol using the following primers: iNOS (179 base pairs, bp), 5'- CCTCAAGTCTTATTTCTCAAC-3' (sense) and 5'-TCAGCAGCAAGTTC-CATC -3' (antisense), glyceraldehyde-3-phosphate dehydrogenase (Gapdh) (121 bp), 5'- TTCAACGGCACAGTCAAG-3' (sense) and 5'-CGACATACTCAGCACCAG-3' (antisense). We performed real-time RT-PCR using SYBR green PCR kit (Takara, Japan) and analyzed the amplification curve. The relative expression of the target gene was represented by the $2^{-\Delta\Delta CT}$ value of the tested sample (CT are cycles at threshold detection fluorescence; $\Delta CT = CT$ value of target gene – CT value of Gapdh).

96.2.5 Western Blot

The proteins were extracted using Protein Extraction Kit (Promega, USA). Thirty μg of proteins were mixed with $2 \times$ sodium dodecyl sulfate/sulphate (SDS)-PAGE sample buffer at the ratio of 1:1. The electrophoresis was performed and the proteins were transferred to the nitrocellulose (NC) film. The film was blocked overnight using a buffer. The NC film was washed thrice using a buffer. The monoclonal Goat Anti-Rat iNOS antibodies (1:400) (Santa, USA) were incubated with NC film and shake at 4 °C overnight. The NC film was washed thrice and the secondary antibody of Rabbit Anti-Goat immunoglobulin (IgG) (1:5,000) was

added. After incubation at 37 °C for 1 h, the NC film was exposed. β -Actin (Santa, USA) was used for normalization.

96.2.6 Statistical Analysis

Data were presented as the mean \pm standard deviation (SD) and analyzed by using Statistical Package for the Social Sciences computer program (SPSS version 13.0). We employed multi-factor variance to analyze the data and performed the comparison by using Student–Newman–Keuls test. Differences were considered statistically significant if P values were less than 0.05.

96.3 Results and Discussion

96.3.1 Immunohistochemistry Assay of iNOS

Studies have shown that *Astragalus* may improve cerebral hypoxia and reoxygenation of hippocampal neurons apoptosis. Ethyl acetate fractions of *Astragalus membranaceus* (Fisch.) Bunge var. *mongholicus* (Bunge) Hsiao (Fabaceae) significantly decreased pro-inflammatory mediators (e.g., NO and PGE(2))[5].

Intermittent hypoxia is also a hypoxia and reoxygenation of the pathophysiology process. Thus, we tried the above findings applied to intermittent hypoxia rat model experiments to investigate the protective effect of *Astragalus* intermittent hypoxia in rat hippocampal neurons.

The negative cells appeared purplish-blue under optical microscope and the cytoplasm of positive cells brownish-yellow. Compared with normoxia group and blank control group, large quantity of brown-yellow particles in hypoxia group were observed. In *Astragalus* group, the brownish-yellow particles decreased, and -blue cells also could be observed (Fig. 96.1). Statistical significant difference was observed between *Astragalus* group and hypoxia group ($P < 0.05$), as indicated in Table 96.1.

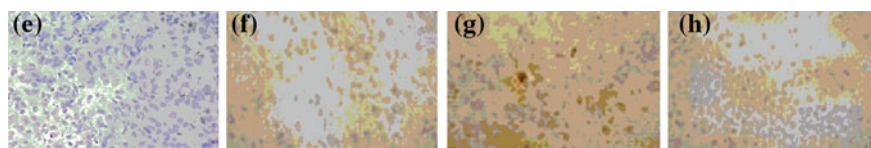


Fig. 96.1 Immunohistochemistry analysis of iNOS in brain of rats. **a** iNOS in control group; **b** iNOS in normoxia group; **c** iNOS in hypoxia group; **d** iNOS in *Astragalus* group

Table 96.1 The IHC assay of iNOS in hippocampal neurons statistically analyzed

Groups	Number of rats	iNOS (mean \pm SD)
The first group (blank control group)	6	1.434 \pm 0.072
The second group (normoxia group)	5	1.366 \pm 0.004
The third group (intermittent hypoxia group)	6	7.803 \pm 0.053
The fourth group (<i>Astragalus</i> group)	10	3.709 \pm 0.046
F value	27	21661.803*
Comparison between the third and the first group		6.369 \pm 0.029*
Comparison between the third and the second group		6.437 \pm 0.029*
Comparison between the third and the fourth group		4.093 \pm 0.029*

* $P < 0.05$, compared with intermittent hypoxia groups

96.3.2 The Expression of iNOS at mRNA Level

As shown in Fig. 96.2, the expressions of iNOS at mRNA level in *Astragalus* group were lower than those in hypoxia group, and the expressions of iNOS in hypoxia group were higher than those in normoxia and blank control groups. Statistical significant difference was observed between *Astragalus* and hypoxia groups ($P < 0.05$), as indicated in Table 96.2.

96.3.3 The Expression of iNOS by Western Blot

The expressions of iNOS in *Astragalus* group were lower than those in hypoxia group. The expressions of iNOS in hypoxia group were higher than those in normoxia and blank control groups, as shown in Fig. 96.3.

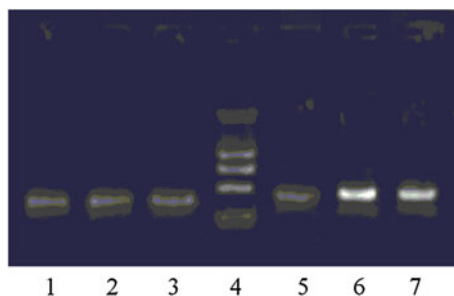


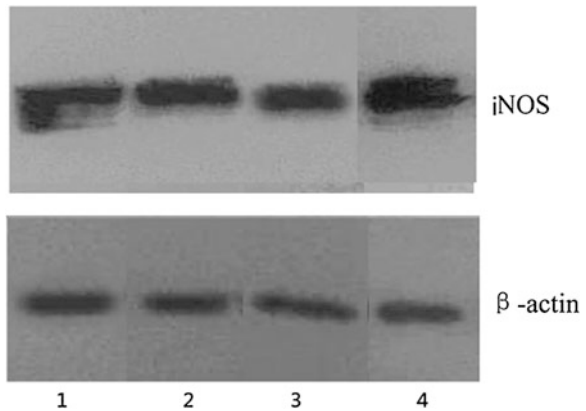
Fig. 96.2 The electrophoretic analysis of PCR products of iNOS in different samples. 1 The band in normoxia group is not clear (179 bp). 2, 3 The band in *Astragalus* group is clear (167 bp). 4 Marker, from bottom to top: 100, 250, 500, 750, 1,000, 2,000 bp. 5 The band in blank control group is 179 bp. 6, 7 The band in hypoxia group is 179 bp

Table 96.2 The expression of iNOS at mRNA level in hippocampal neurons statistically analyzed

Groups	Number of rats	iNOS (mean ± SD)
The first group (blank control group)	6	0.202 ± 0.032
The second group (normoxia group)	5	0.125 ± 0.040
The third group (intermittent hypoxia group)	6	3.394 ± 1.344
The fourth group (<i>Astragalus</i> group)	10	1.121 ± 0.595
F value	27	25.510*
Comparison between the third and the first group		3.192 ± 0.421*
Comparison between the third and the second group		3.269 ± 0.441*
Comparison between the third and the fourth group		2.273 ± 0.376*

**P* < 0.05, compared with intermittent hypoxia groups

Fig. 96.3 The expression of iNOS in hippocampal neurons detected by western blot. The molecular weight of iNOS is 132 kDa. The molecular weight of beta-actin is 43 kDa. 1 blank control group; 2 normoxia group; 3 *Astragalus* treated hypoxia group; 4 non-treated hypoxia group



Our findings showed that the expressions of iNOS at mRNA and protein levels as well as the apoptosis of neurons increased in hippocampus of rats exposed to intermittent hypoxia, but, *Astragalus* decreased the expression of iNOS at mRNA and protein levels and inhibited the apoptosis of neurons in hippocampus. These results are in accordance with previous studies.

Any condition of hypoxia could induce rapidly an abundant expression of HIF-1a. Meanwhile, it was reported that NO generated by iNOS mainly played a cytotoxic role during the process of hypoxia [6]. The apoptosis is one of the important mechanisms to delay neuron death after cerebral ischemia or hypoxia. HIF-1a can regulate the expression of iNOS [7]. *Astragalus* reduced HIF-1a expression. Therefore, it inhibited the production of NO and then avoided the apoptosis of hippocampus neurons and other tissues injury. In our previous research, we found that *Astragalus* could inhibit the expression of HIF-1a (data are published elsewhere).

96.4 Conclusion

Astragalus inhibited the apoptosis of neurons under intermittent hypoxia through down-regulation of the mRNA and protein levels of iNOS. The dose-dependent activity and discovery of the valid parts of *Astragalus* still need to be carried out in the future.

Acknowledgments This work was supported by a grant 10JCYBJC25800 from Natural Science Foundation of Tianjin, a grant 20100132 from Tianjin higher school science and technology development fund project and a grant 2009KY17 from Tianjin Medical University Fund.

References

1. Tohda C, Tamura T, Matsuyama S et al (2006) Promotion of axonal maturation and prevention of memory loss in mice by extracts of *Astragalus mongholicus*. *Br J Pharmacol* 149:532–541
2. Hu JY, Han J, Chu ZG et al (2009) Astragaloside IV attenuates hypoxia-induced cardiomyocyte damage in rats by upregulating superoxide dismutase-1 levels. *Clin Exp Pharmacol Physiol* 36:351–357
3. Gan XL, Hei ZQ, Huang HQ et al (2006) Effect of *Astragalus membranaceus* injection on the activity of the intestinal mucosal mast cells after hemorrhagic shock-reperfusion in rats. *Chin Med J (Engl)*. 119:1892–1898
4. Zhu FF, Yin YY, Li WP (2009) Protective effect of extract of a stragalus against injury induced by hypoxia/reoxygenation in hippocampus neuron. *Chin Pharm Bull.* 25:213–216
5. Chao WW, Kuo YH, Li WC et al (2009) The production of nitric oxide and prostaglandin E2 in peritoneal macrophages is inhibited by *Andrographis paniculata*, *Angelica sinensis* and *Morus alba* ethyl acetate fractions. *J Ethnopharmacol* 122:68–75
6. Iadecola C, Zhang F, Casey R et al (1997) Delayed reduction of ischemic brain injury and neurological deficits in mice lacking the inducible nitric oxide synthase gene. *J Neurosci* 17:9157–9164
7. Palmer LA, Semenza GL, Stoler MH et al (1998) Hypoxia induces type II NOS gene expression in pulmonary artery endothelial cells via HIF-1. *Am J Physiol* 274:212–219

Chapter 97

Prepared and Characterization of 12 β , 15 α -Dihydroxy- 16 α ,17-Epoxyprogesterone

Yibo Wang, Yanbing Shen, Jiajia Ren, Jianmei Luo and Min Wang

Abstract The compound 12 β , 15 α -dihydroxy-16 α , 17-epoxyprogesterone was biotransformed from 16 α , 17-epoxyprogesterone by *Colletotrichum lini* AS3.4486, and its structure was characterized by ^1H NMR, ^{13}C NMR, HREI-MS and single-crystal X-ray diffraction. The crystal of the title compound belongs to monoclinic, space group *R3* with $a = 8.0655(8)$, $b = 12.1955(12)$, $c = 18.589(2)$ Å, $\beta = 90^\circ$, $Z = 4$, $V = 1828.4(3)$ Å³, $D_c = 1.309$ mg/m³, $\mu = 0.092$ mm⁻¹, $F(000) = 776$, $R = 0.0407$ and $wR = 0.0792$. X-ray analysis indicates that intermolecular hydrogen bonds O(2)–H(2)⋯O(5), O(3)–H(3)⋯O(2) are observed.

Keywords Biotransformation · 16 α · 17-epoxyprogesterone · Hydroxylation · *Colletotrichum lini*

97.1 Introduction

16 α ,17 α -epoxyprogesterone (EP, **1**) is an important intermediate of pharmaceutical industry [1, 2]. The production of several high value steroid drugs is mostly derived from the key compounds by microbiological hydroxylation. Biotransformation exhibits higher regio- and stereo-selectivity, may contribute to new derivatives of 16 α , 17-epoxyprogesterone for research of lead compounds.

The literature data indicated the ability of *Colletotrichum lini* AS3. 4486 (*C. lini* AS3.4486) to hydroxylate on steroidal substrates. e. g., The 7 β and 12 β hydroxy

Y. Wang · Y. Shen · J. Ren · J. Luo · M. Wang (✉)

Key Laboratory of Industrial Fermentation Microbiology(Tianjin University of Science and Technology), Ministry of Education; College of Biotechnology, Tianjin University of Science and Technology, Tianjin 300457, People's Republic of China
e-mail: minw@tust.edu.cn

group was introduced to progesterone [3], the 11α , and 15α hydroxy group was introduced to androstenedione [4], and Romano reported that the hydroxylation of the position 7 and 15 of dehydroepiandrosterone (3β -hydroxy-5-androsten-17-one) [5]. In the present paper, we studied the biotransformation of **1** by *C. lini* AS3.4486. Notably, a product 12β , 15α -dihydroxy- 16α , 17 -epoxyprogesterone (**2**) was formed. The introduction of hydroxy group at C12 and C15 position of steroids was very difficult by chemical synthesis. Therefore, it is a mild and selective method that hydroxylated steroid substrates at positions C12 and C15 with *C. lini* AS3.4486.

97.2 Materials and Methods

97.2.1 Apparatus and Reagents

^1H NMR and ^{13}C NMR spectra were measured on a Bruker AV400 Instrument (400 MHz) with DMSO- d_6 as the solvent. Mass spectra were recorded on a Thermo-Finingan mass detector. The single-crystal structure was determined on a Rigaku Saturn CCD area detector. Substrate 16α , 17α -epoxyprogesterone (EP, 98.4 % purity) was obtained from Tianjin Jinjin Pharmaceutical Co., Ltd. All chemical solvents and salts used were of analytical grade or higher.

97.2.2 Preparation of 12β , 15α -Dihydroxy- 16α , 17 -Epoxyprogesterone

Colletotrichum lini AS3.4486 was obtained from Institute of Microbiology, Chinese Academy of Sciences and maintained on PDA agar slants at $4\text{ }^\circ\text{C}$. The microorganism was further cultivated in 250 mL shake flasks containing 50 mL culture medium in two consecutive cultivation steps as previously described by Shen et al. [3].

For the biotransformation, 100 mg of **1** dissolved in 2 mL of ethanol was added to the culture after 24 h for growth and the reaction was allowed to proceed for 48 h. The mycelium was then removed by filtration. The biomass and the broth were extracted separately with EtOAc. All extracts were combined and dried (anhydr. MgSO_4). The solvents after filtration were evaporated under reduced pressure. The crude extracts were purified by Si gel column using dichloromethane/ether/methanol (25:2:1, v/v/v). The white powder was diffused with n-hexane/acetone at room temperature. Colorless prismatic crystals suitable for X-ray analysis were obtained.

97.2.3 Structure Determination

The colorless needle crystal of compound 2 with dimensions of 0.22 mm \times 0.18 mm \times 0.12 mm was selected for X-ray diffraction analysis. The data were collected by a Rigaku Saturn CCD area detector equipped with a graphite-monochromatic MoK α radiation ($\lambda = 0.71073 \text{ \AA}$) using a φ - ω scan mode at 113(2) K. In the range of $2.00 \leq \theta \leq 27.87^\circ$, a total of 19,354 reflections were collected with 4,393 unique ones ($R_{\text{int}} = 0.0559$), of which 2,494 were observed with $I > 2\sigma(I)$ and used in the succeeding refinements. Intensity data were corrected for Lp factors and empirical absorption. The structure was solved by direct methods and expanded by different Fourier techniques with SHELXS-97 program [6]. All of the nonhydrogen atoms were located with successive different Fourier syntheses. The structure was refined by full-matrix least-squares techniques on F^2 using anisotropic thermal parameters for all nonhydrogen atoms. The hydrogen atoms were added according to theoretical models. The final full-matrix least-squares refinement converged at $R = 0.0407$, $wR = 0.0927$ ($w = 1/[\sigma^2(F_o^2) + (0.0428 P)^2 + 0.0000 P]$), where $P = (F_o^2 + 2F_c^2)/3$, $S = 1.020$ ($\Delta\rho$) $_{\text{max}} = 0.185$ ($\Delta\rho$) $_{\text{min}} = -0.229 \text{ e/\AA}^3$ and ($\Delta\sigma$) $_{\text{max}} = 0.000$.

97.3 Results and Discussion

The purified transformation product was characterized by NMR and MS. The detailed results are as follows: HREI-MS: m/z 361.2006 $[M+H]^+$ $C_{21}H_{28}O_5$, Calcd. for 360.1937; ^1H NMR (DMSO- d_6 , 400 MHz): δ (ppm): 0.98 (3H, s, H-18), 1.15 (3H, s, H-19), 2.10 (3H, s, H-21), 4.72 (1H, d, H-12), 4.98 (1H, d, H-15), 5.62 (1H, s, H-4); ^{13}C NMR (DMSO- d_6 , 400 MHz): δ (ppm): 204.89(C-20), 197.95 (C-3), 170.52(C-5), 123.09 (C-4), 71.23 (C-17), 70.28 (C-12), 62.66 (C-15); Rf in dichloromethane/ether/methanol (12.5:2:1, v/v/v): 0.48.

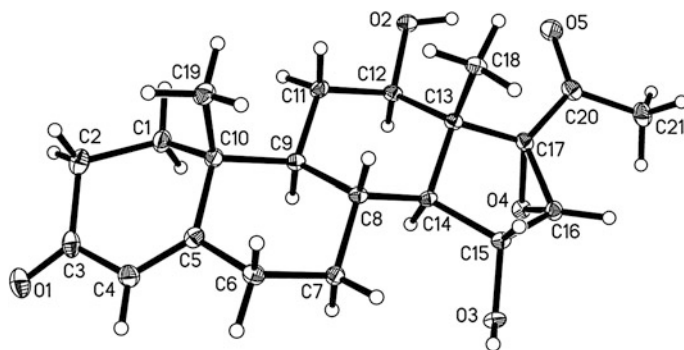
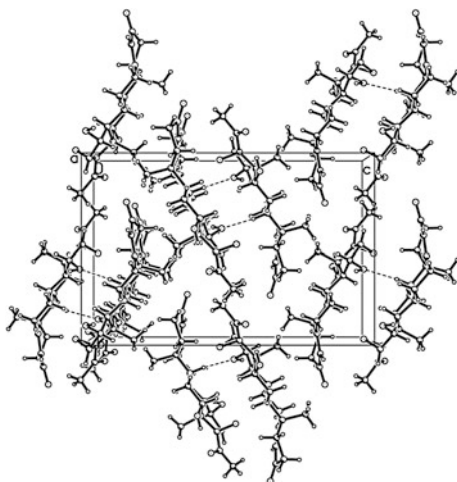


Fig. 97.1 Molecular structure of the compound 2

Fig. 97.2 Crystal packing of the compound 2



The formula weight added 32 to 16 α , 17-epoxyprogesterone from ESI-MS(+). It supposed that the production added two hydroxyls. The molecular structure and perspective view of the crystal packing in a unit cell of compound 2 are shown in

Table 97.1 Selected bond lengths (Å) and bond angles (°) for the compound 2

Bond	Dist.	Bond	Dist.	Bond	Dist.
O(1)–C(3)	1.229(3)	C(5)–C(10)	1.524(3)	C(12)–C(13)	1.525(3)
O(2)–C(12)	1.446(2)	C(6)–C(7)	1.530(3)	C(13)–C(17)	1.542(3)
O(3)–C(15)	1.421(2)	C(7)–C(8)	1.524(3)	C(13)–C(18)	1.544(3)
O(4)–C(16)	1.442(2)	C(8)–C(14)	1.531(3)	C(13)–C(14)	1.547(3)
O(4)–C(17)	1.456(2)	C(8)–C(9)	1.542(3)	C(14)–C(15)	1.537(3)
O(5)–C(20)	1.223(3)	C(9)–C(11)	1.542(3)	C(15)–C(16)	1.512(3)
C(1)–C(10)	1.538(3)	C(9)–C(10)	1.567(3)	C(16)–C(17)	1.479(3)
C(2)–C(3)	1.501(3)	C(10)–C(19)	1.550(3)	C(17)–C(20)	1.501(3)
C(3)–C(4)	1.460(3)	C(11)–C(12)	1.535(3)	C(20)–C(21)	1.501(3)
C(4)–C(5)	1.347(3)				
<i>Angle</i>	(∞)	<i>Angle</i>	(∞)	<i>Angle</i>	(∞)
C(4)–C(5)–C(6)	120.1(2)	C(1)–C(10)–C(19)	110.15(17)	C(18)–C(13)–C(14)	112.31(15)
C(4)–C(5)–C(10)	123.1(2)	C(12)–C(11)–C(9)	114.04(15)	C(8)–C(14)–C(15)	121.05(16)
C(6)–C(5)–C(10)	116.81(16)	C(5)–C(10)–C(9)	107.79(15)	C(8)–C(14)–C(13)	112.88(15)
C(5)–C(6)–C(7)	111.38(16)	C(1)–C(10)–C(9)	108.01(15)	C(15)–C(14)–C(13)	105.13(15)
C(8)–C(7)–C(6)	111.16(16)	C(19)–C(10)–C(9)	112.23(16)	O(3)–C(15)–C(16)	109.93(15)
C(7)–C(8)–C(14)	111.91(15)	O(2)–C(12)–C(13)	112.74(15)	O(3)–C(15)–C(14)	113.14(15)

(continued)

Table 97.1 (continued)

Bond	Dist.	Bond	Dist.	Bond	Dist.
C(7)–C(8)–C(9)	110.75(15)	O(2)–C(12)– C(11)	106.99(15)	C(16)–C(15)– C(14)	102.30(16)
C(14)–C(8)–C(9)	105.95(15)	C(13)–C(12)– C(11)	111.21(16)	C(17)–C(16)– C(15)	109.49(17)
C(8)–C(9)–C(11)	112.18(15)	C(12)–C(13)– C(17)	117.67(16)	C(16)–C(17)– C(20)	121.90(18)
C(8)–C(9)–C(10)	114.71(15)	C(12)–C(13)– C(18)	112.30(16)	C(16)–C(17)– C(13)	107.46(16)
C(11)–C(9)–C(10)	112.55(16)	C(17)–C(13)– C(18)	106.24(15)	C(20)–C(17)– C(13)	124.45(17)
C(5)–C(10)–C(1)	110.30(16)	C(12)–C(13)– C(14)	106.72(15)	C(17)–C(20)– C(21)	118.40(18)
C(5)–C(10)–C(19)	108.35(16)	C(17)–C(13)– C(14)	101.18(15)		

Table 97.2 Hydrogen bonds for shelx [A and deg.]

D–H...A	d(D–H)	d(H...A)	d(D...A)	<(DHA)
O(2)–H(2)...O(4) ^a	0.83(2)	1.96(2)	2.7715(19)	164(2)
O(5)–H(5)...O(1) ^b	0.87(3)	1.95(3)	2.810(2)	166(3)

Symmetry transformations used to generate equivalent atoms

^a $x - 1, y, z$; ^b $-x+3/2, -y+1, z-1/2$

Figs 97.1 and 97.2, respectively. The selected bond lengths and bond angles are listed in Table 97.1.

Compound 2 has three six-membered rings (*A/B/C*) and one five-membered rings (*D*). Ring *A* has a 1 α -sofa conformation. Rings *B* and *C* adopt chair conformations, while the cyclopentane ring *D* adopts a 14 α -envelope conformation. In the crystal structure, there are short intermolecular C–H...O contacts. The title compound was chiral space group. The 12-hydroxy is β configuration with the torsion angles C12–C13–C14–O2 = 175.98(15)°. The 15-hydroxy is α configuration with the torsion angles C13–C14–C15–O3 = –153.64(15)°. The bond lengths and angles are within normal ranges [7, 8]. In the crystal packing (Fig. 97.2), X-ray analysis indicates that intermolecular hydrogen bonds O(2)–H(2)...O(5), O(3)–H(3)...O(2) are observed (Table 97.2).

97.4 Conclusion

The hydroxylated 16 α , 17-epoxyprogesterone was obtained by biotransformation with *Colletotrichum lini* AS3. 4486 and its structure was characterized by ¹H NMR, ¹³C NMR, HREI-MS, and single-crystal X-ray diffraction. In the

view of all these observations, the product should be 12 β , 15 α - dihydroxy-16 α , 17-epoxyprogesterone.

Acknowledgments This work was supported by the National High Technology Research and Development of China (2011AA02A211), the National Natural Science Foundation of China (Nos. 21076158 and 21276196), and Tianjin City High School Science & Technology Fund Planning Project (20120629).

References

1. Wu DX, Guan YX, Wang HQ et al (2011) 11 α -Hydroxylation of 16 α ,17-epoxyprogesterone by *Rhizopus nigricans* in a biphasic ionic liquid aqueous system. *Bioresource Technol* 102:9368–9373
2. Chen K, Tong WY, Wei DZ et al (2007) The 11 β -hydroxylation of 16,17 α -epoxyprogesterone and the purification of the 11 β -hydroxylase from *Absidia coerulea* IBL02[J]. *Enzyme Microb Tech* 41(1/2):71–79
3. Shen Y, Sun H, Fu Y et al (2012) Progesterone hydroxylation with *Colletotrichum lini* AS3. 4486. *Adv Mater Res* 343–344:1070–1073
4. Shen YB, Wang M, Liang QK et al (2011) 11 α ,15 α -Dihydroxyandrost-4-ene-3,17-dione. *Acta Cryst E* 67:o2752
5. Romano A, Romano D, Ragg E et al (2006) Steroid hydroxylations with *Botryodiplodia malorum* and *Colletotrichum lini*. *Steroids* 71:429–434
6. Sheldrick GM (2004) SHELX97. University of Göttingen, Germany
7. Wang S, Wang Y, Nie Q et al (2004) 16 α ,17-Epoxy-4-pregnene-3,20-dione. *Acta Cryst E* 60:o2337–o2338
8. Nie Q, Wang JK, Wang S et al (2005) 16 α ,17-Epoxy-11 α -(p-tolylsulfonyloxy)pregn-4-ene-3,20-dione. *Acta Cryst E* 61:o912–o913

Part IV
Agricultural, Environmental, Marine
Biotechnology and Bio-energy Technology

Chapter 98

Structure Elucidation of Two Triterpenoid Saponins from Leaves of *Schima superba* Gardn. et Champ

Guanghua Huo, Changling Zhang and Yingjun Zhang

Abstract Two new oleanane-type triterpenoid saponins with two angeloyls at C-21, C-22, and a branch of tetrasaccharide moiety (Rha, Cal, Glc, GlcA, or Rha, Xyl, Glc, GlcA) at C-3 were isolated from leaves of *Schima superba* Gardn. et Champ. Their structures were established using one- and two-dimensional NMR and high resolution electrospray ionization mass spectrometry as 21,22-di-*O*-angeloyl-R₁-barrigenol-3-*O*-{ β -D-glucopyranosyl-(1 \rightarrow 2)- β -D-galactopyranosyl-(1 \rightarrow 2)-[α -L-rhamnopyranosyl-(1 \rightarrow 4)]}- β -D-glucuronopyranoside, named schimasuoside A (**1**), 21,22-di-*O*-angeloyl-R₁-barrigenol-3-*O*-{ β -D-glucopyranosyl-(1 \rightarrow 2)- β -D-xylopyranosyl-(1 \rightarrow 2)-[α -L-rhamnopyranosyl-(1 \rightarrow 4)]}- β -D-glucuronopyranoside, named schimasuoside B (**2**). There are strong antifungal effect of their mixture on *Magnaporthe oryzae*.

Keywords *Schima superba* · Schimasuoside A · Schimasuoside B · Structure elucidation

98.1 Introduction

Schima superba Gardn. et Champ (*Theaceae*) is mainly distributed in central and southern China. The plant is commonly cultivated as an ornamental tree, for timber production and as a firebreak planting. Its bark powder is used as a repellent agent to dispel wild pigs and birds from crops in Fujian mountain, to poison fish in

G. Huo (✉) · C. Zhang
College of Bioscience and Engineering, Jiangxi Agricultural University,
330045 Nanchang, People's Republic of China
e-mail: hgh3813899@sohu.com

Y. Zhang
Kunming Institute of Botany, Chinese Academy of Sciences,
650204 Kunming, People's Republic of China

Taiwan, and as an arrow tip toxin by traditional hunters. A methanolic extract of its stem bark is used to kill snails [1], to induce apastia in *Plutella xylostella*, and *Pieris rapae* [2], and to control intestinal parasite. We recently found a strong antifungal effect of an ethanolic extract of *S. superba* leaves on *Magnaporthe oryzae* [3, 4]. The presence of a variety of chemical constituents in its stem such as saponins, flavonoids, lignanoids, have been reported [5, 6]. However, no report on the isolation and identification of saponins from the leaves of *S. superba* was available until now. The current study presents the isolation, structural elucidation of two new saponins from the leaves of *S. superba* in this paper.

98.2 Materials and Methods

98.2.1 General Experimental Procedures

Optical rotations were measured with JASCOP-1020 digital polarimeter (Japan Jasco Pty Ltd). HRESI-MS spectra were acquired on API QSTAR Pulsar LC/TOF mass spectrometer (American AB corp). GC-MS spectra were obtained on Agilent 5973N with Shimadzu GC-14C column gas-mass spectrometer. One- and two-dimensional NMR spectra were recorded on Bruker DRX-500 or Avance III 600 Fourier Transform NMR spectrometer and chemical shifts were given in ppm with TMS as internal standard. UV spectra were measured with Shimadzu UV 2401PC ultraviolet spectrometer. IR spectra were recorded on Bruker Tensor-27 Fourier Transform infrared spectrometer. Preparative and analytical HPLC were performed on HPLC system consisted of Waters 2695 separations module-2,996 photodiode array detector (Auto injection), Waters 600-486 pumps tunable absorbance detector (manual-injection), Water Delta 600-2,487 dual wavelength absorbance detector using Agilent ZORBAX StableBond C-18 (9.4 × 150 mm, 5 μm; 4.6 × 250 mm, 5 μm).

98.2.2 Plant Material

Leaves of *S. superba* were collected from Jiangxi province of China in November 2010 and identified by Prof. X. H. Shi of Forestry College in Jiangxi Agricultural University. Voucher specimens have been deposited at the herbarium of this university.

98.2.3 Extraction and Isolation

Dried and powdered leaves of the plant (10 kg) were extracted with 80 % EtOH. After concentrated under vacuum, the EtOH extract was suspended into water, and

then extracted successively with CHCl_3 and *n*-BuOH. The *n*-BuOH fraction (679.2 g) was subjected to Diaion HP20SS column chromatography (CC) (MeOH– H_2O , 0:100–100:0 v/v) to give eight fractions (Fr.1–8). Fraction 8 (87.68 g) was applied to silica gel CC (CHCl_3 –MeOH– H_2O , 100:0:0–55:45:10) to yield a crude saponin mixture (44.03 g) from the eluate (CHCl_3 –MeOH– H_2O , 6:4:1). The saponin mixture was further purified by RP-18 CC (MeOH– H_2O , 75:25–90:10) to give fractions I–IV (2.29, 3.02, 4.34, 1.59 g). The fraction I was further purified by semi-preparative reversed phase HPLC (MeCN–MeOH– H_2O , 48:16:36, v/v/v) to afford saponin **1** (rt = 24.38 min) and saponin **2** (rt = 24.85 min).

Compound **1**: Amorphous powder $[\alpha]_{\text{D}}^{24} - 15.2$ (c 0.15, MeOH); UV (MeOH); λ_{max} : 203.2 nm; IR (KBr) ν_{max} 3421, 3210, 1720, 1679, 1401, 1207, 1135 cm^{-1} ; ESI-MS (positive ion mode): m/z 1339 $[\text{M} + \text{Na}]^+$; HRESI-MS m/z 1339.6302 $[\text{M} + \text{Na}]^+$ (calcd for $\text{C}_{64}\text{H}_{100}\text{O}_{28}$, 1316.6404); ^1H -, ^{13}C -NMR (pyridine-*d*₅, 600 MHz): Tables 33.1, 33.2.

Compound **2**: Amorphous powder $[\alpha]_{\text{D}}^{24} - 12.3$ (c 0.15, MeOH); UV (MeOH) λ_{max} : 203.4 nm; IR (KBr) ν_{max} 3375, 2924, 1675, 1460, 1206, 1135, 1044 cm^{-1} ; ESI-MS (positive ion mode): m/z 1309 $[\text{M} + \text{Na}]^+$; HRESI-MS m/z 1309.6181 $[\text{M} + \text{Na}]^+$ (calcd for $\text{C}_{63}\text{H}_{98}\text{O}_{27}$, 1286.6283); ^1H -, ^{13}C -NMR (pyridine-*d*₅, 600 MHz): Tables 33.1, 33.2.

98.2.4 Acid Hydrolysis of Saponins

The saponin mixture (30 mg) fraction from RP-18 column chromatography dissolved in 50 % aqueous dioxane (2 mL) and 1.5 N HCl (90 mL) was heated at 96 °C for 6 h. The reaction mixture was extracted twice CHCl_3 and evaporated to dryness. The aglycone (**1a**) was purified by silica gel CC (petroleum ether: EtOAc, 2:1) and detected by HPLC [column Zorbax SB-C18; 4.6 × 250 mm, solvent MeCN– H_2O (3:7–10:0) + 0.1 % TFA; flow rate 1 mL/min; detection wavelength 210 nm; rt = 43.18 min]. The water layer was dried and dissolved in pyridine. The solution was examined for sugars by paper chromatography [*n*-BuOH–HOAc– H_2O (4:1:5)] against standard samples as well as by GC after being converted to their trimethylsilylimidazole derivatives; conditions: [column 30QC2/AC-5 (30 m × 0.32 mm), column temperature; 180 °C/280 °C, temperature-programmed; 3 °C/min, sample temperature; 250 °C, carrier gas; N_2 , retention time D-Glc (18.398 min), L-Glc (18.873 min), D-Gal (19.009 min), L-Gal (19.665 min), D-Rha (15.849 min), L-Rha (14.950 min), D-Xyl (14.285 min), L-Xyl (14.939 min). From the new saponins, rhamnose was in the L-form, while glucuronic acid, glucose, galactose, and xylose were in the D-form.

Compound **1a**: Amorphous powder, $[\alpha]_{\text{D}}^{24} + 8.7$ (c 0.15, MeOH); UV (MeOH), λ_{max} : 207.8, 273.8 nm; IR (KBr) ν_{max} 3,442, 2,959, 2,927, 1,459, 1,385, 1,242,

Table 33.1 ^{13}C NMR data of compounds **1**, **1a** and **2**

Position	1δ	2δ	$1a\delta$	Position	1δ	2δ	$1a\delta$
1	39.3	39.3	38.5		Gal	Xyl	
2	27.1	27.1	26.6	1	100.7	100.8	
3	78.8	78.7	78.6	2	79.6	79.5	
4	37.5	37.3	38.6	3	73.7	78.9	
5	56.0	56.0	54.8	4	71.6	76.7	
6	19.2	19.2	18.5	5	75.8	78.7	
7	36.9	36.9	35.5	6	63.6	–	
8	40.2	40.2	40.8				
9	47.5	47.5	46.5	Glc-1	102.5	102.1	
10	37.0	36.9	36.8	2	76.2	76.2	
11	23.2	23.2	23.4	3	78.6	78.6	
12	124.9	124.9	125.9	4	72.7	72.7	
13	144.5	144.5	141.5	5	78.4	78.4	
14	47.3	47.3	47.1	6	63.7	63.7	
15	67.4	67.4	66.8				
16	73.4	73.4	72.5	Rha-1	102.8	102.5	
17	48.3	48.3	48.1	2	71.2	73.1	
18	39.6	39.6	39.7	3	72.5	73.2	
19	47.5	47.5	45.9	4	73.6	74.3	
20	37.5	37.5	35.6	5	69.8	70.5	
21	79.4	79.4	77.6	6	18.3	17.9	
22	73.5	73.5	72.5				
23	16.3	16.3	15.2		Ang (C-21)	Ang (C-21)	Ang (C-21)
24	27.1	27.1	27.8	1	168.8	167.2	169.1
25	16.3	16.3	15.2	2	129.5	128.2	127.1
26	17.9	17.9	17.6	3	137.3	138.6	138.3
27	20.1	20.3	20.5	4	16.3	16.3	15.2
28	62.6	62.6	62.3	5	21.4	18.8	19.8
29	21.9	21.9	19.4				
30	30.1	30.1	29.0		Ang (C-22)	Ang (C-22)	Ang (C-22)
				1	167.2	167.2	168.2
GlcA-1	105.2	105.1		2	128.2	128.2	127.6
2	81.9	81.9		3	138.6	138.6	139.5
3	76.9	76.9		4	16.3	15.3	15.2
4	76.4	76.3		5	21.4	18.8	19.8
5	78.6	78.5					
6	136.8	136.8					

Compound **1** and **2** δ , in $\text{C}_5\text{D}_5\text{N}$, 600 MHz; Compound **1a** δ , in $\text{C}_5\text{D}_5\text{N}$, 500 MHz

1,165, 1,074, 1,042 cm^{-1} ; ESI-MS (positive ion mode): m/z 693 $[\text{M} + \text{Na}]^+$; ESI-MS (negative ion mode): m/z 705 $[\text{M} + \text{Cl}]^-$; ^1H -, ^{13}C -NMR (pyridine- d_5 , 500 MHz): Tables 33.1, 33.2.

Table 33.2 ^1H NMR data compounds **1**, **2**, and **1a**

Position	1 δ	2 δ	1a δ	Position	1 δ	2 δ	1a δ
1	0.74 s	0.74 s	0.89 s		Gal (1 \rightarrow 2) GlcA	Xyl (1 \rightarrow 2) GlcA	
2	1.71 s	1.71 s	1.51 m	1	6.31 d (10.2)	6.17 d (6.5)	
3	6.67 dd	6.67 dd	3.10 m	2	4.61 s	4.61 s	
4	–	–	–	3	4.42 m	4.36 m	
5	0.71 s	0.71 s	0.67 m	4	4.46 s	4.66 s	
6	1.52 dd	1.52 dd	1.48 m	5	4.51 d	4.35 m	
7	2.08 s	2.08 s	1.57 s	6	4.72 m		
	2.13 dd	2.13 dd	1.65 s				
8	–	–	–				
9	1.65 m	1.65 m	1.48 m		Glc (1 \rightarrow 2) Gal	Glc (1 \rightarrow 2) Xyl	
10				1	5.88 d (6.8)	5.83 d (6.8)	
11	2.08 dd	2.08 dd	1.83 dd	2	4.09 t	4.09 t	
12	7.21 s	7.21 s	5.42 m	3	4.37 m	4.37 m	
13	–	–	–	4	3.99 m	3.99 m	
14	–	–	–	5	6.30 s	6.30 s	
15	4.21 m	4.21 m	3.62 dd	6	4.22 m	4.22 m	
16	3.99 s	3.99 s	3.66 s				
17	–	–	–		Rha (1 \rightarrow 4) GlcA	Rha (1 \rightarrow 4) GlcA	
18	1.29 s	1.29 s	1.29 s	1	6.17 brd (1.8)	6.05 brd (1.8)	
19	1.37 s	1.37 s	1.17 s	2	4.46 s	4.46 s	
	1.64 m	1.64 m					
20	–	–	–	3	4.66 m	4.66 m	
21	6.69 dd	6.69 dd	5.74 dd	4	4.22 s	4.22 s	
22	6.52 s	6.52 s	5.51 dd	5	6.13 s	6.13 s	
23	0.73 s	0.73 s	0.69 s	6	0.96 s	0.96 s	
24	1.06 s	1.06 s	0.89 s				
25	0.77 s	0.77 s	0.68 s		Ang (C-21)	Ang (C-21)	Ang (C-21)
26	0.97 s	0.97 s	0.90 s	1	–	–	–
27	1.28 s	1.28 s	1.29 s	2	–	–	–
28	4.23 s	4.23 s	2.87 s	3	5.80 m	5.80 m	5.98 m
			3.21 s				
29	1.28 s	1.28 s	0.90 s	4	1.95 d (6.8)	1.95 d (6.2)	1.83 s
30	1.07 s	1.07 s	0.82 s	5	1.29 s	1.29 s	1.30 s
Sugar	C-3	C-3					
	GlcA	GlcA			Ang (C-22)	Ang (C-22)	Ang (C-22)
1	4.84	4.84		1	–	–	–
	d (7.2)	d (7.2)					
2	4.81 s	4.81 s		2	–	–	–
3	4.29 s	4.29 s		3	5.96 m	5.96 m	5.98 m
4	4.67 s	4.67 s		4	1.95 d (6.8)	1.95 d (6.2)	1.83 s
5	4.38 m	4.38 m		5	1.29 s	1.29 s	1.30 m
6	7.58 s	7.58 s					

Compound **1** and **2** δ , in $\text{C}_5\text{D}_5\text{N}$, 600 MHz; Compound **1a** δ , in $\text{C}_5\text{D}_5\text{N}$, 500 MHz

98.3 Results and Discussion

The *n*-butanol fraction of the ethanolic extract of *S. superba* leaves was repeatedly chromatographed on Diaion HP20SS, silica gel and reversed phase silica gel (RP-18) columns together with semi-preparative reversed phase HPLC to afford two new triterpenoid saponins (**1**–**2**) (Fig. 33.1).

Part of the saponin mixture of **1** and **2** before purification was hydrolyzed by 1.5 N HCl to give compound **1a** as aglycone, and D-glucose, D-galactose, L-rhamnose, glucuronic acid and D-xylose as sugar moieties, suggesting that **1** and **2** were the glycosides of **1a**. Compound **1a** was a white amorphous powder, and showed positive Libermann–Burchard and Molish reactions, suggesting that **1a** might be a triterpenoid glycoside or a steroidal glycoside. ESI–MS (positive) of **1a** showed a quasi-molecular ion peak at m/z 693 $[M + Na]^+$. The ^{13}C NMR spectrum of **1a** showed characteristic signals for 40 carbons, including two isoprenyl groups [δ_C 127.1 (C-2'), 138.3 (C-3'), 127.6 (C-2''), 139.5 (C-3''), 15.2 (2C, C-4', C-4''), 19.8 (2C, C-5', C-5'')] and two ester carbonyl groups (δ_C 169.1 and 168.2), establishing two angeloyl groups by comparing with those in the literature [7–9], and an oleanane type triterpene with 30 carbons including seven methyls, five quaternary carbons, one double bond [δ_C 125.9 (C-12), 141.5 (C-13)] and six oxygen-bearing methines [δ_C 78.6 (C-3), 66.8 (C-15), 62.3 (C-16), 62.3 (C-28), 77.6 (C-21), 72.5 (C-22)] referring to the literature [10, 11]. In the HMBC spectrum of **1a**, correlations of H-21 and H-22 with the carbonyl carbon in two angeloyls were observed, respectively, indicating the two angeloyls located on C-21 and C-22 of the aglycone. Furthermore, ROESY correlations of H-21 and H-3, H-22 and H-29, H-15, H-16, and H-26, established the relative stereochemistry of each hydroxy group. The above evidences indicated that **1a** was a sapogenin of triterpenoid saponin, named as 21,22-di-*O*-angeloyl-R1-barrigenol [7] (Fig. 33.1(1a)).

Compound **1** was obtained as a white amorphous powder. HR-ESI-MS (positive) of **1** showed the quasi-molecular ion at m/z 1339.6302 $[M + Na]^+$ (calcd. For 1339.6302, $C_{64}H_{100}O_{28}Na$), establishing the molecular formula of **1** as $C_{64}H_{100}O_{28}$ combined with DEPT and ^{13}C NMR spectra. IR spectrum of **1** showed

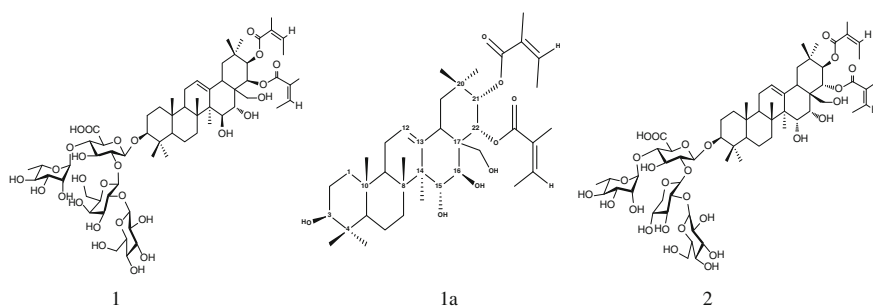


Fig. 33.1 Structures of compounds **1**, **1a** and **2**

characteristic signals for hydroxyl ($3,420\text{ cm}^{-1}$) and carbonyl ($1,720\text{ cm}^{-1}$). Comparison of the ^{13}C NMR spectra data of **1** with those of compound **1a**, suggested **1** to be the 3-*O*-glycoside of 21,22-di-*O*-angeloyl-R1-barrigenol (**1a**). The sugar moieties of **1** were characterized by use of 2D NMR experiments (HSQC, HSQC-TOCSY, and HMBC), as β -D-glucuronopyranosyl, β -D-galactopyranosyl, α -L-rhamnopyranosyl and β -D-glucopyranosyl moieties (anomeric H at δ 4.84 (d, $J = 7.2$ Hz), 6.31 (d, $J = 10.2$ Hz), 6.17 (brd, $J = 1.8$ Hz), 5.88 (d, $J = 6.8$ Hz), respectively). The HMBC correlations verified the sugar linkages of C-3 (δ 78.8) of the oleanolic acid residue with GlcA H-1 (δ 4.84), Rha H-1 (δ 6.17) with GlcA C-4 (δ 76.4), Gal H-1 (δ 6.31) with GlcA C-2 (δ 81.9), and Glc H-1 (δ 5.88) with Gal C-2 (δ 79.6). Therefore the structure of **1** was elucidated as 21,22-di-*O*-angeloyl-R1-barrigenol-3-*O*-{ β -D-glucopyranosyl-(1 \rightarrow 2)- β -D-galactopyranosyl-(1 \rightarrow 2)-[α -L-rhamnopyranosyl-(1 \rightarrow 4)]}- β -D-glucuronopyranoside (Fig. 33.1(1)).

Compound **2**, a white amorphous powder, showed the quasi-molecular ion at m/z 1309.6181 [M + Na] $^+$ (calcd. For 1309.6181, $\text{C}_{63}\text{H}_{98}\text{O}_{27}\text{Na}$) in the HR-ESI-MS (positive), establishing the molecular formula of **2** as $\text{C}_{63}\text{H}_{98}\text{O}_{27}$, combined with DEPT and ^{13}C NMR spectra. Comparison of the ^1H and ^{13}C NMR spectra data of **2** with those of Compound **1**, there were very similar characteristic signals except for the sugar moieties. The sugar moieties of **2** were characterized by analysis of NMR data obtained from the combined use of 2D NMR spectra (HSQC, HSQC-TOCSY, and HMBC). The data allowed identification of a β -D-xylopyranose unit with anomeric proton at δ 6.17 (d, $J = 6.5$ Hz). The remaining unit with the anomeric proton at δ 4.84 (d, $J = 7.2$ Hz), 6.05 (brd, $J = 1.8$ Hz), 5.83 (d, $J = 6.8$ Hz) were characterized as β -D-glucuronopyranosyl, α -L-rhamnopyranosyl, and β -D-glucopyranosyl units, respectively. The branched nature of the tetrasaccharide moiety at the C-3 position of the oleanane moiety was established from the HMBC correlations between C-3 (δ 78.7) and GlcA H-1 (δ 4.84), between Rha H-1 (δ 6.03) and GlcA C-4 (δ 76.3), between Xyl H-1 (δ 6.17) and GlcA C-2 (δ 81.9), and Glc H-1 (δ 5.83) and Xyl C-2 (δ 79.5). Thus, the structure of **2** was deduced to be 21,22-di-*O*-angeloyl-R1-barrigenol-3-*O*-{ β -D-glucopyranosyl-(1 \rightarrow 2)- β -D-xylopyranosyl-(1 \rightarrow 2)-[α -L-rhamnopyranosyl-(1 \rightarrow 4)]}- β -D-glucuronopyranoside (Fig. 33.1(2)).

To the best of our knowledge [12], the oleanane-type triterpenoid saponin bearing two angeloyls at C-21, C-22, and a branch of tetrasaccharide moiety (Rha, Cal, Glc, GlcA, or Rha, Xyl, Glc, GlcA) at C-3 is rarely found in the nature. Therefore, this is the first report on the presence of two triterpenoid saponins above.

Acknowledgments The authors are very grateful to Dr. Min Xu of Kunming Institute of Botany, Chinese Academy of Sciences, for her help in structure identification, Dr. Hongtao Zhu and Dr. Dong Wang of Kunming Institute of Botany, for their help in HPLC facility. This project was supported by National Natural Science Foundation of China (31060250) and the Natural Science Foundation of Jiangxi Province (2009GXN0029).

References

1. Zeng X, Ju J (2005) Molluscidal activity of the methanol extracts of 40 species of plants. *Plant Prot* 31:31–34
2. Deng ZY, Deng YC, Liu YH (2007) Antifeedant activities of the extracts from *Shima superba* against *Plutella xylostella* and *Pieris rapae*. *Pesticide* 46:854–856
3. Huo GH, Zhan WG, Chen MH (2008) Antifungal activities from *Schima superba* and *Camellia oleifera* of Theaceae against *Pyricularia oryzae*. *Acta Agric Univ Jiangxiensis* 30:48–52,72
4. Huo GH, Zhan WG, Fu RH et al (2010) In vitro antifungal activity of saponin extracts from *Schima superba* in combination with *Sapindus mukorossi* against *Pyricularia oryzae*. *Nat Prod Res Dev* 22:755–760
5. Xu W, Zhou GX, Dai Y et al (2010) Chemical constituents in stems of *Schima superba*. *Chin Tradit Herbal Drugs* 41(6):863–866
6. Xu W, Zhou GX, Yao XS (2010) Lignans from the stem of *Schima superba*. *Nat Prod Res Dev* 22(6):945–948
7. Aurada E, Jurenitsch J, Kubelka W (1984) Structure of triterpene-sapogenins of *Aesculus glabra*. *Planta Med* 50(5):391–394
8. Voutquenne L, Guinot P, Froissard C et al (2005) Haemolytic acylated triterpenoid saponins from *Harpullia austro-caledonica*. *Phytochemistry* 66:825–835
9. Fu HZ, Li CJ (2011) Potential anti-inflammatory constituents of the stems of *Gordonia chrysantra*. *J Nat Prod* 74(5):1066–1072
10. Chen CX, Ye HY, Shen YL et al (1997) The chemical constituents from *Schima wallichii*. *Acta Bot Yunnanica* 79(2):201–206
11. Chen WX, Wu D (1977) Studies on sapogenins from *Schima argentea*. *Acta Chim Sinica* 3(36):229–232
12. Zhang ZZ, Li SY, Lian XY (2010) An overview of genus *Aesculus*: ethnobotany, phytochemistry, and pharmacological activities. *Pharm Crops* 1:24–51

Chapter 99

Study on Extraction of Xylan from Bamboo Shoot Shell

Nengfu Yu, Nengliang Wu, Yu Wang and Yegou Tu

Abstract Using bamboo shoot shell as raw material, the experiment utilized the method of alkali extraction after bamboo shoot shell was pretreated. Effects of alkali concentration, extraction temperature, ratio of solid to liquid, and extraction time on yield of xylan were analyzed. The conditions of alkali extraction were: alkali concentration 5 %, ratio of solid to liquid 1:10 (g:mL), extraction time 3 h, extraction temperature 120 °C. The yield of xylan from bamboo shoot shell reached 24.77 %, which shows that bamboo shoot shell is a good raw material with the content of 35.08 % hemicellulose in it.

Keywords Bamboo shoot · Xylan · Bamboo shoot shell · Xylo-oligosaccharide

99.1 Introduction

Bamboo shoot shell (*Bambusa spp*) is one of traditional green vegetables in China. Since ancient times, it is regarded as “food treasures,” “delicacies in the dry frozen ground,” and “the first vegetarian products” [1]. As the bamboo forest and the high yield technology of bamboo forest improved, the fresh bamboo shoot production increased year by year. In 2006, the output of bamboo shoot were more than 5 million tons in China [2]. At present, the output of bamboo shoot in China

N. Yu (✉) · Y. Wang · Y. Tu
Jiangxi Academy of Forestry, Jiangxi 330013 Nanchang, People's Republic of China
e-mail: yunengfu@126.com

N. Wu
Agri-tech Service Station of Bajiang Township Yongfeng County Jiangxi Province, Ji'an
331500 Jiangxi, People's Republic of China

ranks first in the world. Because of short and focused shooting time, about 60 % of the bamboo shoot was produced to bamboo shoots and dried bamboo shoot as raw material. Bamboo shoot shell also known as bamboo sheath, is the bulk waste in the processing of bamboo shoot. In recent years, because the processing of bamboo shoot was weeping development, the bamboo shoot shell as waste piled up like a mountain on annual shooting season. Due to the high moisture content and very easy to decay, the fresh bamboo shoot shell becomes the main pollution source in the processing of bamboo shoot. It may bring hidden trouble to the ecological environment of the bamboo shoot producing area [3, 4]. In China, studying bamboo shoot shell as food is rare. It is mainly used to shoes, caps, and packaging. It is also made into bamboo shell silk, so it can be the raw materials of sofa and be made into straw sandals [5–7]. It reported that bamboo shoot shell can be made to feed [8]. But it did not form dimensions production. Or there were some problems in technology, product quality, and environmental pollution. Besides the economic benefits was indistinctive.

Xylan is a complex polysaccharide which is linked by β -1, 4 wood glycosidic linkage. And its main chain is D-xylose residues. Its main chain is connected to a variety of glucuronic acid, arabinose, acetyl, p-coumaric acid, ferulic acid, and other side chain substituent groups [9, 10]. We can get xylo-oligosaccharides (XOS) which is a kind of functional food through the degradation of xylan.

Due to its unique physicochemical properties and on bifidobacteria selective proliferation XOS is much attention in numerous functional food. XOS can be used as low-calorie food additives. It can also be used as humectant in food applications. It was added to baked goods to preserve moisture and change the rheological properties of dough. Another XOS can be widely used in medicine because it has a surface active site which can adsorb the toxic substances and pathogenic bacteria in human intestinal tract to increase body resistance to disease and activate the immune system. Because of difficult digestion, XOS can prevent and treat diarrhea and reduce the incidence of otitis media on early children. In addition, it is a good effect of feed additives [11–14]. But the raw materials for the preparation of XOS relatively lacked. It reported that corn cob, rice hulls, peanut shells, and cotton seed shell were materials for the preparation of XOS [15–18]. Bamboo shoot shell rich in hemicellulose whose main component is the multipentose, can be used to produce XOS [3, 4, 16, 19, 20]. In this study, the bamboo shoot shell is collected from Nanping City, Fujian Province. We got xylan by preparation of holocellulose and the alkali extraction method. In this paper, we analyzed different alkali concentration, temperature, solid–liquid ratio, and time on the yield of hemicellulose pentosan. That laid the foundation for the preparation of XOS, and provided the basic data support for the comprehensive utilization of bamboo shoot shell.

99.2 Experimental Methods

99.2.1 *Experimental Materials, Reagents, and Apparatus*

Experimental materials: Bamboo shoot shell collected from Pucheng County Nanping City, Fujian Province.

Reagents: sodium hydroxide, phenol, 3,5-dinitrosalicylic acid, anhydrous sodium sulfite, sulfuric acid, hydrochloric acid (All of above reagents were analytical grade.), industrial alcohol;

Instruments: biofuge stratos (Beckman), centrifuge (Thermo), UV/ visible spectrophotometer (Amersham Bioscience, Ultrospec 2100 pro).

99.2.2 *The Extraction of Xylan*

Xylan extraction range is roughly: alkali concentration is 1–10 %, temperature is 60–130 °C, time is 1–12 h.

99.2.3 *Determination of Total Sugar in Xylan*

We determined the total sugar content in xylan by 3,5-dinitrosalicylic acid (DNS) method.

99.2.3.1 *Preparation of Standard Curve by DNS Method*

Preparation of DNS reagent: 6.3 g DNS and 262 mL 2 mol/L sodium hydroxide solution were added to 500 mL hot aqueous solution containing 185 g sodium tartrate, then added 5 g sodium sulfite and 5 g crystalline phenol. After cooling, added 1000 mL distilled water. At last put them on a dark place to be saved for a week [16]. Standard xylose solution whose concentration was 1 mg/mL was compounded. The preparation of standard curve: Draw 0, 0.2, 0.4, 0.6, 0.8, 1.0, 1.2, 1.4, 1.6 mL 1 mg/mL standard xylose in 25 mL colorimetric tube which had plug. And added water to 2 mL. Then added 3 mL DNS reagent. Next put the colorimetric tubes in boiling water to heat for 5 min. Then rapid cool them with water. Next added boiled water to make the volume to 25 mL. At last determined their absorbance under the conditions of a wavelength of 480 nm by UV spectrophotometer. Drew standard curve according to the result. The regression equation is following.

$$y = 0.658x - 0.0336, R^2 = 0.9975 \quad (34.1)$$

99.2.3.2 Determination of Total Sugar in the Xylan

Added 8 % H_2SO_4 solution whose volume is as much as xylan solution in a certain volume of xylan solution, and remain constant temperature at 121 °C for 1 h. And then it was neutralized by 20 % NaOH solution to pH about 7. Added boiled water to make the sugar mass concentration in 0.2–2 g/L. Determined the reducing sugar concentration C (g/L) in neutralization liquid by the DNS method. Then the concentration of the total reducing sugar in the measured sample (C_T) is computed according to (34.2).

$$C_T = C \times \text{diluted multiples} \times 0.9 \quad (34.2)$$

99.2.4 Calculation of Xylan Yield

$$\begin{aligned} \text{Xylan ratio} = & \text{total quality of reducing sugar} / \text{quality of dry raw materials} \\ & \text{of xylan} \times 100 \% \end{aligned} \quad (34.3)$$

99.3 Results and Discussion

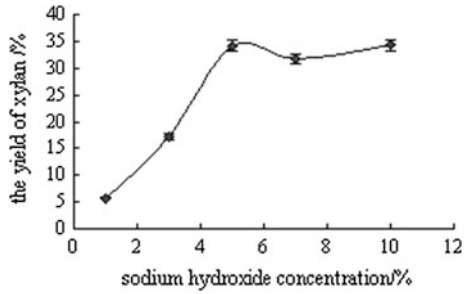
99.3.1 Different Extraction Conditions on the Yield of Xylan

Crushed bamboo shoot shell to powder whose size is 100 mesh. Took a certain amount of bamboo shoot shell powder in a flask. Then added sodium hydroxide solution whose solid–liquid ratio is 1:10 and the mass fraction is 5 % into the flask. After that, made the flask remain constant temperature at 80 °C for 3 h. Repeated the experiment for 3 times. So we can get the average value. Changing the conditions to investigate different factors on the yield of xylan.

99.3.1.1 The Effect of the Concentration of Alkali Solution

As you can see from Fig. 34.1 the yield of xylan increased with sodium hydroxide concentration increasing. However, when the mass fraction of sodium hydroxide is greater than 5 % the increase of xylan yield is not obvious. Considering getting rid of the alkali commodiously and cost control, we selected the mass fraction of 5 % of the alkali to extract xylan.

Fig. 34.1 Effect of alkali solution concentration



99.3.1.2 The Effect of Temperature

As can be seen from Fig. 34.2, the yield of xylan swell during 80–120 °C, peaking at 120 °C. As the temperature raised, the yield of xylan declined slightly before 80 °C, but after 120 °C it declined sharply. With the increase of temperature part of xylan may degrade into xylose, leading to the decrease in xylan content .

99.3.1.3 The Ratio of Solid to Liquid on the Yield of Xylan

We can see from Fig. 34.3 that shows the yield of xylan increased remarkably from 10.44 % at 1:5 to 19.96 % at 1:10. However the solid–liquid ratio increased the yield of xylan declined slightly. Therefore, the solid–liquid ratio was selected at 1:10.

99.3.1.4 The Impact of Soaking Time on the Yield of Xylan

It can be seen from Fig. 34.4 that the yield of xylan took place with an increasing number during 1–3 h. But after 3 h the yield of xylan raised at a slower rate. In order to save time and energy, we consider choosing the best time that is 3 h.

Fig. 34.2 The influence of temperature on yield of xylan

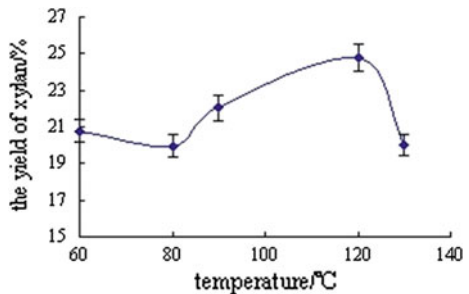


Fig. 34.3 The ratio of solid to liquid on the yield of xylan

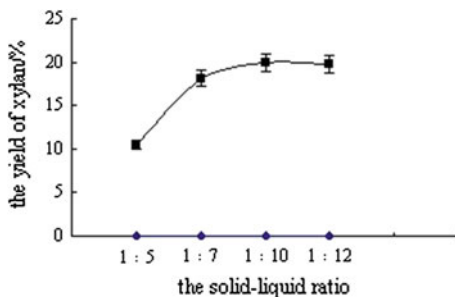
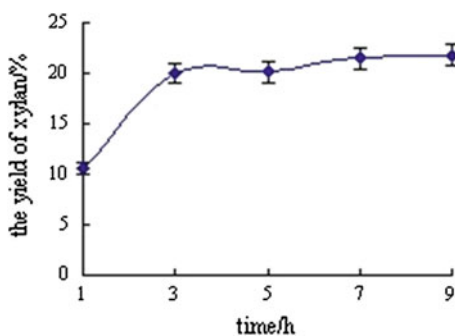


Fig. 34.4 The impact of soaking time on the yield of xylan



99.4 Conclusion

We select bamboo shoot shell as the raw material in this study, which shows that: bamboo shoot shell is a good raw material with the content of 35.08 % hemicellulose in it. The content of hemicellulose in the bamboo shoot shell is higher than that in raw rice husk, peanut shell, and cotton seed shell which were the raw material of current production of XOS. There was no difference between the content of hemicellulose in the bamboo shoot shell and corn cob [21]. Producing XOS by bamboo shoot shell has broad application prospect. The conditions of alkali extraction were : alkali concentration 5 %, ratio of solid to liquid 1:10 (g:mL),extraction time 3 h, extraction temperature 120 °C. The yield of xylan from bamboo shoot shell reached 24.77 %.

Acknowledgments The authors thank Jiangxi Science and Technology Support Programme (2011ZBBF6005) for funding.

References

1. Jianxian Z (1995) Functional food. China Light Industry Press, Beijing, pp 68–72
2. Weisu H, Boyi L (2008) Bamboo shoot deep processing technology status and trends. For Sci 44(8):118–123

3. Yanfang J, Weiyong S (2011) Chemical compositions and natural cellulose fiber characteristics of several bamboo shoot shells. *J Zhejiang Univ (Agric Life Sci)* 37(3):338–342
4. Yanfang J, Weiyong S (2011) Effects of different additive treatments on fermentation quality of bamboo shoot shell silage. *J Zhejiang Agric Sci* 2:341–343
5. Junyan Z (1991) Arts and crafts made of a bamboo shoot shell heap painting. China: 91106716.7
6. Songqiang Z (2003) Bamboo shell slippers. China: 02314598.6
7. Jiaqing H (2006) The production of bamboo shell insole. China: 200510006579.3
8. Xiaoqin W, Jianxin L (1999) Conservation and feeding value of bamboo shoot shell ensilaged with rice straw and wheat bran. *Chin J Anim Nutr* 11(1):53–55
9. Stephen AM (eds) (1985) The polysaccharides (Aspinall, G. O. ed.), Academic Press, Orlando, pp 98–193
10. Puls J and Poutanen K (eds) (1989) Enzyme systems for lignocellulose degradation (Coughlan, M. P. ed.), Elsevier Applied Science, Barking, England, pp 151–166
11. Huiliang W (2004) Chemical products production technology. Jiangxi, China
12. Xin Y (2004) Functional oligosaccharides production and application. Beijing, China
13. Alejandra M, Raimundo G-A, Rafael R (2005) Molecular and microbiological analysis of caecal microbiota in rats fed with diets supplemented either with prebiotics or probiotics. *Int J Food Microbio* 98(3):281–289
14. Cherie JZ, Glenn R (1998) An overview of probiotics, prebiotics and synbiotics in the functional food concept: perspectives and future strategies. *Int Dairy J* 8:473–479
15. Na S, Changhe D, Lite L (2007) Study on Production of xylooligosaccharides from corncob with steaming and enzymatic hydrolysis. *Food Ind* 5:1–4
16. Baoliang L, Guizhen F (2005) Study on extraction of xylan from rice hull. *Chem Ind For Prod* 25:121–124
17. Xiaoyan X, Fusheng C, Dongquan G, Chongbin J (2007) Enzymatic preparation of peanut shells XOS. *Food Ferment Ind* 33:118–120
18. Xinwei Z, Zhusheng L (2007) Research of isolation and purification of xylooligosaccharides from cotton seed husk. *Cereal and Oil Processing* 9:89–91
19. Weimin W, Guanmu Z, Gensheng L, Bingqi L, Zude H (1992) Comprehensive development and utilization of fresh bamboo shoot shell. *Prod Dev Guide* 1:12–13
20. Zhaoxiang Z, Jingxiang T, Chungen L et al (1991) Chemical compositions of bamboo shoot shel. *J Zhejiang For Univ* 8(1):54–59
21. Ruijin Y, Ying X, Zhang W et al (2000) The functional properties of the enzymatic production of XOS. *Chin Food Addit* 2:89–93

Chapter 100

Study on Preparation of Low Alcoholic Wine from Tomato

Kai-ye Deng and Er-na Li

Abstract Tomato is the most popular fruit in the world and the largest tomato growing field is in China. In the present study, tomato juice was used as raw material, which is available in the region were selected for wine production. The conditions for inoculums concentration, fermentation temperature, and initial sugar degree were optimized. The results showed that the tomato juices were similar to grape juice in terms of sugar and acidity. After fermentation, the ethanol concentration was 6–7 % w/v. Enzymatic hydrolysis and fermentation conditions were optimized for producing tomato low alcohol wine. The results demonstrated that the pectase amount 2 %, temperature 50 °C, and enzymolysis period 4 h, initial sugar content 15 %, inoculums size of yeast 5 %, temperature 22 °C, fermentation period 7 days, and clarified agents amount 5 mL. The alcohol content of tomato wine was 6–7 degrees with similar sugar content and acidity of the tomato juice. The product was clear, no precipitation, and in good flavor.

Keywords Food sensory evaluation · Optimization · Tomato · Wine production

100.1 Introduction

Grapes are the main raw materials that have been used for wine production for many years. A lot of research groups have investigated the suitability of fruits other than grapes like cajá [1], banana [2], pupunha [3], mango [4], acerola [5], cocoa, [6] and apple [7–9] for the purpose of wine-making.

Tomato belongs to the nightshade family. The plants typically grow up to 1–3 meters in height and have a weak stem that often sprawls over the ground and

K. Deng (✉) · E. Li
College of Light Industry and Food, Zhongkai University of Agriculture and Engineering,
Guangzhou 510225, People's Republic of China
e-mail: dengkaiye1968@126.com

vines over other plants. The tomato fruit is consumed in various ways, including raw, as an ingredient in considerable dishes and sauces, and in drinks. The fruit is rich in lycopene, which may have beneficial health effects [10].

Tomato has high nutrition and miraculous efficacy. Tomatoes are now eaten freely in the world, and their consumption is believed to benefit the heart, among other organs. Tomato is rich in Vitamin (A, B₁, B₂, C, and P), mineral elements (calcium, phosphor, iron, and zinc), amino acid, carotene, and lycopene, one of the most powerful natural antioxidants. In some studies, lycopene, especially in cooked tomatoes, has been found to help prevent prostate cancer and reduce the harmful effect on the skin by radiation or ultraviolet rays [11–17].

With the global market saw a steady rise in the strength of the wine, the reaction is proportional to the growth. Many consumers favor wines at 13 % or below and technology appears to be accommodative of these desires. In view of this, it was initiated to investigate the suitability of tomato fruit for low alcoholic wine production. The tomato alcohol wine keeps the nutrition value of tomato and has health function at the same time which tastes well and smells sweet. Therefore, it can be accepted by customers especially by the females. It is worthwhile to study the tomato low alcohol wine.

100.2 Materials and Methods

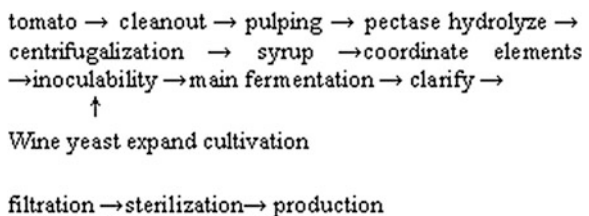
100.2.1 Materials

Fresh tomato and white sugar bought in the market; wine yeast zk-1 was screened and stored in biology lab in Zhongkai University.

100.2.2 Processing

See Fig. 100.1.

Fig. 100.1 Technological process of low wine from tomato



100.2.3 The Influence of Pectase on the Juice Yield

Powered composite complex pectase was used as main materials. Enzymolyzed conditions were determined through the studies of amounts, temperature, and the quantity of tomato juice [18–20].

100.2.4 Determination of Processing Conditions of Wine

100.2.4.1 Determination of Inoculums' Concentration

Different inoculums' concentrations, 2, 5, 10, and 15 %, were added in 100 mL tomato juice with 13 % sugar degree, pH = 3.5, fermented at 25 °C for 7 days, deployed and sensory evaluated, inoculums' concentration was determined.

100.2.4.2 Determination of Fermentation Temperature

Different temperatures, 20, 25, 30, 35 °C, were adopted to fermentation for 7 days with 13 % sugar degree, pH = 3.5, deployed and sensory evaluated, fermentation temperature was determined.

100.2.4.3 Determination of Initial Sugar Degree

Different initial sugar degrees, 5, 10, 15, 20 %, were adjusted in tomato juice, fermented at 25 °C for 7 days, deployed and sensory evaluated, initial sugar degree was determined.

100.2.4.4 Optimization of Fermentation Conditions

According to the above results, orthogonal experiment method was adopted to optimize the producing conditions. The best fermentation conditions can be determined.

100.2.5 Determination of the Dosage of Clarified Agent

Select gelatin as clarified agent. Gelatin was placed into cold water first, then heated in bath until the gelatin clarified, swelled, and then washed in cold water.

When 50 ml wine was mixed with 2–10 ml gelatin liquor in a graduated cylinder clarified gelatin was observed and the bulk of deposit measured to determine the dosage of the gelatin [21–23].

100.2.6 Quality Evaluation

100.2.6.1 Sensory Evaluation

Seven people were chosen to evaluate the quality of tomato low alcohol wine according to the standards in Table 100.1.

100.2.6.2 Examination of Physicochemical Characteristics and Microorganisms

Sugar degree, total acid, pH value, alcohol content, and the rate of juice yield were examined. Total number of bacteria, number of *Escherichia coli* and *Lactobacillus* were examined.

Table 100.1 Standards of sensory evaluation of tomato low-alcohol wine

Opinion	
Color (10 %)	With light yellow or yellow, limpid and clarify and bright, the score is 10
	With limpid and clarify, the brightness is slightly worse, the score is 8–9
	Slightly limpid and clarify, the brightness is worse, the score is 4–7
Smell (25 %)	Turbidity, without brightness, the score is 0–3
	With a full bodied faint scent, mellow and fragrant smell, the score is 25
	With faint scent, mellow and fragrant smell, the score is 22–24
Flavor (50 %)	With faint scent, slight mellow, the score is 19–21
	With smelly, the score is 0–5
	With sour and sweet taste, mellow and a soft aftertaste, the score is 50
	With faint scent, strange mellow and slightly freeze, the score is 44–45
Wine (15 %)	With slightly faint and bitter alcohol and maturity, the score is 35–44
	With faint, bitter and strange sour alcohol, the score is 25–34
	Gentle and fleshy wine, which has the special style of tomato alcohol that the score is 15
	Dissonancy wine, which have tomato alcohol style that the score is 12–14
	Slightly dissonancy wine, which sweet and soul out of place that the score is 5–11
	With strange sour, the score is 0–4

100.3 Results and Discussion

100.3.1 The Effect of Pectase on the Juice Yield

100.3.1.1 Determination of the Addition of Pectase

The addition of pectase was determined through the rate of juice yield. The effects of addition of the pectase and tomato juice yield (%) are shown in Fig. 100.2.

With the increase in addition of pectase, tomato juice yield also increased. Juice yield was 75.5 and 75.7 % when addition of pectase was 2 and 3 %, respectively. Considering the producing cost, 2 % addition of pectase was determined.

100.3.1.2 Determination of the Enzymolyzed Temperature

Temperatures of 40, 45, 50, and 55 °C were chosen to ferment tomato juice for 3 h with the addition of pectase 2 %. The effects of the enzymolyzed temperature and tomato juice yield (%) are shown in Fig. 100.3.

With the increase in fermentation temperature, tomato juice yield increased. Juice yield reached the peak when temperature was 50 °C, and then declined. So 50 °C was determined as fermentation temperature.

Fig. 100.2 The effect of the addition of the pectase on the rate of tomato juice yield

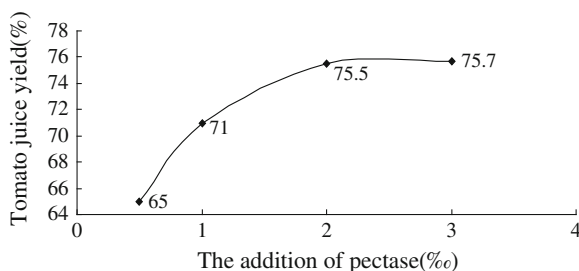


Fig. 100.3 The effect of the enzymolyzed temperature on the rate of tomato juice yield

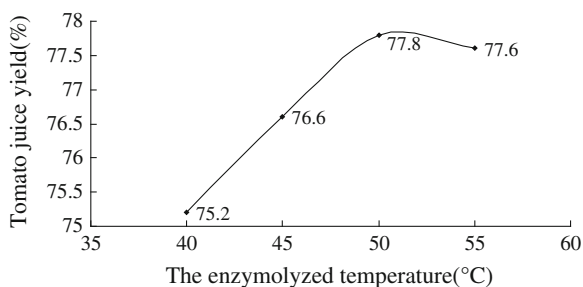
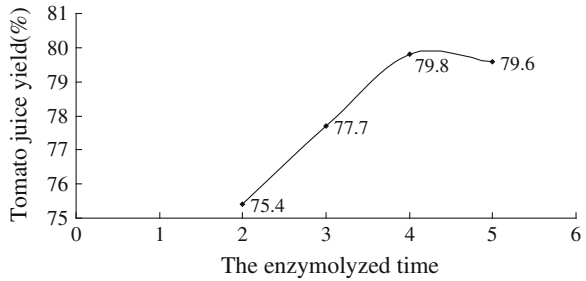


Fig. 100.4 The effect of the enzymolyzed time on the rate of tomato juice yield



100.3.1.3 Determination of the Enzymolyzed Time

Enzymolyzed times of 2, 3, 4, and 5 h were chosen to ferment tomato juice at 50 °C with the addition of pectase 2 %. The effects of the enzymolyzed time and the tomato juice yield (%) are shown in Fig. 100.4.

With the extended enzymolyzed time, tomato juice yield increased. Juice yield reached the peak when time was 4 h, and then declined. Therefore, 4 h was determined as fermentation period.

100.3.2 Optimization of Processing Conditions of Wine

100.3.2.1 Determination of Inoculums' Volume

Inoculums' volume has a significant impact on fermentation period and flavor of wine. Less inoculums' volume will lead to prolong fermentation period, however, more inoculums' volume make fermentation rate excessive against flavor formation.

The results in Table 100.2 showed that fermentation period and flavor of wine was better than the others when inoculums' volume was 5 %.

Table 100.2 Sensory evaluation of tomato low alcohol wine for inoculums' volume

Inoculum volume (%)	Flavor	Mouthfeel
2 %	With fruit flavor, not enough mellow	Less sour, a bit acerbity
5 %	With fruit flavor, have mellowed.	With sour and strong alcohol flavor
10 %	With fruit flavor, rather mellowed	A little sour and strong alcohol flavor
15 %	Not enough fruit flavor	Too sour

Table 100.3 Sensory evaluation of tomato low alcohol wine for temperature

Temperature (°C)	Flavor	Mouthfeel
20	With fruit flavor, not enough mellow	Weak taste and less sour
25	With fruit flavor and mellow	Sweet and sour moderate
30	With fruit flavor, too much mellow	Sweet and sour moderate, strong alcohol flavor
35	Not enough fruit flavor	Too sour

100.3.2.2 Determination of Fermentation Temperature

Temperature changes have profound effects upon tomato wine. Chemical reactions within yeast are facilitated by enzymes, which are large organic catalysts. Each enzyme has an “optimal temperature range”, a temperature range at which it performs best. For many enzymes, the optimal temperature range is to make the best wine.

The results in Table 100.3 showed that fermentation temperature at 20 °C with less flavor production and alcohol. It was at 35 °C fermentation rate was too quick, with sour in alcohol. So 25 °C was chosen as proper fermentation temperature.

100.3.2.3 Determination of Initial Sugar Degree

Most fruits contain sugars that will be fermented when combined with yeasts; sugars are the most common substrate of fermentation. Less sugar may make wine taste not so good, mouthfeel would be light. But too much sugar to make wine was so sweet. The optimal initial sugar degree is the most important factor to make a wine with good flavor.

The results in Table 100.4 showed that initial sugar degree at 10–15 % was better. Less or more initial sugar degree makes mouthfeel too light or too sweet.

100.3.2.4 Optimization of Fermentation Conditions of Low Alcoholic Wine

According to the initiative fermentation experiments, the different inoculum's volume, fermentation temperature and the initial sugar degree of liquor have the most effective taste on the flavor of wine, so the orthogonal test could be used to

Table 100.4 Sensory evaluation of tomato low alcohol wine for initial sugar degree

Initial sugar degree (%)	5	10	15	20
Mouthfeel	Too light	Just enough	Just enough	Too sweet

Table 100.5 Factor and level table of orthogonal test

Level factor			
	A Inoculums' volume (%)	B Fermentation temperature (°C)	C Initial sugar degree (%)
1	3	22	11
2	5	25	13
3	8	28	15

Table 100.6 Design and analysis of orthogonal test of fermentation conditions

No.	A Inoculums' volume (%)	B Fermentation temperature (°C)	C Initial sugar degree (%)	Opinion	Wine degree
1	1	1	1	83.00	5.0
2	1	2	2	82.75	7.3
3	1	3	3	83.00	5.5
4	2	1	2	83.75	6.5
5	2	2	3	83.25	7.5
6	2	3	1	84.00	4.5
7	3	1	3	85.25	6.5
8	3	2	1	81.25	4.6
9	3	3	2	81.38	6.5
K ₁	248.75	252.00	248.25		
K ₂	251.00	247.25	247.88		
K ₃	247.88	248.38	251.25		
\bar{K}_1	82.91	84.00	82.75		
\bar{K}_2	83.67	82.42	82.63		
\bar{K}_3	82.63	82.80	83.75		
R	1.04	1.58	1.21		
Factors lever	B > A > C				
The better lever	A ₂	B ₁	C ₃		

optimize the fermentation conditions according to the color, smell, flavor, and wine (Table 100.5).

Optimum conditions were optimized through orthogonal test, the sensory evaluation was as target, and the results were shown in Tables 100.6 and 100.7.

The results showed that the fermentation temperature could affect the quality of wine most. The initial sugar degree affected lightly. Optimum fermentation conditions were as follows: inoculums' volume 5 %; fermentation temperature 22 °C, and initial sugar degree 15 %. The conditions from the evaluations were inoculums' concentration 8 %, fermentation temperature 22 °C, and initial sugar degree 15 %. However, the two kinds of conditions were inconsistent, the results from optimized tests should be verified.

Table 100.7 Variance analysis for the experimental results of orthogonal array design

Variance source	Sum of square	Degree of freedom	Estimator of variance	F Value	Significance
A	1.728	2	0.864	6.14054*	F0.05(2, 8) = 5.14
B	4.105	2	2.053	7.46842*	F0.01(2, 8) = 10.92
C	2.645	2	1.322	8.81104*	
Total	8.48	6			

100.3.3 The Validation Experiment of the Orthogonal Test

Preparation of low alcoholic wine was fermented under the conditions as fermentation period 7 days, fermentation temperature 22 °C, pH 4.0, and initial sugar degree 15 %. The inoculums’ volume was 5 and 8 %.

From Table 100.8, the low alcoholic wine had the best color, taste when fermentation conditions were used as inoculums’ volume 5 %, fermentation temperature 22 °C, and initial sugar degree 15 %.

100.3.4 Clarification of Low Alcoholic Wine from Tomato

Gelatin was placed into cold water before using it. At this step, the impurity of gelatin would be removed when it sops up and swells.

Heat gelatin in water bath until it began to turn into a clear solution. The dosage of gelatin was determined by the kind of alcohol and gelatin.

Table 100.8 Analysis of proof test results

No.	Inoculums’ concentration (%)	Temperature (°C)	Initial sugar degree (%)	Wine degree (%)	Score
1	8	22	15	6.5	84.55
2	5	22	15	6.5	86.23

Table 100.9 The effect of dosage of gelatin low alcoholic wine

Gelatin (mL) in 50 mL wine	Clarify impaction
3	Wine admixture and the bulk with 8.5 mL deposit
4	Wine admixture white granular and the bulk with 8.5 mL deposit.
5	Wine is limpid and clarifies; the bulk of deposit was 17 mL deposit.
6	Wine admixture white granular with 5 mL deposit.
7	Wine is limpid and clarifies with 11 mL deposit.

When 50 mL wine was mixed with 3–7 mL gelatin liquor in a graduated cylinder, the degree of clarification was observed.

From Table 100.9, the gelatins' volume was 5 mL to clarify tomato wine because wine was clear and the volume of deposit was the largest.

100.3.5 The Qualitative Index of the Produce

Tomato alcohol wine was light yellow, clear, and with no deposition. Its flavor was full of tomato's special flavor and tastes well; meanwhile. The low alcoholic tomato wine with total acidity 7.0 g/L, alcohol degree 7 V %, number of colony 89/mL, *E. Coli* and pathogenic bacteria were not detected.

100.4 Conclusion

The rate of tomato juice yield could reach 80 % under the optimum conditions. The optimum enzymolysis conditions of low alcoholic tomato wine were amount of pectase 2 %, pH 4.0, and the enzymolyzed time was 4 h. The optimum fermentation conditions were fermentation time 7 days, temperature 22 °C, pH 4.0, initial sugar degree 15 %, amount of inoculums' volume 5 %, and volume of gelatin 5 mL. The sensory evaluation showed that tomato wine has new characteristics in smell and taste. Tomatoes are grown very widely as choicest fruits, but used in the preparation of wine still goes a long way. Once the production of tomato wine is successful for commercial use, it will be beneficial for tomato production all around the world.

References

1. Dias DR, Schwan RF, Lima LCO (2003) Metodologia para elaboração de fermentado de cajá (*Spondias mombin* L.). *Cienc Tecnol Alimentos* 23:342–350
2. Akubor PI, Obio SO, Nwodomere KA et al (2003) Production and quality evaluation of banana wine. *Plant Foods Hum Nutr* 58:1–6
3. Andrade JS, Pantoja L, Maeda RN (2003) Melhoria do rendimento do processo de obtenção da bebida alcoólica de pupunha (*Bactrisgasipaes* Kunth). *Cienc Tecnol Alimentos* 23:34–38
4. Reddy LVA, Reddy OVS (2005) Production and characterization of wine from mango fruit (*Mangifera indica* L.). *World J Microbiol Biotechnol* 21:1345–1350. doi:10.1007/s11274-005-4416-9
5. Santos CS, Almeida SS, Toledo AL et al (2005) Elaboração e análise sensorial do fermentado de acerola (*Malpighia puniceifolia* L.). *Braz J Food Technol* 10:47–50
6. Dias DR, Schwan RF, Freire ES, Serôdia RS (2007) Elaboration of a fruit wine from cocoa (*Theobroma cacao* L.). *Int J Food Sci Technol* 42:319–329. doi:10.1111/j.1365-2621.2006.01226.x

7. Joshi VK, Bhutani VP (1991a) The influence of enzymatic clarification in fermentation behavior and qualities of apple wine. *Science des Aliments* 11:491–498
8. Joshi VK, Bhutani VP, Sharma RC (1990) Effect of dilution and addition of nitrogen source in chemical, mineral and sensory qualities of wild apricot wine. *Am J Enol Vitic* 41:229–231
9. Joshi VK, Sandhu DK, Attri et al (1991) Cider preparation from apple juice concentrate and its consumer acceptability. *Indian J Hort* 48:321
10. Liu Z, Meng L, Jiang H (2005) Study on quality improvement of tomato juice beverage. *Food Sci* 07:149–151
11. Rao AV, Agarwal S (1998) Bioavailability and antioxidant properties of lycopene from tomato products. *Nutr Cancer* 31:199–203
12. Minhthy L Nguyen, Schwartz Steven J (1999) Lycopene: chemical and biological properties. *Food Technol* 02:38–43
13. Li Zhang, Zheng-jun Wang (2009) Lycopene health function review. *Chin Condiment* 09:98–100
14. Stahlw Siesh (1995) Vitamins E and C, β_2 carotene and other carotenoids as antioxidants. *Am J Clin Nutr* 62(6):1315–1321
15. Sharma SK, Mangeur ML (1996) Kinetics of lycopene degradation in tomato pulp solids under different processing and storage condition. *Food Res Int* 29:309–3151
16. Johnn Andrews (2006) Risk assessment for the carotenoids lutein and lycopene. *Regul Toxicol Pharm* 45(5):289–298
17. Nguyen ML, Schwartz SJ (1999) Lycopene: chemical and biological properties. *Food Technol* 2:38–43
18. Chen J, Kan J, Du M et al (2006) Pectinase preparation and its application in pulp's producing-juice and juice clarifying. *Chin Food Addit* 3:119–124
19. Wang W, Sun Y (2006) Pectinase and its application in fruit and vegetable juice processing. *Food Res Dev* 11:222–226
20. Joshi VK, Chauhan SK, Lal BB (1991) Extraction of juices from peaches, plums and apricots by pectinolytic treatment. *J Food Sci Technol* 28(1):64–65
21. Lin J, Wan Z, Guo Z et al (2012) Effects of multiple clarifiers on flavor of Shatangju wine. *Food Res Dev* 02:51–54
22. Wang Y, Zeng Q, Chen S et al (2009) Effects of different clarifiers on clarification of mulberry fruit wine. *J Storage Process* 04:52–54
23. Ni Z, Xiao Z, Niu Y et al (2012) Effects of three common clarificants on clarification of cherry wine. *J Food Ind* 01:25–28

Chapter 101

Effects of Glucose Assimilation on Lutein and Chlorophyll Biosyntheses in the Green Alga *Chlorella pyrenoidosa*

Tao Li, Yi-han Liu, Fu-ping Lu and Yue Jiang

Abstract Glucose assimilation caused a significant decrease of lutein and chlorophyll accumulation in *Chlorella pyrenoidosa* cultivated in low nitrogen medium, which are in line with the previously reported glucose-bleaching effect on the green alga *Chlorella protothecoides* cultivated in nitrogen deficient medium. Our study showed that an excessive lipid production induced by nitrogen deficiency was expected to be responsible for the decrease of lutein and chlorophyll accumulation in *C. pyrenoidosa* under heterotrophic conditions. When *C. pyrenoidosa* was cultivated in high nitrogen medium, the lutein and chlorophyll biosyntheses acted very differently: lutein content still decreased markedly whereas chlorophyll content remained stable. In addition, when we inhibited chlorophyll biosynthesis with levulinic acid, the chlorophyll a (chl a) and chlorophyll b (chl b) contents decreased markedly, but the lutein biosynthesis was not influenced at all. It was concluded that lutein and chlorophyll biosyntheses were possibly not coordinated in *C. pyrenoidosa* under heterotrophic conditions.

Keywords Lutein · Chlorophyll · *Chlorella pyrenoidosa* · Heterotrophic

T. Li
Basic Science Department, Tianjin Agricultural University, Tianjin 300384,
People's Republic of China

T. Li · Y. Jiang (✉)
Department of Biology and Kwong Living Trust Food Safety and Analysis Lab,
Hong Kong Baptist University, Kowloon Tong, Hong Kong,
People's Republic of China
e-mail: yjiang@hotmail.com.hk

Y. Liu · F. Lu
The College of Biotechnology, Tianjin University of Science and Technology,
Tianjin 300457, People's Republic of China

101.1 Introduction

Chlorella pyrenoidosa is a nonmotile, unicellular freshwater green alga [1]. It can grow not only under photoautotrophic conditions but also in darkness by making use of glucose as carbon and energy sources. Lutein, chlorophyll a (chl a), chlorophyll b (chl b), and other photosynthetic pigments can also be produced by *C. pyrenoidosa* under darkness [2–5].

In plant and green alga, lutein, and other carotenoids bind the light harvesting complexes which are located in the thylakoids membrane of chloroplast. So the biosynthesis of carotenoid must be coordinated with the formation of other photosynthetic components [6]. Chlorophyll and lutein biosyntheses are coordinated and regulated through the action of phytochrome and blue/UV receptors in plant and green alga under photoautotrophic conditions [7]. Besides, the presence of chlorophyll is prerequisite for the biosynthesis of carotenoid in the plastid of *Sinapis alba* [8]. So it was reported that the accumulation of carotenoids was inhibited when the chlorophyll biosynthesis was arrested in the green alga *Chlamydomonas* [9]. Other researchers even indicated that carotenoid biosynthesis was also under the control of factors which participated in the regulation of chlorophyll biosynthesis in tomato seedlings [10].

Soluble sugars have been proven as a negative regulator in the photosynthesis process [11]. So far plenty of studies focused on the repression of photosynthesis by carbohydrate have been reported [11–15]. However, little work has been conducted to study the effects of sugar assimilation on carotenoid biosynthesis in plant and green alga. The chlorophyll content decreased significantly in *Chlorella protothecoides* cultivated in low nitrogen medium under heterotrophic conditions [12]. This phenomenon was called “glucose-bleaching”. Moreover soluble carbohydrate was reported to repress the expression of genes involved in carotenoid biosynthetic pathway and limit the accumulation of carotenoid in tomato leaves [6]. But sucrose also showed the effect in stimulating carotenoid accumulation in tomato fruit pericarp discs [16].

In this study we investigated the influence of glucose assimilation on lutein and chlorophyll biosyntheses in *C. pyrenoidosa* under heterotrophic conditions. We also studied the relationship between lutein and chlorophyll biosyntheses in *C. pyrenoidosa* grown in the dark. Our study provided preliminary information for understanding the biosynthesis of photosynthetic pigments in *C. pyrenoidosa* under heterotrophic conditions.

101.2 Materials and Methods

101.2.1 Microalga and Culture Conditions

The algal strain *C. pyrenoidosa* was purchased from Carolina Biological Supply Co., Burlington, USA. The basic medium was the same as that used in the previous report and the potassium nitrate concentration is 1.25 g L^{-1} [3]. The heterotrophic

cultivation was realized by culturing the algal cells in the basic medium supplemented with 40 g L^{-1} glucose at $28 \text{ }^\circ\text{C}$ with orbital shaking at 180 rpm under darkness. For the cultivation of the algal cells in high nitrogen medium, the concentration of potassium nitrate was 8.25 g L^{-1} . The autotrophic cultivation was performed by incubating the algal cells in the basic medium under a light intensity of $100 \text{ } \mu\text{E m}^{-2} \text{ s}^{-1}$ produced by two fluorescent lamps with a 16:8 of light to dark photoperiod. The mixotrophic mode was the same as the autotrophic cultivation except for supplementing 40 g L^{-1} glucose in the medium. As to the inhibition experiment, the inhibitors were added into the culture after 48 h incubation. No inhibitor was added in the control.

101.2.2 Biomass and Pigments Analyses

For the biomass measurement, 5 mL culture was filtered through the pre-dried filter paper (Walkman) and the cell pellets were rinsed twice with deionized water. Then cell pellets were dried at $105 \text{ }^\circ\text{C}$ to a constant weight.

For the measurement of lutein content, the lyophilized cells were ground after freezing with liquid nitrogen. Extraction was carried out with acetone until the cell debris became colorless. $20 \text{ } \mu\text{L}$ of extract was separated on a Waters Spherisorb $5 \text{ } \mu\text{m}$ ODS $4.6 \times 250 \text{ mm}$ analytical column (Waters, Milford, MA, USA) following the previous method [17]. Individual carotenoids were identified by comparing their absorption spectra to those of standards (Sigma-Aldrich, USA). The concentration of pigment was calculated with corresponding standard curve.

101.2.3 Glucose Concentration Measurement

The concentration of residual glucose in the culture was measured by 3, 5-dinitrosalicylic acid (DNS) method [18].

101.2.4 Cell Composition Analysis

The lyophilized algal powder was resuspended in 1 M NaOH and then boiled for 10 min. The total protein concentration in the supernatant obtained after centrifuging the mixture at 3000 g for 5 min was quantified using the DC protein assay kit (Bio-Rad, USA) [19].

The cellular starch content was analyzed by following the method from other researchers [20]. Briefly, the algal powder was resuspended in 100 % ethanol and boiled for 30 min. Then the suspension was centrifuged at 3000 g for 5 min and the debris was dried. Afterwards the starch was extracted by boiling the cell debris

in 0.2 M NaOH for 30 min and the mixture was neutralized with 1 M acetic acid. Then the mixture was digested with amyloglucosidase at 37 °C over night. The starch level was calculated by measuring the glucose concentration in the supernatant by DNS method after centrifuging the digested mixture at 3000 g for 5 min.

The total lipids were assayed by following the reported method [21]. Briefly the lyophilized algal cells were resuspended in the extraction solution (chloroform:methanol = 2:1, by vol.) and disrupted with a Ultra-Turrax T25 homogenizer (IKA, Germany) at 20000 rpm. The extracted lipids dissolved in the chloroform phase were dried in a rotary evaporator and then weighed.

101.2.5 Transmission Electronic Microscope (TEM) Experiment

The ultrathin sections of algal cells were examined with a Philips EM 208S transmission electron microscope at 80 kV. The section images were obtained by a Gatan 794 Camera System (Gatan Inc., CA) [22].

101.2.6 Statistical Analysis

The data are expressed as averages \pm S.D. Statistical significance was evaluated by independent paired two sample *t*-test (OriginPro 7.0) when comparing two groups. $p < 0.01$ was considered as significant.

101.3 Results

101.3.1 Time Course of Lutein and Chlorophyll Accumulation in C. pyrenoidosa Cultivated in Low Nitrogen Medium

After comparing the cell dry weight under three cultivation modes, we found that glucose assimilation by *C. pyrenoidosa* was in favor of biomass production under both mixotrophic and heterotrophic conditions (Table 101.1). The cell dry weight achieved 16.2 g L⁻¹ after 120 h cultivation under heterotrophic conditions, four times as high as that obtained under autotrophic conditions. But light irradiation was more favorable for the accumulation of lutein and chlorophyll. The pigment contents in *C. pyrenoidosa* under autotrophic and mixotrophic conditions were much higher than that under heterotrophic conditions (Table 101.1). In addition, glucose assimilation by *C. pyrenoidosa* caused marked decrease of cellular lutein

Table 101.1 Cell growth and pigments content of *C. pyrenoidosa* under three cultivation modes

Mode	Biomass (g L ⁻¹)	Lutein (mg g ⁻¹)	Chl a (mg g ⁻¹)	Chl b (mg g ⁻¹)
Autotrophy	4.09 ± 0.07	13.9 ± 0.1	20.3 ± 0.07	14.49 ± 0.1
Mixotrophy	10.78 ± 0.11	5.16 ± 0.05	5.39 ± 0.22	3.87 ± 0.03
Heterotrophy	16.2 ± 0.05	1.47 ± 0.02	0.77 ± 0.02	1.07 ± 0.02

and chlorophyll contents (Figs. 101.1, 101.2). The cellular lutein content decreased by 36.6 and 39.6 % respectively during the period in which the algal cells assimilated glucose rapidly under heterotrophic and mixotrophic conditions. The cellular chlorophyll content also decreased by 61.5 and 60.5 % respectively under heterotrophic and mixotrophic conditions (Figs. 101.1, 101.2).

The transmission electronic microscope images show that the ultrastructure of *C. pyrenoidosa* cultivated under mixotrophic and heterotrophic conditions are different from those cultured under autotrophic conditions (Fig. 101.3a, b, and c). Compared with the autotrophic algal cell, the amount of C-shape chloroplast in the mixotrophically and heterotrophically cultivated cells were almost negligible, especially in the latter. Besides, large amounts of starch granules were present in the mixotrophic and heterotrophic cells. The lipid content in the mixotrophic and heterotrophic cells also increased sharply, especially in the latter in which the total lipid content reached as high as 43.7 % of cell dry weight (Table 101.2). Moreover, the algal culture became etiolated during the period when the glucose was assimilated rapidly by algal cells. This phenomenon called “glucose-bleaching” effect was also observed in *C. protothecoides* cultivated in nitrogen deficient medium [12]. So we investigated the influence of glucose assimilation on lutein and chlorophyll accumulation in *C. pyrenoidosa* cultured in nitrogen-enriched medium further.

101.3.2 Time Course of Lutein and Chlorophyll Accumulation in *C. pyrenoidosa* Cultivated in High Nitrogen Medium

Lutein and chlorophyll biosyntheses acted very differently when *C. pyrenoidosa* was cultured in high nitrogen medium under heterotrophic conditions (Fig. 101.4). The chlorophyll content remained stable, the chlorophyll a and b content obtained at 120 h decreased by 6.5 and 15.3 % compared with the value at 36 h (chl a, $p > 0.01$; chl b, $p > 0.01$). However, lutein content decreased significantly, by 38.9 % ($p < 0.01$).

As to the cell composition, the image of algal cell ultrastructure shows that plenty of starch granules still occupy large inner space in *C. pyrenoidosa* cultivated in high nitrogen medium under heterotrophic conditions (Fig. 101.3d). However the lipid production was greatly repressed, the lipid content decreased to 25.6 % of cell dry weight (Table 101.2).

Fig. 101.1 Glucose consumption and the pigments accumulation in *C. pyrenoidosa* cultivated in low nitrogen medium under mixotrophic conditions. Data points are expressed as averages \pm S.D. of triplicates (filled square chl a; open triangle chl b; open circle lutein; filled triangle glucose)

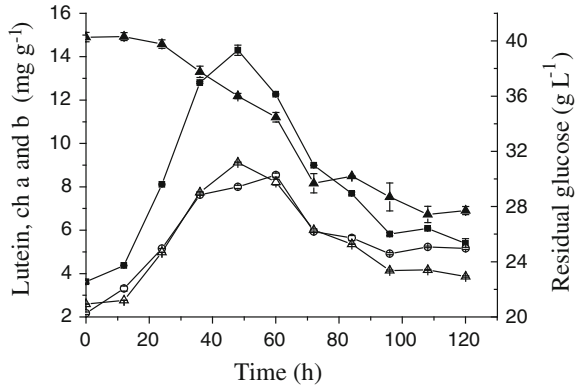
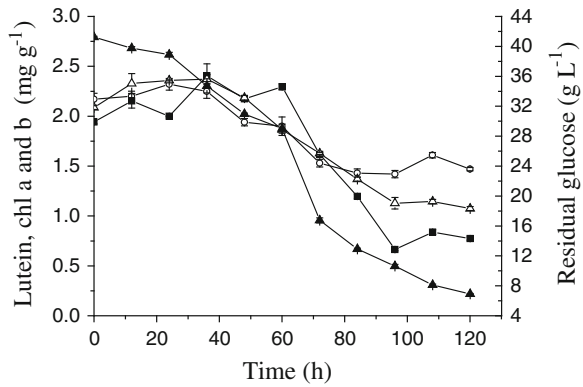


Fig. 101.2 Glucose consumption and the pigments accumulation in *C. pyrenoidosa* cultivated in low nitrogen medium under heterotrophic conditions. Data points are expressed as averages \pm S.D. of triplicates (filled square chl a; open triangle chl b; open circle lutein; filled triangle glucose)



Based on the results shown in Fig. 101.4, we thought that the biosynthesis of lutein and chlorophyll in *C. pyrenoidosa* under heterotrophic conditions were expected to be non-coordinated. So we conducted another experiment to validate the relationship between lutein and chlorophyll biosyntheses in *C. pyrenoidosa* under heterotrophic conditions.

101.3.3 Relationship Between Lutein and Chlorophyll Biosyntheses in *C. pyrenoidosa* Under Heterotrophic Conditions

Levulinic acid and fluridone has been proven to be effective inhibitors for chlorophyll and lutein biosynthesis respectively in green alga [25, 26]. In our work we used these two chemicals to regulate chlorophyll and lutein biosyntheses in *C. pyrenoidosa*.

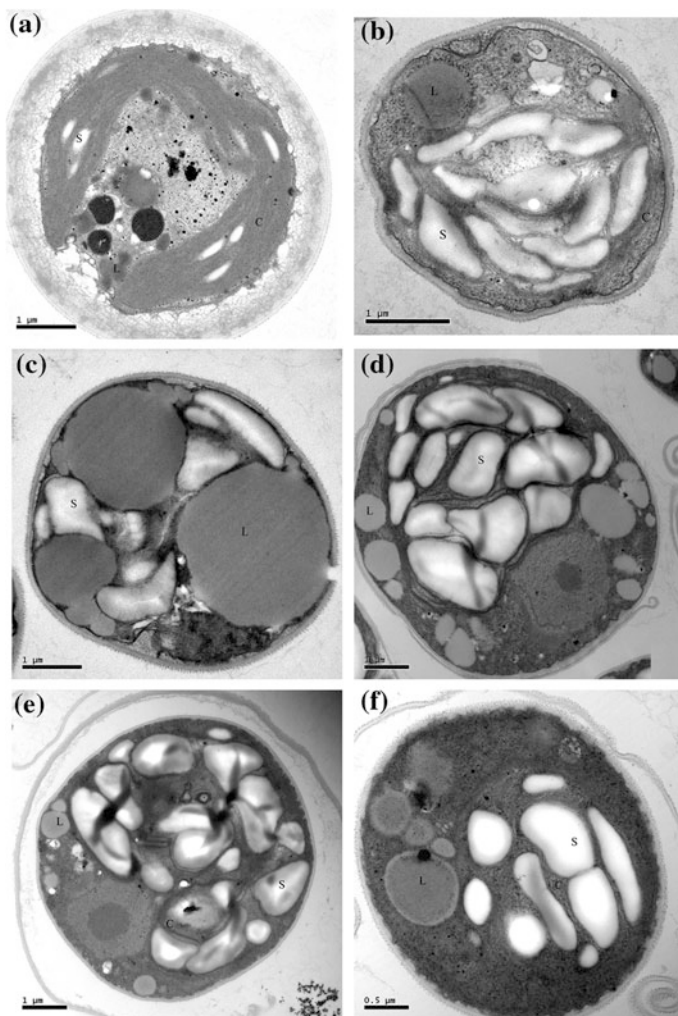
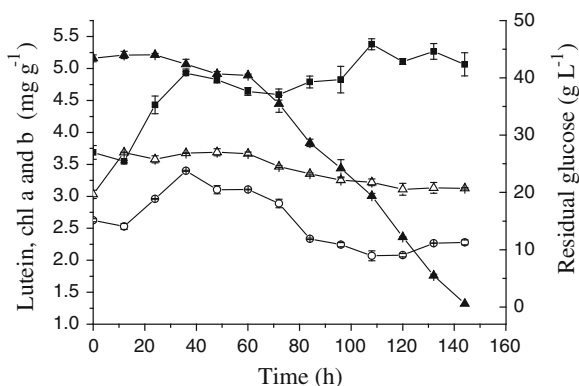
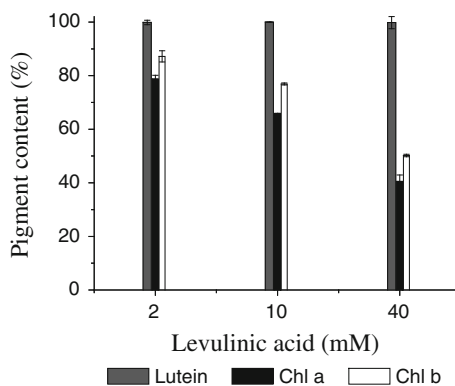


Fig. 101.3 Ultrastructure of *C. pyrenoidosa*. Algal cells used in this experiment were cultivated for 120 h. **a** Autotrophic cell cultivated in low nitrogen medium. **b** Mixotrophic cell cultivated in low nitrogen medium. **c** Heterotrophic cell cultivated in low nitrogen medium. **d** Heterotrophic cell cultivated in high nitrogen medium. **e** Heterotrophic cell treated with 40 mM levulinic acid. **f** Heterotrophic cell treated with $20 \mu\text{g mL}^{-1}$ fluridone. Cellular components: *C* chloroplast; *L* lipid body; *S* starch granule. The cellular components were identified according to the previous reports [23, 24]

Although chl a and b contents decreased markedly after inhibiting chlorophyll biosynthesis, especially for the treatment with high concentration of levulinic acid (40 mM), but the lutein content did not change at all compared with the control (Fig. 101.5), whereas, the inhibition of lutein biosynthesis also caused the decrease

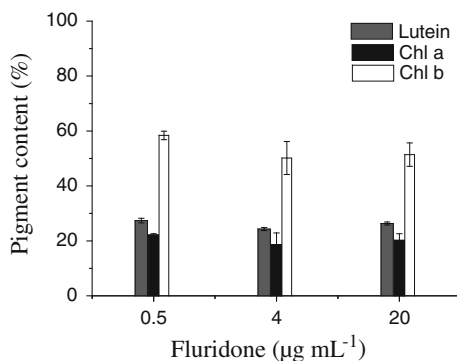
Table 101.2 Cell composition of *C. pyrenoidosa* cultivated in high and low nitrogen medium under heterotrophic conditions

Medium	Lipid (%)	Protein (%)	Starch (%)
Low nitrogen	43.7 ± 0.7	6.5 ± 0.1	44.3 ± 0.5
High nitrogen	25.6 ± 2.4	15.9 ± 0.5	48.8 ± 1.6

Fig. 101.4 Glucose consumption and the pigments accumulation in *C. pyrenoidosa* cultivated in high nitrogen medium under heterotrophic conditions. Data points are expressed as averages ±S.D. of triplicates (filled square chl a; open triangle chl b; open circle lutein; filled triangle glucose)**Fig. 101.5** Changes of lutein and chlorophyll contents in *C. pyrenoidosa* under heterotrophic conditions after inhibiting chlorophyll biosynthesis with levulinic acid. Content (%) of lutein and chlorophyll respect to the control in which no levulinic acid was added. Data are expressed as averages ±S.D. of triplicates

of chlorophyll content. The contents of cellular lutein, chlorophyll a and b decreased by 73.7, 79.8, and 48.6 %, respectively when treating *C. pyrenoidosa* with 20 $\mu\text{g mL}^{-1}$ of fluridone (Fig. 101.6). The decrease of cellular lutein and chlorophyll contents after treatment with fluridone also caused the change of algal cell ultrastructure (Fig. 101.3f). The amount of filamentous chloroplast in fluridone treated algal cell decreased markedly compared with untreated *C. pyrenoidosa* (Fig. 101.4d). But for levulinic acid treated algal cell, the ultrastructure did not show big difference with that of untreated *C. pyrenoidosa* (Fig. 101.3d, e).

Fig. 101.6 Changes of lutein and chlorophyll contents in *C. pyrenoidosa* under heterotrophic conditions after inhibiting lutein biosynthesis with fluridone. Content (%) of lutein and chlorophyll respect to the control in which no fluridone was added. Data are expressed as averages \pm S.D. of triplicates



101.4 Discussion

101.4.1 Effects of Glucose Assimilation on Lutein and Chlorophyll Accumulation in *C. pyrenoidosa* Cultivated in Low Nitrogen Medium

Sugars have been reported to repress the biosynthesis of chlorophyll and photosynthesis efficiency, limit the development of photosynthesis apparatus [27]. In this study, large amounts of C-shape chloroplast disappeared when *C. pyrenoidosa* was cultivated in the medium containing glucose. Assimilation of glucose by *C. pyrenoidosa* cultivated in low nitrogen medium accompanied with a profound decrease of cellular lutein and chlorophyll contents under both heterotrophic and mixotrophic conditions. Our results were consistent with the reported “glucose-bleaching” phenomenon that was thought to be caused by the metabolites produced in the “glucose respiration” process [12].

In our study we found that the lipid content in *C. pyrenoidosa* cultivated in low nitrogen medium was much higher than that cultured under high nitrogen conditions, but the protein content was much lower. Besides, the images of the algal cell ultrastructure show that small amounts of filamentous chloroplasts which can be observed in *C. pyrenoidosa* cultivated in high nitrogen medium was almost negligible under low nitrogen conditions. But the starch content had no obvious change. Other researchers have shown the evidence that sugars repressed the expression of photosynthetic genes [11]. The content of D1 protein of PS II reaction center decreased significantly when the leaf was incubated in the medium supplied with glucose [15]. Moreover, the decrease of D1 protein caused breakdown of light harvesting complex II and decrease of chlorophyll content. In green alga, the organic carbon source is mainly converted into proteins, lipid, and carbohydrate [28]. Based on our experiment results and the previous reports we proposed that more carbon flux channeled to lipid biosynthetic pathway when *C. pyrenoidosa* was cultivated in low nitrogen medium compared with the normal

conditions (high nitrogen conditions). As a result, the protein production decreased and accordingly an aggravated negative influence of glucose assimilation on the chloroplast development took place. Because of this, the content of chlorophyll, which is a required component of chloroplast protein complexes, decreased markedly and the glucose bleaching occurred. So we think that an enhanced lipid production induced by low nitrogen is expected to be responsible for the occurrence of “glucose-bleaching” in the green alga *C. pyrenoidosa*. In tomato leaves the decrease of carotenoids caused by sugar accumulation was related to the reduction of chlorophyll content [6]. In our study, we found that lutein and chlorophyll biosyntheses were not coordinated in *C. pyrenoidosa* under heterotrophic conditions. Lutein accumulation was not affected after inhibiting chlorophyll biosynthesis. So the decrease of lutein accumulation is expected to be nonrelated to the reduction of chlorophyll content in *C. pyrenoidosa* cultivated in low nitrogen medium under heterotrophic conditions.

101.4.2 Effects of Glucose Assimilation on Lutein and Chlorophyll Accumulation in C. pyrenoidosa Cultivated in High Nitrogen Medium

The etiolated *C. protothecoides* cultured in low nitrogen medium turned green after being transferred into the high nitrogen medium [29]. In our experiment, marked decrease of chlorophyll content was also not observed any more when *C. pyrenoidosa* was cultivated in high nitrogen medium. But lutein content still decreased significantly during the period in which *C. pyrenoidosa* consumed glucose rapidly.

In photoautotrophic plant cells, chlorophyll and lutein are required components of light harvesting complexes of photosystems. So their biosyntheses are coordinated and regulated by light through phytochrome receptors [7, 30]. Besides, factors which participate in the regulation of chlorophyll biosynthesis are also likely to control the accumulation of carotenoid [11]. The pool of free carotenoids depended on the amounts of chlorophyll in *S. alba* [8]. The content of carotenoids in tomato seedlings decreased after inhibiting chlorophyll biosynthesis with gabaculine [10]. However, the chloroplast was not the energy supplier any more in green alga grown in the dark and our results showed that lutein and chlorophyll biosyntheses were not coordinated in *C. pyrenoidosa* under heterotrophic conditions. When we inhibited chlorophyll biosynthesis, the lutein accumulation was not influenced at all. However, when we blocked lutein biosynthesis with fluridone, the chlorophyll content also decreased markedly. So it is expected that the biosynthesis of chlorophyll is controlled by the accumulation of lutein which drains the pool of chlorophyll by complex formation in *C. pyrenoidosa* under heterotrophic conditions.

101.5 Conclusion

In conclusion, we demonstrate that an excessive lipid production is likely to be responsible for the occurrence of glucose bleaching on *C. pyrenoidosa* cultivated in low nitrogen medium under heterotrophic conditions. Glucose assimilation leads to a significant decrease of lutein accumulation in *C. pyrenoidosa*. Lutein and chlorophyll biosyntheses are expected not to be coordinated in *C. pyrenoidosa* under heterotrophic conditions.

Acknowledgments The research was supported by Research Grant Council of Hong Kong SAR. The TEM experiment was conducted in EM unit of the University of Hong Kong. We would like to thank for their assistance.

References

1. Bold HC, Wynne MJ (1984) Introduction to the algae, 2nd edn. Prentice-Hall, New Jersey
2. Chen F (1996) High cell density culture of microalgae in heterotrophic growth. Trends Biotechnol 14:421–426
3. Shi XM, Chen F, Yuan JP, Chen H (1997) Heterotrophic production of lutein by selected *Chlorella* strains. J Appl Phycol 9:445–450
4. Lee YK (2001) Microalgal mass culture systems and methods: their limitation and potential. J Appl Phycol 13:307–315
5. Wu ZY, Shi XM (2006) Optimization for high-density cultivation of heterotrophic *Chlorella* based on a hybrid neural network model. Lett Appl Microbiol 44:13–18
6. Mortain-Bertrand A, Stammitti L, Telef N et al (2008) Effects of exogenous glucose on carotenoid accumulation in tomato leaves. Physiol Plant 134:246–256
7. Mohr H, Schopfer P (1995) Plant physiology. Springer, Berlin
8. Frosch S, Mohr H (1980) Analysis of light-controlled accumulation of carotenoids in mustard (*Sinapis alba* L.) seedlings. Planta 148:279–286
9. Plumley FG, Schmidt GW (1995) Light-harvesting chlorophyll a/b complexes: interdependent pigment synthesis and protein assembly. Plant Cell 7:689–704
10. Corona V, Aracri B, Kosturkova G et al (1996) Regulation of a carotenoid biosynthesis gene promoter during plant development. Plant J 9:505–512
11. Gibson SI (2005) Control of plant development and gene expression by sugar signaling. Curr Opin Plant Biol 8:93–102
12. Matsuka M, Hase E (1965) Metabolism of glucose in the process of “glucose-bleaching” of *Chlorella protothecoides*. Plant Cell Physiol 6:721–741
13. Schäffer C, Simper H, Hofmann B (1992) Glucose feeding results in coordinated changes of chlorophyll content, ribulose-1,5-bisphosphate carboxylase-oxygenase activity and photosynthetic potential in photoautotrophic suspension cultured cells of *Chenopodium rubrum*. Plant Cell Environ 15:343–350
14. Krapp A, Hofmann B, Schäfer C, Stitt M (1993) Regulation of the expression of *rbcS* and other photosynthetic genes by carbohydrates: a mechanism for the ‘sink regulation’ of photosynthesis. Plant J 3:817–828
15. Kilb B, Wietoska H, Godde D (1996) Changes in the expression of photosynthetic genes precede loss of photosynthetic activities and chlorophyll when glucose is supplied to mature spinach leaves. Plant S 115:225–235

16. Telef N, Stammitti-Bert L, Mortain-Bertrand A et al (2006) Sucrose deficiency delays lycopene accumulation in tomato fruit pericarp discs. *Plant Mol Biol* 62:453–469
17. Baroli I, Do AD, Yamane T, Niyogi KK (2003) Zeaxanthin accumulation in the absence of a functional xanthophyll cycle protects *Chlamydomonas reinhardtii* from photooxidative stress. *Plant Cell* 15:992–1008
18. Miller GL (1959) Use of dinitrosalicylic acid reagent for determination of reducing sugar. *Anal Biochem* 31:426–429
19. Illman AM, Scragg AH, Shales SW (2000) Increase in *Chlorella* strains calorific values when grown in low nitrogen medium. *Enzyme Microb Technol* 27:631–635
20. Izumo A, Fujiwara S, Oyama Y et al (2007) Physicochemical properties of starch in *Chlorella* change depending on the CO₂ concentration during growth: comparison of structure and properties of pyrenoid and stroma starch. *Plant S* 172:1138–1147
21. Christie WW (2003) Lipid analysis: isolation, separation, identification, and structural analysis of lipids. Oily Press, Bridgwater
22. Yamada T, Sakaguchi K (1982) Electron microscopic studies of *Chlorella ellipsoidea* protoplast formation. *J Gen Appl Microbiol* 128:1319–1327
23. Pino Plumed M, Villarejo A, Róos A et al (1996) The CO₂-concentrating mechanism in a starchless mutant of the green unicellular alga *Chlorella pyrenoidosa*. *Planta* 200:28–31
24. Libessart N, Maddelein ML, Koornhuysen N et al (1995) Storage, photosynthesis, and growth: the conditional nature of mutations affecting starch synthesis and structure in *Chlamydomonas*. *Plant Cell* 7:1117–1127
25. Samuel IB (1971) Studies on the biosynthesis and metabolism of δ -Aminolevulinic acid in *Chlorella*. *Plant Physiol* 48:316–319
26. Patricia EG, John EM (1986) Inhibition of carotenoid accumulation and abscisic acid biosynthesis in fluridone-treated dark-grown barley. *Eur J Biochem* 160:117–121
27. Pego JV, Kortstee AJ, Huijser C, Smeekens SCM (2000) Photosynthesis, sugars and the regulation of gene expression. *J Exp Bot* 51:407–416
28. Li YT, Han DX, Hu GR, Sommerfeld M, Hu Q (2010) Inhibition of starch synthesis results in overproduction of lipids in *Chlamydomonas reinhardtii*. *Biotechnol Bioeng* 107:258–268
29. Aoki S, Hase E (1964) De- and re-generation of chloroplasts in the cells of *Chlorella protothecoides* I. Synthesis of nucleic acids and protein in relation to the process of regeneration of chloroplast. *Plant Cell Physiol* 5:473–484
30. Von Lintig J, Welsch R, Bonk M et al (1997) Light-dependent regulation of carotenoid biosynthesis occurs at the level of phytoene synthase expression and is mediated by phtochrome in *Sinapis alba* and *Arabidopsis thaliana* seedlings. *Plant J* 12:625–634

Chapter 102

RNA Interference and Applications in Plants

Yunrong An, Zhongyou Pei, Nan Xin and Haifeng Wang

Abstract RNA interference (RNAi) inhibits gene expression in a very specific way. It has a vital significance in the regulation of gene expression, the defense of viral infection, the controlling of jumping genes. In recent years, RNAi has become an important method of studying gene function with its high specificity, efficiency, heritability and other significant advantages and has been used in the study of functional genomics and traits improvement. This paper simply introduces the RNAi mechanism and discusses the applications of RNAi in plant functional genomics, crop quality improvement, and resistance of disease and insect.

Keywords Crop quality improvement · Disease and insect resistance · Functional genomics · RNA interference

102.1 Introduction

RNA interference (RNAi) is a new technology of studying genetic function. It has gradually become one of the useful tools in studying molecular biology and cell biology since 1990s. Now, RNAi has been widely used in the research of plant functional genomics and plants traits improvement. RNA is the sequence-specific gene silencing induced by double-stranded RNA, which means that RNAi provides

Fund project: project supporting by science and technology in Tianjin, sweet sorghum polymer molecular breeding (10ZCKFNC00100).

Y. An · Z. Pei (✉) · N. Xin · H. Wang
Department of Agronomy, Tianjin Agricultural University, Tianjin 300384, People's
Republic of China
e-mail: peizhy@126.com

a rapid mean of depleting mRNAs by introducing double-stranded RNA. The double-stranded RNA could degrade its homologous mRNA in intracellular, thus inhibit the expression of corresponding gene specifically and efficiently to get the effect “gene knockout.” RNAi is a common phenomenon in organisms, initially found in some plants, and then in nematodes, flies, zebrafish, and mammalian cells. It has shown its great prospects in functional analysis of genes in animal and plant, crop quality improvement as a new gene blocking technology. It is an important protection mechanism for organisms against external infection. Therefore, RNAi was awarded as one of the important achievements in 2001 by Science, and as one of the major scientific and technological achievements in 2002 by Nature. This paper has reviewed the function mechanism of RNAi and its application in plant.

102.2 Mechanism of RNAi

In 1995, Guo and Kemphues found that the introduction of sense or antisense RNA to par-1 mRNA resulted in degradation of the par-1 message RNA in *Caenorhabditis elegans* in the experiment [1], which challenged the traditional explanation of antisense RNA, because antisense was one of the most attractive means of eliminating gene expression at that time. In 1998, Fire and Xu found that mRNA of target genes degrades when they introduce double-stranded RNA (dsRNA) into cells [2], proving that highly purified dsRNA could effectively and specifically block the corresponding gene expression, and at least two orders of magnitude higher than single-strand RNA in efficiency. It reveals the phenomenon Guo and Kemphues met for the first time, namely, RNAi. Hereto, as a regulation mechanism of gene expression, it gradually revealed its mysterious veil, opened a new field for life science research.

The mechanism of RNAi, as an important research method, has a rapid development. At present, what has been widely recognized is that dsRNA will be processed into the 21–23 nucleotide small interfering RNAs (siRNAs) by a particular enzyme called Dicer (Dicer enzyme belongs to RNase III family), and could identify double-stranded RNA specifically, cut double-stranded RNA which is exogenously imported, transgenic, or virus-infected. In 1999, Hamilton and Baulcombe proved that siRNAs are the key mediators in RNAi [3]. In 2001, Bernstein completed the cloning of Dicer—the RNase III-like enzyme [4]. These siRNAs were incorporated into a nuclease complex labeled the RNA-induced silencing complex (RISC). The activated RISC targets and cleaves mRNA which is complementary to the siRNA, thus make the specific gene which corresponds to the mRNA transcriptional silence [5]. From then on, RNAi mechanism research gradually goes to mature.

102.3 The Application of RNAi in Plant Research

102.3.1 *The Application of RNAi in Plant Functional Genomics Research*

As the mechanism of RNAi gradually matures, RNAi has been widely used in the plant functional genomics research. In the research, RNAi can be used as a powerful tool because RNAi has a highly sequence specificity. It could make the specific gene silence, and lose its function or reduce its expression in order to validate its function. In 2000, in the flower development research, Chuang further verified the function of known functional genes, including AG, CLV3, AP1, PAN by RNAi [6], and pioneered in the application of RNAi in plant functional genomics. In 2004, Padmanaban found two VHA-C genes by RNAi, which supply V-ATPase to cell by active exocytosis, supporting the growth of amplified cells in arabidopsis. It has showed that they are necessary to the growth of arabidopsis cells [7]. In 2005, Moritoh silenced OsGEN-L gene by RNAi, leading to the development of rice early microspore inhibited and pollen difficultly mature [8]. It has showed that it has a close relationship between OsGEN-L gene and the formation of rice pollen. In 2006, Travella successfully inhibited target gene in constructing the transgenic crops of sextuploid wheat by PDS-RNAi and EIN1-RNAi. He thought that RNAi was a good tool in the research of function lack mutations of polyploid plants [9]. In 2009, Li amplified two gene fragments using the CP gene of Y virus in potatoes as template, and then inserted plant expression vector pROK II. Therefore, he established RNAi express carrier pROKY300 that targeted the CP gene of PVY and then turned it into agro bacterium tumefactions EHA105. The result showed that the instantaneous expression of hairpin RNA interfered effectively the PVY infection [10]. In 2011, Zibu constructed the RNAi expression carrier of starch branch enzyme gene *sbe2b* in grain endosperm and turned it into tobacco to detect its influence to the amylose synthesis. The result showed that the expression of *sbe2b* gene was lower than the control. The content of chain starch changed significantly, and amylose content increased than the control but no significant change [11].

102.3.2 *The Applications of RNAi in Crop Quality Improvement*

Although production problem is the most important goal in traditional breeding, people has given more and more attention on improving crop nutrition value. RNAi not only shows its superiority on the expansion of scope in the operated gene, but also on the controllability of the expression of target genes. Researchers have improved plant phenotype and crop quality by using RNAi. It has been a

great success. In 2002, Liu increased the proportion of stearic acid and oleic acid in the cottonseed oil by inhibiting the expression of two critical fatty acids desaturase genes. He raised the stearic acid content from 2–3 to 40 % and the oleic acid content from 15 to 77 % respectively. He got the plant which could raise stearic acid and oleic acid content at the same time by hybridizing the offspring [12]. In 2003, Ogita inhibited the expression of CaMXMT1 gene which could code theobromine synthase in coffee plants. It has made theobromine content decreased 30–80 % and caffeine content decreased 50–70 %, which reduced the stimulation caffeine to sensitive people [13]. In 2004, Tang knocked out 22 kDa maize storage protein gene (a protein of low lysine content) by RNAi and got a mutation plant of high lysine content [14]. In 2004, Fukusaki inhibited the expression of key enzymes—CHS gene, which is necessary to biosynthesis of flower pigments and flavonoid. He successfully changed the original color, blue, to white and pink and created new commodity flowers [15]. In 2007, Chen suppressed the expression of endogenous ACO gene in tomato by RNAi and made the production of ethylene reduced greatly. It has provided reference for extending the shelf life of fruits and vegetables [16]. In 2007, Wan increased the content of lycopene greatly in tomato's fruit by RNAi, which provides references for improving the nutritional value of tomato [17].

102.3.3 The Application of RNAi in Plant Diseases and Insects Resistance

RNAi has been used widely in the study of plant diseases resistance. In 1984, Lichtenstein silenced genes, *iaam*, *ipt*, in *arabidopsis*, and tomato by RNAi. These two genes could cause many perennial fruits, nuts, and appreciation plants getting root cancer. By doing this, these plants could successfully resist root cancer [18–20]. In 1998, Waterhouse first reported the successful application of RNAi in preventing and controlling of potato virus Y [21]. In 1999, Pinto induced gene silence by introducing the enzyme which is needed for copying Rice yellow mottle virus into rice. It has made the plants resisted RYMV [22]. In 2000, Wang successfully got the plant that could resist Barley yell dwarf virus (BYDV) by RNAi [23]. In 2002, Kalantidis successfully got the plant that could resist Cucumber mosaic virus (CMV) by RNAi [24]. In addition, in 2005, Ida proved that RNAi-induced resistance of Beet necrotic yellow vein virus (BNYVV) was more effective in the leaves than in the root [25, 26].

RNAi has also successfully used in agricultural insect control. Researchers used transgenic plants, engineering bacterium, and direct feeding to make insect intake dsRNA to suppress the growth. In 2007, Mao successfully reduced mRNA level of the body cytochrome P450 in tobacco and *arabidopsis* by RNAi [27]. The growth of larvae has been inhibited after being fed two transgenic plants. In 2009, Bautista inhibited the expression of the pigment p450 gene, CYP6BG1, which is highly

expressed in the body of diamondback moth [28]. When diamondback moth that resisted to the synthesis of pyrethrum ester is fed dsRNA solution which made it very sensitive to pyrethroid pesticides.

102.3.4 The Application of RNAi in Plant Male Sterility

Male sterility is a common phenomenon in life activity of higher plants, and has a great application value in agriculture. Many researchers controlled gene expression of plant flowering, studied plant male sterility, and fertility restoration by RNAi. In 2000, Chuang proved genes about flowering development in *Arabidopsis* by RNAi and got the male sterility mutations of stable heredity [6]. In 2005, Cigan directly silenced the promoter MS45 of maize pollen sac gene, inhibiting the formation of pollen sac and forming the male sterility plant. The maize could restore fertility by using different promoter to make the promoter MS45 expressed again [29]. In the same year, Moritoh observed rice plants of OSGEN-L-RNA and found that part of it have a very low sterility and part of it are male sterility, so found the rice male sterility materials [8].

102.4 Prospects

RNAi, as a convenient and practical genome research method, has been widely used in all areas of biological research and made many important achievements. Using RNAi to reveal the inherent law and molecular basis of plant development or make the harmful genes silenced, it has important significance for speeding up the application of molecular breeding technology in crop breeding, selecting different varieties of breeding materials. However, RNAi also has its deficiencies. First of all, they will be interfered by RNAi at the same time if several genes have the same or similar sequence. Therefore, which genes could be interfered cannot be determined. Scientists have not made breakthrough although they have done a lot of work in this respect. Second, the application of RNAi in the study of improving quantitative traits controlled by micro effect gene was little. Even if the function gene is knocked out, the effect is too little. It is hard to find phenotype change because its genetic effects are weak. Finally, since the same or similar genetic background of the polyploid species between different chromosome set, there are also certain difficulties in studying and applying polyploid function genome by RNAi. With the continuous development of technology and method, it will play a significant role on gene function, plant development, traits improvement, and other fields. People will break new ground in the biology research and application and bring greater social value.

References

1. Guo S, Kempthues KJ (1995) Par-1, a gene required for establishing polarity in *C. elegans* embryos, encodes a putative Ser/Thr kinase that is asymmetrically distributed. *Cell* 81(4):611–620
2. Fire A, Xu S, Montgomery MK (1998) Potent and specific genetic interference by double stranded RNA in *Caenorhabditis elegans*. *Nature* 391:806–811
3. Hamilton AJ, Baulcombe DC (1999) A species of small antisense RNA in post-transcriptional gene silencing in plants. *Science* 286:950–952
4. Bernstein E, Caudy A, Hammond SM, Hannon GJ (2001) Role for a bidentate ribonuclease in the initiation step of RNA interference. *Nature* 409:363–366
5. Kim VN (2003) RNA interference in functional genomics and medicine. *Korean Med. Sci.* 18:309–318
6. Chuang C, Meyerowitz EM (2000) Specific and heritable genetic interference by double stranded RNA in *Arabidopsis thaliana*. *Proc Natl Acad Sci USA* 97(9):4985–4990
7. Padmanaban S, Lin XY, Perera I (2004) Differential expression of vacuolar H⁺ 2ATPase subunit c genes in tissues active in membrane trafficking and their roles in plant growth as revealed by RNAi. *Plant Physiol* 134:113
8. Moritoh S, Miki D, Akiyama M (2005) RNAi mediated silencing of OsGEN-L (OsGEN-like), a new member of the RAD-XPG nuclease family, causes male sterility by defect of microspore development in rice. *Plant Cell Physiol* 46:699–715
9. Travella S, Klimm TE, Keller B (2006) RNA interference-based gene silencing as an efficient tool for functional genomics in hexaploid bread wheat. *Plant Physiol* 142:6–20
10. Li Q, Tao G, Qiu Y (2009) RNAi vector construction of potato Y virus gene CP and determination of interference effect. *Genom Appl Biol* 28(3):460–464
11. Zibu W, Qi J (2011) Construction of the RNAi vector and expression of starch branch enzyme gene in wheat grain endosperm. *mol. Plant Breed* 9(4):438–442
12. Liu Q, Singh SP, Green AG (2002) High-stearic and high-oleic Cotton seed oils produced by hairpin RNA-mediated post-transcriptional gene silencing. *Plant Physiol* 129(4):1732–1743
13. Ogita S, Uefuji H, Yube Y (2003) Producing decaffeinated coffee plants. *Nature* 423(19):823
14. Tang G, Galili G (2004) Using RNAi to improve plant nutritional value: from mechanism to application. *Trends Biotechnol* 22(9):463–469
15. Fukusaki E, Kawasaki K, Kajiyama S et al (2004) Flower color modulations of *Torenia hybrida* by down regulation of chalcone synthase genes with RNA interference. *J Biotechnol* 111(3):229–240
16. Chen Y, Li H (2007) The cloning of tomatos ACO gene and inhibition of its RNAi to release ethylene. *J Agri Biotechnol* 15(3):464–468
17. Wan Q, Zhang X, Song M (2007) RNAi specific mediated gene Lcy silenced to increase the content of lycopenein tomatoes. *J Biol Eng* 23(3):429–433
18. Lichtenstein C, Klee H, Montoya A (1984) Nucleotide sequence and transcript mapping of the gene of the pTiANC octopine Ti-plasmid: a bacterial gene involved in plant tumori genesis. *J Mol Appl Genet* 2:354–362
19. Ooms G, Hooykaas PJ, Moolenaar G (1981) Crown gall plant tumors of abnormal morphology, induced by *Agro bacterium tumefaciens* carrying mutated octopine Ti plasmids; analysis of T2 DNA functions. *Gene* 14:33–50
20. Depicker A, van Montagu M, Schell J (1978) Homologous DNA sequences in different Tip lasmids are essential for oncogenicity. *Nature* 275:150–153
21. Waterhouse PM, Graham MW, Wang MB (1998) Virus resistance and gene silencing in plants can be induced by simultaneous expression of sense and antisense RNA. *Proc Natl Acad Sci USA* 95(23):13959–13964
22. Pinto YM, Kok RA, Baulcombe DC (1999) Resistance to rice yellow mottle virus (RYMV) in cultivated African rice varieties containing RYMV transgenes. *Nat Biotechnol* 17:702–707

23. Wang MB, Abbott DC, Waterhouse PM (2000) A single copy of a virus-derived transgene encoding hairpin RNA gives immunity to barley yellow dwarf virus. *Mol Plant Pathol* 1(6):3472356
24. Kalantidis K, Psaradakis S, Tabler M (2002) The occurrence of CMV2 specific short RNAs in transgenic tobacco expressing virus derived double-stranded RNA is indicative of resistance to the virus. *MPMI* 15(8):8262833
25. Tenlado F, Dlaz- Ruffz JR (2001) Double- stranded RNA- mediated interference with plant virus infection. *J Virol* 75(24):12288–12297
26. Andika IB, Kondo H, Tamada T (2005) Evidence that RNA silencing-mediated resistance to Beet necrotic yellow vein virus is less effective in roots than in leaves. *MPMI* 18(3):194–204
27. Mao YB, Cai WJ, Wang JW (2007) Silencing a cotton boll worm P450 monooxygenase gene by plant-mediated RNAi impairs larval tolerance of gossypol. *Nat Biotechnol* 25:1307–1313
28. Bautista M, Tanaka T (2009) RNA interference mediated knockdown of a cytochrome P450, CYP6BG1, from the diamondback moth, *Plutella xylostella*, reduces larval resistance to permethrin. *Insect Biochem Mol Biol* 39:38–46
29. Cigan AM, Unger Wallace E, Collet H (2005) Source transcriptional gene silencing as a tool for uncovering gene function in maize. *Plant J* 43:929–940

Chapter 103

Isolation, Identification and Degradation Characteristics of Three Thick Oil Degrading Bacteria Strains

Chan Tian, Shengyan Tian, Xianbin Liu and Lulu Qin

Abstract In order to find the microbe suited to microbial enhanced oil recovery (MEOR), three bacterial strains DS1, DS2, and DS3 with excellent degrading effect on thick oil were isolated from the thick oil and water reservoir of oil well 51-82# in Erlian Oil Field. The three bacteria were identified as *Acinetobacter* sp., *Enterococcus* sp. and *Brevibacterium* sp. through 16S rDNA sequence similarity search. Viscosity reducing experiment was conducted using thick oil with a viscosity of 1746 mPa·s (50 °C) from Erlian Oil Field as the substrate with the three isolated bacterium alone and their consortium. The viscosity reduced 49.1, 46.6, and 49.0 % by DS1, DS2, and DS3, respectively, during 7 days degradation experiment. However, the reduction rate of viscosity reached 57.0 % with the consortium, which was significantly higher than that of single strain. It demonstrated that viscosity reduced effect was better with the consortium of the three isolated bacteria. The consortium can be applied in MEOR.

Keywords Bacteria · MEOR · Thick oil · Viscosity reducing · 16S rDNA

103.1 Introduction

In contemporary society, energy issue should not be underestimated. The oil has gone deep into all aspects of life as the most important energy substance in modern society. So the oil exploration has become the key of energy issues. Only 5–50 % of the crude oil can be mined by primary and secondary exploitation, and the remaining two-third of the crude oil will be exploited by tertiary oil recovery [1, 2]. At present tertiary oil recovery technology mainly includes heat

C. Tian · S. Tian · X. Liu (✉) · L. Qin

Tianjin Key Laboratory of Marine Resources and Chemistry, Tianjin University of Science and Technology, Tianjin 300457, People's Republic of China

e-mail: lxb0688@tust.edu.cn

flooding, steam flooding, chemical flooding, and microbial enhanced oil recovery (MEOR) [3]. Microbe can metabolize the long-chain saturated hydrocarbons in crude oil to be shorter hydrocarbons, and can produce surfactants, organic acids, and carbon dioxide. The surface tension of crude oil was reduced, the flow properties of crude oil was improved after microbial action [4–6]. Compared to the other tertiary oil recovery, MEOR is a green mining technology with the advantage of low cost, less energy consumption, and minimal damage to the stratum [7]. Usually there is a relatively stable microbial community in the reservoir, which was mostly injected by water. Some of them (Archaea) adapt to the poor strata through self-regulation and can use the limited nutrition in the formation to grow slowly which were there before the reservoir developed [5, 8]. In recent years, the researches of MEOR are increasing, MEOR has become one of the fastest development technology to enhanced oil recovery and it has achieved initial success in field test both at home and abroad [9–13]. In order to find the microbe suited to MEOR, three bacterial strains with excellent degrading effect on thick oil were isolated from the thick oil and water reservoir of oil well 51-82# in Erlian Oil Field. Their identification and degradation characteristics were researched.

103.2 Materials and Methods

103.2.1 Reagent and Medium

The thick oil were collected in 51–82# oil well of Erlian Oil Field which has a density of 0.9078 g/cm^3 ($20 \text{ }^\circ\text{C}$) and a viscosity of $1746 \text{ mPa}\cdot\text{s}$ ($50 \text{ }^\circ\text{C}$).

The medium for enrichment contained the following, in grams per liter of water: yeast extract, 3; K_2HPO_4 , 10; $(\text{NH}_4)_2\text{SO}_4$, 1; KH_2PO_4 , 4; MgSO_4 , 0.25; NaCl, 5; pH 7.2, sterilized at $121 \text{ }^\circ\text{C}$ for 15 min.

LB medium contained the following, in grams per liter of water: peptone, 10; yeast extract, 5; NaCl, 10; pH 7.2, sterilized at $121 \text{ }^\circ\text{C}$ for 15 min.

103.2.2 Enrichment of Thick Oil Degrading Bacterial Consortia

The thick oil was used as the sole carbon to enrich thick oil degrading bacteria strains from water reservoir of oil well 59-82# in Erlian Oil Field. A portion of 10 g thick oil was transferred to a 250 mL conical flask containing 50 mL medium and 50 mL water reservoir. The flasks were shaken on a thermostat incubator at $40 \text{ }^\circ\text{C}$ at a speed of 100 rpm. After 7 days, an aliquot of 5 mL supernatant was then transferred into a 150 mL conical flask containing 50 mL medium and 5 g thick oil. The flasks were shaken on a thermostat incubator at $40 \text{ }^\circ\text{C}$ at a speed of 100 rpm for 7 days. This step was repeated once to attain a thick oil degrading enriched consortium.

103.2.3 Isolation and Identification of Bacterial Strains

At the end of the enrichment, bacterial strains in each consortium were isolated by spreading the 10-fold serial diluted consortium on agar plates coated with LB medium. Bacterial colonies producing clear zones were scored positive and picked up from the plates, further purified by repetitive streaking on nutrient agar plates. The isolated strains were then identified by Gram's stain, scanning electron microscope and 16S rDNA gene sequence.

The total DNA was extracted by kit after pure cultures of bacteria in LB medium. The bacterial 16S rDNA gene fragment was amplified in a 50 μ L reaction containing 25 μ L Mix, 10 μ L of each primer (27F: 5'-AGA GTT TGA TCA TGG CTC AG-3'; 1492R: 5'-CTA CGG TTA CCT TGT TAC GAC-3'), 2 μ L template DNA, and 21 μ L distilled water. The PCR was performed in a thermocycler with the thermal profile: initial denaturing 4 min at 94 °C, followed by 30 cycles of denaturing (94 °C for 1 min); annealing (55 °C for 1 min) and elongation (72 °C for 2 min). The purifying and sequencing of 16S rDNA sequence was finished by BGI Beijing. DNA sequence of the cloned 16S rDNA fragments was compared using BLASTN at <http://www.ncbi.nlm.nih.gov/BLAST/> maintained by National Center of Biotechnology Information (NCBI). The clone sequences were aligned and phylogenetic trees were constructed by the neighbor-joining method with the Molecular Evolutionary Genetics Analysis (MEGA) software and Cluster X.

103.2.4 Biodegradation of Thick Oil by Enriched Consortia and Bacterial Isolates

To start the biodegradation experiment, 2 mL aliquot of the enriched bacterial consortium or single bacterial isolated reaching the late exponential growth phase was aseptically inoculated into 40 mL enrichment medium containing 40 g thick oil, at an initial concentration of 50 g/L. Enrichment medium containing the same amount of thick oil but without any microbial inoculum was used as the control to determine abiotic losses of thick oil. Triplicate flasks were prepared for each enriched consortium and the control. The flasks were shaken in the same way as described above. After 7 days, they were measured by Brookfield viscometer.

103.3 Results and Discussion

103.3.1 Isolation of Strains and Phenotypic Characteristics

In the medium containing thick oil as the sole carbon source, few bacterial colonies were able to grow and resulted in the formation of clear zones. In this study, we focused on three bacterial strains named DS1, DS2, and DS3 which produced

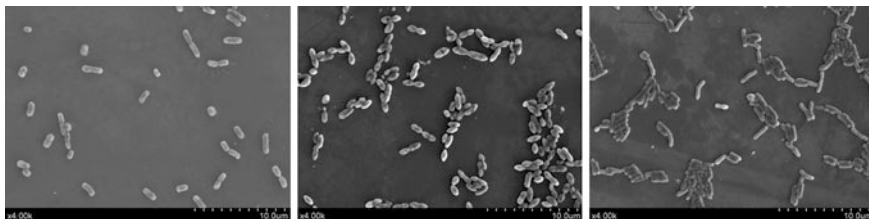


Fig. 103.1 SEM photos of DS1, DS2, and DS3

the largest clear zones on the agar plates. By repeated picking up and dilution of the colony of three strains, pure cultures of these strains were successfully obtained. Microscopic examination of the three strains (DS1: gram-negative, DS2: gram-positive, and DS3: gram-positive) revealed the presence of short bacillus cells, short cocci cells, and short bacillus cells. Cells of strains were nonmotile and shaped $0.6\text{--}0.8 \times 1.2\text{--}1.6 \mu\text{m}$, $0.6\text{--}0.8 \times 1.0\text{--}1.2 \mu\text{m}$, $0.4\text{--}0.6 \times 1.2\text{--}1.4 \mu\text{m}$ cell diameter (Fig. 103.1). Microscopic examination did not reveal any evidence of spores or of swimming motility.

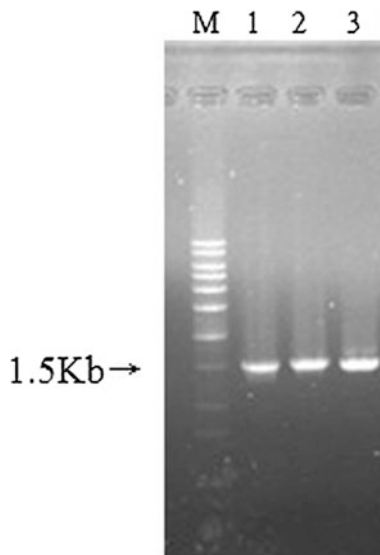
103.3.2 Genotypic Characterization of the Isolated Strains

The taxonomic position of the bacteria has, however, not been known with certainty. We solved this problem by PCR amplification, and subsequent sequencing of the 16S rDNA genes directly from the isolated bacteria. Genomic DNA of three isolates were extracted and used as DNA template for PCR amplification. The single amplified DNA fragments of approximately $\pm 1,500$ bp size were generated as shown in Fig. 103.2. It was accord with the amplification interval in template DNA between the two 16S rDNA primers. It was showed that the amplification products have a high concentration by the clear bandings in electrophoretic test. So the sequencing reaction could be continued.

The three strains were identified on the basis of their 16S rDNA homologies with entries in the GenBank databases. Experimental results showed that three isolated microorganisms were able to grow on thick oil as the sole carbon source. The three isolated strains were named DS1, DS2, and DS3 prior to further analysis for genotypic characteristics using 16S rDNA technique. When examined by BLAST similarity analysis, DS1, DS2, and DS3 were determined to be *Acinetobacter* sp., *Enterococcus* sp. and *Brevibacterium* sp. by the strains which have a similarity more than 98 % to the three strains.

Download the 16S rDNA sequences of the strains that have a high sequence similarity (above 98 %) to the three strains. The clone sequences were aligned and phylogenetic tree was constructed by the neighbor-joining method with the Molecular Evolutionary Genetics Analysis (MEGA) software and Cluster X. DS1,

Fig. 103.2 Agarose gel electrophoresis of 16S rDNA-PCR fragment obtained from the amplification of genomic DNA of the three isolates: *Lane M* (20 Kb DNA ladder); *Lane 1* (isolate DS1); *Lane 2* (isolate DS2); *Lane 3* (isolate DS3)



DS2, and DS3 were closely related to *Acinetobacter haemolyticus*, *Enterococcus gallinarum*, and *Brevibacterium otitidis* with a homology of 99 %, 99 %, and 98 %, respectively (Fig. 103.3).

It has great significance to search and select appropriate microbial strain to enhance oil recovery from the nature as MEOR has got much attention. In this study, we got three strains that can significantly reduce the viscosity of heavy oil and use thick oil as the sole carbon source from authigenous microorganism. It has been reported that petroleum hydrocarbon can be degraded by *Acinetobacter* sp. and *Brevibacterium* sp. It has been found that *Acinetobacter* sp. with perfect adaptive capacity to environment has good effect to remove pristane and phytane in thick oil [14]. *Brevibacterium* sp. was able to degrade polycyclic aromatic hydrocarbons such as anthracene, phenanthrene, pyrene, and naphthalene. The one with the less hoops was easier to be degraded [15]. And it has been found that *Acinetobacter* sp. can produce surface. *Acinetobacter calcoaceticus* can produce a kind of surfactant named HBS-1 which make the surface tension and the oil water interfacial tension reduced [16], and then the flow properties of crude oil was improved. Li Qing's research also showed that surfactant was produced by *Acinetobacter* sp. [17]. Zhang Hao did the MEOR field test with the microorganism of *Brevibacterium* sp. they selected. The result was that 947t oil was gained within half a year [18]. *Enterococcus* sp. also had a great viscosity reduced effect for the thick oil in Erlian Oil Field. While *Enterococcus* sp. on the degradation is rarely reported. The three strains were selected directionally in particular circumstances. Study on the shape, physiological, and biochemical and molecular laid a good foundation for the function gene cloning and expression of the three strains.

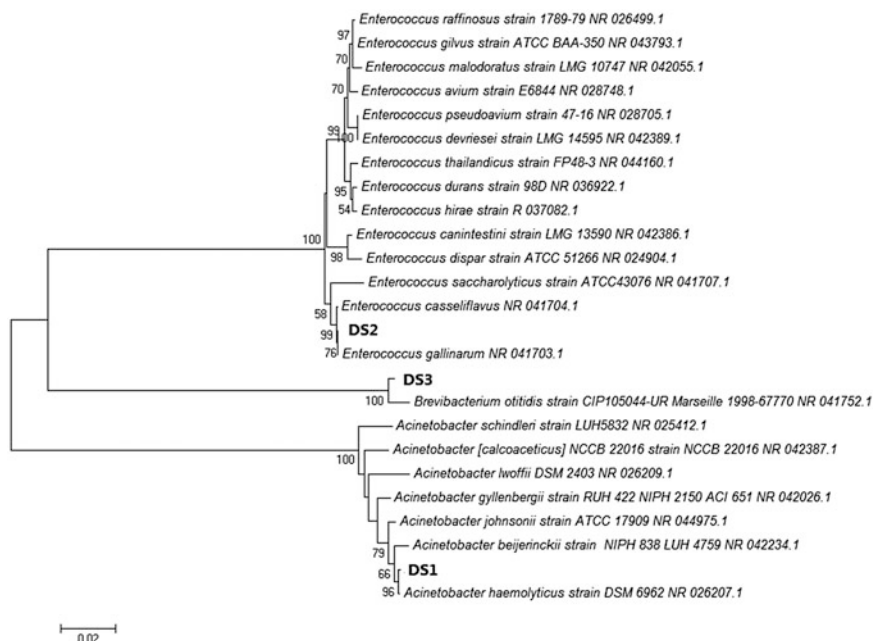
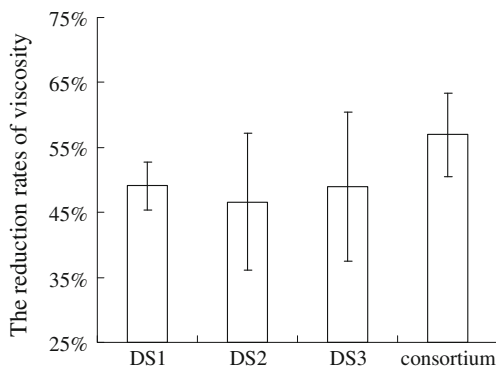


Fig. 103.3 Phylogenetic tree of thick oil degrading bacteria strains. The bacteria strains isolated are highlighted in boldface. The tree was constructed by the neighbour-joining method, with the Kimura two parameter correction factors. Bootstrap values higher than 50 % are shown at the nodes. The scale bar represents substitutions per nucleotide position. The length of the representative T-RF is listed in the end of each clone. Sequences are shown in the phylogenetic tree when they showed high sequence similarity (above 98 %)

103.3.3 Degradation Characteristics of Three Bacteria Strains

The thick oil in experimental group has emulsified by the three isolated bacterium alone and their consortium after 3 days. The viscosity reduced 49.1, 46.6 and 49.0 % by DS1, DS2, and DS3, respectively, during 7 days degradation experiment. The viscosity of crude oil changed after the effect of microbe. The viscosity of crude oil can reduce 10–50 % in normal [19–23], but the reduction rates of viscosity of the three strains we got were more than 45 %. It proved that they are excellent thick oil degrading bacteria strains. However, the reduction rate of viscosity reached 57.0 % with the consortium, which was significantly higher than that of single strain (Fig. 103.4). It demonstrated that viscosity reduced effect were better with the consortium of the three isolated bacteria. The degradation to thick oil with microbe has a strong selectivity [24], so single bacteria strain can only degrades some composition in crude oil selectively. Compared to single strains, the

Fig. 103.4 The reduction rate of viscosity by the three isolated bacterium alone and their consortium



consortium of different bacteria strains can degrade more composition in crude oil. And different strains produced different surfactants, organic acid, as well as enzyme composition. They respectively act on different petroleum hydrocarbon fractions to reduce the surface tension of the thick oil, so the liquidity is changed. The bacteria strains applied to MEOR should be able to produce metabolites such as gases, acids, surfactants that benefit to oil displacement. They also should be adaptable of anaerobic survival, high temperature, high pressure, different pH, and salinity conditions. For a single strain, it is too difficult to satisfy these requirements, so the consortium should be used in MOER [25]. She Yuehui's study also found that the viscosity reduced effect of consortium is better than the single strain [26]. The consortium can be applied in MEOR.

103.4 Conclusion

Three bacterial strains DS1, DS2, and DS3 with excellent degrading effect on thick oil were isolated from the thick oil and water reservoir of oil well 51–82# in Erlian Oil Field. The three bacteria were identified as *Acinetobacter* sp., *Enterococcus* sp., and *Brevibacterium* sp. through 16S rDNA sequence similarity search.

The viscosity reduced 49.1, 46.6, and 49.0 % by DS1, DS2, and DS3, respectively, during 7 days degradation experiment. However, the reduction rate of viscosity reached 57.0 % with the consortium. The consortium can be applied in MEOR.

Acknowledgments This work was supported by the Project of Prospering Ocean with Science and Technology of Tianjin Municipality (No. KJXH2012-23).

References

1. Sen R (2008) Biotechnology in petroleum recovery: the microbial EOR. *Prog Energy Combust* 34:714–724
2. Youssef N, Elshahed MS, McInerney MJ (2009) Microbial processes in oil fields: culprits, problems, and opportunities. *Adv Appl Microbiol* 66:141–251
3. Sui CH, Li H, Bi XZ (2010) The situation and development trend of tertiary oil recovery around the World. *Foreign Oilfield Eng* 26:13–16 (in Chinese)
4. Zhou LG, Xiang YS, She YH (2004) Development of microbial enhanced oil recovery in Qinghai oil field. *Biotechnology* 14:58–59 (in Chinese)
5. Yang ZY, Shi M, Wang DW et al (2006) Study on authigenous microorganism community distribution and oil recovery mechanism in daqing oilfield. *Acta Petrolei Sinica* 27:95–100 (in Chinese)
6. Belyaev SS, Borzenkov IA, Nazina TN et al (2004) Use of microorganisms in the biotechnology for the enhancement of oil recovery. *Microbiology* 73:590–598 (in Chinese)
7. Hao CL, Liu YJ, Wang DW (2007) Advance of research for MEOR in oil reservoir after polymer flooding. *Biotechnology* 17:87–90 (in Chinese)
8. Xiang YS, Feng QX, Nazina NT et al (2004) Mechanism of indigenous Microbial enhancement of oil recovery and pilot test. *Acta Petrolei Sinica* 25:63–67 (in Chinese)
9. Van Hamme JD, Singh A, Ward OP (2003) Recent advances in petroleum microbiology. *Microbiol Mol Biol Rev* 4:503–549
10. She YH, Yi SJ (2002) The technology of petroleum and environmental microbe. China University of Geosciences Press, Beijing, pp 64–88 (in Chinese)
11. Wang H, Lu Y, Yin XY (2003) The summarization of microbial enhanced oil recovery technology. *Petrol Geol Oilfield Dev Daqing* 22:49–52 (in Chinese)
12. Hao GY, Xu YT, Huang MS (2004) Application and developing trends of microbial enhanced oil recovery. *Energy Environ Prot* 18:8–13 (in Chinese)
13. Wang CM (2007) Separation and study of degradation characteristics of polycyclic aromatic hydrocarbon bacteria and their effects on heavy oil in MEOR. Sichuan University (in Chinese)
14. Jia QC, Guo CL, Lu GN et al (2011) Isolation and identification of two strains efficiently degrading heavy oil and their degradation characteristics. *Chinese J Environ Eng* 5:1181–1186 (in Chinese)
15. Nie MX, Zhang ZJ, Lei P (2001) Biodegradation of polycyclic aromatic hydrocarbons by a preponderant *Brevibacterium*. *Environ Sci* 22:83–85 (in Chinese)
16. Luo Q (2008) Studies on synthesis of biosurfactant HBS-1 and function of viscosity-reduced by emulsification on nanbao 35-2 heavy crude oil. Southwest Petroleum University (in Chinese)
17. Li Q, Shao ZZ (2008) Components in bioemulsifier produced by *Acinetobacter* strains. *Chinese J Appl Environ Biol* 14:553–557 (in Chinese)
18. Zhang H, Zhao B, Chen JM et al (2003) Recover heavy oil and extra heavy oil by MEOR. *Oil Drill Prod Technol* 25:49–50 (in Chinese)
19. Wu PC, Ju QY, Li CL et al (1998) A study on effects of microbes on crude oil in microbial enhanced oil production. *Oilfield Chem* 15:362–365 (in Chinese)
20. Zhang TS, Lan GZ, Deng L et al (2001) Experiments on heaving oil degradation and enhanced oil recovery by microbial treatments. *Acta Petrolei Sinica* 22:54–57 (in Chinese)
21. Zhang TS, Ren ZM, Lan GZ et al (2003) Microbial degradation influences on heave oil characters. *J Southwest Petrol Inst* 25:1–4 (in Chinese)
22. He ZG, Xiang TS, Mei BW et al (1999) Lab research of enhancing oil recoveru with microorganism. *Oil Drill Prod Technol* 21:95–99 (in Chinese)
23. Wang CM, Li DP, Liu SG (2007) Effects of biophysiological and biochemical characteristics of a strain of *Microbacterium* sp. on properties of thickened oil. *Acta Petrolei Sinica* 28:89–92 (in Chinese)

24. Bao JP, Zhu CS, Ma AL et al (2002) Quantitative study of biomarker composition in biodegraded oils. *J Jiangnan Petrol Inst* 24:22–26 (in Chinese)
25. Donaldson EC, Chilingarian GV, Yen TF (1989) *Microbial enhanced oil recovery*. Elsevier Science Publishers B.V., Amsterdam, pp 7–11
26. She YH, Xia J, Huang JF et al (2009) Characteristics of indigenous microorganisms for enhancing oil recovery after polymer flood in Daqing oilfield. *Oilfield Chem* 26:98–101 (in Chinese)

Chapter 104

Effect of Anti-Nematode Preparations on Physiological Traits of Cucumber Leaves Affected by Root-Knot Nematode

Shuchang Lu

Abstract This paper was to study the effects of anti-nematode preparations with different mechanisms on changes of enzyme systems and membrane permeability of cucumber leaves, so as to provide reference basis for effective control of soil root-knot nematode in greenhouse. With cucumber seedlings affected by root-knot nematode as material, changes of superoxide dismutase (SOD), peroxidase (POD), relative conductivity in cucumber were tested after the seedling soil was treated by preparations of Wuxianmei, Hailvsu, Duxiandna, and Avermectin. After treated by different preparations, SOD and POD activity of cucumber leaves were higher than control, and that treated by Wuxianmei was the highest. In addition to Duxiandna, the relative conductivity content of other treatments were significantly lower than control. When cucumbers were planted for 70 days, the effect of Avermectin against root-knot nematode was the best of 64.7 %. After cucumbers were infected by root-knot nematode, different preparation treatments all had certain control effect, which made the physical indicators of cucumber have obvious change.

Keywords Cucumber · Root-knot nematode · Preparation · Leaf · Physiological trait

104.1 Introduction

The damage of soil root-knot nematode in the main vegetables producing areas is increasingly serious in China, and it shows significant aggravation trend especially in northern producing area of off-season protected vegetables, being a serious obstacle restricting the production of protected vegetables.

S. Lu (✉)

Department of Agronomy, Tianjin Agricultural University, 300384
Tianjin, People's Republic of China
e-mail: lsc9707@163.com

According to the survey, the disease has different degrees of occurrence in the main producing areas in Jixian, Wuqing, and Jinghai of Tianjin City, especially in Jixian, root-knot nematode disease has caused great harm on the local vegetable production [1]. When root-knot nematode infects the roots of cucumber, the enzyme systems and membrane permeability of root system will change, thus affecting the physiological traits of aboveground leaf tissue. This not only directly affects the growth and development of vegetables, causing the production decline and quality reduce, but also exacerbates the occurrence of bacterial and fungal diseases such as *Fusarium* wilt [2].

Currently, the mechanisms for the prevention of soil root-knot nematodes are as follows: (1) using preparations to kill root-knot nematode; (2) using preparations to drive root-knot nematodes away from the roots to prevent roots being infected; (3) using root growth promoting preparation to promote the growth of new roots, thus increasing the transportation of soil moisture and nutrients to aerial part [3]. The traditional control against soil root-knot nematode mainly relies on chemical preparations, but many chemical preparations are highly toxic and high residue pesticides, large amount of application will cause serious pollution on soil and groundwater, so the research and development of new preparations and new technologies with high efficiency and low toxicity against root-knot nematode is extremely urgent [4, 5]. How the preparations with different mechanisms affect the soil root-knot nematode and plant physiological traits is rarely reported. To this end, taking cucumber seedlings infected by soil root-knot nematode as the material, the author used several preparations of Hailvsu (root growth promoting preparation), Wuxianmei (botanical nematode driven preparation), Duxiandan (chemical nematicide preparation), and Avermectin (biological nematicide preparation) with different mechanisms to control root-knot nematode, and further analyzed the changes of enzyme systems and membrane permeability of plant leaves after application of preparations, so as to provide reference for effective control of soil root-knot nematode in protected vegetable fields.

104.2 Materials and Methods

104.2.1 Materials

104.2.1.1 Test Crops

The crop used in the test was cucumber, and the variety was Jinyou 35.

104.2.1.2 Preparations

The preparations used in the test were as follows: 2 % Avermectin EC (Jiangsu Gaoyang Agriculture Technology Co., Ltd.), 3 % Duxiandan granules (active

ingredient was 3 % chlorpyrifos, Shandong Qingdao Haibeil Chemical Co., Ltd.), Hailvsu water solvent (algae extract, Beijing New Hefeng agricultural information Co., Ltd.), and Wuxianmei EC (botanical nematode driven preparation, Beijing New Hefeng agricultural information Co., Ltd.).

104.2.1.3 Test Soils

The overwintering soils in cucumber greenhouse with serious damage caused by root-knot nematodes in Xiniantuozui Village in Xiqing District of Tianjin City were collected at the end of 2009 and taken as the test soils, the soil texture was medium loam, and the soil type was alluvial soil.

104.2.2 Methods

104.2.2.1 Experimental Design

Four different types of preparation treatments including Wuxianmei, Hailvsu, Duxiandan, and Avermectin were set in the test, and water irrigation treatment was set as control, each treatment contained three repeats.

The test was started on March 5, 2011. The cucumber seeds were placed in the Petri dishes covered with wet gauze, then the dishes were placed in 25 °C incubator for 5 days. After germination, the seeds were planted in the pots with the diameter of 15 cm, each pot was covered with 500 g semi-wet soil containing nematodes. Two seedlings with vigorous growth were kept after 20 days. 30 days later, 50 mL Wuxianmei 3000 times, Hailvsu 1000 times, Duxiandan 500 times, and Avermectin 1000 times were used to irrigate, respectively, and control group was irrigated with water. The physiological indicators such as enzyme activity, relative conductivity were determined after 40 days, and the number of soil root-knot nematodes was counted after 70 days.

104.2.2.2 Determination of Physiological Indicators

Superoxide dismutase (SOD) was determined using NBT photoreduction method, suppressing 50 % of photoreduction was adopted as an enzyme activity unit; peroxidase (POD) was determined using guaiacol method; conductivity was determined using conductometry. The determination of the above four indicators was carried out according to the method by HAO Zai-bin [6].

104.2.2.3 Determination of the Number of Root-Knot Nematodes in Soil and Calculation of Control Effect

The separation of root-knot nematode in soil referred to Bayesian funnel method. 20 g fresh soil samples were weighed, covered with 4-layer gauze, and placed in the funnel containing 50 mL clean water. The funnel end was connected with a section of rubber tube, the other end of rubber tube was tightly clamped with water clip. After being placed stillly for 48 h, the clip was opened and about 10 mL bottom water sample flew out to centrifuge tube, then the tubes were centrifuged at 2,000 r/min for 2 min. Each sample had two tubes, the upper liquid was abandoned, and 1 mL base liquid was kept. The tubes were placed under microscope to count for three times. The number of soil root-knot nematodes was counted before planting and 70 days after planting, respectively.

Control effect (%) = (number of nematodes in control–number of nematodes in preparation treatment)/(number of nematodes in control–number of nematodes before planting) × 100

104.2.2.4 Data Processing

Experimental data obtained were preliminarily processed using Microsoft Office Excel 2003, and SAS9.1 software was used for statistical analysis (Duncan's method for verification, $\alpha = 0.05$).

104.3 Results and Analysis

104.3.1 *Effect of Different Pesticides on the Content of Chlorophyll in Cucumber Leaves*

After treated by different preparations, the content of chlorophyll in leaves of cucumber seedlings were shown in Fig. 104.1. As shown in Fig. 104.1, contents of chlorophyll a, chlorophyll b, and carotenoids of cucumber leaves treated by hailvsu were the highest, being 11.17, 4.15, 2.49 mg/L, respectively. The content of chlorophyll of cucumber leaves treated by Duxiandan was the lowest. It showed that root-knot nematode affected the photosynthesis of cucumber leaves. After the pesticides application, the photosynthesis of cucumber leaves was improved.

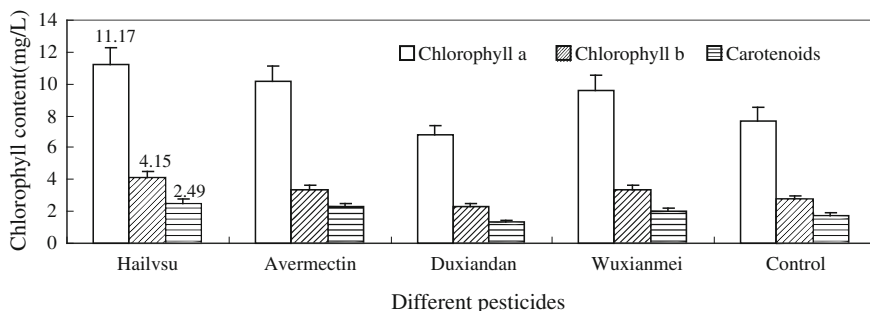


Fig. 104.1 Effect of different pesticides on the content of chlorophyll in cucumber leaves

104.3.2 Changes of SOD and POD Activity in Leaves of Cucumber Seedlings

After treated by different preparations, the changes of SOD and POD activity in leaves of cucumber seedlings were shown in Table 104.1. As shown in Table 104.1, SOD activity of cucumber leaves treated by Wuxianmei was the highest, being 100.7 U/g, and SOD activities of cucumber leaves treated by Wuxianmei, Hailvsu, and Avermectin were significantly higher than control. SOD activity treated by Wuxianmei was higher than other three preparations, indicating that Wuxianmei led to the minimum decrease of SOD activity, thereby maintaining a certain degree of resistance of cucumber. SOD activity of cucumber leaves treated by Duxiandan was the lowest, this indicated that the impact of chemical preparations on physiological traits of cucumber leaves was higher than other biological preparations; POD activity of cucumber leaves treated by Wuxianmei was 260.0 U/g, which was significantly higher than that treated by other three preparations, and was 3.17 times of control. The changes of POD activity after treated by Hailvsu and Avermectin were similar, POD activity of cucumber leaves treated by Duxiandan was the lowest. This indicated that these four preparations could increase POD activity of cucumber leaves, which was conducive to the protection of enzyme system, thus increasing the resistance of cucumber in a certain degree.

Table 104.1 Effect of different preparations on SOD and POD activity of cucumber leaf

Index	Different treatments				
	Wuxianmei	Hailvsu	Duxiandan	Avermectin	Control
SOD (U/g)	100.7 ± 20.1	82.4 ± 26.0	44.1 ± 10.3	66.3 ± 15.7	46.2 ± 10.3
POD (U/g)	260.0 ± 23.2	186.7 ± 20.7	160.2 ± 12.8	190.2 ± 22.2	81.9 ± 11.2

104.3.3 Changes of Relative Conductivity in Leaves and Roots of Cucumber Seedlings

After treated by different preparations, the changes of relative conductivity in leaves and roots of cucumber seedlings were shown in Figs. 104.2 and 104.3. As shown in Figs. 104.2 and 104.3, the relative conductivity in control was the largest of 0.371, and the relative conductivity treated by preparations was lower than control. The conductivity in cucumber leaves treated by Duxiandan was the largest, the conductivity treated by Hailvsu, Wuxianmei, and Avermectin was relatively low, and the difference among them was not significant. This indicated that after treated by these three preparations, cell membrane permeability of cucumber leaves decreased, the leakage of electrolyte reduced, and the damage suffered by cells was also significantly alleviated. The damage degree of roots was higher than ones of leaves, above 0. After the pesticides application, the damage degree of roots was decreased. The effects of Wuxianmei and Avermectin were evident.

104.3.4 Control Effects of Different Preparations Against Soil Root-Knot Nematode

The initial number of root-knot nematodes in semi-wet soil per 100 g after over-wintering was 153. After cucumbers were planted for 70 days, the number of root-knot nematodes in pots greatly increased due to the increase of soil temperature. After treated by four preparations, the number of root-knot nematodes in soil was significantly lower than control. The control effect of Avermectin against root-knot

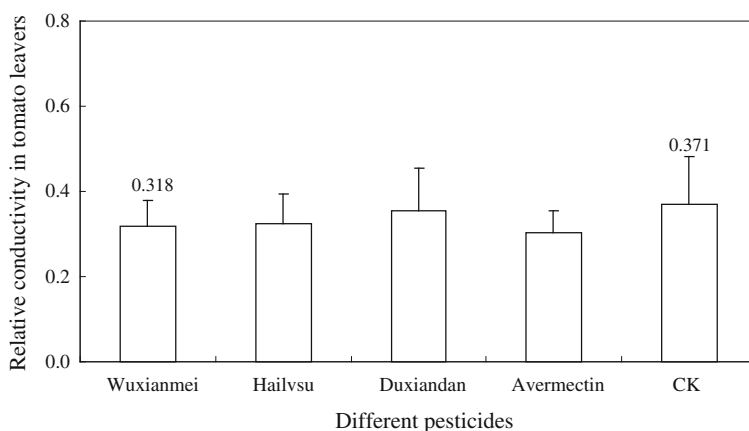


Fig. 104.2 Effect of different preparations on relative conductivity of cucumber leaves

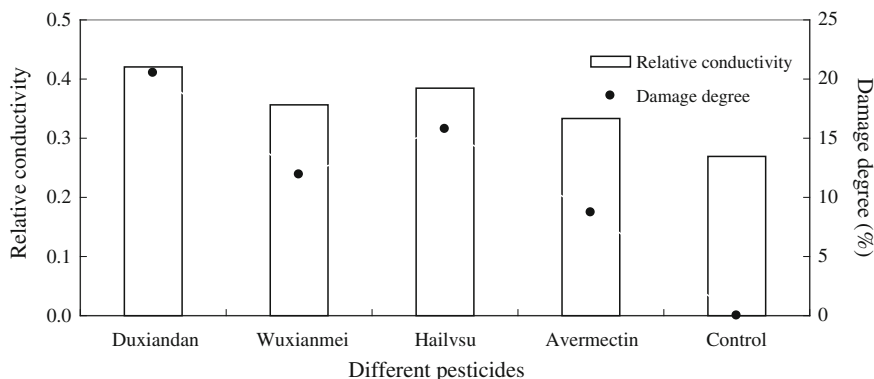


Fig. 104.3 Effect of different preparations on relative conductivity and damage degree of cucumber roots

Table 104.2 Control effect of different pesticides on root-knot nematode

Item	Treatment				
	Wuxianmei	Hailvsu	Duxiandan	Avermectin	Water (CK)
Number of root-knot nematode pre planting (head/100 g)	153	153	153	153	153
Number of root-knot nematode after the pesticides use (head/100 g)	826	945	760	534	1203
Control effect (%)	35.9	26.7	43.8	64.7	-

nematode was the best, reaching 64.7 %. The control effect of Wuxianmei was lower than Avermectin and Duxiandan, but it was non-toxic and had no pollution on environment, which could be used in production. As the root growth promoting preparation, Hailvsu also increased the plant resistance against root-knot nematode, which had certain control effect (Table 104.2).

104.4 Conclusion and Discussion

The metabolic balance of generation and elimination of reactive oxygen species in plant is damaged under adversity stress, and excess reactive oxygen species can cause and aggravate peroxidation of membrane lipids, thus destroy the structure and function of membrane. The results showed that SOD activity and POD activity of cucumber leaves treated by preparations were significantly higher than control, biological preparation, and root growth promoting preparation had better improvement effect on leaf physiological traits of cucumber infected by root-knot nematode than chemical preparations. SOD and POD are the key enzymes in

protective enzyme systems for eliminating reactive oxygen species [7]. These all indicated that the antioxidant system of cucumber changed after treated by preparations, and the level of POD activity could better reflect the strength of free radical elimination or antioxidant capacity [8].

After infection for 70 days, the number of root-knot nematode significantly increased, but the increase in control was significantly larger than preparation treatments. This indicated that preparations had certain control effect against root-knot nematode, Avermectin had better control effect, while Wuxianmei and Hailvsu mainly improved the resistance of soil against root-knot nematode via driving root-knot nematode and promoting root growth. Although the control effect of Wuxianmei is not as good as other two nematicides, it is pollution-free and safe, which can be combined with other preparations for integrated use in practice, and control the damage caused by root-knot nematode from different mechanisms. So, the preparation of integrated agents will have a very broad development prospect.

Acknowledgments This work was financially supported by special fund for basic application and cutting-edge technology research projects of Tianjin City (09JCYBJC08600).

References

1. Huang GM, Wang JC, Liu P et al (2009) Study on plant nematodes in Tianjin vegetable base. In: Peng YL, Zhu YL (eds) 2009 Conference papers of Chinese society of plant pathology. Chinese Agric ScienTech Press, Beijing
2. Zhang SS, Hu L, Liu ZL et al (2006) Relationship between the disease defense related enzymes and the disease resistance of plants. *J Anhui Agric Sci* 12:48–49
3. Huang CD, Ren T, Dong LL et al (2010) The application effectiveness of integrated control techniques for root knot nematode in intensive vegetable production fields. *China Veg* 21:23–25
4. Dui H, Zheng G, Lv HP et al (2009) Effect control of sever kinds of pharmacy on the root-knot nematode of cucumber. *Gansu Agric ScienTech* 12:40–49
5. Kounobor RD, Saliou N, Sabine F et al (2005) Influence of irrigation on the distribution and control of the nematode *Meloidogyne javanica* by the biocontrol bacterium *Pasteuria penetrans* in the field. *Biol Fert Soils* 41:205–211
6. Hao ZB, Cang J, Xu Z (2004) Plant physiology experiments. Harbin Industrial University Press, Heilongjiang
7. Jaizme MC, Tenoury PJ (1997) Interactions between the root-knot nematode *Meloidogyne incognita* and *Glomus mosseae* in banana. *Plant Soil* 196:27–35
8. Wang HH, Lin QY, Xie LH (2001) The effects of three cucumber mosaic virus isolates on the defendant enzymes and cell membrane permeability in tobacco cells. *Acta Phytopathol Sin* 31:39–43

Chapter 105

Enzymolysis and Microbial Transformation of Geniposide in *Gardenia Jasminoides* into Genipin by *Aspergillus niger*

Yu Li, Wenbin Jin, Wei Jing, Mengcheng Yao, Yanyang Tang and Fuping Lu

Abstract A filamentous fungi strain, *Aspergillus niger*, producing β -glucosidase was screened to transform geniposide in traditional Chinese medicine *Gardenia jasminoides* into genipin. The conversion rate of *Gardenia* hydrolyzed by β -glucosidase which had been extracted from fermentation broth of *A. niger* could reach 15 % at the enzyme concentration of 5 %, enzyme digestion time of 40 min, temperature at 50 °C. On the other hand, genipin was achieved with the method of microbial cell transformation. The optimum conversion conditions by cells were: β -glucosidase activity dose 10.12 U/mL at a fermentation time of 96 h, rotation speed of 180 r/min, medium capacity of 50 mL and *Gardenia* concentration of 10 %. By HPLC analysis, the maximum conversion efficiency of 22 % was achieved. By this way, conversion efficiency was increased by 7 % and the extraction process was saved compared with enzymatic hydrolysis method.

Keywords Genipin · *Gardenia* · Microbial transformation · Enzymatic hydrolysis

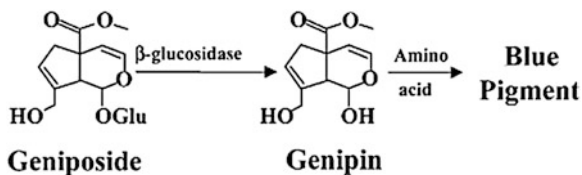
105.1 Introduction

The fruit of *Gardenia* (*Gardenia jasminoides* Ellis) is an oriental folk medicine which has been included in traditional formulations [1, 2]. The chief effectual components of *Gardenia* are geniposide and genipin. The pharmacokinetic study of *Gardenia* showed that geniposide could be changed into genipin quickly in vitro by human intestinal flora [3]. Genipin has obvious effects used for the treatment of inflammation [4], jaundice, hepatic disorders. Additionally, genipin is a natural

Y. Li · W. Jin · W. Jing · M. Yao · Y. Tang · F. Lu (✉)

Key Laboratory of Industrial Fermentation Microbiology, Ministry of Education, National Engineering Laboratory for Industrial Enzymes, The College of Biotechnology, Tianjin University of Science and Technology, 300457 Tianjin, People's Republic of China
e-mail: lfp@tust.edu.cn

Fig. 105.1 The mechanism of blue pigment formation in gardenia fruit



cross-linking agent with advantages of low toxicity and high biocompatibility. Thus it has been widely applied in a variety of medical fields such as nerve regeneration [5] and drug delivery [6]. According to this, in *Gardenia jasminoides* the compound genipin is much more preferred to geniposide, however, the concentration of genipin is very low in gardenia fruits (about 0.005–0.01 %), while geniposide presents abundantly (about 3.06–4.12 %) [7]. It is difficult to extract genipin from gardenia fruits directly, so the methods of enzymatic hydrolysis and microbial transformation have been used to replace the traditional method. The two conversion methods were optimized in this paper to find out the most suitable conditions for maximum industrial production of genipin from gardenia by using the *Aspergillus niger*.

Geniposide from gardenia fruit is hydrolyzed by β -glucosidase to produce genipin. Geniposide has specific absorbance at 340 nm, but this specific absorbance is disappeared after the transforming from geniposide into genipin [8, 9], so they pose difficulties to the testing of genipin. While other researches suggested that genipin became blue when being reacted with amino acids (Fig. 105.1) [10, 11]. Even though the mechanism of the blue pigment formation has not been clear [12, 13], genipin could produce blue colored pigments with amino acids that provided a simpler, safer, sensitive and stable alternative method for the colorimetric detection of genipin. The blue pigments were stable in alkaline (pH 9.0) and remained stable after 10 h at 60–90 °C [14]. Furthermore, the absorbances of blue pigments possessed stability and high sensitivity [15, 16].

105.2 Materials and Methods

105.2.1 Materials

Gardenia (extracted from gardeniae fruits, contains 3 % of geniposide by HPLC); DNS reagent (3,5-dinitrosalicylic acid 1 %, phenol 0.2 %, sodium sulfite 0.05 %, NaOH 1 %, sodium potassium tartrate 20 %); genipin standard (Seebio Biotechnology); glycine and salicin (Sangon Biotech).

105.2.2 Strain Screening

Try to follow the type sizes and typefaces specified in Table 105.1 as best as your can. The whole paper should use Times New Roman font with 10 pts in the main text. Use 14 pts bold characters for the paper title, and capitalize the first letter of each substantive in the title. Author names should use 12 pts characters and separated by commas. Capitalize the surnames and the first letters of the first names. Use superscript on the right if authors' sequence numbers are necessary. Use 10 pts characters for the main text and author's affiliations, please be sure that there are sequence numbers in front of them. Capitalize the first letter of the beginning word for each section title and subheading. Use 12 pts bold Roman characters for section titles and 10 pts bold Roman characters for subheadings.

105.2.3 Extraction and Activity Detection of β -glucosidase

The cell culture was centrifuged at 5,000 r/min and 4 °C for 10 min. The supernatant was mixed with sodium acetate buffer (pH 4.0) and then the supernatant was concentrated by ultrafiltration. The crude enzyme would be used for the determination of β -glucosidase activity.

The measurement of activity of crude enzyme was performed by the DNS method [17]. The determination method of β -glucosidase was as follows: salicin solution (0.3 mL), 0.05 M sodium acetate buffer (pH 5.0, 0.7 mL) and suitable amount of the crude β -glucosidase were mixed and incubated in water bath (50 °C) for 30 min. Then the reaction was stopped by adding DNS reagent (1 mL). Color was developed by heating for 5 min in a boiling water bath. The tubes were cooled with running tap water and solution was dilute to 10 mL. Then 0.05 M sodium acetate buffer (pH 5.0) was taken as a blank control and the solution was monitored at 550 nm by UV-Vis.

Table 105.1 Levels of factors for the best enzymatic hydrolysis efficiency of geniposide from gardenia fruit

Factors	Enzyme concentration (% V/V)	Enzyme digestion time (min)	Temperature (°C)
Level 1	1.0	20	40
Level 2	2.0	40	50
Level 3	5.0	60	60
Level 4	10.0	90	70
Level 5	20.0	120	80

105.2.4 Analytical Methods

Thin layer chromatography (TLC) analysis of genipin, which was the fermentation product, was carried out on silica gel GF254 TLC plate (50 mm × 100 cm) with mobile phase of the mixture of ethyl acetate and petroleum ether (2:1, V/V). Gardenia in water and genipin standard were used as controls. Then it was detected under UV light (254 nm).

High Performance Liquid Chromatography (HPLC, Agilent) was used to determine the content of genipin [18]. The mobile phase consisted methanol and water with a ratio of 45:55 and a flow-rate of 1 mL/min. The samples were filtered by 0.45 μm microporous filtering membrane before injection. The assay was carried out after injecting 20 μL sample to HPLC with the ODS-2HPERSIL C18 chromatographic column (4.6 mm × 250 mm, 5.0 μm) temperature of 25 °C and the detection wavelength of 238 nm. The linear regression equation for genipin was $Y = 7858.9x - 389.19$ ($R^2 = 0.993$).

$$\text{Productivity of genipin (\%)} = \frac{\text{Actual yield of genipin(mol)}}{\text{Theoretical yield of genipin(mol)}} \text{ times } 100\% \quad (105.1)$$

105.2.5 Optimization of Hydrolysis of Gardenia Using β -glucosidase from *Aspergillus niger*

The crude β -glucosidase (10 mL), 1 % gardenia solution (10 mL), phosphate buffer (pH 5.0, 250 mL) were mixed and incubated in water bath (50 °C) for 40 min. Then glycine was added into the system and the mixture was reacted in 80 °C water bath for 1 h. After the reaction, it was detected under UV light (590 nm). Geniposide from gardenia fruit was hydrolyzed by β -glucosidase to produce genipin and genipin became blue when being reacted with amino acids. Based on this mechanism, the absorbances could represent the concentration of genipin a large extent [19].

The factors, including the enzyme concentration, enzyme digestion time, and fermentation temperature were optimized for the best enzymatic hydrolysis efficiency of geniposide from gardenia fruit. The levels of factors were showed in Table 105.1.

105.2.6 The Optimization of Microbial Transformation Conditions

Spores of strain were inoculated into a 250 ml flask in which liquid media of tap water and the powder of gardenia were added, and then cultivated. After 4 days,

Table 105.2 Levels of factors for the best conversion conditions by cells

Factors	Fermentation time (h)	Rotation speed (r/min)	Medium capacity (mL)	Gardenia concentration (% V/V)
Level 1	48	150	5	5
Level 2	72	160	10	10
Level 3	84	180	30	15
Level 4	96	190	50	20
Level 5	120	200	70	25

glycine was added into the system and the mixture was reacted in 80 °C water bath for 1 h. After the reaction, it was detected under UV light (590 nm). Geniposide from gardenia fruit was hydrolyzed by β -glucosidase to produce genipin and genipin became blue when being reacted with amino acids. Based on this mechanism, the absorbances could represent the concentration of genipin a large extent.

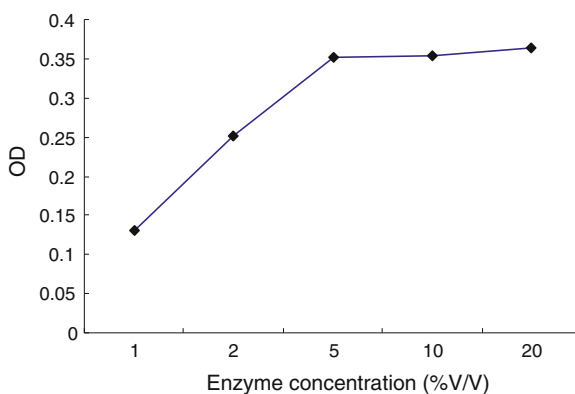
The conditions of fermentation were established by one-factor-at-a-time method. The influencing factors, including the fermentation time, rotation speed, medium capacity and gardenia concentration were optimized for the best conversion conditions by cells. The levels of factors were showed in Table 105.2.

105.3 Results and Discussion

105.3.1 Screening Strains of High Transformation Activity

Genipin can react with amino acids to form a blue pigment, thus microbial transformation of genipin can be evaluated by the size of the blue circle formed on the screening plate. The strain B-4 with high microbial transformation capacity was screened easily and fast. The strain B-4 was identified as *A. niger*, based on its

Fig. 105.2 Effect of enzyme concentration on the hydrolysis of geniposide



morphological properties and the sequence of 18S rDNA. Used the method of DNS, enzyme activity was determined at 10.12 U/mL.

105.3.2 The Optimization of Hydrolysis of *Gardenia* Using β -glucosidase

The crude β -glucosidase which had been extracted from fermentation broth of *Aspergillus niger* was evaluated for its capability to hydrolyze geniposide from gardenia fruit. Attempts were made to increase the overall conversion efficiency by optimizing the reaction parameters (enzyme concentration, enzyme digestion time and temperature). The optimum hydrolysis condition by β -glucosidase was determined according to the method described in Sect.105.2.5.

As Figs. 105.2 and 105.3 showed that when the enzyme concentration increased to 5 %, and enzyme digestion time was 40 min, the enzymatic reaction was completed and the yield of genipin had not obvious improvement.

Figure 105.4 summarized the influence of temperature on the degree of hydrolysis of geniposide. During this period, the activity of β -glucosidase increased gradually till reaching the maximum value of 10.12 U/ml at 50 °C, and the conversion rate increased along β -glucosidase activity. Because the maximum activity of β -glucosidase was observed at pH 6.0 at 50 °C, and β -glucosidase was stable at 50 °C [20].

Taking all the influencing factors and the results into consideration, the optimal transformation conditions by the crude β -glucosidase which had been extracted from fermentation broth of *A. niger* was considered as follows: the enzyme concentration of 5 %, enzyme digestion time of 40 min, temperature at 50 °C. By HPLC analysis, the maximum conversion efficiency of 15 % was achieved.

Fig. 105.3 Effect of enzyme digestion time on the hydrolysis of geniposide

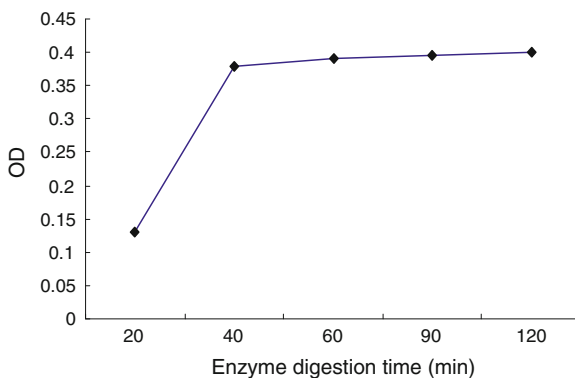
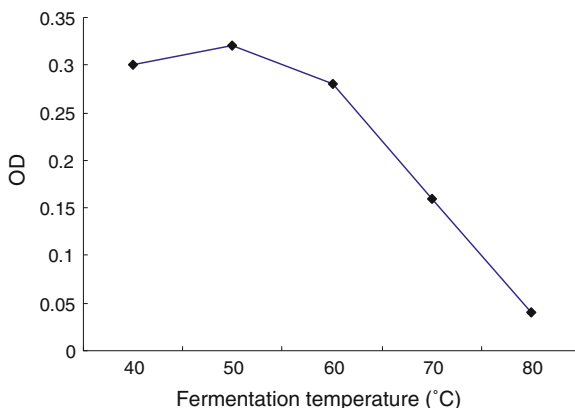


Fig. 105.4 Effect of temperature on the hydrolysis of geniposide



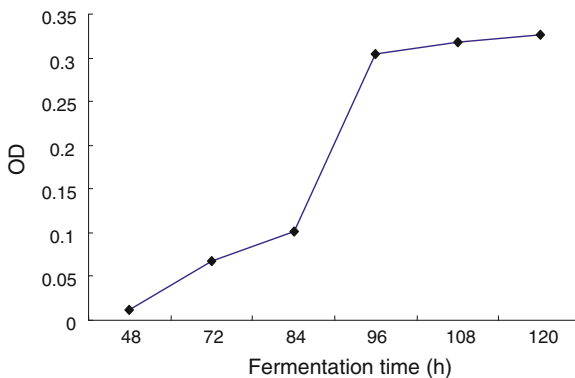
105.3.3 The Optimization of Fermentation Condition by Cells

The effect of fermentation conditions of the strain on genipin production has been studied. The optimum fermentation condition by cells has been determined according to the method described in [Sect.105.2.6](#).

The absorbances of blue pigments were assayed in different fermentation time (48, 72, 84, 96, 120 h). As [Fig. 105.5](#) showed, the geniposide mostly converted into genipin after 96 h. Due to the instability of genipin and the reactions of genipin with amino acids, the longer fermentation times the more yield of genipin lost [21]. As a result, the most suitable time of fermentation termination was 96 h.

As [Figs. 105.6](#) and [105.7](#) showed that when the rotating speed increased to 180 r/min and capacity at 50 mL, the conversion rate was at its maximum. The probable reason was that *Aspergillus niger* was an aerobic microorganisms and dissolved oxygen concentration had the greatest influence on fungus growth [22]. As a result, the dissolved oxygen was not enough when the speed below 180 r/min, and the mycelium in the medium was ruptured at excessive speed. Those were not conducive to the growth of microorganisms.

Fig. 105.5 Effect of fermentation time on the conversion rate of geniposide



The absorbances of blue pigments was assayed in different gardenia concentration (5, 10, 15, 20, 25 % V/V). As Fig. 105.8 showed that when the gardenia concentration at 10 %, the yield reached maximum. The cost of the medium is a crucial factor in determining the feasibility of a fermentation process. Because there was no other nutrient added in the fermentation medium, it was expected that the production would be cost efficient.

Taking all the influencing factors and the results into consideration, the optimal transformation conditions by cells was considered as follows: fermentation time of 96 h, rotation speed of 180 r/min, medium capacity of 50 mL and gardenia concentration of 10 %.

105.3.4 Fermentation Production Analysis

During the fermentation by B-4, the results by TLC showed that sample III (pre-fermentation) did not show any blue spots while sample II (after fermentation) showed a clear blue spot with Rf 1.5, and the Rf of sample II was consistent with

Fig. 105.6 Effect of rotational speed on the conversion rate of geniposide

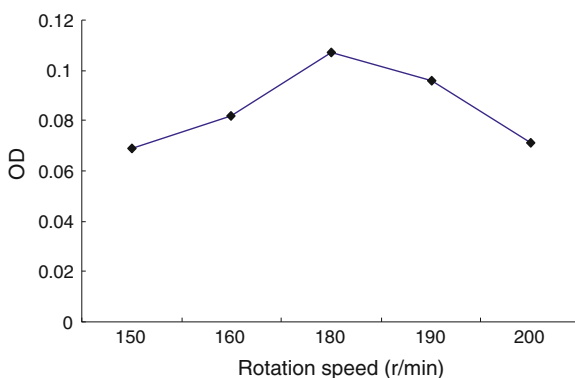


Fig. 105.7 Effect of medium volume on the conversion rate of geniposide

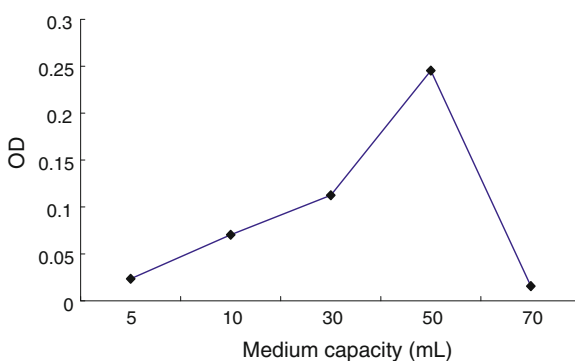


Fig. 105.8 Effect of gardenia concentration on the conversion rate of geniposide

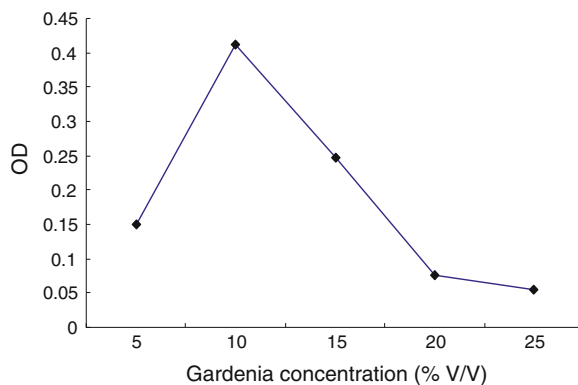


Fig. 105.9 Products of the fermentation detected by TLC

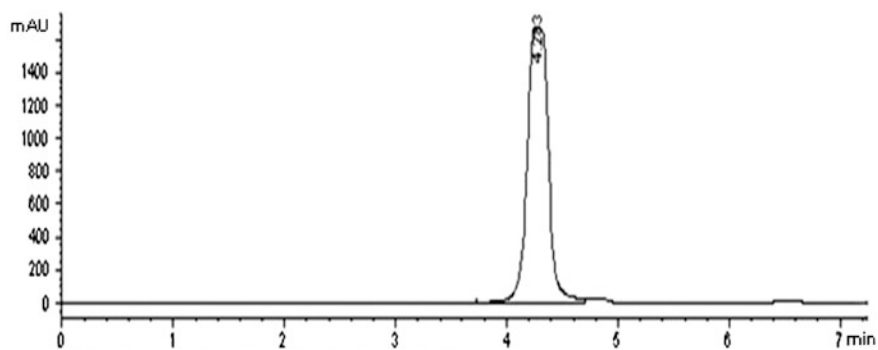


Fig. 105.10 Genipin standard products analyzed by HPLC

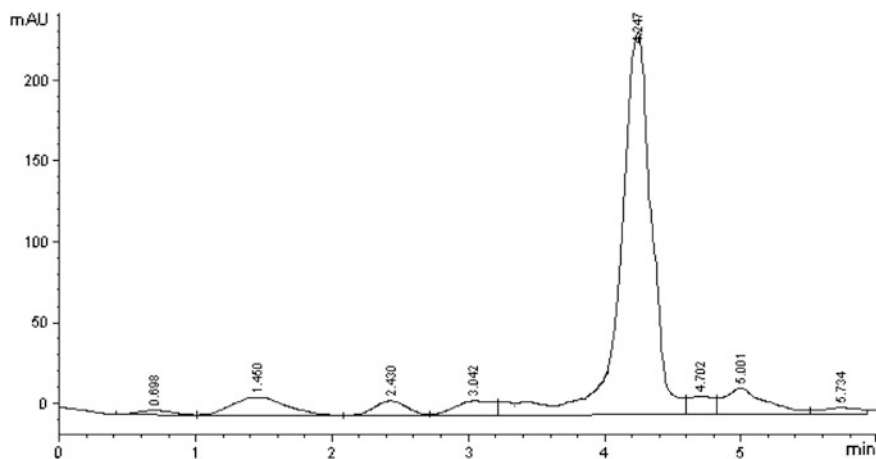


Fig. 105.11 Sample analyzed by HPLC

sample I (standard of genipin). It indicated that substrate geniposide had been transformed into the product genipin (Fig. 105.9).

The fermentation samples by *A. niger* B-4 used gardenia fruit as substrate were subjected to HPLC analysis. As Figs. 105.10 and 105.11 showed, the fermentation of B-4 strain and gardenia converted, and the conversion rate of geniposide to genipin could reach 22 % by the method of peak area spectrophotometry. With this method, conversion efficiency was increased at 7 % and the extraction process was saved compared with enzymatic hydrolysis method.

105.4 Conclusion

A strain of *A. niger* was obtained to transform geniposide in gardenia into genipin successfully, and β -glucosidase from the strain was used to hydrolyze gardenia. The conversion rate could reach 15 % at the enzyme concentration of 5 %, enzyme digestion time of 40 min, temperature at 50 °C.

In this study, the fermentation technology used traditional Chinese medicine Gardenia as the medium composition to transform geniposide into genipin. No extra nutrient was needed in the fermentation medium. By the method of microbial cell transformation, the conversion rate could reach 22 % under the optimized fermentation conditions (a fermentation time of 96 h, rotation speed of 180 r/min, medium capacity of 50 mL and gardenia concentration of 10 %). Therefore the method of microbial transformation had the potential to be applied on industry. Our study supplied new information for the optimization and development of microbial production of genipin from gardenia.

Acknowledgments The authors gratefully acknowledge the support of Tianjin Municipal Science and Technology Committee (10ZCKFNC01700) and the National High-tech Research and Development Program (863 Program), NO.2012AA021502.

References

1. Zheng HZ (2000) Modern research and application of Chinese Traditional Medicine. Beijing 4:3166–3172
2. Ni HY, Zhang ZH, Fu HZ (2006) Research and development of Fructus Gardeniae. China J Chin Mat Med 31:538–541
3. Mie I, Satoshi M, Atsushi M et al (2004) Japanese herbal medicine inchin-ko-to as a therapeutic drug for liver fibrosis. J Hepatol 41:584–591
4. Peng J, Qian ZY, Liu TZ et al (2003) Comparative studies on hepatic protective and choleric effect of geniposide and crocetin. Chin New Drug 12:105–108
5. Chen YH, Chang JY, Cheng CY et al (2005) An in vivo evaluation of a biodegradable genipin-crosslinked gelatin peripheral nerve guide conduit material. Biomaterials 26:3911–3918
6. Chen SC, Wu YC, Mi FL et al (2004) A novel pH-sensitive hydrogel composed of N, O-carboxymethyl chitosan and alginate cross-linked by genipin for protein drug delivery. J Control Release 96:285–300
7. Cao JP, Wang YL, Jia YJ (2001) Simultaneous determination of geniposide and genipin in Gardenia jasminoides Eillis by high performance liquid chromatography. J Dalian Med Univ 23:61–62
8. Yao XS, Wu LJ, Wu JZ (2004) Natural medicine chemistry, vol 220, 4th edn. People's Medicinal Publishing House, Beijing
9. Park JE, Lee JY, Kim HG (2002) Isolation and characterization of water-soluble intermediates of blue pigments transformed from geniposide of gardenia jasminoides. Agric and Food Chem 50:6511–6514
10. Paik YS, Lee CM, Cho MH et al (2001) Physical stability of the blue pigments formed from geniposide of gardenia fruits: effects of pH, temperature and light. J Agric Food Chem 49:430–432
11. Lee SW, Lim JM, Bhoo SH et al (2003) Colorimetric determination of amino acids using genipin from Gardenia jasminoides. Anal Chem Acta 480:267–274
12. Park JE, Hahn TR, Park YS (2001) Separation and characterization of water soluble blue pigments formed from geniposide of gardenia fruits. J Agric Chem Biotechnol 44:190–193
13. Park JE, Lee JY, Kim HG et al (2002) Dietary blue pigments derived from genipin, attenuate inflammation by inhibiting LPS-induced iNOS and COX-2 expression via the NF- κ B inactivation. Agric Food Chem 50:6511
14. Paik YS, Lee CM, Cho MH et al (2003) Colorimetric determination of amino acids using genipin from Gardenia jasminoides. Anal Chim Acta 480:267–274
15. Fujikawa S, Fukui Y, Koga K et al (1987) Brilliant skyblue pigment formation from Gardenia fruits. Agric Food Chem 65:419–424
16. Fujikawa S, Nakamura S, Koga K et al (1987) Continuous blue pigment formation by gardenia fruit using immobilized growing cells. J. Ferment Tech 65:711–717
17. Paik YS, Lee CM, Cho MH et al (2001) Physical stability of the blue pigments formed from geniposide of gardenia fruits: effects of pH, temperature, and light. J Agric Food Chem 49:430–432
18. Lu Y, Zhang T, Tao JS (2008) Study on processing of hydrolyzing geniposide with β -glucosidase. Acta Univ Trad Med Sinensis Pharmacol Shanghai 22:76–78
19. Lee SW, Lim JM, Bhoo SH et al (2003) Hahn. Colorimetric determination of amino acids using genipin from Gardenia jasminoides. Anal Chim Acta 480:267–274

20. Kaur J, Chadha BS, Kumar BA et al (2007) Purification and characterization of β -glucosidase from *Melanocarpus* sp. MTCC 3922. *Electron J Biotechnol* 10:260–270
21. Djerassi C, Nakano T, Zalkow L et al (2004) Genipin—a novel fingerprint reagent with colorimetric and fluorogenic activity. *J Forensic Sci* 49:1192–1194
22. Zhang QB, Xiao AF, Ni H et al (2012) Effects of oxygen conditions on naringinase production in *Aspergillus niger* DB056 fermentation. *Food Science Technol* 37:7–10

Chapter 106

Study on the Application of a Thermotolerant *Saccharomyces cerevisiae* in the Production of Bio-ethanol

Yueqiang Li, Yefu Chen, Jian Dong, Xinxin Zhang, Tong Shen and Dongguang Xiao

Abstract Bio-ethanol has attracted extensive attention because of its advantages response to energy crisis and environment pollution. However, the ethanol production could be decreased due to the high temperature created by the exothermic reactions during the fermentation process of bio-ethanol. In this study, the thermotolerant *Saccharomyces cerevisiae* strain constructed in our precious work was applied to the very high gravity fermentation (VHG) process for the production of bio-ethanol. The ethanol production of F3 and the control strain AY12 via different fermentation techniques were tested. Our results illustrate that the F3 strain exhibits higher ethanol production compared to the strain AY12 in different temperatures, and that the fermentation technique of simultaneous saccharification and fermentation (SSF) possesses the predominance among the four. The orthogonal test was also performed to optimize the fermentation conditions. Finally, the ratio of nutriment and water 1:2.6, inoculum size 25 ml, fermentation period 56 h were identified as the optimal fermentation conditions and the ethanol production was 12.2 % (v/v).

Keywords Bio-ethanol · *Saccharomyces cerevisiae* · SSF · VHG

Y. Li · Y. Chen · J. Dong · X. Zhang · T. Shen · D. Xiao (✉)
Key Laboratory of Industrial Fermentation Microbiology, Ministry of Education, Tianjin Industrial Microbiology Key Laboratory, College of Biotechnology, Tianjin University of Science and Technology, Tianjin 300457, People's Republic of China
e-mail: xdg@tust.edu.cn

106.1 Introduction

Due to rising focuses on the environmental problems and the periodic crises in some of the larger oil exporting countries, bio-ethanol has become a viable and realistic alternative energy in the global market [1–4]. Highly concentrated bio-ethanol production means less volume in fermentation tanks and consumes less distillery energy. The very high gravity (VHG) technology is attracting more and more interests due to its economic value [5–8].

The analog fermentation technique is a diminution of the current ethanol industry production processes. In this process, the incubate temperature rise when fermentation enter the peak period. Judging from the cost of production, raw material fermentation technique is minimal in all of the techniques. However, since the starch material has not been liquefied and saccharified, the free glucose concentration is low in the mash and this would be an inhibition to the ethanol fermentation. Now the ripe fermentation process is the most sophisticated fermentation process, but at the same time, the energy cost is very high because of the large amount of cooling water which is used to maintain the temperature of the mash. In simultaneous saccharification and fermentation, two different processes (saccharification and fermentation) were carried on in the same bioreactor at the same time [9, 10]. As the single saccharification step is saved, the cost of production can be significantly reduced. Considering about the large scale of the bio-ethanol industry, simultaneous saccharification and fermentation is more suitable to the actual production. At the same time, the cooling energy consumption will significantly reduce if thermotolerant strain which can work normally at high temperature in the fermentation process is used.

Due to the advantages of thermotolerant strain, it was broadly studied in recent years. Several breeding methods such as physical and chemical mutagenesis [11, 12], adaptation [13], protoplast fusion [14], evolution engineering [15], global transcription machinery engineering [16], and genome shuffling [17], had been previously used to improve the thermotolerance and ethanol production of yeast. D'Amore et al. screened numerous yeast strains for glucose fermentation at 40 °C [18]. In another study, Banat's yeast (*Saccharomyces cerevisiae*) showed a maximum ethanol production of 7.0 % and 6.9 % (w/v) at 37 °C and 40 °C, when 14 % (w/v) glucose used as substrate [19]. *S. cerevisiae* F111, which can grow at temperatures up to 50 °C, has been isolated and applied to industrial scale fermentation. *S. cerevisiae* NPO1 produced 11.3 % of ethanol from sweet sorghum juice medium containing 24.8 % of total sugar (89 % theoretical ethanol yield) [6, 20]. As the properties of yeast thermotolerance are controlled by so many genes and mediated through so many pathways, the achievements of previous studies were not efficient adequately.

In this study, the ethanol production of thermotolerant yeast F3 constructed through genome shuffling and its control strain AY12 was measured by four techniques at different temperature to verify the advantages of F3. Then the fermentation conditions were optimized by orthogonal test.

106.2 Material and Method

106.2.1 Strain and Incubate Conditions

In this study, *S. cerevisiae* AY12 used is an industrial diploid strain. *S. cerevisiae* F3 is a thermotolerant yeast constructed through genome shuffling based on AY12.

The first stage seed medium: 0.5 % yeast extract is added to 8°Brix corn hydrolyzate. It is sterilized at 100 °C for 15 min and then cooled to room temperature before used.

The second stage seed medium: 0.5 % yeast extract is added to 12°Brix corn hydrolyzate. It is sterilized at 100 °C for 15 min and then cooled to room temperature before used.

Raw material fermentation medium: 60 g corn flour is in a 250 ml flask, then add 130 ml water (60–70 °C), 20 min later, 30 µl (10 U/g) amylase, 90 µl (150 U/g) glucoamylase, 1.2 ml acid protease (15 U/g), 1 ml nutrient solution (150 g MgSO₄/L, 75 g KH₂PO₄/L, 81 g CON₂H₄/L) is added. The mash is cooled to room temperature before used.

The ripe material fermentation medium: 60 g corn flour is in a 250 ml flask, then add 130 ml water (60–70 °C), 20 min later, 30 µl (10 U/g) amylase is added and incubated at 85–90 °C for 1.5 h in a water bath incubator, 90 µl (150 U/g) glucoamylase is added and incubated at 55–60 °C for 20 min in a water bath incubator, 1.2 ml acid protease (15 U/g), 1 ml nutrient solution is added and incubated at 55–60 °C for 20 min in a water bath incubator. The mash is cooled to room temperature before used.

Analog technique fermentation medium: It is the same as the ripe material fermentation medium. Simultaneous saccharification and fermentation medium: 60 g corn flour is in a 250 ml flask, then add 130 ml water (60–70 °C), 20 min later, 30 µl (10 U/g) amylase is added and incubated at 85–90 °C for 1.5 h in a water bath incubator, 90 µl (150 U/g) glucoamylase, 1.2 ml acid protease (15 U/g), 1 ml nutrient solution is added. The mash is cooled to room temperature before used.

106.2.2 Fermentation Technique

The seed culture process of four kinds of techniques in our study is same. Firstly, the strain is inoculated into tube with 4 ml sterilized the first stage seed medium, static culture for about 24 h. Then put it all into 250 ml flask with 36 ml sterilized the second stage seed medium, static culture for 16–17 h. Then the inoculum is added to fermentation medium by size of 10 %. The mash is incubated at the given temperature. In the process of analog technique, the mash is firstly incubated at 30 °C during the initial 11 h, then at 40 °C for the rest time (about 61 h). Ethanol was removed from the fermented mash via distilling apparatus at the end of fermentation.

106.3 Result and Discussion

106.3.1 Effect of Different Temperature on the Ethanol Production of F3 and AY12

In order to investigate the effect of different temperature on the ethanol production of AY12 and F3 which was constructed through genome shuffling in our previous work, we separately tested their ethanol productions in temperatures of 30 °C, 35 °C, 38 °C, 40 °C, 42 °C, respectively, and the results are showed in Fig. 106.1.

As can be seen from Fig. 106.1, the ethanol production of AY12 and F3 were almost the same at 30 °C. While the performance of F3 was better than AY12 at 35 °C, 38 °C, 40 °C, when the incubate temperature rise to 42 °C, the ethanol production of these two strains was almost identical. Though the ethanol production of both strains decreased as the increase of the incubate temperature, it is obvious that the ethanol production of F3 was higher than AY12 at almost all the temperatures. According to the results above, it is obvious that the thermotolerance of the strain was increased compared with the control strain AY12. In conclusion, the strain F3 constructed through genome shuffling displays a higher thermotolerance compared with strain AY12.

106.3.2 Effect of Fermentation Technique and Temperature on the Ethanol Production of F3 and AY12

In order to determine the most appropriate fermentation technique of the thermo-tolerant strain F3, experiments were carried on through different techniques (raw material fermentation technique, ripe material fermentation technique, analog fermentation technique, simultaneous saccharification, and fermentation technique)

Fig. 106.1 Effect of ethanol production of AY12 and F3 at different incubate temperature

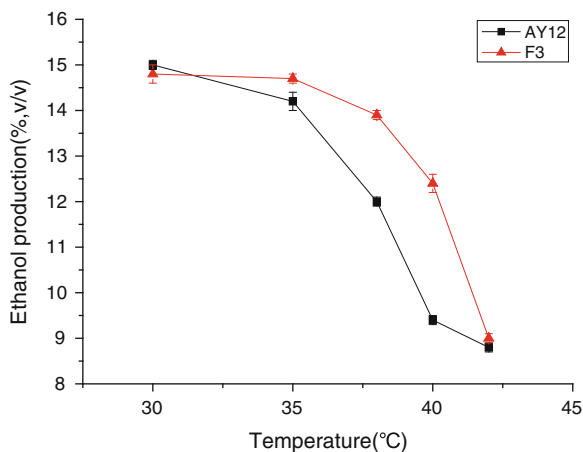


Table 106.1 Fermentation result of AY12

Ethanol production (%v/v)	Techniques			
	Raw material fermentation technique	Ripe material fermentation technique	Simultaneous saccharification and fermentation technique	Analog fermentation technique
Temperature (°C)	30	38	40	
	8.0	10.1	9.3	
	15.0	13.9	10.0	
	15.0	11.2	10.6	
	15.0	12.0	9.5	

Table 106.2 Fermentation result of F3

Ethanol production (%v/v)	Techniques			
	Raw material fermentation technique	Ripe material fermentation technique	Simultaneous saccharification and fermentation technique	Analog fermentation technique
Temperature (°C)	30	38	40	
	9.5	10.1	8.8	
	15.0	14.3	10.2	
	15.0	12.2	11.1	
	14.8	13.9	12.4	

at different temperatures. 30 °C, 38 °C, 40 °C had been selected as the fermentation temperatures. The results are showed in Tables 106.1 and 106.2.

According to the results above, the ethanol production of ripe material fermentation technique (15, 14.3, 10.2) was highest of all four fermentation techniques, and that of raw material fermentation technique (9.5, 10.1, 8.8) was the lowest of all these technique at temperature of 30 °C, 38 °C, 40 °C, respectively. At 38 °C, the ethanol production of raw material fermentation technique increased first compared with that at 30 °C, and then decreased when the temperature rise to 40 °C. But we all know that the production cost of ripe material fermentation technique is very high and this is not suitable to actual production. Therefore, considering both of the production cost and fermentation results, simultaneous saccharification and fermentation is the best technique for the ethanol production of F3.

106.3.3 Optimization of the Fermentation Conditions of F3 Through Simultaneous Saccharification and Fermentation Technique

In order to save the material and shorten the fermentation time, here we studied the optimum fermentation conditions of F3. We tested three factors that influence simultaneous saccharification and fermentation condition for ethanol production via single-factor test. The three factors are ratios of material to water, inoculum

concentration and fermentation time. And then, we optimized the fermentation process through orthogonal test.

106.3.3.1 Effect of Ratios of Water to Material on Alcohol Production

Ratios of water to material were adjusted to 2.4, 2.6, 2.8, 3.0, and 3.2; the experimental data is shown in Fig. 106.2. As presented, the yield of ethanol exhibits a basically stable situation when ratio of water to material is in the range of 2.2–2.8. However, as the ratios of water to material rise above 2.8, the ethanol production was significantly decreased.

106.3.3.2 Effect of Inoculum Concentrations on Alcohol Production

Inoculum concentration also plays an important role in ethanol production. Fermentation time will be extended if the inoculum concentration is too small. However, large inoculum concentration leads to a high inoculum cost. 10 ml, 15 ml, 20 ml, 25 ml inoculum were added to the mash. Results are showed in Fig. 106.3. As we can see, the ethanol production will be not increased when the inoculum concentration rise above 15 ml.

106.3.3.3 Effect of Fermentation Time on Alcohol Production

Shorter fermentation time means lower cooling cost, higher equipment utilization, and business profits, so the fermentation time was optimized. As results presented in Fig. 106.4, the ethanol production rise slower than previous time after 48 h. The production would not increase if fermentation time was prolonged.

Fig. 106.2 Effect of ratios of water to material on alcohol production

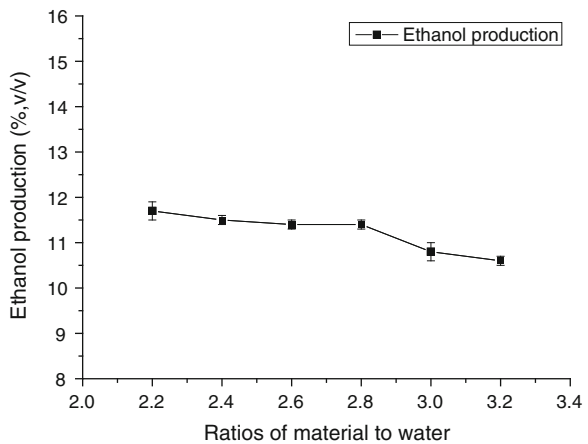


Fig. 106.3 Effect of inoculum concentrations on alcohol production

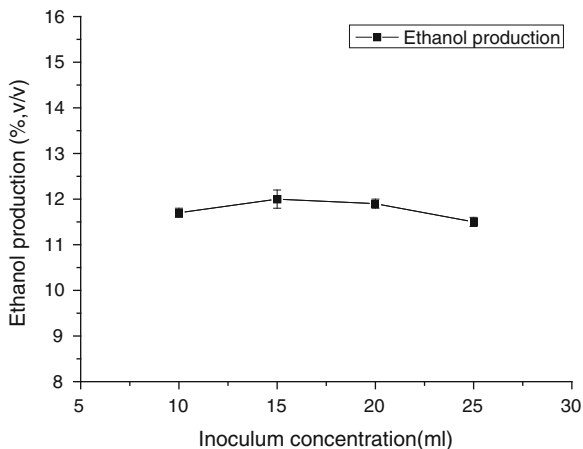
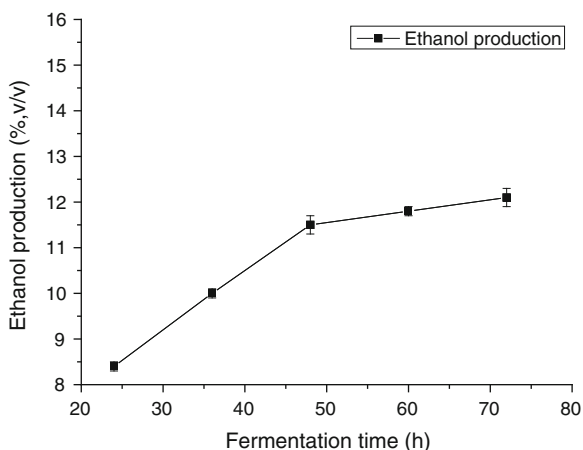


Fig. 106.4 Effect of fermentation time on alcohol production



106.3.3.4 Orthogonal Test

According to the results of the single-factor tests, ratios of water to material, inoculum concentration, and fermentation time were optimized by orthogonal experiment. Ratios of water to material 2.8, inoculum concentration 15 ml, fermentation time 48 h were used as intermediate level in the orthogonal tests. The experimental design and results of analysis are showed in Tables 106.3 and 106.4.

Based on the results of experiments, the influence of factors on the ethanol production was ordered from larger to little as the amount of. As can be seen from Table 106.4, the best combination was $A_1B_3C_3$, revealing that the optimized fermentation conditions are as follow: ratios of water to material 2.6, inoculum concentration 25 ml, fermentation time 56 h.

Table 106.3 Factors and levels of orthogonal test

Level	Ratios of water to material (A)	Inoculum concentration (B)	Fermentation time (C)	Blank
1	1:2.6	15	48	
2	1:2.8	20	52	
3	1:3.0	25	56	

Table 106.4 Results of orthogonal test

Test No.	Factors					Result
	Ratios of water to material (A)	Inoculum concentration (B)	Fermentation time (C)	Blank		
1	1	1	1	1	1	11.2
2	1	2	2	2	2	11.8
3	1	3	3	3	3	12.2
4	2	1	2	3	3	11.5
5	2	2	3	1	1	11.9
6	2	3	1	2	2	11.7
7	3	1	3	2	2	11.8
8	3	2	1	3	3	11.2
9	3	3	2	1	1	11.5
Mean1	11.733	11.500	11.367	11.533		
Mean2	11.700	11.633	11.600	11.767		
Mean3	11.500	11.800	11.967	11.633		
Pole difference	0.233	0.300	0.600	0.234		
Order	Fermentation time > ratios of water to material > inoculum concentration					
Optimized factor	A ₁	B ₃	C ₃			
Optimized combination	A ₁ B ₃ C ₃					

Table 106.5 Results of verification testing

	1	2	3	Average
Ethanol production (% vol)	12.1	12.1	12.2	12.1

At last, three parallel experiments which have been carried out on ethanol fermentation by the optimal technique to verify the orthogonal test result (Table 106.5). The ethanol productions of them were 12.1, 12.1, 12.2, respectively, and the average was 12.1.

106.4 Conclusion

From all the experiments above, we have verified the advantage of the thermotolerant strain F3 compared with its control strain AY12. Simultaneous saccharification and fermentation technique has been identified to be the proper technique for F3 through the ethanol production comparison of four techniques. The fermentation conditions were optimized via single-factor test and orthogonal test. The optimal fermentation conditions are as follows, the ratio of nutriment and water 1:2.6, inoculum size 25 ml, fermentation period 56 h.

Acknowledgments This work was financially supported by the program of the National Agricultural Research Projects Fund (Grant No. 2012AA021505), the Cheung Kong Scholars and Innovative Research Team Program in University of Ministry of Education, China (Grant No. IRT1166), and Tianjin Municipal High School Science and Technology Development Fund Program, China (No. 20110625).

References

1. Matsushika A, Inoue H, Murakami K et al (2009) Bioethanol production performance of five recombinant strains of laboratory and industrial xylose-fermenting *Saccharomyces cerevisiae*. *Bioresour Technol* 100:2392–2398
2. Bothast RJ, Schlicher MA (2005) Biotechnological processes for conversion of corn into ethanol. *Appl Microbiol Biotechnol* 67:19
3. Najmul AR (2003) Optimization and Cost Estimation of Novel Wheat Biorefining for Continuous Production of Fermentation Feedstock. *Biotechnol Bioeng* 23:872–880
4. Basso LC, De Amorim HV, De Oliveira AJ et al (2008) Yeast selection for fuel ethanol production in Brazil. *FEMS Yeast Res* 8:1155–1163
5. Cardona CA, Sánchez ÓJ (2007) Fuel ethanol production: Process design trends and integration opportunities. *Bioresour Technol* 98:2415–2457
6. Abdel W, Fattah R (2000) Isolation of thermotolerant ethanologenic yeasts and use of selected strains in industrial scale fermentation in an Egyptian distillery. *Biotechnol Bioeng* 68:531–535
7. Limtong S, Sringiew C, Yongmanitchai W (2007) Production of fuel ethanol at high temperature from sugar cane juice by a newly isolated *Kluyveromyces marxianus*. *Bioresour Technol* 98:3367–3374
8. Kida K, Kume K, Morimura S et al (1992) Repeated-batch fermentation process using a thermotolerant flocculating yeast constructed by protoplast fusion. *J Ferment Bioeng* 74:169–173
9. Shen Y, Tang Q, Wu TX (2010) Optimization of clear liquid fermentation condition for ethanol production from *Canna edulis* Kerl. *Natural Science* 2:115–119
10. Claassen PAM, Lier JB, Lopez AM et al (1999) Utilisation of biomass for the supply of energy carriers. *Appl Microbiol Biotechnol* 52:741
11. Sridhar M, Kiran N, Venkateswar L (2002) Effect of UV radiation on thermotolerance, ethanol tolerance and osmotolerance of *Saccharomyces cerevisiae* VS1 and VS3 strains. *Bioresour Technol* 83:199–202
12. Rajoka MI, Ferhan M, Khalid AM (2005) Kinetics and thermodynamics of ethanol production by a thermotolerant mutant of *Saccharomyces cerevisiae* in a microprocessor-controlled bioreactor. *Lett Appl Microbiol* 40:316–321

13. Balakumar S, Arasaratnam V, Balasubramaniam K (2001) Isolation and improvement of a thermotolerant *Saccharomyces cerevisiae* strain. *World J Microbiol Biotechnol* 17:739–746
14. Sakanaka K, Yan W, Kishida M et al (1996) Breeding a fermentative yeast at high temperature using protoplast fusion. *J Ferment Bioeng* 81:104–108
15. Petek Z, Akar U (2002) Evolutionary engineering of multiple-stress resistant *Saccharomyces cerevisiae*. *FEMS Yeast Res* 5:569–578
16. Ratnam BVV, Narasimha Rao M, Damodar Rao M et al (2005) Optimization of fermentation conditions for the production of ethanol from sago starch using response surface methodology. *World J Microbiol Biotechnol* 19:523–526
17. Shi D, Wang C, Wang K (2009) Genome shuffling to improve thermotolerance, ethanol tolerance and ethanol productivity of *Saccharomyces cerevisiae*. *J Ind Microbiol Biotechnol* 36:139–147
18. D'Amore T, Celotto G, Russell I et al (1989) Selection and optimization of yeast suitable for ethanol production at 40 °C. *Enzyme Microb Technol* 11:411–416
19. Banat IM, Nigam P, Marchant R (1992) Isolation of thermotolerant, fermentative yeasts growing at 52 °C and producing ethanol at 45 °C and 50 °C. *World J Microbiol Biotechnol* 8:259
20. Laopaiboon L, Nuanpeng S, Srinophakun P et al (2009) Ethanol production from sweet sorghum juice using very high gravity technology: Effects of carbon and nitrogen supplementations. *Bioresour Technol* 100:4176–4182

Chapter 107

Different Chemicals Stimulate Diapause Termination of *Artemia* Embryos

Yuqing Chen and Bo Zhang

Abstract This paper studied the effect of the chemicals on the diapause termination of the *Artemia* cysts, including reactive oxygen species (ROS) producing reagent CaO₂, reactive nitric species (RNS) producing reagent NO, and antioxidant reagents tea polyphenol (TP) and ascorbic acid (VC). The results showed that all the tested chemicals could significantly promote *Artemia* cysts development, and the optimum range for CaO₂, TP, VC, and sodium nitroprusside (SNP, NO generators) was 38–94, 50–150, 625–2500, and 25–100 mg/L, respectively. The hatching percentage (H %) was raised from 20 % for the control group to 86 % for the CaO₂ treated group, 86 % for the TP treated group, 85 % for the VC treated group, and 67 % for the SNP treated group, respectively. An analysis of trehalose consumption and glycerol accumulation of the *Artemia* cysts was also performed during incubation.

Keywords *Artemia* cysts · Chemical stimulation · Diapause termination · Trehalose

107.1 Introduction

To survive from harsh environment, *Artemia* tends to release encysted gastrulae (cysts) instead of swimming larvae (nauplii). The cysts usually have low level of development and remarkable tolerance to hypoxia, anoxia, and temperature

Y. Chen · B. Zhang

College of Marine Science and Engineering, Tianjin University of Science and Technology, Tianjin 300457, People's Republic of China

B. Zhang (✉)

Tianjin Key Laboratory of Marine Resources and Chemistry, College of Marine Science and Engineering, Tianjin University of Science and Technology, Tianjin 300457, People's Republic of China
e-mail: zhangbo@tust.edu.cn

variations [1–3]. It has been reported that in a short period after cysts being released, they remain in diapause and the hatching percentage (H %) is very low, even under the optimal environmental conditions [4].

Eggs remaining in diapause stage need specific stimuli and right environmental conditions to resume development [5]. Physical factors, such as dehydration/rehydration, freezing/thawing, and light alone or in combination, are considered as useful tools to terminate diapause and promote development of *Artemia* cysts [6–9], though the intracellular molecular changes driven by these factors are not yet known. Compared to the physical process, chemical treatments are easily to control.

Three kinds of chemical stimulations have been confirmed having apparent effects on the hatching of encysted gastrulae, including oxidants (e.g., hydrogen peroxide, H_2O_2 and/or calcium peroxide, CaO_2) [10, 11] antioxidants (e.g., tea polyphenol, TP) [12], and second messenger nitric oxide (NO) [13]. The oxidants are regarded as reactive oxygen species (ROS) signal producer. However, the antioxidants are well known for clearance of ROS. NO is related to reactive nitric species (RNS). Interestingly, all of them play key roles in promoting the development of *Artemia* cysts.

In this work, chemicals including CaO_2 , NO, TP, and vitamin C (VC) were applied to investigate their induction on diapause termination and development of *Artemia* embryos. To our best knowledge, this is the first time to introduce vitamin C in similar researches.

107.2 Materials and Methods

Cysts from a parthenogenetic *Artemia* strain were harvested in Seitien, Kazakhstan in September, 2011. After the removal of impurities (such as empty shells and debris), the cysts were soaked in brine (salinity of 150) for 2 h, and then collected with a 0.125 mm sieve. The purified cysts were stored at $-20\text{ }^\circ\text{C}$.

107.2.1 Hatching Assays

Four chemicals, including NO generator sodium nitroprusside (SNP), H_2O_2 supplier (CaO_2), TP, and VC, were added into hatching medium at the beginning of incubation. Their final concentrations in the medium were selected within the range from 5–250 mg/L for SNP, 2–113 mg/L for CaO_2 , 3–250 mg/L for TP, and 10–2500 mg/L for ascorbic acid (VC), respectively. As the addition of VC remarkably reduced the medium acidity, NaOH was used to adjust pH to 7.5. The pH values remained constant when the cysts were treated by TP, SNP and CaO_2 . Briefly, cysts were immersed in brine (salinity of 30) for 20 min after unfrozen for 24 h and then hatched under the standard hatching conditions [14]: the salinity of

25, pH 8.0, the temperature of 28 ± 1 °C, the density of about 2.5 g cysts dry matter per liter, the illumination of 2000 lux, and continuous aeration. The hatching percentage (H %) was recorded after 24 h incubation unless otherwise stated.

107.2.2 Analysis of Trehalose and Glycerol Contents in Decapsulated Cysts

To analyze the content of trehalose and glycerol in the cysts at each time point after the chemical treatment, the sample was collected and rinsed thoroughly with running water to remove traces of chemicals after incubation of 0, 2, 4, 6, 8, 10 h. Each sample was divided into two parts, one part was further hatched in seawater to assay H % and the other was decapsulated and the contents of trehalose and glycerol were analyzed. About 0.5 g decapsulated cysts were homogenized in 4.5 mL 72 % ethanol on ice, and then centrifuged at $\times 800$ g (0 °C) for 10 min to remove the insoluble fragments. The supernatants were to 5 mL with the addition of 72 % ethanol, and the contents of trehalose and glycerol were analyzed by high-performance liquid chromatography (HPLC) [15]. The results were recorded as the percentage of mg trehalose/glycerol per mg dry weight of decapsulated cysts.

107.3 Results and Discussions

107.3.1 Chemicals Induction Analysis

As shown in Fig. 107.1, similar hatching efficiencies were obtained by the addition of CaO₂, TP, and VC to the hatching medium respectively. The optimal concentrations for achieving the highest hatching percentage were 75 mg/L for CaO₂ and TP, and 1250 mg/L VC. While maximum cyst development obtained with SNP was about 67 %. When SNP concentration reached to 250 mg/mL, H % dropped to zero. This inhibition may be due to the harmful effect of SNP. To our knowledge, this is the first time to point that VC could improve diapause termination greatly, which is another example of ROS elimination.

107.3.2 Analysis of Diapause Termination

As the proceeding of incubation, the amount of trehalose dropped significantly from 2–10 h. The reduction percentage was 14.1 % (control group), 50.2 % (H₂O₂ treated group), 68.8 % (CaO₂ treated group) and 71.9 % (TP treated group)

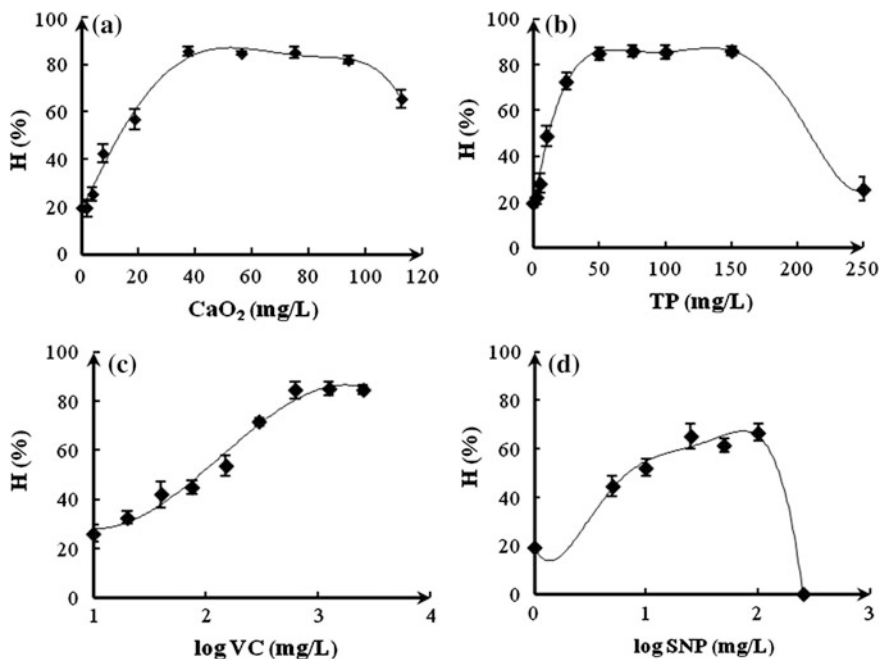


Fig. 107.1 Hatching percentage of *Artemia* cysts treated by different chemicals. 0.5 g of cysts in non-supplemented sea water added with CaO_2 (a), TP (b), VC (c) or SNP (d) were hatched with rotation for 24 h. Results are presented as the mean values of three replicates with error bars representing standard deviation, and the X-axis for C and D is \log_{10} . The data were analyzed by a non-linear regression. If the error bars are not shown, the error is smaller than the symbol

(Fig. 107.2a). The results indicated that trehalose deduction might correlate with hatching rate of each sample. The content of glycerol increased from 5.7–9.0 % at first 6 h and reduced to 5.0 % at 10 h with 85 larvae developed per 100 cysts induced by TP (Fig. 107.2b). Before 6 h, the longer TP and CaO_2 accompanied cysts during incubation, the higher H % presented. However, the H % remained at about 61 % by H_2O_2 treatment and at 10 % of control sample (Fig. 107.2c). At first 2 h, the increase rate of trehalose was 6.5 % for control sample, 13.7 % for H_2O_2 treatment, 6.5 and 5.5 % for CaO_2 and TP treatment respectively. The results for each time point were subjected to two-way analysis of variance (ANOVA) followed by F-test. Both trehalose ($P < 0.05$) and glycerol ($P < 0.01$) had increased at first 2 h, which indicated diapause had been terminated and metabolic process had started in this period. It has been reported that when diapause was broken [7], the trehalose metabolism would be initiated, undergoing complete oxidation and serving as a substrate for glycogen and glycerol synthesis [8, 16]. The result in this study indicated that the consumption of trehalose started from 2 h. In consideration of short treatment time of H_2O_2 , molecular switch might have been triggered before hatching, and that suggested that trehalose might not be the

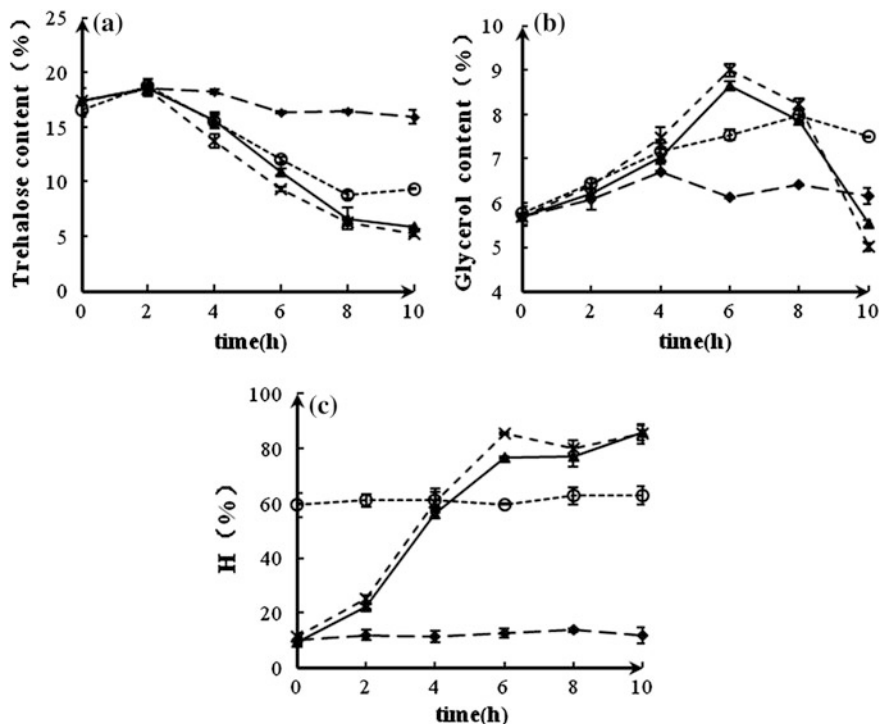


Fig. 107.2 Different performance by varying stimulation. With different stimulation, trehalose (a), glycerol (b), and H % (c) yielded various changes at each time point during the incubation. The aliquot treated by H₂O₂ was prehydrated in water for 60 min. Before hatching in non-supplemented sea water, these cysts were collected on a sieve and rinsed thoroughly with running water to remove traces of H₂O₂. The last two were hatched with CaO₂ and TP added separately at the beginning of incubation. ◆—control sample, ○—H₂O₂ (3 %, w/w, 10 min), ▲—CaO₂ (75 mg/L), ×—TP (60 mg/L)

key of switch. There may be another unknown energy system functioning immediately after diapause termination.

No direct evidence was provided here, but Clegg's research on diguanosine (Gp4G) has supported this assumption [17]. Wang et al. reported the activation of cellular was ignited as early as 0.5 h after rehydration [18], which confirmed the changes in some substance in the first 2 h. Studies suggested that diapause was triggered by external and internal signals, and the molecular switches, playing regulatory roles, were considered as the central issues in the study of diapause [19]. More researches have been conducted to investigate the potential mechanisms and the characteristics of the chemicals as the specific stimuli of diapause termination. The studies mainly focused on the investigation of gene expression, differential mRNA, and proteomic profiling during post-diapaused embryonic development of *Artemia franciscana* [18, 20, 21], but there is a lack of these investigations after chemical stimulation.

107.4 Conclusion

This work studied the effect of the chemicals (CaO₂, TP, VC, and SNP) on the diapause termination of the *Artemia* cysts. The results showed that the tested chemicals significantly promoted *Artemia* cysts development, and the optimum range for CaO₂, TP, VC, and SNP was 38–94, 50–150, 625–2500, and 25–100 mg/L, respectively. The hatching percentage (H %) was raised from 20 % for the control group to 86 % for the CaO₂ treated group, 86 % for the TP treated group, 85 % for the VC treated group, and 67 % for the SNP treated group, respectively. Additionally, the rate of trehalose consumption and glycerol accumulation inside the *Artemia* cysts was also measured.

Acknowledgments This study was supported by the International Cooperation Research Program of the Ministry of Science & Technology of China (grant number CK08-03 and 2010DFA32300).

References

1. Clegg JS (1997) Embryos of *Artemia franciscana* survive four years of continuous anoxia: the case for complete metabolic rate depression. *J Exp Biol* 200:467–475
2. MacRae TH (2003) Molecular chaperones, stress resistance and development in *Artemia franciscana*. *Semin Cell Dev Bio* 14:251–258
3. Clegg JS (2007) Protein stability in *Artemia* embryos during prolonged anoxia. *Biol Bull* 212:74–81
4. Clegg JS, Conte FP (1980) A review of the cellular and developmental biology of *Artemia*. In: Persoone G, Roels O, Jaspers E (eds) *The brine shrimp Artemia*. Universa Press, Wetteren, Belgium
5. Kostal V (2006) Eco-physiological phases of insect diapause. *J Insect Physiol* 52:113–127
6. Li Y (2008) Differential proteomic analysis in different development stages of *Artemia sinica*. Master thesis, Liaoning Normal University (in Chinese)
7. Drinkwater LE, Clegg JS (1991) Experimental biology of cyst diapause. In: Browne RA, Sorgeloos P, Trotman CNA (eds) *Artemia* biology. CRC Press, Boca Raton
8. Boulton AP, Huggins AK (1977) Biochemical changes occurring during morphogenesis of the brine shrimp *Artemia salina* and the effect of alterations in salinity. *Comp Biochem Physiol A: Mol Integer Physiol* 57:17–22
9. Clegg JS (1986) The physical properties and metabolic status of *Artemia* cysts at low water contents. In: Leopold AC (ed) *Membranes, metabolism and dry organisms*. Cornell University Press, Ithaca
10. Van Stappen G, Lavens P, Sorgeloos P (1998) Effects of hydrogen peroxide treatment in *Artemia* cysts of different geographical origin. *Adv Limnol* 52:281–296
11. Naessens E, Trackaert W, Van NL et al (2002) Method for producing free swimming *Artemia* nauplii and packaged cysts for use in that method. European, EP1195088A1, 10.04.2002
12. Fan XY (2008) Method to hatch free swimming nauplii from *Artemia* cysts. China, ZL200710137409.8, 05.12.2008 (in Chinese)
13. Robbins HM, Van Stappen G, Sorgeloos P et al (2010) Diapause termination and development of encysted *Artemia* embryos: roles for nitric oxide and hydrogen peroxide. *J Exp Biol* 213:1464–1470

14. Lavens P, Sorgeloos P (eds) (1996) Manual on the production and use of live food for aquaculture. FAO fisheries technical paper, Rome
15. Yue ME, Niu X (2009) Determination of trehalose and glycerin in *Artemias* by high performance liquid chromatography. *Chem. Reagents* 31:375–376 (in Chinese)
16. Clegg JS (1964) The control of emergence and metabolism by external osmotic pressure and the role of free glycerol in developing cysts of *Artemia salina*. *J Exp Biol* 41:879–892
17. Warner AH, Clegg JS (2001) Diguanosine nucleotide metabolism and the survival of artemia embryos during years of continuous anoxia. *Eur J Biochem* 268:1568–1576
18. Wang WW, Meng B, Chen WH et al (2007) A proteomic study on postdiapaused embryonic development of brine shrimp (*Artemia franciscana*). *Proteomics* 7:3580–3591
19. MacRae TH (2010) Gene expression, metabolic regulation and stress tolerance during diapause. *Cell Mol Life Sci* 67:2405–2424
20. Tate WP, Marshall CJ (1991) Post-dormancy transcription and translation in the brine shrimp. In: Browne RA, Sorgeloos P, Trotman CNA (eds) *Artemia* biology. CRC Press, Boca Raton
21. Chen WH, Ge XM, Wang WW et al (2009) A gene catalogue for post-diapause development of an anhydrobiotic arthropod *Artemia franciscana*. *BMC Genomics* 10:52

Chapter 108

Dominant Bacteria TCCC15005 Used for Treatment of Alkaline Wastewater from Oil Refinery in a SBR

Jing Yang, Hua Zhao, Xi Wang, Xin Feng and Xinhua Wang

Abstract Biological treatment was an important and integral part of any wastewater treatment plant that treats wastewater from either municipality or industry. In this study, dominant bacteria TCCC15005 was used for treating alkaline wastewater from oil refinery in a SBR system. Subsequently, the optimized treatment conditions were investigated. The result indicated that the optimized treatment conditions were 0.5 % corn mill, 1.0 % corn steep liquor, 0.2 % $\text{MgSO}_4 \cdot 7\text{H}_2\text{O}$, 1.03 g/L inoculation amount, 35 °C, pH 7.5. And the treatment time was 28 h. Under the optimal conditions, the removal rate of COD can reach 84.16 %.

Keywords Alkaline wastewater · Dominant bacteria · Sequencing batch reactor (SBR) · Treatment conditions

108.1 Introduction

In the process of oil refining, the alkaline wastewater was mainly resulted from the process of removing acid liquid of straight-run diesel and gasoline by alkaline cleaning [1]. Such alkaline wastewater contained a lot of material of environmental pollution, and even many carcinogens. The main components were sodium hydroxide, naphthenic acid sodium, phenol sodium, sodium carbonate, sodium sulfide and so on [2]. If this kind of alkaline wastewater was discharged directly, it would contaminate the environment gravely; if it entered the wastewater treatment system without disposal, it would have seriously impacted on both the subsequent disposal process and water quality [3].

J. Yang · H. Zhao (✉) · X. Wang · X. Feng · X. Wang
Key Laboratory of Industrial Microbiology, Ministry of Education,
College of Bioengineering, Tianjin University of Science and Technology,
Tianjin 300457, People's Republic of China
e-mail: zhaohua@tust.edu.cn

Petrochemical production technology had grown more sophisticated in recent years. Organic substances in alkaline wastewater tended to be prosperous, which caused a great burden to traditional treatment process [4]. Nowadays most of alkaline wastewater disposal techniques was based on the recovery of the naphthenic acid sodium and phenol sodium [5, 6] while the alkaline residue wastewater should be processed after the recovery [7].

Biotechnology of treating alkaline wastewater had a long history [8]. Modern biotechnology, especially selecting and cultivating dominant bacteria, could enhance the biological systems removal capability to refractory organics [9]. Comparing with other methods, this method had many advantages, such as lower cost, higher efficiency, easier to be handled and without secondary pollution. All those characteristics attracted a great of attention from all over the world. There had been many relevant searches on this issue in different fields, including printing and dyeing, chemical waste water and so on [10]. The sequencing batch reactor (SBR) system was a fill-and-draw activate-sludge treatment system that could be applied to treat piggery wastewater, either in aerobic/anoxic conditions [11], or in anaerobic digestion [12], domestic sewage [13], industrial sewage [14–16] and so on.

Now, feasibility of using combined dominant bacteria and SBR for oilfield wastewater treatment had been reported [17]. The present work was focused on optimization of treatment condition, namely carbon source, nitrogen source, inorganic salt, inoculum concentration, pH, temperature and the treating time. The biological treatment conditions could provide data and technical support to practical application in alkaline wastewater.

108.2 Materials and Methods

108.2.1 *Microorganisms and Culture Medium*

One bacterial strain, TCCC15005 was isolated from sludge nearby a petroleum smelter [18]. The culture medium was LB medium containing tryptone $10 \text{ g}\cdot\text{L}^{-1}$, yeast extract $5 \text{ g}\cdot\text{L}^{-1}$, sodium chloride (NaCl) $10 \text{ g}\cdot\text{L}^{-1}$, the pH values of the media were adjusted to the optimum pH values of 7.0. Prior to use, the media were sterilized in an autoclave at $121 \text{ }^\circ\text{C}$ for 20 min. The flasks were incubated at $37 \text{ }^\circ\text{C}$ in a rotary shaker at 120 r/min [19]. After 24 h, centrifuging at 4,000 r/min for 10 min, cleaning twice, collecting bacteria and blending with sterilized bran, then drying it, and keeping in $4 \text{ }^\circ\text{C}$.

108.2.2 *Pretreated Alkaline Wastewater*

Alkaline wastewater obtained from oil refinery should be pretreated. Firstly, 5.5 % sulfate acids was added. 24 h later, the sublayer liquid was collected and used as experimental material. Table 108.1 showed the properties that the sublayer liquid and their values after these pretreatment operations.

Table 108.1 Composition of sublayer liquid

Properties	pH	COD (mg/L)	Sulfide (mg/L)	Phenol (mg/L)
Values	6.13	58016	10196	41.39

108.2.3 Sequencing Batch Reactor (SBR)

The SBR process was presented in Fig. 108.1.

One 1.5-L reactor, as shown in Fig. 108.1, was used in the experiments. The dominant bacteria was inoculated in the SBR reactors and pretreated alkaline wastewater was added (final volume of 1.0 L). During the feeding of the wastewater, the reaction system was fully aerated and the aeration continued for 22 h. The reaction process was then shut down for 5 h. After full settling of the bio-sludge, the 1/2–2/3 supernatant was removed. Then the alkaline wastewater was filled into the reactor up to the final volume of 1.0 L and the above operation was repeated [20, 21].

108.2.4 Method of COD Determination

The COD in alkaline wastewater was determined by potassium dichromate method [22].

108.2.5 Determination of the Optimized Treatment Condition and Treating Time

Carbon sources, nitrogen sources, inorganic salt, inoculum concentration, pH, temperature and the treating time were varied accordingly in the optimization

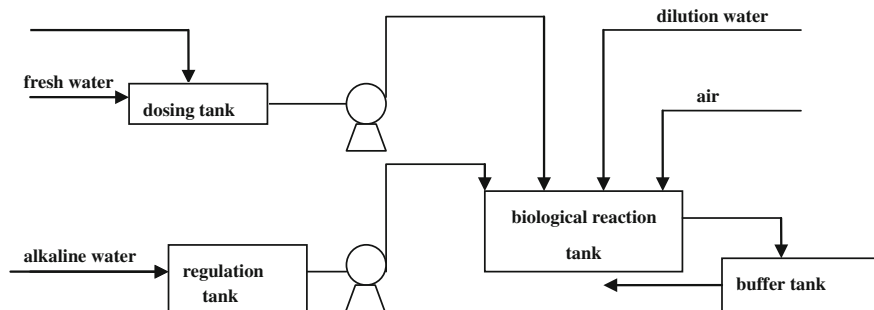


Fig. 108.1 SBR process

experiments, carbon sources each at 0.5 %, nitrogen sources each at 1.0 %, and inorganic salt each at 0.2 %, temperature range of 10–60 °C, pH range of 6–8.5. At the same time, different inoculum concentration, treating time and consecutive treatment were investigated.

108.3 Results and Discussion

108.3.1 *Effects of Nutrient Substance on the Cod Removal Rate*

In the process of treating alkaline wastewater, bacteria took all kinds of organic pollutant as nutrition for their growth. But nutrients of pretreated alkaline wastewater may not completely meet the need of bacteria, in that case, some extra nutrients should be added.

108.3.1.1 Effects of Carbon Sources on the Cod Removal Rate

In order to research the effect of adding carbon sources on the COD removal rate, we chose glucose, sucrose, starch, maltose and corn mill as carbon source. It could be concluded from the results presented graphically in Fig. 108.2 that TCCC15005 can use various carbon sources, but the best carbon source was corn mill and additive amount was 0.5 %.

108.3.1.2 Effects of Nitrogen Sources on the Cod Removal Rate

The influence of nitrogen sources and additive amount on the COD removal rate was investigated. In the treatment process, adding nitrogen source can increase the COD removal rate, the COD removal rate was illustrated as Fig. 108.3. Because of its high COD removal rate and economic applicability, corn steep liquor was chosen as nitrogen source and its optimal additive amount was 1 %.

108.3.1.3 Effects of Inorganic Salt on the Cod Removal Rate

Inorganic salt was the indispensable substances of microbial life activities, so different inorganic salt magnesium sulfate ($\text{MgSO}_4 \cdot 7\text{H}_2\text{O}$), sodium dihydrogen phosphate ($\text{NaH}_2\text{PO}_4 \cdot 12\text{H}_2\text{O}$), potassium phosphate (K_3PO_4), calcium chloride (CaCl_2), manganese sulfate (MnSO_4) were added to increase COD removal rate. It was showed that the optimum inorganic salt was magnesium sulfate ($\text{MgSO}_4 \cdot 7\text{H}_2\text{O}$) and its additive amount was 0.2 % (Fig. 108.4).

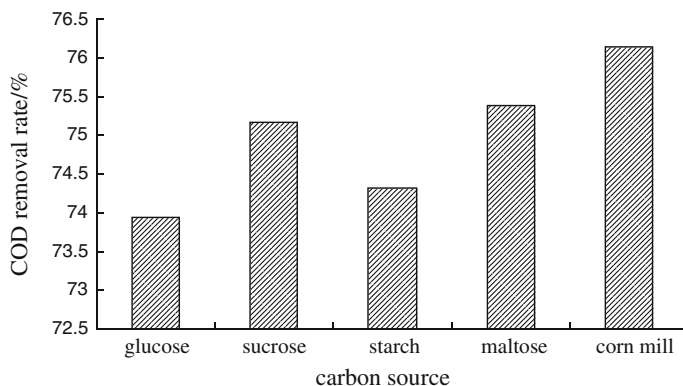


Fig. 108.2 Effects of carbon sources on the COD removal rate. TCCC15005 was inoculated into SBR reactor. 0.5 % (m:m) glucose, sucrose, starch, maltose and corn mill was added respectively. 0.50 g inoculum concentration. Then cultured at pH 7.0 at 37°. 25 h later, the COD value was measured

108.3.2 Effects of Inoculum Concentration on the Cod Removal Rate

At the same time, the effect of inoculum concentration on COD removal rate was tested. It was obvious from the data presented graphically in Fig. 108.5 that the optimum inoculum concentration for TCCC15005 was 1.03 g at which the COD removal rate is up to 81.65 %. When inoculum concentration was low, the degradation was not obvious. With the inoculum concentration increased, the COD removal rate increased gradually. When inoculum concentration was more than 1.03 g, COD removal rate was up to 81.65 %, about 10.46 % higher compared with that of modified before. But the increment of COD removal rate was not obvious if inoculum concentration continued to increase. So the optimum inoculum concentration was 1.03 g considering comprehensively the degrading efficiency and economy.

108.3.3 Effects of Treating Condition on the Cod Removal Rate

108.3.3.1 Effects of Temperature on the Cod Removal Rate

The effect of temperature on the COD removal rate of combined TCCC15005 and SBR was studied at temperatures ranging from 10 to 60 °C (Fig. 108.6). It was showed that the optimum treatment temperature for TCCC15005 with SBR was

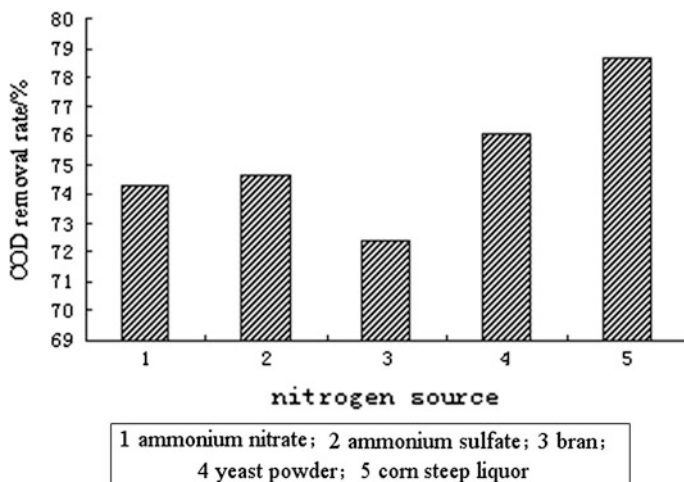


Fig. 108.3 Effects of nitrogen sources on the COD removal rate. TCCC15005 was inoculated into SBR reactor. 1.0 % (m:m) ammonium nitrate, ammonium sulfate, bran, yeast powder, corn steep liquor was added respectively. 0.5 % (m:m) corn mill was used as carbon source. The culture condition was as following, 0.50 g inoculum concentration, pH 7.0, 37°. 25 h later, the COD value was measured

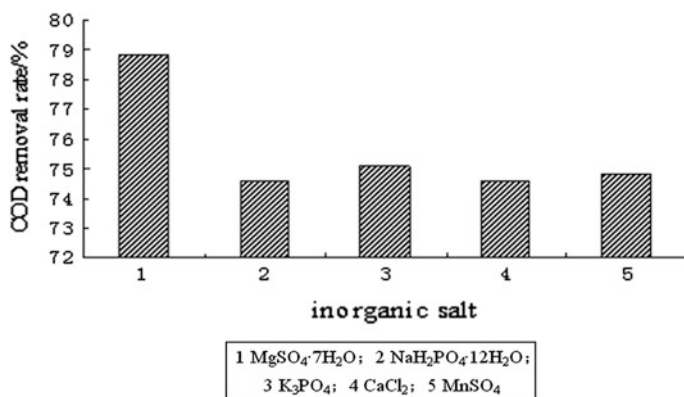


Fig. 108.4 Effects of inorganic salt on the COD removal rate. TCCC15005 was inoculated into SBR reactor. 0.2 % (m:m) different inorganic salt ($MgSO_4 \cdot 7H_2O$, $NaH_2PO_4 \cdot 12H_2O$, K_3PO_4 , $CaCl_2$, $MnSO_4$) was added respectively. 0.5 % corn mill was used as carbon source and 1.0 % corn steep liquor was used as inorganic salt. The culture condition was as following, 0.50 g inoculum concentration, pH 7.0, 37 °C. 25 h later, the COD value was measured

35 °C, as in this case, the COD removal rate was up to 82.08 %. When the temperature was less than 25 °C or more than 40 °C, the COD removal rate decreased significantly.

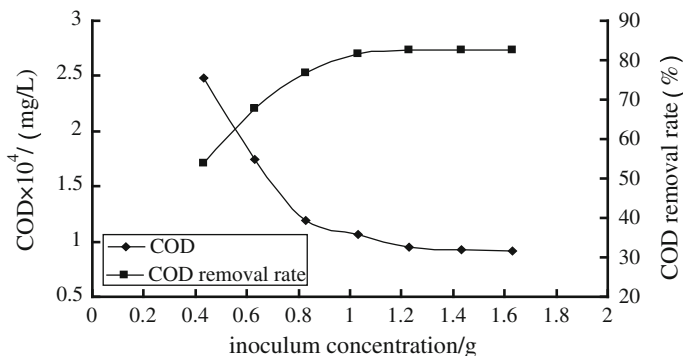


Fig. 108.5 Effects of inoculum concentration on the COD removal rate. TCCC15005 was inoculated into SBR reactor according to six different inoculum concentrations (0.43, 0.63, 0.83, 1.03, 1.23, 1.43, 1.63 g). The culture condition were 0.5 % corn mill, 1.0 % corn steep liquor, 0.2 % $\text{MgSO}_4 \cdot 7\text{H}_2\text{O}$, pH 7.0, 37 °C. 25 h later, the COD value was measured

108.3.3.2 Effects of pH on the Cod Removal Rate

The influence of pH on the COD removal rate was investigated. Seven different pH(6.0, 6.5, 7.0, 7.5, 8.0, 8.5) were test. It could be concluded from the results presented graphically in Fig. 108.7 that pH would have a major influence to bacteria breeding and COD removal rate. The optimum pH value for TCCC15005 with SBR was 7.5 at which the COD removal rate is up to 82.27 %. When pH < 6.5, COD removal rate was not obvious and less than 50 %. If pH was more than 6.5, with pH increased, the COD removal rate also increased rapidly, until pH is 7.5, COD removal rate reached the peak. If pH > 7.5, the COD removal rate decreased dramatically. So the optimum pH was 7.5.

108.3.4 Effects of the Treating Time on the Cod Removal Rate

The treating time of SBR also affect the COD and COD removal rate. We get COD and COD removal rate every 4 h. It could be concluded from the results presented graphically in Fig. 108.8 that the optimum treating time was 28 h. At the beginning, COD was higher than original alkaline wastewater because of adding bacteria. After 12 h, COD variation was not obvious because of bacterial extension and logarithm. But from 12 to 28 h, bacteria was in stable phase and they has exuberant metabolism, so COD removal rate increased dramatically and COD removal rate was up to 84.16 %. But the increment of COD removal rate was not obvious if treating time continued to increase because of decline phase. So we determined that the treating time of SBR was 28 h.

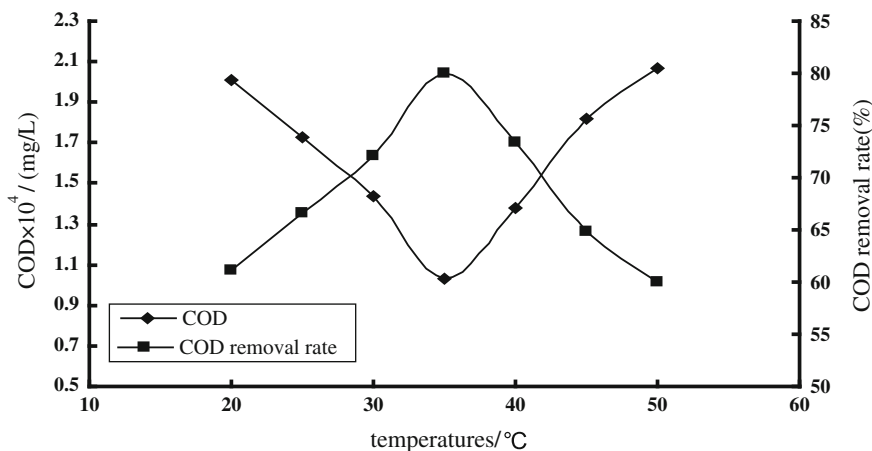


Fig. 108.6 Effects of temperature on the COD removal rate. TCCC15005 was inoculated into SBR reactor and cultured at different temperatures which were ranging from 10 to 60 °C. The culture condition was as following, 0.5 % corn mill, 1.0 % corn steep liquor, 0.2 % $MgSO_4 \cdot 7H_2O$, 1.03 g inoculum concentration, pH 7.0. 25 h later, the COD value was measured

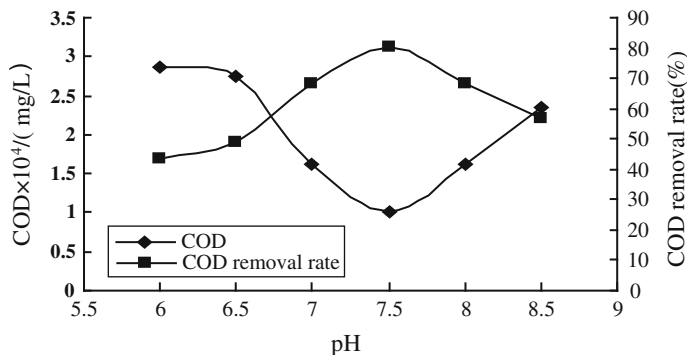


Fig. 108.7 Effects of pH on the COD removal rate. TCCC15005 was inoculated into SBR reactor. The condition of culture was as following, the volume of the alkaline wastewater which was prepared at pH 6.0, 6.5, 7.0, 7.5, 8.0 and 8.5. The culture condition were 0.5 % corn mill, 1.0 % corn steep liquor, 0.2 % $MgSO_4 \cdot 7H_2O$, 1.03 g inoculum concentration, 35 °C. 25 h later, the COD value was measured

108.3.5 Effects of Consecutive Treatment on the Cod Removal Rate

In summary, dominant bacteria with SBR was used to treat alkaline wastewater from oil refinery, the COD of alkaline wastewater decreased perceptibly under the optimized condition after 28 h. But wastewater was polluted seriously and its initial COD was high, so the COD of treated wastewater was still extremely high.

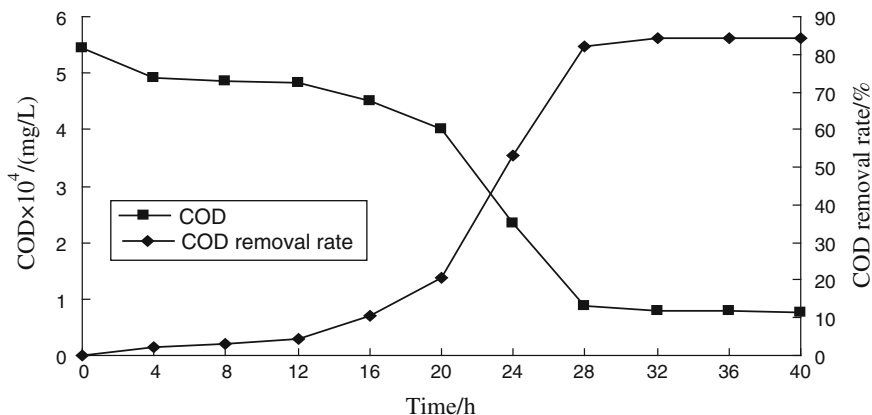


Fig. 108.8 Effects of the processing time on the COD removal rate. TCCC15005 was inoculated into SBR reactor. The culture condition was as following, 0.5 % corn mill, 1.0 % corn steep liquor, 0.2 % MgSO₄·7H₂O, pH 7.5, 35 °C, 1.03 g inoculum concentrations. Every 4 h, the COD value was measured

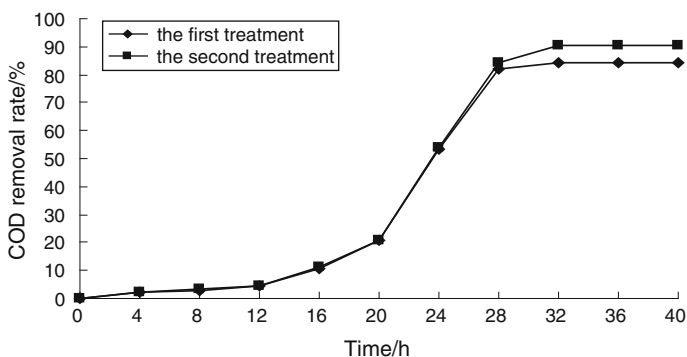


Fig. 108.9 Effects of consecutive treatment on the COD removal rate. TCCC15005 was inoculated into SBR reactor. The culture condition was as following, 0.5 % corn mill, 1.0 % corn steep liquor, 0.2 % MgSO₄·7H₂O, pH 7.5, 35 °C, 1.03 g inoculum concentrations. Every 4 h, the COD value was measured. Then centrifuging treated alkaline wastewater at the speed 4,000 r/min, 10 min, and taking 30 mL clear liquid to 250 mL flask. The above step was repeated

The effect of consecutive treatment on the COD removal rate was researched. According to the data presented graphically in Fig. 108.9, we know that the COD removal rate was up to 84.16 % after the first treatment, and on that basis, by the second treatment the COD removal rate was up to 90.69 %, which was 7.75 % higher than a single disposal process. Through the second disposal process, the COD removal rate increased unobviously. It appeared likely that alkaline wastewater contained large amounts of sulfide and phenol which were harmful to

bacterial growth. So we can consider that reducing COD of alkaline wastewater by removing toxic substances in order to achieve better results. Further studies were necessary in this direction.

108.4 Conclusion

Through optimizing treating conditions with dominant bacteria into SBR, the optimized conditions was ensured as follows: 0.5 % corn mill, 1.0 % corn steep liquor, 0.2 % $\text{MgSO}_4 \cdot 7\text{H}_2\text{O}$, 1.03 g/L inoculation amount, 35 °C, pH 7.5. And treating time was 28 h. In such optimized conditions, the removal rate of COD can be up to 84.46 % and almost 13.85 % higher than before. So the method that treating alkaline wastewater with dominant bacteria with SBR is feasible, the treating efficiency was good. Moreover, the dominant bacteria still can use cheap culture medium to degrade the alkaline wastewater, so it had important applicable value and became foundation for industrial production.

References

1. Sublette KL (1997) A preliminary cost analysis of the biotreatment of refinery spent-sulfidic caustic. *Appl Biochem Biotech* 63(1):695–696
2. Strom AD, Danilevskaya IP, Ptitsa RP et al (1970) Experiments in the biological purification of petroleum refinery wastewater. *Chem Technol Fuels Oils* 6(4):277–280
3. Xie WY, Zhong L, Ren W et al (2009) Technological advances in treatment of alkaline wastewater from petrochemical industry. *Mod Chem Ind* 29(6):28–31
4. Balcioglu IA, Ötker M (2003) Treatment of pharmaceutical wastewater containing antibiotics by O_3 and $\text{O}_3/\text{H}_2\text{O}_2$ process. *Chemosphere* 50(1):85–95
5. Cheng LH, Chen JJ, Liu HB et al (2006) Commercial tests for alkaline wastewater treatment by biologic catalytic oxidation. *Pet Ref Eng* 36(7):59–62
6. Cheng LH, Chen JJ, Zhong HW et al (2006) Pretreatment of alkaline wastewater from refinery by biologic catalytic oxidation process. *Pet Process Petrochem* 37(3):64–67
7. Milan P, Miroslav S, Mirjana S et al (2008) Influence of the waste oil concentration in water on the efficiency of the aeration process in refinery wastewater treatment. *J Mech Eng* 54(10):675–684
8. Matveev MS (1996) Biological purification of waste water from oil refineries. *Chem Technol Fuels Oils* 2(5):329–332
9. Speece RE (1983) Anaerobic biotechnology for industrial wastewater treatment. *Environ Sci Technol* 17(9):416–427
10. Eigenson AS, Loakimas EG, Lukinskaya NT et al (1974) Prospects for development in water usage and water discharge in petroleum refineries and petrochemical plants. *Chem Technol Fuels Oils* 10(9):665–667
11. Jern NW (1987) Aerobic treatment of piggery wastewater with the sequencing batch reactor. *Biol Wastes* 22(4):285–294
12. Masse DI, Patni NK, Droste RL et al (1996) Operation strategies for psychrophilic anaerobic digestion of swine manure slurry in sequencing batch reactor. *Can J Civil Eng* 23(6):1285–1294

13. Song JN (2012) Experimental research on ABR-SBR process for the treatment of domestic sewage. *China Rural Water Hydropower* 0(2):75–77
14. Wei N, Ji K, Yu XQ et al (2012) Effects of pollutants removal by multi-stage sequencing batch reactor (SBR) processes. *Water Pur Technol* 31(1):42–46
15. Han HJ, Zhou FX, Liu YS et al (2012) Experimental study of oil hydrocarbons in coal chemical wastewater by SBR process. *Water Wastewater Eng* 38(2):57–60
16. Cai XP, Liu LC (2012) Study on the treatment of liquor-making wastewater by SBR. *Liquor-making Sci Technol* 1:98–99
17. Li SC, Liu ZH, Li Z et al (2006) Treatment of oilfield produced wastewater with SBR + concentrated microorganisms. *Urban Environ Ecol* 16(S1):74–75
18. Zhao H, Cao QQ, Liu K et al (2009) Degrading conditions of the optimized strains in the alkaline wastewater biological treatment. *Appl Chem Ind* 38(2):229–232
19. Banerjee A, Ghoshal AK (2010) Isolation and characterization of hyper phenol tolerant *Bacillus sp.* from oil refinery and exploration sites. *J Hazard Mater* 176(1–3):85–91
20. Sirianuntapiboon S, Preeyatum A (2006) Some properties on the application of *Candida utilis* TISTR No. 5001 into sequencing batch reactor (SBR) System. *Afr J Biotechnol* 5(23):2377–2387
21. Berent N, Delgenes N, Akunna JC et al (2000) Combined anaerobic-aerobic SBR for the treatment of piggery wastewater. *Water Res* 34(2):611–619
22. Rocenkery M (1993) The fast method of the COD determination. *Anal Lett* 26(9):2025–2030

Chapter 109

Isolation and Characterization of a New Moderately Halophilic Bacterium Strain SM. 200-5 from Solar Saltern Ponds

Gaochao Xu, Yuangao Deng, Donghui Song and Liying Sui

Abstract A new moderately halophilic bacterium strain SM. 200-5 was isolated from the solar saltern ponds with salinity 200 in Hangu Saltworks, Tianjin, China. The cells of the strain SM. 200-5 were rods and Gram-negative. They could grow in a salinity range of 30–150 and initial pH 6–11, with optimum of salinity 100 and initial pH 7. 16S rDNA alignment showed that the strain SM. 200-5 had 93–95 % similarity with those sequences of genus *Salimicrobium* sp.. Biochemical characterization analysis via API 20E system indicated that biochemical characters of the strain SM. 200-5 were partially different from *Salimicrobium* sp. ISL-25, which was its closest member in the phylogenetic tree. Therefore, the strain SM. 200-5 proposed a new species of *Salimicrobium*.

Keywords Halophilic bacterium · Phylogenetic analysis · *Salimicrobium* sp. · 16S rDNA

109.1 Introduction

Halophilic bacteria are defined as those microorganisms inhabiting hypersaline environments such as salt lakes, salt mines, solar saltern ponds, and salted food [1, 2]. Moderately halophilic bacteria manifest optimal growth in salinity 30–150 [3]. In response of the hypersaline environment, halophilic bacteria usually have special physiological structures and produce valuable active compounds, such as poly- β -hydroxybutyrate (PHB), extracellular polysaccharides, ectoine, and thus possess the potential of biotechnological utilization [4–7]. Recent years many researches have focused on the taxonomy [8, 9] and biodiversity [10–13] of the

G. Xu · Y. Deng · D. Song · L. Sui (✉)

Tianjin Key Laboratory of Marine Resources and Chemistry, Tianjin University of Science and Technology, Tianjin 300457, People's Republic of China

e-mail: suily@hotmail.com

halophilic bacteria, as well as their metabolites (e.g., bacteriorhodopsin, halocins) [14–17] and the ability to degrade pollutants (e.g., azo dye, hydrocarbon) [18, 19].

Halophilic bacteria play an important role in decomposing organic compounds in solar saltern ponds. High density of halophilic bacteria reduces the viscosity of the brine and enhances absorption of solar energy, and thus accelerates the evaporation rate of the brine and improves the quality and quantity of the salt yield [20]. A few studies have conducted in aspect of halobacterium in solar saltern ponds. Yoon et al. [21] isolated a halophilic bacterial strain MSS-155 from a marine solar saltern of the Yellow Sea in Korea; Montalvo-Rodríguez et al. [22] isolated three strains of halobacteria in the solar salterns in Cabo Rojo, Puerto Rico; Chen et al. isolated and identified moderately halophilic bacteria from solar saltern in Shandong, China and investigated their potential antimicrobial and antitumor activities [23]. Yeon et al. [12] evaluated the diversity among the isolated halophiles from the local solar salterns via RFLP analyses of PCR-amplified 16S rDNAs, and followed by phylogenetic analysis of the partial 16S rDNA sequences.

In this study, we isolated and indentified a strain named SM. 200-5 from solar saltern ponds (salinity 200) in Hangu Saltworks, Tianjin, China. The purpose of this study is to provide basic information for further investigation and application of halobacterium in saltern ponds.

109.2 Materials and Methods

109.2.1 Collection of Samples

Sediment sample was collected from solar saltern ponds (salinity 200) in Hangu Saltworks, Tianjin, China in March, 2011. It was kept in sterile plastic bags and stored in the refrigerator at 4 °C.

109.2.2 Selection of Culture Medium

Before insulating the bacterial colony, the growth of bacteria in three kinds of culture medium with different formulations (Table 109.1) was compared in order to select the optimal culture medium for the halophilic bacteria. The modified CM and Gibbons medium were prepared with brine water taken from the same salt pond to ensure that the ionic composition of the medium was consistent with the bacterial living conditions. The brine water was treated with NaClO and autoclaved previous to use.

1 g of sediment sample was added in the Erlenmeyer flask containing 49 mL culture medium. The flasks were incubated in an orbital shaker (150 rpm) at 37 °C

Table 109.1 Formulation of the culture medium

	Modified CM medium [24]	Modified Gibbons medium [25]	Gauze's No.1 medium [26]
Carbon resource (g/L)	yeast extract 10.0	yeast extract 10.0	soluble starch 20.0
Nitrogen resource (g/L)	acid hydrolyzed casein 7.5	acid hydrolyzed casein 5.0	KNO ₃ 1.0
Inorganic salts (g/L)	Brine water	peptone 5.0 Brine water sodium citrate 3.0 KCl 2.0 MgSO ₄ ·7H ₂ O 20.0	NaCl 20.0 FeSO ₄ ·7H ₂ O 0.01 MgSO ₄ ·7H ₂ O 0.5 K ₂ HPO ₄ 0.5
Salinity	200	200	200
pH	7.2–7.4	7.2–7.4	7.2–7.4

for 30 min, 2 mL supernatant was then added to 98 mL culture medium, respectively. OD₆₀₀ was determined after 3 days incubation.

109.2.3 Isolation of Bacterial Colony

Bacteria were isolated from sediment sample with the method above, and 100 µL plating dilutions were then streaked onto agar of the modified CM medium. The agar plates were incubated for 5–7 days. The single colony was picked up on the basis of differences in morphology and inoculated into the modified CM liquid medium, and was incubated in an orbital shaker (150 rpm) at 37 °C for 5–7 days. The above procedure was repeated three times for purification.

109.2.4 DNA Extraction and PCR Amplification of the 16S rDNA Gene

DNA was extracted from the isolated bacteria using AxyPrep Bacterial Genomic DNA Miniprep Kit (Axygen, USA), and stored at -20 °C for later use. The 16S rDNA gene was amplified with two general bacterial primers: 27 f (5'-AGAGTTTGATCCTGGCTCAG-3') and 1525 r (5'-AAAGGAGGTGATCCAGCC-3'). The PCR amplification contained 1 µL of each primer, 4 µL dNTP, 5 µL 10 × buffer, 0.5 µL Taq (TaKaRa, Japan), and 1 µL template DNA, in a final volume of 50 µL. The following conditions were used in the amplification of the 16S rDNA genes: 94 °C for 5 min, followed by 30 cycles of 94 °C for 30 s, 55 °C for 30 s, 72 °C for 3 min, and with a final 10 min extension at 72 °C. Amplified PCR products were

checked by 1 % agarose gel electrophoresis. Sequencing of 16S rDNA gene was done by BGI (China).

109.2.5 Phylogenetic Analysis

Sequences of the isolated bacterial strains were compared to the 16S rDNA gene sequences in the GenBank database, via BLAST searches. Alignment of sequences was carried out with CLUSTAL X software. A phylogenetic tree was constructed using the neighbor-joining method as implemented within the MEGA 5.0, and bootstrap consensus trees were inferred from 1000 permutations of the datasets.

109.2.6 Morphological, Physiological, and Biochemical Characterization

Based on the phylogenetic analysis results, morphological characterizations of the isolated strain SM. 200-5 was determined through Gram-stain [27] and electron microscope (SU-1510, Hitachi, Japan).

Salt tolerance for bacterial growth was tested by adding fresh bacterial culture into the modified CM medium with salinities of 0, 30, 50, 100, 150, 200, and 250, respectively, in a proportion of 1:10³. Growth at different pHs was evaluated using the modified CM medium with initial pH of 5, 6, 7, 8, 9, 10, and 11, respectively. The bacterial growth was determined at OD₆₀₀ after incubating for 24 h at 37 °C.

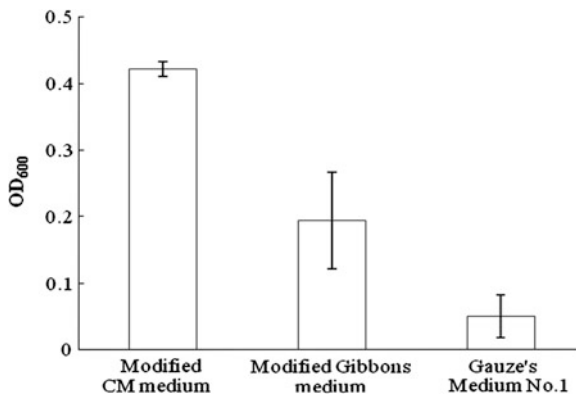
API 20E Bacterial Identification Kit (Biomérieux, France) was used to determine the biochemical characterization of the isolated strain SM. 200-5. The kit contained 20 biochemical indicators, such as enzymes, acid production, etc.

109.3 Results and Discussion

109.3.1 Optimal Culture Medium

Bacterial growth in three culture media was shown in Fig. 109.1. The results showed that the growth of halophilic bacteria in the modified CM medium was the fastest, followed by modified Gibbons medium and those in the Gauze's No.1 medium was the slowest. Therefore, the modified CM medium was chosen as the optimal medium for later isolation and characterization of the halobacteria. The inferior bacterial growth in Gauze's No.1 medium indicated that the carbon (starch) and inorganic nitrogen (KNO₃) could not sustain the halobacterial growth. The higher concentration of nitrogen resources (acid hydrolyzed casein) and

Fig. 109.1 Bacterial growth in different culture medium



similar ionic composition with their living environment in the modified CM may be more suitable for halophilic bacteria growth comparing with the modified Gibbons medium.

109.3.2 Phylogenetic Analysis

16S rRNA gene sequence (about 1.5 kb nucleotides) of the five isolate were determined for this study. 16S rDNA fragments of the five isolated strains were aligned to those closely related species in the database. In the phylogenetic tree, strain SM. 200-5 fell within the clade comprising *Salimicrobium* species (Fig. 109.2). The homology assay indicated that four isolates were related to the genus *Halomonas* (97–99 % similarity), while the strain SM. 200-5 showed 95 % identity to *Salimicrobium flavidum* sp. ISL-25, which was a member of the genus *Salimicrobium*.

109.3.3 Phenotypic Characterization of the Strain SM. 200-5

Colony of the strain SM. 200-5 was circular, pale yellow, smooth, slightly convex, opaque, and 0.5–1 mm in diameter. The cells were rods, (0.3–0.4) $\mu\text{m} \times$ (1.8–3.0) μm , Gram-negative (Fig. 109.3). *Salimicrobium flavidum* sp. ISL-25 was its closest-related strain, while the cells of it were coccoids, ovoids, or rods, (0.4–1.3) $\mu\text{m} \times$ (0.8–9.0) μm , gram-variable-staining [28]. Morphological analysis showed that the strain SM. 200-5 had differences with *Salimicrobium flavidum* sp. ISL-25 on cell morphology and size (Table 109.2).

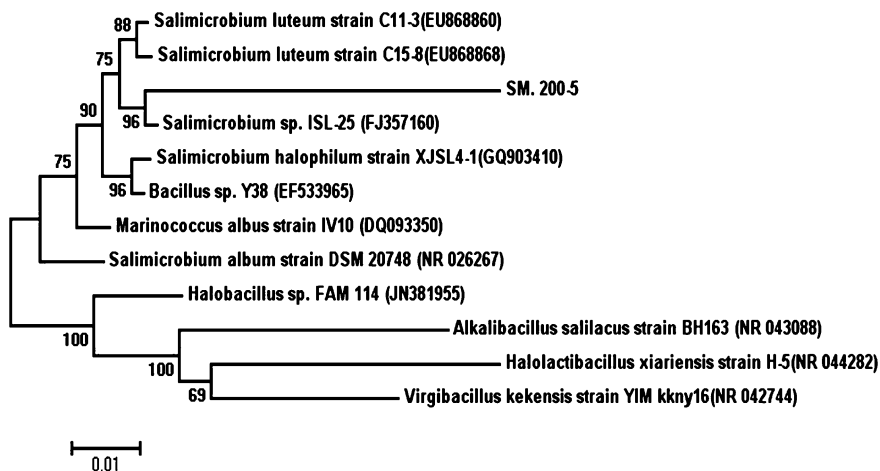
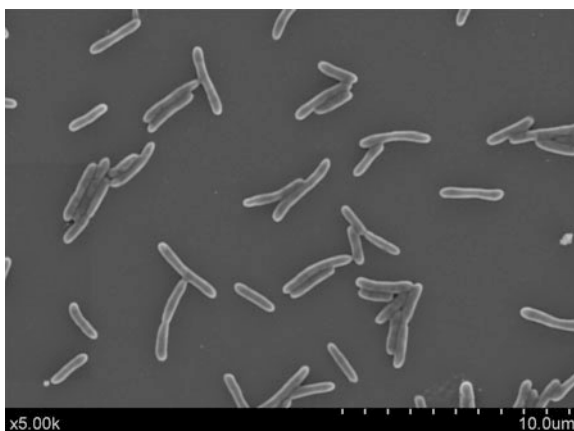


Fig. 109.2 Phylogenetic tree of the strain SM. 200-5 and other closely related bacteria based on partial 16S rDNA sequence

Fig. 109.3 Electron microscopic image of the strain SM. 200-5 ($\times 5000$)



109.3.4 Physiological and Biochemical Characterization

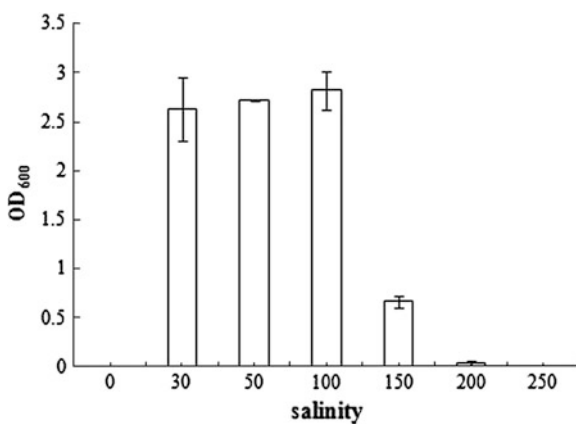
The strain SM. 200-5 could grow in a range of salinity 30–200 and initial pH 6–11, with the optimum of salinity 100 and initial pH 7 (Figs. 109.4 and 109.5). This is consistent with *Salimicrobium flavidum* sp. ISL-25, whose optimal salinity and pH was 100 and pH 7–8 as indicated in Table 109.2.

In assays with the API 20E system, H_2S could be produced. D-glucose, L-rhamnose, laetrile, L-arabinose were fermented and D-mannite, myoinositol, D-sorbierite, D-sucrose, D-melibiose were weakly present, whereas β -galactosidase, arginine dihydrolase, lysine decarboxylase, ornithine decarboxylase, tryptophan

Table 109.2 Comparison of morphological and biochemical characteristics of the strain SM. 200-5 and *Salimicrobium flavidum* sp. ISL-25

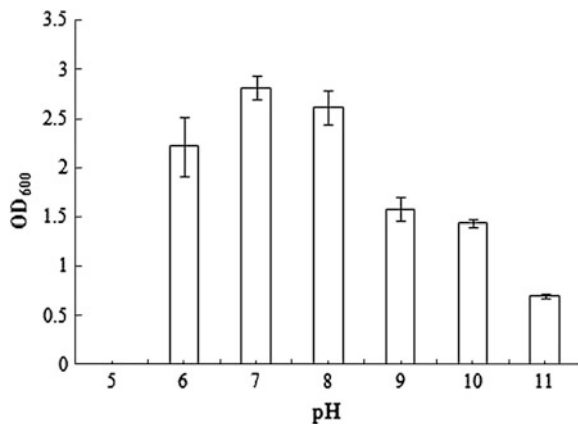
Characteristics	SM. 200-5	<i>Salimicrobium flavidum</i> sp. ISL-25 [28]
Cell morphology	Rods	Cocci, ovals or rods
Cell size (μm)	$(0.3\text{--}0.4) \times (1.8\text{--}3.0)$	$(0.4\text{--}1.3) \times (0.8\text{--}9.0)$
Salinity range for growth	30–200	10–260
Optimal salinity	100	100
pH range for growth	6.0–11.0	ND
Optimal pH	7.0	7.0–8.0
H ₂ S produce	+	–
Enzymes produce		
Gelatinase	–	–
β -galactosidase	–	\pm
Acid production from		
L- rhamnose	+	–
L- arabinose	+	–
Myoinositol	\pm	–
D- mannite	\pm	+
D- sucrose	\pm	+
D- melibiose	\pm	+
D- sorbierite	\pm	–

* +: positive, -: negative, \pm : weakly positive; ND: not determined

Fig. 109.4 Growth of the strain SM. 200-5 at different salinities

deaminase, urease, and gelatinase were absent, indole and acetoin were not produced and citrate were not used. The results indicated that the strain SM. 200-5 and its closest strain *Salimicrobium* sp. ISL-25 had differences in producing H₂S, fermenting rhamnose and arabinose to produce acid (Table 109.2).

Fig. 109.5 Growth of the strain SM. 200-5 at different pH



109.4 Conclusions

The isolated strain SM. 200-5 was a member of the genus *Salimicrobium*, which grow in a salinity range of 30–150 and pH 6–11 with optimum of salinity 100 and initial pH 7. The strain SM. 200-5 had a 95 % similarity with *Salimicrobium flavidum* sp. ISL-25 in terms of 16S rDNA sequencing. Strain SM. 200-5 was distinguished from *Salimicrobium flavidum* sp. ISL-25, by cell shape, ranges of salinity and pH for growth, biochemical characteristics, and acid production, as shown in Table 109.2. On the basis of its phenotypic and genotypic properties, strain SM. 200-5 represented a novel species of the genus *Salimicrobium*. Therefore, we proposed that the strain SM. 200-5 is a new species of *Salimicrobium*.

Acknowledgments This study was supported by the International Cooperation Research Program of the Ministry of Science & Technology of China (grant number 2010DFA32300); the International Cooperation Research Program of the Bureau of Science & Technology of Tianjin (grant number 09ZCGHHZ01200); Key program of Natural Science Foundation of Tianjin (grant number 09JCZDJC25400).

References

1. Oren A, Larimer F, Richardson P et al (2005) How to be moderately halophilic with broad salt tolerance: clues from the genome of *Chromohalobacter salexigens*. *Extremophiles* 4:275–279
2. Ashrafaddin S, Ali AK, Ferdous RJ (2005) Identification and characterization of salt-inducible polypeptide in *Paenibacillus* sp., a moderately halophilic bacterium. *J Biosci Bioeng* 5:573–575
3. Rodríguez-Valera F, Ventosa A, Juez G (1985) Variation of environmental features and microbial populations with salt concentrations in a multi-pond saltern. *Microb Ecol* 2:107–115

4. Oren A (2008) Microbial life at high salt concentrations: phylogenetic and metabolic diversity. *Saline Syst* 1:2–14
5. Liu JJ, Chen QZ, Zeng JN et al (2007) Advances in the research of bioactive substances from marine microorganisms. *J Mar Sci* 1:55–65 (Chinese)
6. Lv JS, Huang HQ, Cong M et al (2006) Identification for a marine bacterium and preliminary study on purification of metabolite from the bacterium. *Acta oceanol sin* 5:173–178
7. Oren A (2002) Diversity of halophilic microorganisms: environments, phylogeny, physiology, and applications. *J Ind Microbiol Biotechnol* 1:56–63
8. Boudjelal F, Zitouni A, Mathieu F et al (2011) Taxonomy and antimicrobial activities of two novel halophilic *Saccharomonospora* strains isolated in Algerian Sahara soils. *Ann Microbiol* 2:299–305
9. Das Sarma P, Das Sarma S (2008) On the origin of prokaryotic “species”: the taxonomy of halophilic Archaea. *Saline Syst* 4:5–9
10. Wang J, Dang HY, Yang GP et al (2009) Physiochemical and phylogenetic analysis of moderately halophilic bacteria halomonadaceae in deep-sea sediments of the Southern Okinawa Trough. *J Mar Sci* 5:17–22 (Chinese)
11. Tang J, Zheng AP, Bromfield ESP et al (2011) 16S rRNA gene sequence analysis of halophilic and halo-tolerant bacteria isolated from a hypersaline pond in Sichuan, China. *Ann Microbiol* 2:375–381
12. Yeon SH, Jeong WJ, Park JS (2005) The diversity of culturable organotrophic bacteria from local solar salterns. *J Microbiol* 1:1–10
13. Zahran HH (1997) Diversity, adaptation and activity of the bacterial flora in saline environments. *Biol Fert* 3:211–223
14. Brown LS (2001) Proton transport mechanism of bacteriorhodopsin as revealed by site-specific mutagenesis and protein sequence variability. *Biochemistry* 11:1249–1255
15. Habden X, Tohty D, Wu M et al (2007) Studies on bacteriorhodopsin gene and sequence of 16S rRNA encoding genes of halophilic archaea of Xinjiang Aibi Lake. *J Biotechnol* 1:46–50 (Chinese)
16. Lanyi JK, Schobert B (2003) Mechanism of proton transport in bacteriorhodopsin from crystallographic structures of the K, L, M₁, M₂, and M₂' intermediates of the photocycle. *J Mol Biol* 2:439–450
17. Kis-Papo T, Oren A (2000) Halocins: are they involved in the competition between halobacteria in saltern ponds. *Extremophiles* 1:35–41
18. Guo JB, Zhou JT, Wang D et al (2008) A novel moderately halophilic bacterium for decolorizing azo dye under high salt condition. *Biodegradation* 1:15–19
19. Litchfield CD (2011) Potential for industrial products from the halophilic Archaea. *J Mol Biol* 10:1635–1647
20. Sorgeloos P, Takaert W (1990) Roles and potentials of *Artemia* in coastal saltworks. In: Cheng L (ed) *Proceeding of International Symposium on Biotechnology of Saltponds*, Tanggu, Tianjin, pp 69–77
21. Yoon JH, Kang KH, Oh TK et al (2004) *Halobacillus locisalis* sp. nov., a halophilic bacterium isolated from a marine solar saltern of the Yellow Sea in Korea. *Extremophiles* 1:23–28
22. Montalvo-Rodríguez R, Ruíz-acevedo A, Ló pez-Garriga J (1997) New isolates of extremely halophilic Archaeobacteria (Halobacteria) from Puerto Rico and the Caribbean. *Caribbean J Sci* 1:98–104
23. Chen L, Wang GY, Bu T et al (2010) Identification of a moderately halophilic bacterium whb45 and screening of its antimicrobial and antitumor activity. *Microbiol China* 1:85–90 (Chinese)
24. Gochnauer MB, Kushner DJ (1969) Growth and nutrition of extremely halophilic bacteria. *Canadian J Microbiol* 10:1157–1165
25. Sehgal SN, Gibbons NE (1960) Effect of some metal ions on the growth of *halobacterium cutirubrum*. *Canadian J Microbiol* 2:165–169

26. Feng EM, Su HY, Wang L (2010) Isolation, identification and phylogenetic analysis of moderately halophilic bacterium isolated from Yantai Sea area. *Mar Sci Bul* 1:52–58 (Chinese)
27. Dong XZ, Cai MY (2001) *Common bacterial identification manual*. Science Press, Beijing
28. Yoon JH, Kang SJ, Oh KH et al (2009) *Salimicrobium flavidum* sp. nov., isolated from a marine solar saltern. *Int J Syst Evol Microbiol* 11:2839–2842

Chapter 110

Preparation of Wetting Powder for Biocontrol *Bacillus Subtilis*

Fang Chen, Shangjing Guo, Haiying Shi, Deduo Han, Yuanjun Kang,
Yu Zheng and Min Wang

Abstract *Bacillus subtilis* is considered as one kind of beneficial strains which can effectively inhibit the pathogenic fungus of the plants and promote plant growth. *B. subtilis* wetting powder exhibited better prevention and cure of powdery mildew, phytophthora blight, gray mold, and plant growth promoting ability. *B. subtilis* wetting powder was formulated using diatomite and calcium carbonate as carrier, sodium dodecyl sulfate, PVA, and CMC–Na as co-formulants, soluble starch, sucrose, and sodium glutamate as protective agent. Optimal formulation recipe and processing technology of *B. subtilis* wetting powder were developed. The best composition was diatomite 5 %, calcium carbonate 5 %, SDS 5 %, CMC-Na 5 %, soluble starch 0.5 %, sucrose 0.5 %, and sodium glutamate 0.5 %. Quality index analysis revealed that the wetting powder reached the biological pesticide standards.

Keywords *Bacillus subtilis* · Wetting powder · Stability · Preparation

This research was supported by the Natural Science Foundation of Tianjin, China (Project No. 09JCZDJC19100). Scientific Research foundation for Doctor, Liaocheng University, China (Project No. 3010)

F. Chen · S. Guo · H. Shi · D. Han · Y. Kang
School of Pharmaceutical, Liaocheng University, Liaocheng, 252059 Shandong, China

Y. Zheng · M. Wang (✉)
Key Laboratory of Industrial Fermentation Microbiology, Ministry of Education,
Collage of Biotechnology, Tianjin University of Science and Technology, Tianjin 300457,
China
e-mail: minw@tust.edu.cn

110.1 Introduction

There is increasing market demand for the environmental friendly biopesticide. Antagonistic bacteria are considered as an important functional group of beneficial bacteria used for biological control as well as for promoting plant growth [1, 2]. Recently, biological control has become an important approach to suppress many plant pathogens [3–6]. *Bacillus subtilis* is considered to be an excellent biocontrol agent not only due to its ability on inducing plant systematic resistance, but also on producing various hydrolytic enzymes and antibiotics [7–14]. From the large amount of antimicrobials produced, lipopeptides stand among the most representative. These antifungal peptides have been proved safe to people and no pollution to environment [15, 16]. So, they have high potential for being used in biological control, food antisepsis, medicine, and so on.

As *B. subtilis* has the characteristics of omnipresence in soils, thermal tolerance, rapid growth, and ready formation of resistant spores, it is considered to be a good biological control agent. Hot air was used in process of spray drying. Temperature was thought to be a main factor for the bacteria. In the process of dehydration, the bacteria cells were smaller than that of freeze-drying. So the species of protective agent in spray drying played an important role. Protective agents are usually used according to the optimized formulation, because single protective agent cannot meet the requirement. Various composition of the optimized protective agent formulation had its own effect in spray drying; also they had a synergistic effect. The maximum protection effect was achieved only when the formulation had an optimized proportion and concentration, based on the structure and size of the cells.

B. subtilis B579 (deposition number CGMCC No. 2270) was isolated from rhizosphere of cucumber in Tianjin, China. It could effectively inhibit the growth of pathogenic *Fusarium oxysporum*, *Rhizoctonia solani*, *Fusarium gramineum*, *Phytophthora capsici*, and *Fusarium solani* on Potato Dextrose Agar (PDA) plates using the dual plate assay [17]. The experiments in glasshouse showed that *B. subtilis* B579 could effectively control Fusarium wilt of cucumber caused by *F. oxysporum* f. sp. *Cucumerinum*. The percentage of germination of seeds and the vigor index of the plants, also the weight of fruits were improved by treating the plant or seed with the fermentation broth of *B. subtilis* B579 indicating a potential biocontrol agent [18]. Two kinds of lipopeptide antifungal compounds of B579 were identified. Genes involved in the biosynthesis of six antifungal compounds were detected in genomic DNA [19]. In this paper, the best composition of the biocontrol agent of *B. subtilis* B579 was developed. Wetting powder was made using the method of spray drying. The suspensibility, wetting time, fineness, and thermal stability of the wetting powder were tested.

110.2 Materials and Methods

110.2.1 Microorganism and Medium

B. subtilis B579 (conserved in our laboratory) is maintained at 4 °C on slant of LB agar medium. *F. oxysporum* is stored at 4 °C on the eggplant bottle containing potato dextrose agar (PDA) medium. Seed medium was comprised of peptone 10 g/L, glucose 5 g/L, yeast extract 5 g/L, beef extract 5 g/L, and NaCl 5 g/L (pH7.0). Fermentation medium used for batch cultivation is composed with yeast extract 6 g/L, soluble starch 11 g/L, glucose 6 g/L, soy bean meal 13.9 g/L, beef extract 8.9 g/L, and maize meal 12.6 g/L (pH 7.0).

110.2.2 Fermentation of *B. Subtilis* B579

A 250-mL Erlenmeyer flask containing 30 mL of seed medium was inoculated with one inoculating loop of *B. subtilis* B579. The seed culture was performed at 37 °C and 180 rpm on a rotary shaker for 12 h. A 7 L bioreactor (Baosheng Ltd., Shanghai, China) with a working volume of 5 L was used for *B. subtilis* B579 cultivation. The batch fermentation was initiated with 5 % inoculums from seed culture. Cultivation temperature, aeration rate, and the agitation rate were maintained at 37 °C, 2 L/min and 500 rpm, respectively. The pH was adjusted with 1 mol/L NaOH when required.

110.2.3 Preparation of Wetting Powder

The fermentation was ended after about 26 h cultivation, and 5 L broth was harvested. The diatomite and calcium carbonate as carrier, sodium dodecyl sulfate, PVA and CMC–Na as co-formulants, soluble starch, sucrose, and sodium glutamate as thermal protective agent. The optimal formulation recipe was optimized by response surface methodology. The wetting powder was obtained by spray-dried [20]

110.2.4 Dual Plate Assay of Biocontrol Agent

The antagonism of biocontrol agent against *F. oxysporum* was tested on PDA plates using the dual plate assay. The biocontrol agent was diluted to 0, 1, 2, 5, and 10 g/L, respectively. The pathogen *F. oxysporum* was inoculated to the center of PDA plates. The inhibition zones of the agent solution with different concentration

were compared. Then pathogens were incubated on the center of PDA plates at 28 °C for 3 d. The sterile-distilled water was served as control. Three replications were carried out for each treatment.

110.2.5 Quality Index Analysis of Biocontrol Agent

Quality index of wetting powder was analyzed according to the wetting powder quality national standard of China [20–22]. The effective composition of wetting powder is not less than the marked content; fineness (44 μm test sieve) ≥ 95–98 % (National standard of China GB/T 16150-1995). Wetting time was 1–2 min (GB/T 5451-2001), and moisture content generally is not more than 3 % (GB/T 1600-2001). Suspension rate was about 70 % (GB/T 14825-2006). The value of pH was neutral, according to the requirement of stability, and the pH was sometimes 5–9 (GB/T 1601-1993). Hot storage stability was stored at 54 ± 2 °C for 14 d, and the effective component decomposition rate was less than 10 % (GB/T 19136-2003).

110.2.6 Analytical Methods

One gram of biocontrol agent was suspended in 9 mL of sterile distilled water and treated in a blender (IKA, Germany) for 10 min. Serial dilutions of the cell suspension from 10^{-7} to 10^{-10} were prepared. Appropriate dilution of 100 μL was spread on solid LB media with 3 replicates. Plates were incubated at 37 °C for 24 h, and then the colony forming units (CFU) were counted. Response surface methodology was used by SAS 6.0 software.

110.3 Results and Discussion

110.3.1 Preparation of Wetting Powder

The fermentation broth was collected and the optimal formulation recipe was developed by response surface methodology. The best composition was diatomite 5 %, calcium carbonate 5 %, SDS 5 %, CMC-Na 5 %, soluble starch 0.5 %, sucrose 0.5 %, and sodium glutamate 0.5 %. The obtained agent of *B. subtilis* B579 as shown in Fig. 110.1 indicated that the agent of *B. subtilis* B579 with even and small particle size could be successfully prepared by the method of spray drying. The viable count of the agent was 1.2×10^9 CFU/g.

Fig. 110.1 Picture of wetting powder of *B. subtilis* B579



The solution was spray-dried with temperature 180° at paste entrance, 70° at outlet, pump rate 60 mL/min and the atomization was controlled at an air pressure of 0.1 MPa.

110.3.2 Inhibitory Effect Assay of Wetting Powder

Cylinder-plate method was used to verify the inhibitory effect of the prepared agent against *F. oxysporum*. The inhibition zones for different biocontrol agent concentrations were 0, 9, 17, and 20 mm, respectively. So, the effective concentration of the wetting powder for use was 2–5 g/L.

110.3.3 Quality Index Analysis of Wetting Powder

Quality index of wetting powder was analyzed. The transmission rate of wetting powder through 44 µm test sieve was 98 %. The wetting time was 110 s. The moisture content was 2.8 %. The suspension rate was as high as 83 %. The value of pH was neutral, which was 7.3. The wetting powder was stable to hot, and the effective component decomposition rate was 6 % after hot storage for 14 d. Quality index of wetting powder reached the biological pesticide standards.

110.4 Conclusion

The optimal formulation recipe and processing technology of *B. subtilis* B579 wetting powder were developed. The best composition was diatomite 5 %, calcium carbonate 5 %, SDS 5 %, CMC-Na 5 %, soluble starch 0.5 %, sucrose

0.5 %, sodium glutamate 0.5 %. The wetting powder was obtained by spray-dried with temperature 180° at paste entrance, 70° at outlet, pump rate 60 mL/min and the atomization was controlled at an air pressure of 0.1 MPa. Quality index analysis revealed that the wetting powder reached the biological pesticide standards. The effective concentration of the wetting powder for use was 2–5 g/L.

References

1. Fravel D, Olivain C, Alabouvette C (2003) *Fusarium oxysporum* and its biocontrol. *New Phytol* 157:493–502
2. Chung S, Kong H, Buyer JS et al (2008) Isolation and partial characterization of *Bacillus subtilis* ME488 for suppression of soilborne pathogens of cucumber and pepper. *Appl Microbiol Biotechnol* 80:115–123
3. Uppal AK, Hadrami AE, Adam LR et al (2008) Biological control of potato Verticillium wilt under controlled and field conditions using selected bacterial antagonists and plant extracts. *Biol Control* 44:90–100
4. Siddiqui IA, Shaikat SS (2004) Systemic resistance in tomato induced by biocontrol bacteria against the root-knot nematode, *Meloidogyne javanica* is independent of salicylic acid production. *J Phytopathology* 152:48–54
5. Ahn IP, Chung HS, Lee YH (1998) Vegetative compatibility groups and pathogenicity among isolates of *Fusarium oxysporum* f. sp. *cucumerinum*. *Plant Dis* 82:244–246
6. Wang SL, Shih IL, Wang CH et al (2002) Production of antifungal compounds from chitin by *Bacillus subtilis*. *Enzyme Microbial Technol* 31:321–328
7. Thilagavathi R, Saravanakumar D, Ragupathi N et al (2007) A combination of biocontrol agents improves the management of dry root rot (*Macrophomina phaseolina*) in greengram. *Phytopathol Mediterr* 46:157–167
8. Lee HJ, Park KH, Shim JH et al (2005) Quantitative changes of plant defense enzymes in biocontrol of pepper (*Capsicum annuum* L.) late blight by antagonistic *Bacillus subtilis* HJ927. *J Microbiol Biotechnol* 15:1073–1079
9. Kavitha S, Senthilkumar S, Gnanamanickam S et al (2005) Isolation and partial characterization of antifungal protein from *Bacillus polymyxa* strain VLB16. *Process Biochem* 40:3236–3243
10. Stover AG, Driks A (1999) Secretion, localization, and antibacterial activity of TasA, a *Bacillus subtilis* spore-associated protein. *J Bacteriol* 181:1664–1672
11. Hwang SF, Chakravarty P (1992) Potential for the integrated control of Rhizoctonia root-rot of *Pisum sativum* using *Bacillus subtilis* and a fungicide. *J Plant Dis Prot* 99:626–636
12. Chu IM, Lee C, Li TS (1992) Production and degradation of alkaline protease in batch cultures of *Bacillus subtilis* ATCC 14416. *Enzyme Microbial Technol* 14:755–761
13. Brannen PM, Kenney DS, Kodiak (1997) A successful biological-control product for suppression of soil-borne plant pathogens of cotton. *J Ind Microbiol Biotech* 19:169–171
14. Choudhary DK, Johri BN (2009) Interactions of *Bacillus* spp. and plants—with special reference to induced systemic resistance (ISR). *Microbiol Res* 164(5):493–513
15. Chen H, Yuan CL, Cai KZ et al (2008) Purification and identification of iturin A from *Bacillus subtilis* JA by electrospray ionization mass spectrometry. *Acta Microbiologica Sinica* 48:116–120
16. Tsuge K, Inoue S, Ano T et al (2005) Horizontal transfer of iturin A operon, *itu*, to *Bacillus subtilis* 168 and conversion into an iturin A producer. *Antimicrob Agents Chemother* 49:4641–4648

17. Wang M, Chen F, Zheng Y et al (2009) Identification and characterization of antifungal compounds produced by *Bacillus subtilis* B579. In: International conference of natural products and traditional medicine (TCNPTM'09), conference proceedings, pp 291–295
18. Chen F, Wang M, Zheng Y et al (2010) Quantitative changes of plant defense enzymes and phytohormone in biocontrol of cucumber Fusarium wilt by *Bacillus subtilis* B579. *World J Microbiol Biotechnol* 26(4):675–684
19. Chen F, Han D, Wang M et al (2012). Production and identification of antifungal compounds produced by *Bacillus subtilis* B579. In: 2012 international conference on bioinformatics and biomedical engineering, vol 4. pp 87–90
20. Wang J, Wang N, Gao G et al (2010) Research on wetting powder of *Bacillus subtilis* with each gram 20 billion spores. *Agrochemicals* 49(7):486–489
21. Collins DP, Jacobsen BJ (2003) Spatial and temporal population dynamics of a phyllosphere colonizing *Bacillus subtilis* biological control agent of sugar beet cercospora leaf spot. *Biol Control* 26(2):153–161
22. Shoda M (2000) Bacterial control of plant diseases. *J Biosci Bioeng* 89(6):515–521

Chapter 111

Isolation and Characterization of s-Butanol Tolerant Microorganisms

Litao Shi, Hongjiang Yang, Qian Li and Xuying Qin

Abstract s-butanol can be produced indirectly from biomass by fermentation. To construct recombinant strains producing s-butanol directly, microbes naturally with high tolerance to s-butanol are required for metabolic engineering. In this study, totally 30 s-butanol tolerant microorganisms were isolated from different environmental soil samples by screening and enrichment method. Among the isolates, strains S-2, S-9, S-24, and S-26 were able to tolerate 15 g/L s-butanol. Additionally, s-butanol tolerance mechanisms were also studied by quantitatively analyzing degradation ability of the isolates. The results indicated that strains S-9 and S-24 possessed relatively low levels of s-butanol degrading enzyme activity and might be used as native tolerant strains for metabolic engineering. Strain S-13 showed the highest s-butanol degradation efficiency (72.7 %) in LB medium, suggesting that strain S-13 disrupted s-butanol via a way of co-metabolism and suitable for bioremediation of the chemical under more complicated environments. Furthermore, the isolated strains were identified by comparative analysis of the 16S rRNA gene sequences.

Keywords s-butanol · Screening · Tolerance · Identification

111.1 Introduction

S-butanol has many applications including industrial solvents, emulsifiers, dyes, dispersants, dehydrating agents, paint removers, and industrial detergents. Also s-butanol can be used as gasoline octane components, plasticizers, mineral processing agents, and herbicides [1].

L. Shi · H. Yang (✉) · Q. Li · X. Qin
College of Biotechnology, Tianjin University of Science and Technology,
Tianjin 300457, People's Republic of China
e-mail: hongjiangyang@tust.edu.cn

S-butanol is industrially manufactured by the hydration of 1-butene or 2-butene on a large scale. The production level of s-butanol reached 9,00,000 tons/year, and manufacturers are mainly located in Europe and the United States [2].

A number of strains of *Lactobacillus* spp. have been reported to be able to convert meso-2, 3-butanediol into s-butanol in a few studies [3]. However, no further genetic and biochemical evidences have been obtained to prove the existence of s-butanol synthesis pathway in bacteria. The s-butanol can be produced indirectly with microbial fermentation, and the production process practically involves the fermentation processes and the chemical reaction. First, various carbon sources were converted to 2, 3-butanediol via a series of metabolic pathways[4]. Second, 2, 3-butanediol was dehydrated into methyl ethyl ketone (MEK) efficiently through enzymatic bioconversion without purification. Third, MEK was transformed to s-butanol through hydrogenation, the chemical reaction [5].

Although no known pathway involving in s-butanol synthesis available in isolated microbes, attempts have been making to construct recombinant strains with the ability to produce s-butanol directly during fermentation process [6]. The candidate strains suitable for metabolic engineering would meet the certain criteria, and s-butanol tolerance would be a critical variable affecting s-butanol production level of the engineered microbes [6].

In this paper, s-butanol tolerant microorganisms were isolated via screening and enrichment method. The isolates were characterized for their growth rate in the presence of s-butanol and their degradation ability of s-butanol. With the comparative analysis of the 16S rRNA gene sequences, some of the isolated strains were identified.

111.2 Materials and Methods

111.2.1 Experimental Materials

The soil and sludge samples were collected from various environmental sites, and they were stored in sterile sealed bags at 4 °C refrigerator ready for use.

111.2.2 Media

LB medium was used for routine cultivation of bacteria, and it was composed of NaCl 10 g/L, Peptone 10 g/L, and Yeast extract 5 g/L. The medium was adjusted to pH 7.0.

Enrichment medium was used for the isolation of s-butanol tolerant microorganisms, and it was composed of KH_2PO_4 0.5 g/L, K_2HPO_4 0.5 g/L, $\text{FeSO}_4 \cdot 7\text{H}_2\text{O}$ 0.01 g/L, MgSO_4 0.2 g/L, NaCl 9 g/L, Peptone 5 g/L, and Glucose 30 g/L. The

medium was adjusted to pH 7.0 [7]. Before cultivation, s-butanol was added to the medium for the enrichment and selection of s-butanol tolerant strains.

To analyze the s-butanol degradation efficiency of the isolates, two media was used for cultivation the isolates, the basic medium and LB medium. The basic medium (pH 7.0) was composed of KH_2PO_4 0.5 g/L, K_2HPO_4 0.5 g/L, $\text{FeSO}_4 \cdot 7\text{H}_2\text{O}$ 0.01 g/L, MgSO_4 0.2 g/L, NaCl 9 g/L, and $(\text{NH}_4)_2\text{SO}_4$ 5 g/L [7]. Before cultivation, s-butanol was added to the media to the certain concentration.

111.2.3 Enrichment and Isolation of s-Butanol Tolerant Bacteria

Add soil and sludge samples (10 g) to 150 mL enrichment medium (supplement with 5 g/L s-butanol) in 250 mL flask sealed with a solid cap. The mixture was incubated at 37 °C with a shaking speed 220 rpm. After 24 h incubation, 10 mL supernatant was transferred to 150 mL fresh enrichment medium (supplement with 5 g/L s-butanol), the mixture was cultured for another 24 h under the same conditions. The enrichment step was repeated for three more times [8].

After enrichment, take 1 mL enrichment culture and make serial dilutions. Take 150 μL of each dilution and spread on solid enrichment medium supplementing with s-butanol (5 g/L). The Petri dishes were incubated at 37 °C for 72 h [9].

111.2.4 Growth Rate Analysis

The isolated bacteria were inoculated in 5 mL LB medium and incubated at 37 °C overnight. The cultures were transferred into 5 mL fresh LB medium at 5 % inoculum size. S-butanol was added to the cultures at the concentrations of 0.5, 1, and 1.5 %, respectively. After incubation at 37 °C for 24 h with shaking speed of 220 rpm, the cell optical density at wavelength of 600 nm (OD_{600}) was measured [10, 11].

The isolates were also inoculated on L-agar plates supplementing with s-butanol (0.5, 1, and 1.5 %, respectively). The growth was observed after 48 h incubation at 37 °C [12].

111.2.5 Degradation Efficiency Analysis

Degradation efficiency analysis was performed as described previously [13]. In brief, the isolated strains were inoculated in 5 mL LB medium and incubated at 37 °C overnight. The cultures were transferred into 5 mL fresh LB medium at 5 %

inoculum size. One percent of s-butanol was added to the cultures, while sterile saline buffer was used as control. After 24 h incubation at 37 °C, s-butanol level in the fermentation broth was subjected to gas chromatography analysis. Basic medium was also used to replace LB medium for degradation efficiency analysis [14].

Gas chromatography (Agilent 7890A) with column HP-INNOWAX was used to determine the remaining amount of s-butanol in the fermentation broth. The detailed procedure as described according to the manual with modifications [15–17]. Briefly, column temperature was held at 45 °C for 1 min, and then programmed at 8 °C/min to 155 °C and held for 1 min; flow rate: 1 mL/min; Inlet was 180 °C; Detector was 200 °C; The flow rate of nitrogen gas, hydrogen gas, and air were 35, 35, and 350 mL/min, respectively. Isoamyl alcohol was used as internal control standard [18, 19].

111.2.6 Identification of the Isolated Strains

Bacterial genomic DNA was extracted as described previously [20]. To amplify bacterial 16S rRNA gene fragments, specific primers 27F and 1492R were adopted and their sequences were as follows [21]:

27F: 5'-AGAGTTTGATCCTGGCTCAG-3'

1492R: 5'-GGTTACCTTGTTACGACTT-3'

PCR reaction system was 50µL and the parameters were heating at 94 °C for 5 min, 1 cycle; heating at 94 °C for 40 S, annealing at 51 °C for 2 min, extension at 72 °C for 3 min, 30 cycles; 72 °C for 10 min.

PCR products were purified from gel and subjected to sequencing analysis with the same primers used in PCR. Sequence homology search was carried out with BLAST provided by NCBI to identify the isolates. The isolates were classified to genus level with Classifier (Ribosomal Database Project II) [22].

111.3 Results and Discussion

111.3.1 Isolation of s-Butanol Tolerant Strains

As described in Materials and methods, the 5 d enriched culture was diluted and spread on L-agar medium supplementing with 5 g/L s-butanol. Totally, 30 strains with different morphologies were obtained from various environmental samples.

111.3.2 Growth Rate Analysis under Various s-Butanol Concentrations

The isolated strains were subjected to growth rate analyzing. The experiment results showed that strains S-2, S-9, S-24, and S-26 still grew well in the presence of 15 g/L s-butanol. Their relative growth rates were 0.58, 0.64, 0.31, and 0.29, respectively, compared with the corresponding cultures without supplementing with 15 g/L s-butanol. The relative growth rates were below 0.13 in the remaining 26 strains. In the medium supplementing with 5 g/L and 10 g/L s-butanol, the relative growth rate of 30 strains had no significant difference (Fig. 111.1a, b, and c).

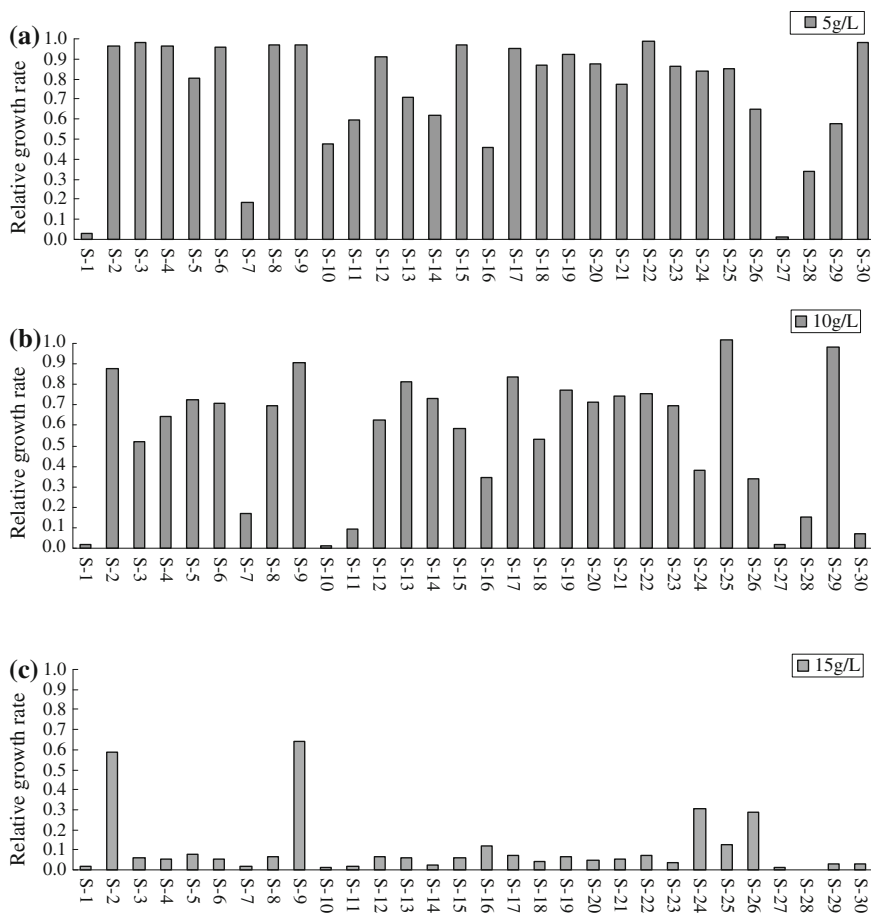


Fig. 111.1 The relative growth rate analysis of the 30 isolated strains. **a** the relative growth rates of the isolates in the presence of 0.5 % s-butanol; **b** the relative growth rates of the isolates in the presence of 1 % s-butanol; **c** the relative growth rates of the isolates in the presence of 1.5 % s-butanol

On L-agar plates supplementing with 5, 10, and 15 g/L s-butanol, respectively, only strains S-2, S-9, S-24, and S-26 formed colonies similar to the results obtained from the relative growth rate analysis. To our best knowledge, no study has been reported on isolation of s-butanol tolerant microorganisms [23, 24].

111.3.3 Degradation Efficiency Analysis of the Isolated Strains

Solvent tolerance mechanisms have been studied in microbes [24]. Several structures were involved in such a functionality, including cellular membrane lipid barrier, efflux pumps, cellular membrane protein contents, and enzymes digesting solvents [25]. In this work, we investigated s-butanol tolerance mechanism by analyzing their s-butanol degradation efficiency in both LB medium and basic medium, respectively.

Strains S-2, S-9, S-24, and S-26 thrived in the medium with 1.5 % s-butanol (Fig. 111.1c). Their s-butanol degradation efficiency was 56.4, 8.2, 17.0, and 21.4 %, respectively, in the basic medium (Fig. 111.2b); while in LB medium the corresponding degradation efficiency was 63.7, 22.0, 17.2, and 54.1 %, respectively (Fig. 111.2a). These data suggested that the dominated mechanism for strains S-2 and S-26 tolerating s-butanol might be due to the existence of

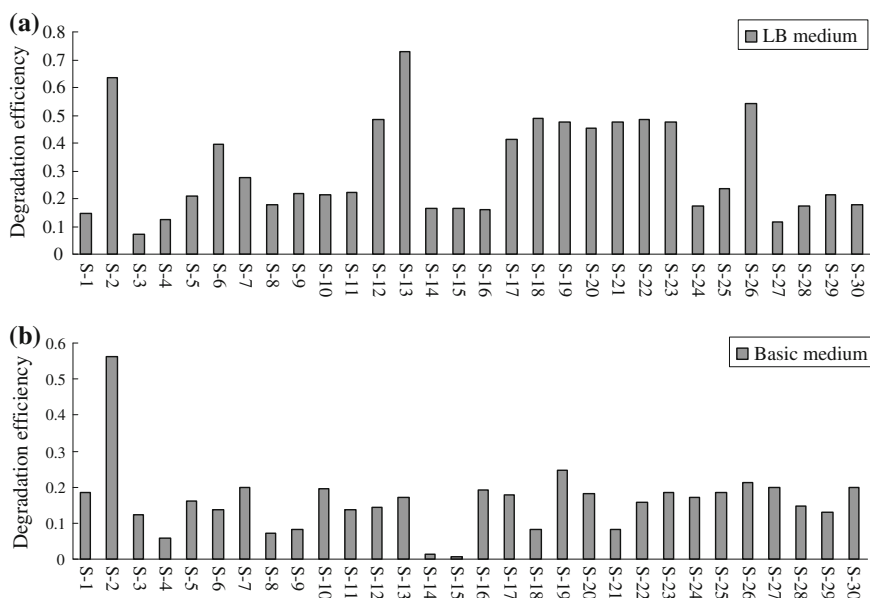


Fig. 111.2 S-butanol degradation efficiency of the isolates incubated in different media. **a** the related analysis in LB medium; **b** the related analysis in the basic medium

Table 111.1 Homology analysis and classifications of the isolated strains

Strains	Most similar strains (accession no.)	Similarity %	Genus ^a
S-2	<i>Arthrobacter luteolus</i> (DQ486130.1)	100	Arthrobacter
S-9	<i>Bacillus aryabhatai</i> (HQ242766.1)	100	Bacillus
S-13	<i>Lysinibacillus fusiformis</i> (FJ973545.1)	100	Lysinibacillus
S-24	<i>Bacillus tequilensis</i> (JF411311.1)	100	Bacillus
S-26	<i>Bacillus tequilensis</i> (JF411311.1)	100	Bacillus

^a Classification results by classifier from RDPII [22]

enzyme(s) degrading s-butanol, and both strains might be used as bioremediation strains; while strains S-9 and S-24 should have relatively low levels of s-butanol degrading enzymatic activity, and they might be used as native s-butanol tolerant strains for construction of s-butanol producing strains via metabolic engineering. Among the tested strains, S-13 showed the highest s-butanol degradation efficiency 72.7 % within 24 h incubation in LB medium. This suggested that strain S-13 disrupted s-butanol via a way of co-metabolism and suitable for bioremediation of s-butanol under more complicated environments [26].

111.3.4 Identification of the Isolates

Extract chromosome DNA of the isolated bacteria and then amplify their 16S rRNA gene with primers 27F and 1492R [27]. The obtained 16S rRNA gene sequences were analyzed with BLAST program in the NCBI and Classifier in RDPII [28, 29]. As shown in Table 111.1, with similarity of 100 %, strain S-2 was highly homologous to *Arthrobacter luteolus*, S-13 was highly homologous to *Lysinibacillus fusiformis*, S-9 was highly homologous to *Bacillus aryabhatai*, and S-24 and S-26 were highly homologous to *Bacillus tequilensis*, respectively. It is interesting to find that strains S-9, S-24, and S-26 all belong to the genus of *Bacillus* but with different aspects for s-butanol tolerance. This is the first study on s-butanol tolerant strains isolation [30–32]. Strains S-9 and S-24 might be engineered for construction of recombinant microbes producing s-butanol directly via fermentation [6].

111.4 Conclusion

S-butanol cannot be synthesized directly from biomass by fermentation. Construction of recombinant strains producing s-butanol directly could be an alternative to indirectly production via fermentation, and isolation of microbes naturally with high tolerance to s-butanol is required for metabolic engineering. In this work, totally 30 s-butanol tolerant microorganisms were isolated, and strains

S-2, S-9, S-24, and S-26 were able to tolerate 15 g/L s-butanol. To investigate s-butanol tolerance mechanisms, the degradation ability of the isolates was quantitatively analyzed. Strains S-9 and S-24 possessed relatively low levels of s-butanol degrading enzymatic activity and might be used as native tolerant strains for construction of s-butanol directly producing strains via metabolic engineering. Strain S-13 showed the highest s-butanol degradation efficiency in LB medium. This suggested that strain S-13 disrupted s-butanol via a way of co-metabolism and suitable for bioremediation of s-butanol under more complicated environments.

Acknowledgments This work was partly supported by The National Natural Science Foundation of China (Grant No. 30970114) and The National Key Technology R&D Program of China (Grant No. 2011BAC11B05).

References

1. Baertsch Chelsey D, Kenny T, Komala et al (2002) Genesis of Bronsted acid sites during dehydration of 2-butanol on tungsten oxide catalysts. *J Catal* 212:44–57
2. Huichang Z (1989) S-butanol production by water legitimate directly. *Jiangsu chemical* 17(3):50–53
3. Ching THOU, Ramesh PATEL, Nancy BARNABR et al (1981) Stereospecificity and other properties of a novel secondary-alcohol-specific alcohol dehydrogenase. *Biochem* 119:359–364
4. Yu EC, Levitin N, Saddler JN (1982) Production of 2,3-butanediol by *Klebsiella pneumoniae* grown on acid hydrolyzed wood hemicellulose. *Biotchnol Lett* 4(11):741–746
5. Kaoutar E, Mohamed K, Mahfoud Z et al (2004) Cobalt-exchanged hydroxyapatite catalysts: magnetic studies, spectroscopic investigations, performance in 2-butanol and ethane oxidative dehydrogenations. *J Catal* 187:16–24
6. Robin E. Osterhout, San Diego et al (1011) Microorganisms and methods for carbon-efficient biosynthesis of MEK and 2-butanol: US, 0008858[P]
7. Taosheng C, Qizu L (1991) Fermentation of acetone and butanol production technology, vol 14. Chemical Industry Press, Beijing, pp 18–21
8. Zvaigzne AI, Acree WE Jr (1994) Solubility of anthracene in binary alkane + 2-butanol solvent mixtures. *Chem Eng J* 39:114–116
9. Chou Junpeng, Yan Xu, Ruan Wenquan et al (2004) Metabolic regulation of breeding and fermentation of L-lactic acid fermentation influence factors. *Microbiology* 34(5):929–933
10. Liu J, Fan LT et al (2004) Downstream process synthesis for biochemical production of butanol ethanol, and acetone from grains: eneration of optimal and near optimal flow sheets with conventional operating units. *Biotechnology* 20(5):1518–1527
11. Hartmanis MGN, Klason T, Gatenbeck S (1984) Uptake and aivation of acetate and butyrate in *Clostridium acetobutylicum*. *Microbiol Biotechnol* 20:66–71
12. Anan H, Keke C, Yan S et al (2009) Strain selection and medium optimization of the metabolism of glycerol yielding lactic acid. *Microbiology* 36(8):1195–1199
13. Huang WC, Ramey DE, Yang ST (2004) Continuous production of butanol by *Clostridium acetobutylicum* immobilized in a fibrous bed bioreactor. *Appl Biochem Biotechnol* 22(16):113–116
14. Martin JR, Petitdemange H, Ballongue J, Gay R (1985) Effects of acetic and butyric acids on solvents production by *Clostridium acetobutylicum*. *Biotechnol Letters* 2:89–94
15. Jingchuan H (2009) Acetone butanol producing strain breeding and fermentation process. Biological and Environmental Engineering College of Zhejiang. Zhejiang University

16. Ruonong F, Yongfu C (1989) Gas chromatography and thermal analysis techniques, vol 34. National Defence Industry Press, Beijing, pp 11–12
17. Qureshi N, Schripsema J, Lienhardt J et al (2000) Continuous solvent production by *Clostridium beijerinckii* BA101 immobilized by adsorption onto brick. *World J Microbiol Biotechnol* 16(4):377–382
18. Smith Christy A, Hyman Michael R (2004) Oxidation of methyl ter-butyl ether by alkane hydroxylase in dicyclopropylketone-induced and n-octane-gro-grown *Pseudomonas putida* GPo1. *Appl environ microb* 70(8):4544–4550
19. Bennett GN, Scotcher MC (2007) Blocking sporulation by inhibiting SpoIIE. US, 0020740
20. Sambrook J, Russell DW (2001) Molecular cloning: a laboratory manual, 3rd edn. Cold Spring Harbor Press, New York, pp 1.31–1.38
21. Hendrickson ER, Payne JA, Yong RM et al (2002) Molecular analysis of dehalococcoides 16S ribosomal DNA from chloroethene-contaminated sites throughout north America and Europe. *Appl environ microb* 68(2):485–495
22. Qing W, Garrity GM, Tiedje JM et al (2007) Naive Bayesian classifier for rapid assignment of rRNA sequence into the new bacterial taxonomy. *Appl Environ Microbiol* 73(16):5261–5267
23. Macfie Sheila M, Cossins Edwin A, Taylor Gregory J (1994) Effects of excess manganese on production of organic acids in acids in Mn-tolerant and Mn-sensitive cultivars of *Triticum aestivum* L (Wheat). *J Plant Physiol* 143:135–144
24. Hongzhi M, Qunhui W, Dayi Q (2009) The utilization of acid-tolerant bacteria on ethanol production from kitchen garbage. *Renewable Energy* 34:1466–1470
25. Folsom BR, Chapman PJ (1990) Phenol and trichloroethylene degradation by *Pseudomonas cepacia* G4: kinetics and interactions between substrates. *Appl Environ Microbiol* 56:1279–1285
26. Yuquan X, Wei Z (2000) Isolation and identification of a phenol-degrading bacterial strain. *Acta Scientiae Circumstantiae* 20:4
27. Hendrickson ER, Payne JA, Yong RM et al (2002) Molecular analysis of dehalococcoides 16S ribosomal DNA from chloroethene-contaminated sites throughout north America and Europe. *Appl environ microb* 68(2):485–495
28. Sambrook J, Russell DW (2001) Molecular cloning: a laboratory manual, 3rd edn. Cold Spring Harbor Press, New York, pp 1:31–1.38
29. Jinghui Z, Madden TL (1997) PowerBLAST: a new network BLAST application for interactive or automated sequence analysis and annotation. *Genome Res* 7(6):649–656
30. Papoutsakis ET, Alsaker KV, Borden J (2005) Understanding butanol and butyrate toxicity and tolerance in clostridia at the genomic scale. United States: 229th ACS National Meeting, San Diego
31. Eric P, Knoshaug Min Zhang (2009) Butanol tolerance in a selection of microorganisms. *Appl Biochem Biotechnol* 153:13–20
32. Liyanage Hemachandra, Young Michael, Kashket Eva R (2000) Butanol tolerance of *Clostridium beijerinckii* NCIMB 8052 associated with down-regulation of *gldA* by antisense RNA. *Microbiol Biotechnol* 2:87–93
33. Atsumi S, Canan AF, Connor MR et al (2007) Metabolic engineering of *Escherichia coli* for 1-butanol production. *Metab Eng* [Epub ahead of print] 10(6):305–311
34. Inui M, Suda M, Kimura S et al (2008) Expression of *Clostridium acetobutylicum* butanol synthetic genes in *Escherichia coli*. *Appl Microbiol Biotechnol* 77(6):1305–1316

Chapter 112

Application of Support Vector Machine in Base Liquor Classification

Junsen Lu, Liping Du, Haimei Ding, Ziping Du and Dongguang Xiao

Abstract Considering the deficiency of the traditional liquor classification method, a novel method for liquor classification based on support vector machine is discussed in this paper. Liquor chromatographic data is used as basis and the LIBSVM toolbox is used as classification tool in this method. Two different grades of 490 base liquor samples (containing 242 samples of ordinary base liquor, 248 samples of high-quality base liquor) were used to test the method. In the experiment, 180 samples of ordinary base liquor and 184 samples of high-quality base liquor were selected as the training set to build the model and the remaining base liquor were used as the testing set to test the accuracy of the model. The model accuracy could reach 98 % without the correlation parameter optimization. The results show that the method can achieve a higher accuracy, and prove the correctness and effectiveness of the method.

Keywords LIBSVM · Support vector machine · Base liquor · Classification

112.1 Introduction

With thousand years of history and culture heritage, liquor is endemic to China. At present, the identification of liquor classification is not only tested by physical and chemical character, but also, in most cases, dependent on the experts, who are well

J. Lu · L. Du · H. Ding · D. Xiao (✉)

Key Laboratory of Industrial Fermentation Microbiology Ministry of Education, Tianjin Industrial Microbiology Key Laboratory, College of Biotechnology, Tianjin University of Science and Technology, Tianjin 300457, People's Republic of China
e-mail: xiao99@tust.edu.cn

Z. Du

College of Economics and Management, Tianjin University of Science & Technology, Tianjin 300457, People's Republic of China

trained and experienced. Based on the observation, analysis, and description, the experts evaluate liquor product from many aspects such as color, flavor, taste and style, and finally give a comprehensive report, which can be the important evidence for liquor classification assessment [1]. However, this subjective method leads to the result that the judging results vary with each individual. Even the same wine taster can give the different results due to different physical status, environment, and emotions. In practice, the same wine taster can hardly obtain the same result of samples of the same batch. Moreover, the accuracy of evaluation cannot be guaranteed in case of giving quick comment for large number of liquor samples [2]. Because of the demands of nondestructive and intelligent rapid detection technology, in the meantime, in order to achieve the fairness and accuracy for further of liquor classification with a strict and consistent standard, using instrument to measure alcohol substance contend and using scientometric indicators to evaluate liquor have been one of the necessary means [3].

The Support Vector Machine (SVM) method was proposed by Vapnik [4, 5] in AT&T Bell laboratory in 1963 is a new promising classification technology. SVM researches machine learning problems with limited number of samples, whereas the traditional statistical recognition method can only achieve theory-guaranteed performance in the case of large number of sample. Therefore, SVM has obvious advantages [6, 7]. Compared with Artificial Neural Networks (ANNs), SVM has no overfitting problems; instead, it has better generalization ability [8]. LIBSVM toolbox, which is developed based on MATLAB by associate professor Lin Chin-Jen from National Taiwan University, is an effective tool using SVM as theory for classification. There are a lot of default parameters and few parameters need to be input in the toolbox, which can be used to solve many problems conveniently [9].

In this paper, we focus on the application of SVM in base liquor classification. In the experiment, the data from the liquor gas chromatography (GC) were divided into the training set and the test set. The training set was used to build the model by SVM and the test set was for testing the classification accuracy of the model. The results showed that different samples of base liquor were well separated.

112.2 Materials and Methods

112.2.1 Data Sources

The liquor samples were provided by Sitir Liquor Co., Ltd. containing 242 samples of ordinary base liquor and 248 samples of high-quality base liquor. The contents of main substance in each base liquor were analyzed by gas chromatography (GC). Each sample included the content of 16 attributes. The attributes were ethyl acetate, ethyl acetate, ethyl acetate, ethyl lactate, ethyl ester, ethyl ester, ethyl acetate, acetic acid, propionic acid, butyric acid, caproic acid, lactic acid, propyl alcohol, isobutyl alcohol, isoamyl alcohol, and methanol.

112.2.2 Method

The experiment process as Fig. 112.1:

112.2.3 Data Preprocessing [10]

In the process of using LIBSVM toolbox, we found that data preprocessing had significant impact on the model predicting accuracy. However, at present, there was no improved theory to support how to choose preprocessing method, and uniform standards had not yet been discovered. So, in the experiment, three different methods were adopted and the model with the highest accuracy would be chosen.

- (a) Raw data without any processing
- (b) [0,1] normalization

The mapping function used in this method shows as follow:

$$f : x \rightarrow y = \frac{x - x_{\min}}{x_{\max} - x_{\min}} \tag{1}$$

In the formula, $x_{\min} = \min(x)$, $x_{\max} = \max(x)$. The raw data is normalized within the range of [0, 1].

- (c) [-1,1] normalization

The mapping function used in this method was as follows:

$$f : x \rightarrow y = 2 \times \frac{x - x_{\min}}{x_{\max} - x_{\min}} + (-1) \tag{2}$$

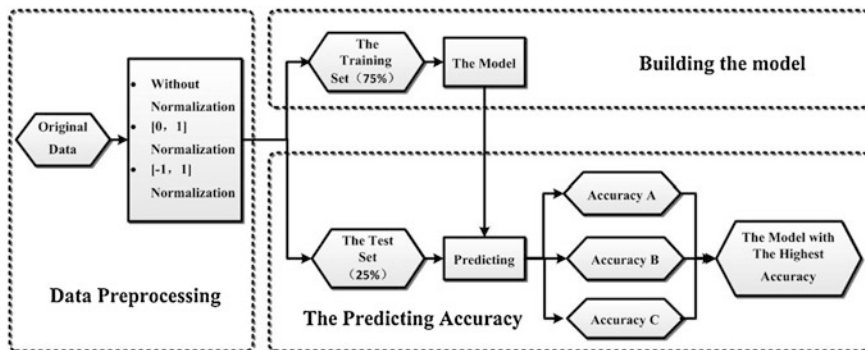


Fig. 112.1 The process map of application of SVM in base liquor classification

In the formula, $x_{\min} = \min(x)$, $x_{\max} = \max(x)$. The raw data is normalized to the range of $[-1, 1]$.

In MATLAB, the normalization can be achieved by the “mapminmax” function.

112.2.4 Building the Model

According to the percentage of 75 %, 180 samples of ordinary base liquor and 184 samples of high-quality base liquor were selected as the training set. The label “1” represented the ordinary base liquor and the label “2” represented the high-quality base liquor. In the model, the parameter “c” in LIBSVM was selected in 5 and the parameter “g” was selected in 2. The following MATLAB codes built the model.

```
wine_labels = wine (:,1);
wine_data = wine (:,2:end);
train_wine = [wine_data (1:180,:);wine_data(243:426,:)]; % Selecting the training set
train_wine_labels = [wine_labels(1:180,:);wine_labels(243:426,:)]; % Extracting the training set labels
model = svmtrain (train_wine_labels, train_wine, '-c 5 -g 2') % Building the model
```

112.2.5 The Predicting Accuracy

The remaining 25 % liquor samples (62 samples of ordinary base liquor and 64 samples of high-quality base liquor) as the test set were used to predict the accuracy of the model we built. The following MATLAB codes predicted the accuracy.

```
test_wine = [wine_data(181:242,:);wine_data (427:490,:)]; % Selecting the test set
test_wine_labels = [wine_labels (181:242,:); wine_labels (427:490,:)]; % Extracting the test set labels
[predict_label, accuracy] = svmpredict (test_wine_labels, test_wine, model); % The predicting accuracy
```

112.3 Results and Discussion

The accuracy of the predicting results with three different preprocessing methods is shown in Table 112.1 and Fig. 112.2.

From Table 112.1 and Fig. 112.2, it could be seen the predicting accuracy by $[0,1]$ normalization was the highest, which was up to 98.41 %. Only 2 of 126

Table 112.1 The accuracies of the model with three different processing methods

No.	Preprocessing methods	Predicting accuracy (%)	Predicting accuracy of ordinary base liquor (%)	Predicting accuracy of high-quality base liquor (%)
1	Raw data without Normalization	94.44 (119/126)	96.77 (60/62)	92.18 (59/64)
2	[0,1] Normalization	98.41 (124/126)	98.38 (61/62)	95.31 (61/64)
3	[-1,1] Normalization	96.03 (121/126)	93.54 (58/62)	98.43 (63/64)

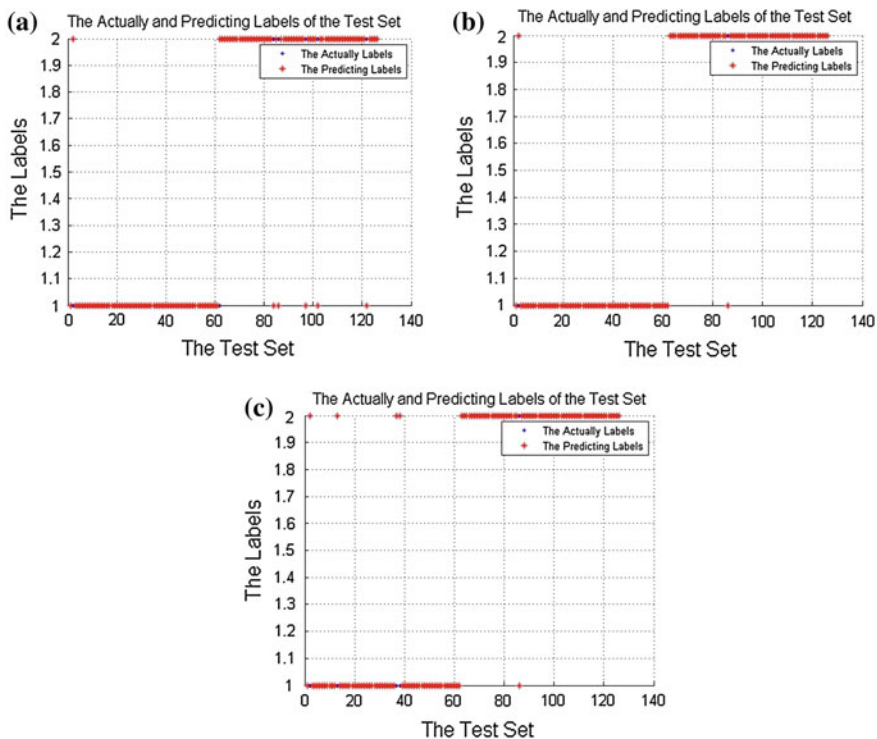


Fig. 112.2 The actually and predicting labels of the test set with three different processing methods, **a**: raw data without normalization, **b**: [0,1] Normalization, **c**: [-1,1] Normalization

samples were misclassified. The predicting accuracy of ordinary base liquor was 98.38 % and the predicting accuracy of high-quality base liquor was 95.31 %. The predicting accuracy still reached to 94.44 % when the raw data without normalization was used. Thus, base liquor classification was accurately realized by SVM and the experiments obtained some satisfied results.

112.4 Conclusion

Results obtained from experiments showed that the proposed approach had the merits of high learning efficiency, classification accuracy, and generalization capability. This method performed well and fast, it was suitable for practical application. In the future, how to improve the predictive accuracy of the model by parameter optimization of “c” and “g” is worthy to be studied. This method could be widely used with the step of continual study.

References

1. Shen Y (2006) The history and development of Chinese liquor sensory quality and evaluation technology [J]. *Liquor Mak* 33(4):3–4 (in chinese)
2. Jiang A, Peng J, Peng S et al (2010) Research on SVM-based liquor infrared spectrum analysis method. *Comput Appl Chem* 27(2):233–236 (in chinese)
3. Zhang J, Zhao L, Ouyang Y et al (2007) Applications of modern equipment analytical techniques in sensory evaluation of liquor [J]. *Food Sci* 10:561–565 (in chinese)
4. Vapnik VN (1998) *Statistical learning theory*. John Wiley and Sons, Inc., New York
5. Vapnik VN (2000) *The nature of statistical learning theory*. Springer, New York
6. Burges CJ (1998) A tutorial on support vector machines for pat tern recognition. *Data Min Knowl Discov* 2:127–167
7. Cristianini N, Shaw a-Taylor J (2000) *An introduction of support vector machines and other kernel based learning methods*. Cambridge University Press, New York
8. Wang L, Lin J (2006) Development and application of Support Vector Machine [J]. *Automat PetroChem Ind* 3:34–38 (in chinese)
9. Chang CC, Lin CJ (2010) LIBSVM: LIBSVM—A library for support vector machines. 2011. software available at <http://www.csie.ntu.edu.tw/~cjlin/libsvm/>
10. Shi F, Wang X, Yu L et al (2010) *Analysis of 30 neural network cases by MATLAB* [M]. Beihang University Press (in chinese), Beijing

Chapter 113

Isolation and Characterization of *n*-Butanol Tolerant Microorganisms

Yue Yu, Hongjiang Yang, Qun Li and Xuying Qin

Abstract *n*-butanol is produced traditionally by acetone butanol ethanol (ABE) fermentation with relatively low productivity. To improve *n*-butanol synthesis level, microbes naturally with high tolerance to *n*-butanol are required for metabolic engineering. In this study, a total of 30 *n*-butanol tolerant microorganisms were isolated from various environmental samples by screening the enriched cultures. Ten of them were able to tolerate more than 2 % (v/v) *n*-butanol, and strain YY-23 even thrived in the presence of 3 % (v/v) *n*-butanol. In addition, *n*-butanol tolerance mechanisms were investigated by quantitatively analyzing degradation ability of the isolates. The results showed that strains YY-13, YY-14, YY-15, and YY-18 didn't metabolize *n*-butanol in LB medium, suggesting that they didn't have *n*-butanol degrading enzymes and all of them might be used as candidates for construction of high *n*-butanol producing strains. Strains YY-10 and YY-29 showed strong *n*-butanol degradation efficiency (31 and 20 %, respectively), and might be used for *n*-butanol bioremediation. Furthermore, the isolated strains were identified by the 16S rRNA gene sequences comparative analysis.

Keywords Characterization · Degradation · *n*-butanol · Tolerance

113.1 Introduction

Butanol is an important fine chemical raw material, mainly used in the production of dibutyl phthalate (DBP) and butyl acrylate (BA) [1]. More importantly, butanol is regarded as good bio-fuel because it has high energy content, high miscibility with gasoline, high octane rating, and low volatility [2, 3]. Studies have shown that

Y. Yu · H. Yang (✉) · Q. Li · X. Qin
College of Biotechnology, Tianjin University of Science and Technology,
Tianjin 300457, People's Republic of China
e-mail: hongjiangyang@tust.edu.cn

equal volume of butanol could release twice as much energy as ethanol did when burning [4]. With the shortage of the fossil oil fuel resources and the increasing greenhouse effect, biofuels especially n-butanol have been attracting growing attentions [5, 6].

Traditionally n-butanol was produced by *Clostridium acetobutylicum* and related variants by using starch or sugars under anaerobic condition [7–9], and the process was usually known as acetone butanol ethanol (ABE) or solvent fermentation [10]. Acetone, butanol, and a small amount of alcohol and other solvents can generally be produced by several clostridia species, and the mainly n-butanol producing strains currently used in industrial production are *C. acetobutylicum*, *C. beijerinckii*, *C. saccharobutyl-aceticum*, and *C. saccharobutylicum* [11, 12].

ABE fermentation had been adopted for n-butanol production for a long time. However, its yields, productivity and final concentrations were too low for bio-production to compete economically with chemical synthesis [13–15]. To improve the productivity of n-butanol by microbial fermentation, various approaches have been applied in strains breeding, including synthetic biology, mutagenesis, genetic engineering, metabolic engineering, cell immobilizations, and the continuous n-butanol removal during fermentation process [16]. Due to the slow growth rate and stringent equipments requirements for ABE fermentation, n-butanol synthesis pathways have been and cloned into various industrial microbes for heterologous expression, including *Escherichia coli*, *Pseudomonas putida*, *Bacillus subtilis*, and *Lactobacillus brevis* [17–19]. These microbes have relatively higher tolerance to n-butanol and much faster growth rate compared with clostridia species.

In this work, to get more strains natively against n-butanol, we selected n-butanol tolerant microorganisms from various environmental samples. The isolates were further characterized for their n-butanol tolerance abilities and their degradation efficiency of n-butanol. The isolates will be native candidates for further metabolic engineering to produce n-butanol heterologously.

113.2 Materials and Methods

113.2.1 Environmental Samples

The soil and sludge samples were collected from 36 different environmental sites, and they were stored in sterile sealed bags at 4 °C refrigerator ready for use.

113.2.2 Media

Luria–Bertani (LB) medium was used for routinely cultivation and maintenance of bacteria, and it was composed of NaCl 10 g/L, peptone 10 g/L, and yeast extracts

5 g/L. The medium was adjusted to pH 7.0. To make the solid medium, 15 g/L agar is added to LB medium.

Enrichment medium was used for the isolation of *n*-butanol tolerant microbes, and it was composed of KH_2PO_4 0.5 g/L, K_2HPO_4 0.5 g/L, $\text{FeSO}_4 \cdot 7\text{H}_2\text{O}$ 0.01 g/L, MgSO_4 0.2 g/L, NaCl 9 g/L, Peptone 5 g/L, and Glucose 30 g/L. The medium was adjusted to pH 7.0 [20]. Suitable amount of *n*-butanol was added to the medium for the enrichment and selection of *n*-butanol tolerant strains.

The basic medium and LB medium were used for cultivation of the isolates to analyze the *n*-butanol degradation efficiency. The basic medium (pH 7.0) was composed of KH_2PO_4 0.5 g/L, K_2HPO_4 0.5 g/L, $\text{FeSO}_4 \cdot 7\text{H}_2\text{O}$ 0.01 g/L, MgSO_4 0.2 g/L, NaCl 9 g/L, and $(\text{NH}_4)_2\text{SO}_4$ 5 g/L. Suitable amount of *n*-butanol was added to the media for the analysis.

113.2.3 Enrichment and Isolation of n-Butanol Tolerant Strains

Add soil and sludge samples (20 g) to 150 mL sterile saline buffer and shake for 30 min. After keep the mixture statically for 15 min, transfer 10 mL supernatant to 150 mL enrichment medium (supplement with 10 g/L and 50 g/L *n*-butanol, respectively) in 250 mL flasks sealed with solid caps. The mixtures were incubated at 35 °C. After 24 h incubation, 10 mL supernatant was transferred to 150 mL fresh enrichment medium (supplement with 10 g/L and 50 g/L *n*-butanol, respectively), the mixtures were continuously cultured for another 24 h under the same conditions. Repeat the enrichment step three more times. At the end of enrichment, take 1 mL enrichment culture and make serial dilutions. Take 150 μL of each dilution and spread on solid enrichment medium supplementing with *n*-butanol (10 g/L). The Petri dishes were incubated at 35 °C for 72 h for observation.

113.2.4 Tolerance Analysis

The isolated strains were continuously cultivated in 5 mL LB medium at 35 °C to prepare primary and secondary seeding cultures. The secondary seeding cultures were transferred into test tubes with 5 mL fresh LB medium at 5 % inoculum sizes. *n*-butanol were added to the cultures at the concentration of 1, 2, and 3 %, respectively. After incubation at 35 °C for 24 h with shaking speed of 220 rpm, the cell optical density at wavelength of 600 nm (OD_{600}) was determined [21].

113.2.5 Degradation Efficiency Analysis

Degradation efficiency analysis was performed as described previously [22]. In brief, the isolated strains were inoculated in 5 mL LB medium and incubated at 35 °C overnight. The cultures were transferred into 5 mL fresh LB medium at 5 % inoculum size. One percent of n-butanol was added to the cultures, while sterile saline buffer was used as control. After 24 h incubation at 35 °C, n-butanol level in the fermentation broth was subjected to gas chromatography analysis. Basic medium was also used for degradation efficiency analysis.

Agilent 7890A with column HP-INNOWAX (30 m*0.32 mm*0.25 µm) was used. Sample preparation includes centrifugation and filtering with 0.25 µm filter. The main parameters were set up according to the manual with modifications [23]. Briefly, the temperature of column oven was held at 45 °C for 1 min, and then programmed at 8 °C/min to 155 °C and held for 1 min; the flow rate of nitrogen gas, hydrogen gas, and air were 35, 35, and 350 mL/min, respectively. The injection port temperature was maintained at 180 °C and the dual hydrogen flame ionization detector temperature was 200 °C. Isoamyl alcohol was used as internal control standard [13].

113.2.6 Identification of the Isolated Strains

Bacterial genomic DNA was extracted as described previously [24]. Specific primers 27F and 1492R were used to amplify bacterial 16S rRNA gene fragment, and their sequences were as follows:

27F: 5'-AGAGTTTGATCCTGGCTCAG-3' (corresponding to *Escherichia coli* positions 8–27).

1492R: 5'-GGTTACCTTGTTACGACTT-3' (corresponding to *Escherichia coli* positions 1,507–1,492).

The PCR reaction system was 50µL and the parameters include denaturation at 94 °C for 5 min, 1 cycle; denaturation at 94 °C for 1 min, annealing at 53 °C for 45 s, and extension at 72 °C for 1 min, 33 cycles; 72 °C for 10 min.

PCR products were purified from gel and subjected to sequencing analysis with the same primers used in PCR. Sequence homology search was carried out with BLAST provided by NCBI to identify the isolates [25]. The isolates were classified to genus level with Classifier (Ribosomal Database Project II) [26].

113.3 Results and Discussion

113.3.1 Enrichment and Isolation of n-Butanol Tolerant Strains

Totally 30 strains with different morphologies were selected from various environmental samples. Among them, 25 strains were screened out from the enriched culture in presence of 10 g/L *n*-butanol, and 5 strains were screened out from the enriched culture in the presence of 50 g/L *n*-butanol.

113.3.2 Tolerance Analysis

Solvents have natural toxicity to microbes [27]. *n*-Butanol toxicity is a crucial factor affecting the production level of fermentation [28, 29]. The tolerance ability of the 30 isolates was quantitatively determined by measuring the relative growth rate of different strains in the presence of 1, 2, and 3 % *n*-butanol, respectively. Almost all the isolated strains grew well in the medium supplementing with 1 % *n*-butanol, indicating they can tolerate 1 % *n*-butanol during growth (Fig. 113.1a). In the presence of 2 % *n*-butanol, the relative growth rates of 10 strains were over 40 % of their corresponding controls (Fig. 113.1b). Among them, strain YY-23 had the highest relative growth rate 67.8 %. Even in the presence of 3 % *n*-butanol, strain YY-23 still thrived though the relative growth rate was only 30 % of the control (Fig. 113.1c). Its tolerance ability was similar to the strains isolated previously [30].

113.3.3 Degradation Efficiency Analysis

The mechanisms of *n*-butanol tolerance in microbes have been explored, and mainly including the barrier by cell membrane lipid, expulsion by efflux pumps, adjustment in cellular membrane protein content, and degradation of *n*-butanol [31–33]. In this work, we investigated *n*-butanol tolerance mechanisms of the isolated strains by analyzing their *n*-butanol degradation efficiency in LB medium and the basic medium, respectively.

As described in Materials and methods, remaining *n*-butanol in LB medium was tested. Strains YY-13, YY-14, YY-15, and YY-18 didn't digest *n*-butanol at all, while strains YY-4, YY-8, YY-16, YY-30, and YY-10 degraded more than 20 % *n*-butanol, especially strain YY-10 can remove as much as 31 % *n*-butanol within 24 h incubation (Fig. 113.2a).

The degradation efficiency was also investigated in the basic medium supplement with *n*-butanol as sole carbon source. As shown in Fig. 113.2b, strains YY-2,

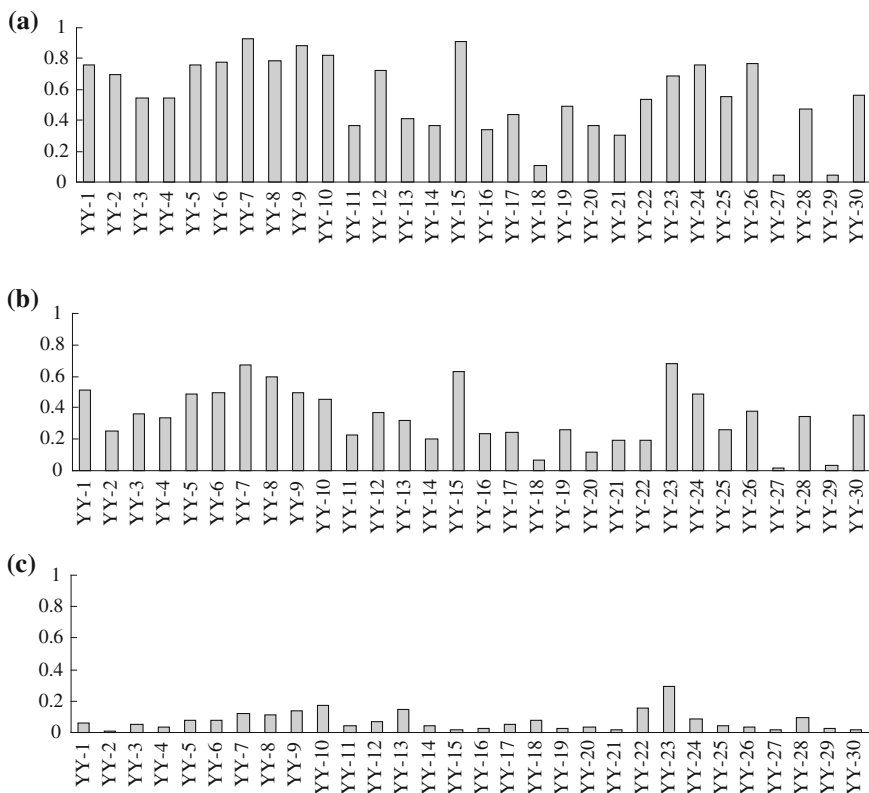


Fig. 113.1 Relative growth rates of the isolates. **a** The relative growth rates of the isolates in the presence of 1 % n-butanol. **b** The relative growth rates of the isolates in the presence of 2 % n-butanol. **c** The relative growth rates of the isolates in the presence of 3 % n-butanol

YY-7, YY-11, YY-21, and YY-29 digested more than 25 % n-butanol within 24 h, especially strain YY-29 remove as much as 31.7 % n-butanol in the basic medium within 24 h (Fig. 113.2b).

Strains YY-10 and YY-29 showed high n-butanol degradation efficiency in LB and the basic medium. Both of them could be used in bioremediation of n-butanol associated contaminations. Especially strain YY-10 could digest n-butanol even in the presence of other carbon sources, indicating it might disrupt n-butanol in a way of cometabolism and suitable for bioremediation in more complicated environments [34]. No degradation of n-butanol was observed in strains YY-13, YY-14, YY-15, and YY-18, the mechanisms of their n-butanol tolerance might not be related with degradation, and these strains might be more suitable for metabolic engineering to construct high level n-butanol producing strains.

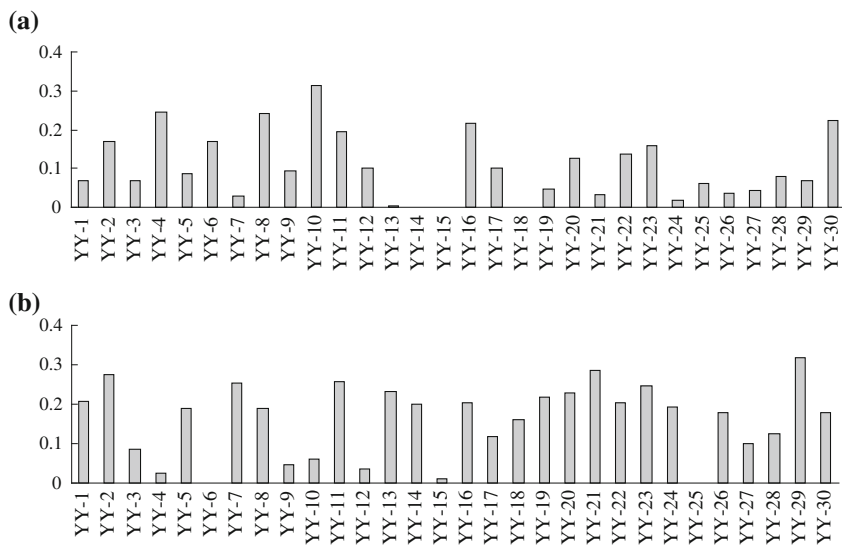


Fig. 113.2 Degradation efficiency of the isolated strains. **a** Remaining *n*-butanol analysis in LB medium **b** Remaining *n*-butanol analysis in the basic medium

113.3.4 Identification of the Isolates

Strains YY-10, YY-13, YY-14, YY-15, YY-18, YY-23, and YY-29 are selected for identification. Their genomic DNA was used as templates for PCR to amplify 16S rRNA gene fragments. PCR products were purified and subjected to sequencing analysis. Homology searches were performed via BLAST provided by NCBI [25]. Their taxonomy classifications were carried out by the program Classifier of RDPII [26]. Both analyses gave similar results, strains YY-10, YY-14, and YY-29 were homologous to *Bacillus subtilis* with the similarity of 100, 99, and 100 %, respectively, strain YY-13 was homologous to *Bacillus cereus* with the similarity of 99 %, strain YY-15 was homologous to *Bacillus tequilensis* with the similarity of 99 %, strain YY-18 was homologous to *Bacillus methylotrophicus* with the similarity of 99 %, and strain YY-23 was homologous to *Pseudomonas stutzeri* with the similarity of 99 % (Table 113.1). Previously, *Escherichia coli*, *Zymomonas mobilis*, *Saccharomyces cerevisiae*, and *Lactobacillus* had been reported to resist to 1–3 % *n*-butanol [30, 35, 36]. However, their *n*-butanol tolerance mechanisms were not studied [30]. For *n*-butanol producing strain construction, tolerant strains which showed high *n*-butanol degradation efficiency should be expelled from the candidate list.

Table 113.1 Homology analysis and classifications of the isolated strains

Strains	Accession no.	Most similar strains (accession no)	Similarity (%)	Genus ^a
YY-10	JX575604	<i>Bacillus subtilis</i> (JQ039972.1)	100	Bacillus
YY-13	JX575605	<i>Bacillus cereus</i> (GQ462534.1)	99	Bacillus
YY-14	JX575606	<i>Bacillus subtilis</i> (FJ263018.1)	99	Bacillus
YY-15	JX575607	<i>Bacillus tequilensis</i> (JX077105.1)	99	Bacillus
YY-18	JX575608	<i>Bacillus methylotrophicus</i> (JN700125.1)	99	Bacillus
YY-23	JX575609	<i>Pseudomonas stutzeri</i> (AB680456.1)	99	Pseudomonas
YY-29	JX575604	<i>Bacillus subtilis</i> (JQ039972.1)	100	Bacillus

^a Classification results by classifier from RDPII [26]

113.4 Conclusions

Tolerance was a crucial factor affecting synthesis level of n-butanol producing strains. To construct n-butanol high producing recombinant strains, native n-butanol tolerant strains are required for metabolic engineering. In this work, totally 30 strains tolerant to n-butanol were isolated. Strains YY-13, YY-14, YY-15, and YY-18 didn't metabolize n-butanol in LB medium, strain YY-23 had the highest relative growth rate even in the presence of 3 % butanol with relatively low n-butanol degradation efficiency, and all of them might be used as candidates for genetic engineering to construct high n-butanol producing strains. Their n-butanol tolerance mechanisms needed to be further investigated. Strains YY-10 and YY-29 showed strong n-butanol degradation efficiency and could be used for n-butanol bioremediation.

Acknowledgments This work was partly supported by The National Natural Science Foundation of China (Grant No. 30970114) and The National Key Technology R&D Program of China (Grant No. 2011BAC11B05).

References

1. Lee SY, Park JH, Jang SH et al (2008) Fermentative butanol production by Clostridia. *Biotechnol Bioeng* 101(2):209–228
2. Schwarz WH, Gapes JR (2006) Butanol-rediscovering a renewable fuel. *BioWorld Europe* 1:16–19
3. Riehard VN (2008) Biobutanol enters battle of the alcohols. *Chem World-UK* 5(2):21
4. Ladisch MR (1991) Fermentation-derived butanol and scenarios for its uses in energy-related applications. *Enzym Microbiol Technol* 13:280–283
5. Shota A, Anthony FC et al (2008) Metabolic engineering of *Escherichia coli* for 1-butanol production. *Metab Eng* 10:305–311
6. Jiang M, Wei P et al (2006) Consideration on the development of industrial biotechnology of post-petroleum epoch. *Chem Ind Eng Prog* 25(10):1119–1123
7. Qureshi N, Blaschek HP (2001) Recent advances in ABE fermentation: hyper-butanol producing *Clostridium beijerinckii* BA101. *J Ind Microbiol Biotechnol* 27(5):287–291

8. Parekh M, Formanek J, Blaschek HP (1998) Development of a cost-effective glucose-corn steep medium for production of butanol by *Clostridium beijerinckii*. *J Ind Microbiol Biotechnol* 21:187–191
9. Madihah MS, Ariff AB (2001) Direct fermentation of gelatinized sago starch to acetone-butanol-ethanol by *Clostridium acetobutylicum*. *World J Microbiol Biotechnol* 17:567–576
10. Karakashev D, Thomsen AB, Angelidaki I (2007) Anaerobic biotechnological approaches for production of liquid energy carriers from biomass. *Biotechnol Lett* 29:1005–1012
11. Papoutsakis ET (2008) Engineering solventogenic clostridia. *Curr Opin Biotechnol* 19(5):420–429
12. Keis S, Shaheen R, Jones DT (2001) Emended descriptions of *Clostridium acetobutylicum* and *Clostridium beijerinckii*, and descriptions of *Clostridium saccharoperbutylacetonicum* sp. Nov. and *Clostridium saccharobutylicum* sp. Nov. *Int J Syst Evol Microbiol* 51:2095–2103
13. Woods DR (1995) The genetic engineering of microbial solvent production. *Trends Biotechnol* 13(7):259–264
14. Linden JC, Moreira AR, Lenz TG (1985) *Comprehensive biotechnology*. Pergamon Press, Oxford
15. Jones DT, Woods DR (1986) Acetone-butanol fermentation revisited. *Microbiol Rev* 50(4):484–524
16. Jin X, Wang G, He B (2007) Research progress and high yield strategy of acetone-butanol fermentation. *Chem Ind Eng Prog* 26:1727–1732
17. Nair RV, Papoutsakis ET (1944) Expression of plasmid-encoded aad in *Clostridium acetobutylicum* M5 restores vigorous butanol production. *J Bacteriol* 176(18):5843–5846
18. Harris LM, Blank L, Desa IRP et al (2001) Fermentation characterization and flux analysis of recombinant strains of *Clostridium acetobutylicum* with an inactivated solR gene. *J Ind Microbiol Biotechnol* 27(5):322–328
19. Tomas CA, Welker NE, Papoutsakis ET (2003) Overexpression of groESL in *Clostridium acetobutylicum* results in increased solvent production and tolerance, prolonged metabolism, and changes in the cell's transcriptional program. *Appl Environ Microbiol* 69(8):4951–4965
20. Chen Taosheng, Qizu Lu (1991) *Fermentation of acetone and butanol production technology*. Chemical Industry Press, Beijing
21. Liu J, Fan LT et al (2004) Downstream process synthesis for biochemical production of butanol, ethanol, and acetone from grains: Generation of optimal and near optimal flow sheets with conventional operating units. *Biotechnol Prog* 20(5):1518–1527
22. Huang WC, Ramey DE, Yang ST (2004) Continuous Production of butanol by *Clostridium acetobutylicum* immobilized in a fibrous bed bioreactor. *Appl Biochem Biotechnol* 22(16):113–116
23. Jingchang He (2009) Study on the selecting of high acetone and butanol production strain and its new fermentation technology, Zhejiang University of Technology, Zhejiang
24. Sambrook J, Russell DW (2001) *Molecular Cloning: A Laboratory manual*, 3rd edn. Cold Spring Harbor Press, New York
25. Zhang Jinghui, Madden TL (1997) Power BLAST: A new network BLAST application for interactive or automated sequence analysis and annotation. *Genome Res* 7(6):649–656
26. Wang Qing, Garrity GM, Tiedje JM et al (2007) Naive Bayesian classifier for rapid assignment of rRNA sequence into the new bacterial taxonomy. *Appl Environ Microbiol* 73(16):5261–5267
27. Clark DP, Beard JP (1979) Altered phospholipid composition in mutants of *Escherichia coli* sensitive or resistant to organic solvents. *J Gen Appl Microbiol* 113:267–274
28. Bowles LK, Ellefson WL (1985) Effects of butanol on *Clostridium acetobutylicum*. *Appl Environ Microbiol* 50:1165–1170
29. Papoutsakis ET, Alsaker KV, Borden J (2005) *Understanding butanol and butyrate toxicity and tolerance in clostridia at the genomic scale*. United States: 229th ACS National Meeting, San Diego
30. Knoshaug EP, Zhang M (2009) Butanol tolerance in a selection of microorganisms. *Appl Biochem Biotechnol* 153(1–3):13–20

31. Baer SH, Blaschek HP, Smith TL (1987) Effect of butanol challenge and temperature on lipid composition and membrane fluidity of butanol-tolerant *Clostridium acetobutylicum*. *Appl Environ Microbiol* 53:2854–2861
32. Ramos JL et al (2002) Mechanisms of solvent tolerance in gram-negative bacteria. *Annu Rev Microbiol* 56:743–768
33. Weber FJ, Bont JA (1996) Adaptation mechanisms of microorganisms to the toxic effects of organic solvents on membranes. *Biochim Biophys Acta* 1286:225–245
34. Yuquan Xu, Zhang Wei (2000) Isolation and identification of a phenol-degrading bacterial strain. *Acta Sci Circumst* 20(4):450–455
35. Luong JHT, Nguyen AL (1986) Diffusion in κ -carrageenan gel beads. *Biotechnol Bioeng* 29:242–248
36. Antoce OA et al (2007) A calorimetric method applied to the study of yeast growth inhibition by alcohols and organic acids. *Am J Enol Viticult* 48(4):413–422

Chapter 114

Effects of Dual-Frequency Ultrasound with α -amylase on the Properties and Structure of Mung Bean Starch

Aijun Hu, Jing Lu, Jie Zheng, Xiaoqing Zhang, Ying Zhang, Tong-Cun Zhang, Qian Li and Lin Yang

Abstract In this paper, we focus on the effects of dual-frequency ultrasound (40 and 80 kHz) with α -amylases (5U/g) on the properties and structure of mung bean starch. The reducing sugar value and starch solubility in the treated starch slurry under ultrasound enzyme were studied. Scanning electron microscopy (SEM) and Fourier transform infrared spectrometer (FTIR) were used to measure the apparent structure and crystal texture of starch. The results indicated that compared with the results of single-frequency ultrasound treatment, dual-frequency ultrasound promoted the starch hydrolysis by amylase and increased the starch solubility remarkably. More channels and holes were found on the surface of treated starch granule by SEM. The results of FTIR analysis showed the FTIR peak shape of ultrasonic treated starch was different from that of the control starch.

Keywords Ultrasound · Mung starch · Property · Structure · α -amylases

A. Hu (✉) · L. Yang · J. Zheng · Y. Zhang · Q. Li · J. Lu
Key Laboratory of Food Nutrition and Safety (Tianjin University of Science & Technology),
Ministry of Education, College of Food Engineering and Biotechnology, Tianjin University
of Science & Technology, Tianjin 300457, People's Republic of China
e-mail: huaijun@tust.edu.cn

X. Zhang
Modern Analytic Technique Research Center, Tianjin University of Science & Technology,
Tianjin 300457, People's Republic of China

T.-C. Zhang
Key Laboratory of Industrial Microbiology, Ministry of Education, College of
Bioengineering, Tianjin University of Science & Technology, Tianjin, China

114.1 Introduction

As a renewable resource and a carbohydrate, starch is very abundant, and its yield is only less than cellulose in nature [1]. It is often used as an important raw material in many fields such as food, chemical, paper, and textile industry [2]. Because of the defects in structure and properties, for example, insoluble in cold water, easy to be aged, native starch is limited to wide applications. In order to improve them and to meet the requirement of modern industrial processing, many technologies are applied to modify starch, including chemical modification, physical modification, and biochemical medication [3]. In many cases, chemical modification is replaced by environmental friendly technologies considering its chemical contamination, safety, and solvent residue in the product. Of which, two green modifications, ultrasonic and enzymatic method are focused in the relevant area.

Ultrasound is a mechanic wave with the frequency of above 20 kHz [4]. It can be divided into three types: power ultrasound, high frequency ultrasound, and diagnostic ultrasound [5]. The power ultrasound is usually used in textile industry, pharmaceutical, and food processing, such as ultrasonic extraction, disinfecting, emulsification, pasteurization, crystallization, degassing of liquids, defoaming, and sonochemical reaction [6, 7]. These applications are introduced mainly owing to three effects of ultrasound, physical effect, thermal effect, and cavitation effect [8, 9].

Ultrasonic Cavitation is the momentary creation of vacuum “bubbles” in the fluid which immediately and violently implode to produce millions of microscopic jets of liquid. In addition, a local temperature near this activity has been shown to be as high as 10,000 °C, and the pressure produced may be as high as 10,000 PSI. It is considered as the main reason that ultrasound is successfully used in many fields and sonochemical reaction takes place. And it has been studied extensively from the mid-twentieth century owing to its importance for ultrasonic applications [10]. Ultrasound treatment of corn starch could distort the crystalline region, and destruct the granular structure [11].

Enzyme is a biological catalyze with many varieties such as α -amylases, β -amylase, and protease. α -amylases are very important in biological reactions such as fermentation, germination, or digestion, and also widely used in starch processing industry. α -amylases only attack the α , 1–4 glycosidic bond in starch granules, produce a small quantity of glucose which raises the dextrose equivalent. Moreover, it can cause starch granules surface some little holes or other kinds of damage with no change of starch X-ray pattern or the crystal structures [12, 13].

Nowadays ultrasonic and enzymatic application are paid more interests and focuses, however till now, no researches are found on the effects of dual-frequency ultrasonic with enzyme on starch. The aim of this work was to research the effects of dual-frequency ultrasound with α -amylases on properties and structure of mung bean starch (MBS), which provides a theoretical and experimental background for dual-frequency ultrasonic application in starch and enzymic hydrolysis.

114.2 Materials and Methods

114.2.1 Materials and Equipment

Commercially available MBS (13 % moisture) was obtained from Jin Cheng Co., Ltd, (Shandong, China). Sodium hydroxide, AR, was supplied by the Tianjin DeEn Chemical Reagent Company (Tianjin, China). Fehling reagent was obtained from Sigma Company (American). α -amylase (2,000U/mL) was supplied by Imperial Jade Bio-Technology Co.,Ltd (Ningxia, China). Ultrasonic cleaner was supplied by Scientz Biotechnology Co.,Ltd (Ningbo, China). Electronic analytic balance (FA1604S) was supplied by Weighing Scales Instrument Factory (Shanghai, China). pH Meter (PHS-3C) was supplied by LEICI Instrument Company (Shanghai, China). Electric blast oven (DGG-101-2) was supplied by Tianjin Tianyu Instrument Company (Tianjin, China). Electric heated water bath (HW-SY21-K) was supplied by Beijing Changfen Instrument Company (Beijing, China). Electronic balance (TD1200) was supplied by Tianjin Tianma Instrument Company (Tianjin, China). Scanning Electron Microscope SU-1510 was obtained from Hitachi Ltd (Tokyo, Japan). Infrared spectrometer Vector22 was obtained from Bruker spectrometer (Germany).

114.2.2 Sample Preparation Method

Sample suspensions were prepared by stirring 100 g mung starch and 900 mL distilled water. Sodium hydroxide was used to neutralize the solution (pH = 6.0) and then mixed with α -amylases according to 5U per 1 g starch. Calcium chloride (0.2 %) was applied to protect the enzyme activity. Prepared samples were placed into the bath and ultrasonic treated with 40 kHz, 80 kHz, and 40 + 80 kHz for 90 min in 60 °C, respectively. Treatments without the ultrasound were used as controls. The preparation of sonicated mung starch was performed in triplicate.

114.2.3 Determination of Reducing Sugar

The reducing sugar of suspension was determined, using the titrimetric method according to GB/T5009.7-2008. Dextrose equivalent (DE) was used to examine the degree of hydrolysis of starch. DE was calculated as follows:

$$DE = \frac{\text{Reducingsugar expressed glucose}}{\text{g dry solid weight}} \times 100\% \quad (114.1)$$

114.2.4 Determination of Starch Solubility

Five starch suspensions of 1 % (w/w) were separately prepared in a flask and were heated to 95 °C for 30 min with shaking every 5 min and left for cooling to room temperature (30 ± 2 °C) and centrifuged for 15 min at 3,000 g. The supernatant was decanted, and the residual volume was determined. The solid part was dried in an oven for 2 h at 130 °C [14]. The result was expressed as the mean of the determination results of above suspensions.

114.2.5 Scanning Electron Microscopy

The samples were sprinkled on double-sided adhesive tape and mounted on an aluminum stub, and then coated with a thin gold film. Optical sections of granules were obtained by scanning electron microscope [15].

114.2.6 Fourier Transforms Infrared (FTIR) Spectroscopy

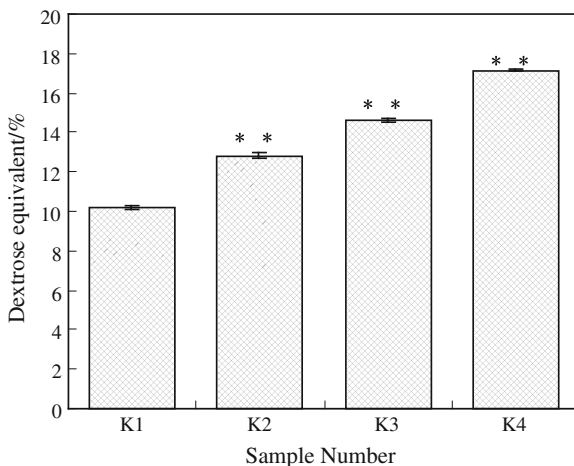
FTIR spectra of samples in KBr pellets (1 mg/30 mg) were measured on a spectrophotometer with a DTGS detector and OMNIC 7.0 software using 64 scans at resolution of 4 cm^{-1} . The spectra were recorded over the wave number range between 4,000 and 500 cm^{-1} . The samples were dried at 105 °C for 4 h before analysis to avoid interference by moisture [16].

114.3 Results and Discussion

114.3.1 Effect of Ultrasound and Amylase on Reducing Sugar

Figure 114.1 indicated that ultrasound had a remarkable effect on DE of the starch hydrolysate. Ultrasound promoted amylase action on the starch granules to produce smaller molecules and reducing sugar, as a result, the DE increased. As the ultrasonic frequency was increased, the effect on DE was more obvious. DE of K4 treated by dual-frequency was bigger than the others. This may be explained that dual-frequency ultrasonic treatment can create more bubbles and cavitations which contribute to the enzymatic hydrolysis and the decomposition of starch granules [17].

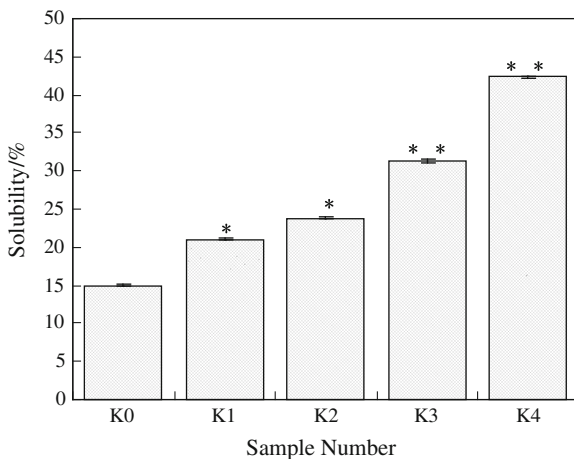
Fig. 114.1 Effect of ultrasound and α -amylase treatment on dextrose equivalent (K1 was treated only with amylase; K2, K3, K4 were treated respectively by 40, 80, and 40 + 80 kHz ultrasound with amylase). “***” difference is extremely significant ($P < 0.01$)



114.3.2 Effect of Ultrasound and Amylase on Samples Solubility

It can be shown from Fig. 114.2 that starch solubility was affected by both ultrasound and amylase. Compared with K0, the solubility of K1 and K2 increased, however, K3 and K4 had greater solubility. The structure of starch may be destroyed by ultrasound and amylase, thus its internal soluble matter can be easier to release [18]. Dual-frequency ultrasound acts starch granule more seriously and the solubility reached the maximum. This trend was consistent with DE.

Fig. 114.2 Effect of ultrasound and α -amylase treatment on solubility (K0 was native starch, K1 was treated only with amylase; K2, K3, K4 were treated, respectively by 40 kHz, 80 kHz, and 40 + 80 kHz ultrasound with amylase). “*” Difference is significant ($P < 0.05$). “***” Difference is extremely significant ($P < 0.01$)



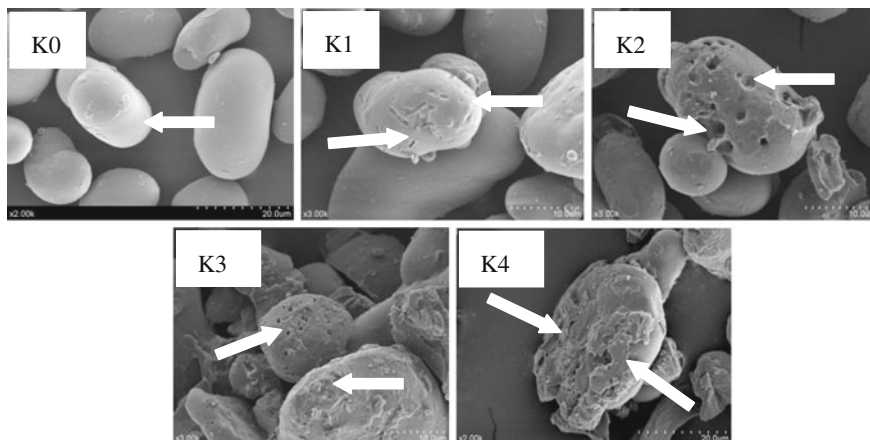


Fig. 114.3 Effect of ultrasound and α -amylase treatment on apparent structure (K0 was native starch, K1 was treated only with amylase; K2, K3, K4 were treated respectively by 40 kHz, 80 kHz, and 40 + 80 kHz ultrasound with amylase)

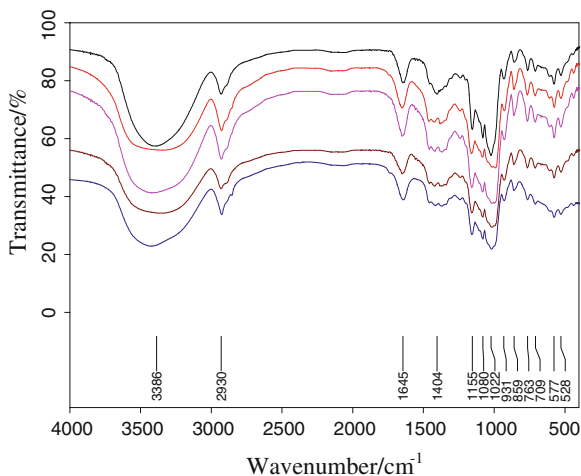
114.3.3 Influence of Ultrasound and Amylase on Apparent Structure of Samples

As shown in Fig. 114.3 that native starch granule was oval or kidney-shaped and some attachments could be seen on the surface of granule, which may be protein (K0) [19]. After treated with only amylase, some little holes and channels were found on the surface of granules (K1). Both 40 kHz and 80 kHz ultrasonic treatment with amylase made the holes or channels bigger and deeper. K4 clearly indicated that starch granule was broken seriously and parts of structure were separated from granule. This was probably because of the more powerful cavitation of dual-frequency ultrasound [20].

114.3.4 Influence of Ultrasound and Amylase on Crystal Structure of Samples

FTIR spectroscopy was used to verify the change in the crystal structure of sample molecules resulting from ultrasound and amylase. The FTIR spectra of K0, K1, K2, K3, and K4 are shown in Fig. 114.4. It could be seen that the spectrum of five samples had a little difference at about $1,390\text{ cm}^{-1}$. In every sample spectrum, the bands $3,386$ and $2,930\text{ cm}^{-1}$ correspond to OH and CH stretching, respectively, while the bands at $1,645\text{ cm}^{-1}$ correspond to the scissoring of two O–H bonds of water molecules [21]. Compared to K0, FTIR spectra of K1, K2, K3, and K4 have similar profiles indicating that the ultrasound and amylase had effect on the crystal

Fig. 114.4 Effect of ultrasound and α -amylase treatment on crystal structure (K0 was native starch, K1 was treated only with amylase; K2, K3, K4 were treated respectively by 40 kHz, 80 kHz, and 40 + 80 kHz ultrasound with amylase)



structure. The spectra of K1, K2, K3, and K4 provide evidence of ultrasonic effect by showing the presence of important band at $1,404\text{ cm}^{-1}$ (C–H). These C–H bands were from glucoses which were produced by both amylase and ultrasound. That was consistent with the conclusion of DE.

114.4 Conclusion

Both single-frequency (40 and 80 kHz) and dual-frequency ultrasound (40 + 80 kHz) can promote amylase to act on the starch granule to increase the dextrose equivalent. Also ultrasonic treatment with amylase can increase the solubility. Ultrasonic treatment could produce many holes and channels on the surface, and dual-frequency treatment destroyed the integrity of the particles, but did not change the crystal structure. Compared to single-frequency ultrasound, dual-frequency ultrasonic treatment has more significant effect on the properties and structure of mung bean starch.

Acknowledgments The authors acknowledge the financial support from the National Natural Science Foundation of China (Project No.: 31071608), the Science and Technology Innovation Funded Project of Dongli District, Tianjin (Project No.:2010312), the 863 (Hi-tech research and development program of China) program under contract NO.2012AA021505 and the National Natural Science Foundation of China (Project No.: 31201354).

References

1. Liu XZ, Luo ZG, Hu ZH et al (2008) Effect of ultrasonic treatment on rheological properties of corn starch. *Mod Food Sci Technol* 4:316–321
2. Yoshinobu I, Takehisa K, Toshiyuki W (1994) Ultrasound degradation of waxy rice starch. *Biosci Biotech Biochem* 58:1799–1802
3. Ji GQ, Shao XZ, Wang YT (2010) Application of ultrasound technology in the modification of starch. *Cereals Oils* 1:1–5
4. Melissa ML, Samir KK, Larson DJ et al (2010) Ultrasonic pretreatment of corn slurry for saccharification, a comparison of batch and continuous systems. *Ultrason Sonochem* 17:939–946
5. Anet RJ, Zoran H, Drago S (2010) Ultrasound effect on physical properties of corn starch. *Carbohydr Polym* 79:91–100
6. Devon KC, Ya JW (2006) Application of protease and high-intensity ultrasound in corn starch isolation from degermed corn flour. *Cereal Chem* 83:506–509
7. Cao C, Liu BL (2009) Application and prospect of high-frequency ultrasound technique in food industry. *J Anhui Agric Univ* 37:18143–18144
8. Kamaljit V, Richard M, Raymond M et al (2006) Ultrasonic recovery and modification of food ingredients. *Chem Mater Sci*. doi:[10.1007/978144197472313](https://doi.org/10.1007/978144197472313)
9. Feng Z, Jiang FY, He TL (2010) Application of ultrasound in the food processing. *J Wu Yi Univ* 34:21–26
10. Brennen CE (1995) *Cavitation and Bubble Dynamics*. New York: Oxford University Press
11. Anet RJ, Zoran H, Drago S (2010) Ultrasound effect on physical properties of corn starch. *Carbohydr Polym* 79:91–100
12. Zhou Y, Hoover R, Liu Q (2004) Relationship between α -amylase degradation and the structure and physicochemical properties of legume starches. *Carbohydr Polym* 57:299–317
13. Georges T, Anders VN, Agnes RS (2010) Hydrolysis of concentrated raw starch, a new very efficient α -amylase from *Anoxybacillus flavothermus*. *Carbohydr Polym* 87:46–52
14. Luo ZG, Lu JJ (2010) Effect of ultrasound treatment on the thermal properties of maize starch. *Mod Food Sci Technol* 7:666–668
15. Wang LF, Wang YJ (2003) Application of high-intensity ultrasound and surfactants in rice starch isolation. *Cereal Chem* 81:140–144
16. Zhang B, Cui DP, Liu MZ et al (2012) Corn porous starch: Preparation, characterization and adsorption property. *Int J Biol Macromol* 50:250–256
17. Mason TJ, Paniwnyk L, Lorimer JP (1996) The uses of ultrasound in food technology. *Ultrason Sonochem* 3:253–260
18. Renate CB, Bozena R, Salah L et al (2005) Degradation of chitosan and starch by 360 kHz ultrasound. *Carbohydr Polym* 60:175–184
19. Zhao YL, Liao DL, Zhang YQ et al (2007) The ultrasound effect on the properties and structure of cassava starch. *Chin J Process Eng* 7:1138–1143
20. Huang Q, Li L, Fu X (2007) Ultrasound effects on the structure and chemical reactivity of cornstarch granules. *Starch—Starke* 59:371–378
21. Zhang LM, Zuo BM, Wu PL (2012) Ultrasound effect on the acetylation of dioscorea starch isolated from *Dioscorea zingiberensis* C. H. Wrigh. *Chem Eng Process* 54:29–36

Chapter 115

Relationship Between Diet and Stable Carbon and Nitrogen Isotope Composition in Beef Tissues

Fengmei Sun, Guangyu Shi, Huiwen Wang and Shuming Yang

Abstract The effect of the amount of C₄ plants in diets on the carbon and nitrogen stable isotope composition of different types of beef tissues was investigated. Eighteen young bulls were randomly divided into six groups and fed with a diet consisting of different content of C₄ plant material. At the end of experiment, the $\delta^{13}\text{C}$ values of cattle tail hair, defatted muscle, and crude fat all become enriched and significantly correlated with increasing proportions of C₄ constituents in the diet. However, the $\delta^{15}\text{N}$ values of beef tissues did not increase regularly with the change of diet, but the correlation among $\delta^{13}\text{C}$ and $\delta^{15}\text{N}$ values of above tissues were highly correlated. Based on these results, it is possible for the proportion of C₄ plant material to be estimated from the $\delta^{13}\text{C}$ values of the different tissue samples. And, cattle tail hair instead of muscle in beef origin is available.

Keywords $\delta^{13}\text{C}$ · $\delta^{15}\text{N}$ · Beef · Diet · Stable isotope

F. Sun (✉) · G. Shi

Department of Food Science, Hebei North University, Zhangjiakou 075131, People's Republic of China

e-mail: Shiliu0616@163.com

F. Sun · S. Yang

Institute of Quality Standard and Testing Technology for Agro-Product, Chinese Academy of Agricultural Science, Beijing 100081, People's Republic of China

H. Wang

Department of Animal Husbandry and Engineering, Hebei North University, Zhangjiakou 075131, People's Republic of China

115.1 Introduction

Food safety has become a focus of public concern. Because of diseases such as bovine spongiform encephalopathy (BSE) and foot and mouth disease (FMD), consumers are demanding to know the truth about provenance of animal products. The Swiss Federal Office of Public Health carried out an investigation that showed 82 % of customers purchased their food based on knowing the origin of the product [1]. Since January 2005, EU regulations have mandated that all food and feed should be traced at all stages of production, processing, and distribution in order to sell food and feed products in EU countries [2]. Therefore, a comprehensive tracing system is urgently needed for beef.

During the past 30 years, stable isotope ratio analysis (SIRA) has been successfully used in some areas of food production to determine the authenticity of food and to verify the geographic origin of food such as honey, fruit, and wine, etc. [3–5]. Some methods for food authentication have been officially acknowledged by institutions such as the European Commission for Normalization (CEN) or the Association of Official Analytical Chemists (AOAC) [6]. In recent years, SIRA has been regarded as a potential tool for tracing the geographic origin of animal food such as milk, cheese, butter, lamb, beef [7–12], and beef diet [13–15]. Previous studies have shown that the stable carbon and nitrogen composition of diets influence the $\delta^{13}\text{C}$ and $\delta^{15}\text{N}$ values of animal tissue, where the former is varying with proportions of C_3 or C_4 photosynthetic plant, and the latter is affected by many other factors, but to some extent to reflect the legumes and cultivation density of feed. Thus those of values of tissue are good indicators of diet [16]. Today, maize is largely used as cow and cattle feed to increase milk production or weight. Boner [12] and Schmidt [10] have reported the $\delta^{13}\text{C}$ values of defatted beef muscle could be used to distinguish organic from conventional cattle farming, because the fodder of organic cattle farming mainly consists of C_3 plants whereas the C_4 plants are more typically used in conventional cattle farming. Increasingly, SIRA techniques are being developed as a quantitative tool for inferring the proportion of C_3/C_4 plant components in cattle diets [15].

This study investigated the effect of different diets on the stable carbon ($\delta^{13}\text{C}$) and nitrogen ($\delta^{15}\text{N}$) stable isotope composition of different bovine tissues with the aim of establishing a quantitative relationship between the dietary C_4 plant intake and $\delta^{13}\text{C}$ of bovine tissues.

115.2 Materials and Methods

115.2.1 Animals and Experimental Designing

Eighteen (12–14 months old) young bulls were randomly divided into six treatment groups of three animals each. Two dietary formulas were given to the cattle,

Table 115.1 Dietary formula on a dry mass basis

Basic diet (%)			C ₄ diet (%)	
Maize silage	C ₄ plants	44	Maize silage	30
Maize meal		8	Distiller maize	63
Soybean meal	C ₃ plants	16	Maize meal	7
Wheat bran		12		
Wheat flower		11		
Cottonseed cake		9		
Total		100		100

a basal diet and a diet consisting of entirely of C₄ plants (Table 115.1). Initially, these two kinds of diets were prepared, then the following portions, 0, 20, 40, 60, 80 and 100 %, of the C₄ diet were mixed with 100, 80, 60, 40, 20, 0 % of the basal diet for the six treatments, respectively. Where ultimately the C₄ components accounts for 52.0, 61.6, 71.2, 80.8, 90.4, 100 % of the total diet for the group 1 through 6, respectively. All animals were slaughtered after feeding for 132 days.

115.2.2 Feed Samples

During the study, feed samples were collected and stored at -20°C before SIRA. Each individual composite sample was oven-dried at 60°C for 48 h and triturated. The roughage feed (maize silage) and other materials were then sieved using 0.177 and 0.149 mm mesh screen, respectively.

115.2.3 Cattle Tail Hair

Prior to the commencement of the study and the start of the new diets, a strand of tail hairs was cut close to the skin of each cattle. A sample was then taken in the same way from the same position at the end of the experiment. The hair of entire cattle tail was first soaked and was rinsed in deionized water and then dried at 60°C for 12 h. Then the samples were soaked in methanol/chloroform (2:1) for 2 h to removal fat and then rinsed and soaked in deionized water for another 30 min. Finally, the samples were rinsed with deionized water, dried at 60°C , and cut into 1 ~ 2 mm [14, 16, 17].

115.2.4 Meat and Fat Samples

Buttock muscles were collected at 48 h after post-mortem and stored at -20°C . The sample preparation followed a common preparation approach. Briefly, a

minimum 50 g sample is cut into small pieces with a ceramic scissors and dried completely with the aid of a lyophilizer (freeze-drier). The dried pieces are homogenized with a mortar and pestle. The resulting dry powder is extracted with diethyl ether for 6–8 h in a Soxhlet apparatus. Afterwards the fat-free dry mass (raw protein) is sieved through a 0.074 mm mesh screen and the lipid fractions (after evaporating the solvent) for each beef sample is stored at 4 °C until analysis.

115.2.5 Stable Carbon and Nitrogen Isotope Analysis

Pretreated samples (1 mg) were weighed into tin capsules and introduced into the elemental analyzer (Flash EA1112) by an autosampler, where the samples were combusted into CO₂ and N₂. The gas was separated using a gas chromatograph and analyzed using a Thermal Finnigan DELTA^{Plus} XL). The uncertainty of measurements was typically ± 0.2 ‰ for δ¹³C and δ¹⁵N. The values of the isotopic ratios were expressed in δ ‰ according to the following general formula:

$$\delta = \left[\left(R_{\text{sample}} / R_{\text{standard}} \right) - 1 \right] \times 1,000 \quad (115.1)$$

Where R_{sample} and R_{standard} represent the abundance ratio of ¹³C/¹²C and ¹⁵N/¹⁴N isotopes in the sample and the standard respectively. The standard used in this study was the international standard V-PDB (Vienna Pee Dee Belemnite) for δ¹³C and air for δ¹⁵N.

115.3 Results and Discussion

115.3.1 Feedstuff

The δ¹³C and δ¹⁵N values of the various feed materials are presented in Table 115.2. Plants are divided into three types of C₃, C₄, and CAM according to their different photosynthetic pathways. Maize silage, distiller maize, and maize meal are all typical C₄ plants which have enriched δ¹³C values. Soybean meal, wheat bran, wheat flower, and cottonseed cake are C₃ plants, and their δ¹³C values

Table 115.2 The δ¹³C and δ¹⁵N values of feed material

Feedstuff	δ ¹³ C (‰)	δ ¹⁵ N (‰)
Maize meal	-12.10 ± 0.14	1.14 ± 0.18
Distiller maize	-13.00 ± 0.35	1.92 ± 0.27
Cottonseed cake	-25.47 ± 0.38	1.84 ± 0.25
Wheat bran	-26.21 ± 0.22	-0.64 ± 0.11
Wheat flower	-27.65 ± 0.09	-0.19 ± 0.04
Maize silage	-13.10 ± 0.64	0.60 ± 0.13
Soybean meal	-25.41 ± 0.29	-0.60 ± 0.11

Table 115.3 The $\delta^{13}\text{C}$ values of cattle tissues and corresponding C_4 content (mean \pm SD), $N = 3$

Groups	C_4 content (%)	^a Diets $\delta^{13}\text{C}$ (‰)	Cattle tail hair $\delta^{13}\text{C}$ (‰)	Defatted muscle $\delta^{13}\text{C}$ (‰)	Crude fat $\delta^{13}\text{C}$ (‰)
1	52.0	-19.28	-18.17 \pm 0.93	-18.58 \pm 1.15	-21.11 \pm 0.24
2	61.6	-18.02	-17.22 \pm 0.39	-18.15 \pm 1.11	-19.31 \pm 1.90
3	71.2	-16.75	-16.36 \pm 0.18	-17.91 \pm 0.86	-19.65 \pm 0.17
4	80.8	-15.49	-14.91 \pm 0.31	-16.46 \pm 0.38	-18.87 \pm 0.63
5	90.4	-14.23	-13.41 \pm 0.12	-14.70 \pm 0.45	-17.49 \pm 0.29
6	100	-12.97	-12.02 \pm 0.14	-14.72 \pm 0.68	-17.55 \pm 0.45

a. these values were calculated based on the proportions of C_3 and C_4 plants and measured isotope compositions of each.

Table 115.4 The $\delta^{15}\text{N}$ values of cattle tissues in different C_4 content

Groups	C_4 content (%)	Diets $\delta^{15}\text{N}$ (‰)	Cattle tail hair $\delta^{15}\text{N}$ (‰)	Defatted muscle $\delta^{15}\text{N}$ (‰)
1	52.0	0.15	4.82 \pm 0.26	4.50 \pm 0.10
2	61.6	0.42	5.30 \pm 0.16	4.62 \pm 0.10
3	71.2	0.68	5.23 \pm 0.19	4.66 \pm 0.32
4	80.8	0.94	4.61 \pm 0.24	3.31 \pm 0.18
5	90.4	1.21	5.11 \pm 0.37	4.93 \pm 0.59
6	100	1.47	4.48 \pm 0.18	3.84 \pm 0.19

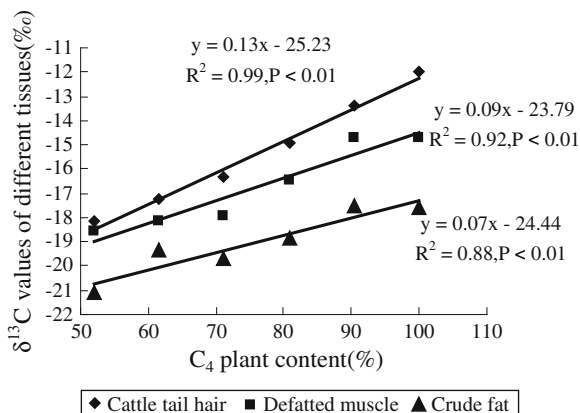
are depleted. More materials for feed were manually mixed in most occasions, and roughages such as grass silage and straw were difficult to be homogenized. Therefore, the $\delta^{13}\text{C}$ values of medley of each group were calculated based on the $\delta^{13}\text{C}$ values of feed ingredient and its proportion in the total diet (Table 115.3).

Generally, the $\delta^{15}\text{N}$ value of grass is higher than that of corn feed, and nitrogen-fixing plants such as soybean, alfalfa are lower (close to atmospheric nitrogen 0 ‰ or much lower). However, the $\delta^{15}\text{N}$ value of alfalfa was high in this study. The $\delta^{15}\text{N}$ values of plants are affected by many factors, such as soil conditions, the intensity of agricultural land use and nitrogen fertilizer [15, 18]. The $\delta^{15}\text{N}$ values of medley of each group were calculated according to the same method (Table 115.4).

115.3.2 Stable Carbon Isotope

Table 115.3 shows the $\delta^{13}\text{C}$ values of cattle tail hair, defatted muscle and crude fat, all enrich in ^{13}C with the increasing proportions of C_4 constituents in the diet. Moreover, all $\delta^{13}\text{C}$ values of the various beef tissues are significantly correlated with the content of C_4 plant material (Fig. 115.1). The correlation coefficient between the $\delta^{13}\text{C}$ values of cattle tail hair and C_4 plant content in the diet was the highest ($R^2 = 0.99$, $P < 0.01$), followed by defatted muscle ($R^2 = 0.92$, $P < 0.01$)

Fig. 115.1 Relationship between C_4 content and $\delta^{13}C$ values of the different tissue types



and the crude fat ($R^2 = 0.88$, $P < 0.01$). A Previous investigation found that the $\delta^{13}C$ values of different tissues taken at slaughter such as kidney fat, liver, blood, plasma, and muscle are highly correlated ($R^2 = 0.92$ – 0.99) with the calculated $\delta^{13}C$ values of the diet given [14]. Another study showed that there was a strong linear relationship between maize carbon in the diet and $\delta^{13}C$ values of lipid-free muscle ($R^2 = 0.98$) and lipid ($R^2 = 0.93$) [16]. However, in the other two studies, feed were constantly changed with the growth stages of cattle, and the feed ingredients are very different at every stage. The significant correlations were showed between $\delta^{13}C$ values of cattle tail hair segment and feeds, and they were significantly correlated with the proportion of C_4 plant of feeds, but there were no significant correlation between $\delta^{13}C$ values of whole cattle tail hair and feeds [14, 19]. The cattle tail hair mainly consists of keratin that is a kind of structure protein. Once the keratin structure is formed, hair tissue metabolism will stop [16]. Therefore, the isotopic information recorded by every section of the hair reflects the diet for growth at that time, and cattle tail hair can be regarded as an isotopic archive recording feeds changes. In this study, the diet of each group was not changed during the whole experiment, thus, the $\delta^{13}C$ values of cattle tail hair at the end of the experiment should essentially have the same isotopic information throughout the hair. Based on these results, the proportion of C_4 plant material could be estimated from the $\delta^{13}C$ values of different beef tissue samples.

As shown in Table 115.3 and Fig. 115.1, the $\delta^{13}C$ values of cattle tail hair is the most enriched followed by defatted muscle, and then the crude fat, and the correlation among them is significant. The correlation coefficients between defatted muscle and tail hair and crude fat were separately 0.90 ($P < 0.001$) and 0.87 ($P < 0.001$). Meanwhile, the correlation coefficients between hair and crude fat was 0.81 ($P < 0.001$). These results were similar to a previous study that showed the $\delta^{13}C$ values of hair, defatted muscle, and crude fat similarly decreased, and the $\delta^{13}C$ values between them are significant [17]. In another study, the $\delta^{13}C$ values declined in order of hair, muscle, plasma, blood, liver, and kidney fat [14]. Because of the discrimination against ^{13}C during the process of lipid synthesis, the $\delta^{13}C$ values of crude fat

are more depleted than that of diet, but $\delta^{13}\text{C}$ of muscle, hair, liver, blood, and plasma are more enriched relative to the diet. In this study, the correlation coefficient between defatted muscle and crude fat was not as high as found in previous studies, $r = 0.976$ and 0.98 [15, 20]. The reason maybe that the lipid extraction methods were different, or non-lipid fractions were mixed into crude fat when being transferred, and therefore leading to a lower correlation coefficient.

115.3.3 Stable Nitrogen Isotope

The nitrogen isotope in the feed was not controlled. The result (Table 115.4) showed that $\delta^{15}\text{N}$ values of the feed had nothing to do with the content of C_4 plants, and $\delta^{15}\text{N}$ values of cattle hair, defatted muscle did not increase regularly with the change of feed. However, in each group, the $\delta^{15}\text{N}$ values of muscle were lower than that of cattle tail hair, the correlation between them was significant ($P < 0.01$), and the correlation coefficient was 0.732 . As mentioned earlier, the nitrogen isotope in the feed was affected by a number of factors which resulted in $\delta^{15}\text{N}$ values of animal tissue without regularity. Nevertheless, the nitrogen isotope in tracing the origin of beef will provide additional information. Guo reported that cattle could be distinguished from pastoral or agricultural areas with $\delta^{15}\text{N}$ values, and the correct classification rate of beef origin could be significantly improved by $\delta^{13}\text{C}$ and $\delta^{15}\text{N}$ values complement each other [21].

The correlation among $\delta^{13}\text{C}$ and $\delta^{15}\text{N}$ values of cattle tail hair, defatted muscle, and crude fat were highly correlated, and indicating that tail hair instead of muscle in beef origin was available. According to the report, the lowest growth rate of tail hair is 0.51 mm/d [22]. Therefore, the appropriate section of tail hair in the light of fattening time is clipped from the root for analysis, which reflects the feed of cattle fattening period. Thus, it will make the isotope traceability technology easier.

115.4 Conclusion

The $\delta^{13}\text{C}$ values of cattle tail hair, defatted muscle, and crude fat all enhanced with the increment of the proportions of C_4 constituents in diet. Moreover, all $\delta^{13}\text{C}$ values of different tissues were significantly correlated with the content of C_4 plant material, so the proportion of C_4 plant material could be estimated from the $\delta^{13}\text{C}$ values of tissues. At the same time, $\delta^{15}\text{N}$ values of cattle hair, defatted muscle did not increase regularly with the change of feed. And the correlation among $\delta^{13}\text{C}$ and $\delta^{15}\text{N}$ values of cattle tail hair, defatted muscle, and crude fat were highly correlated. Thus, tail hair instead of muscle in beef origin is available.

Acknowledgments This research was financially supported by the Ministry of Science and Technology of the People's Republic of China. The project was tracing technology of beef.

References

1. Franke BM, Gremaud G, Hadorn R et al (2005) Geographic origin of meat-elements of an analytical approach to its authentication. *Eur Food Res Technol* 221:493–503
2. Schwägele F (2005) Traceability from a European perspective. *Meat Sci* 71:164–173
3. Croft LR (1987) Stable isotope mass spectrometry in honey analysis. *TrAC, Trends Anal Chem* 6:206–209
4. Simpkins WA, Patel G, Harrison M (2000) Stable carbon isotope ratio analysis of Australian orange juices. *Food Chem* 70:385–390
5. Roßmann A, Schmidt HL, Hermann A et al (1998) Multielement stable isotope ratio analysis of glycerol to determine its origin in wine. *Z Lebensm Unters Forsch A* 207:237–243
6. Roßmann A (2001) Determination of stable isotope ratios in food analysis. *Food Rev Int* 17:347–381
7. Renou JP, Deponge C, Gachon P et al (2004) Characterization of animal products according to geographic origin and feeding diet using nuclear magnetic resonance and isotope ratio mass spectrometry: Cow milk. *Food Chem* 85:63–66
8. Manca G, Franco MA, Versini G et al (2006) Correlation between multielement stable isotope ratio and geographical origin in Peretta cows' milk cheese. *J Dairy Sci* 89:831–839
9. Rossmann A, Haberhaue G, Hölzl S et al (2000) The potential of multielement stable isotope analysis for regional origin assignment of butter. *Eur Food Res Technol* 211:32–40
10. Schmidt O, Quilter JM, Bahar B et al (2005) Inferring the origin and dietary history of beef from C, N and S stable isotope ratio analysis. *Food Chem* 91:545–549
11. Camin F, Bontempo L, Heinrich K et al (2007) Multi-element (H, C, N, S) stable isotope characteristics of lamb meat from different European regions. *Anal Bioanal Chem* 389:309–320
12. Boner M, Forstel H (2004) Stable isotope variation as a tool to trace the authenticity of beef. *Anal Bioanal Chem* 378:301–310
13. Gebbing T, Schellberg J, Kühbauch W (2004) Switching from grass to maize changes the C isotope signature of meat and fat during fattening of steers. *Proceedings of the 20th General Meeting of the European Grassland Federation. Grassland Science in Europe, vol 9. Luzern, pp 1130–1132*
14. De Smet S, Balcaen A, Claeys E et al (2004) Stable carbon isotope analysis of different tissues of beef animals in relation to their diet. *Rapid Commun Mass Spectrom* 18:1227–1232
15. Bahar B, Monahan FJ, Moloney AP et al (2005) Alteration of the carbon and nitrogen stable isotope composition of beef by substitution of grass silage with maize silage. *Rapid Commun Mass Spectrom* 19:1937–1942
16. Schwertl M, Auerswald K, Schnyder H (2003) Reconstruction of the isotope history of animal diets by hair segment analysis. *Rapid Commun Mass Spectrom* 17:1312–1318
17. Guo BL, Wei YM, Pan JR et al (2006) Study on the change of stable carbon isotope composition in cattle tissues. *Sci Agric Sini* 39:1885–1890 (Chinese)
18. Ghidini S, Ianieri A, Zanardi E et al (2006) Stable isotopes determination in food authentication: A review. *Ann Fac Medic Vet di Parma XXVI*: 193–204
19. Guo BL, Wei YM, Pan JR (2008) Study on the changing law of stable carbon isotope composition in cattle tail hair. *Sci Agric Sini* 41:2105–2111 (Chinese)
20. Piasentier E, Valusso R, Camin F (2003) Stable isotope ratio analysis for authentication of lamb meat. *Meat Sci* 64:239–247
21. Guo BL, Wei YM, Pan JR et al (2007) Application of carbon and nitrogen isotope in beef origin traceability. *Sci Agric Sini* 40:365–372 (Chinese)
22. Schwertl M, Auerswald K, Schäufele R et al (2005) Carbon and nitrogen stable isotope composition of cattle hair: ecological fingerprints of production system? *Agric Ecosyst Environ* 109:153–165

Chapter 116

Expression and Sequence Analysis of *ChRpS3*, a Ribosomal Protein S3 cDNA, and its Potential Role in Ovary Development of *Cymbidium hybridum*

Xiaoqiang Chen, Xiulan Li, Ning Sun and Wenqin Song

Abstract A full length cDNA sequence, *Ch-RpS3*, was isolated by RT-PCR and further characterized by sequencing and expression analysis. The cDNA fragment was 1,003 bp in length and contained a complete open reading frame of 786 bp, encoding a protein of 261 amino acid residues with high sequence homology to RpS3 from other plants such as monocotyledon *Oryza sativa* (91 %). Phylogenetic analysis at the amino acid level also confirmed that *Ch-RpS3* belonged to the monocot-specific RpS3 clade. Furthermore, spatial and temporal expression analysis with RT-PCR indicated that *Ch-RpS3* was highly expressed in ovaries 2 days after pollination and is predicted to encode a novel member of RPS3 participating in cell growth and proliferation. It is deduced that this 40S ribosomal S3 like protein is involved in initiating ovary development of *C. hybridum*, which might provide novel insights into the molecular mechanism of ovary and floral development.

Keywords *Cymbidium hybridum* · Differential display RT-PCR · Floral development · 40S ribosomal S3 protein (RPS3)

116.1 Introduction

Floral development is one of the most complicated processes in phanerogam development. Floral development in *Arabidopsis* and other plants has been the focus of classic and molecular genetic analyses in recent years [1, 2]. With the

X. Chen (✉) · N. Sun

Department of Agronomy, Tianjin Agricultural University, Tianjin 300384, People's Republic of China
e-mail: chenxiaoqiang@tjau.edu.cn

X. Li · W. Song

College of Life Sciences, Nankai University, Tianjin 300071, People's Republic of China

development of molecular biology tools and theories, many floral development genes and floral homology genes have been isolated and cloned from a lot of plant species such as the fern, gymnosperm, and angiosperm [3]. Through the research on interactions of these genes, rapid progress is being made in elucidating the molecular mechanisms involved in the floral development of flowering plants.

C. hybridum is a member of the family orchidaceae, one of the largest and most diverse families of flowering plants. Being different from the flowers in other flowering plants, the nearly identical shape of sepals and petals as well as the production of a unique large lip (labellum) and a gynostemium or column in orchid flowers make it as a very special plant species in the study of floral development [4]. Furthermore, for other flowering plants, ovaries are mature before pollination [5], whereas ovule development of orchids only starts after successful pollination. So the ovary of orchids is an ideal tissue material to study flower ovule initiation and development [6, 7]. However, molecular studies on orchid ovary development are still too limited [8, 9]. Therefore, the isolation of more new variant ovary genes in orchids and further studies of their roles in orchid floral development are necessary.

The ribosome is a large ribonucleoprotein machine that synthesizes proteins from transcribed mRNA. Ribosomal protein S3 (RpS3) is a member of ribosomal small subunit and is also well known to be involved in the initiation of translation. Several ribosomal proteins have also been found to play roles in the translational apparatus which seems to be a major function and other extraribosomal functions [10–13] including induction of apoptosis, suppression of tumors, regulation of development, and DNA repair, and RPS3 is no exception.

Here, a cDNA fragment, CDD-470, was isolated by using Differential Display RT-PCR (DDRT-PCR) methods to study the changes of gene expression between the non-pollinated ovaries and the pollinated ones in *Cymbidium hybridum*. According to its sequences, a full-length cDNA with an open reading frame of 786 nucleotides, *Ch-RpS3*, encoding a protein of 261 amino acids has been obtained by RT-PCR. The amino acid sequence predicted from the corresponding region of the cDNA of *C. hybridum* exhibited significant homology with that of other RpS3 proteins. The similarities between RpS3 and the corresponding region in *C. hybridum* suggest that the homologous sequence, *Ch-RpS3*, in *C. hybridum* is a novel gene that is functionally homologous to RpS3. Its function was predicted in this paper.

116.2 Materials and Methods

116.2.1 Plant Materials

Cymbidium hybridum used in this study was grown in greenhouses under natural light and controlled temperature ranging from 23 to 27 °C. Various organs of these orchids (the petals, the sepals, the labellums, and the columns), roots, stems, and vegetative leaves, were separately dissected, immediately frozen in liquid nitrogen, and stored at –80 °C.

116.2.2 RNA Extraction and mRNA Purification

Frozen materials of the pollinated flowers and the untreated ones were ground in liquid nitrogen and simultaneously extracted using TRIZOL[®] (BBI, Markham, Canada), according to the manufacturer's instructions. The possible contaminated DNA was digested by RNase free DNase I (Takara, Shiga, Japan) for 30 min at 37 °C. The RNA was checked for quality and quantity by agarose gel electrophoresis (1.2 % formaldehyde denaturing agarose gel) and fluorimetry (ND-1000, NanoDrop, Wilmington, USA). Poly (A)+ RNA was isolated and purified by using Oligotex mRNA Mini kit (Qiagen, Valencia, USA).

116.2.3 Cloning of cDNA for CDD-700

The total RNA extracted from ten individual materials was equivalently pooled and subjected to the following reactions. 2 µg samples in every reaction were reverse transcribed using 0.05 µg reverse primers of M11 (5'-AAGCTTTTTTTTTTA-3') and 200 unit M-MLV reverse transcriptase under conditions specified by the enzyme supplier (Promega, Madison, USA) in a final volume of 0.01 cm³. Following reverse transcription, PCR amplifications were performed in 0.025 cm³ of a reaction mix with 0.001 cm³ of the reverse-transcribed cDNA, 0.5 µmol/L of each forward DD-17 (5'-GATCCAGTAC-3') and reverse primer (M11), 200 µmol/L dNTPs, 1x polymerase buffer and 1 U Taq DNA polymerase (Takara). PCR amplification reactions were performed in the MG5331 thermal cycler (Eppendorf, Hamburg, Germany) using the following program: after denaturation at 94 °C for 5 min, amplification was performed with 40 cycles of 30 s at 94 °C, 2 min at 40 °C, and 1 min at 72 °C, followed by a final extension at 72 °C for 10 min. Amplified PCR products were separated on a 6 % (w/v) polyacrylamide gel (PAGE). After silver staining, the gel was dried in room temperature and photographed. A 100-bp ladder was used to estimate the molecular size of fragments. All reactions were performed in triplicate to avoid false-positive results.

116.2.4 Cloning of cDNA for Ch-RpS3

Single-stranded cDNA was synthesized from purified mRNA with QIAEXII Gel Extraction Kit (Qiagen) according to the supplier's instructions. To isolate the RpS3 genes which may be involved in ovary development, the synthesized cDNAs of the pollinated ovaries of orchid *C. hybridum* were used as templates in PCR experiments. PCR amplification was performed by touchdown program using Plant RpS3 gene degenerate primer RpS3-S1 (5'- G(G\A)AG(A\C\G)A(A\G)CAA CCATGGCGT-3') and RpS3-A1 primer (5'- ACACCAAATCTTCCTTGTA

TCT -3') which was designed according to CDD470. The conditions for PCR amplification were as follows: 94 °C for 3 min; 16 cycles at 94 °C for 30 s, 0.5 °C/cycle from 65 °C to 58 °C for 45 s and 72 °C for 1 min; Another 20 cycles of PCR amplification were used after touchdown program. The denaturing step was 94 °C for 30 s, the annealing step was 58 °C for 45 s, and the extension step at 72 °C for 1 min; A final extension was at 72 °C for 10 min.

A PCR product about 700 bp long was purified by the QIAEXII Gel Extraction Kit (Qiagen), ligated to the pUCmT-easy vector (BBI) and then transformed into competent cells of *Escherichia coli* DH5 α by heat shock. Positive clones were identified by PCR methods and subsequently sequenced as described below.

According to the sequence that joins together the 700 bp fragment with CDD470 above, the full length cDNA for *Ch-RpS3* was amplified using specific 5' primer RpS3-S2 (5'-GAAGAAGCAACCATGGCCGT-3') and 3' primer RpS3-A2 (5'-GTAAATGCTCATGAACACAATCCAA-3') as described above with 32 cycles of PCR amplification were used, 94 °C for 30 s, 50 °C for 45 s, and 72 °C for 1 min, followed by a final extension at 72 °C for 10 min.

Sequencing and sequence analysis: Clones were sequenced at the Sangon (Shanghai, China) using the PRISM Ready Reaction DyeDeoxy Termination cycle sequencing kit with an ABI-3700 DNA Sequencer (Applied Biosystems, USA).

Pairwise comparisons and multiple alignments of nucleotide sequences and deduced amino acid sequences were performed using the Align program [14] and CLUSTAL W version 1.8 [15], with default cost settings for opening and extending gaps.

116.2.5 Construction of Phylogenetic Trees

The phylogenetic tree was constructed with the neighbor-joining method [16] with the Poisson correction distance [17]. The reliability of the tree was established by conducting 1,000 neighbor-joining bootstrap sampling steps [18].

116.2.6 RT-PCR

Total RNA was isolated from various organs of *C. hybridum*. 2 μ g RNA was reverse-transcribed in a 0.02 cm³ reaction mixture in every reaction using 0.05 μ g M11. PCR amplification reactions were performed in the MG5331 thermal cycler using the programme as described above. β -actin is as a control. The PCR product was analyzed by electrophoresis in 1.5 % agarose gels.

In addition, a reaction without reverse transcriptase was included as a control for each cDNA first-strand synthesis. PCR amplifications of these latter controls gave no amplified fragments indicating that the RNA preparations were free from

contaminating DNA. RT-PCR products were directly sequenced as described below. Primers specific for Ch-RpS3: RpS3-S2 and RpS3-A2. Primers specific for β -actin:

β -s, 5'- GCAGCTCCTCTGTTGAGAAGAAC-3'.

β -a, 5'- TTCTGGGCAACGGAATCTCT -3'.

116.2.7 Reverse Northern Blot Analysis

Reverse northern blot was performed as described by Vögeli et al. [18, 19] and Li et al.[20]. with some modifications. 0.001 cm³ PCR products of positive clones from differential displayed bands were dotted and fixed in duplicate sets onto nylon membranes (Pall, NY, USA). After the total cDNA from the non-pollinated or the pollinated ovaries that had been labeled with digoxigenin (DIG)-11-dUTP by using the Random Primer DNA Labeling System (Roche, Basel, Switzerland), reverse northern hybridization and detection were performed following the instructions of the Roche DIG High Prime DNA Labeling and Detection Starter Kit II. The membranes were then hybridized at 42 °C overnight, high-stringency washed twice in 2 × SSC–0.5 % SDS at 42 °C for 30 min, and washed twice in 0.5 × SSC–0.52 % SDS at 65 °C for 15 min. β -actin was used as positive control and distilled H₂O was used as negative control.

116.3 Results

116.3.1 Isolation of the Full Length cDNA Sequences of Ch-RpS3 from Cymbidium Hybridium

CDD-470 (DQ159867) was determined and compared with those published sequences in the GenBank database by BLAST searches. On the basis of the deduced amino acid sequence, CDD-470 showed homology with sequences encoding components of 40S ribosomal S3 proteins (RPS3) [21]. According to the sequence of CDD-470, two primers

(RpS3-S1 and RpS3-A1) have been designed to amplify a cDNA fragment of about 700 bp using mRNA from the pollinated ovaries of *C. hybridium* as a template. The full-length cDNA sequence for *C. hybridium* RpS3 gene, *Ch-RpS3* (accession No. DQ683575), was isolated and characterized with primers RpS3-S2 and RpS3-A2 according to sequence joining together the 700 bp fragment with the CDD470.

116.3.2 Sequence and Phylogenetic Analysis of Ch-RpS3

Ch-RpS3 is 1,003 bp long with a 786 bp ORF that encodes a putative protein consisting of 261 amino acids. Sequence comparison (Fig. 116.1) of the putative *Ch-RpS3* protein with other published plant RpS3 proteins indicates that *Ch-RpS3* shows extensive similarity to plant RpS3 proteins, with the highest identity (91 %) with monocotyledon *Oryza sativa* (P49397). To determine the evolutionary relationship between *Ch-RpS3* and the RPS3 genes from other species, a phylogenetic tree (Fig. 116.2) based on analysis of RPS3 amino acid sequence of *Ch-RpS3* and its homologous from other ten species was constructed. According to the parameters used, the phylogenetic analysis showed that these ten species with *Ch-RpS3* had been divided into 4 large groups, i.e., animals (*Drosophila melanogaster*, *Rattus norvegicus*, *Homo sapiens*), dicotyledons (*Arabidopsis thaliana*, *Helianthus annuus*, *Solanum tuberosum*, *Medicago truncatula*, *Cicer arietinum*), monocotyledons (*Oryza sativa*, *Cymbidium hybridium*), and yeast (*Schizosaccharomyces pombe*). It was evident that *Ch-RpS3* fell into the clade of plant ribosomal protein S3 genes and it was phylogenetically closely related to the RPS3 of *Oryza sativa* (P49397) which belonged to monocotyledons.

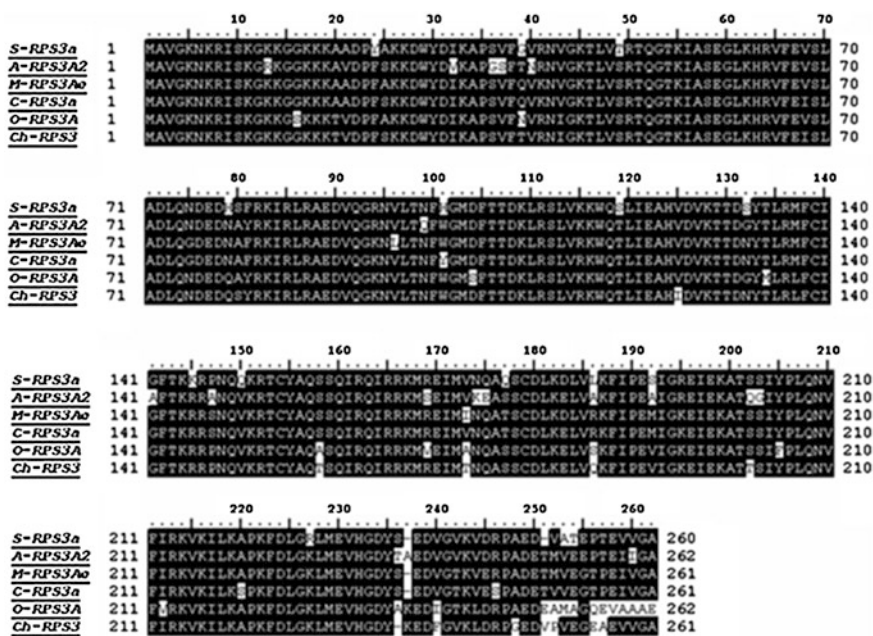


Fig. 116.1 Alignment of the translated *Ch-RpS3*, along with the known RPS3a from other plants, using CLUSTAL W 1.8 [15]. Identical amino acids are highlighted by black boxes. GenBank/EMBL/DDJB Nucleotide Sequence Databases, accession numbers: *A-RpS3A2* (Q42262), *S-RpS3a* (ABB72801), *M-RpS3Ao* (ABE88517), *C-RpS3a* (AJ515028), and *O-RpS3a* (P49397)

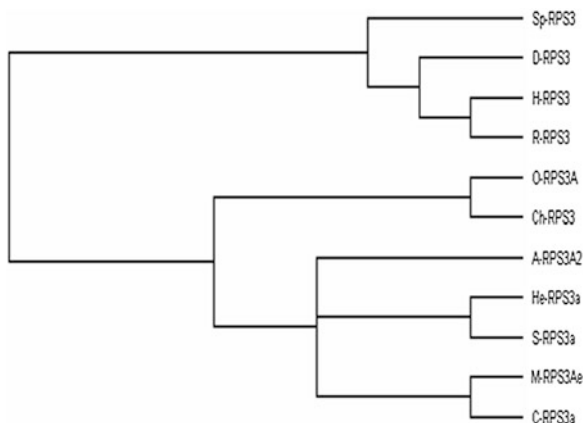
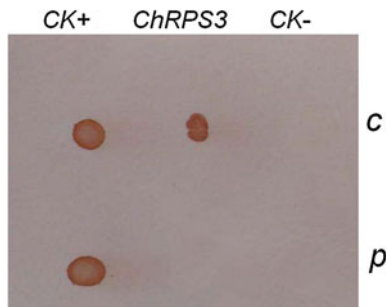


Fig. 116.2 Phylogenetic tree showing the relationship between the Ch-RpS3 and various ribosomal proteins S3 of other species. A-RPS3a from *Arabidopsis thaliana* (GenBank accession No. Q42262); D-RPS3 from *Drosophila melanogaster* (P55830); Sp-RPS3 from *Schizosaccharomyces pombe* (Q09781); H-RPS3 from *Homo sapiens* (AAH04981); R-RPS3 from *Rattus norvegicus* (CAA53004); O-RPS3a from *Oryza sativa* (P49397); He-RPS3a from *Helianthus annuus* (P49198); *Ch-RpS3* from our study (DQ159867); S-RPS3a from *Solanum tuberosum* (ABB72801); M-RPS3Ae from *Medicago truncatula* (ABE88517); C-RPS3a from *Cicer arietinum* (AJ515028)

116.3.3 Reverse Northern Blot Analysis of Ch-RpS3

We probed the PCR fragments against complex cDNA probes made from RNA isolated from the non-pollinated and the pollinated ovaries. As shown in Fig. 116.3, *Ch-RpS3* was successfully confirmed by reverse northern blot to be true differentially expressed cDNA band in the pollinated ovaries.

Fig. 116.3 Reverse Northern blot analysis of isolated differentially expressed cDNA fragments *Ch-RpS3*. CK+: positive control from β -actin; CK-: negative control from distilled H₂O; P: with pollinated ovary cDNA probe; C: with non-pollinated ovary cDNA probe



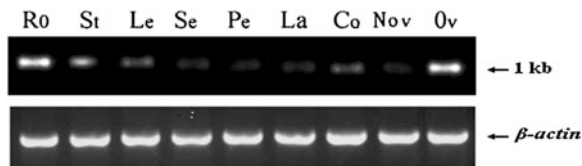


Fig. 116.4 Detection of the *ChRPS3* expression by RT-PCR in different tissues and flower organs. Total RNA was extracted from roots (*Ro*), stems (*St*), leaves (*Le*), sepals (*Se*), petals (*Pe*), labellum (*La*), column (*Co*), and ovary (*ov*). cDNA reverse transcribed from mRNA was, respectively, used as template. β -actin was used to show the amount of cDNA used for each RT-PCR reaction

116.3.4 Expression Pattern of Ch-RpS3

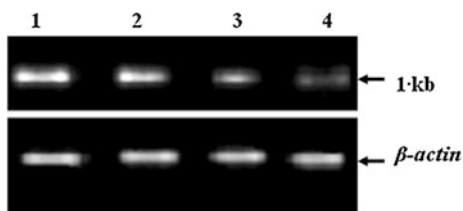
RT-PCR was used to analyze the expression pattern of *Ch-RpS3*. Total RNA was prepared from roots, stems, leaves, ovaries (the non-pollinated and different stages of the pollinated), and the different floral organs of *C. hybridum*.

A single band of the same size as the *Ch-RpS3* cDNA (approximately 1 kb) was detected. As shown in Fig. 116.4, *Ch-RpS3* was highly expressed in roots and the pollinated ovaries, but detected in non-pollinated ovaries, floral organs (the petals, the sepals, the labellum, and the column), and two vegetative tissues (stems and leaves) quite weakly. Toward different stages of pollinated ovaries, *Ch-RpS3* was highly expressed at the 2 days stage, with a subsequent decrease in abundance in 8 and 16 days developmental stages (Fig. 116.5).

116.4 Discussion

The molecular mechanisms involved in floral development are largely unknown and, currently, the interactions between genes related to floral development are poorly understood. Only recently, applications of molecular methods to the study of plant development, genes involved in floral development have begun to be identified [3]. We have carried out DDRT-PCR analysis to isolate a cDNA fragment differentially expressed in the pollinated ovaries of *C. hybridum*, CDD-470. The full length cDNA sequence of *Ch-RpS3* was isolated by RT-PCR. *Ch-RpS3*

Fig. 116.5 RT-PCR analysis of *ChRPS3* in different stages of pollinated ovaries. 1, 2, 3, 4 on the top indicated pollinated ovaries on 2, 4, 8, 16 days, respectively



was composed of a 1,003 bp fragment containing an ORF capable of encoding a protein of 261 amino acids. Sequence analysis showed that it was homologous to the ribosomal protein S3. It is reported that several higher plant RP genes show size diversity in comparison to the prokaryote counterparts, but RPs of homologous proteins from different sources have similar sizes [22]. And the length of the *Ch-RpS3* is similar to that of other homologous RPS3 proteins.

Furthermore, Rps3 genes from plants to mammals not only have highly conserved protein size, but also code similar amino acid sequences [23]. The sequence alignment of *Ch-RpS3* performed with other plant Rps3 s using CLUSTAL W also confirmed this (Fig. 116.1). Of all the similar proteins, the predicted gene product from *C. hybridum* yielded the highest identity with the *Oryza sativa* proteins (91 %) (P49397). The strong homology suggested that *Ch-RpS3* and plant RPS3 gene especially monocot *Oryza sativa* encoded proteins of similar function. The phylogenetic analysis (Fig. 116.2) based on analysis of amino acid sequence of *Ch-RpS3* and its homologous from other ten species also showed *Ch-RpS3* fell into the clade of plant ribosomal protein S3 genes and it was phylogenetically closely related to the RPS3 of *Oryza sativa* (P49397) which belonged to monocotyledons.

The ribosome is a large ribonucleoprotein machine that synthesizes proteins from transcribed mRNA. The 80 s eukaryotic ribosomes contain at least 30 proteins in the small subunit (40 s) and 40 in the large (60 s) subunit [24]. Ribosomal proteins are in general highly conserved in evolution [10]. In addition to their role in ribosomal functions, several ribosomal proteins have also been found to play roles in the translational apparatus and other extraribosomal functions such as regulation of development [25–27]. The fact that mutations in several genes encoding ribosomal proteins in arabidopsis result in morphological alterations and a significant delay in development [28, 29] indicated the important roles of ribosomal proteins in plant development.

Ribosomal protein S3 (RPS3) is no exception. It is one of the ribosomal proteins in the 40S subunit and is located on the surface of the 40S ribosomal subunit. It is a multifunctional ribosomal protein and it is highly conserved between distantly related species [30]. Consistent with its location, several studies indicated that expression of S3a gene and/or its homologues is required for cell growth and proliferation in various evolutionarily distant species. It is known that RPS3 functions as a DNA repair endonuclease and ribosomal protein S3 [31, 32]. Chang [27] reported a third function of RPS3, induction of apoptosis. In synchronously cultured *Catharanthus roseus* cells, the *rps3* (encoding S3a homologue in plants) is preferentially and transiently expressed at the G1/S boundary [33]. LmS3arp, a component of the small ribosomal 40S subunit, was also involved in a number of cellular processes including cell proliferation, differentiation, and apoptosis. In our study, the mRNA for *Ch-RpS3* which was detected and expressed in the pollinated ovaries was confirmed by cDNA reverse northern blot (Fig. 116.3). The genes from plants are expressed in the locations where they ultimately perform their function, so the possibility cannot be excluded that *Ch-RpS3* function in the development of the pollinated ovaries. A possible mechanism by which the ovary development is triggered by enhancing RPS3a expression can be explained, at

least in part, in terms of the role of RPS3a in cell growth and proliferation. However, interestingly, RT-PCR in this study (Fig. 116.4) further showed that *Ch-RpS3* was also highly expressed in roots other than pollinated ovary in *Cymbidium hybridum*. It is reported that some genes also specifically expressed in the roots except in their relative tissues [34, 35]. The function is not identified so far. Since roots are the tissue in which cell division is active, it appeared that there was a strong correlation between RPS3a expression levels and cell division and proliferation. To clarify its molecular mechanism and physiological significance, further research would be required. Furthermore, to detect temporal pattern of expression of *Ch-RpS3* in ovaries at different pollinated stages, we performed cDNA reverse Northern blots (data not shown). It is found *Ch-RpS3* showed relative higher levels at the 2 days stage, with a subsequent decrease in abundance in 8 and 16 days developmental stages, which was also verified by RT-PCR experiments (Fig. 116.5). This is similar to the report that ribosomal protein genes Rps3 had proportionately lower steady-state mRNA levels in later stages of seedling development [36]. Apoptosis could be induced by sequential alterations in RPS3a expression involving enhancement from an initially low constitutive level, followed by suppression [27]. Whether the development of ovary could also be induced by sequential alterations in RPS3a expression needs further study.

So far, little information is available on the functional role of ribosomal protein S3 in plant development especially in monocotyledonous species [37, 38]. In this study, the fact that *Ch-RpS3* isolated from *C. hybridum* was homologous to the ribosomal protein S3 genes and deduced to play a role in the development of ovary provides novel insights into the conservation and diversification of ribosomal protein S3 genes in the floral development of a highly evolved monocotyledonous species. It is tempting to suggest the possible functional diversification between the monocot and the dicot during the evolutionary development of flowering.

Acknowledgments The authors are grateful for the generous support provided by Profs. Chengbin Chen and Ruiyang Chen. The work was supported by the Natural Science Foundation of Tianjin (10JCYBJC09000).

References

1. Coen ES, Meyerowitz EM (1991) The war of the whorls: genetic interaction controlling flower development. *Nature* 353:31–37
2. Weigel D, Meyerowitz EM (1994) The ABCs of floral homeotic genes. *Cell* 78:203–209
3. Moriyah Z, Vivian FI (2003) Flower development: initiation, differentiation, and diversification. *Annu Rev Cell Dev Biol* 19:119–140
4. Yu H, Goh CJ (2000) Identification and characterization of three orchid MADS-Box genes of the AP1/AGL9 subfamily during floral transition. *Plant Physiol* 123:1325–1336
5. Bouman F (1984) The ovule in embryology of angiosperm. In: Johri BM (ed) Springer, Berlin. p 123–157
6. Wang L, Zhang X (1999) Expression and sequence analysis of a cDNA relative to orchid ovule development. *Acta Bot Sinica* 41(3):276–279

7. Zhu GF, Guo ZF (2004) Progress on molecular biology of main ornamental orchidaceae. *Chinese Bull Bot* 21(4):471–477
8. Lu ZX, Wu M, Loh CS, Yeong CY et al (1996) Nucleotide sequence of a flower-specific MADS box cDNA clone from orchid. *Plant Mol Biol* 23:901–904
9. Bui AQ, O'Neill SD (1998) Three 1-aminocyclopropane -1-carboxylate synthase genes regulated by primary and secondary pollination signals in orchid flowers. *Plant Physiol* 116: 419–428
10. Wool IG, Chan YL, Gluck A (1995) Structure and evolution of mammalian ribosomal proteins. *Biochem Cell Biol* 73:933–947
11. Wool IG (1996) Extraribosomal functions of ribosomal proteins. *Trends Biochem Sci* 21:164–165
12. Kim J, Chubatsu LS, Admon A et al (1995) Implication of mammalian ribosomal protein S3 in the processing of DNA damage. *J Biol Chem* 270:13620–13629
13. Naora H, Naora H (1999) Involvement of ribosomal proteins in regulating cell growth and apoptosis: translational modulation or recruitment for extraribosomal activity? *Immunol Cell Biol* 77(3):197–205
14. Myers EW, Miller W (1988) Optimal alignments in linear space. *Comp Appl Biosci* 4:11–17
15. Thompson JD, Gibson TJ, Plewniak F et al (1997) The clustal X windows interface flexible strategies for multiple sequence alignment aided by quality analysis tools. *Nucleic Acids Res* 24:4876–4882
16. Saitou N, Nei M (1987) The neighbor-joining method: a new method for reconstructing phylogenetic trees. *Mol Biol Evol* 4:406–425
17. Nei M, Kumar S (2002) *Molecular evolution and phylogenetics*. Oxford University Press, New York
18. Felsenstein J (1985) Confidence limits on phylogenesis: an approach using the bootstrap. *Evolution* 39:783–791
19. Vögeli LR, Bürckert N, Boller T (1996) Rapid selection and classification of positive clones generated by mRNA differential display. *Nucleic Acids Res* 4:1385–1386
20. Li Z, Chen S (1998) Rapid screening and classification of positive cDNA clones generated by differential display. *High Tech Bull* 8:44–48
21. Chen XQ, Wang CG, Zhang Y et al (2007) Identification and sequence analysis of cDNA fragments relative to ovary development of *Cymbidium hybridum* after pollination. *Biol Plant* 51(2):249–256
22. Chan YL, Olvera J, Paz V et al (1996) The primary structures of rat ribosomal proteins S3a (the V-Fos transformation effector) and of S3b. *Biochem Biophys Res Commun* 228:141–147
23. Fingen-Eigen M, Domdey H, Kohrer K (1996) The ribosomal protein gene RPS3 is an essential single copy gene of the yeast *Saccharomyces cerevisiae*. *Biochem Biophys Res Commun* 223:397–403
24. Moore PB (1998) The three-dimensional structure of the ribosome and its components. *Annu Rev Biomol Struct* 27:35–38
25. Wilson DM, Deutsch WA, Kelley MR (1994) *Drosophila* ribosomal protein S3 contains an activity that cleaves DNA at apurinic/aprimidinic sites. *J Biol Chem* 269:25359–25364
26. Lim Y, Lee SM, Lee JY et al (2002) Complete genomic structure of human rpS3: Identification of functional U15b snoRNA in the fifth intron. *Gene* 286:291–297
27. Chang YJ, Jae YL, Joon K (2004) RPS3, a DNA repair endonuclease and ribosomal protein, is involved in apoptosis. *FEBS Lett* 560:81–85
28. Ito T, Kim GT, Shinozaki K (2000) Disruption of an Arabidopsis S-13 homologous gene by transposon-mediated mutagenesis causes aberrant growth and development. *Plant J* 22:257–264
29. Weijers D, Franke-van Dijk M, Venken RJ et al (2001) An Arabidopsis minute-like phenotype caused by a semi-dominant mutation in a ribosomal protein S5. *Genes Dev* 128:4289–4299
30. Andersson S, Sæbøe-Larssen S, Lambertsson A et al (1994) A *Drosophila* third chromosome Minute locus encodes a ribosomal protein. *Genetics* 137:513–520

31. Yacoub A, Augeri L, Kelley MR et al (1996) A *Drosophila* ribosomal protein contains 8-oxoguanine and abasic site DNA repair activities. *EMBO J* 15:2306–2312
32. Sandigursky M, Yacoub A, Kelley MR et al (1997) The *Drosophila* ribosomal protein S3 contains a DNA deoxyribophosphodiesterase (dRpase) activity. *J Biol Chem* 272:17480–17484
33. Kodama I, Ito M, Hattori T (1991) Isolation of genes that are preferentially expressed at the G1/S boundary during the cell cycle in synchronized cultures of *Chararanthus roseus* cells. *Plant Physiol* 95:406–411
34. Villand P, Aolen R, Olsen OA (1992) PCR amplification and sequences of cDNA clones for the small and large subunits of ADP-glucose pyrophosphorylase from barley tissues. *Plant Mol Biol* 19(3):381–389
35. Zhou DX, Bisanz-Seyer C, Mache R (1995) Molecular cloning of a small DNA binding protein with specificity for a tissue-specific negative element within the rps1 promoter. *Nucleic Acid Res* 23(7):1165–1169
36. Li-Pook-Than J, Carrillo C, Bonen L (2004) Variation in mitochondrial transcript profiles of protein-coding genes during early germination and seedling development in wheat. *Curr Genet* 46:374–380
37. Gao J, Kim SR, Chung YY (1994) Developmental and environmental regulation of two ribosomal protein genes in tobacco. *Plant Mol Biol* 25:761–770
38. Braun HP, Emmermann M, Mentzel H (1994) Primary structure and expression of a gene encoding the cytosolic ribosomal protein S4 from potato. *Biochim Biophys Acta* 1218:435–438

Chapter 117

Lichen Flora on the Genera *Alectoria*, *Pseudephebe*, and *Sulcaria* (Lichenized Ascomycota, Parmeliaceae) from the Hengduan Mountains in China (4)

Xinyu Wang, Dong Liu, Jianwen Li, Hiroshi Harada
and Lisong Wang

Abstract Alectorioid lichen specimens used in this study were collected since 1981, mainly from the Hengduan mountain region, all the specimens were examined using standard microscopic techniques and hand-sectioned under dissecting microscope, secondary metabolites were identified by TLC. After detailed taxonomical and chemical study of our specimens and the type specimens, *Sulcaria virens* var. *forrestii* is found to have same diagnostic characters with *S. virens* except for the diameter of the main branch, thus, it is treated as the synonym of *S. virens*. *Alectoria ochroleuca*, *Pseudephebe pubescens*, and *S. virens* have rather restricted distribution in Hengduan Mountains, they are considered as rare lichens. Taxonomic characters together with distribution map and key to Alectorioid lichens are provided in this paper. All the specimens involved in this study are deposited in Herbarium of Kunming Institute of Botany (KUN).

Keywords Alectorioid · Lichenized fungi · Hengduan mountains · Taxonomy · Species revision

X. Wang · L. Wang (✉)

Key Laboratory of Biodiversity and Biogeography, Kunming Institute of Botany,
Chinese Academy of Sciences, Kunming 650201, China
e-mail: wanglisong@mail.kib.ac.cn

D. Liu · J. Li

Yunnan University of Traditional Chinese Medicine, Kunming 650500, China

H. Harada

Natural History Museum and Institute, Chiba 2608682, Japan

117.1 Introduction

The genera *Alectoria* Ach., *Pseudephebe* M. Choisy and *Sulcaria* Bystr. belong to the family Parmeliaceae (Lecanorales) [1], they are characterized by fruticose or caespitose thallus, mat-shaped, erect, or pendulous, without axils in the medulla, apothecia lecanorine type [2]; mainly distributed in alpine region. Hengduan Mountain is located in the Southwest of Qingzang highland, including east of Xizang, Northeast of Yunnan, and west of Sichuan, including a land of about 500,000 sq. kms, it is the biodiversity hot spot in China. There were very few reports on these genera in Hengduan Mountain region [3–8].

Sulcaria virens var. *forrestii* was published by Hawksworth [9] based on two specimens collected from Yunnan Dali and Deqin, they were collected by G. Forrest in 1912 and 1914, this species variety is published based on the diameter difference of the main branches with *S. virens*. After the examination of the type specimens (Holotypus 13271, Paratypus 20808) and 50 new specimens collected from the original habitat, the authors discovered more varieties of the main branch diameter, it is not a stable character, thus, it should not be treated as a key taxonomic character, detailed discussion, and the results are shown below.

117.2 Materials and Methods

Two hundred and seventy one specimens were collected from 1981 to 2011, including 13 *Bryoria*, 254 *Sulcaria*, and 4 *Pseudephebe*, these collections covered 41 counties from Hengduan Mountain central area, and are deposited in the Herbarium of Kunming Institute of Botany, China (KUN). We also examined the type specimens of *S. virens* var. *forrestii* (Holotypus 13271, Paratypus 20808) from Royal Botanic Garden Edinburgh (E), and *Pseudephebe* specimens from North America and Finland as comparison.

The dried specimens were examined using standard microscopic techniques and hand-sectioned under NIKON 102 dissecting microscope. All measurements were made on material mounted in GAW (glycerol: ethanol: water = 1:1:1); anatomical descriptions are based on observations of these preparations under a NIKON E 200 microscope. Secondary metabolites were identified by TLC as described by Culberson [10].

117.3 Results and Discussion

117.3.1 Key to *Alectorioid* Lichen

1. Thallus surface with longitudinal furrow, holdfast present in the base	<i>Sulcaria</i>
2.. Thallus surface without longitudinal furrow, holdfast absent	2
3.. Ascus containing 1 spore, spores muriform	<i>Oropogon</i>
4.. Ascus containing 2–8 spores	3
5. 2-4 spores per ascus, spores brown when mature	<i>Alectoria</i>
6. 8 spores per ascus, spores hyaline	4
7. Thallus closely attach to the substrate, mat-shaped, without secondary compounds	<i>Pseudephebe</i>
8. Thallus erect or pendulous, medulla P+, K+	<i>Bryoria</i>

117.3.2 The Genus *Alectoria* Ach. in Luyken, *Tent. Hist. Lich.: 95 (1810)*. Brodo and Hawksw., *Opera Bot. 42:56. (1977)*

Type species: *Alectoria sarmentosa* (Ach.) Ach.

Thallus fruticose, erect to pendent, attach to the substrate by a holdfast in the base part; branching variable, dichotomously to irregularly branched, tips pointed; surface grayish white to dull yellow, covered with speckled pseudocyphellae; cortex composed of periclinal, conglutinate hyphae; medulla without axis, medullary hyphae loosely composed, usually ornamented; apothecia lecanorine-type, 2–4 (–8) spores per ascus, ascospores 1-celled, ellipsoid, turning brown or dark brown at maturity; photobiont green algae; containing usnic, diffractaic, and alectronic acid as main compounds.

This genus is characterized by fruticose, grayish white to yellow thallus, having speckled pseudocyphellae, medullary hyphae verrucose, 2–4 spores per ascus, spores 1-celled and brown when mature, containing usnic acid as main compound. It differs from *Sulcaria* by having no longitudinal furrow on the surface, it could be distinguished from *Oropogon* and *Bryoria* by having brown spores and usnic acid.

Eight species were reported worldwide [2], including 2 from China [11].

Alectoria ochroleuca (Hoffm.) Mass., Sched. Crit. Lich. Ital.: 47. 1855. (Fig. 117.1a–c)

≡ *Usnea ochroleuca* Hoffm., Descr. Adunbr. Pl. Lich. 2(1): 7. 1791.

Diagnostic characters: Thallus fruticose, erect to decumbent, 5–15 cm tall, main branches 1–3 mm in diam., branching anisotomic dichotomous or irregular, apices pointed; surface grayish yellow, tips turning brown to black, without soredia or isidia; pseudocyphellae speckled, elongate fusiform, conspicuous,

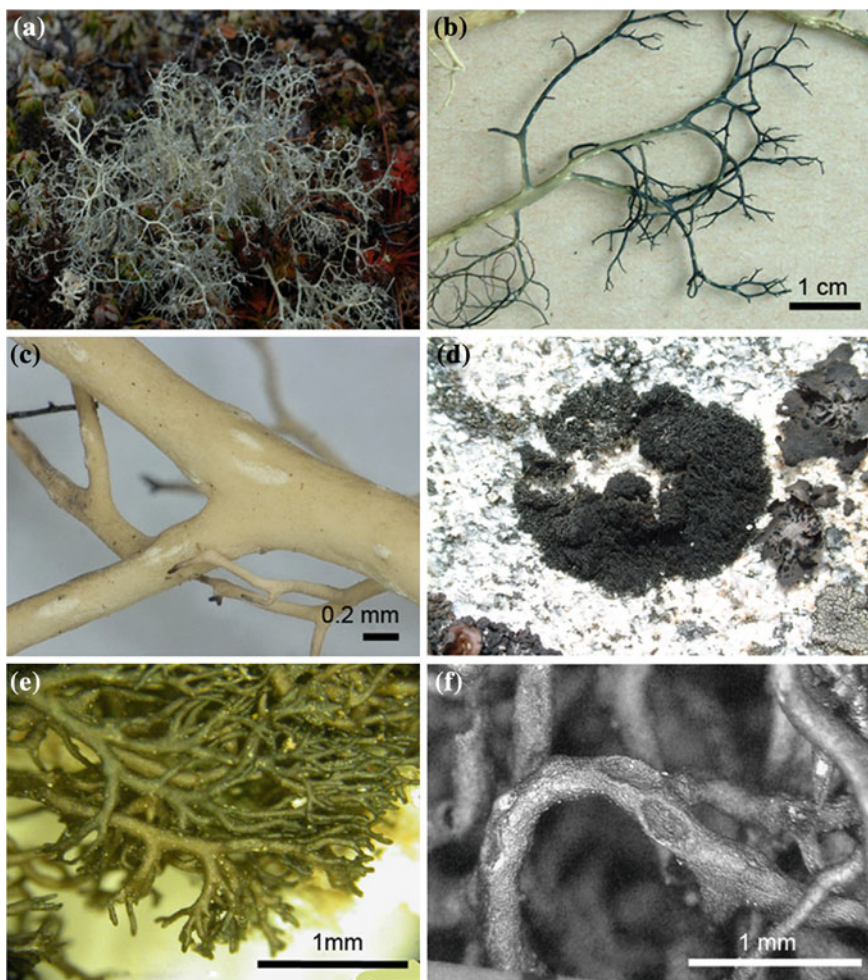


Fig. 117.1 a–c Habit of *Alectoria ochroleuca*. d–f Habit of *Pseudephebe pubescens*

usually more than 1 mm long; medullary hyphae 5 μm in diam., verrucose on the surface; apothecia not seen.

Chemistry: Cortex K–, P–, C–, KC+ yellow, medulla K–, P–, C–, KC+ yellow, CK+ gold yellow. Containing usnic, diffractaic, and alectoronic acid.

Ecology and distribution: Growing on the alpine grassland, rocky area or sometimes on the bark of *Rhododendron impeditum* and *Juniperus indica*, altitude varies from 4,000 to 5,000 m.

It has been reported from Inner Mongolia and Heilongjiang Prov [11], new to Yunnan and Tibet, Worldwide distribution: Nepal, India [12], Japan [6], Korea peninsula [13, 14], North America, Canada, New Zealand, and Europe [2].

Usage: Antibiotics, material for litmus reagent [5].

Remarks: This species is characterized by the dull yellow surface with blackened apices; white and conspicuous pseudocyphellae, medullary hyphae verrucose, and containing usnic acid as the main compound. It is similar with *Sulcaria sulcata*, but the latter species differs in having longitudinal furrow on the surface and without usnic acid.

Specimens examined: Yunnan Prov., Deqin Co., Mt. Baima, 4,000–4,800 m, under *Rhododendron* shrub, *Li S. Wang* 94-15,361, 93-13,500, 81-22,849, 85-8,898, 81-22,850, 85-8,891, 84-41a. Tibet Prov., Demula Co., alt. 5,000 m, *Mu Zang* 9,419; Yadong Co., alt. 4,760 m, on rock, *Mu Zang* 44.

117.3.3 The Genus *Pseudephebe* M. Choisy, Icon. Lich. Univ. ser. 2, fasc. 1: (sine pag.) (1930)

Type species: *Pseudephebe pubescens* (L.) M. Choisy.

Diagnostic characters: Thallus fruticose, mat-shaped, compacted, and closely adnate to the rock, 0.5–1 cm tall; main branches cylindrical to compressed, branching isotomic dichotomous to irregular; surface dark brown to black, without pseudocyphellae, isidia or soredia; cortex 2-layered, outer layer verrucose, inner layer composed of compact longitudinally orientated hyphae; medulla without axis, medullary hyphae smooth; photobiont green algae; apothecia lecanorine-type, 8-spores per ascus, ascospores ellipsoid, hyaline, 1-celled, 7–12 × 6–8 μm; lichen compounds absent.

Arctic and alpine distribution.

The genus is characterized by brown mat-shaped thallus closely attached to the substrate, cortex 2-layered, spores hyaline, and without lichen substrate; It is similar with *Bryoria*, but differs that *Bryoria* erect or pendulous, usually more than 5 cm long, cortex 1-layered, and containing lichen compounds.

2 species are known worldwide [2], 1 is reported from China [15].

Pseudephebe pubescens (L.) M. Choisy, Icon. Lich. Univ., ser. 2, 1:(sine pag.)(1930) (Fig. 117.1d–f)

≡ *Lichen pubescens* L., Sp. Pl. 2: 1155 (1753)

Diagnostic characters: Thallus fruticose, rather slim, mat-shaped and closely attached to the substrate, roundish or irregular, 3–12 cm in diam., dark brown to black, shiny; main branch 0.1–0.2 mm in diam., curved with roundish pit on the surface, but not forming pseudocyphellae or perforation, without spinules, isidia or soredia; apothecia not seen.

Chemistry: All reaction negative, no lichen substances present.

Ecology and distribution: Growing on the surface of alpine rocks between 4,300 to 5,070 m, usually mixed with *Umbilicaria indica*, *Ophioparma ventosa*, *Rhizoplaca chrysoleuca*, and *Rhizocarpon* spp.

It has been reported from Sichuan and Tibet Provinces [15]; worldwide distribution: Europe [16], North America [2, 17], and Japan [6].

Remarks: This species is characterized by mat-shaped thallus closely adnate, dark brown to black, and with no lichen substrates, it is rather similar with *P. minuscula* from North America and Europe, but the latter species differs in having broader main branches (0.2–0.5 mm), apices flattened, with numerous short lateral branches, and thallus surface verrucose.

117.3.4 *The Genus Sulcaria* Bystr. *Ann. Univ. Mariae Curie-Sklodowska, C. 26: 275 (1971); Brodo and Hawksw., Opera Bot. 42: 146 (1977)*

Type species: *Sulcaria sulcata* (Lev.) Bystr. ex Brodo and D. Hawksw.

Thallus fruticose, erect, or pendulous, 5–50 cm long, attached by a holdfast in the base; surface with longitudinal furrow, usually expose the white medulla, without pseudocyphellae; medullary hyphae loose, hyphae surface verrucose, without axis; apothecia lecanorine type; ascus clavate, 8-spored, ascospores ellipsoid, 1-cell and hyaline when young, 2–3(–4) celled and brown at maturity; containing atranorin as main compound.

The genus is characterized by having longitudinal furrow on the surface, brown, and 2–3 celled spores.

4 species are known worldwide, *S. isidiifera* and *S. badia* mainly distribute in North America [2, 18], 2 species and 1 variety are known in China [11].

Key to the speceis of *Sulcaria*

1. Thallus pendulous, 10–30 cm long, surface yellowish green, containing vulpinic acid	<i>S. virens</i>
2. Thallus shrub-like, erect or suberect, 5–15 cm tall	2
3. Thallus grayish white to grayish brown, apices blackened, containing psoromic acid	<i>S. sulcata</i> f. <i>sulcata</i>
4. Thallus yellowish green, containing vulpinic acid	<i>S. sulcata</i> f. <i>vulpinoides</i>

117.3.4.1 *Sulcaria sulcata* f. *Sulcata* (Lev.) Bystr. ex Brodo and D. Hawksw., *Opera Bot. 42:156.1977. (Fig. 117.2a–b)*

≡ *Cornicularia sulcata* Lev., in Jacquin, Fr.-Voy. Inde, Descr. Coll. 4: 179 (1844).

—*Alectoria sulcata* (Lev.) Nyl., Mem. Soc. Imp. Sci. Nat. Cherbourg 5: 98 (1857).

—*Alectoria sulcata* var. *barbata* D. Hawksw., Taxon 19: 242 (1970).

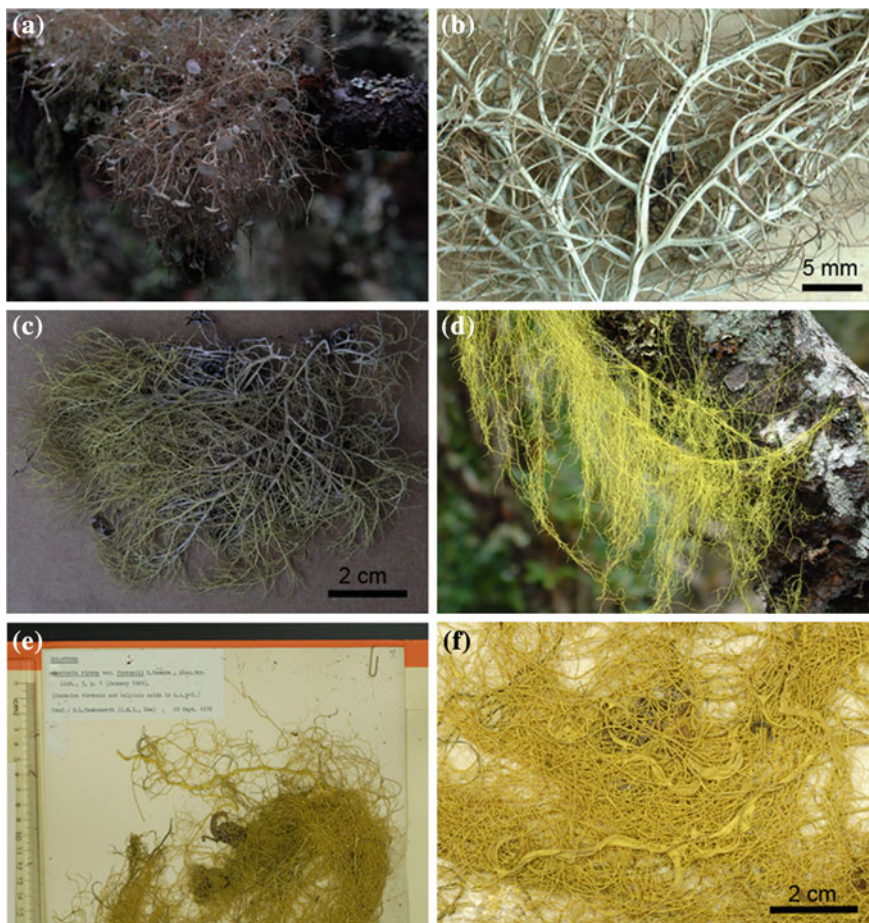


Fig. 117.2 a–b Habitat of *Sulcaria sulcata* f. *Sulcata*; c Habitat of *Sulcaria sulcata* f. *vulpinoides*. d, f Habitat of *Sulcaria virens*; E Holotype of *Sulcaria virens* var. *forrestii*

Diagnostic characters: thallus erect or suberect, 5–15 cm tall, attached to the substrate at the base; main branch cylindrical, partly flattened, c. 3 mm in diam.; branching dichotomous or irregular, angle between branches varies from 30 to 80°, apices pointed; surface of the thallus grayish white to grayish brown, smooth and shiny, apices blackened; longitudinal furrow present, usually exposing the white medulla, without soredia, isidia, or pseudocyphellae; apothecia disc-like, 0.3–1 cm in diam., growing near the apices, margin complete, without spinules or cilia; disc light brown to brown, usually covered with white pruina; medullary hyphae verrucose; apothecia clavate, 8-spored, ascospores ellipsoid, 1-celled and hyaline when young, 2–3-celled and brown at maturity, 25–35 × 10–15 µm.

Chemistry: Cortex K+ yellow, Medulla K–, C–, KC–, P+ deep yellow. Containing atranorin, virensic acid, ethyl hematommate, 2-methoxypsoromic acid, and olivetoric acid.

Ecology and distribution: Usually growing on the bark of *Quercus* spp., *Rhododendron* spp., *Salix* sp. and *Sorbus* sp., rarely on *Pinus densata*, *P. yunnanensis*, *Picea*, *Abies* and *Tsuga*, altitude varies from 1,700 to 3,700 m.

It has been reported from Yunnan, Shanxi, Sichuan, Hubei, Zhejiang, Anhui and Taiwan [11], it is new record for Guizhou and Tibet; Worldwide distribution: India, Bhutan, Nepal [12], Japan [6], Korea peninsula [13, 14].

Usage: It is used as food and medicine by local people in Yunnan.

Remarks: This species is characterized by fruticose thallus and surface grayish white to grayish brown, surface with longitudinal furrow, exposing the white medulla, it could be distinguished by these characters easily.

Specimens examined: Yunnan Prov., Lijiang Co., Jiuhe Village, Laojunshan Mt., 26° 39' N 99° 46' E, alt. 3,500–3,750 m, on *Rhododendron* sp., *Li S. Wang* 00-20,166, 05-24,409, 05-24,403, 05-25,074. Yulong Snow Mt., 27° 04' N 100° 12' E, ganheba, 2,700–3,450 m, on bark of *Pinus densata* and *Quercus* sp., *Li S. Wang* 04-2,777, 04-23,506, 93-13,607, 88-11,052, 85-0208, 85-145a, *Z. A. Sheng* 14, 1,882, *Lix-9*, *J. X. Xi* 0103, 0104, 0113, 0114, *X. J. Li* 80-1,509, *Ahti* 87-46,467, 87-46,257, *M. Zang* 25,109a; Lidiping Village, alt. 3,250 m, *Li S. Wang* 0163, 0175; Yunlong Co., Caojian Village, Ziben Mt., 24° 55' N 98° 45' E, alt. 2,400–3,150 m, on *Salix* sp., *Li S. Wang* 00-18,897, 00-18,822, 00-19514, 05-24,317, 05-24,389, 05-24,376, 05-24,634, *J.X. Xi* 0326, 0337, 0360; Gongshan Co., Bingzhongluo Village, Songta snow mountain, 28° 09' N 98° 33' E, alt., 2,400–2,600 m, *Li S. Wang* 82-733, 82-752a, 82-736, 82-743, 788a, 00-19,229, 00-19,652, 00-19,208, 00-19,601; Binchuan Co., Jizushan Mt., alt. 3,000 m, on decaying bark, *Li S. Wang* 96-15,953; Dali Co., Cangshan Mt., *S.E. Liu* 018004a, 22,090, 22,090a, *Ga By* 20c; Deqin Co., Meili snow mountain, Xiaonong village, alt. 3,100–3,500 m, on *Salix*, *Picea* and *Quercus*, *Li S. Wang* 94-15014, 94-15016, 94-15391, 94-15411; Sichuan Prov., Huili co., Longzhou Mt. alt. 3,000–3,500 m, on *Rhododendron* and *Jasminum*, *Li S. Wang* 97-18,133, 96-17,969, 97-18,133, 96-18,059, 97-17923; Wolong Co., Wolong village, on shrub, *Li S. Wang* 96-17,698; Luding Co., Gongga Mt., 29° 20' N 101° 30' E, alt. 2,450–3,000 m, on *Sorbus* sp., and stump, *Li S. Wang* 96-16186, 96-16,119, 96-16,978; Guizhou Prov., Jiangkou Co., Fanjing Mt., alt. 2,300 m, on *Rhododendron* sp., *Li S. Wang* 88-233; Anhui Prov., Huangshan Mt., *D. A. Lu* 520, 511, 485, 553, 522, 2,618; Zhejiang Prov., Tianmu Mt., *D. A. Lu* 279.

117.3.4.2 *Sulcaria sulcata* f. *vulpinoides* (Zahlbr.) D. Hawksw., Opera Bot. 42:156.1977. (Fig. 117.2c)

≡ *Alectoria sulcata* var. *vulpinoides* Zahlbr., in Handel-Mazzetti, Symb. Bot. Sin. 3: 202 (1930).

Diagnostic characters: This form differs from f. *sulcata* by the bright yellow-green thallus surface, and containing vulpinic and psoromic acid.

Ecology and distribution: Growing on the bark of *Quercus* sp., *Rhododendron* sp., *Salix* sp., or *Pinus densata*, altitude varies from 2,000–3,600 m.

This species is endemic to Hengduan mountain area, it has been reported from Yunnan and Sichuan Provinces.

Specimens examined: Yunnan Prov., Lijiang Co., Wenhai Village, alt. 3,200 m, on bark, *Li S. Wang* 04-2,3474; Heibaishui Village, alt. 2,750 m, *Li S. Wang* 94-14,628, 98-18,176; Laojunshan Mt., 26° 39' N 99° 46' E, alt. 3,500 m, *Li S. Wang* 00-20,142; Hongshan Village, under *Abies* sp., alt. 3,500, *M. Zang* 10,149; Yulong Mt., on *Pinus densata*, alt. 3,200 m, *Li S. Wang* 85-0165, on *Quercus* sp. 85-0107, *S. G. Wu* 128, 4087c; Zhongdian Co., Haba Mt., 27° 20' N 100° 04' E, alt. 2,800–3,600 m, on *Picea* sp., *Li S. Wang* 02-22,167, 02-22,068; Wenshui Village, Daxueshan Mt., 28° 30' N 99° 49' E, alt. 3,400 m, on *Rhododendron* sp. and *Quercus* sp. *Li S. Wang* 00-19,902, 00-20,067; Shigashan Mt., alt. 3,600–3,780 m, *S. Q. Wang* 98-18,421, 96-17,142, *Li S. Wang* 1982; Hongshan Mt., alt. 3,400–3,600, on *Quercus pseudosemicarpifolius*, *Li S. Wang* 81-22b, *M. Zang* 10,552; Tianchi lake, 27° 37' N 99° 33' E, alt. 3,200–3,600, on *Quercus* sp., *Li S. Wang* 04-23,296, on *Rhododendron* sp., *Li S. Wang* 98-18,164, 98-18,455; Baishuitai, 27° 39' N 100° 01' E, alt. 3,350 m, on *Picea* sp., *Li S. Wang* 94-14,686; Napahai Village, 27° 55' N 98° 37' E, alt. 3,350–3,580 m, on *Pinus densata* and *Quercus* sp. *Li S. Wang* 03-22,817, 81-1,972, 81-8, *X.J. Li* 1970; Deqin Co., Meili Mt., Yupeng Village, 28° 24' N 98° 48' E, alt. 3,100–3,500 m, on *Quercus* sp. and *Salix* sp., *Li S. Wang* 94-15,407, 94-15,148, 94-15,016; Kunming, Songming Co.; Sichuan Prov., Muli Co., on bush, alt. 2,000 m, *Li S. Wang* 83-2,436.

117.3.4.3 *Sulcaria virens* (Tayl.) Bystr. ex Brodo and D. Hawksw., Opera Bot. 42:156.1977. (Fig. 117.2d–f)

≡ *Alectoria virens* Tayl., Hook. Lond. J. Bot. 6: 188 (1847).

—*Alectoria virens* v. *forrestii* Hawksw. Misc. Bryol. Lichenol., Nichinan 5: 1 (1969);

—*Sulcaria virens* var. *forrestii* (D. Hawksw.) D. Hawksw., Opera Bot. 42:156 (1977); —*Sulcaria virens* f. *decolorans* (Asah.) Hawksw., in Brodo and Hawksw., Opera Bot. 42:156 (1977);

—Wei Jiang-chuen, in An enumeration of lichens in China (1991).

Diagnostic characters: Thallus pendent, soft, and long, 10–25(–30) long, attached to the substrate by the basal holdfast; main branch cylindrical to flat, 0.5–4 mm in diam.; branching isotomic dichotomous, axil part usually flattened, surface light yellow to lemon yellow, smooth and dull, with longitudinal furrow, usually exposing the white medulla, without soredia, isidia or pseudocypbellae; medullary hyphae loose, partly hollow, surface verrucose; apothecia not seen.

Chemistry: Thallus K–, medulla K–, P+ red, containing vulpinic acid, atranorin and evernic acid.

Ecology and distribution: Usually on the bark of *Rhododendron* and *Quercus*, or on the tree crown and bark of *Pinus yunnanensis*, *P. densata*, *Picea likiangensis* and *Abies* sp., rarely on rock, altitude varies from 1,900–3,900 m.

It has been reported from Yunnan, Sichuan, Tibet and Taiwan [11], endemic in Himalaya region [12, 19, 20].

Usage: This species is first reported in *Shaanxi Chinese Medicine* named as ‘Jinsidai’, later on, it is cited in other books such as *Chinese Medical Dictionary* and son on. Although the description of the species in the book *Shaanxi Chinese Medicine* is same with *Sulcaria virens*, but from the geographical aspect, the species is not supposed to be present in Shaanxi, the species in this book might be actually *Lethariella zahlbruckneri*, more research on the medical use of the species is needed.

Remarks: *Sulcaria virens* is characterized by soft and long pendulous thallus, up to 20–30 cm long, 0.5–4 mm in diameter, surface bright yellow and containing vulpinic acid; *S. sulcata* f. *vulpinoide* differs from this species by the fruticose, erect thallus; Genera with pendulous thallus such as *Bryoria*, *Lethariella* and *Usnea* could be distinguished from this species by the dull thallus color, not bright yellow but brown or gray to yellowish, without longitudinal furrow on the surface, and different secondary compounds.

Specimens examined: Yunnan Prov., Bijiang Co., Gaoligongshan Mt., *Li S. Wang* 5,779; Dali Co., Zhonghesi Temple, alt. 3,620 m, on *Rhododendron* sp.; Dongchuan Co., Luoxue Village, on rock, alt. 4,020 m, *Li S. Wang* 09-30573; Gongshan Co., Dulongjiang Village, alt. 2,600 m, on *Picea* sp., *Li S. Wang* 05-24,307, 99-18,493, 05-25,793; Yeniugu Village, alt. 2,400 m, on bushes, *Li S. Wang* 00-19,556, 00-19,300, 00-19,365; Tengchong Co., Guyong Village, alt. 2,200 m, *Li S. Wang* 83-2,609; Zhongdian Co., Tianbao Mt., alt. 3,580 m, *Li S. Wang* 81-24; Lijiang Co., Lidiping, alt. 3,270 m, *Li S. Wang* 06-26,363,07-28,793,82-15,06-26,363; 82-15, 1,982-10-1; Jiuhe Village, Laojunshan Mt., alt. 3,450 m, on *Abies* sp., *Li S. Wang* 05-25,015, 05-2,5311, 03-22,666, 05-24,408, 02-21,270, 05-24,756, 05-24,306, 99-18,708, 05-2,4631; Sichuan Prov., Dukou Co., Daheishan Mt., alt. 2,450 m, on *Quercus*, *Li S. Wang* 83-22,520.

117.4 Conclusion

Sulcaria virens var. *forrestii* published by Hawksworth was based on two specimens collected from Yunnan Dali and Deqin, this species is characterized by flat main branch, 2.5–4 mm in diam., containing vulpinic acid, while the main branches of *S. virens* is no wider than 1.5 mm. After the examination of the type specimens (Holotypus 1,3271, Paratypus 20,808) and 50 new specimens collected from the original habitat, the authors discovered 41 specimens which has a diameter less than 1.5 mm, 6 of them is between 1.5–2.6 mm, only 4 of them has diameter wider than 2.6 mm. All those specimens share the same morphological, anatomical, and chemical characters, except for the diameter of the main branch, about 12 % of the specimens have a diameter between 1.5–2.6 mm, so the value of

the diameter might not be a good character to distinguish these two varieties, thus, it is suggested that *S. var. forrestii* is treated as synonym of *S. virens*.

And three lichen species: *Alectoria ochroleuca*, *Pseudephebe pubescens*, and *Sulcaria virens* have rather restricted distribution in Hengduan Mountains and they are considered as rare lichens.

Acknowledgments This study was supported by a grant from the National Natural Science Foundation of China (No. 31170023), Foundation of Key Laboratory, CAS (KLBB-201210) and Flora Lichenum Sinicorum (KSCX2-EW-Z-9).

References

1. Tehler A, Wedin M (2008) Systematics of lichenized fungi. In: Nash III (ed) Lichen Biology. Cambridge University Press, Cambridge, p 336–352, doi:[10.1017/CBO9780511790478.018](https://doi.org/10.1017/CBO9780511790478.018)
2. Brodo IM, Hawksworth DL (1930) *Alectoria* and allied genera in North America. Opera Bot 42:1–164
3. Zahlbruckner A (1930) Lichens in Handel-Mazzetti. Symb Sin 3:1
4. Wei JC, Jiang YM (1986) Lichens of Tibet. Scientific press, Beijing, pp 62–65
5. Wu JN, Wang LS (1992) Alectoriaceae and Anziaceae lichens from Yunnan Lijiang region. Acta Bot Yunnanica 14(1):37–44
6. Harada H, Wang LS (2004) Thallial branch connection to create a loop in the filamentous lichen *Sulcaria virens*. Lichenology 3(1):29–30
7. Zhou ZY, Wang LS, Wang F, Liu JK (2007) Chemical compound of *Sulcaria virens*. Acta Bot Yunnanica 29(5):586–590
8. Wang LS, Harada H (2008) Ethnic uses of lichens in Yunnan (2), *Sulcaria sulcata*. Lichenology 7(1):31–34
9. Hawksworth DL (1969) A new variety of *Alectoria virens* Tayl. From Yunnan province, China. Misc Bryol Lichenol 5(1):1–3
10. Culbertson CF (1972) Improved conditions and new data for the identification of lichen products by a standardized thin-layer chromatography method. J Chromatogr 72:113–125. doi:[10.1017/CBO9780511790478.018](https://doi.org/10.1017/CBO9780511790478.018)
11. Wei JC (1991) An Enumeration of Lichens in China. International Academic Publishers, Beijing
12. Singh KP, Sinha GP (2010) Indian Lichens: An Annotated Checklist. Botanical Survey of India Ministry of Environment and Forests: 68
13. Lee YJ (1988) Cryptogam of North Korea 7. Scientific dictionary press, Pyongyang
14. Hur JS, Koh YJ, Harada H (2005) A checklist of Korean lichens. Lichenology 4(2):65–95
15. Wang LS, McCune B (2010) Contributions to the lichen flora of the Hengduan mountains, China 1. Genus *Pseudephebe* (lichenized Ascomycota, Parmeliaceae). Mycotaxon 113:431–437. doi:[10.5248/113.431](https://doi.org/10.5248/113.431)
16. Hawksworth DL (1972) Regional studies in *Alectoria* (Lichenes) II. The British species. Lichenologist 5:181–261. doi:[10.1017/S002428297200026X](https://doi.org/10.1017/S002428297200026X)
17. Thomson JW (1979) American Arctic Lichens, vol 1. The University of Wisconsin Press, Wisconsin
18. Brodo IM (1986) A new species of the lichen genus *Sulcaria* (Ascomycotina, Alectoriaceae) from California. Mycotaxon 27:113–117
19. Awasthi G, Awasthi DD (1985) Lichen genera *Alectoria*, *Bryoria* and *Sulcaria* from India and Nepal. Candollea 40(1):305–320
20. Obermayer W, Elix JA (2002) Notes on chemical races in *Sulcaria sulcata* from southeastern Tibet and adjacent regions. Bibl Lichenol 86:33–46

Chapter 118

Discussion on the New and the Old Country Mark in Detecting the Coliform Bacteria

Lin Huang, Chunxia Wang, Ying Zhang, Fan Mei, Yan Huang,
Jinpeng Wang and Bo Zheng

Abstract For the application of the new country mark in practice detection, the lactose method and the LST method were compared. Lactose method and LST method were used to determine the different consistence bacterium fluid of the coliform bacteria and pollution-free eggs, beverages and tablewares, which had 110 samples in all. The result of two different detection methods had no difference in statistics. Within the MPN 95 % confidence interval, lactose method and LST method were credible and accurate. Compared with lactose method, the unqualified rate of LST method in sample detection was increased by an average of 48.4 %. Although there was no difference between these two kinds of methods in statistics, the unqualified rate of LST method was absolutely higher than lactose method. This result showed that LST method could reduce the rate of false negatives in sample detection.

Keywords Coliform bacteria · Difference · Lactose method · LST method

118.1 Introduction

Recently, some food testing departments, factories and experiment course in colleges are still using the lactose bile salts method in country mark GB/T4789.3-2003 [1] to detect coliform numbers in samples. In 2008, our country health

L. Huang (✉) · C. Wang · F. Mei · Y. Huang · J. Wang · B. Zheng
Key Laboratory of Ministry of Education Industrial Fermentation Microbiology, Tianjin
Key Laboratory of Industrial Microbiology, Tianjin University of Science and Technology,
Tianjin 300457, People's Republic of China
e-mail: huanglin731@tust.edu.cn

Y. Zhang
China National Research Institute of Food and Fermentation Industries, Beijing 100027,
People's Republic of China

department made the new test standard GB/T4789.3-2008 [2], which was similar with coliform detection method of the export food, LST method, but it hasn't been widespread used by most detection departments [3]. And then, China published new detection standard GB4789.3-2010 [4] in 2010. Compared with the edition in 2003, new method has more changes in the part of culture medium, detection method and detection time et al. This paper aims to explore the difference in two detection methods.

118.2 Materials and Methods

118.2.1 Bacteria Sources

Escherichia coli was obtained from type culture collection of Tianjin university of science & technology.

118.2.2 Sample Sources

Pollution-free eggs samples were collected from supermarket and sour milk beverages samples were obtained from one company. Tableware samples were collected from our college dining room in different dining time. Different concentrations of bacteria standard liquid were made of *E. coli*.

118.2.3 Cultural Media

GB/T4789.3-2003: lactose bile broth (incipient medium), eosin-methylene blue agar medium (EMB), lactose broth (recurrence medium);

GB 4789.3-2010: lauryl tryptose broth (LST), brilliant green lactose bile broth (BGLB);

118.2.4 Culture Experiment

A loopful activated *E.coli* was transferred to a 100 mL triangular flask containing 50 mL broth liquid medium, and incubated for 24 h at $(36 \pm 1) ^\circ\text{C}$. Sterile saline solution was used for serial dilution with 1 mL overnight suspension culture. Colony forming unit (CFU) of each dilution was counted by VRBA method in

country mark GB4789.3-2010 [5]. Repeated the experiment procedure above, and then obtained the consistence result of each dilution gradient.

1 mL known concentration bacterium fluid were transferred to 49 mL sterile water, and this liquid were used as sample for later detection. The same sample's CFU results of VRBA method, coliform numbers of lactose method and LST method were recorded. The lactose method's results were unified divided by 100, in order to compare with LST method's results(MPN/mL).

118.2.5 Sample Experiment

Samples, pollution-free eggs, beverages and tablewares were detected coliform by using method in country mark GB/T4789.3-2003 and GB4789.3-2010, then recording the results.

GB/T4789.3-2003: (i) lactose fermentation experiments: samples were diluted and three consecutive dilutions were chosen. Portion liquid of each dilution were transferred to three same tubes respectively, which containing lactose ferment broth. Then incubated the tubes at $(36 \pm 1) ^\circ\text{C}$ for (24 ± 2) h, observing acid and gas production about every tube; (ii) separated culture: transferred suspension of the tube, which had acid and gas production, to eosin methylene blue plate. Incubated the plates at $(36 \pm 1) ^\circ\text{C}$ for $(18-24)$ h, observing the colony morphology and choosing the typical colonies [6]; (iii) verification experiment: picked suspicious colonies on the plate for gram staining, and then observed them under a microscope; at the same time, a loopful of bacterium suspension was transferred to a tube containing lactose broth. Incubated the tubes at $(36 \pm 1) ^\circ\text{C}$ for (24 ± 2) h, results of acid and gas production were recorded. Reported experimental results: according to the positive pipe number in verification experiment, most probable number (MPN) of each sample was calculated, coliform MPN value per 100 mL (g) was recorded.

GB4789.3-2010: (i) incipient experiment: the pH value of samples mix liquid were regulated between 6.5 and 7.5. Samples were diluted and three consecutive dilutions were chosen. Portion liquid of each dilution were transferred to three tubes respectively, which containing LST broth, incubated at $(36 \pm 1) ^\circ\text{C}$ for (48 ± 2) h; (ii) recurrence experiment : bacterium fluid of tubes, which had gas production, were transferred to BGLB tubes, incubated at $(36 \pm 1) ^\circ\text{C}$ for (48 ± 2) h, and then results of gas production about each tube was recorded. Reported experimental results: according to the positive pipe number of verification experiment, MPN of each sample was calculated, and coliform MPN value per 1 mL(g) was recorded. In order to compare with industry standard, the results of samples experiment were unified multiplied by 100 (MPN/100 mL).

118.3 Results and Discussion

118.3.1 *E. coli* Standard Liquid Test Results By Lactose Method and LST Method

Bacteria liquid of *E.coli* were prepared different concentration of 0–100 cfu/mL, 100–1,100 cfu/mL and greater than 1,100 cfu/mL. Totally there were 45 samples, which were detected coliform numbers by VRBA plate method, lactose method and LST method. The 0–100 cfu/mL concentration test results were listed in Table 118.1, 100–1100 cfu/mL results were shown in Table 118.2 and greater than 1100 cfu/mL results were shown in Table 118.3.

Results of 0–100 cfu/mL concentration were analyzed the otherness. The actual number of colonies, detected by VRBA plate method, were found in the MPN 95 % confidence interval of the two detection methods. This phenomenon

Table 118.1 Results of VRBA plate method, lactose method and LST method (0–100 cfu/mL concentration)

Number	VRBA plate method (cfu mL)	Lactose method(MPN mL)	LST method(MPN mL)
1	2	<3	<3
2	3	<3	<3
3	3	4	3
4	5	7	3
5	8	12	9.4
6	6	7	7.4
7	30	24	27
8	22	29	20
9	45	42	43
10	41	42	38
11	33	42	38
12	35	42	38
13	40	53	43
14	100	95	93
15	1	<3	<3
16	3	3	3
17	2	<3	<3
18	4	3	3
19	4	<3	<3
20	16	12	15
21	18	19	15
22	16	20	16
23	93	95	93
24	44	39	43
25	47	36	43

Table 118.2 Results of VRBA plate method, lactose method and LST method (100–1100 cfu/mL concentration)

No.	VRBA plate method (cfu mL)	Lactose method (MPN mL)	LST method(MPN mL)
1	110	93	93
2	145	120	150
3	120	150	120
4	250	240	210
5	200	160	160
6	115	120	93
7	321	290	290
8	477	460	460
9	224	240	240
10	208	160	150

Table 118.3 Results of VRBA plate method, lactose method and LST method (≥ 1100 cfu/mL concentration)

No.	VRBA plate method (cfu mL)	Lactose method (MPN mL)	LST method(MPN mL)
1	Cannot be counted	1100	>1100
2	Cannot be counted	>2400	>1100
3	Cannot be counted	>2400	>1100
4	1200	>2400	>1100
5	Cannot be counted	>2400	>1100
6	Cannot be counted	>2400	>1100
7	Cannot be counted	1100	>1100
8	1132	>2400	>1100
9	Cannot be counted	>2400	>1100
10	Cannot be counted	>2400	>1100

confirmed that *E. coli* bacteria liquid test results of two methods were credible and accurate. According to Table 118.1, the otherness of two detection methods by T inspection method was compared. Established hypothesis as followed, $H_0: \mu\alpha = 0$, mean that lactose method and LST method had no otherness, $H_1 \mu\alpha \neq 0$, level of significance is $\alpha = 0.05$.

Calculated datas as formula (118.1) and (118.2) showed:

$$Sd = \sqrt{\frac{\sum d^2 - (\sum d)^2/n}{n - 1}} \tag{118.1}$$

$$t = \frac{\bar{d}}{Sd/\sqrt{n}} \tag{118.2}$$

$$\sum d = 32.2; \bar{d} = 32.2/25 = 1.29; n = 25; \sum d^2 = 376.92$$

$$Sd = \sqrt{\frac{376.92 - (32.2)^2/25}{24}} = 3.74$$

$$t = \frac{1.288}{3.74 \cdot \sqrt{25}} = 1.72, v = n - 1 = 24$$

$\alpha = 0.05$, $t_{0.05}(24) = 2.064$ was read from T test critical value table. In this case, $t < t_{0.05}(24)$, so $P > 0.05$, mean it isn't refused to H_0 . This result explained lactose method and LST method had no significant difference in statistics, when the bacteria liquid concentration was 0–100 cfu/mL. But it still could not be considered that the value and actual significance of the two methods were just the same.

Results of 100–1100 cfu/mL concentration were analyzed the otherness. As Table 118.2 shown, the actual number of colonies by VRBA plate method also were found in the MPN 95 % confidence interval. Therefore results of two methods also were credible and accurate. The otherness of two detection methods under this concentration (100–1100 cfu/mL concentration) was compared. Established hypothesis as followed, $H_0: \mu x = 0$, $H_1: \mu x \neq 0$, level of significance is $\alpha = 0.05$. Calculations' result was $t = 1.15$. When α was 0.05, $t_{0.05}(9)$ read from table was 2.262. In this situation, $t < t_{0.05}(9)$, so $P > 0.05$, mean it isn't refused to H_0 either. This result explained two detection methods had no significant difference in statistics, when the bacteria liquid concentration was 100–1100 cfu/mL.

According to datas in Table 118.3, when LST method detected bacteria liquid concentration just over 1,100 MPN/mL, lactose method's results always displayed great than or equal to 2,400 MPN/mL. That was far beyond the reality number, however, these results of VRBA plate were still in 95 % confidence interval. But the otherness of two methods could not be calculated accurately.

118.3.2 Sample Test Results of Lactose Method and LST Method

Three kinds of samples, pollution-free eggs, sour milk beverages and tablewares, totally 65 samples in all, were respectively detected coliform numbers by lactose method and LST method, testing whether they exceed corresponding standard of themselves. The test results were shown in Table 118.4 and Table 118.5.

Results of samples were analyzed the otherness. As data were shown in Table 118.4, paired sample T test was used, and established hypothesis as followed, $H_0: \mu x = 0$, $H_1: \mu x \neq 0$, level of significance α was 0.05. Calculations result, t was 0.80. When α was 0.05, $t_{0.05}(29)$ read from T test critical value table was 2.045. In this case, $t < t_{0.05}(29)$, so $P > 0.05$, which mean it isn't refused to H_0 . This result explained lactose method and LST method had no significant difference in statistics, which was also conformed with standard liquid detection

Table 118.4 The detection results of pollution-free eggs detected by lactose method and LST method

Number	Lactose method (MPN 100 mL)	LST method (MPN 100 mL)
1	40	30
2	60	30
3	90	110
4	70	<30
5	90	94
6	90	72
7	110	140
8	90	74
9	120	140
10	<30	<30
11	<30	<30
12	<30	<30
13	<30	<30
14	<30	<30
15	<30	<30
16	60	30
17	40	30
18	70	62
19	60	61
20	90	94
21	90	94
22	90	74
23	30	30
24	<30	<30
25	<30	<30
26	<30	<30
27	<30	<30
28	<30	<30
29	<30	<30
30	30	30

Table 118.5 The unqualified results of coliform detected by lactose method and LST method

Sample used	Number of samples	Lactose method		LST method	
		Number of unqualified	Rate of unqualified (%)	Number of unqualified	Rate of unqualified (%)
Egg	30	2	6.7	3	10
Beverage	10	0	0	0	0
Tableware	25	2	8	3	12
Total	65	4	6.2	6	9.2

results. According to coliform requirements in pollution-free eggs health standard NY5039-2005, coliform numbers in qualified samples are less than or equal to 100 MPN/100 mL. According to this standard, 30 samples of pollution-free eggs in this paper, had different unqualified rates with lactose method and LST method.

The beverages and tablewares detected results were relatively small, hence, they could not be compared by statistics method. However, standard of sour milk beverage health GB16321-2003 and standard of food (drink) disinfection hygiene GB14934-94 are issued standards of qualified coliform numbers in samples. (qualified beverage: ≤ 3 MPN/100 mL, qualified tableware: ≤ 3 MPN/100 cm \times 100 cm). According to these standards, results were shown in Table 118.5, 25 samples of tablewares in this paper, unqualified rate of LST method was absolutely higher than lactose method. Although there was no difference with two methods in statistics, actual samples' qualified rate had significant difference. Compared with lactose method, the unqualified rate of LST method in sample detection was increased by an average of 48.4 %.

118.4 Conclusion

118.4.1 Conclusions

Bacteria liquid with different concentration, 0–100 cfu/mL, 100–1100 cfu/mL and greater than 1,100 cfu/mL, totally 45 samples in all were respectively detected coliform number by VRBA plate method, lactose method and LST method. The results were shown that, within MPN 95 % confidence interval, lactose method and LST method were credible and accurate. Meanwhile, two detection methods were analyzed by statistical analysis, and the results had no significant difference in statistics. Three kinds of samples, pollution-free eggs, beverages, tablewares, totally 65 samples in all, were detected by lactose method and LST method, and the results indicated that the value had no statistical meaning and the unqualified rate of LST method was higher than lactose method, average higher 48.4 %.

118.4.2 Discussion

- (1) The MPN index of LST method and lactose method are different. MPN index are not established on large number of previous test results, they are calculated from the Poisson distribution [7–9]. The intercommunity about two detection methods' MPN index was researched by Tan et al. [10]. Through the series calculations comparison, under three consecutive dilution gradients, two methods' MPN index could be interchangeable used. In this paper, a problem was found, when the positive tube numbers are 1–2–3 or 2–1–3, the corresponding results

couldn't be found in LST method's MPN index, but could be found in lactose's MPN index. MPN index of LST method indeed lack some positive tube numbers' corresponding results. We think that indications lack in LST method's MPN may be consisted in the 95 % confidence interval of adjacent positive tube readings. And if the conclusions as Tan et al. described, when MPN value can't be found in LST method, it can be obtained from lactose method's MPN index.

- (2) Two methods' mediums are different. Tryptone in LST method's medium is superior to peptone and better for the coliform group to absorb nitrogen source. Lauryl sodium sulfate (bacteriostatic agent) in LST method medium has surface activity effect. And this bacteriostatic agent is easier for thalli dispersion. The activity of gram-negative bacteria also cloud be improved by this bacteriostatic agent [11]. Buffer in LST medium was the mixed solution of dipotassium phosphate and monopotassium phosphate, which can keep medium pH relative stability.
- (3) Two methods' steps are different. The pH should be controlled during sample treatment in LST method. Although this step was operated under aseptic condition, it still may be polluted by small amount bacteria. Pollution may also exist during fussy operation process in lactose method, especially during the step of gram stain and picking typical colonies [12–14]. Incipient time of LST method last (48 ± 2) h, that is more than lactose method's incipient time. It was found that extended the time of incipient process was benefit for the damaged cells getting recovery, and reducing the rate of residual. The result in this paper that unqualified rate of LST method was higher than lactose method just coincided with the theory above [15–17].

In general, it was found that lactose method and LST method had no difference in statistics in this research. But the unqualified rates of LST method were obvious higher than lactose method. Those conclusions fit with Zheng and Wang's researches [18–20]. In addition, national health standards of most samples are still using MPN value unit, MPN per 100 mL(g), that is one reason why the new country mark can't be applied in most filed. We hope the related departments will take some appropriate adjustments in future.

References

1. GB/T4789.3-2003 Microbiological examination of food hygiene, coliform group determination
2. Mu YJ (2010) GB/T4789.3-2008 coliform count method. Beer Sci Tech 7:16–18 (in Chinese)
3. Song HH (2007) The comparison of country mark method and industry standard method. Food Saf Guide1:58–60(in Chinese)
4. GB4789.3-2010, The national food safety standards microbiology test coliform group determination
5. Yang LH, Liu L, Wang HJ (2011) Intensified the contrastion between the number of colonies and most probable number in food detection. Heilongjiang Med J 24:588–589 (in Chinese)

6. Qian CR, Huang YX (1997) Microbiology experiment course. Beijing University Press, Haidian, p 196
7. Jin PH (2003) Medical statistics. Fudan University Press, Shanghai, pp 207–209
8. Shen B, Wang YQ, Xu JH (2009) Data evaluation about the TEMPO instrument detection coliform in food using MPN theory. *J Insp Quar* 19:39–40 (in Chinese)
9. Xu BJ (1985) The theory of probability about MPN of coliform. *Environ Prot Tech* 10:1–5 (in Chinese)
10. Tan Z, Wei YX, Luo DP et al (2012) The intercommunity discussion about GB 4789.3-2010 and GB/T4789.3-2003 MPN index. *Guangxi J Light Ind* 4:121–122 (in Chinese)
11. Liu JZ, Huang K, Chen WL (2003) Medium affect the total bacterial count and its improvement. *Food Sci* 24:105–108 (in Chinese)
12. Zhang P, Zhang JQ, He XS (2003) Coliform detection problems in food detection. *Agric Tech* 23:33–34 (in Chinese)
13. Wang XJ, Zhao L, Jiao AY (2000) Problem study in total bacterial count and total coliform group detection. *J Shandong Environ (supplement)*:130 (in Chinese)
14. Lu SB (2003). Development trend of food intestinal bacteria family detection. *China Food Ind* 11:56–57 (in Chinese)
15. Zhang Y, Liu HC, Yin QZ et al (2005) A study on the method of recovering the freeze-injured *Escherichia coli* at—20°. *Chinese J Health Lab Tech* 15:289–292 (in Chinese)
16. Nakagawa H, Hara KY, Kojina T et al (2000) Detection of freeze-injured *Escherichia coli* O157:H7 cells from foods by resuscitation prior to selectice enrichment. *Int J Food Microbiol* 60:107–110
17. Hara KY, Ikedo M, Kodaka H et al (2000) Selective enrichment with a resuscitation step for isolation of freeze-injured *Escherichia coli* O157:H7 from foods. *Appl Environ Microb* 66:2866–2872
18. Zheng ES (2010).The Country Mark GBT4789. 3- 2003 and GBT4789. 3- 2008 examination is intelligent sex research. *Anhui Agric Sci Bull* 16:227, 276 (in Chinese)
19. Wang Q (2011) Research of the otherness in detecting the coliform bacteria from lactose method and LST method. *Food Sci Tech* 36:22–26 (in Chinese)
20. Li Q (2010) Discussing the difference between GB 4789.2-2003 and GB 4789.2-2010, GB 4789.3-2003 and GB 4789.3-2010. *Food Ferment Tech* 46:69–71 (in Chinese)

Chapter 119

Screening Autotetraploid Plantlets of *Glycyrrhiza uralnesis* Fisch by Colchicine-Treated Bud Culture

Xinglin Li, Junting Lu, Xuefei Cao, Na Zhao, Yang Han, Aijia Cao, Jie Ding and Jun Zhao

Abstract To screen effective and useful autopolyploid of *Glycyrrhiza uralnesis* Fisch, the buds were used to dip in the medium with colchicine at different concentrations for different times. The treated buds were transferred to pots with perlite to grow at room temperature. After 2 weeks, the root tips from the cultured seedlings were cut to observe their cell morphology and chromosome counts, and the individual contained four chromosome groups harvested as an autotetraploid. The results indicated that, the colchicine of low concentration might promote the bud's development, whereas high concentration colchicine is harmful for the buds of *Glycyrrhiza uralnesis* Fisch. Moreover, over 30 % autotetraploids might be obtained using 0.15 or 0.20 % of colchicine for 12–36 h, but in comparison with the diploids, the plantlets of many autotetraploids became badly weak at first generation. Therefore, the autotetraploids preliminary obtained will be faced to strictly screen according to agricultural traits and effective component.

Keywords Autotetraploid · Chromosome counts · Chromosome doubling · Colchicine · *Glycyrrhiza uralnesis* Fisch

119.1 Introduction

Polyploidy plants usually grow bigger than those of the diploid plant, thus they can increase the biomass or product yields [1–3]. Research on the induction, identification, and chemical analysis of the polyploidy plantlets of *Salvia miltiorrhiza* was reported by Gao et al. [4], and the selected 61-2-22, an excellent autotetraploid plant, was higher than the control in major chemical compounds and developed

X. Li (✉) · J. Lu · X. Cao · N. Zhao · Y. Han · A. Cao · J. Ding · J. Zhao
Industrial Fermentation Microbiology, Ministry of Education, Tianjin University of Science and Technology, Tianjin 300457, People's Republic of China
e-mail: lxlszf@tust.edu.cn

into a new variety for large-scale production. *Glycyrrhiza uralnesis* Fisch is also a kind of traditional Chinese medicinal plant with many important usages, whose roots have glycyrrhizinic acid, glycyrrhizin, and glycyrrbetinic acid [5–9]. However, owing to low induction ratio of the autotetraploid, for further study, lack of abundant mutants will become one of the biggest problems. In this paper, the aim is to optimize mutant condition to screen more autotetraploid of *G. uralnesis* Fisch by different concentrations of colchicine.

119.2 Materials and Methods

119.2.1 Culture Procedure

Seeds of *G. uralnesis* Fisch were purchased from the medicinal market in Tianjin. In this paper, from seed treatment to bud induction, the culture procedure was performed as described by Gao et al. [4, 10].

119.2.2 Induction of Autopolyploid Seedlings

All buds were inoculated in MS inorganic medium containing different concentrations of colchicine (0.1, 0.15, 0.2, and 0.3 %, w/v) at different times (12, 24, 36, and 48 h). Then the treated buds were transferred to the inorganic medium of MS and cultured at 25 °C. After two weeks, the root tips of the seedlings were used for chromosome determination.

119.2.3 Chromosome Observation

The chromosome observation of the root tips of seedlings was performed as described by Gao et al. [4]. No less than three roots per seedling were tested in all trials except for less than three roots.

119.2.4 Data Analysis

Actual survival ratio (ASR,%) = survival number/(treatment seed number × survival ratio of CK); Mutation ratio (MR,%) = mutation number/survival number.

119.3 Results and Discussion

119.3.1 Effect of Colchicine on Growth of the Seedlings

Colchicine can obviously affect seeds' bourgeon of *G. uralnesis Fisch.* At early stage, the treated seeds by 0.10 % colchicine germinated better than that of other treatments, and 0.3 % of colchicine for a long time would significantly inhibit the bud growth (Fig. 119.1). Thus, in order to harvest more original materials, the concentration of colchicine should be of low levels for a short time [5, 11–13].

119.3.2 Effect of Colchicine on Chromosome Counts and Cell Morphology of Seedling Roots

The roots treated were observed under microscope. Figure 119.2 shows the differences of the cells between normal and over-treated root tips. The cell formation from the latter was mostly changed into rotundity, in which the cells will have difficulty in distinguishing chromosome count and morphology. Optimizing treatment condition of root tip, all tested materials were assayed by individual

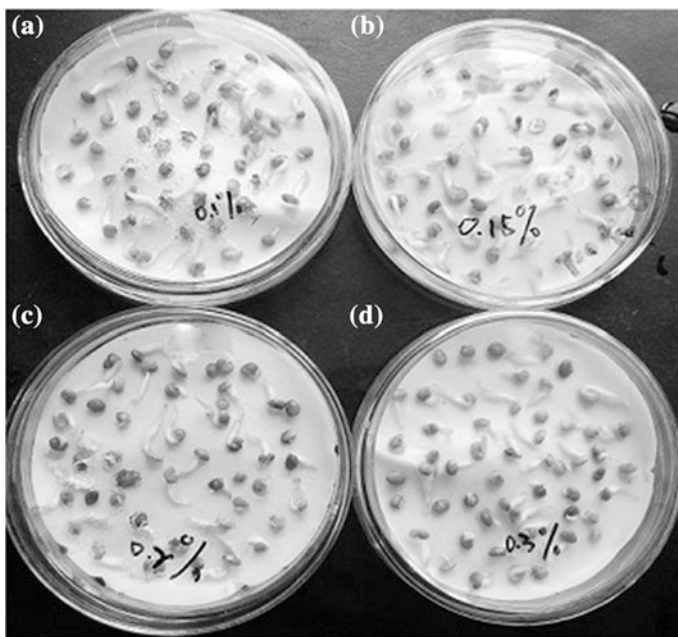


Fig. 119.1 The seeds bourgeon observation at different concentrations of colchicine: **a** 0.10 %; **b** 0.15 %; **c** 0.20 %; **d** 0.30 %

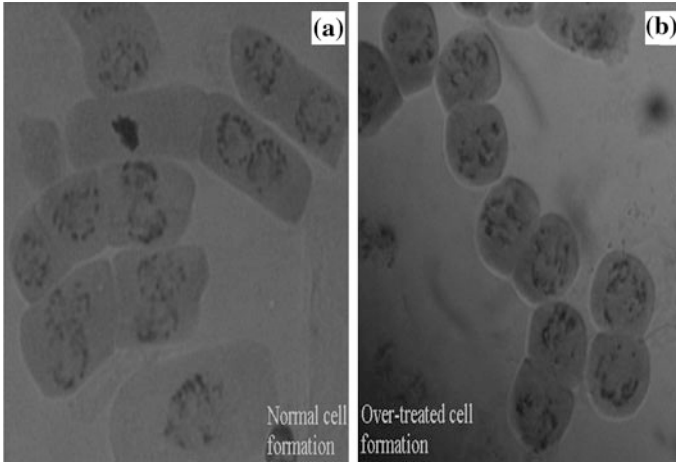


Fig. 119.2 Two kinds of cells treated by dyeing and standing agents: **a** normal cell formation; **b** over-treated cell formation

plant, and the cells divided into many mutants are lined in Fig. 119.3, in which the variation consisted of the chromosome bridge, the sectorial chimera, and the autopolyploid, respectively.

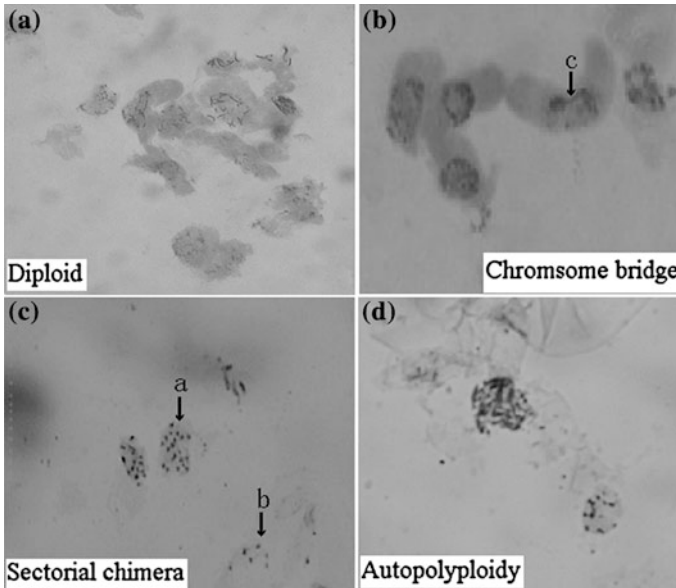


Fig. 119.3 Chromosome counts and morphological observations of the root tip cells from *G. uralensis* Fisch: **a** shows the chromosome of the diploid cells; **b**, **c**, and **d** show the chromosome of the mutant cells

119.3.3 Effect of Colchicine on Survival Ratio and Autopolyloid Ratio of Seedlings

After transferring to medium with perlite for 2 weeks, the number of survival buds, the actual survival ratio, and the mutant ratio of all seedlings were counted and analyzed according to treatment time and concentration of colchicine (Table 119.1). Over 30 % autotetraploids might be obtained using 0.15 or 0.20 % of colchicine for 12–36 h, whereas other treatments were very low at both actual survival ratio and mutant ratio.

Table 119.1 Effect of colchicum on survival ratio and mutant ratio of seedlings

Treatment of colchicum		Number of buds tested	Number of survival buds	Number of mutants	Actual survival ratio (%) ^a	Mutant ratio (%) ^b
Time (hrs)	Concentration (% w/v)					
CK		100	78	0	100	0
12	0.1	100	27	5	34.6	18
	0.15	100	25	6	32.1	24
	0.2	100	16	5	20.5	31
	0.3	100	9	2	11.5	22
	Subtotal/Mean	400	77	18	24.7	23.4
24	0.1	100	24	4	30.8	21
	0.15	100	20	7	25.6	35
	0.2	100	13	3	16.7	23
	0.3	100	5	1	6.4	20
	Subtotal/Mean	400	62	15	19.9	24.2
36	0.1	100	19	4	24.4	21
	0.15	100	10	3	12.8 ^c	30
	0.2	100	7	1	9.0	14
	0.3	100	2	0	2.6	0
	Subtotal/Mean	400	38	8	12.2	21.1
48	0.1	100	10	1	12.8	10
	0.15	100	4	0	5.2	0
	0.2	100	1	0	1.3	0
	0.3	100	0	0	0	0
	Subtotal/Mean	400	15	1	4.8	6.7
Total/Mean not containing CK		1600	192	42	15.4	21.9

^a Actual survival ratio (ASR, %) = survival number/(treatment seed number × survival ratio of CK);

^b Mutation ratio (MR, %) = mutation number/survival number

119.3.4 Morphological Comparison Between the Diploid and the Autopolyploid from *G. uralnesis* Fisch

All well-developed seedlings were classed by chromosome numbers and registered their morphological characteristic. Figure 119.4 and Table 119.2 show the difference between the diploid and the autopolyploid from *G. uralnesis* Fisch. In comparison with diploids, plantlets of many autotetraploids became badly weak at first generation, especially, it was short of fibril roots [4, 10–12]. For further study, obtaining useful and effective autopolyploid of *G. uralnesis* Fisch will need to be screened again in subsequent generations.

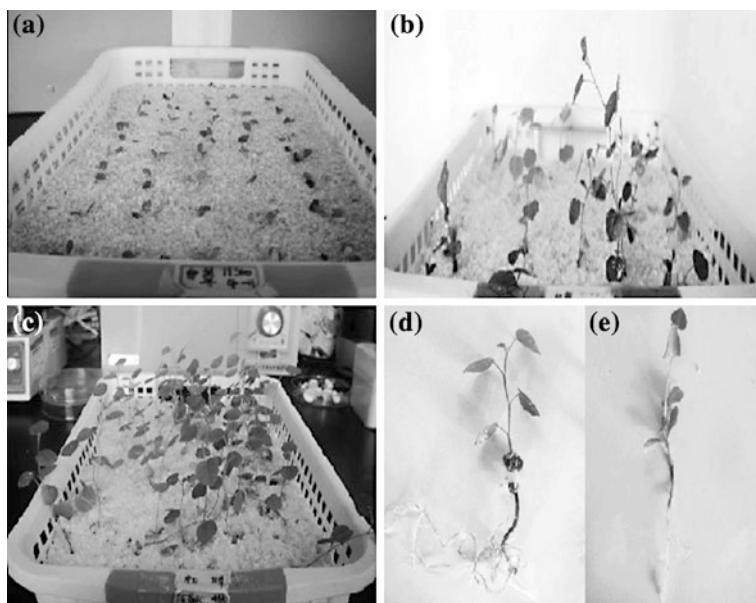


Fig. 119.4 Morphological comparisons between the diploid and autopolyploid from *G. uralnesis* Fisch: **a** and **d** show the diploids; **b**, **c**, and **e** show the autotetraploids

Table 119.2 Biological comparison of the characteristics between diploids and autotetraploids of *G. uralnesis* Fisch

Plantlet types	Seedling height (cm)	Root length (cm)	Leaf color	Distance between leaves	Axilla buds	Stem perimeter	Stem color
Diploids(2×, CK)	>7.0	>9.0	Thin green	Long	Little	Wide	Poppy
Autotetraploids (4×)	3.0–5.0	2.0–3.0	Thick green	Short	Much	Narrow	Red

119.4 Conclusion

Colchicine of low concentration for a short time can promote bud development, whereas high concentration colchicine for a long time is harmful for buds of *G. uralnesis Fisch.* Moreover, over 30 % autotetraploids might be obtained using 0.15 or 0.20 % of colchicine for 12–36 h, but in comparison with diploids, the plantlets of many autotetraploids became badly weak at first generation. Therefore, the autotetraploids preliminary obtained will be faced to strictly screen according to agricultural traits and effective component.

Acknowledgments The work was supported by “National Training Project of College Students’ Innovative and Pioneering Work in Tianjin” and “Natural Science Funds of Tianjin University of Science and Technology (20100209).”

References

1. Itokawa H, Morris-Natschke S, Akiyama T, Lee K (2008) Plant-derived natural product research aimed at new drug discovery. *J Nat Med* 62:263–280
2. Jian WW, Jian YW (2010) Tanshinone biosynthesis in *Salvia miltiorrhiza* and production in plant tissue cultures. *Appl Microbiol Biotechnol* 88:437–449
3. Yan Y, Wang Z (2007) Genetic transformation of the medicinal plant *Salvia miltiorrhiza* by *Agrobacterium tumefaciens*-mediated method. *Plant Cell Tissue Organ Cult* 88:175–184
4. Gao S, Zhu D, Cai Z, Xu D (1996) Autotetraploid plants from colchicine-treated bud culture of *Salvia miltiorrhiza Bge.* *Plant Cell Tissue Organ Cult* 47:73–77
5. Chandler RF (1985) Liquorice, more than just a flavour. *Can Pharm J* 118:420–424
6. Badam L, Amagaya S, Pollard B (1997) In vitro activity of licorice and glycyrrhetic acid on Japanese encephalitis virus. *J Commun Dis* 29:91–99
7. Fuji H, Tian J, Luka C (1986) Effect of glycyrrhetic acid on influenza virus and pathogenic bacteria. *Bull Chin Mater Med* 11:238–241
8. Guo N, Takechi M, Uno C (1991) Protective effect of glycyrrhizine in mice with systemic *Candida albicans* infection and its mechanism. *Acta Academiae Medicinae Sinicae* 12:380–383
9. Salari M, Sohrabi N, Kakhoda Z, Khalili M (2003) Antibacterial effects of enoxolone on periodontopathogenic and capnophilic bacteria isolated from specimens of periodontitis patients. *Iran Biomed J* 7:39–42
10. Gao S, Chen B, Zhu D (2002) In vitro production and identification of autotetraploids of *Scutellaria baicalensis*. *Plant Cell Tissue Organ Cult* 70:289–293
11. Dhooghe E, Laere K, Eeckhaut T, Leus L, Huylenbroeck J (2011) Mitotic chromosome doubling of plant tissues in vitro. *Plant Cell Tissue Organ Cult* 104:359–373
12. Huang H, Gao S, Chen L, Jiao X (2008) In vitro induction and identification of autotetraploids of *Dioscorea zingiberensis*. *Vitro Cell Dev Biol-Plant* 44:448–455
13. Kim Y, Hahn E, Murthy H, Paek K (2004) Effect of polyploidy Induction on biomass and ginsenoside accumulations in adventitious roots of ginseng. *J Plant Biol* 47:356–360

Chapter 120

Screening of Antimicrobial Marine Microorganisms and Purifying of Its Bioactive Substances

Zhiwen Liu, Qiankun Ruan, Sirigulen Qian and Lina Cong

Abstract A bacterium HS-A38 with antimicrobial activities was isolated from the intestine of wild sea cucumbers in Dalian sea area. Based on the analysis of morphological, physiological, and 16S rDNA sequence, the strain HS-A38 was identified as *Bacillus subtilis*. Two bioactive substances (1 and 2) were purified from the fermented broth of the *Bacillus subtilis* HS-A38 using the methods of fractional sedimentation with ammonium sulfate, CM-52 ion-exchange chromatography and Sephadex G-75 column. The SDS-PAGE analysis indicated that the relative molecular weight of these bioactive substances were 41 kDa and 28 kDa, respectively. The antibacterial spectra showed that substance 1 could only inhibit Gram-positive bacteria, whereas substance 2 could significantly inhibit both the Gram-positive and negative bacteria.

Keywords Antibacterial activities · Antimicrobial marine microorganisms · Bioactive substance · Purification

120.1 Introduction

Bioactive substances are believed to play a key role in microbial interactions by mediating antagonistic activity and intercellular communication [1]. In addition, many microbial natural products have biotechnological potential as antibiotics,

Zhiwen Liu and Qiankun Ruan contributed equally to this work.

Z. Liu · Q. Ruan · S. Qian · L. Cong (✉)
College of Bio & Food Technology, Dalian Polytechnic University, Dalian 116034,
Liaoning, People's Republic of China
e-mail: conglu@dlpu.edu.cn

biosurfactants, antifungal, or anticancer agents [2]. Sequences of microbial genomes revealed that only a small fraction of the natural product diversity is known, which highlighted the potential for finding novel bioactive compounds in environmental microorganisms [3]. The need for novel antimicrobials to combat increasing antibiotic resistances in pathogenic bacteria has stimulated the exploration of other than the traditional sources, such as terrestrial actinomycetes or fungi [4].

The marine environment harbors bacteria with antagonistic traits [5, 6], and marine microorganisms are a potential source of novel antimicrobials [7]. Antagonistic marine bacteria have been isolated from surface and deep waters [8, 9], but the majority originated from biotic surfaces such as sponges [10], zooplankton and macroalgae [11], corals [12], and bryozoans [13]. Bioactive bacterial strains predominantly belong to *Pseudoalteromonas* spp [14], the *Roseobacter* clade [15], and *Actinobacteria* [16]. A number of marine derived antimicrobials have been characterized in greater detail, including halogenated and sulfuric compounds [17, 18], depsipeptides and lipopeptides [19, 20], glycolipids [21], as well as high molecular weight structures such as amino acid oxidases [22].

An emerging source of new bioactivity may result from the many recent studies of microbial diversity in the marine environment, particularly those microbes associated with marine plants and animals [23,24]. Several studies have demonstrated that “living surfaces” represent an environment rich in epibiotic microorganisms that produce bioactivity [25,26]. Nevertheless, the vast biotechnological potential of marine epibiotic microorganisms remains mostly unexplored. This study mainly explores new sources with potential bioactivity from marine microorganism host and isolates the bioactive substance producing by microorganisms.

120.2 Materials and Methods

120.2.1 Isolation of Bacterial Strains from Sea Cucumber Intestin

Fresh sea cucumber intestine was grinded, shook, and mixed fully under the sterile environment. The supernatant of the samples were progressively diluted with sterilized ddH₂O by gradient diluents of 10⁻¹, 10⁻², 10⁻³, 10⁻⁴, and 10⁻⁵. Each 0.2 ml of them was spread onto marine agar 2216 media, incubated at 25 °C for 2 days, and then selected the single cell colony based on the differences of the sample and the morphological of the strains.

120.2.2 Screening of Strains with Antibacterial Activity

Screening of strains with antibacterial activity was conducted by the method of agar well diffusion. All isolated strains were respectively inoculated in 5 mL LB liquid medium and cultured on a rotary shaker (150 rpm) at 28 °C for 2 days. The fermented broth was spun down at 8,000 g for 10 min, whereas the supernatant was passed through a 0.45 µm Millipore filter. The indicator strains in this test are *Micrococcus lysodeikticus*, *Staphylococcus aureus*, *Vibrio parahaemolyticus*, and *Pseudomonas aeruginosa*. Wells of 5 mm diameter were punched in Brain Heart Infusion agar plates seeded with indicator organisms. The fermented broth (200 µl) was added in the wells. Plates were then incubated at 30 °C for 48 h. Where upon inhibitory activity was detected as a zone of clearing in the turbid agar around the wells containing antibacterial activity (positive samples). The diameter of the clearing zones was measured in (mm) to obtain a semi-quantitative determination of the concentration of the antibacterial compound.

120.2.3 Identification of the Selected Strain

The marine selected bacteria strain with higher antibacterial activity than others was selected and identified by chemotaxonomic, morphological characters, and its 16S rDNA gene sequence. The sequence was initially analyzed on the NCBI (<http://www.ncbi.nlm.nih.gov/>) using the BLAST tool and corresponding sequences were retrieved. A similarity matrix was prepared using Dnadist program in PHYLIP analysis package using Jukes-Cantor corrections. The phylogenetic tree was constructed by the neighbor-joining method using the MEGA software package.

120.2.4 Preparation of Bioactive Substance Suspension

The strain was incubated in 2216E broth for 16 h at 28 °C and 150 rpm. Then 2 % of the seed culture was inoculated to fermentation media containing soluble starch 1.25 %, beef extract 2.5 %, steep water 1 %, Tween-80 0.01 %, and cultured on a rotary shaker (150 rpm) at 28 °C for 48 h. The cultured bacteria were centrifuged at 8,000 rpm for 10 min and the supernatants were reserved.

120.2.5 Preliminary Authentication of the Bioactive Substances

In order to identify the composition of bioactive substance, 500 µl fermentation supernatants mixed with 20 µl Protease k and kept at temperature 50 °C for 1 h,

whereas the supernatants without Protease k were used as a control. The antibiotic activity of the two supernatant samples was tested by the method of ager well diffusion.

120.2.6 Ammonium Sulfate Precipitation

Crude proteins were precipitated by adding ammonium sulfate to the final concentration of 60 % (w/v), and proteins were harvested by centrifugation (12,000 rpm for 30 min at 4 °C). The pellet was dissolved in sterilized water and dialyzed to desalt crude protein using dialysis membrane (MWCO: 12–14,000). Antimicrobial active of the crude proteins were assayed by the methods of ager well diffusion.

120.2.7 Ion-Exchange Chromatography and Gel Filtration

The clear supernatant was subjected to purify by CM-52 ion-exchange chromatography pre-equilibrated with 20 mM PBS (pH 5.0). The proteins were fractionated with a 0.1–0.6 M step gradient of NaCl in 20 mM PBS buffer and flow rate of 1 ml/min. Eluted fractions were collected and measured. Eluted fractions (2 mL) were collected and the OD280 was measured for every fraction. All fractions were used in the bioassay to check the antimicrobial activity, and then the fractions with bioactivity were dried with a vacuum concentrator and weighed.

The above dried samples were diluted and the fractions were subjected to purify by Sephadex G-75 column pre-equilibrated with 10 mM PBS (pH 7.0). The column was eluted with 10 mM PBS at a flow rate of 0.6 ml/min. Eluted fractions (2 ml) were collected and the OD280 was measured for every fraction. All the fractions were used in the bioassay to check the antimicrobial activity and the fractions were dried and weighed.

120.2.8 Protein Assay and Analysis of SDS-PAGE

The protein concentration was measured by the methods of Bradford using bovine serum albumin. 15 % SDS–polyacrylamide gel electrophoresis (SDS-PAGE) was performed to detect the purified bioactive substances.

120.3 Results

120.3.1 Screening of Antimicrobial Marine Microorganisms

200 marine bacteria strains were isolated and tested for their antimicrobial activities against *M. lysodeikticus*, *S. aureus*, *V. parahemolyticus*, and *P. aeruginosa*. The results showed that 13 strains (accounting for 6.5 %) possessed antimicrobial activities. As shown in Table 120.1, the strain HS-A38 exhibited the strongest inhibitory effects against the four indicator strains. The inhibition zone of the strain reached 24.6, 32.4, 36.0, 18.0 mm, respectively.

120.3.2 Identification of the Strain HS-A38

The strain HS-A38 was identified through morphological and molecular tools. It was strictly aerobic, motile, Gram-positive, spore forming, and rod-shaped (Fig. 120.1). Its 16S rDNA gene sequence with 1,648 bp showed 100 % similarity with *Bacillus* sp (AB195282). The 16S rDNA sequence was submitted to GenBank under the accession number GQ 466597. The NJ-based phylogenetic tree showed that it stood with *Bacillus* sp clade (Fig. 120.2). Hence, the strain HS-A38 selected in the present study was identified as *Bacillus* sp.

Table 120.1 Strains with strongest antibacterial activities

Strain no	Inhibition zone (mm)			
	ML	SA	VP	PA
A9-4	22.6	26.6	26.8	–
A8-5	26.6	30.0	29.7	15.0
A1-15	23.0	22.0	28.1	–
A8-3	25.4	30.4	17.8	–
A8-20	25.4	28.0	18.0	–
A8-4	23.4	32.0	18.0	–
C6-7	23.2	26.0	27.0	–
C8-11	24.0	27.0	27.0	–
C7-17	21.5	26.7	26.2	–
C7-21a	22.0	24.7	28.5	–
C7-21b	20.0	25.3	31.2	–
C7-18	21.5	27.0	27.7	–
HS-A38	24.6	32.4	36.0	18.0

ML *Micrococcus lysodeikticus*, SA *Staphylococcus aureus*, VP *Vibrio parahemolyticus*, PA *Pseudomonas aeruginosa*

Fig. 120.1 Morphology of the strain HS-A38 ($\times 1,000$)

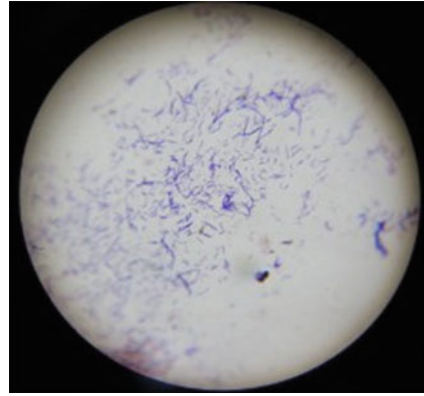
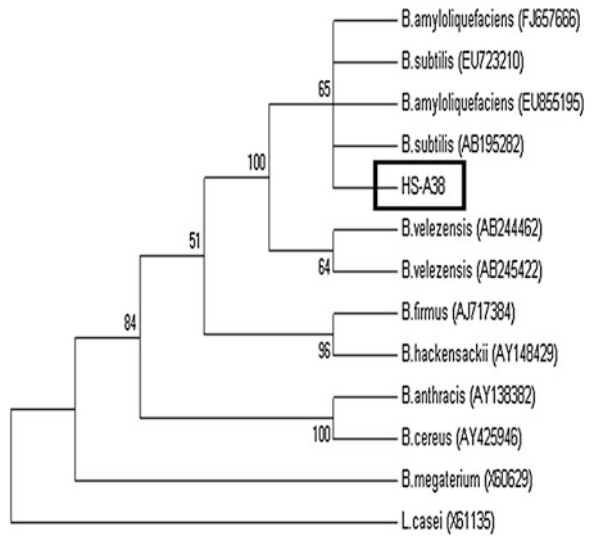


Fig. 120.2 Phylogenetic tree of HS-A38 based on the 16S rDNA sequence



120.3.3 Preliminary Authentication of Bioactive Substances

Compared with the no Protease k, the bacteria inhibition zone of the supernatant with Protease k significantly diminished (Fig. 120.3). The results demonstrated that the composition of the bioactive substances should contain proteins.

Fig. 120.3 Antibacterial result of the extracted liquid processed by Protease k



120.3.4 Purification of Bioactive Substances

The crude extracts from the supernatant of HS-A38 was precipitated by 60 % ammonium sulfate solution and dialysed. The dialysate was supplied to CM-52 ion-exchange chromatography for purification (Fig. 120.4a). The fractions possessing antimicrobial activities were collected and rechromatographed on the Sephadex G-75 column, and it showed that two peaks of bioactive substances (Fig. 120.4b).

Each of the fractions was designated as substances 1 and 2, respectively. They were collected and independently estimated its purity by SDS-PAGE. The results showed that both of substances 1 and 2 exhibited a single band with the molecular weight of 41 kDa and 28 kDa, respectively (Fig. 120.5).

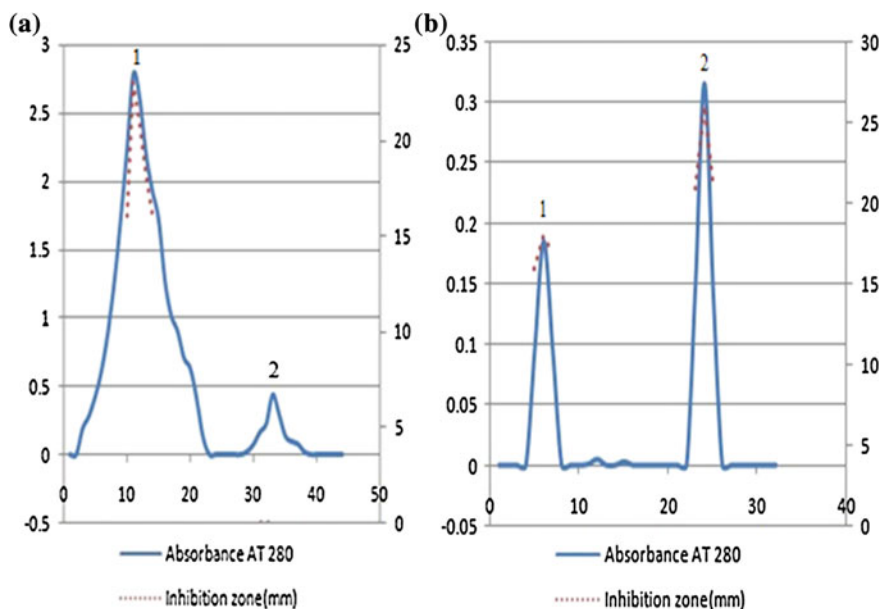
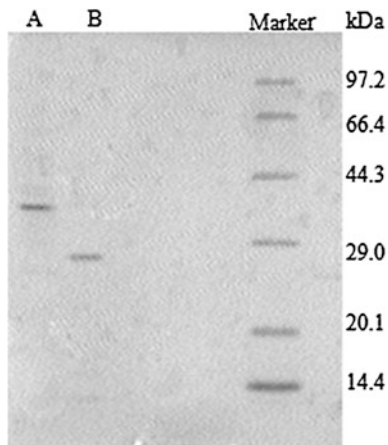


Fig. 120.4 CM-52 anion-exchange chromatography (a) and the chromatography of Sephadex G-75 (b)

Fig. 120.5 SDS-PAGE assay of purified protein after chromatography of Sephadex G-75. **a** substance 1, **b** substance 2



120.3.5 Antimicrobial Activities Assay

The antimicrobial activities of substances 1 and 2 were tested with four indicator strains (Fig. 120.6). The results showed that substance 1 exhibited inhibitory effects against Gram-positive strains and substance 2 against both Gram-positive and -negative bacteria (Table 120.2).

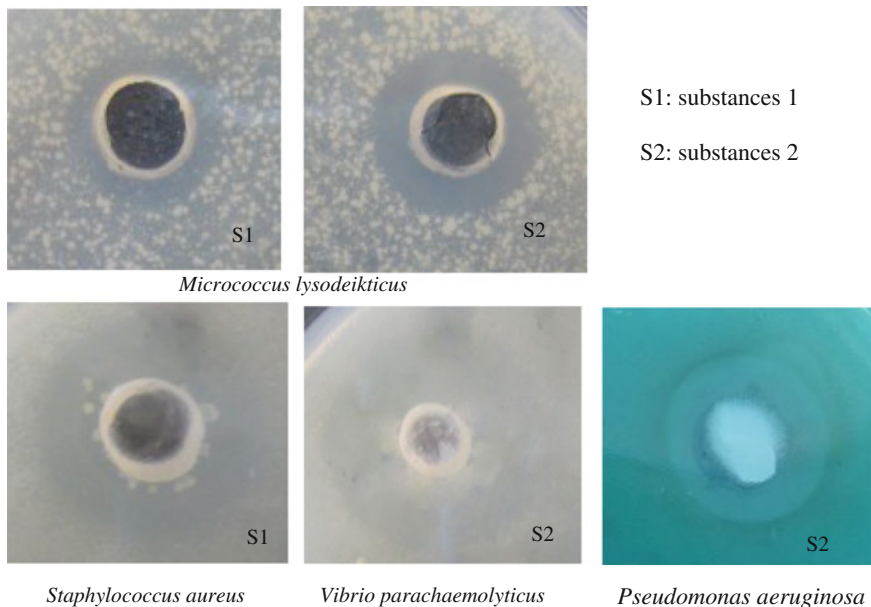


Fig. 120.6 Antibacterial results of bioactive substances 1 and 2

Table 120.2 Antibacterial spectrum of bioactive substances

Substance no	Inhibition zone (mm)			
	ML	SA	VP	PA
1	14.0	17.2		–
2	23.1		33.1	17.0

ML *Micrococcus lysodeikticus*; SA *Staphylococcus aureus*; VP *Vibrio parahemolyticus*; PA *Pseudomonas aeruginosa*

120.4 Discussion

The widespread occurrence of antibiotic-resistant human pathogens and the paucity of effective antifungal drugs have created an urgent need for new antimicrobial agents. Marine microorganisms have proved to be rich sources of bioactive substances, and numerous with potent biological activities and unique chemical structures were isolated. The large numbers, and diversity, of marine microorganisms such as bacteria, fungi, and cyanobacteria suggest that this resource will be of significant importance in the discovery of new antimicrobial agents and other drugs, and are expected to compete with terrestrial microorganisms in this aspect in the near future. In addition, compared with other marine organisms, marine microorganisms own their superiority that is easy to realize industrialization by fermentation, we can optimistically predict unique metabolites will be mass-produced by cultivation of genetically modified microbes. It is no doubt that study of marine microorganisms will have a vast range of prospects.

In this project, we report the screen of antimicrobial marine microorganisms and purification of its bioactive substances. The strain HS-A38 with obvious antimicrobial activity was isolated from sea cucumber intestine. It was identified by chemotaxonomic and morphological characters and its 16S rDNA sequence. The results showed that it belongs to *Bacillus* sp. Two bioactive substances were purified from the selected strain with the methods of ammonium sulfate sedimentation, CM-52 ion-exchange chromatography, and Sephadex G-75 column. The molecular mass of purified bioactive substances detected on SDS-PAGE was 41 kDa and 28 kDa, respectively. Substance 1 exhibited antibacterial activities against *M. lysodeikticus* and *S. aureus*, whereas substance 2 mainly focused on the killing *V. parahemolyticus*, *M. lysodeikticus*, and *S. aureus*. The N-terminal amino acid sequence will be analyzed for further study. We are planning to conduct future studies in analyzing the gene responsible for bioactive substance 2 and to overexpress it in a suitable recombinant expression system [27].

Acknowledgments This research was supported by the Natural Science Foundation of China (Grant no. 31072224), Natural Science Foundation of Liaoning Province of China (Grant no. 20102009), and Foundation of Liaoning Educational Committee for Innovation Team (Grant no. LT2010012).

References

1. Hibbing ME, Fuqua C, Parsek MR et al (2010) Bacterial competition: surviving and thriving in the microbial jungle. *Nat Rev Microbiol* 8:15–25
2. Demain AL, Sanchez S (2009) Microbial drug discovery: 80 years of progress. *J Antibiot* 62:5–16
3. Fischbach MA (2009) Antibiotics from microbes: converging to kill. *Curr Opin Microbiol* 12:520–527
4. Berdy J (2005) Bioactive microbial metabolites. *J Antibiot* 58:1–26
5. Nair S, Simidu U (1987) Distribution and significance of heterotrophic marine bacteria with antibacterial activity. *Appl Environ Microbiol* 53:2957–2962
6. Long E, Azam F (2001) Antagonistic interactions among marine pelagic bacteria. *Appl Environ Microbiol* 67:4975–4983
7. Zhang LX, An R, Wang JP et al (2005) Exploring novel bioactive compounds from marine microbes. *Curr Opin Microbiol* 8:276–281
8. Gram L, Melchiorson J, Bruhn JB (2010) Antibacterial activity of marine culturable bacteria collected from a global sampling of ocean surface waters and surface swabs of marine organisms. *Mar Biotechnol* 12:439–451
9. Hohmann C, Schneider K, Bruntner C et al (2009) Caboxamycin, a new antibiotic of the benzoxazole family produced by the deep-sea strain streptomyces sp NTK 937. *J Antibiot* 62:99–104
10. Taylor MW, Radax R, Steger D et al (2007) Sponge-associated microorganisms: evolution, ecology, and biotechnological potential. *Microbiol Mol Biol Rev* 71:295–347
11. Wiese J, Thiel V, Nagel K et al (2009) Diversity of antibiotic-active bacteria associated with the brown alga laminaria saccharina from the baltic sea. *Mar Biotechnol* 11:287–300
12. Rypien KL, Ward JR, Azam F (2010) Antagonistic interactions among coral-associated bacteria. *Environ Microbiol* 12:28–39
13. Herndl H, Wiese J, Thiel V et al (2010) Phylogenetic diversity and antimicrobial activities of bryozoan-associated bacteria isolated from mediterranean and baltic sea habitats. *Syst Appl Microbiol* 33:94–104
14. Bowman JP (2007) Bioactive compound synthetic capacity and ecological significance of marine bacterial genus pseudoalteromonas. *Mar Drugs* 5:220–241
15. Martens T, Gram L, Grossart HP et al (2007) Bacteria of the roseobacter clade show potential for secondary metabolite production. *Microb Ecol* 54:31–42
16. Bull JE (2007) Stach marine actinobacteria: new opportunities for natural product search and discovery. *Trends Microbiol* 15:491–499
17. Andersen RJ, Wolfe MS, Faulkner DJ (1974) Autotoxic antibiotic production by a marine chromobacterium. *Mar Biol* 27:281–285
18. Geng HF, Bruhn JB, Nielsen KF et al (2008) Genetic dissection of tropodithetic acid biosynthesis by marine roseobacters. *Appl Environ Microbiol* 74:1535–1545
19. Romanenko LA, Uchino M, Kalinovskaya NI et al (2008) Isolation, phylogenetic analysis and screening of marine mollusc-associated bacteria for antimicrobial, hemolytic and surface activities. *Microbiol Res* 163:633–644
20. Das P, Mukherjee S, Sen R (2008) Antimicrobial potential of a lipopeptide biosurfactant derived from a marine bacillus circulans. *J Appl Microbiol* 104:1675–1684
21. Kiran GS, Thomas TA, Selvin J (2010) Production of a new glycolipid biosurfactant from marine nocardiosis lucentensis MSA04 in solid-state cultivation. *Colloids Surf B Biointerfaces* 78:8–16
22. Gomez D, Espinosa E, Bertazzo M et al (2008) The macromolecule with antimicrobial activity synthesized by pseudoalteromonas luteoviolacea strains is an L-amino acid oxidase. *Appl Microbiol Biotechnol* 79:925–930

23. Penesyan A, Marshall-Jones Z, Holmstrom C et al (2009) Antimicrobial activity observed among cultured marine epiphytic bacteria reflects their potential as a source of new drugs: research article. *FEMS Microbiol Ecol* 69:113–124
24. Hentschel U, Schmid M, Wagner M et al (2001) Isolation and phylogenetic analysis of bacteria with antimicrobial activities from the mediterranean sponges *aplysina aerophoba* and *aplysina cavernicola*. *FEMS Microbiol Ecol* 35:305–312
25. Muscholl-Silberhorn A, Thiel V, Imhoff J (2009) Abundance and bioactivity of cultured sponges-associated bacteria from the mediterranean sea. *Microb Ecol* 55:94–106
26. Egan S, Thomas T, Kjelleberg S (2008) Unlocking the diversity and biotechnological potential of marine surface associated microbial communities. *Curr Opin Microbiol* 11:219–225
27. Cong LN, Yang XJ, Wang XX et al (2009) Characterization of an i-type lysozyme gene from the sea cucumber *stichopus japonicus*, and enzymatic and nonenzymatic antimicrobial activities of its recombinant protein. *J Bios Bioeng* 107:583–588

Chapter 121

Determination of Dichloromethane in Waste Water Using Headspace Gas Chromatography

Chaozheng Zhang, Huijing Xu, Yutao Li and Fuhai Wang

Abstract A method for the detection of dichloromethane (DCM) in waste water was developed by using head-space gas chromatography with FID detection. The calibration curve was linear in three orders of magnitude range of DCM levels and the linear correlation coefficient was 0.9995. The limit of detection was 0.004 mg/l and the limit of quantitation was 0.01 mg/l. The system and method precision were both accord with the requirement. The method, practiced in the quantitative determination of DCM in waste water, solved many problems as such and high water content in sample. Many impurities which impacted the detection of DCM were separated visibly.

Keywords Determination · Dichloromethane · Headspace gas chromatography · Waste water

121.1 Introduction

Dichloromethane (DCM) is a toxic pollutant, widely used as a solvent in pharmaceuticals industry [1]. DCM has been extensively used for several decades, first applied in paint removal [2]. It has showed dogged persistence in water

C. Zhang (✉) · F. Wang

Key Laboratory of Ministry of Education Industrial Fermentation Microbiology, Tianjin
Key Laboratory of Industrial Microbiology, Tianjin University of Science and Technology,
Tianjin 300457, People's Republic of China
e-mail: zhangchaozheng@tust.edu.cn

H. Xu

Tianjin Product Quality Inspection Technology Research Institute, Tianjin 300384,
People's Republic of China

Y. Li

Tianjin Trustworthy Biotechnology Limited, Tianjin 300200, People's Republic of China

(half-life over 700 years) and atmosphere (half-life 79 days). Thus, it is difficult to remove DCM from contaminated water [3]. DCM is toxic to the central nervous system at high exposure levels in air [4]. Carcinogenicity of DCM has been also reported in the mouse lung and liver and there is suspected carcinogenicity in human liver and kidney [5]. Therefore, the researchers are very interested in biodegradation of DCM [1, 6–8]. But, it is very important how to detect the concentration of DCM during biodegradation experiments.

The analysis of volatile organic compounds in aqueous using gas chromatography has been performed by some researchers [9–13]. They often use head space and solid phase microextraction as inject sources [14–18]. Ibrahim A. Wasfi detected the ethanol and abused inhalants in blood using headspace gas chromatography (HS-GC)-mass spectrometry method [19]. M. Guardia Rubio analyzed the pesticides in washing waters by solid-phase extraction-gas chromatography [20].

The aim of this study is to establish a method of detecting the concentration of DCM in the waste water using HS-GC. The standard curve and its limit of quantitation (LOQ) and limit of detection (LOD) are investigated.

121.2 Materials and Methods

121.2.1 Chemicals and Reagents

HPLC-grad DCM was purchased from Concord (Tianjin, China). The waste water was got back from a Wastewater treatment plant of pharmaceutical company. The wastewater was boiled for 30 min prior to using blank solution and diluents.

121.2.2 Gas Chromatography Determination

An agilent 7890 gas chromatography with a flame ionization detector was used. The column was a DB-624 (30 m × 0.53 mm, 3 μm film thickness) from Agilent Corporation. The injector was G1118 head-space injection resource. The carrier gas was nitrogen gas. The method was as follows: the column flow is 3.0 ml/min, constant flow mode; the split ratio was 5:1; the inlet temperature was 180 °C; the detector temperature was 250 °C; the temperature program was 40 °C for 4 min followed ramp at 10 °C/min to 200 °C.

121.2.3 Head-Space Method

A 10 ml sample contained DCM was put into a 20 ml HS-GC vial (Agilent USA). The head-space sampler conditions were: vial pressure is 14 psi, sample shaker is

high, extractions per Vial is 2, oven temperature is 60 °C, loop temperature is 75 °C, transfer line temperature is 100 °C, GC cycle time is 35 min, vial equilibration time is 15 min, vial pressurization time is 0.1 min, loop fill time is 0.15 min, loop equilibration time is 0.05 min, sample injection time is 1 min.

121.2.4 Calibration Solutions

A stock solution of DCM standard in boiled sewage was prepared at 8 mg/l and stored in refrigerator. The calibration standard solutions were prepared in boiled waste water at 0.05, 0.1, 0.5, 1, 2, 4, 8 mg/l for HS-GC. All the solutions were diluted with boiled waste water and always made extemporaneously.

121.2.5 Solution of the System and Method Precision

Accurately weighed DCM standard sample 20 mg to 100 ml volumetric flask, dissolved by dilution and take to volume. Transfer 1.0 ml above solution to 100 ml volumetric flask and take to volume with dilution as the system precision solution.

Accurately weighed DCM 10 mg to 100 ml volumetric flask, dissolved by dilution and take to volume. Transfer 1.0 ml above solution to 100 ml volumetric flask and take to volume with dilution as the sample solution. Prepare six solutions use the same batch DCM.

121.3 Results and Discussion

121.3.1 Optimization of the HS Conditions

For the sampling of DCM from the waste water, HS was preferred to direct sampling for several reasons: equilibrium time was less than SPME; the contact of the fiber with the sample was avoided. For this study, the oven temperature and the vial equilibration time were observed and studied. Five temperatures (50, 60, 70, 80, 90 °C) were investigated and the result was shown in Fig. 121.1. The vial equilibration time was studied at 5, 8, 10, 15, 20, 25 min and Fig. 121.2 showed the finding.

Figure 121.1 indicates that the head-space concentration of DCM was increasing as the oven temperature was ascending. There was no increase when the oven temperature exceeded 60 °C. The result is related with the boiling point of DCM. It is 39.75 °C. Figure 121.2 shows that a equilibration time of 15 min gives satisfactory results; a longer time did not result in increasing of the concentration in the head space of vial. Therefore, 60 °C and 15 min were used for heated temperature and equilibration time of the vial, respectively.

Fig. 121.1 Relationship between oven temperature and peak area at vial equilibration time 15 min (the DCM concentration was 2 mg/l)

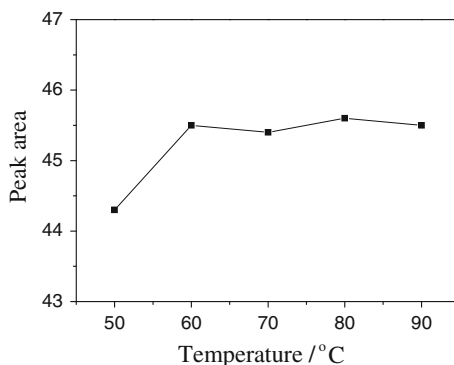
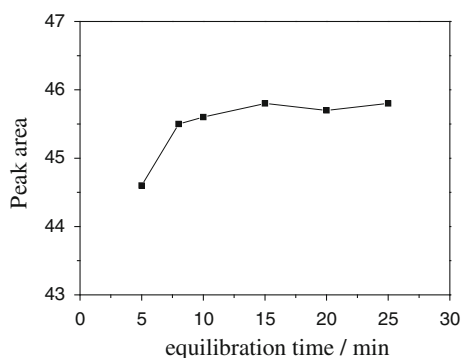


Fig. 121.2 Relationship of vial equilibration time and peak area at oven temperature 70 °C (the DCM concentration was 2 mg/l)



121.3.2 Selectivity of GC Method

We have optimized the different steps of the GC to higher the resolution and lower the limit of detection. To examine the specificity of the method, we injected three samples: blank solution, blank solution with DCM, and waste water. The chromatograms are shown in Fig. 121.3. The blank solution, waste water boiled 30 min, is not obvious responded on the chromatographic condition. The response time of DCM is 7.806 min. The resolution of DCM and other impurities are all more than 1.5.

121.3.3 Quantization by Calibration Curve

Calibration standards should approximate the composition of the sample to be analyzed not only with respect to the analyte concentration but also with regard to the concentrations of the other impurities in the sample matrix. In particular, the sample matrix plays an important role in the head space analysis. The waste water is just like this.

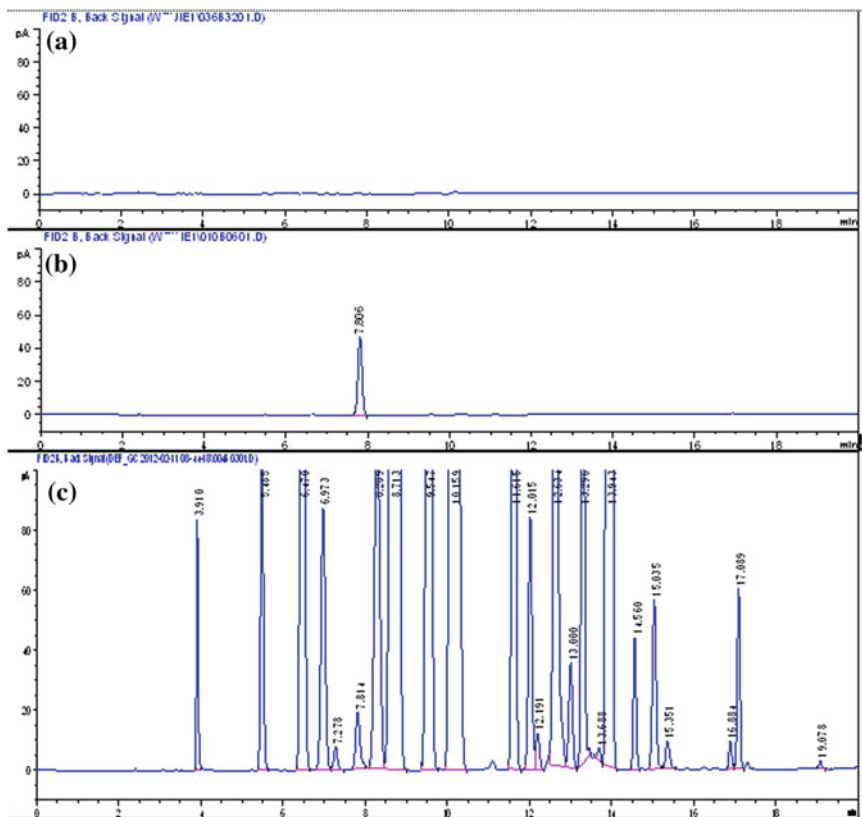


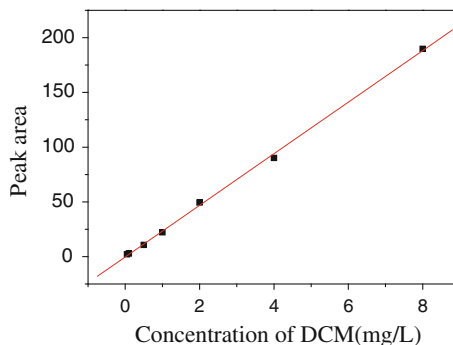
Fig. 121.3 Chromatogram under the method condition. **a** the blank solution, **b** the blank solution with DCM, **c** the waste water

In our study, the calibration curve in the concentration rang from 0.05 to 8 mg/l of DCM in the matrix was prepared. In order to overcome the problem of the matrix effect, the standard solutions were prepared by boiled waste water. The linear relation between peak area and the DCM concentration in waste water is presented in Fig. 121.4. The values for the intercept and slope for the regression line $y = a + bx$ were calculated to be $a = -0.28 \pm 1.15$, $b = 23.56 \pm 0.33$ for seven points ($n = 7$) at the 95 % confidence limit. The correlation coefficient of the line was calculated to be $R = 0.9995$. From this regression line DCM concentration in waste water were calculated.

121.3.4 System and Method Precision

The 2 mg/l DCM solution was used as the system precision solution. Six replicate injections of the system precision solution were injected in the chromatograph and

Fig. 121.4 Calibration curve by linear regression



recorded the retention time and peak area responses. The RSD % of retention time and peak area responses was calculated. The RSD % of peak area and retention time is not more than 2.0 %. The result is in line with the requirement of system precision.

The 1 mg/l DCM solution was used as the method precision solution. Two replicate injections of each sample solution, record the peak area of DCM. The assay of DCM RSD % is not more than 2.0 %. The result accords with the requirement of method precision.

121.3.5 LOD and LOQ of the Method

Gradually dilute the solution of method precision injected in chromatograph, inspected the signal-to-noise ratio. When diluted the solution to 100 times, the signal-to-noise ratio is 10.5, between 9 and 11. The signal-to-noise ratio is 2.6, between 2 and 3, when diluted the concentration of method precision to 250 times. Therefore, the LOQ and LOD is 0.01 and 0.004 mg/l respectively.

121.4 Conclusion

For the determination of DCM in waste water, the head space gas chromatographic procedure was verified. The head space procedure was investigated and the result was fine. In the concentration rang between 0.05 and 8 mg/l of DCM, a linear response was observed. The correlation coefficient was 0.9995 for the calibration plot. The system and method precision were in line with the requirement (RSD < 2.0 %). The LOD and LOQ, observed in this study, were 0.01 and 0.004 mg/l, respectively.

In comparison with extraction and adsorption procedures for DCM in waste water, the head space method is faster and more accurate when the DCM concentration is obviously low. Nevertheless, the precision measured by head space method was reduced.

This study verified that the procedure described in this paper can be successfully used for the determination of DCM in waste water in pharmacy industry.

Acknowledgments The financial support of the Tianjin science and technology plan project (Science and technology innovation fund for small and medium-sized enterprises NO. 11ZXCXGX16300) is gratefully acknowledged.

References

1. Krausova VI, Robb FT, Gonzalez JM (2003) Bacterial degradation of dichloromethane in cultures and natural environments. *J Microbiol Methods* 54:419–422
2. U.S. International Trade Commission (1986) Synthetic organic chemicals. U.S. production and sales. U.S. International Trade Commission, Washington, pp 1970–1985
3. Mackay DM, Cherry JA (1986) Groundwater contamination: pump-and-treat remediation. *Environ Sci Technol* 23:630–636
4. WHO Working Group (1996) In: Methylene chloride-environmental health criteria 164. World Health Organization, Geneva, p. 21
5. Sakai T, Morita Y, Wakui C (2002) Biological monitoring of workers exposed to dichloromethane, using head-space gas chromatography. *J Chromatogr B* 778:245–250
6. Edwards RR, Campbell J, Milne GS (1982) The impact of chloromethanes on the environment part 2, methyl chloride and methylene chloride. *Chem Ind* 41:619–627
7. Gälli R, Leisinger T (1985) Specialized bacterial strains for the removal of dichloromethane from industrial waste. *Conserv Recycl* 8:91–100
8. Freedman DL, Gossett JM (1991) Biodegradation of dichloromethane and its utilization as a growth substrate under methanogenic conditions. *Appl Environ Microbiol* 57:2847–2857
9. Kuráň P, Soják L (1996) Environmental analysis of volatile organic compounds in water and sediment by gas chromatography. *J Chromatogr A* 773:119–141
10. Ashley DL, Bonin MA, Frederick L et al (1992) Determining volatile organic compounds in human blood from a large sample population by using purge and trap gas chromatography/mass spectrometry. *Anal Chem* 64(9):1021–1029
11. Cassada DA, Zhang Y, Snow DD et al (2000) Trace analysis of ethanol, MTBE, and related oxygenate compounds in water using solid-phase microextraction and gas chromatography/mass spectrometry. *Anal Chem* 72(19):4654–4658
12. Sarafraz-Yazdi A, Mosadegh M, Amiri A (2011) Determination of volatile organic compounds in environmental water samples using three solid-phase microextraction fibers based on sol-gel technique with gas chromatography-flame ionization detector. *Anal Methods* 3:1877–1886
13. Leong MI, Huang SD (2012) Determination of volatile organic compounds in water using ultrasound-assisted emulsification microextraction followed by gas chromatography. *J Sep Sci* 35:688–694
14. Cervera MI, Beltran J, Lopez FJ et al (2011) Determination of volatile organic compounds in water by head space-solid-phase microextraction gas chromatography coupled to tandem mass spectrometry with triple quadrupole analyzer. *Anal Chim Acta* 74:87–97
15. Li YT, McCarty CL, George EdJ (2011) Determination of selected semi-volatile organic compounds in water using automated online solid-phase extraction with large-volume injection/gas chromatography/mass spectrometry. *Fron Env Sci Eng* 5(3):417–425 (in chinese)

16. Zhang ZM, Wang QT, Li GK (2012) Fabrication of novel nanoporous array anodic alumina solid-phase microextraction fiber coating and its potential application for headspace sampling of biological volatile organic compounds. *Anal Chim Acta* 727:13–19
17. Cervera MI, Beltran J, Lopez FJ, Hernandez F (2011) Determination of volatile organic compounds in water by headspace solid-phase microextraction gas chromatography coupled to tandem mass spectrometry with triple quadrupole analyzer. *Anal Chim Acta* 704:87–97
18. Vera H, Raquel S, José Luís M et al (2012) Response surface optimisation applied to a headspace-solid phase microextraction-gas chromatography-mass spectrometry method for the analysis of volatile organic compounds in water matrices. *Int J Environ An Ch* 92(2):166–189
19. Wasfi IA, Al-Awadhi AH, Naser Z et al (2004) Rapid and sensitive static headspace gas chromatography–mass spectrometry method for the analysis of ethanoland abused inhalants in blood. *J Chromatogr B* 799:331–336
20. Guardia Rubio M, Ruiz Medina A, Pascual Reguera MI et al (2007) Multi residue analysis of three groups of pesticides in washing waters from olive processing by solid-phase extraction-gas chromatography with electron capture and thermionic specific detection. *Microchem J* 85:257–264

Chapter 122

Simulation of Bio-syngas Production from Biomass Gasification via Pressurized Interconnected Fluidized Beds

Fei Feng, Guohui Song, Laihong Shen and Jun Xiao

Abstract Bio-syngas production from biomass gasification via pressurized interconnected fluidized beds was described. The interconnected fluidized beds technology separates the gasification and combustion processes of biomass, and the heat is transferred from combustor to gasifier by bed materials, while extra heat needed in gasification process is provided by additional biomass burning in the combustor. The simulation of the whole process was carried out with Aspen Plus software. The effects of gasification temperature (T_g), gasification pressure (p_g) and steam to biomass ratio (S/B) on bio-syngas production were studied. The results showed that gasification temperature, gasification pressure, and S/B had great influences on the bio-syngas composition and to achieve high carbon conversion and yield of high-quality bio-syngas, the suitable gasification temperature is around 750 °C, and the gasification pressure and S/B could not too high.

Keywords Pressurized · Interconnected fluidized beds · Bio-syngas · Simulation · Biomass gasification

122.1 Introduction

Since biomass is one kind of renewable, clean energy, and can achieve the goal of CO₂ zero-emission and reduce the greenhouse effect during its industrial utilization, its development and employment has obtained great attentions all over the

F. Feng · G. Song · L. Shen (✉) · J. Xiao

Key Laboratory of Energy Thermal Conversion and Control of Ministry of Education,
School of Energy and Environment, Southeast University, Jiangsu 210096,
People's Republic of China
e-mail: lhshen@seu.edu.cn

F. Feng

Department of Mechanical Technologies, Nanjing College of Chemical Technologies,
Jiangsu 210048, People's Republic of China

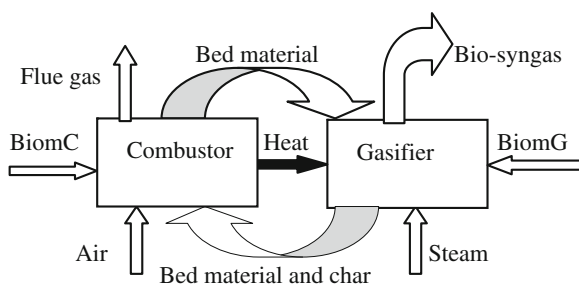
world [1]. Biomass gasification is considered as a key technology in reaching targets for renewable energy and CO₂ emissions reduction [2]. After proper purification and conditioning, bio-syngas from biomass gasification composed mainly of CO and H₂ can be synthesized to methane, methanol, gasoline, and diesel oil [3–6]. So many researchers have done a lot of work about the bio-syngas production from biomass gasification, including gasification agents, reactors, catalysts, and so on. For instance, the oxygen-rich air was used as the gasification agents to avoid the dilution of bio-syngas with the inert nitrogen of air, while some researchers used a mixture of air and steam as gasification agents to produce bio-syngas with relatively higher H₂/CO ratio to meet the requirements of the further synthetic reactions [7–9].

This article intends to study the laws of bio-syngas production with biomass gasification from a new perspective of simulation. The process simulation with Aspen Plus software was carried out to demonstrate the effects of operating parameters, like gasification temperature, gasification pressure and the ratio of steam to biomass fed into the gasifier (*S/B*), on the bio-syngas composition, yield, and carbon conversion of biomass. These results provided reference data for the further study of biomass gasification.

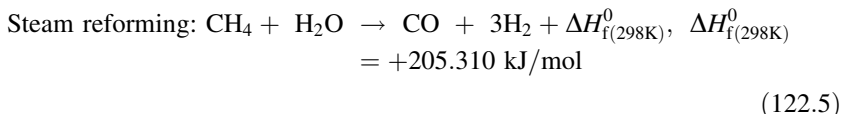
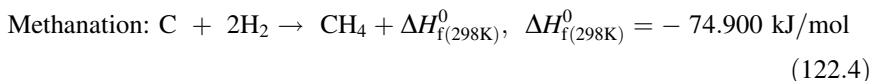
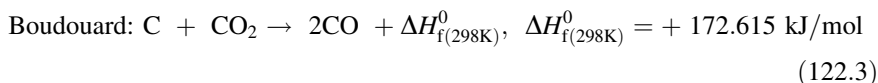
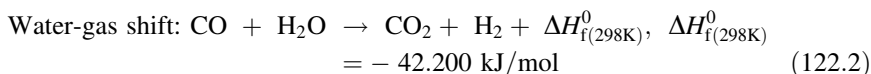
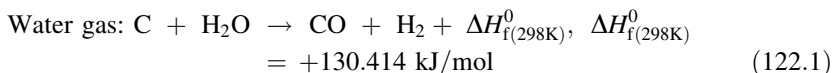
122.2 Materials and Methods

Gasifier is the core equipment of the biomass gasification process, which can be classified as fixed bed gasifiers and fluidized bed ones. The interconnected fluidized beds gasifiers are evolved from the conventional fluidized bed gasifiers [10]. The scheme of biomass gasification in interconnected fluidized beds is illustrated in Fig. 122.1 [11]. It is in a loop with end-to-end configuration composed of a circulating fluidized bed as a combustor, and a bubbling fluidized bed as a gasifier. The circulating fluidized bed is designed for combustion fed with air as gasification agent and the bubbling fluidized bed for biomass gasification fed with steam as gasification agent. The gasification-required heat is achieved by means of the circulation of bed particles (sand, ash, etc.), which serve as the heat carrier and circulate in the system. In this way, the gasification and combustion processes are separated from each other [12, 13].

Fig. 122.1 Bio-syngas production from biomass gasification in interconnected fluidized beds



The whole biomass fed into the interconnected fluidized beds is divided into two parts, which are BiomC and BiomG, respectively. One part (BiomG) is fed into the bubbling fluidized bed (gasifier), where the biomass mixes with the steam and hot bed particles, and the intense exchange of heat and mass occurs. Then the volatile compounds in the biomass evaporate, followed by the pyrolysis of the biomass. The reactions between gaseous product after pyrolysis combined with solid residual and steam occur, where gases such as CO and H₂ are generated [12]. The reactions occurring in the gasifier include [14, 15]:



The other part (BiomC) is burnt in a circulating fluidized bed (combustor) where the bed particles carry a great deal of heat. The flue gas carrying hot bed particles from the combustor passes through a separator, where the hot particles are separated from the flue gas and pass into the gasifier, providing the heat needed for the biomass gasification. The unseparated particles are expelled from the system in the form of flowing ash with the flue gas. The char mixed with the cold bed particles in the gasifier is back-passed into the combustor to combust.

122.3 Process Simulation

Based on the application of Aspen Plus software, the following assumptions were made [12, 16]:

- (1) The combustor and the gasifier were operated under a steady state, and the reactions reached the chemical equilibrium.
- (2) Pressure losses in the combustor and the gasifier were not considered.

- (3) The product gas of biomass gasification included H_2 , CO , CO_2 , CH_4 , H_2O , N_2 , H_2S , NH_3 , COS , and SO_2 and the solid products were ash and unburnt carbon. Tar was not taken into account.
- (4) Ash in biomass and bed particles (sand) were inert and would not participate in the chemical reactions.

The simulation flowchart of bio-syngas production from biomass gasification in pressurized interconnected fluidized beds was shown in Fig. 122.2. The whole model mainly consisted of two basic modules, a gasification module and a combustion module. The gasification module was composed of a pyrolyzer and a gasifier, and the combustion module included a decomposer and a combustor. The pyrolyzer block corresponded to Ryield block of Aspen Plus, whose function was to decompose biomass into simple components. Unreacted char from the gasifier was separated by a cyclone, and sent to the combustor of the combustion module. The bed materials from the combustor (sand) were circulating, whereby the heat was carried from the gasification module to the combustion module. Water was heated in the steam generator with the flue gas from the combustor to provide the gasifier with steam as the gasification agent.

The whole model of gasification module and combustion module was based on the principle of minimization of Gibbs free energy, which originated from the Rgibbs block of Aspen Plus. The Gibbs free energy is minimal when the chemical equilibrium for the process is achieved [17]. Based on mass balance, chemical equilibrium, and energy balance between the gasifier and the combustor, the mathematical model for the gasification process was set up.

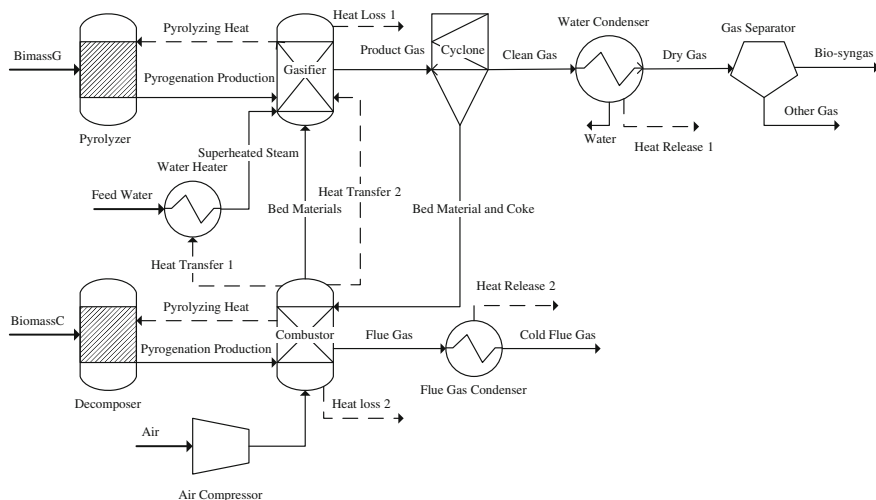


Fig. 122.2 Simulation flowchart of bio-syngas production from biomass gasification in pressurized interconnected fluidized beds

122.4 Operating Conditions and Primary Parameters

The biomass sample was the pine sawdust from Jiangsu Province, China. The proximate analysis and the ultimate analysis of biomass were illustrated in Table 122.1.

The operating conditions and primary parameters in the simulation were shown in Table 122.2.

122.5 Results and Discussion

122.5.1 Influences on Product Gas Composition

The product gas from biomass gasifier was mainly composed of bio-syngas ($H_2 + CO$), CO_2 and CH_4 . Figures 122.3, 122.4, 122.5 showed the influences on its composition.

The product gas composition was shown as a function of gasifier temperature in Fig. 122.3. In the case where the gasifier pressure remained 0.4 MPa and the S/B was 0.6, the bio-syngas content was varied around 60–90 mol % at the gasifier temperature range of 650–950 °C and with the rise of gasifier temperature, it increased and kept nearly constant at the temperature of about 800 °C, whilst the CO_2 and CH_4 content decreased correspondingly. The product gas composition in the biomass gasifier is the result of the combination of a series of complex and

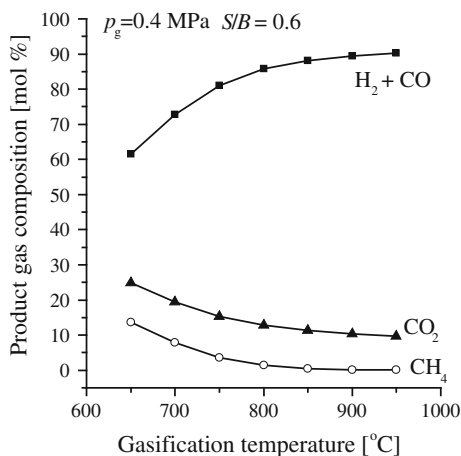
Table 122.1 Proximate and ultimate analysis of biomass

Proximate analysis (wt%)		Ultimate analysis (wt%)	
Moisture	7.89	C	40.06
Fixed carbon	14.77	H	5.61
Volatile	75.78	O	43.88
Ash	1.56	N	0.90
Low heating value (MJ/kg)	14.47	S	0.10

Table 122.2 Input data for the process simulation

Parameters	Value
Room temperature	25 °C
Biomass-flow rate of gasifier	3 kg/h
Air inlet temperature	25 °C
Air flow rate	7 m ³ /h
Combustor temperature	750–1,050 °C
Gasifier temperature	650–950 °C
Feed water inlet temperature	25 °C

Fig. 122.3 Effect of gasification temperature on product gas composition



competing reactions, as given in reactions (122.1)–(122.5). Reactions (122.1), (122.3), and (122.5) occurring in the gasifier are intensive endothermic processes, while the reactions (122.2) and (122.4) are exothermic ones. As a result, higher temperatures favor the endothermic reactions and the production of bio-syngas.

The effect of gasification pressure on product gas composition was shown in Fig. 122.4, which indicated that as the gasification temperature was 750 °C and S/B was 0.6, with the increase of gasification pressure, the bio-syngas content decreased, while the CO_2 and CH_4 content increased correspondingly. This was because the increase of pressure would promote the gasification reactions toward the direction that led to volume reduction, which favored the reaction (122.4), while led the reactions (122.3) and (122.5) to the opposite direction.

Fig. 122.4 Effect of gasification pressure on product gas composition

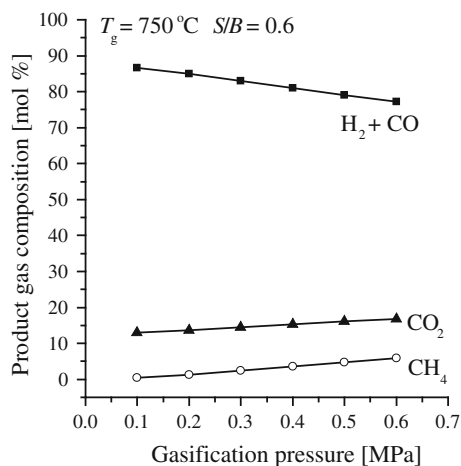


Fig. 122.5 Effect of S/B on product gas composition

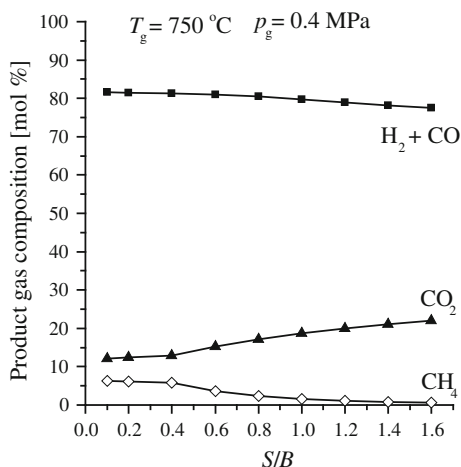


Figure 122.5 indicated the influence of S/B on product gas composition. When the gasification temperature was $750\text{ }^\circ\text{C}$ and the gasification pressure remained 0.4 MPa , as the S/B increased, the bio-syngas content was not affected so evidently, while CH_4 content decreased and the CO_2 content increased. More S/B meant more steam participated in the reactions, which would promote reactions (122.1), (122.2), and (122.5) toward the right direction.

122.5.2 Influences on Carbon Conversion of Biomass

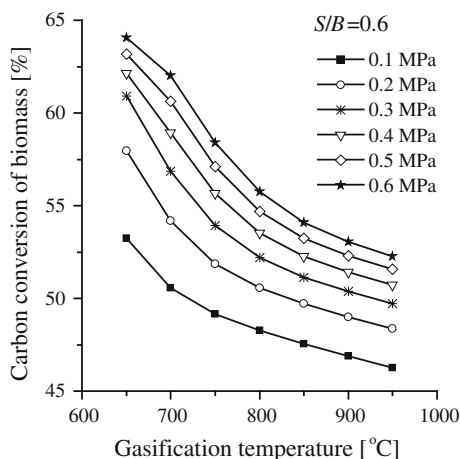
One parameter of carbon conversion of biomass can be used to investigate the effect of different operating parameters in the gasifier on the gasification process. The carbon conversion of biomass was defined in Eq. (122.6).

$$\text{Carbon conversion of biomass} = \frac{\text{gasified carbon in the gasifier (kg)}}{\text{carbon of biomass fed into the system (kg)}} \quad (122.6)$$

The effect of gasification temperature on carbon conversion at different gasification pressure was indicated in Fig. 122.6. When S/B was kept 0.6 , with the rise of gasification temperature, the carbon conversion of biomass decreased correspondingly at the same gasification pressure. This was because higher gasification temperature meant more biomass was fed into the combustor and less biomass into the gasifier, which resulted in a decrease of carbon conversion.

Figure 122.6 also showed that at the same gasification temperature, with the increase of gasification pressure, the carbon conversion of biomass increased, too, which indicated that higher gasification pressure favored the carbon conversion.

Fig. 122.6 Effect of gasification temperature on carbon conversion of biomass at different gasification pressure



S/B also had great influence on the carbon conversion of biomass. As shown in Fig. 122.7, in the case where gasification temperature was 750 °C and the gasification pressure was 0.4 MPa, with the increase of S/B , the carbon conversion increased and then decreased, and reached maximum for the S/B of about 0.4.

As the S/B was lower than 0.4, there was not enough steam to react with the biomass, and reactions (122.1), (122.2), and (122.5) may not reach a state of completion. With the increase of S/B , more steam took part in the above reactions and made the carbon conversion increase. However, larger S/B meant excessive water was fed into the system, which resulted in more carbon that was needed in the combustor to provide heat to make the water evaporate and overheat. Thus, less biomass went into the gasifier, which led to a decrease of the carbon conversion correspondingly.

Fig. 122.7 Effect of S/B on carbon conversion of biomass

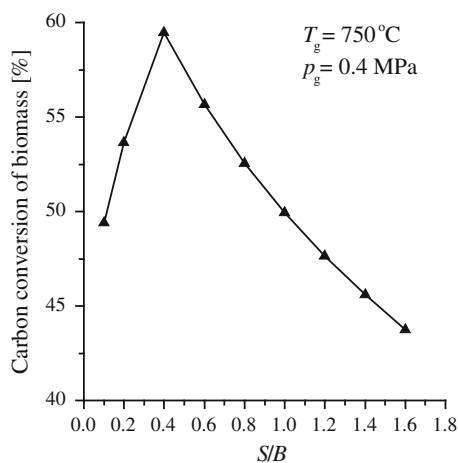
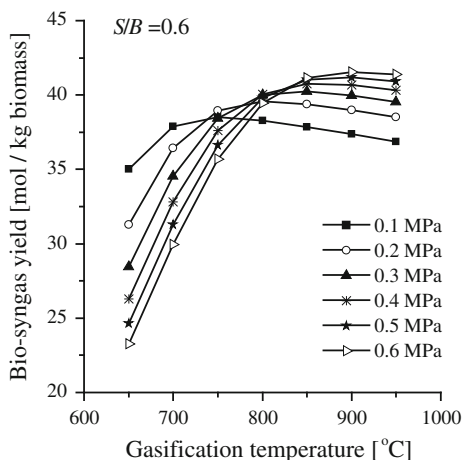


Fig. 122.8 Effect of gasification temperature on bio-syngas yield at different gasification pressure



122.5.3 Influences on Bio-Syngas Yield

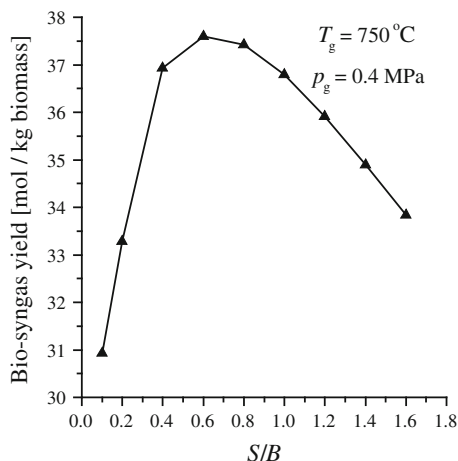
Bio-syngas yield is another important parameter to describe the gasification process of biomass, which can be defined as

$$\text{Bio-syngas yield} = \frac{\text{bio-syngas in the gasifier (mol)}}{\text{biomass fed into the system (dry and ash free, kg)}} \quad (122.7)$$

Figure 122.8 showed the influence of gasification temperature on bio-syngas yield at different gasification pressure. In the case where S/B was 0.6, bio-syngas yields all increased with the rise of gasification temperature and almost kept a high value after the temperature reached 750 °C and above. The reason was that higher temperature favored the bio-syngas production, while the gasification pressure had a weak effect on it at high temperature.

S/B also had great influence on the bio-syngas yield, as shown in Fig. 122.9. In the case where the gasification temperature maintained 750 °C and the gasification pressure was 0.4 MPa, bio-syngas yield increased at first, reached the maximum value when S/B was around 0.6, and then decreased. The reason was somewhat the same as the explanation of the variant of carbon conversion of biomass. With the increase of S/B , more steam participated in the biomass gasification process and promoted the bio-syngas production, while the larger S/B value meant more water was needed in the system and resulted in the reduction of biomass fed in the gasifier. As a result, the bio-syngas yield decreased as S/B was larger than 0.6.

Fig. 122.9 Effect of S/B on bio-syngas yield



122.6 Conclusions

With the Aspen Plus software, simulation of bio-syngas production from biomass gasification via pressurized interconnected fluidized beds was carried out. Some valuable results were obtained as follows.

- (1) Bio-syngas content in the product gas was influenced by the gasification temperature, pressure, and S/B . It increased with the gasification temperature rising, while the gasification pressure and S/B had a weak effect on it.
- (2) When S/B remained 0.6, the carbon conversion of biomass decreased with the increase of gasification temperature at the same gasification pressure, while it increased with the rise of gasification pressure at the same gasification temperature. In the case where gasification temperature was $750\text{ }^\circ\text{C}$ and the gasification pressure 0.4 MPa , with the increase of S/B , the carbon conversion increased and then decreased, and reached maximum as the S/B was about 0.4.
- (3) When S/B was kept 0.6, bio-syngas yield almost increased with the increase of gasification temperature at different gasification pressure. It kept a high value as the gasification temperature was higher than $750\text{ }^\circ\text{C}$.
- (4) To achieve a high content of bio-syngas and high carbon conversion and bio-syngas yield, the gasification temperature could be higher than $750\text{ }^\circ\text{C}$, and the gasification pressure and S/B could not be too high.

Acknowledgments This work was supported by the National Natural Science Foundation of China (2010CB732206).

References

1. Fatih M, Mustafa B, Havva B (2009) Potential contribution of biomass to the sustainable energy development. *Energy Convers Manag* 50:1746–1760
2. Turn S, Kinoshita C, Zhang Z et al (1998) Experimental investigation of hydrogen production from biomass gasification. *Int J Hydrogen Energy* 23:641–648
3. Pengmei L, Zhenhong Y, Chuangzhi W et al (2007) Bio-syngas production from biomass catalytic gasification. *Energy Convers Manag* 48:1132–1139
4. Jan K, Tilman JS, Serge MAB (2010) Production of synthetic natural gas (SNG) from coal and dry biomass-technology review from 1950 to 2009. *Fuel* 89:1763–1783
5. Zhang XT, Chang J, Wang TJ et al (2006) Investigation into methanol synthesis from biomass derived syngas over Cu-Zn-Al-Li catalysts. *Chi J Pro Eng* 6:104–107 (in Chinese)
6. Lu YX, Wang TJ, Li YP et al (2008) Direct synthesis of liquefied petroleum gas from biomass synthesis gas. *J Fuel Chem Tech* 36:246–249 (in Chinese)
7. Dennis YCL, Yin XL, Wu CZ (2004) Review on the development and commercialization of biomass gasification technologies in China. *Renew Sust Energy Rev* 8:565–580
8. Su DR, Zhou ZQ, Xie JJ et al (2011) Biomass oxygen enriched-steam gasification in an atmospheric fluidized bed for singes production. *Trans Chin Soc Agric Mach* 42:100–104 (in Chinese)
9. Song FE, Tan YS, Xie HJ et al (2009) Study on preparation of dimethyl ether from biomass-derived syngas. *Mod Chem Ind* 29:306–308 (in Chinese)
10. Jose' C, Jose' M, Gregorio M (2007) Review on dual fluidized-bed biomass gasifiers. *Ind Eng Chem Res* 46:6831–6839
11. Christoph P, Reinhard R, Hermann H (2004) In-bed catalytic tar reduction in a dual fluidized bed biomass steam gasifier. *Ind Eng Chem Res* 43:1634–1640
12. Yanan Z, Jun X, Laihong S (2009) Simulation of methanol production from biomass gasification in interconnected fluidized beds. *Ind Eng Chem Res* 48:5351–5359
13. Bischi A, Langørgenb øy, Saanum I et al (2011) Design study of a 150kWth double loop circulating fluidized bed reactor system. *Int J Greenh Gas Con* 5:467–474
14. Ajay K, David D, Milford AH (2009) Thermochemical biomass gasification: a review of the current status of the technology. *Energies* 2:556–581
15. Hugo D, Enrique S, Jahirul M et al (2011) Catalytic steam gasification of biomass: catalysts, thermodynamics and kinetics. *Chem Rev* 111:5404–5433
16. Gao Y, Xiao J, Shen L (2008) Hydrogen production from biomass gasification in interconnected fluidized beds. *Acta Energiæ Solaris Sinica* 29:894–899 (in Chinese)
17. Qu YX (2011) Numerical simulation and software for chemical processes. *Chem Ind Press, Beijing* (in Chinese)

Chapter 123

Research on Salt-tolerant Gene *GPD1* in *Zygosaccharomyces rouxii*

Lihua Hou, Yanfei Yu, Cong Wang and Chunling Wang

Abstract To better understand the osmo-adaption mechanism, salt-tolerant gene *GPD1* coding for glycerol-3-phosphate dehydrogenase was evaluated in the wild-type *Zygosaccharomyces rouxii* (S). Genomic DNA of S was used for PCR reaction to amplify the *GPD1* gene. The PCR products were sent into sequencing vector pUC19 to achieve the plasmid pUC19-*GPD1*. The engineered strain W303-YEp195-S and the control strain W303-YEp195 were constructed, respectively. It was observed that the overexpression of *SGPD1* can obviously increase the tolerance of salt compared to the control. Identification, and over-expression of *SGPD1* from the S play an important role for the osmo-adaption mechanism of salt-tolerant yeasts used in soy sauce fermentation.

Keywords Salt tolerance · *GPD1* · *Zygosaccharomyces rouxii*

123.1 Introduction

Soy sauce, a traditional oriental food condiment with a salty taste and distinct fragrance, is becoming more and more popular worldwide. Soy sauce fermentation includes high-salt liquid fermentation mostly used in Japan and low-salt solid fermentation usually applied in China. During soy sauce fermentation processes salt-tolerant yeasts, such as *Zygosaccharomyces rouxii*, *Torulopsis versatilis* and *Candida versatilis* are very important for flavor formation [1]. The concentration of salt is 18 % in the high salt liquid fermentation of soy sauce, which causes high osmotic stress [2]. In this environment, the metabolic activity of the yeast is low

L. Hou (✉) · Y. Yu · C. Wang · C. Wang
Ministry of Education, Key Laboratory of Food Nutrition and Safety (Tianjin University of Science and Technology), Tianjin 300457, People's Republic of China
e-mail: lhhou@tust.edu.cn

due to the high salt content of the soy sauce mash, where yeasts need to have the ability of adjustment to the poor condition [3].

The gene *GPD1* plays an important role in the adaptation to the hyper-osmotic stress dependent on signal transduction pathways, and especially the transcription controlled by the yeast High Osmolarity Glycerol (HOG) response pathway that mediates cellular adaptation to hyperosmotic stress and is responsible for the production of glycerol in yeast [4]. The gene *GPD1* encodes the glycerol-3-phosphate dehydrogenase (GPDH) which is related to glycerol synthesis [5]. The transcriptional change in *GPD1* seems to revolve around metabolism and is similar to that caused by other stresses although Gpd1p in glycerol production and active glycerol uptake is among those upregulated in a Hog1-dependent manner [6]. In case of hyper-osmotic stress, yeast cells must react to the presence of external osmolytes that alter the osmotic pressure acting on the cell. Part of the response consists of the production of the intracellular osmolyte glycerol, a compatible solute, to increase the internal osmolarity of the cell [7].

In the present work, *SGPD1* was cloned and expressed in *Saccharomyces cerevisiae* to analyze the cellular impact on salt tolerance and glycerol. Growth characteristics, osmotic tolerance, and fermentation performance conditions of the engineered strains were studied in the present work.

123.2 Materials and Methods

123.2.1 Strains and Media

The *Z. rouxii* (S yeast) and *S. cerevisiae* strain W303-1A (*MATa leu2 ura3 trp1 his3 ade2 can1*) were used in this study. The yeast cells were cultivated with shaking after pre-cultivation for 2–3 days at 30 °C in YPD medium (1 % yeast extract, 2 % peptone and 2 % glucose) and YPDN (6–18 % NaCl dissolved in normal YPD substrate) or CM-URA medium (0.67 %w/v yeast nitrogen base without amino acids, 2 % glucose and 0.192 % CM-URA powder). The high fidelity *E.coil* Top 10 was used for plasmid propagation, grown with shaking in LB (0.5 % yeast extract, 1 % peptone, 1 % NaCl pH = 7.2) medium at 37 °C. The X-Gal LBA plate (50 ng/ml ampicillin, 0.5 mmol/l IPTG and 40 ug/ml X-Gal) was used to screen the colonies. The plasmids were transformed into the strain W303-1A by the lithium acetate method [8].

123.2.2 Plasmids and Strains Construction

PCR was performed using high-fidelity *Pfu* DNA polymerase to clone the *SGPD1* with the primers *GPD1*-up(GCGCATGCTACGGTATAAAGGGTGTACA) and *GPD1*-dn(GCAAGCTTTTCAATTCCCAGCTTATTC). PCR products of

SGPDI was digested with *SphI* and *HindIII* and then inserted into the sequencing vector pUC19 to achieve the plasmids pUC19-S. The sequence of plasmids pUC19-S was confirmed by DNA sequence analysis. Simultaneously, *SGPDI* gene was cloned into the plasmid YEp195, constructing the plasmids YEp195-S (Y-S). Subsequently, the plasmids YEp195-S (Y-S) and the plasmids YEp195 were transformed into W303-1A, forming the strains W303-YEp195-S (WYS) and W303-YEp195 (W-Y), respectively.

123.2.3 The Real-time Quantitative PCR

Real-time quantitative PCR is non-competitive, while in the product formation it was tested on. *S* yeast was cultivated in the presence of NaCl (0, 6, 12 and 18 %) at 30 °C. The cells (about 3×10^8) were collected by centrifugation, washed, and recollected. The total RNA was prepared using the trizol made by TransGen Biotech following the manufacturer's instructions. RNA was then treated with DNaseI according to the protocol. The mRNA samples (2 mg) were denatured with formaldehyde. Aliquots (1.0 mg) of total RNA were used in the RT reaction (42 °C 30 min, 85 °C 5 min). QPCR was performed by using the cDNA produced by the RT kit. Then cDNA samples were used for template in the PCR reaction with the primers *GPD1*-R-up (CTGCAGGTGTTGCTGATTTG) and *GPD1*-R-dn (GCCAT TTCAGTGGCTACACG). The length of PCR products *GPD1*-R was 70 bp. 18S (128 bp) was used as internal reference with primers 18 s-up (CCAAGAA-CATGATGGCTGCT) and 18 s-dn (CTTGAAGAGCTCCTGGATGG) [9].

123.2.4 Glycerol Estimation

The cells were grown in YPD media and harvested at 0.5 of OD550 to determine intracellular and extracellular glycerol. The cells were then pre-cultivated in fresh media and incubated for 1 h at 30 °C. Cell extracts were prepared [10] and glycerol was analyzed enzymatically using a glycerol assay kit (Applygen, China).

123.3 Results and Discussion

123.3.1 Sequence Analyses

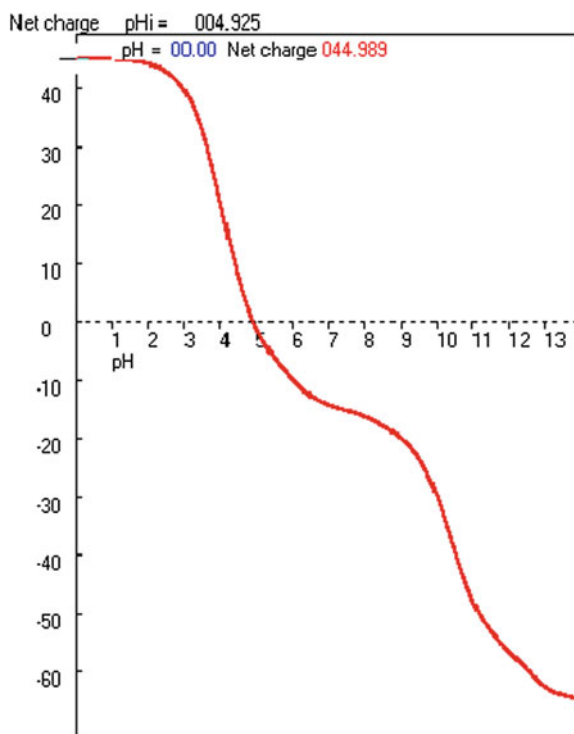
The *GPD1* genes amplified from genomic DNA from *S* yeast was cloned into pUC19 and subsequently sequenced. The results showed the length of open reading frame (ORF) of *SGPDI* was 1167 bp, which encoded a 389 amino-acid

protein, and the sequences of the promoter and the terminator (data now shown). The *GPD1* sequence of S yeast was the same as that of CBS732 (<http://www.genolevures.org/concordance/?search=Zygosaccharomyces+rouxii>) using blastn, which suggests gene *GPD1* present in *Z. rouxii* was conserved and played crucial roles in osmoregulation. In our lab, other salt-tolerant genes of S and S3-2, such as *HOG1* and *FPS1*, are studied.

123.3.2 Structure Analyses

After sequencing, the second structure of *SGPD1* was constituted to analyze the quality of coding proteins for further research. The amino acids sequence of *SGPD1* was determined using Anthepro software. It was found structure composed of all alpha 2.99, all beta 3.34, alpha + beta 2.89, alpha/beta 1.88, and irregular 2.02. As shown in Fig. 123.1, the prediction of isoelectric point of *SGPD1* was 4.925.

Fig. 123.1 The prediction of isoelectric point of *SGPD1*



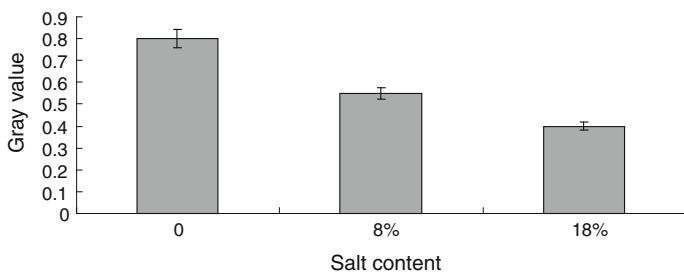


Fig. 123.2 Expression level of *GPD1* under different salts

123.3.3 Expression Level of *GPD1*

The strain S was cultured in the media with salt content of 8, 18 %, and without salt, followed by extraction of RNA. The salt content of 8, 18 %, and without salt was carried out because 8 % NaCl was mostly used in the low-salt solid soy sauce fermentation and 18 % NaCl was usually added during the high-salt liquid soy sauce fermentation. Gray value was IOD of end products/IOD of internal reference. The transcription levels of *SGPD1* was estimated using QPCR analysis with 18s rDNA as endogenous reference. As shown in Fig. 123.2, the transcription level of *SGPD1* in the media was reduced with increase in the salt content.

123.3.4 Salt-tolerant Analyses

The plasmids YEplac195 and Y-S constructed in this study were transformed to strain *S. cerevisiae* (W303-A), forming the engineered strains W-Y and WYS, respectively. The resulting stains were cultivated in YPD with 8 and 18 % salt. Figure 123.3 gives the growth of the strains. The results indicate that the salt-tolerance of WYS was distinctly improved compared to the control W-Y. The salt-tolerant analysis revealed that *GPD1* of S had a significant effect on resistance to high osmolarity in *S. cerevisiae*.

In addition, the glycerol contents in WYS along with the control W-Y grown in YPD media with different salt were measured. WYS and W-Y were cultivated with shaking in YPD media with 0, 8, and 18 % NaCl at 30 °C for 2 or 3 days, respectively. As shown in Fig. 123.4, for the same strain the glycerol content also enhanced with the increase in the salt concentration, which indicated that the glycerol could respond to the changes in external osmotic pressure. For the same salinity, the glycerol content was of the order of WYS and W-Y. Meanwhile, the glycerol content of WYS was higher than the control W-Y. Glycerol synthesis plays significant physiological roles in metabolism of the yeast including

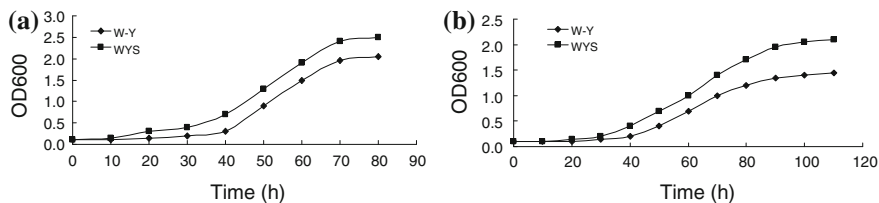


Fig. 123.3 Salt-tolerant analyses of the engineered strains WYS and WY in the presence of 8 % (a) and 18 % NaCl (b)

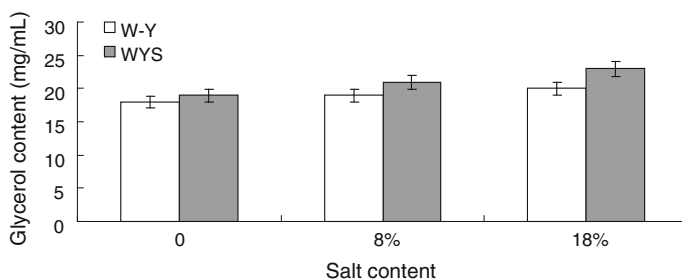


Fig. 123.4 Glycerol concentration of the engineered strains WY and WYS in the presence of 0, 8, and 18 % NaCl, respectively

osmoregulation and maintaining intracellular redox balance under an aerobic condition. In the present work, the results demonstrated that the increase of glycerol was one reason for the salt-tolerant improvement of *S* yeast.

123.4 Conclusion

In conclusion, overexpression of *SGPDI* caused the stronger salt-tolerance compared to the control WY. Identification and overexpression of *SGPDI* from the *S* play an important role for the osmo-adaption mechanism of the salt-tolerant yeasts used in soy sauce fermentation. The utilization of overproducing glycerol is a potentially valuable strategy for producing soy sauce to improve the performance of salt tolerance and the flavor.

Acknowledgments This work was supported by these projects in China (2013AA102106, 2012BAD33B04, 31371819, 2012GB2A100016, 2012AA022108, 31171731, 10ZCZDSY07000, 2012AA021303 and IRT1166).

References

1. Cao XH, Hou LH, Lu MF et al (2010) Genome shuffling accelerated and enhanced flavor formation of soy sauce by improving salt-tolerance of *Candida versatilis*. *Int J Food Sci Tech* 45:17–22
2. Yokotsuka T (1986) Soy sauce biochemistry. *Adv Food Res* 30:195–329
3. Luh BS (1995) Industrial production of soy sauce. *J Ind Microbiol* 14:467–471
4. Hohmann S (2002) Osmotic stress signaling and osmoadaptation in yeasts. *Mol Biol Rev* 66:300–372
5. Albertyn J, Hohmann S, Thevelein JM et al (1994) *GPD1*, which encodes glycerol 3-phosphate dehydrogenase, is essential for growth under osmotic stress in *Saccharomyces cerevisiae* and the high-osmolarity glycerol response pathway regulates its expression. *Mol Cell Biol* 13:4135–4144
6. O'Rourke SM, Herskowitz I (1998) The Hog1 MAPK prevents cross talk between the HOG and pheromone response MAPK pathways in *Saccharomyces cerevisiae*. *Genes Dev* 12:2874–2886
7. Hohmann S, Krantz M, Nordlander B (2007) Yeast osmoregulation. *Methods Enzymol* 428:269–286
8. Schiestl RH, Gietz RD (1989) High efficiency transformation of intact yeast cells using single stranded nucleic acids as carrier. *Curr Genet* 16:339–346
9. Causton HC, Ren B, Koh SS et al (2001) Remodeling of yeast genome expression in response to environmental changes. *Mol Biol Cell* 12:323–337
10. Andre L, Nilsson A, Adler L (1988) The role of glycerol in osmotolerance of the yeast *Debaryomyces hansenii*. *J Gen Microbiol* 144:669–677

Chapter 124

Mutagenic Research on Ciliary Neurotrophic Factor (CNTF) in *Escherichia coli* After Heavy Ions Irradiation

Xiaodong Jin, Qingfeng Wu, Xinguo Liu, Yan Liu, Yong Chen, Jian Lu and Lin Jiang

Abstract Based on the natural human CNTF gene, Ying et al. acquired CNTF-T mutant and constructed *Escherichia coli* expressing CNTF. In order to increase the yield and enhance the protein expression in the constructed *E. coli*, the strains were irradiated with high-LET heavy ions. Some mutants were obtained in this work and the mechanisms underlying the enhanced expression of CNTF in *E. coli* after exposure to heavy ions are discussed in this paper.

Keywords High-LET irradiation · CNTF · Mutant · Molecular characterization

124.1 Introduction

Unlike conventional radiations such as X- and γ -rays, high-LET (linear energy transfer) charged particles lose most of their kinetic energy at the Bragg peak, which is produced near the end of the range [1]. Thus, heavy ion irradiation has been taken as a more effective mutagen compared with low-LET radiations and has been used in mutation breeding widely. To date, the mutation-induction effects of heavy ion beams have been investigated in various organisms [2–5].

Ciliary neurotrophic factor (CNTF) is a 22–26 kD acid protein, which was originally purified from chick eye and characterized as a survivability factor for neurons from chick embryonic ciliary ganglia in vitro [6]. Recent research shows that CNTF, contacting with receptor located in thalamencephalon, decreases fat and loses weight in mice. In diet-induced obesity (DIO) mice model, CNTF has the same function. Noticeably, this model represents the real instance of human

X. Jin (✉) · Q. Wu · X. Liu · Y. Liu
Institute of Modern Physics, Chinese Academy of Sciences, Lanzhou, China
e-mail: jinxd@impcas.ac.cn

Y. Chen · J. Lu · L. Jiang
Lanzhou Institute of Biological Products, Lanzhou, China

obesity. Compared to banting, CNTF has no weight rebound after stopping administration. Therefore, it is promisingly developed to a new-type and a high-efficient anti-obesity product and has a prevalent clinic development future [7, 8]. Based on the natural human CNTF gene, Ying et al. in the Lanzhou Institute of Biological Products acquired CNTF-T mutant and constructed *Escherichia coli* expressing CNTF [9].

In this study, the constructed *E. coli*, which expresses recombinant CNTF, as original strain was used and irradiated with high-LET heavy ions. Mutants with increased yield and enhanced protein expression of CNTF are expected to be obtained.

124.2 Materials and Method

124.2.1 Plasmid and Strain

Recombinant plasmid including CNTF gene and transpeptidase *E. coli* were constructed by the Fourth research department, Lanzhou Institute of Biological Products.

124.2.2 Irradiation

Heavy ion irradiation (neon ions) was performed in the therapy terminal at the Heavy Ion Research Facility in Lanzhou (HIRFL). The dose averaged LET of the neon ion beam on samples was calculated to be 96.6 keV/ μm , and the dose rate was adjusted to be about 2 Gy/min. Doses from 0 to 30 Gy were applied in this work.

124.2.3 Survival Curve

Four hours before irradiation, the strains were spread on the LB plate incubated at 37 °C. After irradiation, the samples were cultured in an incubator at 37 °C until obvious colonies appeared. Single colonies were counted as survivors.

124.2.4 Growth Cycle and Viability Assay

The single colonies were isolated and cultured continuously in a rotary shaker. OD values were detected every 60 min until 16 h. At the same time, the strains were cultured on the LB plate overnight, and single colonies were counted.

124.2.5 Mutation of CNTF Protein Expression

To detect the change in CNTF protein expression after irradiation, we adopted the SDS-PAGE analysis. In brief, the strains were cultured until plateau. IPTG was added and then the strains were cultured for 4 h. The samples were lyzed by ultrasonic. Thirty micrograms of total protein was separated by SDS-PAGE, and then stained by coomassie brilliant blue R-250 and decolorized.

124.2.6 Molecular Characterization of CNTF Induced by Ion Beam Irradiation

The plasmids of the mutants, whose CNTF protein expression was higher or lower compared with control, were isolated and their genomic DNA was extracted. The CNTF gene and its upstream region were amplified with the primers TCTTACTGTCCACTGAGACAGC-. Sequencing was performed by Sangon Biotech (Shanghai) Co. The mutations were detected using Bioedit software.

124.3 Results and Discussion

After the neon ion irradiation, colonies were isolated on plates. As shown in Fig. 124.1, the survival curve exhibits that the survival fraction declined with increasing dose and the 50 % lethal dose was close to 10 Gy. After irradiation, 119 strains having viability irradiated at 10 or 30 Gy were screened. We observed the OD values (strain concentration) at different time points in growth cycle. Compared with control, the concentration of No. 59 was obviously increased by 20 % after 11 h as shown in Fig. 124.2. In viability experiment, we found that the No. 48 strain was more active than control, that the number of colonies was 181 which was much higher than control (143) by a factor of 1.26 (Fig. 124.3).

In order to obtain the mutants of CNTF protein expression, we analyzed the change in CNTF protein expression in strains after irradiation. As shown in Fig. 124.4, we found after heavy ions irradiation, compared with control, CNTF contents in No. 7, 49, and 103 were increased obviously, and the contents were lower in No. 60 and 70 than control.

Sequencing analysis of the CNTF fragments amplified from mutant lines shows that single nucleotide deletions were a principal mutation in each case, and the base substitutions and insertions had also occurred. The distribution of the deleted positions appeared to be dispersed around the promoter. These deleted positions also showed no homology to pET42a, and similar sequences in the host genome were therefore searched using the BLAST algorithm. As a result of this analysis, we found that the most deletion occurred in No. 60 strain, there was G deletion in

Fig. 124.1 Survival fraction of *E. coli* after neon irradiation

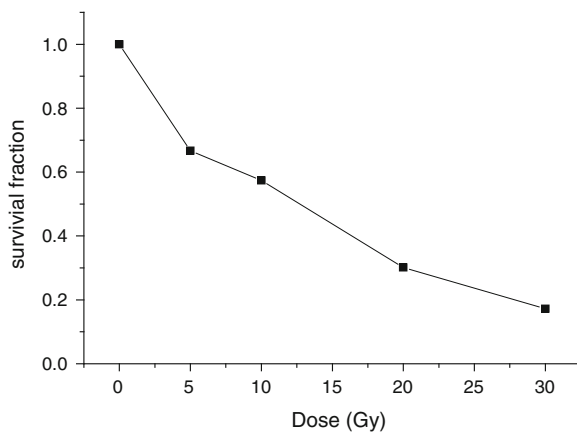


Fig. 124.2 The change of strains concentration in growth cycle irradiated with neon ions

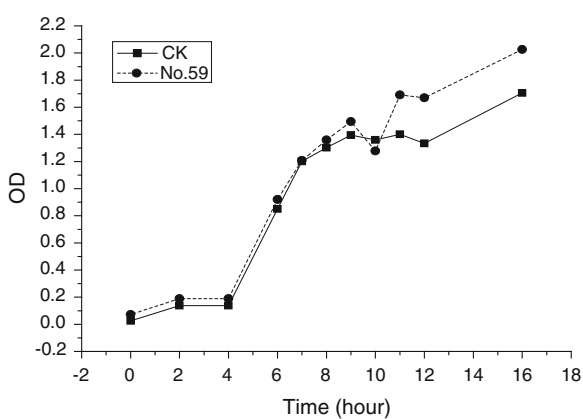
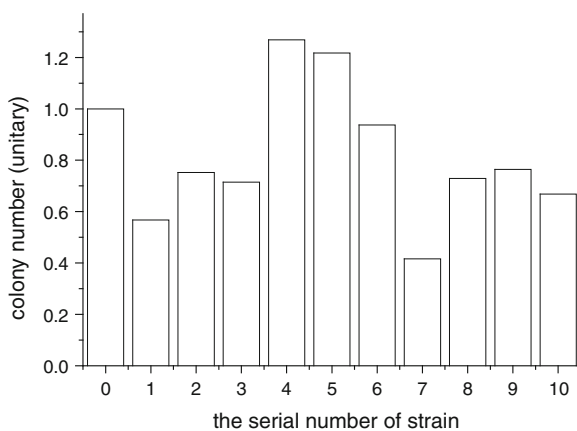


Fig. 124.3 The results of viability experiment, 0 and 4, represent control and No. 48 strains, respectively



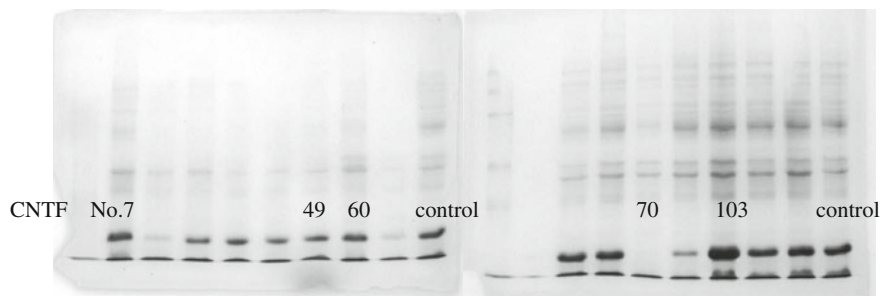


Fig. 124.4 CNTF protein expression in *E. coli* after heavy ions irradiation

the 1685 position, A in 1707, A in 1719, G in 1727, C in 1832, A in 1838, G in 1855, G in 1858, respectively. Moreover, 1727 and 1855 were the hottest mutant positions and G was the highest frequency to lose compared with other positions and bases in our experiments.

In this study, mutants with higher yield and enhanced protein expression compared with the original strain using heavy ion irradiation were obtained. In future studies, quantitative analysis will provide essential information to evaluate the efficiency of ion-beam mutagenesis.

Acknowledgments The authors are grateful to the operating crew of the HIRFL accelerator for supplying the neon ion beam for this experiment. This work is jointly supported by the National Basic Research Program of China (973 Program, No. 2010CB834203), the Western Talents Program of the Chinese Academy of Sciences (O962030XBO), and the National Natural Science Foundation of China (No. 10905080 & No. 11075191).

References

1. Hamada N, Imaok T, Masunaga S et al (2010) Recent advances in the biology of heavy-ion cancer therapy. *J Radiat Res* 51:365–383
2. Matuo Y, Nishijima S, Hase Y et al (2006) Specificity of mutations induced by carbon ions in budding yeast *Saccharomyces cerevisiae*. *Mutat Res* 602:7–13
3. Kiefer J, Stoll U, Schneider E (1994) Mutation induction by heavy ions. *Adv Space Res* 14:257–265
4. Horneck G, Krasavin EA, Kozubek S (1994) Mutagenic effects of heavy ions in bacteria. *Adv Space Res* 14:315–329
5. Hamada N, Hara T, Funayama T et al (2008) Energetic heavy ions accelerate differentiation in the descendants of irradiated normal human diploid fibroblasts. *Mutat Res* 637:190–196
6. Kruttgen A, Grotzinger J, Kurapkat G et al (1995) Human ciliary neurotrophic factor: a structure-function analysis. *Biochem J* 309:215–220
7. Gloaguen I, Coste P, Demartis A et al (1997) Ciliary neurotrophic factor corrects obesity and diabetes associated with leptin deficiency and resistance. *Proc Natl Acad Sci USA* 94:6456–6461

8. Lambert P, Anderson K, Sleeman M et al (2001) Ciliary neurotrophic factor activates leptin-like pathways and reduces body weight gain, even in leptin-resistance obesity. *Proc Natl Acad Sci USA* 98:4652–4657
9. Ying LF, Lei Q, Liang LY et al (2007) Expression and biologic activity analysis of recombinant human ciliary neurotrophic factor (CNTF) mutant. *Biotechnology* 17:16–18

Chapter 125

Molecular Characterization and Expression of Ribosomal Protein L15 Gene (*RPL15*) From *Arachis hypogaea*

Qi Wu, Xiuzhen Wang, Hongtao Yu, Yufei Ding, Fenggao Cui,
Jiancheng Zhang, Yueyi Tang and Chuantang Wang

Abstract RPL15 is a component of the large ribosomal subunit 60S. The sequences of cDNA and DNA of *RPL15* were cloned successfully from *Arachis hypogaea* cultivar Ri Hua 1. These two sequences were analyzed preliminarily. The full length *RPL15* cDNA of *A. hypogaea* contains a 615-bp open reading frame (ORF) which encodes 204 amino acids. The length of *RPL15* gene was 1383 bp with three exons and two introns. Primary structure analysis revealed that the molecular weight of the putative RPL15 protein is 24211.09 Da with a theoretical pI of 11.44. The deduced amino acid sequence of RPL15 (*A. hypogaea* cultivar Ri Hua 1) shared homology with other reported species. The expression of *RPL15* transcript showed that *RPL15* mRNA was expressed mainly in root. The cDNA of *RPL15* was cloned successfully from *A. hypogaea* in this study. It provides scientific material for enriching and improving the *RPL15* gene database.

Keywords Peanut · *Arachis hypogaea* · Ribosomal protein · RPL15 · qRT-PCR

125.1 Introduction

The ribosome of eukaryote is universal and complicated, since it is involved in the process of protein biosynthesis. Ribosomal proteins are the components of ribosome, which shows various functions in DNA repair, apoptosis, drug resistance, and proliferation [1]. Majority studies gradually reveal the physiological functions of ribosomal proteins playing an important role in human disease and development [2].

Q. Wu · X. Wang · H. Yu · Y. Ding · F. Cui · J. Zhang · Y. Tang · C. Wang (✉)
Shandong Peanut Research Institute (SPRI), Qingdao 266100, People's Republic of China
e-mail: chinapeanut@126.com

The basic step to understand the structure and cellular function of ribosome is to characterize the primary structure of the r-proteins according to the nucleotide sequences of the genes and cDNAs. The mechanism of expression and assembly of ribosome components has been studied in prokaryotes. Many studies have been done on the r-proteins in animals and yeast. Most r-protein genes are coordinately transcribed. It is demonstrated that the molecular strategies employed to maintain the coordinate synthesis of r-proteins rely on the change of cellular requirements in different tissues at different developmental stages [3].

RPL15 is a component of the large ribosomal subunit 60S which is encoded by *RPL15* gene belonging to the ribosomal proteins L15e family. This gene has homology with the yeast ribosomal protein *RPL15* gene. It is indicated that the expression of *RPL15* is markedly up-regulated in gastric cancer tissues [1] and over expressed in some esophageal tumors compared to normal matched tissues [4]. It might play a possible role in carcinogenesis of esophagus. *RPL15* gene has been reported in many plants and animals [3, 5, 6]. The expression level of *RPL15* gene is correlative with the rate of growth in petunia. Active transcription of *RPL15* is often detected in young organs [3]. However, *RPL15* from *Arachis hypogaea* has not been reported yet.

In this study, we designed primers according to the available information of homology sequences from other species to get the cDNA and genomic sequence of *RPL15* of peanut to test the relationship among these species.

125.2 Materials and Methods

125.2.1 Experimental Materials

The cultivated *A. hypogaea* L. variety Ri Hua 1 was employed in this study. All seeds were pregerminated and sown then in growth chamber that was maintained at 28 °C, 12 h photoperiod (16,000 lx). For the case of specific tissue expression patterns, we took three samples at the second month after seeding. The root, stem, and leaf organs of each specimen were dissected out and snapped frozen in liquid nitrogen for the experiment.

125.2.2 Full Length cDNA Cloning

Total RNA was extracted from leaf using Trizol Reagent according to the manufacture's protocol (Invitrogen, USA). cDNA was synthesized from total RNA with M-MLV reverse transcriptase (Promega USA) and Oligo(dT) primer. A pair of specific primers RPL15-F1 and RPL15-R1 was designed based on the homologous sequence of *Glycine max* (Glyma05g04870.1) to clone the *RPL15* gene EST

sequence of *A. hypogaea* (Table 125.1). Simple PCR reactions were performed in a Thermal Cycler in a 25- μ L reaction volume containing 12.5 μ L of 2 \times PCR buffer (Tiangen, China), 1.0 μ L of each primer (10 μ mol/L) and 1 μ L of template mix (about 50 ng/ μ L). Lastly PCR-grade water was added to complement the volume into 25 μ L. The PCR temperature profile was 94 $^{\circ}$ C for 5 min, followed by 30 cycles of 94 $^{\circ}$ C for 40 s, 57 $^{\circ}$ C for 40 s, 72 $^{\circ}$ C for 2 min, and the final extension step at 72 $^{\circ}$ C for 10 min. PCR products were analyzed on 1.2 % agarose gel and the target band was purified and cloned into the pMD18-T vector (Takara, Japan). After being transformed into the competent cells of *Escherichia coli* Top10, the positive recombinants were identified through anti-Amp selection and PCR screening with M13-47 and RV-M primers (Table 125.1). The positive clones were sequenced on an ABI3730 Automated Sequencer (Applied Biosystems, USA).

Based on the partial sequence data of *RPL15*, 3' and 5' ends of cDNA were determined by SMART-RACE approaches (Clontech, USA). The 3'-end was cloned by primer RPL15-F2 and UPM primer in the first round PCR, and RPL15-F3 and NUP primers in the second round PCR. For 5' end RACE PCR, the first strand cDNA was tailed at the 5'-end by terminal transferase TdT and dCTP. Primers RPL15-R2 and UPM were in the first round PCR and RPL15-R3 and NUP primers were in the second round PCR (Table 125.1). All the PCR products were cloned and sequenced following the procedures described above.

Table 125.1 Sequences of primers used in this study

Primers	Sequence (5'-3')	Application
RPL15-F1	TTTATGGCAAGCCCACGAACC	Expressed sequence tag
RPL15-R1	GTAAACCCCTGTTAGACTTCC	Expressed sequence tag
M13-47	CGCCAGGGTTTTCCAGTCACGAC	Vector universal primers
R-VM	GAGCGGATAACAATTTACACACAGG	Vector universal primers
RPL15-F2	TATGTGGTCTACCGTGTTCGTGTG	3' RACE first round PCR
RPL15-F3	GCCCACGAACCAGGGTGTACTCA	3' RACE second round PCR
RPL15-R2	GACGAGCCTTGTCGGGGCGGGTTG	5' RACE first round PCR
RPL15-R3	TCTCATTACATCCGATTGCTTCTT	5' RACE second round PCR
UPM	Long: ctaatagactcactatagggcAAGCAGTGGT ATCAACGCAGAGT	3', 5' RACE Universal Primer
NUP	Short: ctaatagactcactatagggc AAGCAGTGGTATCAACGCAGAGT	3', 5' RACE Nested Universal Primer
RPL15-F	ATGGGTGCTTACAAGTATGTTTCGG	Complete cDNA amplify
RPL15-R	TCAACGGTAACGGCGGAGGGAAAGG	Complete cDNA amplify
qRPL15-f	TATGTGGTCTACCGTGTTCGTGTG	RPL15 qRT-PCR
qRPL15-r	TAACACCCTGGTTCGTGGGCTTGC	RPL15 qRT-PCR
Actin-f	TTGGAATGGGTGAGAAGGATGC	Actin qRT-PCR
Actin-r	AGTGGTGCCTCAGTAAGAAGC	Actin qRT-PCR

125.2.3 Cloning the Genomic Sequence of RPL15

The genomic DNA was isolated from leaf using Genomic DNA Purification Kit (Tiangen, China) and dissolved in TE buffer (10 mmol/L Tris/1 mmol/L EDTA, pH8.0) stored at -20°C . According to the full length cDNA of *RPL15* gene from *A. hypogaea* and *G. max* (Glyma05g04870.1), RPL15-F and RPL15-R were designed to amplify the whole sequence of *A. hypogaea RPL15* gene (Table 125.1). Purified PCR products were cloned into the pMD18-T vector (Takara, Japan) and sequenced in both directions as above.

125.2.4 Sequence Analysis, Multiple Sequences Alignment and Phylogenetic Analysis

The homology searches of nucleotide and protein sequences were conducted with BLAST algorithm at the National Center for Biotechnology Information (<http://www.ncbi.nlm.gov/blast>). The nucleotide and deduced amino acid sequences were analyzed using software BioEdit 7.0.9.0 [7]. A multiple sequences alignment was performed with ClustalX 1.83 program [8] and a phylogenetic Neighbor-Joining (NJ) tree was constructed. To derive the confidence value for the phylogeny analysis, bootstrap trials were replicated 1,000 times [9]. The calculated molecular mass and the theoretical isoelectric point were predicted by Protein Mol Wt & AA Composition Calculator (http://www.proteomics.com.cn/proteomics/pi_tool.asp). The motif sequences were searched using the software of SMART (<http://smart.embl-heidelberg.de/>).

125.2.5 RPL15 mRNA Distribution in Different Tissues

The expression of *RPL15* mRNA transcript in root, stem, and leaf were determined by quantitative real-time RT-PCR. Total RNA was extracted according to the protocol of Trizol (Invitrogen, USA). The quantity of total RNA was detected by 1.2 % agarose gel. MMLV reverse transcriptase (Promega, USA) was used to synthesize single-strand cDNA with oligo(dT) primer (Table 125.1). The mixture was incubated at 42°C for 1 h, terminated the reaction by heating at 85°C for 5 min, and subsequently stored at -80°C . The cDNA was diluted 10 times by DEPC-treated water for the next step.

The quantitative real-time RT-PCR assay was carried out in a Roche Light-Cycler 2.0. The PCR was performed in a total volume of 20 μL , containing 10 μL of $2 \times$ SYBR Green Master Mix (Takara, Japan), 2 μL of the diluted cDNA mix, 0.5 μL of each primers ($10 \mu\text{mol l}^{-1}$), and 7 μL of DEPC-water. A 93-bp product was amplified with qRPL15-f and qRPL15-r from cDNA template and then

sequenced to verify the PCR specificity. A pair of β -actin primers, actin-f/actin-r, were used to amplify a 195-bp fragment as an internal control to verify the successful reverse transcription and to calibrate the cDNA template.

The SYBR Green RT-PCR assay was carried out at 95 °C for 30 s, followed by 45 cycles of 95 °C for 5 s, 60 °C for 20 s and 72 °C for 15 s. In a 32-well plate, each sample was run in triplicate along with the internal control gene. Melting curve analysis of amplification products was done at the end of PCR reaction to confirm that PCR product was the only amplified product. To maintain consistency, the baseline was set automatically by the software. The comparative Ct method [10] was used to analyze the relative expression level of *RPL15*. The Ct for the target amplified *RPL15* and the internal control β -actin were determined for each sample. All data were given in terms of relative mRNA expression as mean \pm S.D. The results were subjected to analysis of *t* test, and the *P* values less than 0.05 were considered statistically significant.

125.3 Results

125.3.1 Molecular Characterization of *RPL15* cDNA

The full length cDNA of *RPL15* from *A. hypogaea* (GenBank number JX424591) contains a 615 bp open reading frame (ORF) which encodes 204 amino acids with ATG as initiation codon and TGA as stop codon, which contains 25.37 % A, 23.58 % C, 27.8 % G, and 23.25 % T. The nucleotide sequence and the deduced amino acid sequence are shown in Fig. 125.1. The calculated molecular mass of the deduced mature RPL15 was 24211.09 Da and the protein had a theoretical isoelectric point of 11.44. The analysis with SMART revealed that the *RPL15* gene encodes a novel protein containing a typical ribosomal protein L15e domain (M1 to S170). RPL15 of *A. hypogaea* 3D model was constructed by the SWISS-MODEL Protein Modelling Server (<http://swissmodel.expasy.org/>) (Fig. 125.2). The ratios of structure alpha helix and random coil were 32.84 and 40.20 %, respectively (Fig. 125.2).

125.3.2 Genomic Sequences of *RPL15*

The full length of *RPL15* gene was 1383 bp (GenBank accession no. JX424603), which made up of three exons and two introns. The introns were located within the whole open reading frame. The first intron is 684 bp starting from 172 bp to 855 bp while the second intron is 84 bp from 1054 bp to 1137 bp. And all exon–intron junctions follow the consensus rule of the splice acceptor- AG/GT -splice donor for splicing.

Table 125.2 A listing of the species in this study

Species	Lineage	Accession number
<i>A. hypogaea</i> Ri Hual	Dicotyledon	JX424591
<i>Arabidopsis thaliana</i>	Dicotyledon	NP_193405.1
<i>Vitis vinifera</i>	Dicotyledon	XP_002264206.1
<i>Populus trichocarpa</i>	Dicotyledon	XP_002304285.1
<i>Glycine max</i>	Dicotyledon	Glyma05g04870.1
<i>Oryza sativa Japonica Group</i>	Monocotyledon	NP_001050612.1
<i>Caenorhabditis elegans</i>	Nemathelminthes Invertebrate	NP_499964.1
<i>Chlamydomonas reinhardtii</i>	Chlorophyta	XP_001701780.1
<i>Danio rerio</i>	Osteichthyes Vertebrata	NP_001003447.1
<i>Mus musculus</i>	Rodentia Mammalia Vertebrata	XP_001481087.1
<i>Homo sapiens</i>	Hominoid Mammalia Vertebrata	NP_002939.2

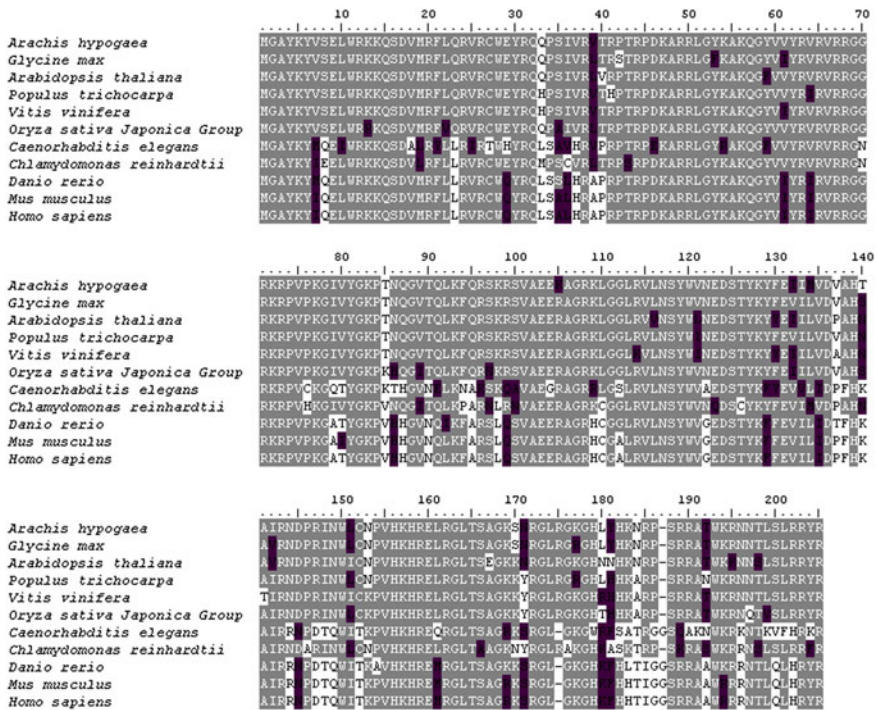


Fig. 125.3 The alignments of deduced amino acid sequences of RPL15 with those from other species. Identical amino acids are marked by gray and dashes mark gaps optimizing sequence alignment. Variant sites are marked by black

showed in Fig. 125.5. *RPL15* mRNA was the most expressed in root and a little bit fewer in leaf and stem. However, no significant differences were found between tissues ($P > 0.05$) (Fig. 125.5).

Table 125.3 The similarity of RPL15 protein sequences between species

Species	A. <i>Hypogaea</i>	G. <i>Max</i>	A. <i>Thaliana</i>	P. <i>Trichocarpa</i>	V. <i>Vinifera</i>	O. <i>Sativa</i>	C. <i>Elegans</i>	C. <i>Reinhardtii</i>	D. <i>Rerio</i>	M. <i>Musculus</i>	H. <i>Sapiens</i>
<i>A. hypogaea</i>	–	0.95	0.911	0.931	0.916	0.906	0.619	0.813	0.721	0.712	0.712
<i>G. max</i>	0.95	–	0.906	0.926	0.901	0.897	0.604	0.799	0.721	0.712	0.712
<i>A. thaliana</i>	0.911	0.906	–	0.892	0.906	0.872	0.619	0.789	0.702	0.697	0.697
<i>P. trichocarpa</i>	0.931	0.926	0.892	–	0.936	0.901	0.624	0.808	0.731	0.721	0.721
<i>V. vinifera</i>	0.916	0.901	0.906	0.936	–	0.901	0.634	0.789	0.731	0.721	0.721
<i>O. sativa</i>	0.906	0.897	0.872	0.901	0.901	–	0.619	0.799	0.712	0.712	0.712
<i>C. elegans</i>	0.619	0.604	0.619	0.624	0.634	0.619	–	0.604	0.75	0.759	0.764
<i>C. reinhardtii</i>	0.813	0.799	0.789	0.808	0.789	0.799	0.604	–	0.687	0.687	0.687
<i>D. rerio</i>	0.721	0.721	0.702	0.731	0.731	0.712	0.75	0.687	–	0.95	0.955
<i>M. musculus</i>	0.712	0.712	0.697	0.721	0.721	0.712	0.759	0.687	0.95	–	0.995
<i>H. sapiens</i>	0.712	0.712	0.697	0.721	0.721	0.712	0.764	0.687	0.955	0.995	–

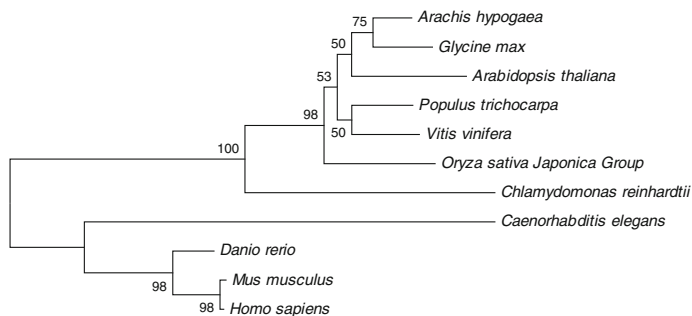


Fig. 125.4 The NJ phylogenetic tree of RPL5 protein sequences from eleven species. The protein sequences used for phylogenetic analysis are as follows: *A. hypogaea* Ri Hua 1 (JX424591), *Arabidopsis thaliana* (NP_193405.1), *Vitis vinifera* (XP_002264206.1), *Populus trichocarpa* (XP_002304285.1), *Glycine Max* (Glyma05g04870.1), *Oryza sativa Japonica Group* (NP_001050612.1), *Caenorhabditis elegans* (NP_499964.1), *Chlamydomonas reinhardtii* (XP_001701780.1), *Danio rerio* (NP_001003447.1), *Mus musculus* (XP_001481087.1), *Homo sapiens* (NP_002939.2)

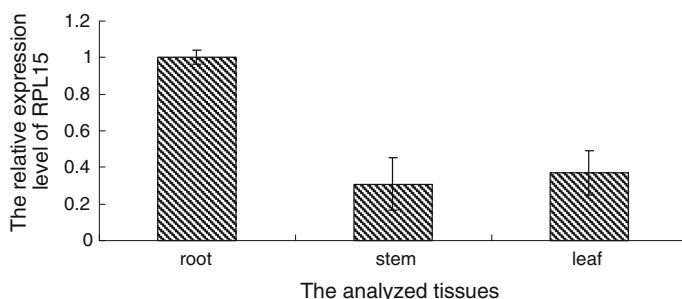


Fig. 125.5 Tissues distribution of the *RPL15* transcripts measured by SYBR Green qRT-PCR. The tissues, including root, stem, and leaf, were collected from three individual *A. hypogaea* cultivar Ri Hua 1. Vertical bars represent the mean \pm S.D

125.4 Discussions

Here, we reported the characterization of cDNA and genomic sequences of *RPL15* gene of *A. hypogaea*. A comparison of the deduced amino acid sequences from eleven species including plants and animals indicated that *RPL15* is highly conserved and remain essentially the same. There is not any deletion or insertion of amino acid residue in alignment sequences. RPL15 is a highly basic ribosomal protein containing a composition of 33 Arg, 19 Lys, 18 Val, 16 Gly and 5 His residues and only 5 Asp and 7 Glu residues, in which the highest content of Arg residues (16.10%), is far higher than other amino acids and Cys content of the

lowest, only 0.98 %. *RPL15* is conserved either in plants or animals. According to the phylogenetic tree, we can see that the division of *RPL15* may be earlier than the formation of plant and animal. It has been forming the specific function for plant and animal to adapt different environment. Protein synthesis in all organisms requires r-proteins and rRNA components into the ribosome complex. In this study, the results of the real-time RT-PCR showed that *RPL15* mRNA was the most expressed in root and a little bit fewer in leaf and stem.

125.5 Conclusions

The characterization of DNA and cDNA clones encoding ribosomal proteins would be beneficial in the study of ribosomal biogenesis and allow the elucidation of structure and regulation of genes encoding ribosomal proteins in eukaryote. These data will enrich and supplement the information about *RPL15*. This paper provides theoretical references for the construction of molecular phylogenetic tree. In addition, it will contribute to the discussion of the genetic polymorphism.

Acknowledgments The authors wish to express their sincere thanks to all the laboratory members for continuous technical advice and helpful discussion. This research was supported from Qingdao Science and Technology Support Program (12-1-4-11-(1)-jch, 11-2-4-9-(3)-jch), and China Agricultural Research System (CARS-14).

References

1. Wang H, Zhao LN, Li KZ et al (2006) Overexpression of ribosomal protein L15 is associated with cell proliferation in gastric cancer. *BMC Cancer* 6:91–98
2. Yang F, Liu WP (2005) Study on the relation of ribosomal protein gene and human diseases. *Chin J Clin Exp Pathol* 3:354–356
3. Lee HS, Mun JH, Kim SG (1999) Characterization of cDNA encoding cytoplasmic ribosomal protein L15 and L27a in petunia (*Petunia hybrida*): Primary structures and coordinate expression. *Gene* 2:155–163
4. Wang Q, Yang C, Zhou J et al (2001) Cloning and characterization of full-length human ribosomal protein L15 cDNA which was overexpressed in esophageal cancer. *Gene* 263:205–209
5. Tom M, Waterman MR, Bocking D et al (1999) Cloning and characterization of the L15 ribosomal protein gene homologue from the crayfish *Orconectes limosus*. *Biochem Biophys Res Comm* 2:313–316
6. Xiang Z, Zhang JN, Song P et al (2006) The study of ribosomal protein L15 cDNA sequences as a molecular marker in the teleostei phylogenetic analysis. *Hereditas (BEIJING)* 28:171–178
7. Hall TA (1999) BioEdit: a user-friendly biological sequence alignment editor and analysis program for Windows 95/98/NT. *Nucleic Acids Symp Ser* 41:95–98
8. Thompson JD, Gibson TJ, Plewniak F et al (1997) The ClustalX windows interface: flexible strategies for multiple sequence alignment aided by quality analysis tools. *Nucleic Acids Res* 25:4876–4882

9. Tamura K, Dudley J, Nei M et al (2007) MEGA4: Molecular Evolutionary Genetics Analysis (MEGA) software version 4.0. *Mol Biol Evol* 24:1596–1599
10. Livak KJ, Schmittgen TD (2001) Analysis of relative gene expression data using realtime quantitative PCR and the $2^{-\Delta\Delta C(T)}$ method. *Methods* 25:402–408

Chapter 126

Optimization of Extraction Conditions for Glycosaminoglycan from *Urechis unicinctus* by Response Surface Methodology

Chunying Yuan, Xu Han, Qingman Cui and Ping Liu

Abstract The enzyme dosage, enzymolysis time, and alcohol precipitation concentration as independent variables and the extraction rate as the response value, the extraction technology of glycosaminoglycan from *Urechis unicinctus* was optimized via response surface methodology on the basis of single-factor experiments. The extraction rate of glycosaminoglycan was affected in the following order: concentration of alcohol precipitation > enzymolysis time > enzyme dosage. The optimal conditions for the glycosaminoglycan extraction were as follows: alcohol precipitation concentration 75 %, enzymolysis time 4 h, and enzyme dosage 0.4 %.

Keywords *Urechis unicinctus* · Glycosaminoglycan · Optimization of extraction conditions · Response surface methodology

126.1 Introduction

Glycosaminoglycans, such as heparin, heparan sulfate, chondroitin sulfate, dermatan sulfate, hyaluronic acid, and keratan sulfate, are polysaccharides containing uronic acid and hexosamine. They not only exhibit anticoagulant, hypolipidemic, antitumor, and antiviral activities, but also enhance the body's immune system [1, 2]. Glycoproteins or glycosaminoglycans have been extracted from *Argopecten irradians*, *Ruditapes philippinarum*, *Simonovacula constricta*, *Scapharca subcrenata*, *Macra veneriformis*, and *Bullacta exarata* et al., and some of their activities have been investigated [3–10]. *Urechis unicinctus* is a species of marine spoon worms, also known as sea intestines, mainly distributed in the Yellow Sea, Bohai Coast. It

C. Yuan (✉) · X. Han · Q. Cui · P. Liu

Key Laboratory for Marine Chemistry and Resource, College of Marine Science and Engineering, Tianjin University of Science and Technology, Tianjin 300457, China
e-mail: cqm80@163.com

is rich in protein and many essential amino acids. Research had shown that the polypeptide extracted from *U. unicinctus* exhibited a certain antitumor activity and improved the immune function of mice, and the fibrinolytic enzyme extracted from the same species had antithrombotic effects [11, 12]. In order to utilize fully the quality resources, we optimized the extraction methods of glycosaminoglycan from *U. unicinctus*.

126.2 Materials and Methods

126.2.1 Materials

U. unicinctus were purchased from farmers' markets in Tianjin Tanggu. Trypsin (enzyme activity, 250 U/g; optimum temperature, 50 °C; optimum pH of 8.0) was purchased from Beijing Solarbio Science & Technology Co., Ltd. A Ds-1 high-speed organization broken machine, a SHA-C water bath oscillator, a T6 new century UV/Vis spectrophotometer, a TGL-16LM high-speed refrigerated centrifuge, a 99-1 magnetic stirrer, a RE-3000 rotary evaporator, and a FD-10-50 vacuum lyophilizer were also used in the experiment.

126.2.2 Methods

126.2.2.1 Glycosaminoglycan Extraction Process

U. unicinctus samples were homogenized and subjected to autolysis and enzymolysis. Subsequently, enzyme inactivation, decoloration, centrifugation, deproteinization, and alcohol precipitation were performed. The samples were then washed with ethanol and acetone before drying.

126.2.2.2 Determination of Glycosaminoglycan Content

Glycosaminoglycan content was determined by Alcian Blue colorimetric assay [13].

126.2.2.3 Experimental Design of the Response Surface

Enzyme dosage, enzymolysis time, and concentration of alcohol precipitation were represented by A, B, and C, respectively. The extraction rate of glycosaminoglycan was expressed as the response value *Y*. The experimental factors and levels obtained in this study are shown in Table 126.1.

Table 126.1 Coded values of experimental factors and levels

Factor	Coded values		
	1	0	-1
A	0.20	3	60
B	0.40	4	70
C	0.60	5	80

126.2.3 Statistical Analysis

The experimental results were analyzed and processed using Design Expert 7.0.

126.3 Experimental Results

126.3.1 Experimental Results and Analysis of Response Surface

The experiment was optimized using a Box–Behnken design. The experimental program and results are detailed in Table 126.2.

Quadratic regression models were fitted, and the regression analysis and results were reported in Tables 126.3, 126.4, 126.5.

As shown in Tables 126.3 and 126.4, the model was very significant ($P < 0.001$), and lack of fit was not significant ($P > 0.05$). These results suggested that the experimental program was reliable, and the selected model fitted the actual situation well.

Table 126.2 Experimental program and results of response surface

Run	A/ %	B/h	C/ %	Y %
1	0.20	3	70	0.03726
2	0.20	5	70	0.03787
3	0.20	4	60	0.03478
4	0.40	3	60	0.03264
5	0.40	5	80	0.06396
6	0.60	4	80	0.04289
7	0.60	3	70	0.03415
8	0.40	5	60	0.03347
9	0.60	4	60	0.02969
10	0.40	4	70	0.07196
11	0.20	4	80	0.05617
12	0.40	4	70	0.06844
13	0.60	5	70	0.04905
14	0.40	3	80	0.06534

According to the P values in Table 126.3, the extraction rate was affected in the following order: concentration of alcohol precipitation > enzymolysis time > -enzyme dosage.

The multiple correlation coefficient and correcting correlation coefficient were 0.9926 and 0.9758 respectively, and the variation coefficient of Y was lower, indicating that the predicted values of the model fitted the experimental values well and the reliability of the experiment was higher (Table 126.5). Therefore, the best extraction conditions could be determined using the regression model, and the regression equation was determined ultimately as follows:

$$Y = 0.072 - 0.002763A + 0.003358B + 0.010C + 0.004798AB - 0.002873AC + 0.002198BC - 0.018A^2 - 0.012B^2 - 0.014C^2$$

Table 126.3 Variance analysis of regression model

Variance source	Sum of square	Degrees of freedom	Mean square	F -value	P -value
Model	0.0027	9	0.0027	59.27	0.0007
A	6.105×10^{-5}	1	6.105×10^{-5}	12.24	0.0249
B	9.018×10^{-5}	1	9.018×10^{-5}	18.08	0.0131
C	0.0008	1	0.0008	165.52	0.0002
AB	9.206×10^{-5}	1	9.206×10^{-5}	18.45	0.0127
AC	3.301×10^{-5}	1	3.301×10^{-5}	6.62	0.0618
BC	1.932×10^{-5}	1	1.932×10^{-5}	3.87	0.1205
A^2	0.0011	1	0.0011	210.56	0.0001
B^2	0.0004	1	0.0004	88.91	0.0007
C^2	0.0006	1	0.0006	122.57	0.0004

Table 126.4 Lack-of-fit test and error analysis of regression model

Variance source	Sum of squares	Degrees of freedom	Mean square	F -value	P -value
Residuals	1.996×10^{-5}	4	4.989×10^{-6}		
Lack of fit	1.984×10^{-5}	3	6.614×10^{-6}	57.41	0.0966
Pure error	1.152×10^{-7}	1	1.152×10^{-7}		
The total deviation	0.027	13			

Table 126.5 Credibility analysis of regression model

Item	Value	Item	Value
Standard deviation	0.0022	Multiple correlation coefficient R^2	0.9926
Mean	0.047	Correcting correlation coefficient R^2	0.9758
Variation coefficient	4.730	Predicting correlation coefficient R^2	0.8814
PRESS	0.0003	The ratio of signal to noise	22.361

126.3.2 Determination of Optimal Extraction Conditions

The response surface analysis charts were plotted based on response surface regression analysis and the regression equation (Figs. 126.1, 126.2, 126.3). The Y values gradually increased with increasing enzymolysis time and enzyme dosage, reached their maximum at certain values of enzymolysis time and enzyme dosage, and then gradually decreased with increasing enzymolysis time and enzyme dosage (Fig. 126.1). A similar phenomenon appeared in Figs. 126.2 and 126.3. Three graphs exhibited an opening downward, convex surface, indicating that maximum response values were obtained. The contour center of these graphs was located in -1 to 1 , revealing that the optimal extraction conditions existed at the levels of the designed factors. The optimal conditions of extraction were as follows: enzyme dosage (A) = 0.38 %, enzymolysis time (B) = 4.16 h, and

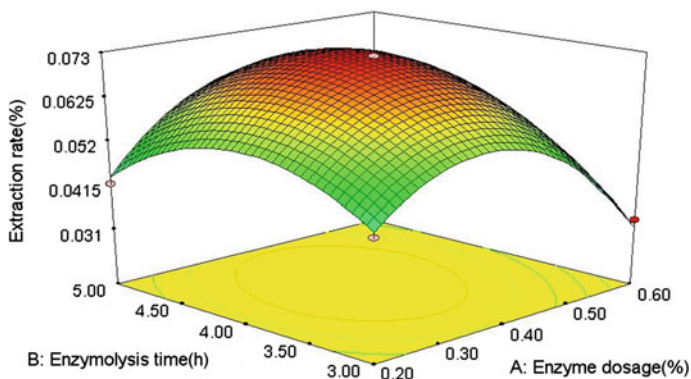


Fig. 126.1 Effects of enzymolysis time and enzyme dosage on the extraction rate of glycosaminoglycan

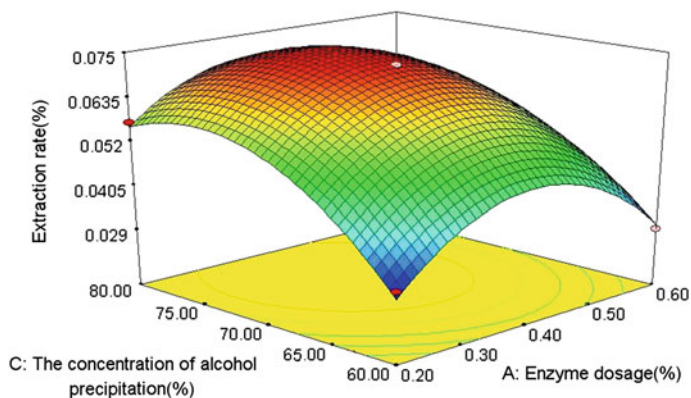


Fig. 126.2 Effects of concentration of alcohol precipitation and enzyme dosage on the extraction rate of glycosaminoglycan

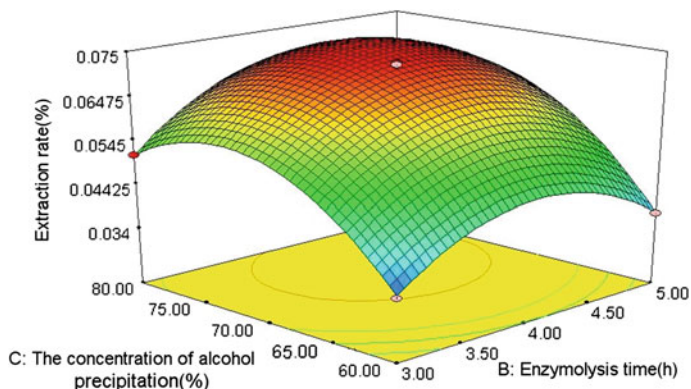


Fig. 126.3 Effects of concentration of alcohol precipitation and enzymolysis time on the extraction rate of glycosaminoglycan

concentration of alcohol precipitation (C) = 73.89 %, the predicted extraction rate was 0.075 %, and the actual extraction rate based on three validation experiments was 0.074 %. The optimal extraction conditions were modified considering operation convenience as enzyme dosage (A) = 0.4 %, enzymolysis time (B) = 4 h, and concentration of alcohol precipitation (C) = 75 %, the actual extraction rate was 0.076 % under these conditions, with only little difference between the actual and theoretical extraction rates, indicating that the parameters of extraction obtained using the response surface method were accurate and reliable, and the model exhibited a higher application value.

126.4 Conclusion

In this paper, we have determined the order of affecting extraction rate of glycosaminoglycan from *U. unicinctus*: concentration of alcohol precipitation > enzymolysis time > enzyme dosage. We have also identified the following optimal extraction conditions using response surface methodology: concentration of alcohol precipitation, 75 %; enzymolysis time, 4 h; enzyme dosage, 0.4 %, and the glycosaminoglycan extraction rate was 0.076 % under these conditions.

Acknowledgments This research was supported by the Tianjin Program of Revitalizing the Sea by Science and Technology (Grant No. KX2010-0003).

References

1. Wang YC, Guan HS, Li BF (1995) Status and prospects of glycosaminoglycan. *Prog Bioeng* 6:2–10
2. Kariya Y, Watabe S, Ochiai Y et al (1990) Glycosaminoglycan from the body wall of sea cucumber, *Stichopus japonicus*. *CompBiochem Physiol* 2:387–392
3. Wang CY, Guan HS (1995) Studies on methods of extraction and purification of glycosaminoglycans from *Argopecten irradians* Larmarck. *J Qingdao Ocean Univ* 4:203–208
4. Wang RF, Wu HM, Fan XP (2008) Purification and monosaccharide composition analysis of glycosaminoglycans of *Ruditapes philippinarum*. *J Guangdong Ocean Univ* 6:25–29
5. Lei XL, Wu HM, Fan XP et al (2004) Extraction and isolation of glycosaminoglycan from *Sinonovacula constricta* and its anti-tumor activity in vitro. *Pharm Biotech* 3:146–149
6. Hu XQ, Wu HM, Lin ZM et al (2008) Preliminary study on physicochemical property of glycosaminoglycan from *Scapharca subcrenata* lisehke and its effects on immune organs of mice. *Mod Food Sci Tech* 8:763–766
7. Yuan CY, Cui QM, Sun XP et al (2011) Optimization of extraction conditions for glycosaminoglycan from *Macra veneriformis* by response surface methodology. *Food Ind* 11:18–21
8. Yuan CY, Cui QM, Sun XP et al (2011) Study on purification and functional activity of glycosaminoglycan from *Macra quadrangularis*. *J Anhui Agric Sci* 10:5882–5884
9. Xu JL, Cui QM, Yuan CY et al (2012) Study on optimization of extraction technology for glycosaminoglycan from *Bullacta exarata* by response surface method. *J Anhui Agric Sci* 6:3559–3561
10. Yuan CY, Xu JL, Cui QM (2011) Purification and analysis of chemical compositions on glycosaminoglycan from *Bullacta exarata*. The 3rd ICBNPTM, Xi An, pp. 186–188
11. Zhao X (2008) Research on purification and characteristics of polypeptides from *Urechis unicinctus*. *Ocean Univ China, Qingdao*, pp. 19–43
12. Chu JX, Cai WD, Han BQ et al (2010) Thrombolytic effect, hemolytic toxicity and acute toxicity of the fibrinolytic enzyme UFEI from *urechis unicinctus*. *Pharm Biotech* 17(4):331–333
13. Glod EW (1979) A simple spectrophotometric method of estimating glycosaminoglycan concentrations. *Anal Biochem* 99:183–188

Chapter 127

Quantitative Trait Loci Mapping of Unstripped Germ Rate in Milled Rice

Shengbin Liu, Fang Wang, Zetian Hua, Meng Meng, Fei Zhao
and Xin Liu

Abstract The objectives of this study were to investigate the genetic factors controlling unstripped germ rate in milled rice using Quantitative trait loci (QTL) analysis. A linkage map consisting of 80 DNA markers was constructed by using 224 recombinant inbred lines (RILs). A total of 8 QTLs located on chromosomes 3, 4, 6, 7, 8, 9, and 12 were detected. These QTLs explained phenotypic variations ranging from 26.44 to 57.28 %. The results and the tightly linked molecular markers that flank the QTL will be useful for improvement of quality in rice breeding.

Keywords QTL · Mapping · Unstripped germ rate · Milled rice · RILs

127.1 Introduction

With the population enlarging, the global demand of cereal grains is increasing. It is estimated that the world population may reach 8.9 billion in 2025 [1], and the total food product needs an increase more than 50 % [2]. As one of the most important staple food crops, rice (*Oryza sativa* L.) plays an important role in food security in China. Rice quality depends on many attributes of the rice grain and is also related to preference among different cultures and habits, its major elements include milling performance, appearance, cooking, eating, and nutrient quality.

With the rapid development in researches of Quantitative trait loci (QTL) based on molecular linkage mapping, many studies have been conducted in recent years that have identified a large number of QTLs for morphological and agronomic

S. Liu · F. Wang · Z. Hua (✉) · M. Meng
College of Food Engineering and Biotechnology, Tianjin University of Science
and Technology, Tianjin 300457, People's Republic of China
e-mail: liushengbin2012@126.com

S. Liu · F. Wang · Z. Hua · F. Zhao · X. Liu
Chinese National Engineering Research Center for Japonica Rice,
Tianjin 300457, People's Republic of China

traits of rice [3–8]. However, to our knowledge, genetic analysis of QTLs associated with unstripped germ rate in milled rice has not been conducted. The objectives of this study were to identify QTLs for unstripped germ rate traits in milled rice using recombinant inbred lines (RILs) from cross Z601 and C14, so to provide basic information for breeding new rice varieties with higher quality through DNA molecular marker techniques.

127.2 Materials and Methods

127.2.1 Plant Materials

The RILs in this study were kindly provided by Professor Zetian Hua of Chinese National Engineering Research Center for Japonica Rice. A set of 224 F₅ RILs, derived from a cross between Z601 (high unstripped germ rate) and C14 (low unstripped germ rate) via single-seed descent, were used in the current study. All plants of the RILs and the two parental lines were planted in the rice cropping season in Tianjin, China and the seeds harvested at maturation were stored at a temperature lower than 10 °C for use.

127.2.2 DNA Preparation and PCR Amplification

DNA was extracted from fresh leaves of 224 RIL individuals and their parents using the SDS method [9–12]. The extracted DNA was dissolved in TE buffer and tested for quality and quantity. Then, these 224 DNA samples were diluted into 25 ng/ml with sterilized double distilled water and stored at 4 °C for the polymerase chain reaction (PCR). PCR [13] was performed with an initial 4 min period at 94 °C, followed by 40 cycles of 30 s of denaturing at 94 °C, 30 s of annealing at 56 °C, and 30 s of extension at 72 °C, and a final 10 min extension at 72 °C. PCR products with large difference were separated on 3 % agarose gel and detected by using a UV-GIS detection system [14].

127.2.3 Linkage Map Construction and Data Analysis

The genotypic constitution of 224 individuals from the RIL population with respect to 80 simple sequence repeats (SSRs) was used to construct a genetic map. This map spanned 1889.15 cM with the mean inter-marker distance of 27.0 cM and involved all 12 rice chromosomes [15]. Composite interval mapping was performed to identify QTL by using the software package QTL IciMapping V3.0, with a LOD threshold of 2.5 for declaring the presence of a putative QTL [16–19]. For the designation of QTL, we followed the rule formulated by McCouch [20].

127.3 Results and Discussion

127.3.1 Distribution of Unstripped Germ Rate in the Segregating RIL Population

10 g rice of every segregating RIL population was dealt with by Detecting System for Appearance Quality of Rice and Seeds. The differences between the two parents Z601(83.62 %) and C14(5.42 %) were rather big, significant differences were observed in the RIL population. The average values of the unstripped germ rate were studied, namely, UGR. Unstripped germ rate of RIL population is presented in Fig. 127.1. In the analyzed data, normal distribution and transgressive segregation in RIL population were observed, indicating that unstripped germ rate was quantitatively inherited and suitable for QTL analysis.

127.3.2 QTLs for UGR

Eight QTLs governing UGR were identified and mapped to chromosomes 3, 4, 6, 7, 8, 9, and 12 (Table 127.1 and Fig. 127.2). These QTLs explained phenotypic variations ranging from 26.44 to 57.28 %.

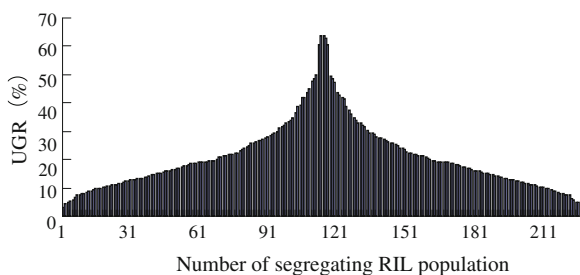
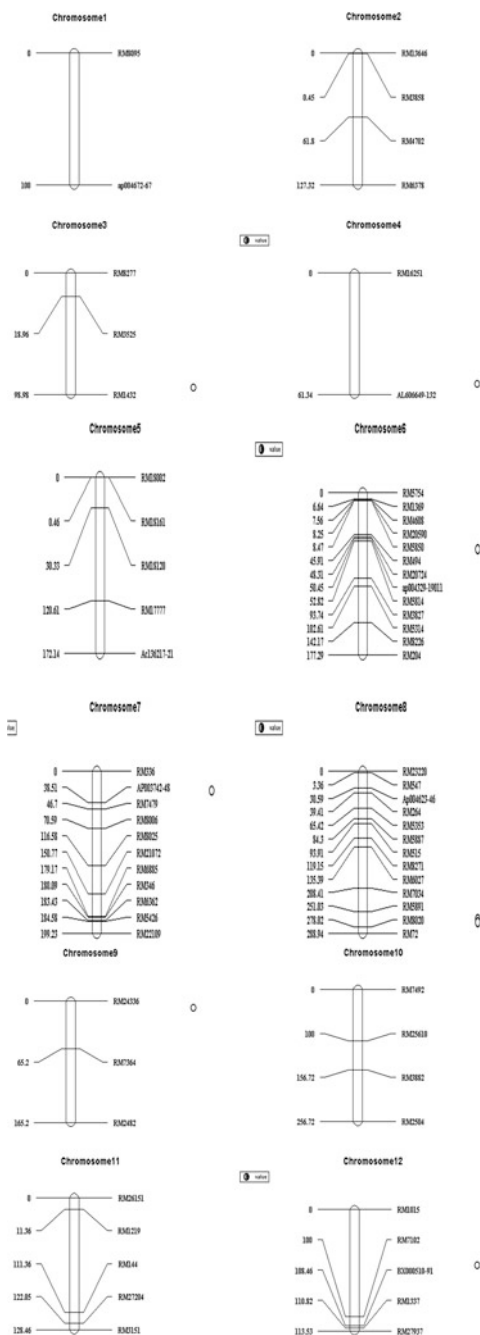


Fig. 127.1 Unstripped germ rate of RIL population

Table 127.1 Location of QTLs for UGR in rice

Number of chromosome	Left maker	Right maker	LOD value	Variation explained (%)
3	RM3525	RM1432	10.36	57.28
4	RM16251	AL606649-132	12.55	54.44
6	RM5850	RM494	10.65	53.63
7	AP003742-48	RM7479	7.05	32.81
8	RM5891	RM8020	7.98	43.52
8	RM8020	RM72	6.21	39.86
9	RM24336	RM7364	10.35	55.35
12	RM7102	BX00050-91	6.09	26.44

Fig. 127.2 Chromosomal locations of QTLs for UGR in RIL population



127.4 Conclusion

Rice is the most important crop in the world, with over 1.5 billion hectares under cultivation and a production of over 583.2 million tons. It is grown in 117 countries and is a staple food for people in 39 countries, which include 2.7 billion people in Asia alone [21]. Thus, it is very important to ensure a balance of grain supply–demand, which can be affected by reduction of cultivated land, sharp population growth, and environmental deterioration.

In this study, we investigate the genetic factors controlling unstripped germ rate in milled rice using QTL analysis. A linkage map consisting of 80 DNA markers was constructed. Eight QTLs were located on chromosomes 3, 4, 6, 7, 8, 9, and 12 were detected. The results will be useful for improvement of quality in rice breeding.

Acknowledgments This work was supported by National High-tech R&D Program of China (863 Program) (Grant No. 2011AA10A101), Natural Science Foundation of Tianjin, China (Grant No.11ZCKFNC01200), and the National Natural Science Foundation of China Grant (No. 31271676).

References

1. Khush GS (2003) Productivity improvements in rice. *Nutr Rev* 61:114–116
2. Khush GS (2001) Challenges for meeting the global food and nutrient needs in the new millennium. *Proc Nutr Soc* 60:15–26
3. Wu WR, Tang DZ, Li WM (2000) Genetic dissection and molecular dissection of quantitative traits. *Acta Agr Sin* 26:501–507
4. Li JZ, He P, Zheng XW et al (1999) Identification and interaction analysis of six agronomic trait loci of rice based on a recombinant inbred population. *Acta Bot Sin* 41:1199–1203
5. McCouch SR, Teytelman L, Xu YB (2002) Development and mapping of 2240 new SSR markers for rice (*Oryza sativa* L.). *DNA Res* 9:199–207
6. Bao JS, Wu YR, Hu B et al (2002) QTL for rice grain quality based on a DH population derived from parents with similar amylose content. *Euphytica* 128:317–324
7. Lu CF, Shen LS, Tan ZB et al (1996) Comparative mapping of QTLs for agronomic traits of rice across environments using a doubled haploid population. *Theor Appl Genet* 93:145–150
8. Guo LP, Luo LJ, Xing YZ et al (2003) Dissection of QTLs in two years for important agronomic traits in rice (*Oryza sativa* L.). *Chin J Rice Sci* 17:211–218
9. Zhang FJ, Zhang ML, Zhu SF (2004) An improved method of DNA extraction in rice. *Plant Q* 18:330–332
10. Peng ST, Yan QC, Wang XD (2002) Research on rice weed DNA extraction and RAPD procedure improvement. *J SJTU* 20:34–41
11. Vanni A, Anfossi L, Giovannoli C (2004) Evaluation of purification procedures of DNA from maize meal samples by exploiting different analytical techniques for the assessment of DNA quality. *Ann Chim* 94:269–280
12. Collardl BCY, Dasa Virkp S L (2004) Evaluation of quick and dirty DNA extraction methods for marker assisted selection in rice (*Oryza sativa* L.). *Plant Br* 126:47–50
13. Zhu SY, Luo TK, Zhang XL (2009) Improvement of SSR-PCR reaction system. *A Agr Sci* 37:3441–3443

14. Xu SB, Tao YF, Yang ZQ et al (2002) A simple and rapid methods used for silver staining and gel preservation. *Hereditas* 24:335–336
15. Jing W, Zhang WW, Jiang L et al (2007) Two novel loci for pollen sterility in hybrids between the weedy strain Ludao and the japonica variety Akihikari of rice (*Oryza sativa* L.). *Theor Appl Genet* 114:915–925
16. Bao JS, Sun M, Zhu LH et al (2004) Analysis of quantitative trait loci for some starch properties of rice (*Oryza sativa* L.): thermal properties, gel texture and swelling volume. *J Cereal Sci* 39:379–385
17. Wu QS, Wan XY, Su N et al (2006) Genetic dissection of silicon uptake ability in rice (*Oryza sativa* L.). *Plant Sci* 171:441–448
18. Churchill GA, Doerge RW (1994) Empirical threshold values for quantitative trait mapping. *Genetics* 138:963–971
19. Wang DL, Zhu J, Li ZK et al (1999) Mapping QTLs with epistatic effects and QTL \times environment interactions by mixed linear model approaches. *Theor Appl Genet* 99:1255–1264
20. McCouch SR, Cho YG, Yano M et al (1997) Report on QTL nomenclature. *Rice Genet Newsl* 14:11–13
21. Sardesai N, Rajyashri KR, Behura SK et al (2001) Genetic, physiological and molecular interactions of rice with its major dipteran pest, gall midge. *Plant Cell Tiss Org* 64:115–131

Chapter 128

The Application of the GSI in the Preservation and Quality Control of Oat Beverage

Yuzhu Liu and Min Zhang

Abstract The purpose of this paper is to introduce the concept of Globle stability index (GSI) in the quality control of oat beverage. The Q10 value of oat beverage was determined by protracting the GSI curve. The results showed that the Q10 were 1.40 and 3.00, respectively, when the temperatures were changed from 28 to 38 °C and 38 to 48 °C. The GSI indicator of oat beverage was established. The key factors of the quality control of oat beverage were total acid, total sugar, viscosity, soluble solids, precipitation, chromatic aberration, and pH. The GSI equation was $y = 0.9889e-0.001x$, $R = 0.9898$. The impact factors of the simplified GSI test through experiments and data processing were determined, included soluble solids, precipitation, color, and pH. The simplified GSI equation was $y = 1.0021e-0.0012x$, $R = 0.9746$. The GSI indicator of oat beverage was established through the application of the two curves. That provided technical preparation for the production of oat beverage.

Keywords Oat beverage · GSI · Q10 · Key factors

128.1 Introduction

In the world's eight major cereal crops, the production of Oat ranked sixth after wheat, rice, corn, barley, and sorghum, so it has huge significance in the food processing [1]. Moreover, it showed various bioactivities, and the main active components are oat polysaccharides and Oat ethanol extracts. The study had indicated that they had the health functions of reducing blood sugar and cholesterol, anticancer, and so on [2]. A new concept is based on the defining and formulating

Y. Liu · M. Zhang (✉)

Key Laboratory of Food Nutrition and Safety, Tianjin University of Science and Technology, Tianjin 300457, People's Republic of China
e-mail: zm0102@tust.edu.cn

a single index called the Global Stability Index (GSI), varying between zero and one and taking simultaneously into account the time variations of all pertinent quality indices proper to the food product under study [3]. In order to evaluate the degradation of the product quality in terms of the sensory, the microbiological and the physicochemical properties, various properties, and quality indices must be experimentally followed as a function of time, depending on the product nature [4]. In this paper, the oat beverage was produced with Oat bran, and the changes of its quality were measured at different storage temperatures.

The concept of GSI was introduced in this process, the Q10 value was calculated through completing the GSI curve. Then the curve coincided with GSI was received through data processing of a single or fewer several indicators. The GSI curve could be simplified, consequently.

128.2 Materials and Methods

128.2.1 Measurement of Coliform Organisms

128.2.1.1 Sample Processing

Oat beverage dope was diluted and three groups of samples were obtained by gradient dilution method, then adjusted the pH to 7.2–7.4.

128.2.1.2 Vaccination

The three groups of samples were inoculated, and each group was inoculated with 1 mL.

128.2.1.3 Proof Test

The inoculated samples would be cultured for 16 – 18 h at 37 °C. The positive number of Coliform organisms for each dilution was recorded, and the corresponding number of coliform organisms was identified according to the coliform MPN table.

128.2.2 Measurement of Total Acid (GB/T 12456-90)

128.2.2.1 Sample Determination

Put the sample of oat beverage (50 mL) in a 250 mL flask, then add 0.2 mL of 1 % PHenolpHthalein solution as indicator and titrate with NaOH solution until a faint

pink color is obtained and do not fade for 30 s. The consumption of NaOH standard titrant (V1) was recorded.

128.2.2.2 Blank Test

The water was applied instead of the test sample, and then the test was carried out according to 2.2.1. The consumption of sodium hydroxide standard titrant (V2) was recorded. 2.2.3 Computational formula:

$$X = C(V1 - V2) \times F / V0 \times 1000$$

128.2.3 Measurement of Total Sugar

128.2.3.1 Sample Processing

Put 1 mL of oat beverage in an Erlenmeyer flask, then 5 mL of hydrochloric acid (6 mol/L) and 20 mL of distilled water were added, then heated in boiling water for 2 h, balanced the pH to 7.0 with 6 mol/L NaOH solution, diluted with water to 100 mL, got the required sample after blending [5].

128.2.3.2 Measurement of Sample

Each of 5 mL alkaline tartaric acid copper liquid A and liquid B were taken to a 250 ml Erlenmeyer flask, then 10 ml of distilled water and three glass beads were added. The sample solution which was less 1 mL than the consumption of test sample solution was added. The sample solution was dropping continually with the speed of 1 drop every 2 s and maintaining the solution boiling within 2 min, until the blue just faded away. The consumption of the total volume of sample solution was recorded.

128.2.3.3 Calculation of Results

$$\text{Formula : } X = (F \times 100) / (V1 \times V2)$$

128.2.4 Measurement of viscosity

The viscosity meter (DV-IIPr) was applied to the determination, the RV2 rotor was selected and measured in the condition of 220 r/min.

128.2.5 Measurement of the Precipitation

After oscillating and mixing, the oat beverage (100 mL) deposited under different conditions was centrifugated at 3,000 r/min for 10 min. The precipitant was added and heated for 2 h at 105 °C, after the supernatant solution was poured out.

128.2.6 Measurement of the Soluble Solids Content

The contents of soluble solids of oat beverage deposited under different conditions were measured by the saccharimeter.

128.2.7 Measurement of pH

The changes of the pH of oat beverage in different preservation conditions were measured by the pH meter.

128.2.8 Measurement of the Chromatic Aberration

The changes of the chromatic aberration of oat beverage in different preservation conditions were measured by using the DC-P3-automatic colorimeter meter.

128.2.9 The Calculation of the GSI

The experiment introduced this formula [3]:

$$V_{ij} = (C_{ij} - C_{i0}) / (L_i - C_{i0}) \quad (128.1)$$

Where C_{ij} is the measured value of the criterion i at time j units; C_{i0} is the initial value of the criterion i , at the start of the experiment ($t = 0$); L_i is the threshold value of criterion i , set by regulations or common practices, i.e., by the user. Finally, we define the Global Stability Index, GSI_j , at any storage time equal to j units, as:

$$GSI_j = 1 - \sum a_i V_{ij} \quad (128.2)$$

where j is the j units of storage time; P is the sum of $i = 1$ to n , n being the total number of the quality degradation criteria; i is the criterion; V_{ij} is the variation of

criterion i at time j units from Eq. 128.2; a_i is a weighting factor reflecting the relative importance of criterion i in terms of describing the quality of the product. It varies between 0 and 1.

128.3 Results

128.3.1 Measured Results of Coliform Organisms

The results of the experiment showed that the coliform bacteria was not detected after had been stored for 180 d, therefore we could ensure that the condition of sterilization in the experiment was consistent with the requirement, and ensured that oat beverage had preserved value during the period.

128.3.2 The Content of Total Acid

The Fig. 128.1 showed that the total acid content would increase gradually with the extension of the time. Under the storage conditions of 48 °C, the total acid content increased quickly, and the total acid content increased gently with the extension of time, while under the storage conditions of 28 and 38 °C, the increase had been gentle relatively.

128.3.3 Measurement of Total Sugar Content

According to the Fig. 128.2, the general trend of the total sugar content was that it would decrease with the extension of the time. The total sugar content had changed obviously, under the storage condition of 48 °C, while it changed more gently under the storage conditions of 28 and 38 °C. It might be that the precipitation had taken away part of the sugar, which led to the decline of the content of total sugar.

128.3.4 Measurement of the Oat Beverage Viscosity

The Fig. 128.3 showed that the viscosity had no obvious trend, only when it was preserved under the conditions of 48 °C, the viscosity had the trend of increase.

Fig. 128.1 Curve of the total acid content

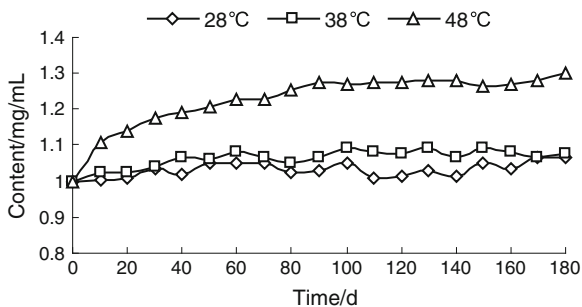


Fig. 128.2 Curve of the total sugar content

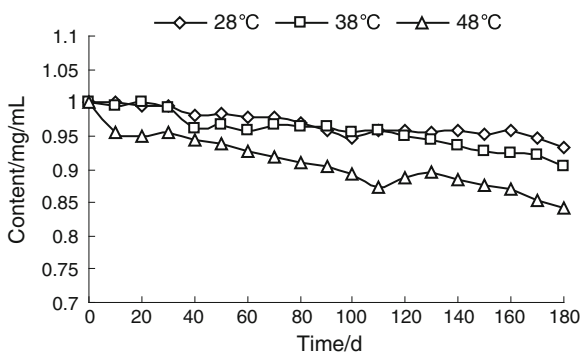
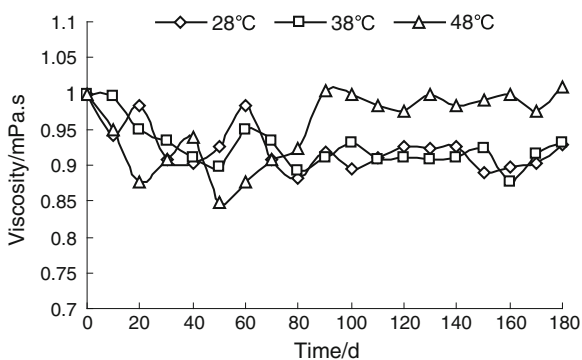


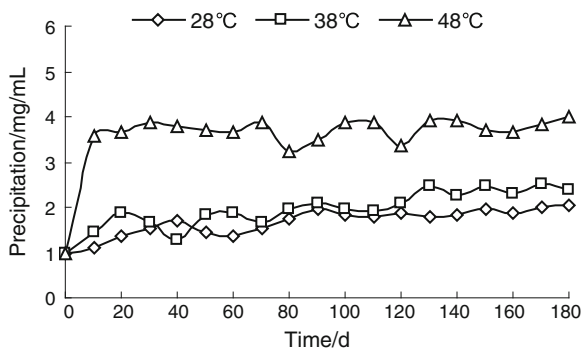
Fig. 128.3 Curve of the viscosity



128.3.5 Measurement of the Oat Beverage Precipitation Amount

According to the Fig. 128.4, the general trend of the precipitation amount was that it would increase with the extension of the time. Under the storage conditions of 48 °C, it had increased obviously in a short time, then gently.

Fig. 128.4 Curve of the precipitation amount



128.3.6 Measurement of the Soluble Solids Content

The Fig. 128.5 showed that the soluble solids content of oat beverage changed gently during experiment of preservation.

128.3.7 Measurement of Oat Beverage pH

The Fig. 128.6 showed that the pH of the oat beverage would decrease with the extension of the time, and it had changed obviously under the storage conditions of 48 °C.

128.3.8 Measurement of the Chromatic Aberration Changes of Oats Beverage

Figure 128.7 The chart showed that the chromatic aberration of oats beverage changed larger with the extension of the time, and the higher its storage-temperature was, the more violently it changed.

Fig. 128.5 Curve of the soluble solids content

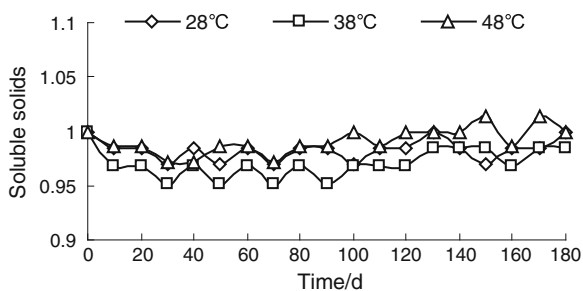
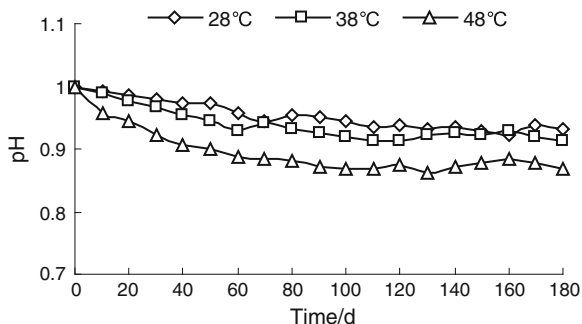
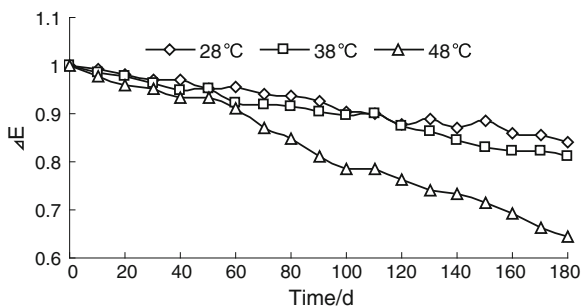


Fig. 128.6 Curve of the pH**Fig. 128.7** Curve of the chromatic aberration

128.3.9 Application of GSI Method in the Results

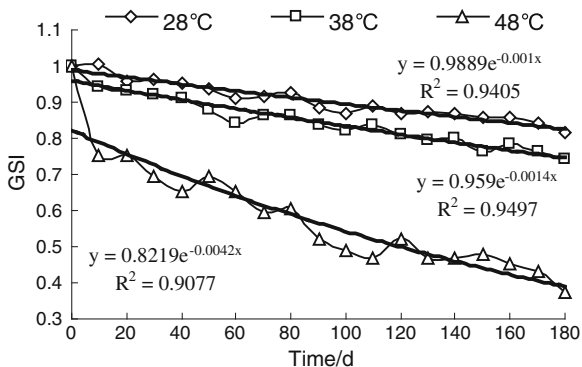
Determination of weight coefficients: MPN value of Coliform group was an important index to reflect the changes of beverage quality. Once the microorganisms exceeded, the beverage would not have value in use. A single experimental result showed that the change of soluble solids content was very little, its weight coefficient was 0.05; while the change of precipitation amount was most obvious during the process of preservation, its weight coefficient was 0.20. The weight coefficients of other indexes were 0.15. The index weight coefficient: {total acid content, total sugar content, viscosity, soluble solid content, precipitation amount, chromatic aberration, pH} = {0.15, 0.15, 0.15, 0.05, 0.20, 0.15, 0.15}.

The GSI was solved by using matrix. According to the kinetic equation [6], we could use the formula $A = A_0 \exp(-Kt)$ to fit the three curves, and the result was shown in Fig. 128.8.

Calculation of the Q10 values which were the temperature coefficients:

- ① when the temperature was from 28 to 38 °C, $KC = 0.001$ and $KC + 10 = 0.0014$, $Q_{10} = KC + 10/KC$, $Q_{10} = 1.40$.
- ② when the temperature was from 38 to 48 °C, $KC = 0.0014$ and $KC + 10 = 0.0042$, $Q_{10} = KC + 10/KC$, $Q_{10} = 3.00$.

Fig. 128.8 Fitting curve of GSI



Data indicate that, when the food had chemical changes in the process of storage, the value of Q10 generally was between 2 and 4 [7]. As mentioned above, the results of the experiment was consistent with the data. Therefore, cryopreservation had great significance to ensure the quality of oat beverage.

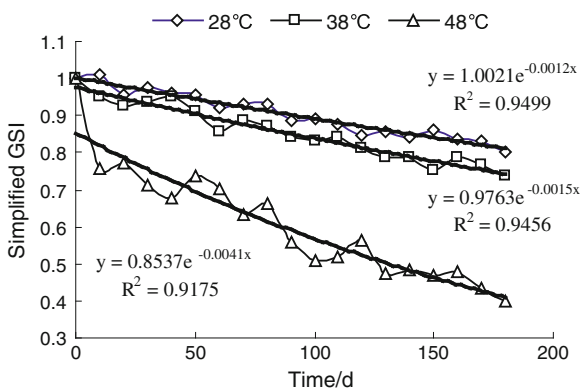
128.3.10 Simplifying the Calculation of GSI of Oat Beverage

The simplified method which was considered comprehensively with chromatic aberration, precipitation, pH, and viscosity was received through a large amount of data process. The weight coefficient was {precipitation, pH, viscosity, chromatic aberration} = {0.3, 0.2, 0.3, 0.2}, then we could process date and fit to get Fig. 128.9.

Calculating the values of Q10 from Fig. 128.9:

- ① when $C = 28\text{ }^\circ\text{C}$ and $C + 10 = 38\text{ }^\circ\text{C}$, $KC = 0.0012$ and $KC + 10 = 0.0015$, $Q10 = KC + 10/KC$, $Q10 = 1.25$.

Fig. 128.9 The curve of simplified GSI



- ② when $C = 28\text{ }^{\circ}\text{C}$ and $C + 10 = 38\text{ }^{\circ}\text{C}$, $KC = 0.0015$ and $KC + 10 = 0.0041$, $Q_{10} = KC + 10/KC$, $Q_{10} = 2.73$.

We could find that the relevant coefficients in Fig. 128.9 were better, and had higher fitting accuracy than others. The Q_{10} values were calculated from Fig. 128.8 and the results were 1.25 and 2.73, that had little difference from the Q_{10} values which were calculated from the general Fig. 128.9, and the detection experiment of index was relatively simple. These indexes included viscosity, precipitation capacity, color, the pH. So we could use the figure to replace the GSI general figure for getting the simplified effect.

128.4 Discussion

The qualitative change of Oat beverage during storage could be reflected by the GSI. The GSI curve could be determined by these seven indicators, including total acid content, total sugar content, viscosity, soluble solids, precipitation, color, and the pH.

The GSI curve equation was $y = 0.9889e - 0.001x$, $R = 0.9898$; we could use four indicators which were viscosity value, precipitation, chromatic aberration, and the pH to get simplified GSI curve, and the simplified GSI equation was $y = 1.0021e - 0.0012x$, $R = 0.9746$.

When the temperature was changed from 28 to 38 °C and 38 to 48 °C, the Q_{10} values which were calculated by GSI curve were 1.40 and 3.00. While the temperature was from 28 to 38 °C and 38 to 48 °C, the Q_{10} values were calculated by the simplified GSI curve were 1.25 and 2.73. The Q_{10} values had a good degree of coincidence before and after simplifying, showed that the simplified GSI curve was a valuable method to measure the quality changes of oat beverage during storage.

References

1. Li J (1993) Nutritional value and health benefits of oats[J]. Xinjiang Agric Sci Technol (in China) 5:38–39
2. Autiok K, Myllymakio O (1987) Flow properties of solution of oat β -glucan[J]. Food Sci 52(5):564–568
3. Achour M (2006) A new method to assess the quality degradation of food products during storage[J]. J Food Eng 75:560–564
4. Labuza, TP (1985) An integrated approach to food chemistry: illustrative cases. Marcel Dekker Inc, New York, Food Chem
5. Wang XP (ed) (2006) Food analysis[M]. Agric Sci (in China), Agric Press, 2–3
6. Labuza TP (1984) Application of chemical kinetics to deterioration of foods. J Chem Educ 61:348–358
7. Zhao JF (ed) (2008) Principles of food technology[M]. China Light Industry Press, china, p 2

Chapter 129

The Effect of Carbon Nanotubes on Rice Seed Germination and Root Growth

Yumei Jiang, Zetian Hua, Yiqing Zhao, Qindai Liu, Fang Wang
and Qin Zhang

Abstract There are few researches available on the effects of carbon nanotubes on rice seed germination and root growth. Aiming at this problem, rice seeds were co-cultured with carbon nanotubes of different concentrations. The rice seedling growth situation was observed including germination percentage rates, length of seeding stem, and root. The absorbance was measured and the root activity was calculated. Experiment results showed that the rice seed germination and root growth were promoted by carbon nanotubes with appropriate concentrations (0 ~ 100 $\mu\text{g/ml}$). When the concentration increased to 150 $\mu\text{g/ml}$, the root length, root activity, and stem length decreased in comparison with the value of 100 $\mu\text{g/ml}$, but still slightly higher than the control, although the root and stem lengths were shorter than the control. Our results demonstrated, for the first time, that carbon nanotubes could promote rice seed germination and root growth at lower concentrations, and may have toxic effects at high concentrations.

Keywords Rice seed · Carbon nanotubes · Germination · Root growth

129.1 Introduction

Materials of particle size less than 100 nm in at least one dimension are generally classified as nanomaterials. The great potential of using nanoscale particles for different biological and medical applications including gene and drug delivery,

Y. Jiang · Z. Hua (✉) · Y. Zhao · Q. Liu · F. Wang · Q. Zhang
College of Food Engineering and Biotechnology, Tianjin University of Science
and Technology, Tianjin 300457, People's Republic of China
e-mail: hzetian@yahoo.com.cn

Y. Jiang
Tianjin International Joint Academy of Biotechnology and Medicine, Tianjin 300457,
People's Republic of China

biosensing, diagnostic, and tissue engineering was widely documented during the last several years.

Most investigations were focused on animals and humans at various levels, and detailed studies and reliable information on the effects of nanomaterials such as carbon nanotubes on plant physiology and plant development at the organism level are very limited. However, there is an extensive interest to investigate the ability of nanoparticles to penetrate plant cell walls and work as smart treatment-delivery systems in plants [1–3]. Rice (*Oryza sativa L.*) is one of the most important food crops worldwide. To achieve the goals of nano-agriculture, detailed studies on the effects of nanotubes on rice seed germination and development of seedlings are needed. This study is the first report, to our best knowledge, that describes the effect of penetration of rice seed coats by carbon nanotubes.

129.2 Materials and Methods

The seeds were the number 294 liao japonica rice seeds. Standard Specification for carbon nanotubes: OD <8 nm, Length ~30 μm , Purity >95wt %, Ash <1.5wt %, SSA >500 m^2/g , EC >102 s/m, MFG Code: M1091016.

Germination of rice seeds. The rice seeds were inoculated on standard agar Murashige and Skoog medium (MS medium) supplemented with different concentrations of carbon nanotubes tubes (50, 100, 150 $\mu\text{g}/\text{ml}$). The MS medium without carbon nanotubes tubes was used for blank control experiments. 16–18 rice seeds were sterilized by 5 min treatment with 0.1 % mercuric chloride and then rinsed five times with sterile water. Sterile rice seeds were placed on MS medium without or with carbon nanoparticles (0, 50, 100, 150 $\mu\text{g}/\text{ml}$) for germination. The rice seeds in the culture bottles were inoculated in biochemical incubator at 28 °C for 6 days. The experiment was repeated twice.

Seed germinations were observed, and the germination rate was calculated. The growth heights of rice seedling stem and the root lengths of rice seedling were recorded everyday according to different concentrations. TTC standard curve was drawn and root activity was calculated according to the root lengths and absorbance of rice seedling in different concentrations for 4.5–6 days.

129.3 Results and Discussion

Addition of carbon nanotubes to agar medium was found to accelerate the process of seed germination and significantly shortened the germination time. Rice seeds placed on medium with carbon nanotubes (50, 100, 150 $\mu\text{g}/\text{ml}$) germinated on the first day, while rice seeds placed on regular MS did not germinate at that time. The germination percentage rates were dramatically higher for seeds treated with

nanoparticles. Seedlings with developed cotyledons and root system were recognized as fully germinated in this experiment.

We observed the growth condition and carried out a variety of parameter determination of rice seedlings for the last 3 days. For different concentrations of carbon nanotubes tubes, there were different values. Carbon nanotubes-exposed rice seedlings (50, 100 $\mu\text{g}/\text{ml}$) had longer and more developed stems and root system compared with blank control seedlings. (Fig. 129.1a, b, c. Tables 129.1, 129.2). With increasing concentration of carbon nanotubes, the positive effect was more and more strong. The positive effect was strongest when the concentration was 100 $\mu\text{g}/\text{ml}$. However, the effect of carbon nanotubes (150 $\mu\text{g}/\text{ml}$) on plant physiology was complex. Rice seedlings (150 $\mu\text{g}/\text{ml}$) had shorter root system compared with blank control seedlings (Fig. 129.1a, d. Table 129.1). Although shorter even than the seeding stem (50 $\mu\text{g}/\text{ml}$), the stem length (150 $\mu\text{g}/\text{ml}$) was still slightly longer than blank control seedlings on the fourth and fifth days. On the sixth day, the length of stem (150 $\mu\text{g}/\text{ml}$) was already shorter than blank control seedlings (carbon nanotubes nontreated) (Fig. 129.1a, d. Table 129.2).

As the culture time increased, the absorption value and root activity of rice seedling roots increased gradually. With the increase in carbon nanotubes concentration (0–100 $\mu\text{g}/\text{ml}$), the root activity also enlarged. When the concentration increased to 150 $\mu\text{g}/\text{ml}$, the root activity decreased less than the value of 100 $\mu\text{g}/\text{ml}$. This result was content with the measured length. However, there was a conflict between the result of root activity and the measured length when they were compared with root activity of the blank control. Root activity was still slightly higher than the control, although the root length was shorter than the blank control (Table 129.3).

Nanomaterials have been applied in various fields such as water purification, wastewater treatment, environmental remediation, food processing and packaging, industrial and household purposes, medicine, and smart sensor development. The majority of applications in these areas had been focused on the significance of the nanomaterials for improved efficiency and productivity. However, in the field of agriculture, the use of nanomaterials is relatively new and needs further

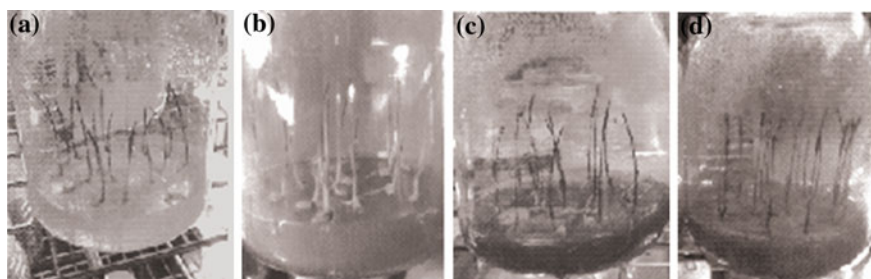


Fig. 129.1 Effect of carbon nanotubes on growth and development of rice seedlings. Four-day-old seedlings were used to show the growth of rice seedling: **a** 0 $\mu\text{g}/\text{ml}$, **b** 50 $\mu\text{g}/\text{ml}$, **c** 100 $\mu\text{g}/\text{ml}$, **d** 150 $\mu\text{g}/\text{ml}$

Table 129.1 The length of seeding root for rice seed (average \pm SE cm)

	0 $\mu\text{g/ml}$	50 $\mu\text{g/ml}$	100 $\mu\text{g/ml}$	150 $\mu\text{g/ml}$
The fourth day	4.922	5.367	5.298	4.289
The fifth day	5.075	5.479	5.680	4.416
The sixth day	5.266	5.694	5.739	4.552

Table 129.2 The length of seeding stem for rice seed (average \pm SE cm)

	0 $\mu\text{g/ml}$	50 $\mu\text{g/ml}$	100 $\mu\text{g/ml}$	150 $\mu\text{g/ml}$
The fourth day	3.116	3.695	4.103	3.249
The fifth day	5.087	5.572	5.912	5.235
The sixth day	9.388	9.716	10.722	9.330

Table 129.3 The absorbance (ab.) and root activity of rice (ra.)

	0 $\mu\text{g/ml}$		50 $\mu\text{g/ml}$		100 $\mu\text{g/ml}$		150 $\mu\text{g/ml}$	
	ab.	ra.	ab.	ra.	ab.	ra.	ab.	ra.
Fourth day	0.143	0.280	0.204	0.407	0.269	0.542	0.172	0.340
Fifth day	0.214	0.428	0.293	0.591	0.336	0.680	0.243	0.488
Sixth day	0.231	0.463	0.313	0.633	0.343	0.695	0.248	0.498

Root activity unit = $C/(1,000 \cdot W \cdot h)$ [mg TTF/(g·h)], absorbance abbreviated as ab., root activity abbreviated as ra.

exploration [1–3]. Till date, only a few plant species and nanomaterials have been studied on seed germination or 15-day-old seedlings. Most of the studies were performed on vegetable seeds. To our knowledge, this is the first report on the effect of nanomaterials on rice seed germination.

Previously, limited reports indicated both positive and negative effects of different nanoparticles on plant physiology [4]. It was demonstrated that nano-TiO₂ treatment in proper concentration accelerated the germination of the aged spinach seeds and increased its vigor [5]. Nanoparticles (Pd, Au at low concentrations; Si, Cu at higher concentrations, and combination of Au and Cu) also had a positive influence on lettuce seed germination, measured in terms of shoot to root ratio and growth of the seedling [6]. Some other studies also support the positive effects of suspensions of nanomaterials on seed germination and root growth of nine different crop species, such as tomato [3], radish (*Raphanus sativus*), rape (*Brassica napus*), rye grass (*Lolium perenne*), lettuce (*Lactuca sativa*), corn (*Zea mays*), cucumber (*Cucumis sativus*) [7], zucchini [8], onion, and cucumber [9].

There were also negative reports of nanomaterials for seed germination and root growth, such as the inhibition effect on ryegrass and corn [7]. Nanomaterials have also been reported to have no influence on the germination and root growth of tomato, cabbage, and carrots [9]. Our results were consistent with the positive reports. Carbon nanotubes were able to penetrate plant seed coat and dramatically affect seed germination and plant growth [3]. The reason for the contradictory

conclusions of different reports may be due to the type of plant species, the nature of nanomaterials, and the concentrations of nanomaterials [7–9]. The higher concentrations (2,000 mg/L) of nanosized Zn (35 nm) and ZnO (w20 nm) inhibited the germination in ryegrass and corn, respectively; this result was similar to the reports of Lin and Xing. They found that the root growth depended on different nanoparticles and their concentrations [7, 10]. In this study, we also found that the ability of rice seed germination and root growth increased with the increasing nanomaterial concentrations before 100 µg/ml. But the ability decreased when the concentrations reached 150 µg/ml. Although the root activity was still slightly higher than the control, the lengths of root and stem (150 µg/ml) were already shorter than blank control. This result means that nanomaterials of high concentrations may have toxic effects on plant. The phytotoxicity of nanomaterials is a question that is gradually attracting more and more attention.

129.4 Conclusion

Our results demonstrated, for the first time, that carbon nanotubes could promote rice seed germination and root growth at lower concentrations, and had toxic effects at high concentrations.

Acknowledgments This work was partially supported by National High-tech R&D Program of China (863 Program) (Grant No. 2011AA10A101), Natural Science Foundation of Tianjin, China (Grant No. 11ZCKFNC01200) and the National Natural Science Foundation of China Grant (No.31271676).

References

1. Rafsanjani MS, Alvari A, Samim M et al (2012) Application of novel nanotechnology strategies in plant biotransformation: a contemporary overview. *Recent Pat Biotechnol* 6:69–79
2. Sozer N, Kokini JL (2009) Nanotechnology and its applications in the food sector. *Trends Biotechnol* 27:82–89
3. Mariya K, Enkeleda D, Meena M et al (2009) Carbon nanotubes are able to penetrate plant seed coat and dramatically affect seed germination and plant growth. *ACS Nano* 3:3221–3227
4. Klaine SJ, Alvarez PJJ, Batley GE et al (2008) Nanomaterials in the environment: behavior, fate, bioavailability, and effects. *Environ Toxicol Chem* 27:1825–1851
5. Zheng L, Hong F, Lu S et al (2005) Effect of nano-TiO₂ on strength of naturally aged seeds and growth of spinach. *Biol Trace Elem Res* 104:83–91
6. Adhikari RM, Shah BK, Palayangoda SS (2009) Solvent dependent optical switching in carbazole-based fluorescent nanoparticles. *Langmuir* 7:2402–2406
7. Lin B (2007) Phytotoxicity of nanoparticles: inhibition of seed germination and root growth. *Environ Pollut* 150:243–250

8. Stampoulis D, Sinha SK, White JC (2009) Assay-dependent phytotoxicity of nanoparticles to plants. *Environ Sci Technol* 15:9473–9479
9. Cañas JE, Long M, Nations S et al (2008) Effects of functionalized and nonfunctionalized single-walled carbon nanotubes on root elongation of select crop species. *Environ Toxicol Chem.* 7:1922–1931
10. Ma Y, Kuang L, He X et al (2010) Effects of rare earth oxide nanoparticles on root elongation of plants. *Chemosphere* 78:273–279

Chapter 130

Study on the Accumulation Laws of Protein in *Japonica* Rice Seed During Development

Fang Wang, Bolian Sun, Chunkai Gu, Jiajia Mi, Qin Zhang and Zetian Hua

Abstract Rice protein is nutritionally superior over most of the other food cereals in terms of amino acid composition. But rice is usually a low protein crop. So, it is important to investigate the change laws of protein for breeding rice with high protein content. The rice seed start to accumulate protein after flowering. In this study, Z601, a *japonica* rice variety, was used as the experimental material. Seeds of five days, ten days, fifteen days, twenty days, and twenty-five days after flowering (DAF) were collected. Protein contents were determined by Kjeldahl method in order to confirm the surge stage in rice seed. The components of rice protein at various development stages were analyzed by SDS-PAGE analysis to find the accumulation law of the individual protein components. The results showed that 15–20 DAF was the surge stage of protein accumulation in rice seed. The protein components in the seeds of 5 DAF did not include albumin and globulin and only contained glutenin and gliadin. After that stage albumin and globulin start to synthesis and the components of protein tended to be stable. The vast majority content of protein during rice seed development was glutenin with about 48 % of the total. The proportion of albumin to total protein content is 20 % and globulin is 15 %, also as gliadin.

Keywords Rice seeds · Protein · Kjeldahl determination · SDS-PAGE

F. Wang · B. Sun · C. Gu · J. Mi · Q. Zhang · Z. Hua (✉)
College of Food Engineering and Biotechnology, Tianjin University of Science and Technology, Tianjin 300457, People's Republic of China
e-mail: hzetian@tust.edu.cn

F. Wang · Z. Hua
China National Japonica Rice R&D Center, Tianjin 300457, People's Republic of China

130.1 Introduction

Rice is the most important cereal crop with about 40 % of total grain production in China. Rice protein is the best among cereals because of the biological value, digestibility, and net protein utilization [1, 2]. But rice is usually a low protein crop compared with other cereals. The protein content depends on the genetic and environmental factor. At present, the way to increase the protein content of rice depends on breeding and applying Nitrogenous fertilizer. Studying the accumulation laws of rice protein during seed development is helpful for early selecting rice variety with high protein content at a particular period never need to wait until the seed maturation. On the other hand, it can be used as a guidance at the time of applying Nitrogenous fertilizer to promote the protein accumulation during rice seed development.

130.2 Materials and Methods

130.2.1 Materials

Z601, the *japonica* rice varieties, was grown in rice growing season in 2011 on the experimental farms of Tianjin rice original seed farm, in Tianjin (39.08 °N, 117.12 °E), China. The seeds were marked on the glume on the flowering day by black marker pen and collected the seeds on 5, 10, 15, 20, 25 DAF, respectively.

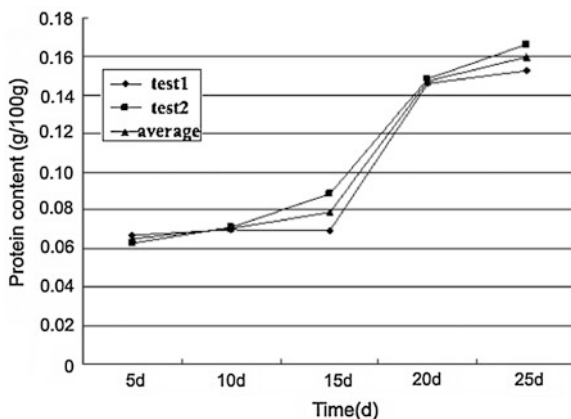
130.2.2 Determination of Protein Content

Protein contents were determined by Hanon K9840 Auto Kjeldahl Analyzer (Jinan Hanon Instruments Co.,Ltd), according to AACC method 46-13 (2000). Each sample was taken 0.2 g and twice repeats were carried out.

130.2.3 SDS-PAGE

Protein component analysis was conducted according to S.Iida [3]. Each seed sample of different developmental stage was taken 0.2 g and ground to powder in liquid nitrogen and then added 2 × SDS-PAGE buffer, vortex several seconds and then it was put on the shaking table at 40 °C for 12 h, and centrifuged at the speed of 8,000 r/min for 20 min at 4 °C. The supernatant was transferred to a new EP tube for analysis by SDS-PAGE or stored at −20 °C until use. Samples of extractable proteins were separated on 15 % SDS-PAGE gels (13 cm length)

Fig. 130.1 The rice seed protein accumulation law



according to [4] and stained with Coomassie Brilliant Blue R250 (Sigma, St Louis, MO, USA) according to [5]. Three repeats of each sample were carried out. Quantitative analysis of polypeptide bands was carried out by Quantity One 4.6.2.

130.3 Results and Discussion

130.3.1 The Accumulation Law of Rice Protein During Seed Development

The rice seeds of 5, 10, 15, 20, 25 DAF were collected to determine protein content by Auto Kjeldahl Analyzer. All the samples were tested twice showing the same trend of protein accumulation during the seed development. The protein content was very low and accumulated slowly in the seeds before 15 DAF. The protein accumulation surge stage was at the period of 15–20 DAF with protein content increasing from 0.0788 to 0.14735 g/100 g, almost enhancing one time, and then the protein accumulation speed slowed down and tended to stable (Fig. 130.1).

130.3.2 SDS-PAGE Analysis of Protein Components

In order to investigate the difference of protein components during seed development in rice, the proteins were extracted from seeds at different developmental stage and assayed by SDS-PAGE (Fig. 130.2).

Further quantitative analysis of polypeptide bands in Fig. 130.2 was carried out by Quantity One 4.6.2 (Bio-Rad Laboratories, Inc.). According to previous report, each polypeptide composition has different molecular weight [6], glutelin

Fig. 130.2 SDS-PAGE analysis of total protein at various stages of rice seed development M, marker; The letters above each lane indicated the day numbers after flowering

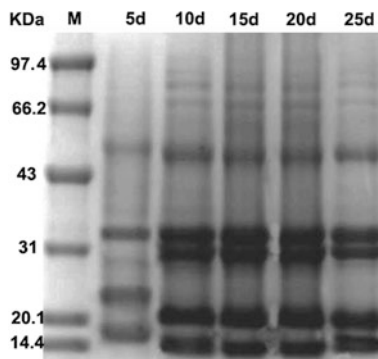


Table 130.1 Percentage of protein components during seed development in rice

DAF (d)	Albumin (%)	Globulin (%)	Glutenin (%)	Gliadin (%)
5			71.13	28.87
10	19.12	14.18	49.00	17.70
15	23.62	13.31	47.46	15.02
20	24.25	14.71	47.46	13.58
25	22.36	14.12	48.07	15.45

(22–23,37–39,57 k Da), albumin (16,76 kDa), globulin (26 kDa), and gliadin (13 kDa).

Table 130.1 showed the percentage of different components. It clearly exhibited the percentage of the main protein component to the total protein. The protein components in the seeds of 5 DAF contained only glutenin and gliadin, albumin and globulin were not detected. Glutenin was easy to detect because of its high content which consists with Tanaka et al. [7]. From 10 DAF, the percentage of protein component tends to be stable. The albumin occupies 20 % and globulin 14 % of the total protein. The proportion of gliadin slowed down from 28 % at 5 DAF to 17 % at 10 DAF and then stayed at about 15 %. The value of glutenin was much higher than the other components during all the developmental stages of rice seeds which could reach about 48 % of total protein.

130.4 Conclusion

This paper provides a protein accumulation profile of seed development in the *japonica* rice variety Z601. The analysis indicated that the developmental stage at 15 DAF can be considered as a change in direction in protein synthesis, peaking at 20 DAF as shown in Fig. 130.1. The study result could be used as guidance for selecting rice variety with high protein content at early stage of 20 DAF and settle the time and amount of applying Nitrogenous fertilizer to promote the protein accumulation for common rice variety.

Acknowledgments This work was supported by National High-tech R&D Program of China (863 Program) (Grant No. 2011AA10A101), Natural Science Foundation of Tianjin, China (Grant No. 11ZCKFNC01200) and the National Natural Science Foundation of China Grant (No.31271676).

References

1. Tanaka K, Sugimoto T, Ogawa M (1980) Isolation and characterization of two types of protein bodies in the rice endosperm. *Agric Biol Chem* 44:1633–1639
2. Cagampang GB, Cruz LJ, Espiritu SG (1966) Studies on the extraction and composition of rice protein. *Cereal Chem* 43:145–155
3. Iida S, Amano E, Nishio T (1993) A rice (*Oryza sativa* L.) mutant having a low content of glutelin and a high content of prolamine. *Theor Appl Genet* 87:374–378
4. Laemmli UK (1970) Cleavage of structural proteins during the assembly of the head of bacteriophage T4. *Nature* 227:680–685
5. Devouge V, Rogniaux H, Nesi N et al (2007) Differential proteomic analysis of four near-isogenic *Brassica napus* varieties bred for their erucic acid and glucosinolate contents. *J Proteome Res* 6:1342–1353
6. Ogawa M, Kumamaru T, Satoh H et al (1987) Purification of protein body-purification of protein body-I of rice seed and its polypeptide composition. *Plant Cell Physiol* 28:15
7. Tanaka K, Sugimoto T, Ogawa M et al (1980) Isolation and characterization of two types of protein bodies in rice endosperm. *Agric Biol Chem* 44:1633–1639

Chapter 131

Prevalence Investigation of Tetracycline Resistant Bacteria in Raw Milk

Xiaomei Zhang and Hongjiang Yang

Abstract To evaluate the prevalence of tetracycline resistant bacteria in raw milk, totally 198 raw milk samples were collected from Hohhot, Inner Mongolia. Preliminary screening results showed that 187 isolated strains were resistant to tetracycline. Fifteen strains were randomly selected for comparative 16S rRNA analysis, and they belonged to different genera including *Serratia* (5), *Pseudomonas* (4), *Bacillus* (1), *Providencia* (1), *Enterobacter* (1), *Staphylococcus* (1), *Acinetobacter* (1), and one unclassified Bacillales strain, respectively. Their tetracycline resistance phenotype was further validated with K–B disk diffusion method, and 11 strains were resistant to tetracycline and 4 isolates intermediate. Tetracycline resistant determinants were investigated by PCR method. Gene *tetAC*, *tetB*, and *tetK* were found in 11, 8, and 1 isolates, respectively. Furthermore, their hemolytic phenotypes were also characterized. The results showed that tetracycline resistant bacteria with a relatively high diversity commonly existed in raw milk with a high prevalence.

Keywords Raw milk · Tetracycline resistant bacteria · Prevalence · Tetracycline resistant determinant

131.1 Introduction

Food-borne illness was caused by various pathogens during every stage of production, and it is mainly related to animal source foods especially milk [1, 2]. Raw milk is natural habitat of *Lactobacillus*, *Pseudomonas*, *Staphylococcus aureus*, *Escherichia coli*, *Micrococcaceae*, and yeast [3, 4].

X. Zhang · H. Yang (✉)

Tianjin Key Laboratory of Industrial Microbiology, Ministry of Education, College of Biotechnology, Tianjin University of Science and Technology, Tianjin 300457, China
e-mail: hongjiangyang@tust.edu.cn

To prevent and control pathogens which may cause infections of cow, a variety of antibiotics are widely used as feed additives in raw milk production. The mainly applied antibiotics included penicillins, tetracycline, amino glycosides, macrolide, and polypeptides [5, 6]. With the extensive application of antibiotics, various resistant bacteria have been isolated from clinical and environmental specimens. Among the antibiotics resistant microbes, methicillin-resistant *Staphylococcus aureus* (MRSA) is resistant to almost all antibiotics treatment and has been heavily studied [7].

Tetracycline was discovered in the 1940s. Due to its broad spectrum of bactericidal activity and low cost, it has been widely used in infection treatment and as feed additives for growth promotion in animal husbandry. In 1953, the first tetracycline resistant strain was isolated during a *Shigella* outbreak in Japan [8]. Currently, with the widely use of tetracycline, tetracycline resistance phenotype has been found in a variety of bacteria including pathogens and commensal flora [9, 10], raising great concerns to human health and food safety issues. The increasing emergence of tetracycline resistance in bacteria is often due to the acquisition of horizontally transferred genes encoding various tetracycline resistance determinants [9].

The tetracycline resistance mechanisms mainly included efflux pumps [8], ribosomal protection [9, 11], enzymatic inactivation, and target modification [9, 12, 13]. Until recently, in both Gram negative and positive microorganisms, there were many genes have been identified relating to the tetracycline resistance phenotype. Most genes are responsible for encoding efflux pumps proteins, such as *tet(AC)*, *tet(B)*, *tet(D)*, *tet(E)*, *tet(G)*, *tet(H)*, *tet(I)*, *tet(J)*, *tet(Z)*, *tet(30)*, *tet(31)*, *tet(K)*, *tet(L)*, *otr(B)*, *tcr3c*, *tetP(A)*, *tet(V)*, and *tet(Y)*. Some genes are responsible for ribosomal protection, such as *tet(M)*, *tet(O)*, *tet(S)*, *tet(W)*, *tet(Q)*, *tet(T)*, *otr(A)*, and *tetP(B)*. Gene *tet(X)* is involved in enzymatic inactivation of the antibiotic [9]. In this study collected 198 raw milk samples and investigated the prevalence of tetracycline resistant bacteria in raw milk samples. Determinants for tetracycline resistance were also identified by PCR method.

131.2 Materials and Methods

131.2.1 Materials

Raw milk samples were collected from Tuoketuo county, which is located at 111°2'30"–111°32'21" E longitude and 40°5'35"–40°35'15" N latitude, north of the Yellow River, in Hohhot, Inner Mongolia. Sampling process was compliance with aseptic procedures strictly. Briefly, rinsing udder with warm water, sterilizing udder with 0.2 % benzalkonium bromide, and disinfecting teat with 75 % alcohol. Hand milking was performed and milk samples were collected in sterile tubes after dumping the first three squirts to clean out the teat [14]. The samples were stored at 4 °C before analyzing.

131.2.2 Screening of Tetracycline Resistant Bacteria

Milk sample was subjected to 10-fold serial dilutions before spreading on plates. In brief, 100 μ L mixtures of diluted samples were spread on Luria–Bertani (LB) agar plates with tetracycline (16 μ g/mL). The plates were incubated at 35 °C for 16–18 h and the results were recorded.

131.2.3 Comparative Analysis of 16S rRNA Gene

Genomic DNA was extracted from bacterial cells harvested from overnight culture of the isolated strains according to methods described previously [15, 16]. The purified chromosome DNA was used as templates for 16S rRNA gene amplified. PCR was performed as described and specific primers used are listed in Table 66.1 [17].

The parameters for PCR included initial denaturation at 94 °C for 5 min, 30 cycles of denaturation at 94 °C for 40 s, annealing at 51 °C for 2 min, and extension at 72 °C for 3 min, and 1 cycle of extension at 72 °C for 15 min. Purified amplification products were subjected to sequencing analysis with the same primers used in PCR [18]. Sequence similarity was analyzed with BLAST provided by NCBI for strains identification [19]. Classifier program was used to classify the isolates based on the 16S rRNA gene sequences [20].

131.2.4 Hemolysis Test

The isolates were tested for their hemolytic properties on blood agar plates [21]. The isolated strains were streaked on the plates and incubated at 35 °C for 24 h. Colony morphology and hemolytic zones around colonies were recorded after incubation.

Table 66.1 Primers sequences

Genes	Primers	Primer sequences	Amplicon size	References
16S rRNA	27F	5' AGAGTTTGGATCATGGCTCAG 3'	~ 1465 bp	[17]
	1492R	5' GGTACCTTGTTACGACTT 3'		[17]
<i>tet(AC)</i>	tetAC–F	5' GCTRTATGCGTTGRTGCAAT 3'	567 bp	[24]
	tetAC–R	5' TCCTCGCCGAAAATGACC 3'		[24]
<i>tet(B)</i>	tetB–F	5' TTGGTTAGGGGCAAGTTTTG 3'	704 bp	[25]
	tetB–R	5' GTAATGGGCCAATAACACCG 3'		[25]
<i>tet(K)</i>	tetK–F	5' CCTGGAATTACAACTGGGT 3'	1080 bp	[26]
	tetK–R	5' CCTCCTACAATTGCTATACC 3'		[26]
<i>tet(M)</i>	tetM–F	5' GTTAAATAGTGTCTTGGAG 3'	657 bp	[27]
	tetM–R	5' CTAAGATATGGCTCTAACAA 3'		[27]

131.2.5 Tetracycline Resistance Validation with K–B Disk Diffusion Method

K–B disk diffusion method was used to test tetracycline resistance phenotype of the isolates and it was performed according the descriptions [22]. In brief, overnight isolate culture was diluted to suspension of 1.5×10^8 cfu/mL with sterile phosphate buffered saline, and 100 μ L was spread on MH agar plate. The tetracycline disk was attached to the premarked position and the diameters of zones of inhibition were measured after 16–18 h incubation at 35 °C. Antibiotic susceptibility was determined according to the manual of Clinical and Laboratory Standards Institute (CLSI) [23].

131.2.6 Tetracycline Resistance Related Genes Screening

A series of genes have been found related to tetracycline resistance in both Gram negative and positive bacteria. With the identification of the isolates by comparative analysis of 16S rRNA, the primers are selected to amplify tetracycline resistance genes based on the previous studies [9]. The sequences of primers and the amplicon sizes are listed in Table 66.1. The PCR reactions are performed according to the previous descriptions [24–27].

131.3 Results and Discussion

131.3.1 Screening of Tetracycline Resistant Bacteria

Diluted milk samples were spread on LB agar plates supplement with 16 μ g/mL tetracycline. Totally, 187 strains were isolated from 198 raw milk samples. Among the isolates, some of them were from the same samples but with different morphologies. Screening results showed that 98 (49.49 %) samples had tetracycline resistant strains, similar to the previous studies [28].

131.3.2 Identification of the Isolates

Fifteen strains were randomly selected for comparative 16S rRNA analysis (Table 66.2). Five strains belonged to the genus *Serratia*. They were harmful human pathogen [29] or insect pathogen [30] (KDZ411). Four strains were homologous to *Pseudomonas aeruginosa*, an opportunistic and important nosocomial human pathogen [31]. Strain KDZ420 was homologous to *Bacillus cereus*

Table 66.2 16S rRNA sequence homology alignments of the isolates

Isolates No.	Homologous strains	Maximum identity (%)
KDZ411	<i>Serratia nematodiphila</i> POT3	99
KDZ412	<i>Serratia marcescens</i> N2.4	99
KDZ416	<i>Serratia marcescens</i> N1.8	99
KDZ418	<i>Serratia marcescens</i> XJCS-MB-3	99
KDZ425	<i>Serratia marcescens</i> N2.4	99
KDZ413	<i>Pseudomonas aeruginosa</i> HNYM41	100
KDZ414	<i>Pseudomonas aeruginosa</i> R13	99
KDZ417	<i>Pseudomonas aeruginosa</i> F1	99
KDZ422	<i>Pseudomonas aeruginosa</i> S2QPS8	99
KDZ415	<i>Bacillus cereus</i> SWFU2816	90 ^a
KDZ420	<i>Bacillus cereus</i> HKS1-1	97
KDZ419	<i>Providencia rettgeri</i> SNCO1_1A	98
KDZ421	<i>Enterobacter cloacae</i> MS2	99
KDZ423	<i>Staphylococcus pasteurii</i> Z1	99
KDZ424	<i>Acinetobacter junii</i> NW123	99

^a Strain KDZ415 is homologous to *Bacillus cereus* SWFU2816 with the similarity of 90 % and it can only be classified to the order of Bacillales with the confidence of 97 %

causing food-borne illness [32]; KDZ419 was *Providencia rettgeri*, also an opportunistic human pathogen [33]; KDZ421 was *Enterobacter cloacae*, an important nosocomial pathogen responsible for various infections [34]; KDZ423 was *Staphylococcus pasteurii*, a Gram positive bacterium emerging as an agent of nosocomial infections [35, 36]; KDZ424 was *Acinetobacter junii*, a rare human pathogen associated with bacteraemia in neonates and pediatric oncology patients [37]. KDZ415 only showed 90 % similarity to the known sequences in databases of GenBank and cannot be assigned to specific genus [38]. After analysis with Classifier in RDPII, strain KDZ415 was tentatively assigned to the order Bacillales with 97 % confidence [39].

131.3.3 Tetracycline Resistance Validation and Hemolysis Test of Part of the Isolates

The tetracycline-resistant phenotypes were validated by K–B disk fusion method. The results showed that 11 isolates resistant to tetracycline (R) and 4 isolates were intermediate (I) (Table 66.3). No strain was found susceptible to tetracycline. The results suggested that LB agar plates with antibiotics were suitable for primary screening of antibiotic resistant bacterial strains from clinical or environmental samples.

To investigate the virulence of the 15 isolates, their hemolytic properties were analyzed with blood agar plates. Beta-hemolysis was observed in 4 strains including one *P. aeruginosa* strain, one *S. marcescens* strain, one *B. cereus* strain,

Table 66.3 Characterization of the tetracycline resistant strains

Isolates	Identity	Resistance genes ^a	Hemolysis	Resistance	<i>tet(AC)</i>	<i>tet(B)</i>	<i>tet(K)</i>	<i>tet(M)</i>
KDZ411	<i>S. nematodiphila</i>	<i>tet(AC)</i> , <i>tet(B)</i>	γ	R	•			
KDZ412	<i>S. marcescens</i>	<i>tet(AC)</i> , <i>tet(B)</i>	γ	I				
KDZ416	<i>S. marcescens</i>	<i>tet(AC)</i> , <i>tet(B)</i>	γ	R	•	•		
KDZ418	<i>S. marcescens</i>	<i>tet(AC)</i> , <i>tet(B)</i>	γ	R	•	•		
KDZ425	<i>S. marcescens</i>	<i>tet(AC)</i> , <i>tet(B)</i>	β	R	•	•		
KDZ413	<i>P. aeruginosa</i>	<i>tet(AC)</i>	α	R	•	•		
KDZ414	<i>P. aeruginosa</i>	<i>tet(AC)</i>	γ	R	•			
KDZ417	<i>P. aeruginosa</i>	<i>tet(AC)</i>	β	R	•			
KDZ422	<i>P. aeruginosa</i>	<i>tet(AC)</i>	γ	R	•			
KDZ415	Unclassified ^b	<i>tet(K)</i> , <i>tet(M)</i>	β	R	•	•		
KDZ420	<i>B. cereus</i>	<i>tet(K)</i> , <i>tet(M)</i>	β	I				
KDZ419	<i>P. rettgeri</i>	<i>tet(B)</i>	γ	R	•	•		
KDZ421	<i>E. cloacae</i>	<i>tet(B)</i>	γ	I	•	•		
KDZ423	<i>S. pasteurii</i>	<i>tet(K)</i> , <i>tet(M)</i>	γ	R		•	•	
KDZ424	<i>A. junii</i>	<i>tet(M)</i>	γ	I				

^a The resistance genes are the main determinants found in the species

^b KDZ415 is an unclassified Bacillales strain

and one unclassified Bacillales strain, α -hemolysis in 1 strain, and γ -hemolysis in 10 strains (Table 66.3), indicating the widely existence of virulence factors in the isolates [29, 33–37].

131.3.4 PCR Screening of Tetracycline Resistance Genes

Primers specific for amplification of genes *tet(AC)*, *tet(B)*, *tet(K)*, and *tet(M)* were used to screen tetracycline resistance determinants in the isolates.

All tetracycline resistant strains had one or two resistance related genes, while the tetracycline intermediate strains were negative in amplification of the target genes except strain KDZ421 which was *E. cloacae* had gene *tet(AC)* and *tet(B)* (Table 66.3). The results indicated gene *tet(AC)* and *tet(B)* were the most discovered genes relating to tetracycline resistance phenotype. Previous studies have shown that gene *tet(A)*, *tet(B)*, *tet(C)*, *tet(D)*, *tet(E)*, *tet(G)*, *tet(H)*, *tet(I)*, *tet(J)*, *tet(Z)*, *tet(30)*, *tet(31)*, *tet(K)*, *tet(L)*, *otr(B)*, *trc3c*, *tetP(A)*, *tet(V)*, and *tet(Y)* were widely distributed among different Gram negative genera [9, 40]. They encoded proteins for various efflux pumps extruding tetracycline out of cells. Among them, the most common *tet* genes identified were gene *tet(AC)* and *tet(B)* [9, 41, 42]. However, Gram positive strains KDZ415 and KDZ423 were shown having tetracycline resistant gene *tet(AC)* and *tet(B)*, suggesting resistance determinants could be horizontally transferred even across far distant species and bringing in a high-profile biosafety issue [43].

131.4 Conclusions

By screening 197 collected raw milk samples, we obtained 187 tetracycline resistant strains from 98 samples and the prevalence rate was as high as 49.49 % (98/197). The resistance phenotypes were further confirmed with K–B disk diffusion method. With the comparative 16S rRNA analysis of 15 randomly selected strains, the isolates were identified belonging to different genera including *Serratia* (5), *Pseudomonas* (4), *Bacillus* (1), *Providencia* (1), *Enterobacter* (1), *Staphylococcus* (1), *Acinetobacter* (1), and one unclassified Bacillales strain, respectively. In addition, *tet* genes were also investigated by PCR method. All tetracycline resistant strains had one or two tetracycline resistance related genes, and gene *tet(AC)* and *tet(B)* were the most discovered genes. Moreover, gene *tet(AC)* and *tet(B)* were even detected in Gram positive strains KDZ415 and KDZ423, suggesting resistance determinants could be horizontally transferred even across far distant species and bringing in a high-profile biosafety issue. Our results showed that tetracycline resistant bacteria with a relatively high diversity commonly existed in raw milk with a high prevalence.

Acknowledgments This work was partly supported by The National Natural Science Foundation of China (Grant No. 30970114) and The National Key Technology R&D Program of China (Grant No. 2011BAC11B05).

References

1. Asao T, Kumeda Y, Kawai T et al (2003) An extensive outbreak of staphylococcal food poisoning due to low-fat milk in Japan: estimation of enterotoxin A in the incriminated milk and powdered skim milk. *Epidemiol Infect* 130:33–40
2. Jorgensen HJ, Mork T, Hogasen HR et al (1999) Enterotoxigenic *Staphylococcus aureus* in bulk milk in Norway. *Appl Microbiol* 99(1):158–167
3. Desmasures N, Bazin F, Gueguen M (1997) Microbiological composition of raw milk from selected farms in the Camembert Region of Normandy. *Appl Microbiol* 83:53–58
4. Desmasures N, GUEGUEN M (1997) Monitoring the microbiology of high quality milk by monthly sampling over two years. *Dairy Res* 64:271–280
5. Yamamoto K, Takagi M, Endoh YS et al (2000) Influence of antibiotics used as feed additives on the immune effect of erysipelas live vaccine in swine. *J Vet Med B Infect Dis Vet Public Health* 47(6):453–460
6. Docic M, Bilkei G (2003) Differences in antibiotic resistance in *Escherichia coli*, isolated from East-European swine herds with or without prophylactic use of antibiotics. *J Vet Med B Infect Dis Vet Public Health* 50(1):27–30
7. Sievert DM, Boulton ML, Stoltman G et al (2002) *Staphylococcus aureus* resistant to Vancomycin—United States. *MMWR* 51(26):565–567
8. Akiba T, Koyama K, Ishiki Y et al (1960) On the mechanism of the development of multiple-drug-resistant clones of *Shigella*. *Jpn J Microbiol* 4:219–227
9. Chopra I, Roberts M (2001) Tetracycline antibiotics: mode of action, applications, molecular biology, and epidemiology of bacterial resistance. *MMBR* 65(2):232–260
10. Roberts MC (1996) Tetracycline resistance determinants: mechanisms of action, regulation of expression, genetic mobility, and distribution. *FEMS Microbiol Rev* 1(19):1–24

11. Burdett V (1986) Streptococcal tetracycline resistance mediated at the level of protein synthesis. *Bacteriol* 165:564–569
12. Ross JI, EADY EA, COVE JH et al (1998) 16S rRNA mutation associated with tetracycline resistance in a Gram-positive bacterium. *ANTIMICROB AGENTS CH* 42:1702–1705
13. Yang W, Moore IF, Koteva KP et al (2004) TetX is a favin-dependent monooxygenase conferring resistance to tetracycline antibiotics. *Biol. Chem.* 279:52346–52352
14. Yuan Y, Zhang Y, Hou Y et al (1991) The isolation and identification procedures of cow mastitis bacteria. *Chin J Vet Sci Technol* 21(2):7–10
15. Fitzgetald JR, Meaney WJ, Hartigani PJ (1997) Fine-structure molecular epidemiological analysis of *Staphylococcus aureus* recovered from cows. *Epidemiol Infect* 119(5):261–269
16. Shinefield HR (2006) Use of a conjugate polysaccharide vaccine in the prevention of invasive staphylococcal disease: is an additional vaccine needed or possible. *Vaccine* 24(2):65–69
17. Hendrickson ER, Payne JA, Yong RM et al (2002) Molecular analysis of dehalococoides 16S ribosomal DNA from chloroethene-contaminated sites throughout North America and Europe. *Appl Environ Microb (AEM)* 68(2):485–495
18. Roe DE, Braham P, Weinbetg A, et al (1995) Characterization of tetracycline resistance in *Actinobacillus actinomycetemcomitans*. *Oral Microbiol Immunol* 10:227–232
19. Tiedje JM, Wang QG, Garrity M et al (2007) Naive Bayesian classifier for rapid assignment of rRNA sequences into the new bacterial taxonomy. *Appl Environ Microb (AEM)* 73(16):5261–5267
20. Janda JM, Sharon L (2007) 16S rRNA gene sequencing for bacterial identification in the diagnostic laboratory: pluses, perils, and pitfalls. *J Clin Microbiol* 45(9):2761–2764
21. Johnson MK, Boese-Marrazzo D (1980) Production and properties of heat-stable extracellular hemolysin from *Pseudomonas aeruginosa*. *Infect Immun* 29(3):1028–1033
22. Kastner S, Perreten V, Bleuler H et al (2006) Antibiotic susceptibility patterns and resistance genes of starter cultures and probiotic bacteria used in food. *Syst Appl Microbiol* 29:145–155
23. CLSI/(NCCLS) (2005) Performance standards for antimicrobial susceptibility testing. Fifteenth Informational Supplement, 25(1):44–51, 110–115
24. Jones CH, Tuclman M, Howe AYM et al (2006) Diagnostic PCR analysis of occurrence of methicillin and tetracycline resistance among *Staphylococcus aureus* isolates from phase 3 clinical trials of tigecycline for complicated skin and skin structure infection. *Antimicrob Agents Chemother* 20(2):505–510
25. Yu Z, Michel FC Jr, Hansen G et al (2005) Development and application of real-time PCR assays for quantification of genes encoding tetracycline resistance. *APPL ENVIRON MICROB (AEM)* 71(11):6926–6933
26. Rahman MH, Sakamoto KQ, Nonaka L et al (2008) Occurrence and diversity of the tetracycline resistance gene *tet (M)* in enteric bacteria of Antarctic adelic penguins. *J Antimicrob Chemoth* 62(3):627–628
27. Liu W-H, Xu Y-D, Guo A-Z, Jia A-Q, Liu J-F, Chen H-C (2006) PCR amplification of *tetB* gene for pathogenic *Salmonella* isolated from diseased pigs. *Chin J Antibiot* 31(11):51–55
28. Huys G, D'Haene K, Collard J-M et al (2004) Prevalence and molecular characterization of tetracycline resistance in *Enterococcus* isolates from food. *Appl Environ Microbiol* 70(3):1555–1562
29. Kurz CL, Chauvet S, Andrès E et al (2003) Virulence factors of the human opportunistic pathogen *Serratia marcescens* identified by in vivo screening. *EMBO J* 22:1451–1460
30. FLYG C, Kenne K, Boman HG (1980) Insect pathogenic properties of *Serratia marcescens*: phage-resistant mutants with a decreased resistance to *Cecropia* immunity and a decreased virulence to *Drosophila*. *Microbiology* 120(1):173–181
31. Pier GB (2002) CFTR mutations and host susceptibility to *Pseudomonas aeruginosa* lung infection. *Curr opin Microbiol* 5(1):81–86
32. BBI (2001) International status of large scale production and use of fuel ethanol in Brazil. World Fuel Ethanol Congress, Beijing

33. Camus AC, HawkeJP (2002) *Providencia rettgeri*-associated septicemia and meningoencephalitis in juvenile farmed American alligators *Alligator mississippiensis*. *J Aquat Anim Health* 14(2):149–153
34. Mezzatesta ML, Gona F, Stefani S (2012) *Enterobacter cloacae* complex: clinical impact and emerging antibiotic resistance. *Future Microbiol* 7(7):887–902
35. Widerström M, Wiström J, Sjöstedt A et al (2012) Coagulase-negative staphylococci: update on the molecular epidemiology and clinical presentation, with a focus on *Staphylococcus epidermidis* and *Staphylococcus saprophyticus*. *Eur J Clin Microbiol* 31(1):7–20
36. Carpaij N, Willems RJL, Bonten MJM et al (2011) Comparison of the identification of coagulase-negative staphylococci by matrix-assisted laser desorption ionization time-of-flight mass spectrometry and *tuf* sequencing. *Eur J Clin Microbiol* 30(10):1169–1172
37. Cayô R, San Segundo LY, del Molino Bernal ICP et al (2011) Bloodstream infection caused by *Acinetobacter junii* in a patient with acute lymphoblastic leukaemia after allogeneic haematopoietic cell transplantation. *J Med Microbiol*, 60(3):375–377
38. Goebel BM, Stackebrandt E (1999) A place for DNA–DNA reassociation and 16S rRNA sequence analysis in the present species definition in bacteriology. *Int J Syst Bacteriol*, 94(44):846–849
39. Cole J et al (2005) The ribosomal database project (RDP-II): sequences and tools for high-throughput rRNA analysis. *Nucleic Acids Res* 33:294
40. Roberts MC (2012) Acquired tetracycline resistance genes. *Antibiot Discov Devel* 3:543–568
41. Costa D, Poeta P, Sáenz Y et al (2008) Prevalence of antimicrobial resistance and resistance genes in faecal *Escherichia coli* isolates recovered from healthy pets. *Vet Microbiol* 127(1–2):97–105
42. Santamaría J, López L, Soto CY (2011) Detection and diversity evaluation of tetracycline resistance genes in grassland-based production systems in Colombia, South America. *Front Microbiol* 2:252
43. Rizzotti L, La Gioia F, Dellaglio F et al (2009) Molecular diversity and transferability of the tetracycline resistance gene *tet(M)*, carried on Tn916-1545 family transposons, in enterococci from a total food chain. *Anton Leeuw Int J G* 96(1):43–52

Chapter 132

Study on Biological Denitrification Removal Technologies Treating Eutrophication Water

Zongzheng Yang, Huan Zhang, Deqiang Zhang and Jinzhao Pang

Abstract In this paper, efficient bacteria including photosynthetic bacteria, nitrifying bacteria, compound bacteria, etc., were applied to degrade pollutants of the urban lakes. The results showed that the removal rates of organic substances, chlorophyll-a and nitrogen compounds were 60, 90, and 50 %, respectively. Moreover, dissolved oxygen (DO) content increased from 1 to 7 mg/L and pH value remained at about eight by adding microbes. The conclusion can be drawn that it is a feasible method for adding microbes into eutrophication water for its decontamination.

Keywords Efficient bacteria · Eutrophication · Sewage decontamination · Bioaugmentation

132.1 Introduction

The urban landscape water is mostly static or closed and the fluidity of the water is poor. Some of them even appear in different degrees of eutrophication, which seriously affects the surrounding natural and living environment, and then the

Z. Yang (✉) · J. Pang

Tianjin Key Laboratory of Pulp and Paper, Tianjin University of Science & Technology,
Tianjin 300457, People's Republic of China
e-mail: yzz3520@163.com

H. Zhang

College of Marine Science and Engineering, Tianjin University of and Technology, Tianjin
300457, People's Republic of China

D. Zhang

Tianjin Qing Shuo Environmental Protection Engineering Co., Ltd, Tianjin 300451,
People's Republic of China

Table 132.1 The quality of the original water

pH	Turbidity (NTU)	NH ₄ ⁺ -N (mg/L)	COD _{Mn} (mg/L)	DO (mg/L)	Chlorophyll-a (mg/m ³)
7.7–8.1	55–65	0.7–1	13–17	0.8–1.5	118–130

function of the landscape water is lost [1]. So it is of significance to study the eutrophication water and protect water environment.

Now, the controlling methods of the landscape water eutrophication include physical, chemical, biological methods, and ecological restoration and the treatments have achieved good results. Zhang et al. used the diving aerating method to remediate the urban landscape water [2]. Yuan et al. used the coagulant which contained aluminum sulfate ($\text{Al}_2(\text{SO}_4)_3 \cdot 18\text{H}_2\text{O}$) and ferric chloride ($\text{FeCl}_3 \cdot 6\text{H}_2\text{O}$) to remove the algae and phosphorus of the eutrophication landscape water [3]. Domaizon and Devaux researched the different densities of silver carps to remove the algae [4]. Joebgen et al. used biological floating island to repair the eutrophication water [5]. In this paper, the bioaugmentation technology was used to control the growth of the algae of the water, to inhibit the growth of the algae by the biodegradation of organic pollutants of the water, to prevent the occurrence of water bloom, and to improve the quality of the landscape water. The removal rate of the organic substances was significantly improved by using the efficient bacteria to treat urban wastewater, and the production of solid substances was reduced. Moreover, nitrification can be enhanced and the denitrification efficiency of sewage can be improved.

132.2 Materials and Methods

132.2.1 Test Water

The serious eutrophicated water was taken from “Jingye Lake” in Tianjin University campus (the quality of lake water was shown in Table 132.1) and subpackaged in 350-L white plastic buckets. The water in Bucket 1 was left untreated and used as the control; while the water in Bucket 2 and 3 was treated successively by nitrifying bacteria, photosynthetic bacteria, and compound bacteria, with the interval of 1d. The total concentration of three kinds of bacteria was 50 mg/L for bucket 1, and 100 mg/L for bucket 2. The total bacteria concentrations of the two buckets were 50 and 100 mg/L, respectively. The water temperature during the test was between 24 and 30 °C.

132.2.2 Test Methods

COD_{Mn} Acidic potassium permanganate index;

Ammonia	Condensed sedimentation pretreatment, Nessler's reagent spectrophotometry;
Chlorophyll-a	90 % acetone extraction, spectrophotometer (722, Shanghai Optical Instrument Factory, China);
Turbidity	Optical turbidity meter (GDS-3B, Shanghai Jianglai Experiment Equipment Co., Ltd., China);
DO	Portable oxygen analyzer (IPB-60T, Shanghai Precision & Scientific Instrument Co., Ltd., China);
pH value	pH meter (PHS-3C, Tianjin Huayi Shengda Instrument Co., Ltd., China)

132.3 Results and Discussion

132.3.1 The Removal of COD_{Mn}

The organic substances were mainly from decomposing plants and animals, domestic sewage, and industrial wastewater discharged. A large number of organic substances in the water caused algae multiplication and DO reduced. Therefore, it is very important to remove COD_{Mn} . COD_{Mn} changed with time is shown in Fig. 132.1.

In Fig. 132.1, it is shown that COD_{Mn} of the untreated water appeared as the maximum value 22.1 mg/L on the 7 day, and this value was much higher than the initial value 13.8 mg/L. Moreover, the fluctuation of the untreated water was much bigger, but the other COD_{Mn} curves with bacteria showed declining trends. Its removal rate was more than 50 % with the bacteria concentration of 100 mg/L on the 5th day. The results showed that efficient bacteria had a good function of COD_{Mn} removal. And it can also be seen that the curve with the bacteria

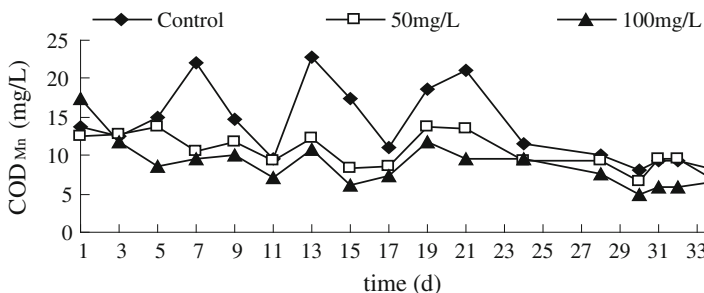


Fig. 132.1 COD_{Mn} changed with time

concentration of 100 mg/L had a much greater decline trend. So it is shown that the removal rate of COD_{Mn} increased with the increasing bacterial concentration.

132.3.2 The Removal of $\text{NH}_4^+\text{-N}$

Ammonia nitrogen in the water was first converted into nitrate nitrogen by nitrifying bacteria, and then nitrate nitrogen was converted into nitrogen by denitrifying bacteria, releasing to the atmosphere. Concentration of $\text{NH}_4^+\text{-N}$ changed with time is shown in Fig. 132.2.

In Fig. 132.2, $\text{NH}_4^+\text{-N}$ value increased to a certain extent during the early days after bacteria inputting. That is because nitrogen compounds were converted into ammonia nitrogen, then ammonia nitrogen was converted into nitrate nitrogen mainly by nitrifying bacteria. Nitrifying bacteria are strict autotrophic bacteria. Moreover, nitrifying bacteria adapt to the environment relatively slow, and the growth rate and metabolism are also very slow. So that $\text{NH}_4^+\text{-N}$ value descend rate was very slow at the beginning of the test. And the growth rate of nitrifying bacteria and nitrification rate were also low at this period. Its removal rate was more than 50 % with the bacteria concentration of 100 mg/L on the 5th day. Furthermore it can also be seen that the curve had a much greater decline trend with bacteria concentration of 100 mg/L, in comparison with that of bacterial concentration 50 mg/L. So it is shown that the removal rate of $\text{NH}_4^+\text{-N}$ increased with increasing bacteria concentration. It can be found that the fluctuation of $\text{NH}_4^+\text{-N}$ and COD_{Mn} value accorded well with each other by comparing Figs. 132.1 and 132.2, because the complex organic substances in the wastewater were decomposed gradually [6].

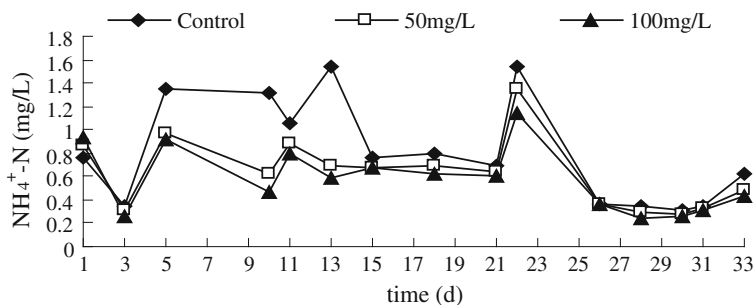


Fig. 132.2 $\text{NH}_4^+\text{-N}$ changed with time

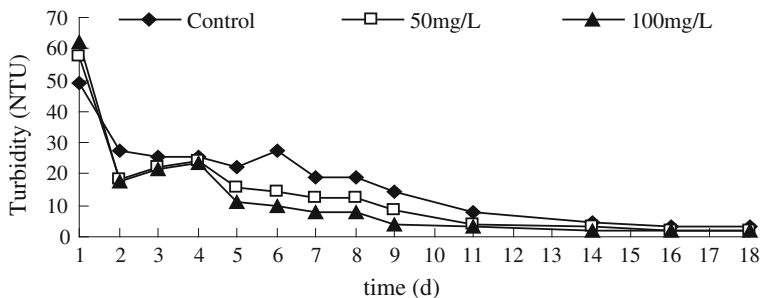


Fig. 132.3 Turbidity changed with time

132.3.3 The Removal of Turbidity

Water turbidity is caused mainly by the substances such as sand, clay, protozoa, algae, bacteria, virus, and organic polymer. Turbidity changed with time is shown in Fig. 132.3.

In Fig. 132.3, water turbidity decreased obviously. Because the organic substances was degraded by efficient bacteria, supernatant turbidity of water sample with the bacteria concentration of 100 mg/L dropped from 62NTU(?) to about 7NTU(?) on the 8th day, and the removal rate of turbidity was about 88 %. The decrease rate of turbidity became faster with increase in bacteria concentration. Turbidity of the untreated water also decreased because of natural settling, but the decline trend was slower than the test.

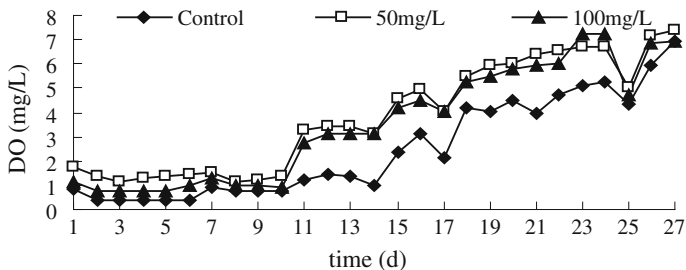


Fig. 132.4 DO changed with time

132.3.4 Effect on DO

In the lakes of the eutrophication, the algae are so dense that it was difficult for the sunlight to penetrate into deep lake, which caused a limited and weakened photosynthesis for deep water. Moreover, the DO value of the source water is decreased due to the accumulation of algae. Next, decomposition of died algae will also consume a lot of DO of in the deep water. But organic substances decrease continuously as they become microbial foodstuffs after the efficient bacterial have been applied, which inhibit the growth of algae. As a result, DO recovers as a result of weakened coverage of algae. DO changed with time is shown in Fig. 132.4.

In Fig. 132.4, DO value was lower than 2 mg/L for the previous 10 days of the test, which was mainly due to growing of nitrifying bacteria at this period. DO value increased steadily from 2 mg/L to about 7 mg/L after the 10th day, which was beneficial for the nitrification, and caused the decreased $\text{NH}_4^+\text{-N}$ value of the water. DO value was about 4.2 mg/L with the bacteria concentration of 50 mg/L on the 15th day. While the DO value of the untreated water was only 2.36 mg/L. It is shown that the bacteria method is superior to natural re-oxygenation. It can be seen from Fig. 132.4 that DO value with higher bacteria concentration was lower than that of lower bacteria concentration. Because the water of the high bacteria concentration decomposed a large number of the organic substances, and then the DO value decreased much slowly.

132.3.5 Changes of Chlorophyll-a

Contents of nitrogen and phosphorus in water are the main factors that affected the multiplication of the algae. The higher the contents of nitrogen and phosphorus are, the more algae become. The contents of nitrogen and phosphorus of the

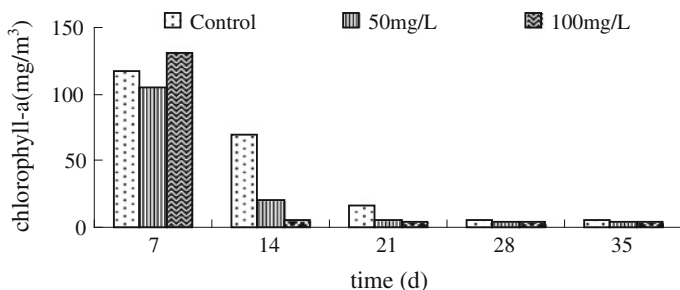


Fig. 132.5 Chlorophyll-a changed with time

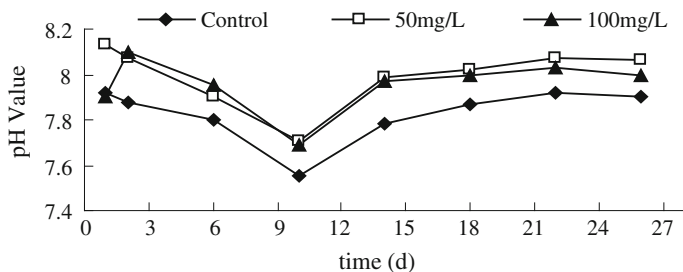


Fig. 132.6 pH value changed with time

sediment increase after the algae died or sank into the lake, since the sediment releases nitrogen and phosphorus into the water, so that the algae grows more quickly, and then a negative cycle is formed. Chlorophyll-a is an important indicator of the algae. Chlorophyll-a changed with time is shown in Fig. 132.5.

In Fig. 132.5, the concentration of chlorophyll-a in three barrels decreased significantly for a week after the bacteria being input. The reason why the control declined was that the water can self-purify without sediment, so that nitrogen and phosphorus of the water reduced and then the concentration of chlorophyll-a decreased. The decreased rate of chlorophyll-a became faster with increase in the bacteria concentration. The color of the water began to change from dark green to clear 2 days after the bacteria treatment and the floating algae on the water also decreased markedly [7].

132.3.6 Change of pH Values

The water maintained alkaline during the test, and the pH value was around eight because the various bacteria coordinated with each other [8]. The pH value changed over time is shown in Fig. 132.6.

The pH value kept stable in the testing duration of 27 days, because photosynthetic bacteria and compound bacteria produced alkali, and nitrifying bacteria consumed alkali in the metabolic activities. The various bacteria maintained good activity and appropriate metabolic conditions, so that the pH was in equilibrium.

132.4 Conclusions

- (1) It was convinced that photosynthetic bacteria, nitrifying bacteria, and compound bacteria behaved well in decontaminating micro-polluted water in this paper.

- (2) The eutrophication of landscape water can be well controlled and decontaminated by inputting microbes, which was very simple to operate. Furthermore, it could not form the secondary pollution or transfer pollutants.

Acknowledgments This work was financed by the Tianjin Binhai New Area Tanggu Science and Technology Development Foundation (2010STHB09-04), China.

References

1. Shan B, Liu H (2008) Field study on usage of bio-eco treatment of circulation & purifying system for polluted scenic water in urban areas. *Chn J Environ Eng* 2(5):702–706
2. Zhang Z, Zheng Z, Zhang P et al (2007) Study on re-oxygenation effect diving aerating device repairing the urban landscape water. *China Water & Wastewater* 20(Supplement):207–210
3. Yuan L, Zhang W, Kong H (2009) Removal test of phosphate and algae from eutrophic landscape water by coagulation. *J Xi'an Univ Archit Technol (Nat Sci edn)* 41(2):236–240
4. Joebgen A, Palm A, Melkonian M (2004) Phosphorus removal from eutrophic lakes using periphyton on submerged artificial substrata. *Hydrobiologia* 528(1–3):123–142
5. Domaizon I, Devaux J (2009) Experimental study of the impacts of silver carp on plankton communities of eutrophic Villerest reservoir. *Aquat Ecol* 33:193–204
6. Zonghua W, Pang J, Xinzheng W et al (2009) Study on dominant consortium treating eutrophication water. *J Nanyang Normal Univ* 8(09):43–45
7. Pang J, Yang Z, Sun Y (2008) Purifying the urban lake by adding dominant bacteria. *China Water Wastewater* 19(6):51–52
8. Lillie SH, Pringle JR (1980) Reserved carbohydrate metabolism in *Saccharomyces cerevisiae*: response to nutrient limitation. *J Bacteriol* 26(4):1384–1394

Chapter 133

Study on Decolorization Effect of Biological Strengthening the Activated Carbon with White Rot Fungi

Zongzheng Yang, Junxia Xu, Peng Yu and Jinzhao Pang

Abstract The colority and Chemical Oxygen Demand (COD) removal rates of biological strengthening the activated carbon with *Phanerochaete chrysosporium* and *Rhodopseudomonas* for papermaking and printing-dyeing wastewater were investigated. With 1 % (v/v) *Phanerochaete chrysosporium*, the colority removal rate for papermaking wastewater reached 80 % at 3 h of retention time, and for printing-dyeing wastewater at 1.5 h of retention time; the COD removal rate was 65.14 and 78.78 % respectively at 3 h of retention time. Having been treated by 1 % *Rhodopseudomonas*, the colority removal rate was lower than that induced by *Phanerochaete chrysosporium*, and the COD removal rate was 71.35 % for papermaking wastewater. Combined strains treatment produced the colority and COD removal rate of 90 and 80 % respectively for papermaking wastewater. The COD removal rate of the biological strengthening activated carbon technique strengthened by *Rhodopseudomonas* first was higher than that strengthened by *Phanerochaete chrysosporium* first.

Keywords *Phanerochaete chrysosporium* · *Rhodopseudomonas* · Biological activated carbon technique · Papermaking wastewater · Printing-dyeing wastewater · The Colority removal rate

Z. Yang (✉) · J. Pang
Tianjin Key Laboratory of Pulp & Paper, Tianjin University of Science and Technology,
Tianjin 300457, People's Republic of China
e-mail: yzz3520@163.com

J. Xu · P. Yu
College of Marine Science and Engineering, Tianjin University of Science and Technology,
Tianjin 300457, People's Republic of China

133.1 Introduction

The pollution of printing-dyeing and papermaking industry wastewater is the major pollution in the industrial wastewater. Both of printing-dyeing wastewater and papermaking wastewater with larger chromaticity contain a variety of toxic and harmful substances, which can cause dying of aquatic creatures and serious environment pollution if they are discharged directly into the natural water system [1, 2]. Discharge standard of water pollutants for pulp and paper industry (GB3544-2008) [3] puts forward more strict effluent standards, which requires $\text{COD} \leq 80 \text{ mg/L}$ and chromaticity less than 50 of the effluent. Sewage emission concentration of textile printing and dyeing enterprise wastewater also has corresponding stipulation ($\text{COD} \leq 100 \text{ mg/L}$, chromaticity less than 50). Therefore, it is very necessary to study the treatment methods for dyeing-printing and papermaking wastewater.

Phanerochaete can damage and eliminate chromophoric accumulation of the printing-dyeing and papermaking wastewater by secreting special degradation enzymes [4]. Jia Rong et al. [5]. treated printing and dyeing wastewater by biocontact oxidation membrane-forming with white-rot fungi, found that the decolorization rate of the mixed dye wastewater reached 79.5 %. Some researchers treated CEH (Chloride, Enzyme treatment, Hypochlorite) bleaching wastewater with *Trichocheerma* sp fixed in RBC (rotating biological contactor), the decolorization rate was 85 % after 3 days [6]. In practice, the treatment effect of the high efficiency degradation immobilized bacterium is better than that of dosing directly [7]. Activated carbon has strong adsorption ability due to its huge specific surface area, so that the contaminants can be removed by the apposition growth microorganism. But the activated carbon needs to be regenerated or replaced after adsorption saturation, which causes a lot of inconvenience. Biological intensifying activated carbon technique is a kind of typical immobilization technology, which can be repeatedly used by putting free microorganism in limited space and making it keep active for a long time by using chemical or physical methods [8, 9]. It is a very practical way that intensifying biological technology was used in combination with the activated carbon, which not only can prolong the service life of the activated carbon, but also can enhance the microbial degradation effect.

In this paper, the treatment effect by biological intensifying activated carbon technique for printing-dyeing wastewater and papermaking wastewater has been discussed. The operating parameters were optimized to achieve ideal efficiency.

133.2 Materials and Methods

133.2.1 Strains

Strain A (*Phanerochaete chrysosporium*) and strain B (*Rhodopseudomonas*) were screened and stored in the Lab of Wastewater Treatment in Tianjin University of Science and Technology.

Table 133.1 The water qualities of the two wastewaters

Item	Papermaking wastewater	Printing-dyeing wastewater
COD (mg/L)	138.24	103.24
BOD (mg/L)	26.27	28.91
BOD/COD	0.19	0.28
pH	6.75	6.23
Chromaticity (multiple)	37	42
Turbidity (Nephelometric turbidity unit)	2.35	25.9

Phanerochaete chrysosporium: slant culture was activated to prepare a suspension. Then it was inoculated in a potato medium, and cultured at 30 °C, 150 r/min to get biomass. The same treatment was applied to *Rhodopseudomonas*.

133.2.2 The Influent Wastewater

The papermaking wastewater was the effluent after secondary treatment of Shandong Huatai Paper Co., Ltd., Dongying, Shandong, China.

The printing-dyeing wastewater was the effluent after anaerobic–aerobic biological film process of a textile factory in Wujiang County, Jiangsu, China. The water qualities for the two wastewaters are listed in Table 133.1.

133.2.3 Methods

The experiment of the printing-dyeing wastewater and papermaking wastewater treatment was carried out in the shaker (HNY-200D, OuNuo Instrument Limited Company, Tianjin, China) at 150 r/min, 30 °C, with 4–8 mesh activated carbon as filler and high efficient fungal strain A (*Phanerochaete chrysosporium*) and bacterial strain B (*Rhodopseudomonas*) as cultured strains. The wastewaters were treated according to Table 133.2. Each sample was operated in duplicate.

133.2.4 Analytical Methods

Chemical Oxygen Demand (COD): potassium chromate method;

Decolorization rate [10, 11]: the relationship between absorbance and wavelength of papermaking wastewater was measured by UV–VIS spectrophotometer. The results showed that the maximum absorption wavelength of papermaking wastewater was at 460 nm. By measuring the absorbance reduction at maximum

Table 133.2 The treatment of wastewater

Sample No	Wastewater	Strain	Inoculation amount (%)
1	Printing-dyeing	A	1
2	Printing-dyeing	B	1
3	Printing-dyeing	A + B	1
4	Papermaking	A	1
5	Papermaking	B	1
6	Papermaking	A + B	1

A Phanerochaete chrysosporium, B Rhodopseudomonas

absorption wavelength of supernatant of the six samples in Table 133.2, the decolorization rates induced by different strains were determined. The supernatant of the wastewaters were monitored every 0.5 h. If the initial absorbance concentration is A, and the residual absorbance concentration is B, then the decolorization rate is calculated by Eq. (133.1).

$$\text{Decolorization rate} = (A - B)/A \times 100 \% \quad (133.1)$$

133.3 Results and Discussion

133.3.1 The Decolorization Effect of Printing-Dyeing Wastewater and Papermaking Wastewater

The samples were taken every 8 h and observed continually under a microscope until there were a few bacteria existing in the water. So it was believed that most of bacteria have been attached on the carriers. The decolorization rate was measured every 1 h; the experimental results are shown in Figs. 133.1 and 133.2.

No. 1 and 3 had good decolorization effect and higher decolorization rate at 90 min. The decolorization effect of No. 2 with only *Rhodopseudomonas* was worst (Fig. 133.1). The mechanism of decolorization by white-rot fungus is attribute to its special enzyme system produced, which catalyze the oxidate redox chromophoric groups and destroy the unsaturated conjugated bonds. *Rhodopseudomonas* has good biological flocculation, which can further facilitate the decomposition of small molecule organic pollutants. But most of the dyes are synthetic macromolecular aromatic compounds that can not be broken down, so it is impossible to achieve the purpose of decolorization, and its decolorization effect should be the function of adsorption. Figure 133.2 shows the decolorization effect of papermaking wastewater, which reflects mainly the same decolorizing law, but the highest decolorization rate was reached in 180 min. According to the above phenomenon, white-rot fungus has good biological decolorizing effect for printing-dyeing wastewater and

Fig. 133.1 Decolorization effect of printing-dyeing wastewater

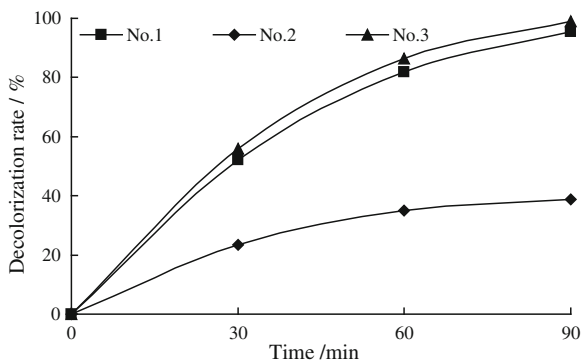
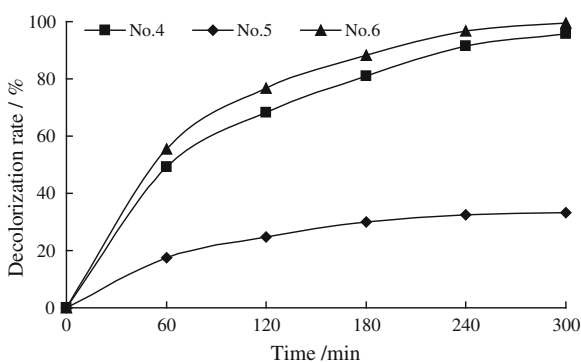


Fig. 133.2 Decolorization effect of papermaking wastewater



papermaking wastewater, which means that white-rot fungus has wide adaptability, non-specificity and the ability of degrading chromophoric accumulation completely.

133.3.2 The COD Removal Effect of Printing-Dyeing Wastewater and Papermaking Wastewater

According to the above decolorization effects, the COD removal effect of the two strains in 180 min was tested respectively; the results are shown in Figs. 133.3 and 133.4.

The COD removal effect of No. 3 and 6 with combined strains was higher than that of the single strain. This can be attributed to extracellular peroxidase (such as lignin peroxidase Lip and manganese peroxidase Mnp) produced by *Phanerochaete chrysosporium*, which can cause a series of free radical reaction, and divide macromolecular complex organic compounds into small molecular substances by opening conjugated bond and benzene rings. *Rhodospseudomonas* has good

Fig. 133.3 Effect of retention time on COD removal rate for printing-dyeing wastewater

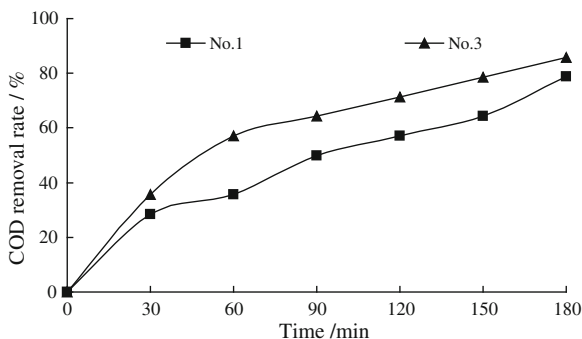
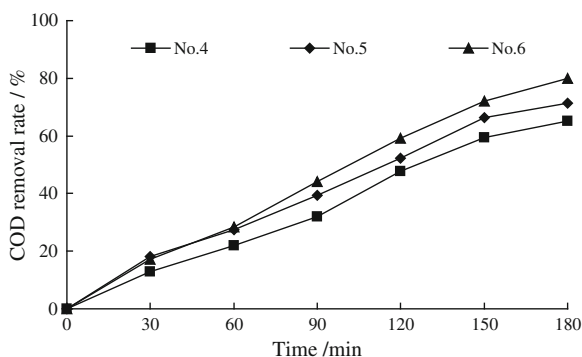


Fig. 133.4 Effect of retention time on COD removal rate for papermaking wastewater



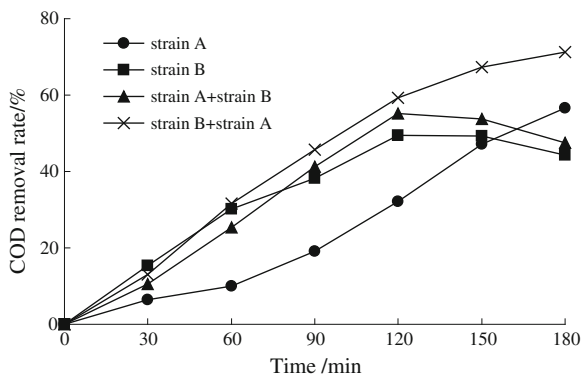
biological flocculation which can further promote small molecule organic pollutants to accelerate the COD removal efficiency.

133.3.3 The Decolorization and COD Removal Effect of Papermaking Wastewater with Combined Strains

The papermaking wastewater was treated respectively by biological activated carbon with strain A, biological activated carbon with strain B, biological activated carbon strengthened by strain A first and then strengthened by strain B, biological activated carbon strengthened by strain B first and then strengthened by strain A. The combination way of the two strains was divided into two stages for 15 min of each stage respectively; the experiment results are shown in Fig. 133.5.

Figure 133.5 shows that the treatment effect of the papermaking wastewater with combined strains was better than that of the single strain at the same time. In the beginning of 60 min, strain B showed the best COD removal effect, while afterwards the beneficial effect of combined strains appeared gradually. Strain B + strain A behaved better than strain A + strain B in terms of COD removal

Fig. 133.5 Comparison of COD removal rate between single strain and combined strains for papermaking wastewater



rate, with about 75 % higher COD removal rate. This is because *Phanerochaete chrysosporium* degraded the macromolecular organic matter, in combination with *Rhodopseudomonas*, which degraded the small molecule organic matters.

133.4 Conclusions

- (1) The function of *Phanerochaete chrysosporium* (strain A) and *Rhodopseudomonas* (strain B) in the advanced treatment of printing-dyeing wastewater and the papermaking wastewater treatments was investigated. The highest decolorization rate can be achieved in 90 min with the treatment of two strains for the printing-dyeing wastewater, and 180 min for the papermaking wastewater.
- (2) The decolorization rates for both wastewaters were higher than 80 %, having been treated by biological activated carbon with the white rot fungus. In the condition of 180 min and 150 r/min shaking speed, the papermaking wastewater effluent COD was 60.82 mg/L with *Phanerochaete chrysosporium*, 49.5 mg/L with *Rhodopseudomonas*, and 33.28 mg/L with the combined strains, which all meet the industrial effluent standards.
- (3) In the treatment of the papermaking wastewater with the combined strains, COD removal rate of the biological activated carbon technique strengthened by *Rhodopseudomonas* first was higher than that strengthened by *Phanerochaete chrysosporium* first.

Acknowledgments This work was financed by the National Science and Technology Planning Project of China under Grant No. of 2011BAC11B04.

References

1. Li ZP, Liu QJ, Lin QT et al (2010) The application study progress of advanced treatment technology of papermaking wastewater. *Trans China Pulp Pap* 25:102–103
2. Gu PJ, Chen WH, Wang PN et al (2006) Considerations on printing-dyeing wastewater treatment. *Pollut Control Technol* 10:52–55
3. GB3544-2008 (2008) Discharge standard of water pollutants for pulp and paper industry. China Standards Press, Beijing
4. Pratima P (2012) Brief description of the pulp and paper making process. In: *Biotechnology for pulp and paper processing*. Springer, New York
5. Zhang RC, Miao XZ, Ma HY et al (2008) A study on advance treatment with bioactive carbon for pulp and paper mill effluent. *China Pulp Pap Ind* 21:54–56
6. Jia R, Zhao F, Wu S et al (2004) Treatment of dyestuff wastewater with white rot fungus bio-contact oxidation technique. *China Environ Sci* 24:205–208
7. Arora DS, Sharma RK (2010) Ligninolytic fungal laccases and their biotechnological applications. *Appl Biochem Biotech* 160:1760–1788
8. Freitas AC, Ferreira F, Costa AM et al (2009) Biological treatment of the effluent from a bleached kraft pulp mill using basidiomycete and zygomycete fungi. *Sci Total Environ* 407:3282–3289
9. Pang JZ, Liu Y (2008) The intensive treatment of paper mill effluent with biological stuffing process. *China Pulp Pap Ind* 29:36–37
10. Kaushik G, Thakur IS (2009) Isolation of fungi and optimization of process parameters for decolourization of distiller mill effluent. *World J Microbiol Biotechnol* 25:955–964
11. Wang A, Xie N, Liang Z (2000) Study on the determination of water colority. *Environ Monit China* 4:37–40

Chapter 134

The Removal of Crude Oil in Waste Drilling Muds by a Constructed Microbial Consortium

Yunkang Chang, Xingbiao Wang, Yifan Han, Manman Wang,
Chenggang Zheng, Yongli Wang and Zhiyong Huang

Abstract Waste drilling muds (WDMs) contain serious pollutants produced by crude oil and gas well drilling. Bioremediation has been known as a useful and cost-effective method for disposal of contaminants in various environments. In this study, an efficient and stable microbial consortium was constructed successfully by successive enrichment of indigenous microorganisms, which can remove oil contaminants from waste drilling muds. Denaturing gradient gel electrophoresis analysis (DGGE) and 16S rRNA gene clone library analysis were used to evaluate the dynamic changes in the microbial consortium in the process. After 7 days' treatment, the main contaminants were removed mostly by constructed microbial consortium than control treatment, which showed that the constructed consortium was of great potential to remediate polluted drilling fields.

Keywords Bioremediation · Crude oil removal · Microbial consortium · Waste drilling muds

Y. Chang · X. Wang · Y. Han · M. Wang · Z. Huang (✉)
Tianjin Key Laboratory for Industrial Biological Systems and Bioprocessing Engineering,
Tianjin Institute of Industrial Biotechnology, Chinese Academy of Sciences,
Tianjin 300308, People's Republic of China
e-mail: huang_zy@tib.cas.cn

M. Wang
College of Biotechnology, Tianjin University of Science and Technology, Tianjin 300457,
People's Republic of China

C. Zheng
Petroleum Exploration and Production Research Institute, SINOPEC, Beijing 100083,
People's Republic of China

Y. Wang
Lanzhou Institute of Geology, Chinese Academy of Sciences, Lanzhou 730000,
People's Republic of China
e-mail: wyl16800@lzb.ac.cn

134.1 Introduction

Waste drilling muds (WDMs) are one of the major pollutants during crude oil and gas well drilling activities in the oil industry. The discharge of WDMs into the environment without any treatment causes problems to the circumjacent soil, groundwater, and human beings due to the harmful ingredients of both organic and inorganic contaminants such as aromatics and heavy metals with carcinogenicity, teratogenicity, and mutagenicity [1–3].

In recent years, researchers pay more and more attention to dealing with WDM contaminants. Some technologies carried out to decrease the environmental damages include thermal disposal [4], microwave treatments [5], supercritical fluid extraction [6], solidification, and stabilization and phytodegradation [7, 8]. However, traditional treatments usually could not overcome some shortcomings in WDMs treatments such as high energy consumption, large land occupation, prohibitive cost, long remediation time, and secondary pollution [9–11].

Bioremediation has been approved by many researchers due to its remarkable advantages such as cost-effectiveness, less land occupation, and no secondary pollution [12]. Hence, researchers have carried out many studies to remediate WDMs using microorganism-related technologies. However, most previous studies only focused on single strain, and the utilized microbial consortium was not stable and not suitable for field application [13, 14].

In this study, the major pollutants of WDMs collected from Dagang oilfield were investigated by X-ray fluorescence spectrometer analysis and total oil extraction analysis. The biodiversity of WDMs sample was investigated by the 16S rRNA gene clone library analysis. Further, a microbial consortium was constructed successfully to remove the oil contaminants from WDMs by successive enrichment of the indigenous microorganisms, and the dynamic changes in the consortium were monitored by DGGE analysis during the enrichment process.

134.2 Materials and Methods

134.2.1 Preparation and Characteristics Of WDMs

134.2.1.1 Physical and Chemical Properties

WDMs were obtained from the drilling field in Dagang Oilfield, southeastern Tianjin, China. The pH, water content, and electrical conductivity of the WDMs were 8.2, 60 % (w/w), 1,796 $\mu\text{s}/\text{cm}$, respectively, which showed that the WDMs were of high water content and weakly saline-alkaline characteristics.

134.2.1.2 Biodiversity of WDMs

Total DNA was extracted from the WDMs sample by UltraClean™ Soil DNA Isolation Kit (Mo Bio Laboratories, Inc., USA) according to the operation manual. The biodiversity of WDMs was tested by 16S rRNA gene amplification and clone library construction, DNA sequencing, alignment, and phylogenetic analysis according to the reported method [15].

134.2.2 Pollutants of WDMs

134.2.2.1 Heavy Metals

Heavy metals of WDM samples were analyzed by X-ray fluorescence spectrometer (PW 4,400/40, PANalytical B.V., Holland) according to the reported method [16].

134.2.2.2 Oil Contaminants in WDMs

According to the reported method [17, 18], the total oil was extracted by dichloromethane and tested by weighing the dry extraction after evaporating the solvent under nitrogen, and then the four fractions (aliphatic, aromatic, resins, and asphaltenes) of the extracted oil were separate by silica gel column chromatography. The fractions were analyzed by gas chromatography–mass spectrometer (GC–MS) (7,890–5,975c, Agilent, USA) equipped with an Agilent HP-5MS fused silica capillary column (60 m × 0.25 mm × 0.25 μm) following the reported method [2].

134.2.3 Construction and Analysis of Microbial Consortium

134.2.3.1 Enrichment of Indigenous Microorganisms

WDMs (10 g, without sterilization) were added to a 250 ml flask containing 50 ml sterile Bushnell–Haas mineral solution (BHM) [19], then 0.05 % (w/v) yeast extract was added to the medium to stimulate the biological activity of indigenous microorganisms of the WDMs. After three days' cultivation at 30 °C, 150 rpm in the shaker, 5 ml of fermentation broth was transferred to 45 ml fresh sterile BHM medium containing 2 % (w/v) crude oil from Dagang Oilfield as the sole carbon source. The culture was enriched through successive inoculum every week over 12 times to obtain a stable microbial consortium with oil-degrading activities.

134.2.3.2 DNA Extraction of Enriched Microorganisms

Bacterial cells of the enriched microbial consortium were collected periodically (0 day, 6, 8, 10, and 12 weeks) in a 2 ml Eppendorf tube by centrifugation at 10,000 g for 5 min. Total DNA of enriched microbial cells was extracted using UltraClean™ Soil DNA Isolation Kit as described above.

134.2.3.3 Primers and 16S rRNA Gene Amplification

The 16S rRNA gene fragments were amplified with primers 341F (5'-CCTACGGGAGGCAGCAG-3') and 518R (5'-ATTACCGCGGCTGCTGG-3'), which targeted universal conserved bacterial 16S rRNA gene sequences [20]. A GC-clamp was attached to the 5' end of primer 341F to prevent complete melting of the DNA fragments during the DGGE analysis [21]. A hot-start PCR was performed at 94 °C for 5 min and a touchdown PCR was performed as follows: the annealing temperature was initially set at 65 °C and then decreased by 0.5 °C every cycle until it decreased to 60 °C, then 18 additional cycles were carried out at 60 °C. Denaturing was carried out at 94 °C for 1 min, and primer annealing was performed at 72 °C for 0.5 min. The final extension step was at 72 °C for 3 min [22].

134.2.3.4 DGGE Analysis

DGGE analysis was performed using a model DCode™ System (Bio-Rad Laboratories Inc., USA) with a denaturing gradient of 40–70 % in a 7.5 % polyacrylamide gel following the manufacturer's instructions. PCR products from the previous step were mixed with the same volume of 2 × Gel loading Dye, and DNA fragments were separated for 12–16 h at 80 V, 60 °C [23]. The gel was stained for 30 min with Super Green I and visualized using a Gel Doc EQ gel documentation system (Bio-Rad Laboratories Inc., USA).

134.2.3.5 Single Bands Excision and PCR Amplification

Single bands from the DGGE gel were excised and placed into 0.5 ml microcentrifuge tubes with 50 µl sterile water. The tubes were incubated overnight at 4 °C. PCR amplifications were carried out with the same program as described above using 1 µl of the DNA eluted from the bands and the same primers. Again, PCR products were used for DGGE analysis to verify whether the excised band was single or not. After that, the true single bands were re-amplified again with the same primers without GC-clamp and the PCR products were sent for sequencing by BGI (<http://www.genomics.cn/index>, China).

134.2.3.6 Analysis of DGGE-Banding Profiles

To assess the dynamic changes in microbial consortium during the enrichment process, DGGE-banding profiles were analyzed by the software Quantityone-1-D (Version 4.6.2) according to the reported method [22].

134.2.4 Crude Oil-Related Experiment

The efficiency of crude oil degraded by constructed microbial consortium was assessed by simulated experiments in the laboratory. WDMs (20 g, without sterilization) were added to 250 ml conical flask containing 80 ml BHM medium and 10 % (v/v) inoculum and incubated at 30 °C, 150 rpm in shaker. The control treatment was the same with microbial flask without inoculum. All the treatments were carried out in triplicate and the average calculated. The degradation rates of crude oil were determined after 7 days' treatment by calculating the weight of the residual oil.

134.2.5 Data Analysis and Chemicals

All the obtained data were subjected to one-way analysis of variance and post hoc Tukey test using the SPSS Version 13.0 statistical package. The results were tested for significance at the 5 % level. All the chemicals used in this study were analytical reagent grade and chromatographic reagent grade.

134.3 Results and Discussion

134.3.1 Microbial Diversity Analysis of WDMs Samples

Phylogenetic analysis (Phylip, Version 3.69) of the partial 16S rRNA gene revealed that indigenous microbial diversity in the WDMs remained a relative high value (Fig. 134.1).

Totally 164 clones were selected and sequenced successfully. After BLAST in NCBI (<http://www.ncbi.nlm.nih.gov/>), the results revealed that sequences mainly grouped with Alpha- and Gamma-proteobacteria (29.88 and 27.44 %, respectively) and Clostridia (16.46 %). In addition, a few clones were affiliated with Beta-proteobacteria (6.71 %) and Delta-proteobacteria (6.71 %) (Fig. 134.2).

Alpha-proteobacteria was the most dominant group in the clone library, which accounted for 29.88 % of the total. These sequences were mainly

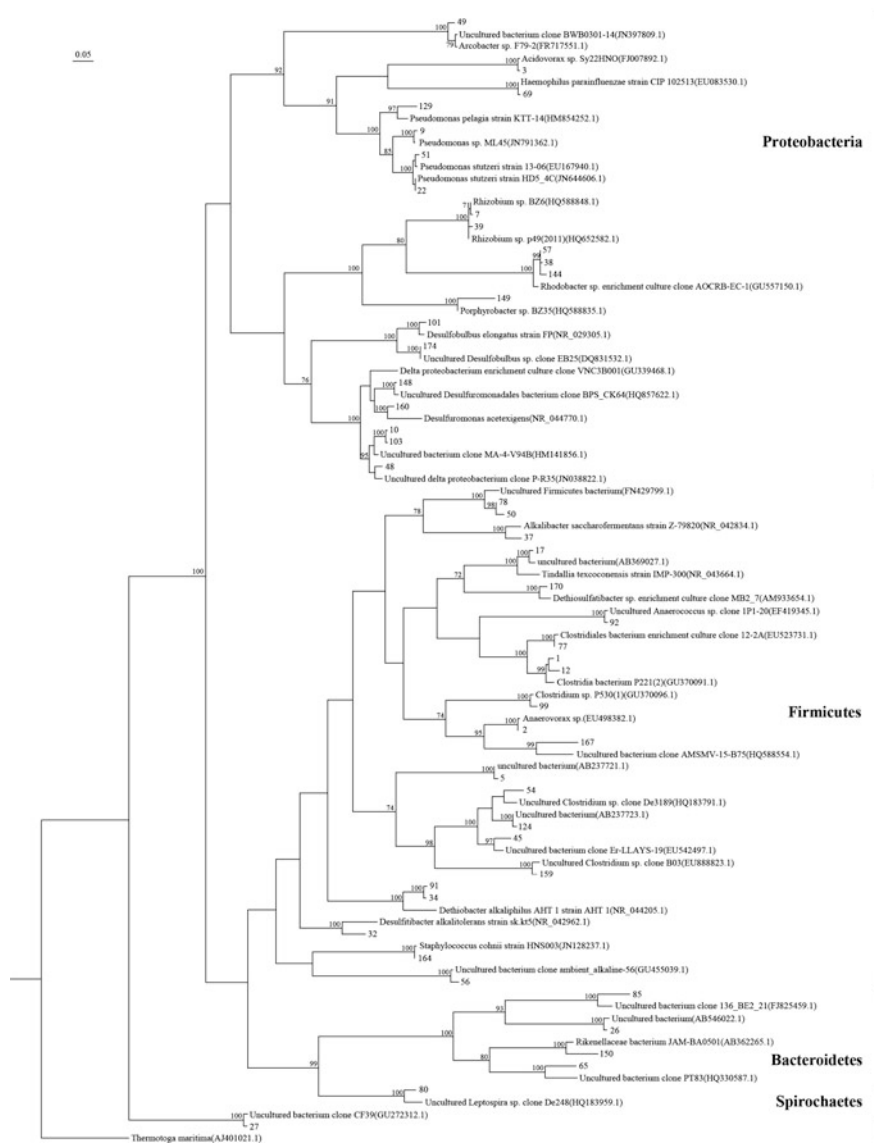


Fig. 134.1 Phylogenetic tree of clones based on partial 16S rRNA gene sequences

grouped and belonged to the genus of *Rhizobium* and *Rhodobacter* (Fig. 134.3). Gamma-proteobacteria was another dominant bacteria, which is of the nearest relationship with the genus of *Pseudomonas*. Many bacteria from these three main genera could degrade petroleum hydrocarbons or their derivatives and play a very important role in oil contaminated environments according to former studies [24–26].

Fig. 134.2 The percentages of different microorganisms of the WDMs

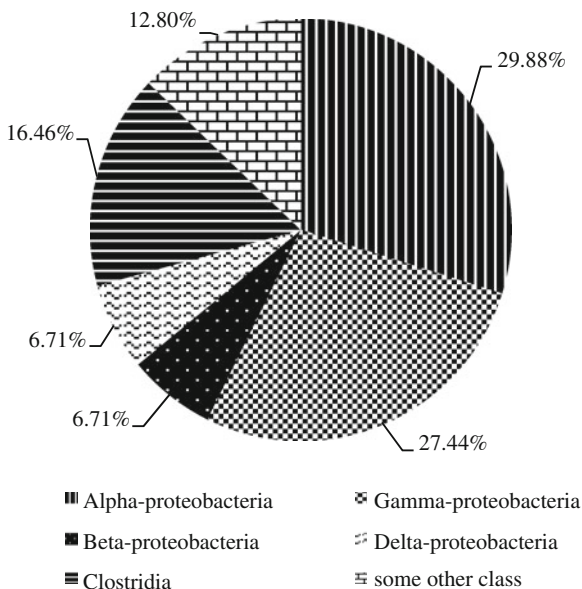
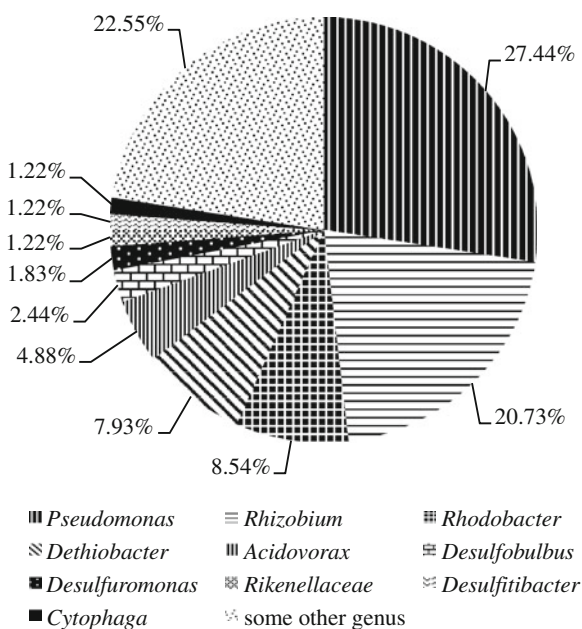


Fig. 134.3 The percentages of microorganisms belong to different genres in the WDMs



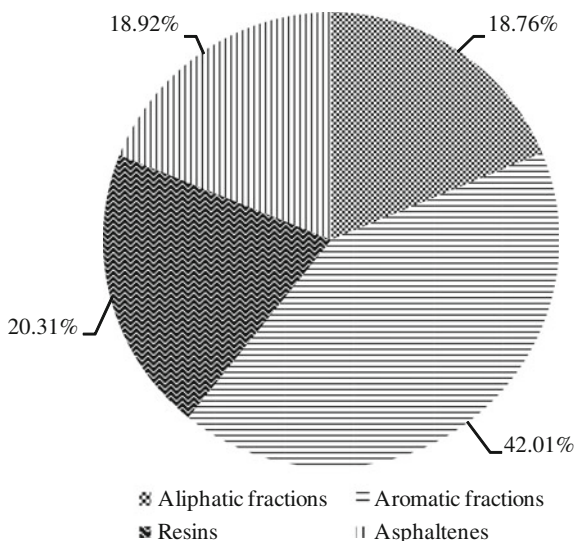
134.3.2 Major Pollutants in WDMs

X-ray fluorescence spectrometers analysis revealed different kinds of heavy metals in the WDMs, including Ba, As, and Pb. Hence, the microorganisms in the WDMs could partly tolerate the toxicity of these heavy metals. However, oil contaminants (containing: aliphatic fractions, 18.76 %, w/w; aromatic fractions, 42.01 %, w/w; resins, 20.31 %, w/w and asphaltenes, 18.92 %, w/w) were determined as the major pollutants according to the oil analysis. The percentage of oil contaminants was about 1.2 ± 0.2 % (w/w), which was quite higher than the threshold of 500 mg/kg set by previous study as serious pollution [27]. The results of silica gel column chromatography analysis revealed that the aromatic fractions were the main part in the contaminated oil of WDMs (Fig. 134.4). The reason may be the aromatic fractions were more difficult to be degraded than aliphatic fractions by indigenous microorganisms and the latter had been degraded at a large scale due to the long time of discard in the drilling field.

In order to study more details of the pollutants in WDMs, further analysis by GC-MS was carried out (Fig. 134.5). The results showed that C₁₄ fraction was the dominant component in the crude oil of WDMs.

Phenanthrene and anthracene were found to be responsible for this result (Fig. 134.6). Similar results were also found by other studies [2, 13]. These two kinds of substances all belonged to polycyclic aromatic hydrocarbons with three cycles, which had been previously reported as environment pollutant for poor bioavailability [28–31], which partially indicated that the WDMs were also of poor bioavailability for microorganisms. The percentages of fractions with carbon

Fig. 134.4 The composition of extracted oil by silica gel column chromatography analysis



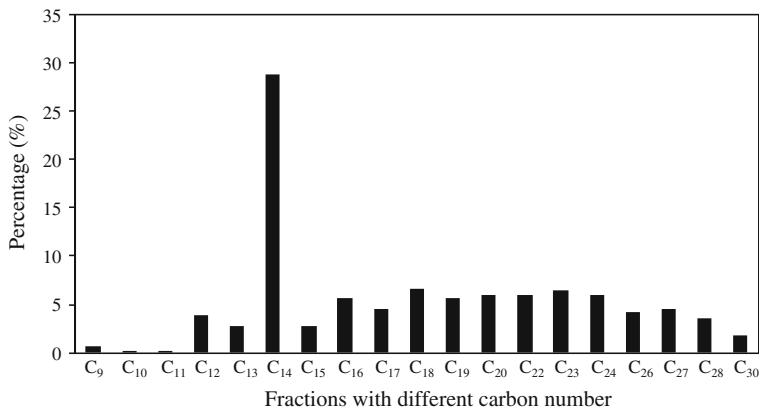
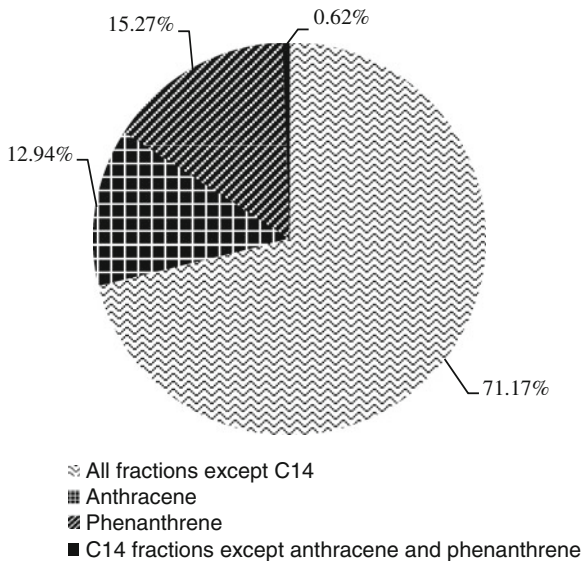


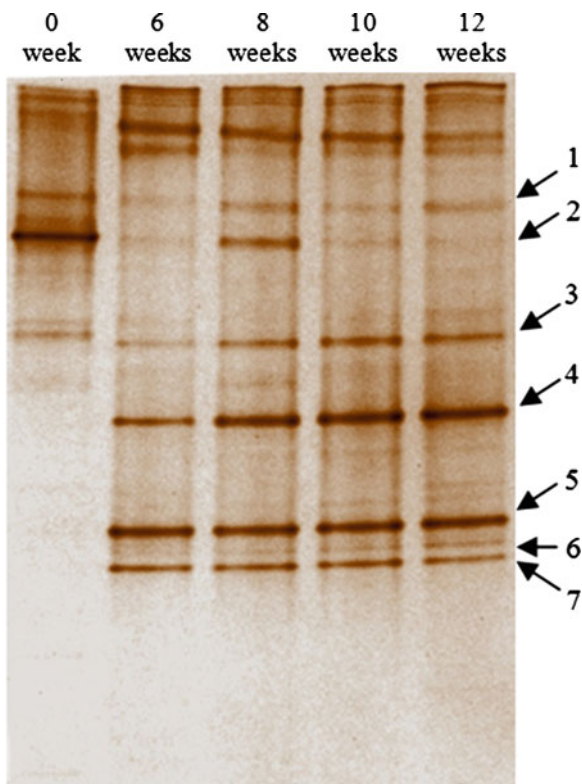
Fig. 134.5 The percentage of fractions with different carbon number by GC-MS analysis

Fig. 134.6 The percentages of phenanthrene and anthracene in oil contaminants



number more than C₁₆ were usually higher than the fractions with carbon number less than C₁₆, which indicated that the long chain hydrocarbon fractions in WDMs were harder to be degraded by microorganisms [32].

Fig. 134.7 DGGE profiles of microbial consortium composition during the enrichment process



134.3.3 Analysis of Enriched Microbial Consortium

Microbial consortium profiles elucidated by DGGE of different times at 0 day, 6, 8, 10, and 12 weeks are shown in Fig. 134.7.

The result revealed that a stable microbial consortium had been constructed after 12 weeks' enrichment. Prominent single band was excised, PCR-amplified and sequenced (Table 134.1). At day 0, the most intensive two bands, band 1 and band 2 were sequenced and identified as *Pseudomonas aeruginosa* and *Pseudomonas*

Table 134.1 Sequence analysis of the major DGGE bands

Band	Systematic affiliation (closest relatives)	Sequence homology (%)	Accession number
1	<i>Pseudomonas aeruginosa</i>	99	DQ459316
2	<i>Pseudomonas stutzeri</i>	100	HQ189757
3	<i>Alishewanella</i> sp.	99	EU287929
4	<i>Alishewanella aestuarii</i>	100	NR_044344
5	<i>Halomonas</i> sp.	100	AB477015
6	<i>Halomonas</i> sp.	100	HM566027
7	<i>Halomonas desiderata</i>	100	AB362300

stutzeri, respectively. It was consistent with the result of 16S rRNA gene clone library. These two species were usually studied in petroleum hydrocarbons degradation experiments [33, 34]. The results showed the intensity of band 1, 3, 4, 5, 7 remained relatively constant during the last 4 weeks' enrichment process from which it could be inferred that these five species were synergistic in this specific environment (Fig. 134.7). At the end of the enrichment process, band 4 and band 5 belonged to the genus of *Alishewanella* and *Halomonas*, tied for the first place in the microbial consortium. *Alishewanella* could typically use multiple electron acceptors to enhance the biodegradation of oil contaminants in anoxic environments [35]. *Halomonas* had been previously studied as good oil contaminant degraders, especially in saline and alkaline environments [36–38].

134.3.4 Degradation Rate of Crude Oil by Microbial Consortium

After 7 days' treatment, nearly 69 % (w/w) of total oil contaminants were successfully degraded, and the degradation rate by the control treatment was only 8 % (w/w). The indigenous microorganisms of the added WDMs may cause oil contaminants degradation in the control treatment, but there was low cell density and poor nutrients in the WDMs, so the degeneration proportion of oil in control treatment was low. By contrast, the added microbial consortium and abundant nutrients caused great power to remove the oil contaminants from WDMs.

134.4 Conclusions

An efficient and stable microbial consortium was constructed successfully by successive enrichment of indigenous microorganisms which were used to remove the oil contaminants from WDMs. DGGE proved to be a very useful method for monitoring the dynamic changes in the constructed active microbial consortium. According to the results, the constructed active microbial consortium was of high genetic stability for the dominant members kept constant in the final stage of enrichment process and remarkable crude oil degradation rate which showed that the microbial consortium was of great potential applied value in polluted drilling fields. A field treatment model will be designed in the future to access the efficiency for field application.

Acknowledgments This work was supported by the Major Project of Tianjin Science and Technology Support Plan (Grant No. 11ZCZDSY09000), the CAS Strategic Priority Research Program (Grant No. XDA05120204), the Knowledge Innovation Program of the Chinese Academy of Sciences (Grant No. KZCX2-EW-104), the NSFC (Grant No. 51104106) and Western Light Joint scholars project.

References

1. Zhao XB, Ji XH, Zhang YH et al (2004) Effect of solvent on the microstructures of nanostructured Bi₂Te₃ prepared by solvothermal synthesis. *J Alloy Compd* 368:349–352
2. Yan P, Lu M, Guan Y et al (2011) Remediation of oil-based drill cuttings through a biosurfactant-based washing followed by a biodegradation treatment. *Bioresour Technol* 102:10252–10259
3. Jacques RJ, Okeke BC, Bento FM et al (2008) Microbial consortium bioaugmentation of a polycyclic aromatic hydrocarbons contaminated soil. *Bioresour Technol* 99:2637–2643
4. Zupan T, Kapila M (2000) Thermal desorption of drill muds and cuttings in Ecuador: the environmental and financially sound solution. *Soc Petrol Eng*. doi:10.2118/61041-MS
5. Robinson J, Kingman S, Snape C et al (2010) Scale-up and design of a continuous microwave treatment system for the processing of oil-contaminated drill cuttings. *Chem Eng Res Des* 88:146–154
6. Street C, Guigard S (2009) Treatment of oil-based drilling waste using supercritical carbon dioxide. *J Can Petrol Technol* 48:26–29
7. Leonard S, Stegemann J (2010) Stabilization/solidification of petroleum drill cuttings: leaching studies. *J Hazard Mater* 174:484–491
8. Ji GD, Yang YS, Zhou Q et al (2004) Phytodegradation of extra heavy oil-based drill cuttings using mature reed wetland: an in situ pilot study. *Environ Int* 30:509–517
9. Vasudevan N, Rajaram P (2001) Bioremediation of oil sludge-contaminated soil. *Environ Int* 26:409–411
10. Benka-Coker MO, Olumagin A (2006) Effects of waste drilling fluid on bacterial isolates from a mangrove swamp oilfield location in the Niger Delta of Nigeria. *Bioresour Technol* 55:175–179
11. Okpokwasili GC, Nnubia C (1995) Effects of oil spill dispersants and drilling fluids on substrate specificity of marine bacteria. *Waste Manage* 15:515–520
12. Mao J, Luo YM, Teng Y et al (2012) Bioremediation of polycyclic aromatic hydrocarbon-contaminated soil by a bacterial consortium and associated microbial community changes. *Int Biodeter Biodegr* 70:141–147
13. Okparanma RN, Ayotamuno JM, Araka PP (2009) Bioremediation of hydrocarbon contaminated-oil field drill-cuttings with bacterial isolates. *Afr J Environ Sci Technol* 3:131–140
14. Toldo JEE, Ayup Zouain RN (2009) Environmental monitoring of offshore drilling for petroleum exploration (MAPEM): a brief overview. *Deep Sea Research Part II: Deep-Sea Res Pt II* 56:1–3
15. Filteau M, Lagacé L, LaPointe G et al (2010) Seasonal and regional diversity of maple sap microbiota revealed using community PCR fingerprinting and 16S rRNA gene clone libraries. *Syst Appl Microbiol* 33:165–173
16. Zarazua G, Ávila-Pérez P, Tejada S et al (2006) Analysis of total and dissolved heavy metals in surface water of a Mexican polluted river by total reflection X-ray fluorescence spectrometry. *Spectrochim Acta, Part B* 61:1180–1184
17. Cai Z, Zhou Q, Peng S et al (2010) Promoted biodegradation and microbiological effects of petroleum hydrocarbons by *Impatiens balsamina* L. with strong endurance. *J Hazard Mater* 183:731–737
18. Bastow TP, van Aarssen BGK, Lang D (2007) Rapid small-scale separation of saturate, aromatic and polar components in petroleum. *Org Geochem* 38:1235–1250
19. Wyndham R, Costerton J (1981) Heterotrophic potentials and hydrocarbon biodegradation potentials of sediment microorganisms within the Athabasca oil sands deposit. *Appl Environ Microb* 41:783–790
20. Luo YR, Tian Y, Huang X et al (2009) Analysis of community structure of a microbial consortium capable of degrading benzo(a)pyrene by DGGE. *Mar Pollut Bull* 58:1159–1163

21. Maarit Niemi R, Heiskanen I, Wallenius K et al (2001) Extraction and purification of DNA in rhizosphere soil samples for PCR-DGGE analysis of bacterial consortia. *J Microbiol Meth* 45:155–165
22. He Z, Zhao Y, Gao F et al (2010) Monitoring bacterial community shifts in bioleaching of Ni-Cu sulfide. *Bioresour Technol* 101:8287–8293
23. Gonzalez N, Simarro R, Molina MC et al (2011) Effect of surfactants on PAH biodegradation by a bacterial consortium and on the dynamics of the bacterial community during the process. *Bioresour Technol* 102:9438–9446
24. Wei GH, Yu JF, Zhu YH et al (2008) Characterization of phenol degradation by *Rhizobium* sp. CCNWTB 701 isolated from *Astragalus chrysopteru* in mining tailing region. *J Hazard Mater* 151:111–117
25. Gemini VL, Gallego A, de Oliveira VM et al (2005) Biodegradation and detoxification of nitrophenol by *Rhodococcus wratislaviensis*. *Int Biodeter Biodegr* 55:103–108
26. Zhang XS, Xu DJ, Zhu CY et al (2012) Isolation and identification of biosurfactant producing and crude oil degrading *Pseudomonas aeruginosa* strains. *Biochem Eng J* 209:138–146
27. Chang W, Dyen M, Spagnuolo L et al (2010) Biodegradation of semi-and non-volatile petroleum hydrocarbons in aged, contaminated soils from a sub-Arctic site: laboratory pilot-scale experiments at site temperatures. *Chemosphere* 80:319–326
28. Ting WTE, Yuan SY, Wu SD et al (2011) Biodegradation of phenanthrene and pyrene by *Ganoderma lucidum*. *Int Biodeter Biodegr* 65:238–242
29. Janbandhu A, Fulekar MH (2011) Biodegradation of phenanthrene using adapted microbial consortium isolated from petrochemical contaminated environment. *J Hazard Mater* 187:333–340
30. Krivobok S, Miriouchkine E, Seigle-Murandi F et al (1998) Biodegradation of Anthracene by soil fungi. *Chemosphere* 37:523–530
31. Jacques RJS, Santos EC, Bento FM et al (2005) Anthracene biodegradation by *Pseudomonas* sp. isolated from a petrochemical sludge landfarming site. *Int Biodeter Biodegr* 56:143–150
32. Das N, Chandran P (2011) Microbial degradation of petroleum hydrocarbon contaminants: an overview. *Biotechnol Res Int* 2011:941810
33. Zhang Z, Zhou Z, Yang C et al (2011) Degradation of n-alkanes and polycyclic aromatic hydrocarbons in petroleum by a newly isolated *Pseudomonas aeruginosa* DQ8. *Bioresour Technol* 102:4111–4116
34. Moscoso F, Deive FJ, Longo MA et al (2012) Technoeconomic assessment of phenanthrene degradation by *Pseudomonas stutzeri* CECT 930 in a batch bioreactor. *Bioresour Technol* 104:81–89
35. Morris JM, Jin S, Crimi B et al (2009) Microbial fuel cell in enhancing anaerobic biodegradation of diesel. *Biochem Eng J* 146:161–167
36. Hassanshahian M, Emtiazi G, Cappello S (2012) Isolation and characterization of crude-oil-degrading bacteria from the Persian Gulf and the Caspian Sea. *Mar Pollut Bull* 64:7–12
37. Dosta J, Nieto JM, Vila J et al (2011) Phenol removal from hypersaline wastewaters in a Membrane Biological Reactor (MBR): operation and microbiological characterisation. *Bioresour Technol* 102:4013–4020
38. Shao ZZ, Cui ZS, Dong CM et al (2010) Analysis of a PAH-degrading bacterial population in subsurface sediments on the Mid-Atlantic Ridge. *Deep-Sea Res Pt I* 57:724–730

Chapter 135

Isolation and Identification of Saline Tolerance Phosphate-Solubilizing Bacteria Derived from Salt-affected Soils and Their Mechanisms of P-solubilizing

Yang Han, Chunmei Wang, Xinglin Li, Xuefei Cao,
Aijia Cao and Na Zhao

Abstract The salt-affected soils of beach from Tianjin China were sampled to screen the saline tolerance phosphate-solubilizing bacteria (SA-T-PSB) using inorganic phosphorous medium. On basis of the phenotypic characterization and 16S rRNA gene sequencing, 4 isolates with the highest PSA, B1114, B1213, B1303, and J101 were identified as *Enterobacter ludwigii*, *Pantoea ananatis*, *Pseudomonas psychrotolerans*, and *Gluconobacter frateurii*, respectively. Subsequently, aimed to assaying the mechanisms of P-solubilizing, organic acid types of the 4 isolates were determined by high performance liquid chromatography. The results showed that all 4 isolates mainly secreted gluconic acid. The effect of carbon and nitrogen source on P-solubilization activity of the strains also indicated that the production of gluconic acid is the main mechanisms of P-solubilizing.

Keywords Microorganism isolation · Microorganism identification · Phosphate-solubilizing bacteria · P-solubilizing mechanisms

135.1 Introduction

Phosphorus as the most essential macronutrients beside N is the second largest agricultural fertilizer limiting the crop yields [1]. However, many soils in the world are P-deficient and thus cannot sustain the good crop yield [2]. Total P in soil generally ranges from 400 to 1,200 mg/kg which is far beyond the plant's requirement [3], but only a small proportion (about 0.1 %) can be efficiently utilized by plant [4]. Most P is precipitated with cations (Ca, Fe, Al) in the form of insoluble P which is unavailable to plant [5]. So the chemical P fertilizer is applied

Y. Han · C. Wang · X. Li (✉) · X. Cao · A. Cao · N. Zhao
Key Lab of Industrial Fermentation Microbiology, Ministry of Education,
Tianjin University of Science and Technology, Tianjin 300457, People's Republic of China
e-mail: lxlszf@tust.edu.cn

to yield, but a large proportion of available phosphate is rapidly transformed into its poorly soluble forms before plant absorbing it [6]. Microorganisms are considered to play a fundamental role in P cycle by biologically mediated processes. Phosphate solubilizing bacteria (PSBs) could dissolve fixed soil P to soluble form which is utilized by plant. Many reports showed that the application of PSBs could increase available P in soil and improve crop yields [7].

But environmental factors might affect severely on the colonization and performance of PSBs. Especially under stress of harsh environment, introduced PSBs cannot survive in quantity or compete with the native organisms in plant rhizosphere [5]. In China, the saline-alkali soil account nearly 4.88 % of the total cultivated area [8]. The saline-alkali soil is characterized with high salt, alkalinity, and low nutrition, which can lead to poor growth and low survival of PSBs [9]. Moreover, this soil with Ca-P as a major phosphorous source has a strong sorption and buffer capacity. The factors above are disadvantageous for the establishment and performance of PSBs [10, 11].

Native stress-tolerant microorganisms isolated from saline-alkali environment might survive and perform better under stress physiology. Therefore, the objective of the present research is to isolate SA-T-PSBs from the salt-affected soils in Tianjin.

135.2 Materials and Methods

135.2.1 Soil Sample and Isolation of Saline-Tolerance Phosphate Solubilizing Bacteria

The soil samples were locally collected from the salt-affected barren land (38°44' North, 117°46' West, Tianjin, China) in sterile plastic bags and conserved at -4 °C. The soils in this area were characterized by EC_e 38.36, organic matter 14.4 g/kg, total N, P 1.02 g/kg, and 1.62 g/kg, respectively, available P 30 mg/kg with pH 7.8. Soil pH was measured using a soil-to-water ratio of 1:2.5. Electrical conductivity (EC) was estimated using a saturation soil extract. To isolate SA-T-PSB, 1 g soil was homogenized in 50 sterile distilled water containing 0.85 % NaCl (w/v) and shaken at 240 rpm for 30 min. The serial dilution was plated on standard NBRIP growth agar mediums [12] amend with different concentrations of NaCl. The plates were incubated at 25 °C for 3 days. The isolates showing clear halo, which indicated P-solubilizing ability, were picked and further purified on NBRIP medium.

135.2.2 Quantitative Assay of Phosphate Solubilization

All purified isolates were estimated qualitatively in NBRIP liquid medium with Ca₃(PO₄)₂ (TCP) as single P source. After 7 days culture, the culture was centrifuged at 10,000 rpm for 10 min and filtered with 0.22 μm syringe filter.

The soluble P in the filtrate was measured by the Mo-blue method with a spectrophotometer at 700 nm [13]. The concentration of P was calculated by a standard curve obtained using KH_2PO_4 .

135.2.3 Physiology Identification of the SA-T-PSBs

The identification of the isolates was performed based on morphology and biochemical reactions including Gram staining, gelatin hydrolysis, oxidase test, methyl red test, Voges–Proskauer (V–P) reaction, and utilization of different carbon sources according to Bergey’s Manual of Systemic Bacteriology [14].

135.2.4 Molecular Identification of the SA-T-PSBs

The isolates were cultured in LB medium at 27 °C for 12 h, and their genomic DNA were extracted using BacteriaGen DNA kit (CW BIO, China). Amplification of the DNA templates was performed using the universal primers Ad (5'-AGA GTT TGA TCC TGG CTCA-3') and rJ (5'-GGT TAC CTT GTT ACG ACT T-3') [15]. The PCR reaction was performed using PCR kit (CW BIO, China). The cycle condition ran in iCycler thermocycler was 5 min of preheating at 95 °C, 30 cycles of 30 s of denaturation at 95 °C, 30 s of primer annealing at 55 °C, 2 min of elongation at 72 °C, and 10 min of extension step at 72 °C. The PCR products were sequenced by sequencing company. The sequences were compared with GenBank data (NCBI) for identification of the SA-T-PSBs.

135.2.5 Gluconic Acid Identification of the SA-T-PSBs

The culture filtrates as described above were diluted ten times and then used for the analysis of gluconic acid by HPLC (Agilent 1100, USA) equipped with KYA TECH HiQ Sil RP-C₁₈ column 250 × 4.6 mm. The mobile phase was 0.05 M KH_2PO_4 containing 5 % methanol with a pH 2.2 [16], the absorption was measured at 210 nm, the column temperature was 25 °C. The identification and estimation of the concentration of gluconic acid in sample were determined by comparing retention times and peak areas of chromatograms with the standards sample of gluconic acid, respectively.

135.2.6 Effect of Carbon and Nitrogen Source on P-solubilizing Activity of Strain J101

To study the effect of different carbon sources on the growth and P-solubilizing activity of strain J101, glucose was replaced with an equal amount (10 g/L) of

fructose or maltose or starch or lactose or sucrose or xylose or mannitol sterilized separately and added to the NBRIP medium. Ammonium sulfate was replaced with 0.5 g/L urea or potassium nitrate or ammonium chloride or ammonium oxalate or ammonium nitrate. The culture filtrate was analyzed for biomass, soluble P, and pH reduction.

135.2.7 Data Analysis

The data was subjected to analysis of variance (ANOVA) with the software SPSS version II. Statistical comparisons of their means were performed by the LSD test at $P \leq 0.05$. All values were the means of three replicates.

135.3 Results and Discussion

135.3.1 Isolation and Characterization of the Selected SA-T-PSBs

A total of 108 saline-tolerance isolates showing clear halos and/or different colonial morphology was selected and purified. The results showed that B1114, B1213, B1303, and J101 denote the highest P-solubilization values, with more than 400 mg/l in medium. And all SA-T-PSBs have the ability of tolerating 2.5 % NaCl stress. B1114, B1303 are able to tolerate 5 % NaCl stress (Table 135.1). The strains B1213 and B1303 have the ability of secreting IAA. The coastal saline-alkali soil in Tianjin was characterized with high salt concentrations and low nutrition which limited growth and performance of microorganisms, especially for some introduced strains. Therefore, the saline tolerance of isolates was considered as one of the main index for screening of PSBs. The initial screening of PSBs was processed in NBRIP plate with a saline stress condition (1.5 %). Four saline-tolerance PSBs which exhibited the highest P solubilizing ability among 108 isolates had a higher P solubilizing activity than those microorganisms of other reports [3, 17]. The SA-T-PSBs could express strong P-solubilization activity in a low available P environments, suggesting that the organisms might be of the adaptability in such a condition or on the basis of the so-called “stress physiology paradigm” proposed by Goldstein et al. [18].

135.3.2 Identification of the Selected SA-T-PSBs

Four selected SA-T-PSBs were shown to be Gram-negative and had small rods. Their colony morphologies were white or/and yellow, circular, smooth, raised and entire edge when observed in LB agar medium. All strains except B1114 are

Table 135.1 Solubilized P, final pH, salinity tolerance, and IAA production by 4 SA-T-PSBs

Isolates	Solubilized P (mg/l) ^a	Salinity tolerance (%)	Final pH ^a	IAA contents (mg/l) ^a
B1114	561 ± 23 a	5.0	4.91 ± 0.13 a	NO
B1213	582 ± 27 a	2.5	4.30 ± 0.07 b	13.47 ± 2.1 a
B1303	441 ± 42 b	2.5	4.16 ± 0.11 b	7.88 ± 0.51 b
J101	612 ± 25 a	1.5	3.37 ± 0.18 d	NO

^a The values were the mean ± SD from three replicates, and there was significant difference ($P \leq 0.05$) between the mean values with different letters by LSD

Gelatin hydrolysis, Oxidase, V-P reaction, Methyl red test positive, and Gelatin hydrolysis negative. B1114 is Gelatin hydrolysis positive. All 4 strains can utilize Glucose, Lactose, Fructose, Maltose, Starch, Sucrose, Glycogen, Mannitol, Glycerol, and Sorbitol as single carbon. By comparing the 16S rRNA gene sequences of the isolates with the GenBank database, it could be indicated that B1114 and B1213 were similar to *E. ludwigii* and *P. ananatis*, respectively, and B1303 and J101 were identified to be *P. psychrotolerans* and *G. frateurii*, respectively (Table 135.2).

135.3.3 Identification of Gluconic Acid

HPLC analysis of the culture filtrates showed that all of 4 SA-T-PSBs could secrete gluconic acid which was probably the major component since there is no other higher peak (Fig. 135.1). Furthermore, gluconic acid might be one of the major organic acids during P-solubilization. J101 with maximum P-solubilization produced the highest content of Gluconic acid (8.47 mM), followed by B1303 which had the lowest P-solubilizing ability (Fig. 135.1). The acidification of medium in process of bacteria-mediated insoluble solubilization suggested the possibility of organic acid produce which was main strategy for dissolution of insoluble phosphate through organometallic complex formation or through metal chelation processes. Particularly for Gram-negative bacteria, production of gluconic acid is the common and efficient organic acid during P solubilizing [19]. In this research, the authors identified and quantified the production of gluconic acid

Table 135.2 Identification of the SA-T-PSBs by 16S rDNA sequencing

Strains	GenBank accession numbers	Most similar organisms	Identity (%)
B1114	JX215328	<i>E. ludwigii</i>	99
B1213	JX215331	<i>P. ananatis</i>	99
B1303	JX215329	<i>P. psychrotolerans</i>	99
J101	JX215330	<i>G. frateurii</i>	99

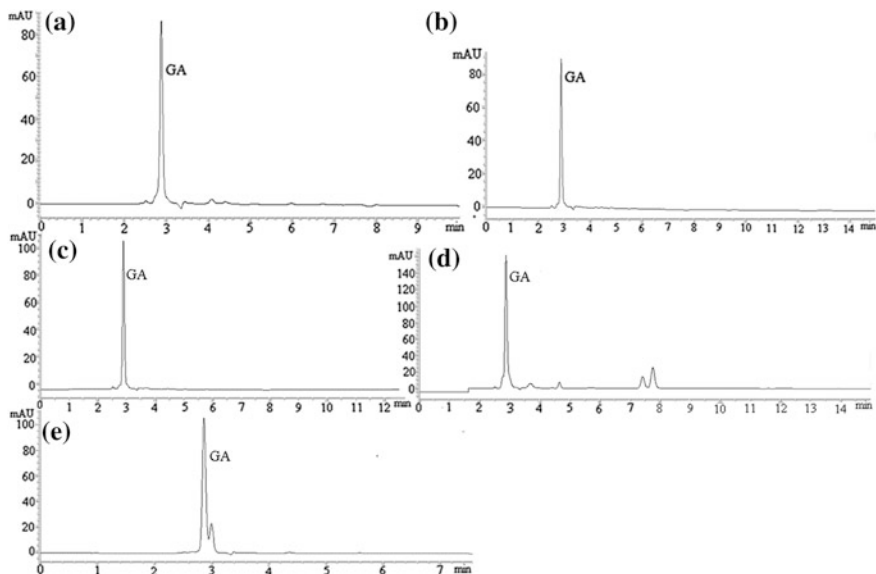


Fig. 135.1 Identification of gluconic acid of the SA-T-PSBs by HPLC

in supernate culture. Gluconic acid is the main organic acid produced by all 4 SA-T-PSBs as previous reports.

135.3.4 Effect of Carbon and Nitrogen Source on P-Solubilizing Activity of Strains J101

As Table 135.3 showed that, the different carbon source had significant effect on the growth, P-solubilizing activity and final medium pH. Different carbon sources in relation to P-solubilization activity were in the following order: glucose > xylose > maltose > mannitol > starch > lactose > sucrose > fructose.

The glucose and xylose were best carbon source for P-solubilizing. Strain J101 was able to grow with all carbon sources. For nitrogen source (Table 135.4), there was no significant effect on the P-solubilization activity of strain J101. The soluble P content released by strain J101 utilizing the glucose as single carbon source far higher than other carbon source, while there was no significant influence on the P-solubilization activity of J101 for various nitrogen source. This result was disagreement with Illmer and Schinner (1995) [20] who suggested that the protons releasing accompanying NH_3^+ assimilation account for the P solubilization. Our result indicated the gluconic acid was the main mechanism for P-solubilizing. There was no relation between the quantities of gluconic acid release by the SA-T-PSBs and the P-solubilizing value, though strain J101 with highest P-solubilization

Table 135.3 Effect of carbon source on P-solubilization value and cell biomass (OD₆₀₀) of strains J101^a

Carbon source	P-solubilization value	OD ₆₀₀	pH
Glucose	618 ± 48	0.62 ± 0.001	3.99 ± 0.07
Fructose	56 ± 2	0.67 ± 0.009	4.78 ± 0.11
Maltose	121 ± 10	0.24 ± 0.01	4.89 ± 0.21
Starch	65 ± 3	0.41 ± 0.008	4.9 ± 0.38
Lactose	63 ± 4	0.51 ± 0.012	4.9 ± 0.11
Sucrose	59 ± 2	0.73 ± 0.009	4.90 ± 0.21
Xylose	347 ± 10	0.69 ± 0.009	4.31 ± 0.13
Mannitol	91 ± 5	1.1 ± 0.012	4.85 ± 0.05

^a Values were the mean ± SD from three replicates

Table 135.4 Effect of nitrogen source on P-solubilization value and biomass (OD₆₀₀) of strains J101^a

Nitrogen source	P-solubilization value	OD ₆₀₀	pH
Ammonium sulfate	625 ± 19	0.536 ± 0.0119	3.66 ± 0.06
Potassium nitrate	504 ± 8	0.328 ± 0.057	3.36 ± 0.04
Ammonium chloride	532 ± 5	0.522 ± 0.0023	3.31 ± 0.03
Ammonium nitrate	613 ± 19	0.419 ± 0.0085	3.33 ± 0.11
Ammonium oxalate	510 ± 20	0.796 ± 0.0141	3.31 ± 0.03
Urea	534 ± 7	0.521 ± 0.0614	3.35 ± 0.03

^a Values were the mean ± SD from three replicates

ability produced the highest amounts of gluconic acid, which was in agreement with Yi Yanmei et al. (2008) [21].

135.4 Conclusion

In this study, we isolated four SA-T-PSB which have high P-solubilizing activity (≥ 400 mg/l). And the P-solubilizing mechanism of 4 strains is mainly to secrete the gluconic acid secretion.

Acknowledgments The work was supported by “National Training Project of College Students’ Innovative and Pioneering Work of Tianjin University of Science and Technology (201210057049)”, “The National Natural Science Foundation of China” and “Spark Plan of Ministry of Science and Technology of China (2012GA610011)”.

References

1. Hameeda B, Harini G, Rupela OP et al (2008) Growth promotion of maize by phosphate-solubilizing bacteria isolated from composts and macrofauna. *Microbiol Res* 163:234–242
2. Hinsinger P (2001) Bio-availability of soil inorganic P in the rhizosphere as affected by root induced chemical changes: a review. *Plant Soil* 237:173–195
3. Malboobi MA, Owlia P, Behbahani M et al (2009) Solubilization of organic and inorganic phosphates by three highly efficient soil bacterial isolates. *World J Microbiol Biotechnol* 25:1471–1477
4. Zou X, Binkley D, Doxtader KG (1992) A new method for estimating gross phosphorus mineralization and immobilization rates in soils. *Plant Soil* 147:243–250
5. Chang CH, Yang SS (2009) Thermo-tolerant phosphate-solubilizing microbes for multi-functional biofertilizer preparation. *Bioresour Technol* 100:1648–1658
6. Sulbarán M, Pérez E, Ball MM et al (2009) Characterization of the mineral phosphate-solubilizing activity of *Pantoea agglomerans* MMB051 isolated from an iron-rich soil in southeastern Venezuela (Bolívar State). *Curr Microbiol* 58:378–383
7. Kumar V, Behl RK, Narula N (2001) Establishment of phosphate-solubilizing strains of *Azotobacter chroococcum* in the rhizosphere and their effect on wheat cultivars under green house conditions. *Microbiol Res* 156:87–93
8. Yang JS (2008) Development and prospect of the research on salt-affected soils in China. *Acta Pedol Sin* 45:837–845
9. Nautiyal CS, Bhadauria S, Kumar P et al (2000) Stress induced phosphate solubilization in bacteria isolated from alkaline soils. *FEMS Microbiol Lett* 182:291–296
10. Gyaneshwar P, Naresh Kumar G, Parekh LJ (1998) Effect of buffering on the P-solubilizing ability of microorganisms. *World J Microbiol Biotechnol* 14:669–673
11. Zhang L, Song FB (2005) Sorption and desorption characteristic of cadmium by four different soil in northeast China. *Chin Geographical Sci* 15:344–347
12. Nautiyal CS (1999) An efficient microbiological growth medium for screening phosphate solubilizing microorganisms. *FEMS Microbiol Lett* 170:265–270
13. Murphy J, Riley JP (1962) A modified single solution method for the determination of phosphate in natural waters. *Anal Chim Acta* 27:31–36
14. Holt JG, Krieg NR, Sneath PHA et al (1994) *Bergey's Manual of Determinative Bacteriology*, 9th edn. Williams & Wilkins, Baltimore
15. Janvier M, Grimont PAD (1995) The genus *Methylophaga*, a new line of descent within phylogenetic branch γ of Proteobacteria. *Res Microbiol* 146:543–550
16. Farhat MB, Farhat A, Bejar W et al (2009) Characterization of the mineral phosphate solubilizing activity of *Serratia marcescens* CTM 50650 isolated from the phosphate mine of Gafsa. *Arch Microbiol* 191:815–824
17. Chen YP, Rekha PD, Arun AB et al (2006) Phosphate solubilizing bacteria from subtropical soil and their tricalcium phosphate solubilizing abilities. *Appl Soil Ecol* 34:33–41
18. Goldstein AH (1995) Recent progress in understanding the molecular genetics and biochemistry of calcium phosphate solubilization by gram negative bacteria. *Biol Agric Hortic* 12:185–193
19. Gulati A, Sharma N, Vyas P et al (2010) Organic acid production and plant growth promotion as a function of phosphate solubilization by *Acinetobacter rhizosphaerae* strain BIHB 723 isolated from the cold deserts of the trans-Himalayas. *Arch Microbiol* 192:975–983
20. Illmer P, Schinner (1995) Solubilization of inorganic calcium phosphates solubilization mechanisms. *Soil Biol Biochem* 27:257–263
21. Yi YM, Huang WY, Ge Y (2008) Exopolysaccharide: a novel important factor in the microbial dissolution of tricalcium phosphate. *World J Microbiol Biotechnol* 24:1059–1065

Chapter 136

Isolation and Characterization of a *Bacillus* Strain for Alkaline Wastewater Treatment

Kun Chen, Wenyu Shi, Jing Yang, Tong-cun Zhang and Hua Zhao

Abstract Biological treatment is one of the considerable choices for removing of organic pollutants present in petrochemical wastewaters. In this study, five strains, named as BS1, BS2, BS3, BS4 and BS5, were isolated from sludge nearby a petroleum smelter. BS5, the isolate with the highest COD removal rate, was identified as *Bacillus flexus*, based on 16S rDNA sequences. Subsequently, the optimized COD removal conditions of BS5 were investigated. It was indicated that the optimal conditions were 0.5 % corn starch, 1 % corn steep liquor, 35 C, pH 7.5, and 10 % (v:v) inoculation size. Under such circumstance, the removal rate of COD can reach 81.04 %. The isolation of *Bacillus flexus* strain BS5 provided an alternative for the bioremediation of alkaline wastewater. Lastly, the study showed that consecutive disposal process may help to reducing COD of wastewater effectively.

Keywords Alkaline wastewater · *Bacillus flexus* · Chemical oxygen demand

K. Chen · W. Shi · J. Yang · T.-C. Zhang · H. Zhao (✉)
Key Laboratory of Industrial Fermentation Microbiology, Ministry of Education,
College of Bioengineering, Tianjin University of Science and Technology, Tianjin 300457,
People's Republic of China
e-mail: zhaohua@tust.edu.cn

T.-C. Zhang · H. Zhao
Tianjin Key Laboratory of Industrial Microbiology, Tianjin 300457,
People's Republic of China

W. Shi
Tianjin Vocational Institute, Tianjin 300410, People's Republic of China

136.1 Introduction

Petrochemical production technology had become more sophisticated in recent years, in turns, organic substances in the sewage tends to be prosperous, which caused a great burden to traditional treatment process [11]. Sewage in petroleum processing industry was mainly resulted from liquid hydrocarbon alkali refining, diesel alkaline cleaning, and ethane pyrolysis gas alkaline cleaning process and so on [4]. Such sewage contained neutral oil, volatile phenol, sulfide and other toxic and detrimental organic substance in abundance [15], which endowed it with a high chemical oxygen demand (COD), high total dissolved solids, high levels of volatile phenol and sulfide, and high alkalinity [8].

The sewage discharged contaminates the environment gravely and also has seriously impacts on the subsequent disposal process [9]. Nowadays, most of sewage disposal techniques based on the recovery of the naphthenic acid and phenol [1], while the alkaline residue wastewater should be processed after the recovery [2].

Modern biotechnology, especially molecular techniques, to select and cultivate the dominant strains so to enhance the biological systems removal capability to refractory organics [12]. Comparing with other methods, this method has many advantages, such as lower cost, higher efficiency, easier to be handled and without secondary pollution [7]. All those characteristics attracted a great attention from all over the world [5]. Many relevant studies had been carried out, including printing and dyeing, chemical waste water and removal characteristics [3].

In this study, bacteria with high efficiency of degrading alkaline wastewater had been screened from sludge nearby a petroleum smelter. Furthermore, a strain with the highest COD removal rate was identified and characterized for the possible applications for environmental management.

136.2 Materials and Methods

136.2.1 Samples

Sludge samples were collected from a petroleum smelter.

136.2.2 Bacteria Screening Culture Medium

Screening culture medium was LB medium which containing a different proportion of pretreated alkaline wastewater.

Alkaline wastewater obtained from the oil refinery should be pretreated. Firstly, 5.5 % sulfate acids was added. 24 h later, the sublayer liquid was collected and

Table 136.1 Composition of the sublayer liquid

Properties	pH	COD(g/L)	Sulfide(mg/L)	Phenol(mg/L)
Values	6.73	58	996	41.39

used as experimental material. The main composition of the sublayer liquid obtained showed as Table 136.1.

136.2.3 Degrading Medium

The degrading medium was consisted of pretreated alkaline wastewater, necessary salts for growth, extra carbon and nitrogen sources. The pH value was adjusted to 7.0. The medium was sterilized at 121 C for 20 min.

136.2.4 Isolation of Strains Degrading Alkaline Wastewater

Enrichment and isolation of bacteria degrading alkaline wastewater were done using bacteria screening culture medium.

136.2.5 Identification of the Bacteria Isolated

DNA extraction was adapted from the protocol previously. The 16S rDNA was amplified by PCR using the following universal primers pairs, 5'-AGTTTG ATCCTGGCTCA-3' and 5'-ACGGCTACCTTGTTACGACTT GCA-3' [2]. The protocol consisted of 30–33 cycles of incubation at 94 C for 30 s, 58 C for 30 s, and 72 C for 1 min, followed by extension for 5 min at 72 C. The 16S rDNA amplified was sequenced and blast before it was submitted to NCBI GenBank.

136.2.6 Method of COD Determination

The COD was determined by potassium dichromate method [14]. Wash culture tubes and caps with 20 % H₂SO₄ before using to prevent contamination. Place sample in culture tube or ampule and add digestion solution. Carefully run sulfuric acid reagent down inside of vessel so an acid layer is formed under the sample-digestion solution layer and tightly cap tubes or seal ampules, and invert each several times to mix completely. Place tubes or ampules in block digester

preheated to 150 C and reflux for 2 h behind a protective shield. Cool to room temperature and place vessels in test tube rack. Some mercuric sulfate may precipitate out but this will not affect the analysis. Remove culture tube caps and add small TFE-covered magnetic stirring bar. Add 0.05 to 0.10 mL (1 to 2 drops) ferroin indicator and stir rapidly on magnetic stirrer while titrating with standardized 0.10 M FAS (ferrous ammonium sulfate titrant). The end point is a sharp color change from blue-green to reddish brown, although the blue-green may reappear within minutes. In the same manner reflux and titrate a blank containing the reagents and a volume of distilled water equal to that of the sample.

136.2.7 Determination of the Optimized Alkaline-Degrading Condition

The effects of different carbon sources, nitrogen sources, pH, temperature, inoculum concentration and consecutive treatment process on COD removal rate were investigated.

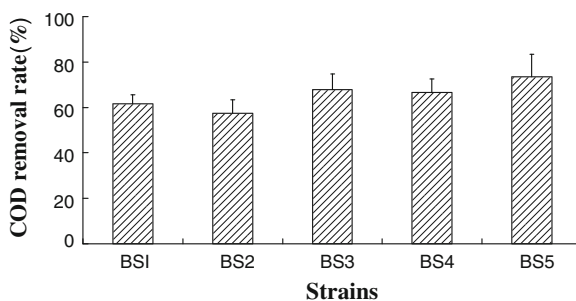
136.3 Results and Discussion

136.3.1 Isolation of Strains with High Alkaline Wastewater Degrading Activity

Five bacteria exhibiting high alkaline wastewater degrading activity were isolated after serial enrichment, which called BS1, BS2, BS3, BS4 and BS5 respectively.

The COD removal rate of the five optimized strains was compared as Fig. 136.1. It was showed that BS5 had the highest COD removal rate, which was up to 73.42 %.

Fig. 136.1 COD removal rate of five strains. The strains were inoculated into pretreated alkaline wastewater, respectively, and then cultured at 35 C at 150 r/min, the pH was control at 7.0. Fifty h later, the COD value was measured



136.3.2 Identification of BS5

The genome DNA of BS5 was extracted and its 16S rDNA was amplified by PCR. The 1067 bp product was sequenced and analyzed. It was identified as *Bacillus flexus*. The 16S rDNA sequence was submitted to NCBI GenBank and the accession number was JX677863.

136.3.3 Effects of Nutrient Substances on the COD Removal Rate of BS5

In the processes of alkaline wastewater treatments, bacteria make use of all kinds of organic pollutant as nutrition for their growth and proliferation. But these nutrients in industry wastewater cannot fully meet the need of these demands. So, some extra nutrition should be added.

136.3.4 Effects of Different Carbon Sources on the COD Removal Rate

Glucose, sucrose, maltose and corn starch were chosen as carbon source, respectively. The group without extra carbon source was used as control. As shown in Fig. 136.2, the addition of carbon source remarkably increased the COD removal rate of the alkaline wastewater. It was proved that the best carbon source was corn starch.

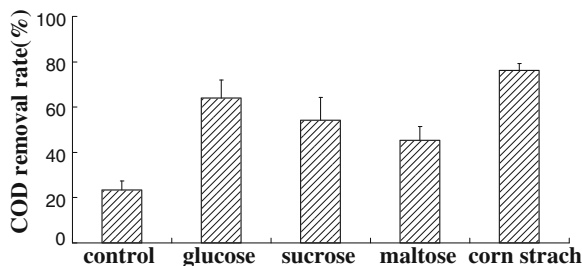


Fig. 136.2 Effects of different carbon sources on the COD removal rate. BS5 was inoculated into degrading medium. 0.5 % (m:m) glucose, sucrose, maltose and corn starch were added respectively, inoculum size 10 %, then cultured at 35 C at 150 r/min, the pH was control at 7.0. 50-h later, the COD value was measured

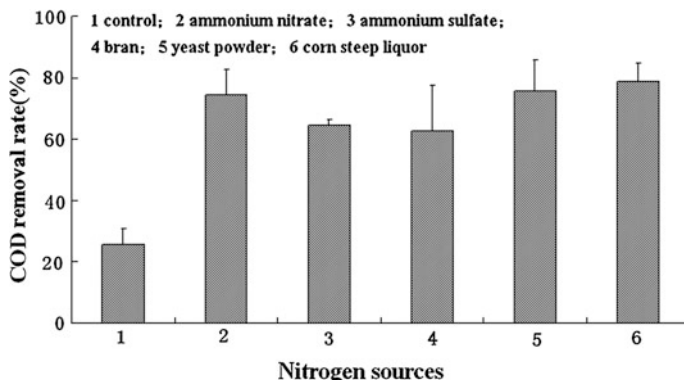


Fig. 136.3 Effects of different nitrogen sources on the COD removal rate. BS5 was inoculated into degrading medium. 1 % (m:m) ammonium nitrate, ammonium sulfate, bran, yeast powder and corn steep liquor was added, respectively. Corn starch (0.5 %) was used as carbon source. The culture condition were inoculum size 10 %, 35 C, pH 7.0, and agitation rate 150 r/min. 50-h later, the COD value was measured

136.3.5 Effects of Different Nitrogen Sources on the COD Removal Rate

Ammonium nitrate, ammonium sulfate, bran, yeast powder and corn steep liquor was selected as extra nitrogen source, respectively. The group without additional nitrogen source was used as control. It was showed that these nitrogen sources can increase the COD removal rate dramatically (Fig. 136.3). Corn steep liquor was performed as the optimal nitrogen source.

Besides nutrition, the physical culture conditions can also have dramatically influences on the wastewater disposal process.

136.3.6 Effects of Temperature on the COD Removal Rate

The effects of temperature on the COD removal rate of BS5 in degrading medium were studied. It was showed that the optimum growth temperature for higher degrading rate was 35 C. When the temperature was less than 25 C or more than 40 C, the COD removal rate decreased significantly (Fig. 136.4).

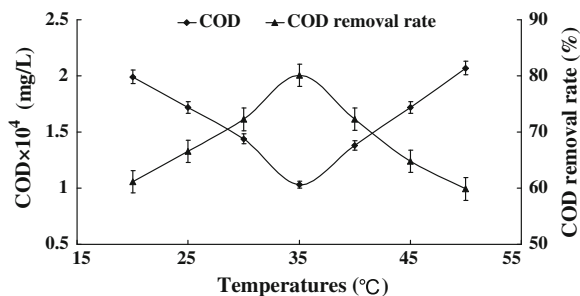


Fig. 136.4 Effects of temperature on the COD removal rate. BS5 was inoculated into degrading medium and cultured at temperatures ranging from 20 °C to 50 °C. The culture condition were 0.5 % corn starch, 1 % corn steep liquor, inoculum size 10 %, pH 7.0, and agitation rate 150 r/min. 50-h later, the COD value was measured

136.3.7 Effects of pH on the COD Removal Rate

The effects of pH on the COD removal rate were tested. It was obviously presented that the optimum pH value for COD removal was 7.5 (Fig. 136.5). When pH < 6.0, COD removal rate was less than 50 %. If pH was higher than 6.0, the COD removal rate increased rapidly while pH increased. Until pH was 7.5, COD removal rate reached its peak. If pH > 7.5, the COD removal rate decreased dramatically.

136.3.8 Effects of Inoculum Size on the COD Removal Rate

The influence of inoculum size on the COD removal rate was investigated. Six different inoculum sizes (4 %, 6 %, 8 %, 10 %, 12 %, 14 %, 16 %) were test. It

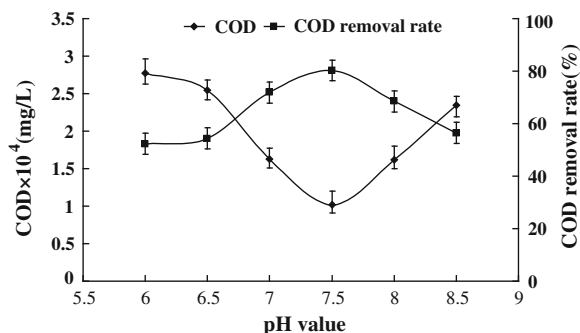


Fig. 136.5 Effects of pH on the COD removal rate. BS5 was inoculated into degrading medium at pH 6.0, 6.5, 7.0, 7.5, 8, and 8.5, respectively. The condition of culture was as following, the volume of the alkaline wastewater was 30 mL/250 mL, 0.5 % corn starch, 1 % corn steep liquor, 10 % inoculum size, then cultured at 35 °C at 150 r/min. 50-h later, the COD value was measured

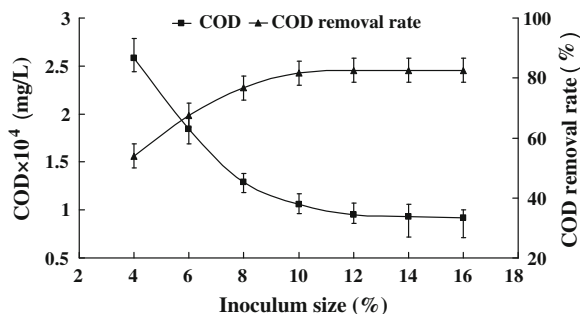


Fig. 136.6 Effects of inoculum size on the COD removal rate. BS5 was inoculated into degrading medium at six different inoculum size (4, 6, 8, 10, 12, 14, and 16 %). The condition of culture was as following, the volume of the alkaline wastewater 30 mL/250 mL, 0.5 % corn starch, 1 % corn steep liquor, then cultured at 35 °C, pH 7.5, at 150 r/min. 50-h later, the COD value was measured

could be concluded from the results presented in Fig. 136.6 that inoculum size would have a major influence on bacteria breeding and COD removal rate. When inoculum size was low, the degradation was lower obviously. When the inoculum size increased, the COD removal rate increased gradually. The COD removal rate reached 81.04 % while the inoculum size was 10 %. But the increment of COD removal rate was not obvious if inoculum size continued to increase. So the optimum inoculum size was set as 10 %.

136.3.9 Effects of Consecutive Treatment on the COD Removal Rate

The performance of optimized strain BS5 was stable by taming. The COD of alkaline wastewater obviously decreased under the optimized condition after 50 h-treatment with the bacteria. But when the initial COD of wastewater was very high, the COD of treated wastewater cannot satisfy the demand of discharge or utilization standards. Take it into account, consecutive treatment processes may be necessary.

The wastewater disposed for one, two or three times process, and the corresponding COD removal rate was showed. According to the data presented in Fig. 136.7, the aim of consecutive treatment on the COD removal rate was achieved. After the first round treatment, the COD removal rate was up to 78.3 %. Whereas, the second round treatment culture enabled the COD removal rate reached 90.5 %. Through a third disposal process, the COD removal rate was 96.2 %. It was considered that consecutive disposal process may help to reducing COD of wastewater effectively.

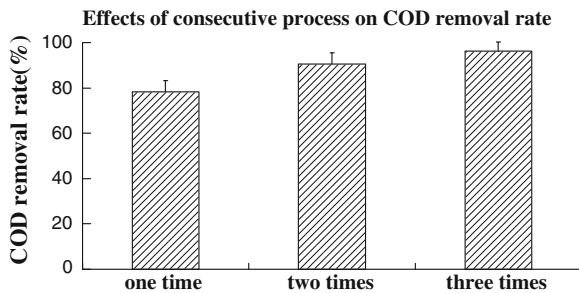


Fig. 136.7 Effects of consecutive process on COD removal rate. Firstly, treated alkaline wastewater at the speed 4000 r/min, 10 min, and take 30 mL clear liquid to 250 mL flask. The culture condition were 0.5 % corn mill, 1 % corn steep liquor, 35 °C, pH 7.5, 10 % inoculum size and agitation rate 150 r/min. 50-h later, the COD value was measured. The wastewater disposed by one, two, three times process, and the correspond COD removal rate was showed

136.4 Conclusion

The organic pollutants in petrochemical and oil refining which are resistant to degradation can be dreadfully hazardous to human health. As they persist in the environment, they are capable of long range transportation, bioaccumulation in human and animal tissue and biomagnification in food chain [13]. Thus treatment of alkaline wastewaters is necessary and biological methods are the most appropriate techniques due to mineralization of toxic organic compounds and inexpensiveness [10].

The use of microbial catalysts in the biodegradation of organic compounds has advanced significantly during the past days. It has been found that large numbers of microbes co-exist in almost all natural environments. Identification of effective microbial species is considered as one of the important priorities for production of the biomass in order to achieve desirable kinetic of biological reactions [6].

At the same time, several external factors can limit the rate of biodegradation of organic compounds. These factors may include temperature, pH, oxygen content and availability, substrate concentration and physical properties of contaminants. Each of these factors should be optimized for the selected organism for the maximum degradation of the organic compound of choice.

In this study, strains degrading alkaline wastewater were isolated from the sludge nearby petroleum smelter and enriched, among which BS5 performed the highest degradation ability. Furthermore, BS5 was identified as *Bacillus flexus* through 16S r DNA and some other data (not shown in this paper). Data presented in this study demonstrated that the strain's optimum disposal condition should be 0.5 % corn starch, 1 % corn steep liquor, temperature 35 C, initial pH 7.5, 10 % inoculation size. In such conditions, the removal rate of COD can be up to 81.04 % and almost 10.38 % higher than before. Meanwhile, successive process was developed to enhance the degradation efficiency.

In conclusion, a *Bacillus flexus* strain characterized stable performance and inexpensive cost in alkaline wastewater treatment was isolated and identified, which has prospective application values in this area.

Acknowledgments This work was supported by the Tanggu Technical Development Foundation Grant of Tianjin in China.

References

1. Choe EK, Son EJ, Lee BS et al (2005) NF process for the recovery of caustic soda and concentration of disodium terephthalate from alkaline wastewater from polyester fabrics. *Desalination* 186(1–3):29–37
2. David AB, Peter RR (1995) Sequence and analysis of the O antigen gene (*rfb*) cluster of *Escherichia coli* 0111. *J. Gene* 164(1):17–23
3. García Becerra FY, Acosta EJ et al (2010) Alkaline extraction of wastewater activated sludge biosolids. *Bioresour Technol* 101(18):6972–6980
4. Garcia GI, Pena PRJ, Venceslada B et al (2000) Removal of phenolic compounds from olive mill wastewater using *Phanerochaete chrysosporium*, *Aspergillus terreus* and *Geotrichum candidum*. *Proc Biochem* 35(8):751–758
5. Leal K, Chacin E, Behling E et al (1998) A mesophilic digestion of brewery wastewater in an unheated anaerobic filter. *Bioresour Technol* 65(1–2):51–55
6. Liu WT, Chan OC, Fang HH (2002) Characterization of microbial community in granular sludge treating brewery wastewater. *Water Res* 36(7):1767–1775
7. Loh KC, Liu J (2001) External loop inversed fluidized bed aircraft bioreactor (EIFBAB) for treating high strength phenolic waste water. *Chem Eng Sci* 56:6171–6176
8. Ma FR, Mu T, Bai B et al (2006) Application of High-concentration Sewage Disposal Technology in Treatment of Diesel Alkaline Residue. *J Environ Protect Oil & Gas Fields* 16(2):19–21
9. Prisciandaro M, Mazziotti di Celso G, Vegliò F (2005) Development of a reliable alkaline wastewater treatment process: optimization of the pre-treatment step. *Water Res* 39(20):5055–5063
10. Prieto MB, Hidalgo A, Rodriguez FC et al (2002) Biodegradation of phenol in synthetic and industrial wastewater by *Rhodococcus erythropolis*. UPV-1 immobilized in air-stirred reactor with clarifier. *Appl Microbiol Biotechnol* 58:833–859
11. Rao AG, Reddy TS, Prakash SS et al (2007) pH regulation of alkaline wastewater with carbon dioxide: A case study of treatment of brewery wastewater in UASB reactor coupled with absorber. *Bioresour Technol* 98(11):2131–2136
12. Richard ES (1983) Anaerobic biotechnology for industrial wastewater treatment. *J Environ Sci Technol* 17(9):416–427
13. Robles A, Lucas R, Cienfuegos AD et al (2000) Phenol oxidase activity in strains of the hyphomycete *Chalara paradoxa* isolated from Olive mill wastewater disposal ponds. *Enzyme Microbial Technol* 26(7):484–490
14. Rocenkery M (1993) The fast method of the COD determination. *Anal Lett* 26(9):2025–2030
15. Xie WY, Tan GQ, Zhong L (2007) Research and application of treatment technology for alkaline waste from oil refinery. *J M Chem Ind* 27(6):10–14